



McErlain, Holly (2022) *The development of novel PET imaging agents for the poly(ADP-ribose) polymerase 1 and synaptic vesicle 2A proteins*. PhD thesis.

<https://theses.gla.ac.uk/83218/>

Copyright and moral rights for this work are retained by the author

A copy can be downloaded for personal non-commercial research or study, without prior permission or charge

This work cannot be reproduced or quoted extensively from without first obtaining permission from the author

The content must not be changed in any way or sold commercially in any format or medium without the formal permission of the author

When referring to this work, full bibliographic details including the author, title, awarding institution and date of the thesis must be given

Enlighten: Theses

<https://theses.gla.ac.uk/>
research-enlighten@glasgow.ac.uk

The Development of Novel PET Imaging Agents for the Poly(ADP-Ribose) Polymerase 1 and Synaptic Vesicle 2A Proteins

Holly McErlain, MChem

A thesis submitted in part fulfilment of the requirements of the degree of Doctor of Philosophy

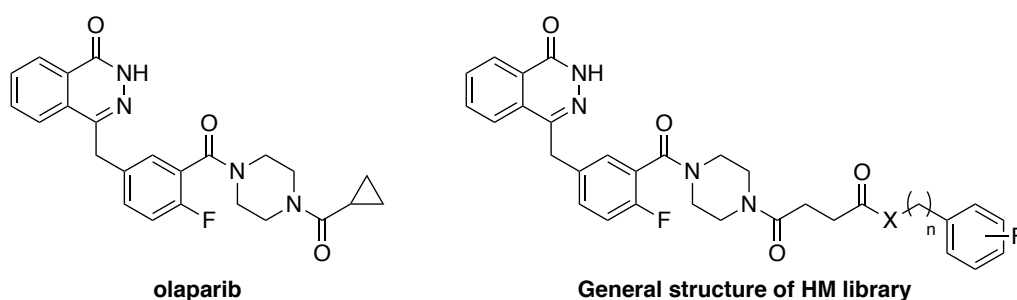


**University
of Glasgow**

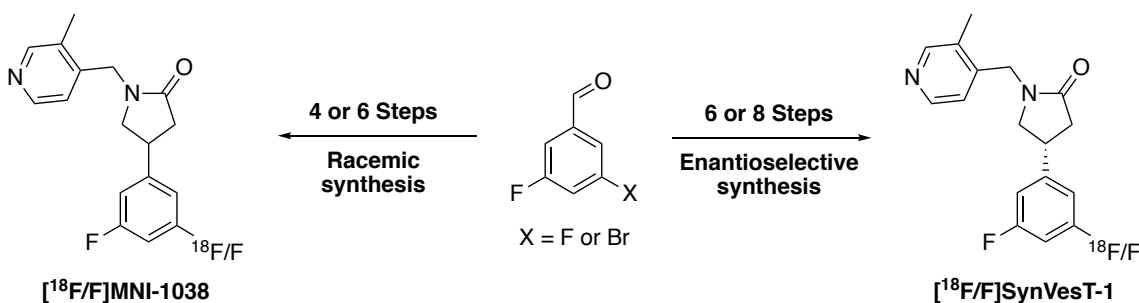
School of Chemistry
College of Science & Engineering
University of Glasgow
July 2022

Abstract

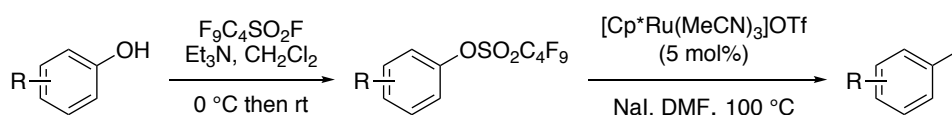
The primary focus of this PhD research was the development and synthesis of several potential PET imaging agents for the PARP-1 and SV2A proteins. The first section of this thesis details the synthesis of a small library of novel PARP-1 inhibitors (HM library) with capacity for application as PET imaging agents. The core structure of these compounds was that of established PARP-1 inhibitor olaparib and was modified with a novel linker to allow incorporation of aromatic units that could undergo late-stage radiolabelling. The physicochemical properties of this library were determined *via* HPLC methodology and subsequently, four candidates were submitted to *in vitro* biological testing of PARP-1 inhibition. Finally, an initial optimisation study for the radiosynthesis of a novel fluorine-18 PET imaging agent for PARP-1 was conducted.



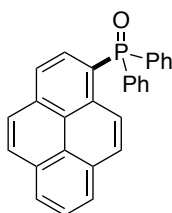
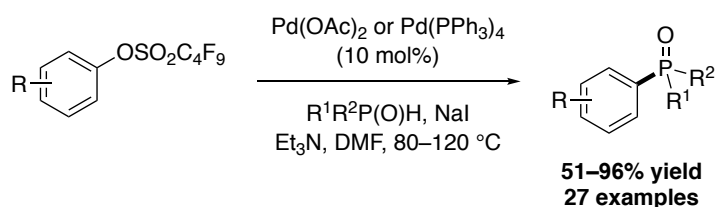
The second section describes a new six-step racemic synthesis of [^{18}F]MNI-1038 an established PET imaging agent for the SV2A protein *via* an organotin precursor, and the fluorine-19 equivalent. Modification of this route and utilisation of asymmetric iminium organocatalysis facilitated the first enantioselective synthesis of the important PET radiotracer [^{18}F]SynVesT-1 in eight steps, and the corresponding fluorine-19 analogue.



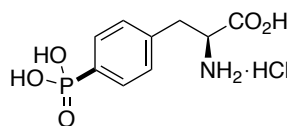
The final section describes the exploration of two novel transition metal-catalysed methods for the transformation of ubiquitous phenols *via* aryl nonafluorobutanesulfonates. Firstly, a new ruthenium-catalysed reaction for the iodination of arenes was examined. This study produced some promising results and demonstrated the potential for application of this methodology in the synthesis of SPECT imaging agents.



Subsequently, a novel sodium iodide-accelerated, palladium-catalysed reaction was developed for the construction of aryl C–P bonds. The synthetic utility of this methodology was then exemplified through the synthesis of various organophosphorus compounds including triarylphosphine oxides, dialkyl arylphosphine oxides, aryl phosphonates and an aryl phosphinate. Furthermore, this reaction was employed for the synthesis of an organic light emitting diode (OLED) material and a phosphonophenylalanine mimic with applications in medicinal chemistry.



OLED material



phosphonophenylalanine
mimic

Table of Contents

Abstract	2
Acknowledgments	7
Author's Declaration	9
Abbreviations	10
1.0 Introduction	15
1.1 Molecular Imaging	15
1.1.1 Positron Emission Tomography Imaging	16
1.1.1.1 PET Imaging Radionuclides	17
1.1.2 Single Photon Emission Computed Tomography Imaging	20
1.1.2.1 SPECT Imaging Radionuclides	20
1.2 Poly(ADP-Ribose) Polymerase 1 (PARP-1)	24
1.2.1 PARP-1 Structure and Function in DNA Damage Response	24
1.2.2 PARP-1 Inhibitors as Cancer Therapeutics	29
1.2.3 PARP-1 Inhibitor-Derived PET and SPECT Imaging Agents	33
1.2.3.1 Rucaparib-Derived PET and SPECT Imaging Agents for PARP-1	34
1.2.3.2 Olaparib-Derived PET and SPECT Imaging Agents for PARP-1	36
1.3 Synaptic Vesicle Glycoprotein 2A (SV2A)	41
1.3.1 Structure, Localisation and Proposed Functions of SV2A	41
1.3.2 SV2A as a Therapeutic Target for Epilepsy	43
1.3.3 PET and SPECT Imaging Agents for SV2A	46
1.4 Conclusion	49
2.0 Results and Discussion	51
2.1 Synthesis of Novel Olaparib-Derived PET Imaging Agents for PARP-1	51
2.1.1 Unpublished Previous Work in the Sutherland Group	51
2.1.2 Proposed Research	54
2.1.3 Synthesis of the Olaparib Core Structure	60
2.1.4 Synthesis of Olaparib-BODIPY FL (37)	66
2.1.5 Synthesis of Novel Olaparib-Derived PARP-1 Inhibitors	70
2.1.6 Physicochemical Properties Evaluation of Novel Olaparib-Derived PARP-1 Inhibitors	73
2.1.6.1 Partition Coefficient	74
2.1.6.2 Plasma Protein Binding	74
2.1.6.3 Membrane Partition Coefficient and Permeability	75
2.1.6.4 Physicochemical Properties of Novel PARP-1 Inhibitors	75
2.1.7 <i>In Vitro</i> Biological Evaluation of Novel Olaparib-Derived PARP-1 Inhibitors	79

2.1.8 Radiochemistry	82
2.1.8.1 Synthesis of Aryl Pinacol Boronic Ester Precursor 74	82
2.1.8.2 Synthesis of Analytical Standard 31 and Precursors 39 and 76	84
2.1.8.3 Development of HPLC Conditions	85
2.1.8.4 Production of [¹⁸ F]Fluoride	89
2.1.8.5 Radiosynthesis of [¹⁸ F]31 from Precursor 39	90
2.1.8.6 Radiosynthesis of [¹⁸ F]31 from Precursor 76	93
2.1.9 Conclusions and Future Work	95
2.2 Novel Enantioselective Synthesis of [¹⁸F]SynVesT-1 ([¹⁸F](<i>R</i>)-24): A PET Imaging Agent for SV2A	99
2.2.1 Proposed Research	99
2.2.2 Initial Enantioselective Synthetic Route to [¹⁸ F]SynVesT-1 ([¹⁸ F](<i>R</i>)-24)	104
2.2.3 Revision of Synthetic Strategy	110
2.2.4 Racemic Synthetic Route to MNI-1038 (24) and [¹⁸ F]MNI-1038 ([¹⁸ F]24)	113
2.2.4.1 Synthesis of MNI-1038 (24)	113
2.2.4.2 Synthesis of 85: Precursor to [¹⁸ F]MNI-1038 ([¹⁸ F]24)	115
2.2.5 Revised Enantioselective Synthetic Route to SynVesT-1 ((<i>R</i>)-24) and [¹⁸ F]SynVesT-1 ([¹⁸ F](<i>R</i>)-24)	120
2.2.5.1 Enantioselective Synthesis of SynVesT-1 ((<i>R</i>)-24)	120
2.2.5.2 Enantioselective Synthesis of (<i>R</i>)-85: Precursor to SynVesT-1 ((<i>R</i>)-24)	125
2.2.6 Radiosynthesis of [¹⁸ F]MNI-1038 ([¹⁸ F]24) and [¹⁸ F]SynVesT-1 ([¹⁸ F](<i>R</i>)-24)	128
2.2.7 PET Imaging of SV2A with [¹⁸ F]MNI-1038 ([¹⁸ F]24) and [¹⁸ F]SynVesT-1 ([¹⁸ F](<i>R</i>)-24)	130
2.2.8 Conclusions and Future Work	133
2.3 Transition Metal-Catalysed Reactions of Aryl Nonaflates	137
2.3.1 Introduction	137
2.3.2 Previous Work in the Sutherland Group	146
2.3.3 Proposed Research	150
2.3.4 Ruthenium-Catalysed Iodination of Aryl Nonaflates	150
2.3.4.1 Synthesis of Aryl Nonaflates	150
2.3.4.2 Investigation of Ruthenium-Catalysed Iodination	153
2.3.4.3 Investigation of an Alternative Ruthenium Catalyst	160
2.3.5 Metal-Free Iodination of Aryl Nonaflates <i>via</i> an S _N Ar Reaction	163
2.3.6 Palladium-Catalysed Iodination of Aryl Nonaflates	165
2.3.7 Iodide-Accelerated, Palladium-Catalysed Phosphorylation Reactions of Aryl Nonaflates	174
2.3.7.1 Background of Metal-Catalysed Aryl Phosphorylation	174
2.3.7.2 Proposed Research	177

2.3.7.3 Synthesis of Supplementary Aryl Nonaflates	178
2.3.7.4 Optimisation and Investigation of Mechanism	179
2.3.7.5 Substrate Scope	187
2.3.7.6 Synthesis of Aryl Phosphorus Compounds with Functionality	190
2.3.8 Conclusions and Future Work	192
3.0 Experimental	197
3.1 General Experimental	197
3.2 PARP-1 Experimental	198
3.3 HPLC Methods for Physicochemical Properties Analysis	229
3.4 SV2A Experimental	232
3.5 Transition Metal-Catalysed Reactions of Aryl Nonaflates Experimental	251
4.0 References	302
5.0 Appendices	327
5.1 Appendix I – Raw Data Obtained from HPLC Determination of Physicochemical Properties	327
5.1.1 Percentage of Plasma Protein Binding (%PPB) <i>via</i> Human Serum Albumin (HSA) Chromatography	327
5.1.2 Membrane Permeability (P_m) and Membrane Partition Coefficient (K_m) <i>via</i> Immobilised Artificial Membrane (IAM) Chromatography	328
5.2 Appendix II – Schematic of FX_{FN} Synthesiser	330
5.3 Appendix III – Chiral HPLC Traces	331

Acknowledgments

Firstly, I would like to thank my supervisor Professor Andy Sutherland for allowing me to undertake this PhD research in his group. Thank you for all your guidance and support that you have given me over the years. I would also like to thank Dr David France for all his help and advice as my second supervisor. I am extremely grateful to the Scottish government for funding my undergraduate studies without which I would not have reached this point. Financial funding for this PhD research was graciously donated by Ian Sword and the University of Glasgow and is gratefully acknowledged.

Thank you to Maria and Professor Anthony Chalmers for performing biological testing of the PARP-1 project. Thank you to all the staff at the West of Scotland PET RPU, Dr Sally Pimlott, Dr Sue Champion and Dr Dmitry Solovyev for being so welcoming. A special thank you to Dr Gavin Brown who supervised and taught me to perform fluorine-18 radiosynthesis. Thank you to Dr Adriana Tavares, Professor Seth Grant, and their respective research groups for collaboration. I would like to express my gratitude to the technical staff of the Joseph Black Building for all their help over the years including, Frank (lab technician), Andy (mass spec), David and Alec (NMR), Karen and Finlay (stores) and Stuart and Arlene (IT support).

Thanks to all past Sutherland group members past, Nikki (for your many helpful chemistry and music chats), Alex, Kerry (for all your amazing stories), Tim, Jonny, Réka (for your lasting friendship), Martyn, Maria and Beckie. A huge thanks to the present members, Leanne, Rochelle, Amy, Nina, Lachlan, and Valeria for the constant laughter and making the lab such an enjoyable place to work. Thanks also to the Hartley group past and present, especially Stuart (for all your advice and one-liners), Joe (for our debates and your jokes), and Becca (for being the best friend I could have wished for to share this experience with).

Outside of the lab, I would like to thank the “Quaranqueens” for your friendship and the many zoom quizzes that saw us through the worst of covid times. Special thanks to Steph and Lee for the last five years of adventures. A massive thank you to Lauren for your love, support, and friendship since we were five years old pretending to be chemists by making lip gloss together! Thank you so much Fraser for

everything you have done over the last five years to support my ambitions. Life is so much better with you, I love you! Thank you to the Andersons for welcoming me into your family, your love and support is amazing! I would like to dedicate this thesis in part to the late Colin Anderson.

I will never be able to thank my family enough, my mum Helen, my dad Thomas, Chris, Emma, Evie, Cora, and Loki. You have all given me invaluable love and support throughout my entire life, especially these last five years. I could not have done any of this without you by my side, I love you always and forever! I would also like to dedicate this thesis to my late dad Thomas McErlain who inspired my career in science.

Author's Declaration

I declare that, except where explicit reference is made to the contribution of others, this thesis represents the original work of Holly McErlain and has not been submitted for any other degree at the University of Glasgow or any other institution. The research was carried out at the University of Glasgow in the Loudon Laboratory under the supervision of Professor Andrew Sutherland between October 2017 and May 2021. Aspects of the work described herein have been published elsewhere as listed below.

E. Dubost, **H. McErlain**, V. Babin, A. Sutherland, T. Cailly, Recent Advances in Synthetic Methods for Radioiodination, *J. Org. Chem.*, 2020, **85**, 8300–8310.

H. McErlain, L. M. Riley, A. Sutherland, Palladium-Catalysed C–P Bond-Forming Reactions of Aryl Nonaflates Accelerated by Iodide, *J. Org. Chem.*, 2021, **86**, 17036–17049.

H. McErlain, E. B. McLean, T. E. F. Morgan, V. K. Burianova, A. A. S. Tavares, A. Sutherland, Organocatalytic Asymmetric Synthesis of SynVesT-1, A Synaptic Density PET Imaging Agent, Accepted for publication in *J. Org. Chem.*, 2022.

Signature

Printed Name

Holly McErlain

Abbreviations

acac	Acetylacetonate
ADME	Absorption, distribution, metabolism, and elimination
ADP	Adenosine diphosphate
AGP	α_1 -Acid glycoprotein
AP	Apurinic/aprimidinic
APE1	Apurinic/aprimidinic endonuclease 1
Ar	Aromatic
ART	ADP-ribosyltransferase
ARTD1	Diphtheria toxin-like ADP-ribosyltransferase 1
A_m	Molar activity
a.u.	Arbitrary units
BBB	Blood-brain barrier
BER	Base excision repair
Boc	<i>tert</i> -Butyloxycarbonyl
br	Broad
BRCA1	Breast cancer type 1 susceptibility protein
BRCA2	Breast cancer type 2 susceptibility protein
Bq	Becquerel
Bu	Butyl
CT	Computed tomography
dba	Dibenzylideneacetone
dppf	1,1'-Bis(diphenylphosphine)ferrocene
CGRP	Calcitonin gene-related peptide
cLog P	Calculated partition coefficient
COSY	Correlated spectroscopy
Cp*	Pentamethylcyclopentadiene
d	Doublet
DBU	1,8-Diazabicyclo[5.4.0]undec-7-ene
DDR	DNA Damage repair
DEPT	Distortionless enhancement polarisation transfer
DIPEA	<i>N,N</i> -Diisopropylethylamine
DMA	<i>N,N</i> -Dimethylacetamide

DMAP	4-Dimethylaminopyridine
DMF	<i>N,N</i> -Dimethylformamide
DMI	1,3-Dimethyl-2-imidazolidinone
DMSO	Dimethylsulfoxide
DNA	Deoxyribonucleic acid
DSB	Double-strand break
EC ₅₀	Half-maximal effective concentration
<i>ee</i>	Enantiomeric excess
EI	Electron impact
EMA	European Medicines Agency
Equiv.	Equivalents
<i>er</i>	Enantiomeric ratio
ESI	Electrospray ionisation
Et	Ethyl
FCC	Flash column chromatography
FDA	The United States Food and Drug Administration
GABA	Gamma-aminobutyric acid
HBTU	<i>O</i> -Benzotriazole- <i>N,N,N',N'</i> - tetramethyluroniumhexafluorophosphate
HER2	Human epidermal growth factor receptor 2
HMBC	Heteronuclear multiple bond correlation
HOBt	Hydroxybenzotriazole
HPLC	High performance liquid chromatography
HR	Homologous recombination
HSA	Human serum albumin
HSQC	Heteronuclear single quantum coherence
HWE	Horner-Wadsworth-Emmons
IAM	Immobilised artificial membrane
<i>i</i> Bu	<i>i</i> so-Butyl
IC ₅₀	Half-maximal inhibitory concentration
impy	Imidazo[1,2- <i>b</i>]pyridazine
<i>J</i>	Coupling constant
K ₂₂₂	Kryptofix [®] 222
<i>K_i</i>	Binding affinity
<i>K_m</i>	Membrane partition coefficient

LIG3	DNA ligase III
Lit.	Literature
LLE	Liquid/liquid extraction
Log <i>P</i>	Partition coefficient
LUMO	Lowest unoccupied molecular orbital
m	Multiplet
<i>m</i> -	<i>Meta</i>
MAR	Mono(ADP-ribose)
Me	Methyl
MeCN	Acetonitrile
Mp	Melting point
MRI	Magnetic resonance imaging
Ms	Mesyl
MW	Molecular weight
<i>m/z</i>	Mass to charge ratio
ⁿ Bu	<i>n</i> -Butyl
NAD ⁺	Nicotinamide adenine dinucleotide
Nf	Nonafluorobutanesulfonyl
NHEJ	Non-homologous end joining
NMP	<i>N</i> -Methyl-2-pyrrolidone
NMR	Nuclear magnetic resonance
<i>o</i> -	<i>Ortho</i>
OBt	O-benzotriazole
OLED	Organic light emitting diode
<i>p</i> -	<i>Para</i>
PAR	Poly(ADP-ribose)
PARP-1	Poly(ADP-ribose) polymerase 1
PBS	Phosphate-buffered saline
PDB	Protein data bank
PEG3400	Polyethylene glycol 3400
PET	Positron emission tomography
Ph	Phenyl
Pin	Pinacol
<i>P_m</i>	Membrane permeability
Pol β	DNA Polymerase beta

ppm	Parts per million
py	Pyridine
q	Quartet
quin.	Quintet
RCP	Radiochemical purity
RCY	Radiochemical yield (decay-corrected unless otherwise stated)
rt	Room temperature
s	Singlet
SAR	Structure-activity relationship
^s Bu	sec-Butyl
SEM	2-(Trimethylsilyl)ethoxymethyl
SPE	Solid phase extraction
SPECT	Single photon emission computed tomography
S _N Ar	Nucleophilic aromatic substitution
SSB	Single-strand break
SUV	Standard uptake value
SV2A	Synaptic vesicle glycoprotein 2A
t	Triplet
TAPS	Tetraarylphosphonium salt
^t Bu	tert-Butyl
^t BuBrettPhos	2-(Di-tert-butylphosphino)-2',4',6'- triisopropyl-3,6-dimethoxy-1,1'-biphenyl
TBAHCO ₃	Tetra- <i>n</i> -butylammonium hydrogen carbonate
TBAF	Tetra- <i>n</i> -butylammonium fluoride
TBAI	Tetra- <i>n</i> -butylammonium iodide
Tf	Trifluoromethanesulfonyl
THF	Tetrahydrofuran
TLC	Thin-layer chromatography
TM	Transmembrane
TMS	Trimethylsilyl
t _r	Retention time
Ts	Tosyl
US	Ultrasound
UV	Ultraviolet

XRCC1	X-Ray repair cross-complementing protein 1
%PPB	Percentage plasma protein binding
Δ	Reflux

1.0 Introduction

1.1 Molecular Imaging

Numerous medicinal imaging technologies have been developed throughout the innovation of modern healthcare including computed tomography (CT), ultrasound (US), magnetic resonance imaging (MRI), positron emission tomography (PET) and single photon emission computed tomography (SPECT). These techniques have been thoroughly examined in multiple review articles.¹⁻⁶ Molecular imaging is a non-invasive technique defined as “the visualisation, characterisation and measurement of biological processes at the molecular and cellular levels in humans and other organisms” by the Molecular Imaging Centre of Excellence (MICOE) Standard Definitions Task Force in 2007.⁷ Molecular imaging agents, also commonly referred to as molecular probes or (radio)tracers, are frequently utilised to generate a signal which can be detected and computed to afford a 2- or 3-dimensional image for visual analysis. In the case of PET and SPECT, nanomolar quantities of tracers containing a radionuclide are generally used to minimise detrimental pharmacological effects. These are commonly known as radiotracers due to the small quantity administered.³ Therefore, PET and SPECT radiotracers must interact with the desired biological target with high potency and specificity to obtain satisfactory images.^{1,8}

One of the key advantages of PET and SPECT is the capability to perform imaging with unlimited depth penetration.⁹ Furthermore, PET and SPECT offer the greatest sensitivity *via* the detection of radiolabelled imaging agents. However, CT and MRI demonstrate superior spatial resolution (Table 1).^{1,2,9} Consequently, hybrid imaging techniques such as PET/CT and SPECT/CT have been utilised more frequently in recent years to combine the detailed anatomical imagery of CT with the highly sensitive radiotracer detection of PET and SPECT.^{10,11} These molecular imaging technologies have been utilised to investigate and/or enhance many factors of modern healthcare including diagnosis, disease pathology, prognosis, and disease state monitoring during the treatment of various conditions such as neurological, oncological and central nervous system disorders.⁹⁻¹⁶ Additionally, drug discovery can benefit from molecular imaging as valuable insight can be obtained into the absorption, distribution, mode of action, metabolism and excretion of novel pharmaceuticals which can be subsequently exploited for dose determination.^{2,17}

Table 1 – Spatial resolution and sensitivity of CT, MRI, PET and SPECT^{1,2,9}

Imaging Technique	Spatial Resolution	Sensitivity
CT	50–200 μm (preclinical) 0.5–1 mm (clinical)	–
MRI	25–100 μm (preclinical) ~1 mm (clinical)	10^{-3} to 10^{-5} M
PET	1–2 mm (preclinical) 5–7 mm (clinical)	10^{-11} to 10^{-12} M
SPECT	1–2 mm (preclinical) 8–10 mm (clinical)	10^{-10} to 10^{-11} M

1.1.1 Positron Emission Tomography Imaging

PET imaging is performed by the administration of a tracer which contains a radionuclide that has an excess of protons. The inherent instability of PET radionuclides is resolved through the conversion of a proton into a neutron, a positron, and a neutrino.¹ The positively-charged positron (β^+) is then emitted from the nucleus in a process known as beta-plus decay. The emitted positron travels a short distance of 0.5–2 centimetres within the surrounding tissue until it collides with a negatively-charged electron (β^-) (Figure 1).¹⁸ The collision of a positron and electron results in a matter-anti-matter annihilation event producing two gamma ray photons (γ -rays) of equal energy and a neutrino particle.¹³ These 511 keV γ -rays are emitted in opposing directions of 180° to each other and are simultaneously detected by photon detectors surrounding the imaging subject. Photon detection cameras employ coincidence detection circuitry to record simultaneously emitted γ -rays of 511 keV to determine lines of coincidence and the approximate location of coincidence events.¹⁰ The data accumulated from numerous coincidence events can then be computed to identify the spatial origin of annihilation events and thus, image where the radiotracer has been distributed in the subject.^{2,18} Furthermore, data can be collected quantitatively as a function of time to provide detailed imagery of radioactivity distribution *in vivo*.^{1,5,10}

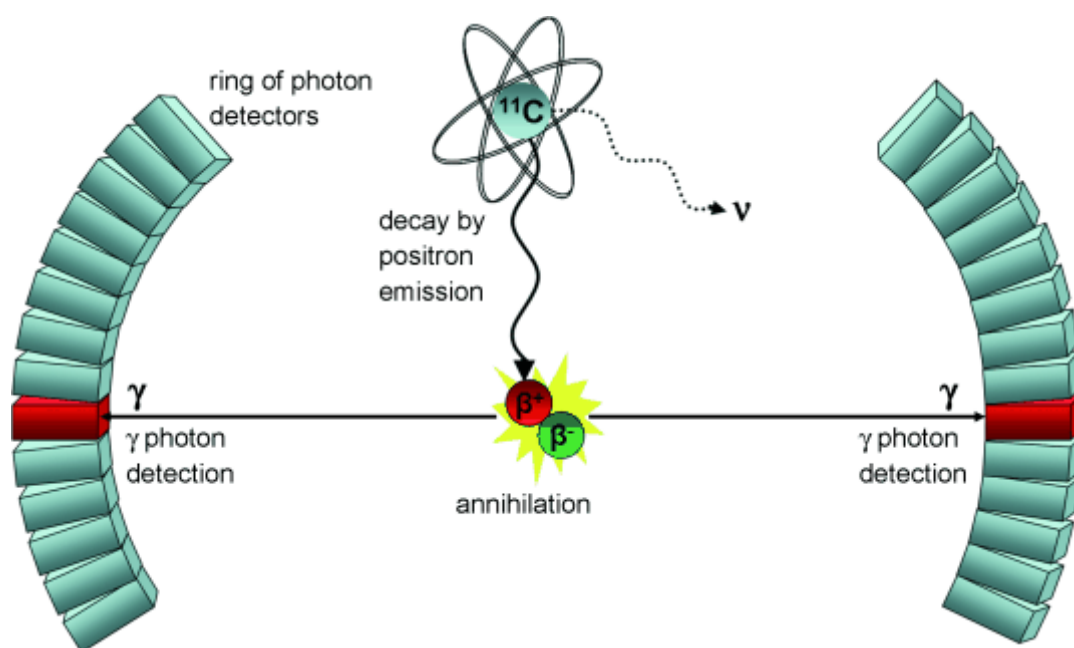


Figure 1 - Positron Emission Tomography.³ (Reprinted with permission from P. W. Miller, N. J. Long, R. Vilar and A. D. Gee, *Angew. Chem. Int. Ed.*, 2008, **47**, 8998–9033. Copyright 2008 John Wiley and Sons.)

1.1.1.1 PET Imaging Radionuclides

A range of radionuclides are employed for PET imaging which decay primarily through positron emission and have short half-lives. A selection of the most frequently used PET radioisotopes is shown in Table 2. Crucially, the radionuclide selected for application must possess a suitable half-life for the time-frame of the desired PET imaging study.¹⁹ Generally, the half-life of a PET or SPECT radiotracer should be shorter than the half-life of the incorporated radionuclide to allow any signals generated by non-specific distribution to be biologically removed and produce a clear image of the specific biological target.² The short half-lives of PET radioisotopes limit the dose of ionising radiation that the subject is exposed to and enable multiple imaging studies to be carried out on a patient within short timescales. Conversely, the use of isotopes with short half-lives demands that PET radiotracers be prepared through fast and efficient synthetic procedures followed by facile purification to limit radioactivity decay as far as practicable.^{18,19} It is widely accepted that the overall preparation time for a PET or SPECT radiotracer be no longer than two to three times the half-life of the chosen radionuclide.⁸ Consequently, most clinical facilities that conduct PET imaging require an on-site

cyclotron for the production of radioisotopes immediately before radiotracer synthesis which incurs significant costs.⁵

Table 2 – PET imaging radionuclides^{2,19}

Radionuclide	Half-life (mins)	Mode of Decay	Maximum Energy (MeV)	Decay Product
¹¹ C	20.3	β ⁺	0.97	¹¹ B
¹³ N	10	β ⁺	1.20	¹³ C
¹⁵ O	2	β ⁺	1.74	¹⁵ N
¹⁸ F	109.7	β ⁺	0.64	¹⁸ O
⁶⁴ Cu	762	β ⁺ /electron capture	0.66	⁶⁴ Ni
⁶⁸ Ga	68.1	β ⁺ /electron capture	1.90	⁶⁸ Zn
⁷⁶ Br	972	β ⁺ /electron capture	4.00	⁷⁶ Se
¹²⁴ I	6019.2	β ⁺ /electron capture	2.14	¹²⁴ Te

The incidence of gallium-68 radiotracers has increased in recent years, however carbon-11 and fluorine-18 remain the most frequently utilised radionuclides in PET imaging agents.^{2,13,20} Carbon-11 is prepared through proton bombardment of [¹⁴N]nitrogen gas within the target of a cyclotron and emission of an alpha particle (equivalent to two protons and two neutrons) known as the ¹⁴N(p,α)¹¹C nuclear reaction. The presence of oxygen or hydrogen within the cyclotron target chamber results in production of [¹¹C]CO₂ and [¹¹C]CH₄ respectively.¹⁷ The majority of carbon-11 radiotracers are prepared from these precursors and given that carbon-11 has a short half-life of 20.3 minutes, the chemical reactions that can be utilised for radiolabelling are limited and synthetically challenging.^{17–19} Recently, a review of carbon-11 radiolabelling methods was published by Kilbourn and Scott in 2021.¹⁷ Furthermore, the synthetic challenges presented by carbon-11 incorporation limit the use of carbon-11 radiotracers to PET centres with a cyclotron.^{2,11,18} However, carbon is the most abundant atom in bioactive compounds and replacement of carbon-12 with carbon-11 results in a negligible isotope effect.² Consequently, the

resultant radiotracer will possess the same biochemical and physicochemical properties as the non-radioactive equivalent.^{6,18}

Fluorine-18 is produced from a cyclotron as either [¹⁸F]fluorine or [¹⁸F]fluoride, for use in electrophilic and nucleophilic radiolabelling reactions respectively. Proton bombardment of a gas target containing [¹⁸O]oxygen (Kr, 50 μmol F₂) (¹⁸O(p,n)¹⁸F nuclear reaction) or deuteron-irradiation of [²⁰Ne]neon (200 μmol F₂) (²⁰Ne(d,α)¹⁸F nuclear reaction) produces carrier-added [¹⁸F]fluorine. The addition of [¹⁹F]fluorine as an isotopic carrier dilutes the molar activity (A_m) of [¹⁸F]fluorine produced. The molar activity is a measurement of radioactivity per mole of compound and is commonly reported as becquerels per micromole (Bq μmol⁻¹). To ensure high quality PET imaging and avoid pharmacological toxicity, it is crucial to obtain radionuclides with high molar activity.²¹ Consequently, the ¹⁸O(p,n)¹⁸F nuclear reaction which affords [¹⁸F]fluorine with molar activity of 0.35–2.00 GBq μmol⁻¹ is commonly favoured over the ²⁰Ne(d,α)¹⁸F nuclear reaction which produces [¹⁸F]fluorine with molar activity of 0.04–0.40 GBq μmol⁻¹.^{22,23} Alternatively, no carrier-added [¹⁸F]fluoride is prepared as an aqueous solution through proton bombardment of [¹⁸O]enriched water (¹⁸O(p,n)¹⁸F nuclear reaction). In recent years, nucleophilic radiofluorination using no carrier-added [¹⁸F]fluoride aqueous solutions has become increasingly favoured due to reports of [¹⁸F]fluoride production with high molar activities of up to 4 × 10⁴ GBq μmol⁻¹ and more facile handling.^{17,21,23} A thorough discussion of radiofluorination methodology is outwith the scope of this thesis. However, multiple extensive reviews of radiofluorination have been published in recent years.^{17,21–23}

Unlike carbon, fluorine is typically not found in naturally occurring biomolecules and so a hydrogen atom or hydroxyl group is commonly substituted with fluorine-18 as a bioisosteric replacement. The resultant fluorine-18 radiotracer exhibits only a slight change in structural steric due to the similar atomic size of fluorine and hydrogen. The addition of fluorine has also been reported to facilitate additional hydrogen-bonding and in some cases even improve potency, with an increasing number of pharmaceuticals incorporating at least one fluorine atom.^{18,23} Furthermore, the C–F bond is the strongest bond in organic molecules and metabolic loss of [¹⁸F]fluoride is unlikely.² PET radiotracers labelled with fluorine-18 are generally favoured over a carbon-11 equivalent due to advantageous properties

of fluorine-18 including a relatively moderate half-life (109.7 mins), high percentage of beta-plus decay (97% β^+ , 3% electron capture) and relatively low maximum emission energy (0.64 MeV).^{18,23,24} The half-life of fluorine-18 is suitably short to limit exposure of PET imaging subjects to ionising radiation, whilst also significantly longer than carbon-11 which allows for a more complex synthetic route and longer PET studies.² Furthermore, the longer half-life of fluorine-18 enables PET centres without a cyclotron to receive a once daily delivery of radiotracer to perform a full day of PET studies without the expense of an on-site cyclotron.^{6,18} Collectively, the high percentage of beta-plus decay, relatively low positron energy (maximal positron range of 2.4 mm) and capacity for longer PET studies of the subject provides higher resolution imaging.^{6,8,18,19,24}

1.1.2 Single Photon Emission Computed Tomography Imaging

Similarly, SPECT imaging requires the administration of a radiotracer. However, unlike PET radiotracers, the radionuclides incorporated into SPECT imaging agents decay through emission of γ -rays directly. These γ -rays are then processed by a lead or tungsten collimator placed in front of a gamma camera which allows only photons at a perpendicular angle of incidence to reach the detector face of the camera.¹ The collimator is essential to identify the spatial origin of the incident rays however, the majority of photons (>99%) do not reach the gamma camera.^{1,9,10} Furthermore, the spatial resolution of SPECT is limited due to the inherent error of the collimator. Consequently, SPECT imaging is several orders of magnitude less sensitive and produces images of lower resolution than PET imaging.² Typically, these gamma cameras are rotated around the imaging subject to obtain projections at multiple defined angles.^{9,13} The data collected from numerous tomographic projections is utilised to produce three-dimensional images. Notably, SPECT imaging has the capability for multiplexing, in which multiple radiotracers containing different radionuclides that emit at distinct energies can be detected to study several biological targets simultaneously.^{1,9,10}

1.1.2.1 SPECT Imaging Radionuclides

Numerous radionuclides undergo gamma-decay and can be utilised for SPECT imaging.^{2,17} A selection of the most frequently used SPECT radioisotopes is shown

in Table 3. Notably, the radionuclides employed for SPECT imaging emit lower energy γ -rays than those produced from the annihilation of PET radioisotopes. As such, SPECT radionuclides possess much longer half-lives than PET radioisotopes and this allows for SPECT imaging agents to be synthesised in longer or more complex routes.² This additional time also enables longer imaging procedures and allows for SPECT studies of slow biological processes.¹³ Furthermore, SPECT radiotracers can be transported from a site of synthesis to the site of imaging without a substantial loss in radioactivity. Consequently, SPECT is widely used in clinical settings since an on-site cyclotron is not compulsory. Additionally, more synthetic flexibility and the lower cost of a gamma camera has made SPECT imaging more widely accessible than PET. Nonetheless, both PET and SPECT are widely used for molecular imaging due to their respective distinct advantages.¹⁰

Table 3 – SPECT imaging radionuclides^{2,17}

Radionuclide	Half-life (h)	Mode of Decay	Primary Energy (MeV)	Decay Product
⁶⁷ Ga	78.3	Electron capture	0.09/0.19/0.30	⁶⁷ Zn
^{99m} Tc	6	Isomeric transition	0.14	⁹⁹ Tc
¹¹¹ In	67.9	Electron capture	0.17/0.25	¹¹¹ Cd
¹²³ I	13.2	Electron capture	0.16	¹²³ Te
²⁰¹ Tl	73.1	Electron capture	0.17	²⁰¹ Hg

Of the suitable radionuclides, technetium-99m and iodine-123 are the most frequently employed for SPECT radiotracers. The majority of SPECT imaging (80%) is currently conducted using technetium-99m radiotracers due to their favourable half-life (6 h) and primary γ -ray emission energy (0.14 MeV).¹⁷ One key advantage of the radioisotope technetium-99m is that it is easily generated through the decay of molybdenum-99 using a commercially available ⁹⁹Mo/^{99m}Tc generator and thus, does not require the use and associated costs of a cyclotron.¹¹ The ⁹⁹Mo/^{99m}Tc generator produces [^{99m}Tc]-pertechnetate with technetium-99 in its highest oxidation state of +7.² The synthetic route required to incorporate technetium-99m into a tracer is more complicated than other SPECT radioisotopes such as iodine-123. However, numerous synthetic kits have been developed for the preparation of technetium-99m radiotracers.¹¹ These kits typically reduce [^{99m}Tc]-pertechnetate

with stannous ions (Sn^{2+}) to afford technetium-99m in the +4 oxidation state which then undergoes chelation with a variety of agents to give a technetium-99m metal complex radiotracer.² The full scope of chelating agents for the preparation of technetium-99m radiotracers is extensive however, multiple reviews of these have been published in recent years.^{17,25} Careful consideration of the resultant technetium-99m metal complex must be made to examine if the biological interactions of the tracer are compromised. One limitation of technetium-99m radiotracers is for SPECT imaging of neurological conditions as the metal complex can exhibit restricted distribution across the blood-brain barrier (BBB).²

Conversely, iodine-123 is commonly utilised for SPECT imaging of neurological conditions. All iodine radioisotopes are prepared as radio-iodide and are commonly distributed as sodium iodide in sodium hydroxide (0.01–0.1 M).² Iodine-123 is produced through a variety of cyclotron mediated nuclear reactions which can be grouped into two distinct categories. The first category produces iodine-123 directly through either alpha, deuteron or proton bombardment of an antimony or tellurium target *via* the $^{121}\text{Sb}(\alpha,2n)^{123}\text{I}$, $^{122}\text{Te}(\text{d},n)^{123}\text{I}$, $^{123}\text{Te}(\text{p},n)^{123}\text{I}$, $^{124}\text{Te}(\text{p},2n)^{123}\text{I}$ nuclear reactions.^{26,27} Notably, these nuclear reactions produce additional iodine radioisotopes such as iodine-124 and iodine-125. These impurities are difficult to remove from the desired iodine-123 product and therefore, limit the application of these methods for iodine-123 production.^{17,27} The second category affords iodine-123 indirectly *via* xenon-123 decay to iodine-123. A target of xenon-124 or iodine-127 can be subjected to proton- or deuteron-irradiation to afford caesium-123 or xenon-123 which naturally decay to give iodine-123. These methods proceed *via* the $^{124}\text{Xe}(\text{p},2n)^{123}\text{Cs} \rightarrow ^{123}\text{Xe} \rightarrow ^{123}\text{I}$, $^{124}\text{Xe}(\text{p},\text{pn})^{123}\text{Xe} \rightarrow ^{123}\text{I}$, $^{127}\text{I}(\text{p},5n)^{123}\text{Xe} \rightarrow ^{123}\text{I}$ and $^{127}\text{I}(\text{d},6n)^{123}\text{Xe} \rightarrow ^{123}\text{I}$ nuclear reactions.^{26,27} Of these reactions, the $^{124}\text{Xe}(\text{p},2n)^{123}\text{Cs} \rightarrow ^{123}\text{Xe} \rightarrow ^{123}\text{I}$ nuclear reaction is widely favoured as iodine-124 and iodine-125 are not produced. Furthermore, xenon-123 is unreactive which allows for its facile isolation from the reaction and can then undergo decay to the desired iodine-123 radioisotope with minimal contamination.^{17,27}

Notably, all strategies for iodine-123 production require the use of a cyclotron. However, the relatively longer half-life of iodine-123 (13.2 h) compared to PET radionuclides allows for commercial production and distribution over larger distances. Another important advantage is the availability of additional iodine

radioisotopes including iodine-124, iodine-125 and iodine-131 which allows one tracer to be radiolabelled with a variety of isotopes with differing applications (Table 4).² Iodine-125 is a longer lived low energy radionuclide (1425.4 h, 0.035 MeV) which can be used for pre-clinical development but does not have sufficient energy for imaging.²⁷ Additionally, iodine-131 has a relatively short half-life of 192 hours and is more commonly used in radiotherapy than imaging due to its emission of higher energy γ -rays of 0.36 and 0.64 MeV.²⁴ Therefore, pre-clinical development of a tracer can be conducted using iodine-125 and the same tracer can then be radiolabelled with iodine-123 and employed to SPECT image thyroid cancer. Moreover, the equivalent iodine-131 compound can be administered for radiotherapy of the tumour. Due to the availability of PET radioisotope iodine-124, the same tracer can also be prepared for applications in PET imaging with greater sensitivity and resolution.²⁷

Table 4 – Iodine radioisotopes^{2,27}

Radionuclide	Half-life (h)	Emission	Gamma Emission Energy (MeV)	Application
¹²³ I	13.2	gamma	0.16	SPECT
¹²⁴ I	100.3	beta/gamma	0.51	PET
¹²⁵ I	1425.4	Auger/gamma	0.035	preclinical development
¹³¹ I	192	beta/gamma	0.36/0.64	radiotherapy

These iodine radioisotopes are generally incorporated into tracers through construction of a covalent bond to a carbon atom of the tracer compound. The synthetic chemistry employed for labelling organic compounds with iodine radioisotopes is discussed further in Section 2.3.1. Typically, a radioisotope of iodine is incorporated into a tracer as a replacement for a hydrogen atom, as is the case for PET radionuclide fluorine-18. When compared with fluorine-18, radioiodine causes a more notable structural change due to its larger atomic radius.² However, radiolabelling with iodine radioisotopes produces a less significant structural change to a tracer than the incorporation of technetium-99m to give a metal complex. Furthermore, a vast array of radioiodination methods have been developed in recent years and prompted a review of this field by Dubost *et al.* in 2020.²⁸

domain (residues 786 to 1014) of PARP-1.^{34,36} PARP-1 was the first of this protein family to be identified during seminal research conducted by Chambon *et al.* from 1963 to 1966. This work focused on the enzymatic consumption of nicotinamide mononucleotide, one of five vital precursors for the biosynthesis of coenzyme nicotinamide adenine dinucleotide (NAD⁺), by a DNA-dependent protein to produce polymeric chains of ADP-ribose.^{37,38} Shortly thereafter, studies from the research groups of Hayaishi^{39,40} and Sugimura^{41–43} corroborated this discovery and initiated the vast research field of ADP-ribosylation and PARP proteins that now exists. One of the major functions of PARP proteins is the catalytic cleavage of an *N*-glycosidic bond within coenzyme NAD⁺ to afford nicotinamide and ADP-ribose (Figure 3). The resultant ADP-ribose units are transferred onto target proteins and DNA in a process known as ADP-ribosylation.^{37,44,45} This enzymatic activity can facilitate addition of a single ADP-ribose unit known as mono-ADP-ribosylation (MARylation). Upon repetition, elongated polymeric branched chains of ADP-ribose (PAR) are formed through poly-ADP-ribosylation (PARylation).⁴⁶ Furthermore, ADP-ribosylation of the PARP automodification domain is referred to as autoPARylation.

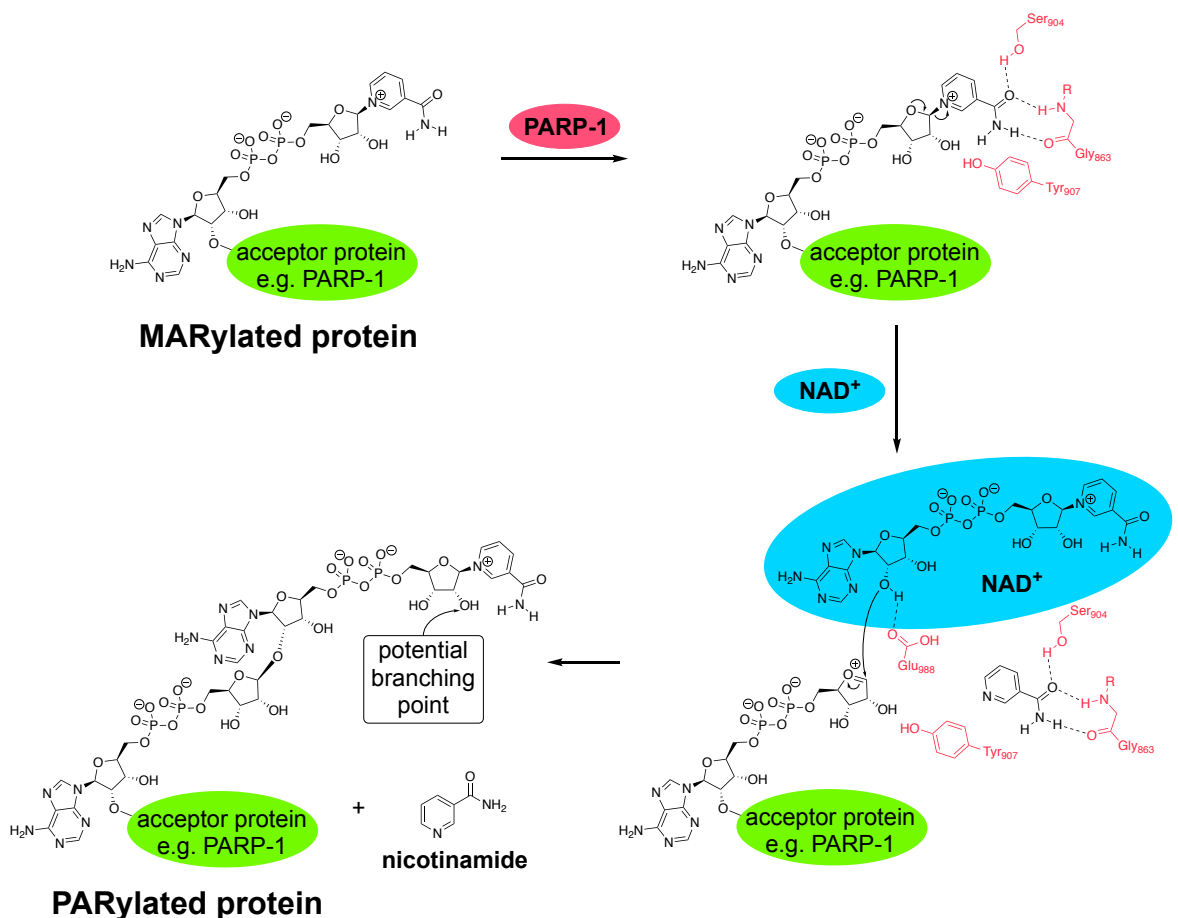


Figure 3 – Poly(ADP-ribosyl)ation mediated by PARP-1

All of the PARP proteins with the exception of PARP-13 exhibit ADP-ribosyltransferase catalytic activity in the form of either MARYlation or PARylation.^{47,48} Although each PARP protein possesses a highly conserved ADP-ribosyltransferase catalytic domain, only PARP-1, PARP-2, PARP-4, PARP-5a (tankyrase 1) and PARP-5b (tankyrase 2) are responsible for PARylation of proteins (PARylation).^{48,49} Notably, it is reported that PARP-1 is responsible for 85–90% of all ADP-ribosylation by the entire PARP family and consequently, has been the most extensively studied of all the PARP proteins.^{44,45,50} The majority of the PARP family perform mono(ADP-ribosyl)ation (MARYlation).⁵¹ MARYlation plays a role in numerous cellular processes such as regulation of the actin cytoskeleton or membrane organelles, signal transduction, and responses to unfolded proteins or cytoplasmic stress.⁵¹ It is believed that both the primary and secondary structure of PARP proteins determines the type of ADP-ribosyltransferase catalytic activity that will be performed.^{48,51} Consequently, the PARP proteins can be more accurately denoted as diphtheria toxin-like ADP-ribosyltransferases (ARTDs).^{29,47,51,52} Furthermore, tRNA 2'-phosphotransferase (TRPT1) is occasionally included as an additional eighteenth member but possesses a significantly derived structure.^{47,52}

Traditionally, this enzymatic activity was regarded solely as a post-translational modification performed on histones and nuclear proteins. However, recent studies have shown that PARP protein mediated ADP-ribosylation is crucial to numerous fundamental cellular functions such as transcription, chromatin structure modulation, recombination and the DNA damage repair (DDR) pathway.^{45,48,53,54} Notably, PARP-1 plays a vital role in the DDR pathway and therefore genome stability.⁴⁵ A variety of exogenous and endogenous factors cause damage to the DNA double helix structure in the form of base modifications, abasic sites, and single- or double-strand breaks (SSBs or DSBs).^{33,55} SSBs are the most common form of DNA damage and if left unrepaired lead to incomplete DNA replication and transcription, genome instability, DSBs and ultimately cell death.³³

PARP-1 mediated PARylation performs an instrumental function in the excision of DNA lesions through the base excision repair (BER) pathway (Figure 4).⁵⁶ When damage occurs to a DNA nucleotide *via* either endogenous or exogenous sources, DNA glycosylase cleaves the *N*-glycosidic bond between the erroneous or damaged nucleotide base and the DNA deoxyribose sugar/phosphate backbone to excise the

base, producing an apurinic/aprimidinic (abasic or AP) site.^{33,55,56} Apurinic/aprimidinic endonuclease 1 (APE1) then excises the abasic/AP site to generate a SSB. PARP-1 rapidly identifies this SSB within milliseconds and binds adjacent to the SSB site using zinc finger 1 and 2, and the tryptophan-glycine-arginine rich domain (WGR).^{31,57,58} The third zinc finger (Zn3) does not partake in binding but forms inter-domain interactions that are vital for PARP-1 catalytic activation.³⁴ Furthermore, the WGR domain interacts with the bound DNA and also partakes in inter-domain interactions.³³ PARP-1 is thought to move between DNA strands through a monkey bar mechanism in which the higher affinity Zn1 and Zn2 domains remain bound to a strand of DNA whilst the lower affinity WGR domain “swings” to a different DNA strand. Subsequent dissociation of Zn1 and Zn2 from the original DNA strand allows PARP-1 to transfer and bind to the second DNA strand.⁵⁹ This can also be referred to as intersegment transfer and is estimated to facilitate a threefold increase in the rate of DNA damage detection than PARP-1 diffusion alone.³⁴

Unbound PARP-1 exists as an autoinhibited structure commonly described as “beads on a string” (Figure **2A**).^{30–32} Upon binding to damaged DNA, PARP-1 undergoes allosteric activation *via* a conformational shift also known as global structural compaction (Figure **2B**).^{30,35} PARP-1 shifts to a significantly more ordered structure in which the N- and C- termini are in close proximity to one another, resulting in an increased number of DNA-protein and protein-protein inter-domain interactions.³⁰ Inter-domain interactions induced by this conformational change result in the destabilisation of the alpha-helical subdomain (HD) within the catalytic domain (CAT) of PARP-1. The displacement of two leucine residues (L698 and L701) from the interior of the HD reduces its stability, prompting loss of PARP-1 autoinhibition and activation of the ADP-ribosyltransferase fold (ART) catalytic function (Figure **2B**).³⁰

Following allosteric activation, the ART domain performs PARylation of arginine, glutamate, aspartate, cysteine, lysine, and serine residues within histones (heteroPARylation), and autoPARylation of the PARP-1 automodification domain (BRCT).³³ The resultant chains of poly(ADP-ribose) (PAR) (consisting of up to 200 monomeric units) act to recruit the scaffolding protein x-ray repair cross-complementing protein 1 (XRCC1). Shortly thereafter, DNA repair enzymes

including DNA polymerase beta ($\text{Pol } \beta$), bifunctional polynucleotide kinase 3'-phosphatase (PNKP) and DNA ligase III (LIG3) are recruited to the SSB site and repair the damaged DNA strand.^{56,57} Additionally, the elongated PAR chains possess a considerable negative charge and steric bulk which promotes chromatin relaxation and successively, facilitates access of the recruited DNA repair enzymes to the SSB site.⁶⁰ Furthermore, it is thought PAR chains prompt the release of autoPARylated PARP-1 from the broken DNA strand *via* electronic and steric repulsion.^{30,33} Following the release of PARP-1 from the DNA strand, PAR chains present on the autoPARylated PARP-1 inhibit DNA binding and enzymatic activity. Subsequently, PAR glycohydrolase (PARG) mediated degradation of these PAR chains restores PARP-1 to the original autoinhibited "beads on a string" state.^{30,57}

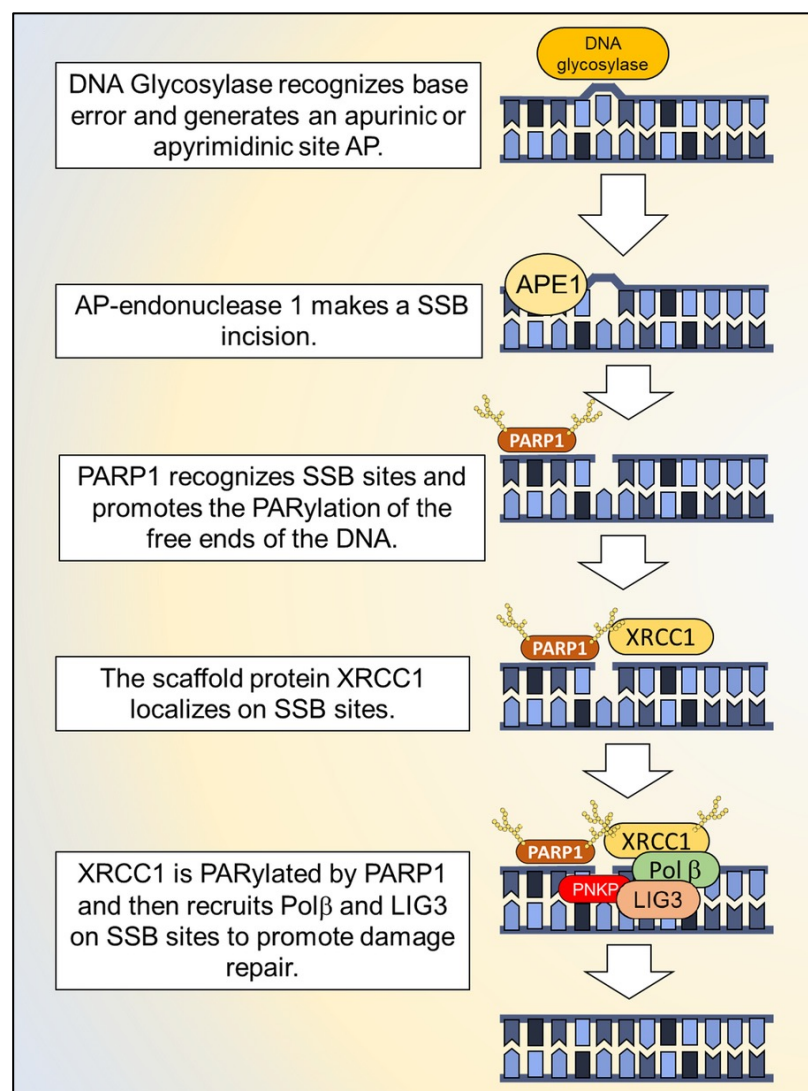


Figure 4 – DNA SSB repair mediated by PARP-1 *via* BER pathway.⁵⁶ (Adapted from Figure 1 of Padella *et al.*, *J. Hematol. Oncol.*, 2022, **15**, 1–21, under the terms of the Creative Commons Attribution 4.0 International License.)

1.2.2 PARP-1 Inhibitors as Cancer Therapeutics

The vital function of PARP-1 in the repair pathway of DNA single strand breaks has made it an attractive target for medicinal chemistry research and particularly, for the treatment of cancer. Current statistics from Cancer Research UK indicate that 50% of UK residents born after 1960 will develop cancer at some stage of their life.⁶¹ This prevalence of disease presents an obvious demand for additional research and development of novel anti-cancer treatments. Furthermore, PARP-1 is highly expressed in numerous forms of cancer due to elevated levels of cellular stress, proliferation and metabolism when compared to normal healthy cells.^{62–64}

The majority of PARP-1 inhibitors developed thus far have been designed to mimic the native ligand coenzyme NAD⁺ and competitively bind to the PARP-1 catalytic domain which obstructs binding of NAD⁺ and therefore inhibits production of poly(ADP-ribose).^{33,65,66} In the presence of a PARP-1 inhibitor, PARP-1 cannot perform PARylation to signal and recruit DNA repair factors which prevents the repair of DNA single strand breaks (SSBs) *via* the BER pathway, as previously described. Subsequently, incomplete DNA replication and transcription creates genome instability and DNA double strand breaks (DSBs) are produced.⁵⁴

PARP-1 inhibitors are typically employed for the treatment of cancer through two distinct strategies. The first technique involves the administration of a PARP-1 inhibitor in combination with chemotherapy or radiation therapy and is an adjuvant or adjunct therapy.^{54,67,68} This therapeutic approach can produce greater efficacy due to the inhibition of PARylation which impedes the repair of therapy induced DNA damage in cancerous cells, in an effect known as chemo/radio-sensitisation.³¹ Conversely, the second strategy applies PARP-1 inhibitors as a single agent or monotherapy for the treatment of BRCA-mutated cell lines through exploiting the genetic concept of synthetic lethality (Figure 5).^{31,69} Due to the inhibition of PARP-1, DNA strands with SSBs inevitably develop DSBs. In normal cell lines, DNA DSBs are repaired *via* the homologous recombination (HR) repair pathway, which utilises a homologous DNA strand to restore the original double-stranded DNA structure and facilitates cell survival.^{55,70} The PARP-1 protein does not serve a direct function in the HR pathway and DSBs can be repaired in normal cell lines despite the inhibition of PARP-1 activity.³³ Conversely, both breast cancer type 1 (BRCA1)

susceptibility protein and breast cancer type 2 (BRCA2) susceptibility protein perform essential functions in the HR pathway.⁷¹ In patients with deleterious heterozygous germline mutations in the BRCA1 and BRCA2 genes, the wild-type BRCA allele is lost during tumorigenesis.³¹ Consequently, DNA DSBs in BRCA-mutated cell lines cannot be repaired through HR and are therefore repaired *via* non-homologous end joining (NHEJ).⁵⁴ However, NHEJ is a nonconservative DNA repair method and ultimately cultivates cell death.^{31,70} In 2005, both Bryant *et al.* and Farmer *et al.* reported that BRCA-mutated cells displayed increased sensitivity to PARP-1 inhibitors due to their deficiency in homologous recombination.^{72,73} Consequently, both groups proposed that PARP-1 inhibitors could be administered for the treatment of patients with BRCA-mutated cancers as a novel higher efficacy yet lower toxicity approach than application of chemotherapy or radiation therapy. This tactic of exploiting PARP-1 inhibitors to force DNA repair through an inherently flawed pathway and promote cell death is termed synthetic lethality.

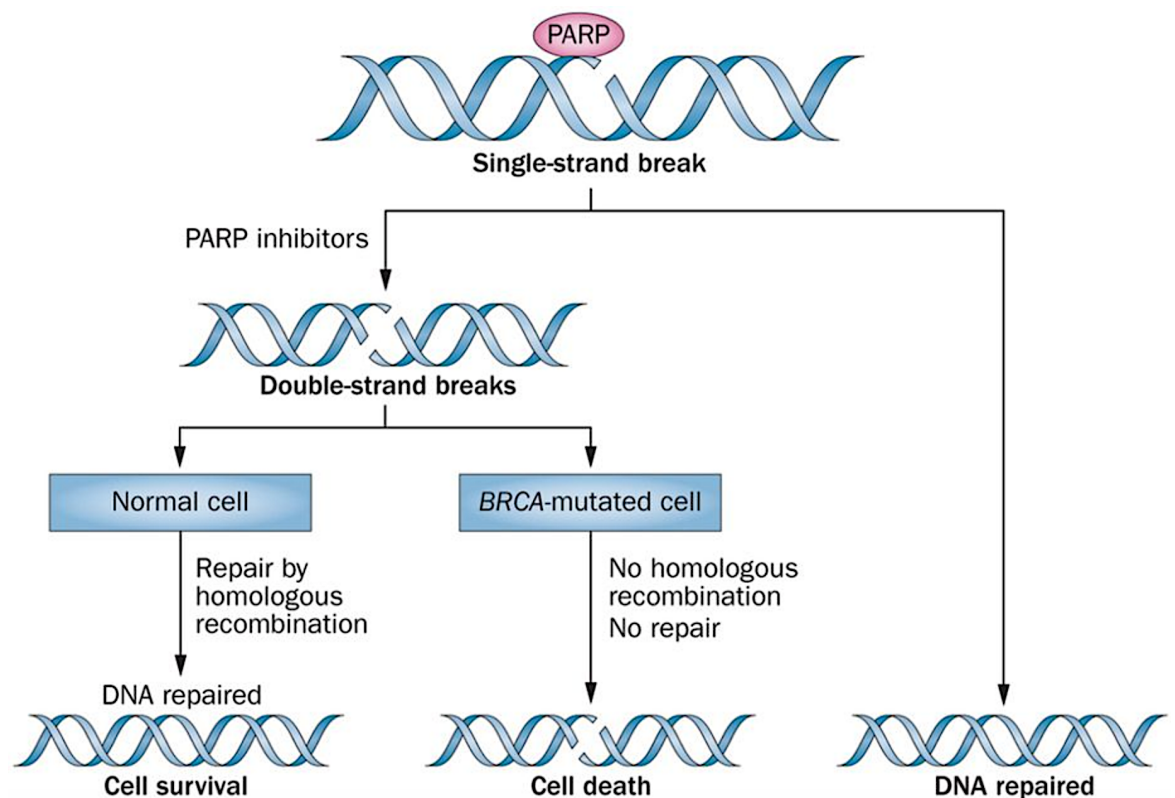


Figure 5 – Synthetic lethality of PARP-1 inhibition in BRCA-mutated cells.⁵⁴

(Reprinted with permission from Springer Nature Customer Service Centre GmbH: Springer Nature, *Nat. Rev. Clin. Oncol.*, An update on PARP inhibitors – moving to the adjuvant setting, A. Sonnenblick *et al.*, Copyright 2015.)

To date, four PARP-1 inhibitors have been granted global approval for the treatment of BRCA-mutated cancers; olaparib (1), rucaparib (2), niraparib (3) and talazoparib (4) (Figure 6). Developed by Menear *et al.* (KuDOS Pharmaceuticals/AstraZeneca) in 2008, olaparib (1) was first granted global approval in 2014.^{74,75} Olaparib (1) was approved by the European Medicines Agency (EMA) for the treatment of relapsed, BRCA-mutated (germline/somatic), high-grade, serous epithelial ovarian, fallopian tube or primary peritoneal cancer following complete or partial response to platinum-based chemotherapy. Furthermore, olaparib (1) was approved by The United States Food and Drug Administration (FDA) for monotherapy in patients with germline BRCA-mutated advanced ovarian cancer following at least three prior lines of chemotherapy. Subsequently, olaparib (1) has received numerous EMA and FDA approvals for the treatment of various cancers including breast, pancreatic and prostate cancer.⁷⁶ Currently, olaparib (1) is the most widely employed PARP-1 inhibitor and the research field concerning further applications is extremely active.

In 2016, rucaparib (2) (Clovis Oncology) was granted global approval as a monotherapy for patients with BRCA-mutated (germline/somatic) advanced ovarian cancer following at least two prior lines of chemotherapy.⁷⁷ Rucaparib (2) approvals were then extended to include maintenance therapy of reoccurring ovarian, fallopian and primary peritoneal cancer and treatment of BRCA-mutated metastatic castration-resistant prostate cancer in 2018 and 2020 respectively.⁷⁶ In addition, niraparib (3) (Merck) received global approval in 2017 for maintenance treatment of patients with recurrent epithelial ovarian, fallopian tube or primary peritoneal cancer who exhibit a complete or partial response to platinum-based chemotherapy.⁷⁸ These approvals were subsequently extended in 2020 to permit the use of niraparib (3) as a late-line treatment in the aforementioned cancers.⁷⁶ Furthermore, talazoparib (4) (Pfizer) received global approval in 2018 for treatment of BRCA-mutated (deleterious germline), HER2-negative, locally advanced or metastatic breast cancer.^{76,79} Notably, talazoparib (4) exhibits higher potency PARP-1 inhibition and trapping than any other PARP-1 inhibitor currently in pre-clinical development or clinical application.^{60,70}

Several PARP-1 inhibitors are currently in clinical development but have not received global approval at this time including fuzuloparib (5), pamiparib (6) and veliparib (7) (Figure 6). Clinical trials of fuzuloparib (5) (Jiangsu Hengrui

Pharmaceuticals) began in 2019 for the treatment of breast, lung, ovarian, and pancreatic cancer.⁷⁶ In 2020, fuzuloparib (**5**) was granted first approval in China for the treatment of BRCA-mutated (deleterious germline), platinum-sensitive, recurrent ovarian, fallopian tube or primary peritoneal cancer following at least two prior lines of chemotherapy.⁸⁰ Similarly, in 2021, pamiparib (**6**) (BeiGene) received first approval in China as a third-line treatment for the same class of carcinomas as fuzuloparib (**5**) following six years of clinical trials.⁸¹ In contrast, veliparib (**7**) (Abbott Laboratories) has not currently gained approval despite extensive investigation in more than one hundred clinical trials since its discovery in 2006. These clinical trials have focused on application of veliparib (**7**) for the treatment of fallopian tube, ovarian, peritoneal, lung and breast cancer.^{82,83}

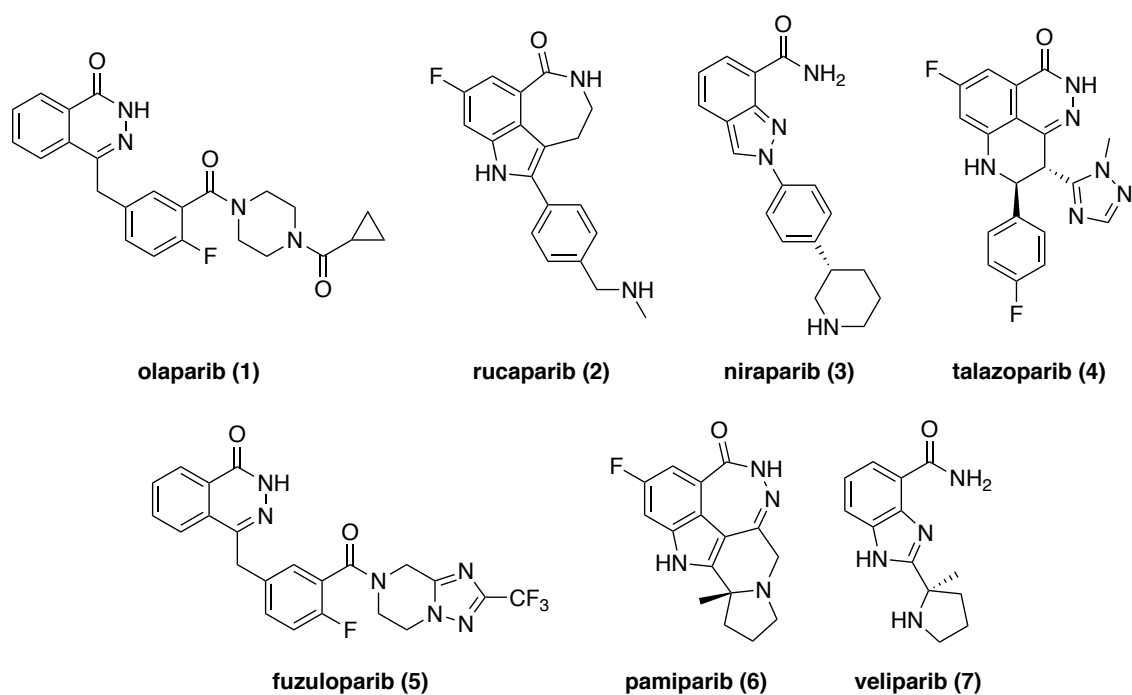


Figure 6 – Structures of approved and clinical candidate PARP-1 inhibitors

Although each of these inhibitors contain a nicotinamide mimetic moiety and bind to the catalytic site of PARP-1, they have presented profiles of PARylation inhibition and cytotoxicity that do not directly correlate. It is now widely accepted that this variation is due to the capacity of each inhibitor to trap PARP-1 on a DNA strand which generates a cytotoxic lesion, replication fork collapse and ultimately cell death.^{31,66,69} The mechanism by which PARP-1 inhibitors facilitate trapping of PARP-1 on DNA strands remains under active investigation. Currently, the widely accepted mechanism postulates that the extent of PARP-1 trapping is dictated by

inhibitor induced allostery. At this time, PARP-1 inhibitors can be classified as type I, II (e.g. olaparib and talazoparib) or III (e.g. rucaparib, niraparib and veliparib).^{33,66} Type I inhibitors impose a strong allosteric effect that destabilises the HD domain and increases trapping of PARP-1 at the site of DNA damage, which in turn generates slow release of PARP-1. Type II inhibitors have minimal effect on the HD domain stability and consequently, on trapping of PARP-1. Conversely, type III inhibitors improve stability of the HD domain which promotes release of PARP-1 from the site of DNA damage and thus exhibit relatively poor PARP-1 trapping.

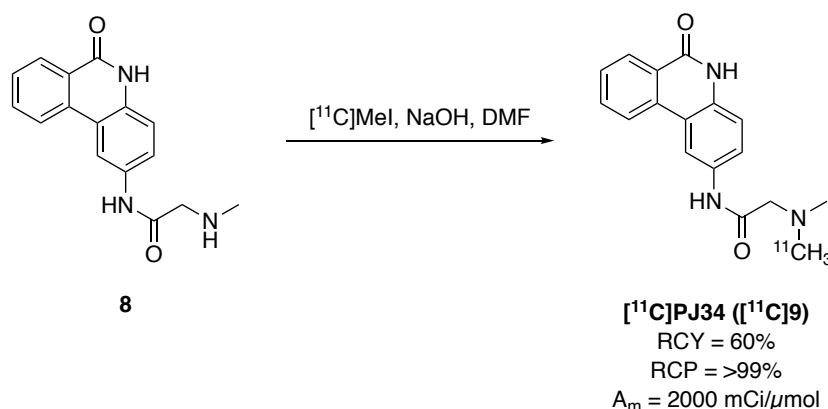
Until recently, PARP-1 inhibitors have primarily been used for the treatment of cancer following multiple lines of chemotherapy. However, the application of PARP-1 inhibitors as a front-line treatment for cancer is a growing field of research.⁸⁴ Significantly, olaparib (**1**) and niraparib (**3**) were approved by the FDA, in 2018 and 2020 respectively, as first-line maintenance treatments for patients with advanced ovarian or metastatic pancreatic cancer.^{84,85} However, the use of PARP-1 inhibitors as a first-line maintenance treatment may also have negative implications on subsequent PARP-1 inhibitor application *via* PARP-1 inhibitor resistance. PARP-1 inhibitor resistance is an area of active research and is believed to develop through numerous mechanisms.^{33,84,85} Emerging fields of research include the application of combination therapies to combat PARP-1 inhibitor resistance and PARP-1 inhibitors as a front-line treatment for BRCA-mutated cancers before or possibly without chemotherapy.^{33,84,85}

1.2.3 PARP-1 Inhibitor-Derived PET and SPECT Imaging Agents

As previously discussed, PARP-1 is highly expressed in tumour cells and thus acts as a biomarker for cancer.⁶⁴ Consequently, radiotracers which bind to PARP-1 present an excellent opportunity for nuclear imaging of numerous cancers. For example, PARP-1 is highly expressed in brain tumours including glioblastoma whilst the surrounding healthy tissue exhibits very low expression.⁶³ Therefore, imaging agents with affinity for PARP-1 can be employed to selectively image glioblastoma tumours within the brain.⁸⁶ Furthermore, PARP-1 imaging agents facilitate non-invasive quantification of *in vivo* PARP-1 expression which can aid prediction of response to PARP-1 inhibitor treatment, prognostic evaluation, tailored therapy dosing and monitoring of cancer treatment response.^{64,87-89} Additionally, given the

numerous PARP-1 inhibitors currently in development it can be advantageous to prepare an equivalent radiotracer to obtain crucial information for drug development such as *in vivo* distribution and pharmacokinetics.⁶⁴ In recent years, interest in this field has grown significantly resulting in the development of multiple PET and SPECT radiotracers that target the PARP-1 protein.^{64,88} The majority of these imaging agents have been structural derivatives of established PARP-1 inhibitors.⁸⁸

The first PET imaging agent based on a PARP-1 inhibitor was a phenanthridinone derivative known as [¹¹C]PJ34 (**[¹¹C]9**) (Scheme 1). The carbon-11 equivalent of potent PARP-1 inhibitor PJ34 (IC₅₀ = 20 nM) was prepared by Tu *et al.* in 2005 via a base-mediated methylation of precursor **8** with [¹¹C]methyl iodide.⁹⁰ The resultant radiotracer [¹¹C]PJ34 (**[¹¹C]9**) was shown to accumulate in necrotic tissue of the pancreas with elevated PARP-1 expression in a rat model of type 1 diabetes.



Scheme 1 – Radiosynthesis of [¹¹C]PJ34 (**[¹¹C]9**)

1.2.3.1 Rucaparib-Derived PET and SPECT Imaging Agents for PARP-1

A series of nuclear imaging agents have been derived from the structure of PARP-1 inhibitor rucaparib (**2**). PET imaging agents include [¹⁸F]FluorThanatrace (FTT) (**[¹⁸F]10**) and [¹⁸F]WC-DZ-F (**[¹⁸F]11**) from Zhou *et al.* in 2014 and 2018 respectively (Figure 7).^{91,92} Of these radiotracers, [¹⁸F]FTT (**[¹⁸F]10**) has been the most studied with numerous phase I clinical trials reported on clinicaltrials.gov for the investigation of multiple cancers including ovarian (NCT03604315, NCT02637934), breast (NCT03846167), pancreatic (NCT03492164), prostate (NCT03334500, NCT05242744), and glioblastoma (NCT04221061), many of which are still active.⁸⁸ Notably, Makvandi *et al.* reported in 2018 that PET imaging with [¹⁸F]FTT (**[¹⁸F]10**)

could be utilised to quantify PARP-1 expression in ovarian carcinomas following a phase I clinical trial (NCT02637934).^{87,93} Phase I clinical trials of [¹⁸F]FTT ([¹⁸F]10) have produced promising results thus far and prompted the progression of this PET radiotracer into phase II trials commencing in April 2022 (NCT05226663). This trial aims to improve nuclear imaging of breast cancer patients through PET/CT imaging with [¹⁸F]FTT ([¹⁸F]10).

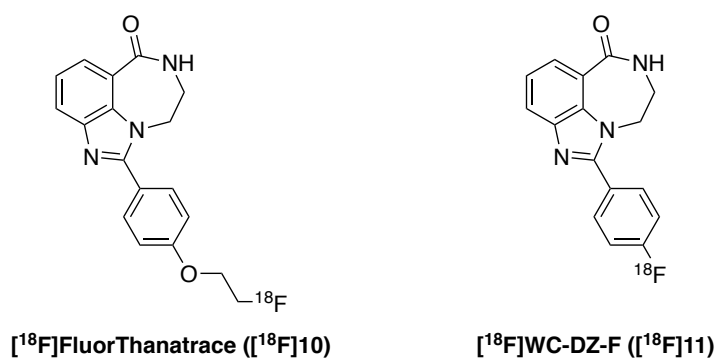
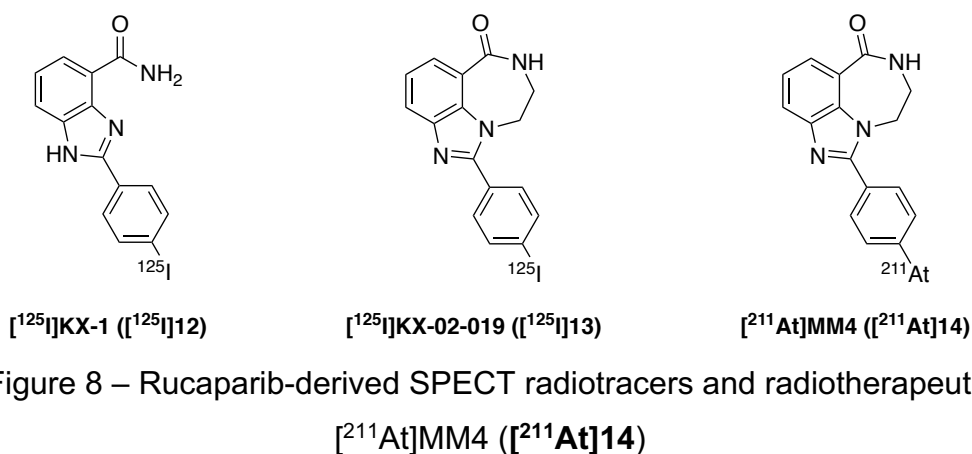


Figure 7 – Rucaparib-derived PET radiotracers

Moreover, SPECT imaging agents have been developed containing the benzimidazole core of rucaparib (2) including [¹²⁵I]KX-1 ([¹²⁵I]12) and [¹²⁵I]KX-02-019 ([¹²⁵I]13) (Figure 8).^{94,95} Promisingly, bicyclic benzimidazole [¹²⁵I]KX-1 ([¹²⁵I]12) showed high uptake and correlation with PARP-1 expression in tumour cells. Notably, pre-injection with olaparib (1) did not reduce radiotracer accumulation which may indicate non-specific biodistribution of [¹²⁵I]KX-1 ([¹²⁵I]12). Furthermore, [¹²⁵I]KX-02-019 ([¹²⁵I]13) was prepared as an iodine-125 equivalent of PET radiotracer [¹⁸F]FluorThanatrace (FTT) ([¹⁸F]10). However, *in vitro* and *in vivo* studies revealed that [¹²⁵I]KX-02-019 ([¹²⁵I]13) exhibits greater affinity for PARP-2 over PARP-1 and produces a five-fold greater accumulation of radioactivity in thyroid tissue than in tumour cells which indicates extensive loss of radioiodine. It is also worth noting that an alpha-emitting astatine-211 equivalent of [¹⁸F]FTT ([¹⁸F]10) and [¹²⁵I]KX-02-019 ([¹²⁵I]13), known as [²¹¹At]MM4 ([²¹¹At]14), was reported by Makvandi *et al.* in 2019 with implications as a novel therapeutic radiopharmaceutical.⁹⁶



1.2.3.2 Olaparib-Derived PET and SPECT Imaging Agents for PARP-1

The majority of nuclear imaging agents developed for the PARP-1 protein have been derived from the 4-substituted phthalazinone core structure of olaparib (**1**) due to the clinical success of this PARP-1 inhibitor. Given the advantages of PET imaging previously discussed, most of the tracers designed to target PARP-1 contain PET radionuclides although some SPECT imaging agents have also been investigated.

In 2011, Weissleder and co-workers reported the olaparib-derived PET radiotracer $[^{18}\text{F}]\text{BO}$ ($[^{18}\text{F}]\text{15}$) in which the 4-*H*-piperazine moiety was substituted with a large terminal multi-ring system containing a pendant fluorine-18 radionuclide (Figure 9).^{97,98} This imaging agent was prepared through a [4+2] inverse-electron-demand Diels-Alder cycloaddition of a terminally tetrazine-substituted olaparib precursor and fluorine-18 radiolabelled *trans*-cyclooctene. Notably, this radiotracer retained moderate PARP-1 inhibition potency ($\text{IC}_{50} = 17.9 \text{ nM}$) *in vitro* when compared to olaparib (**1**) ($\text{IC}_{50} = 5 \text{ nM}$) despite significant structural modification. Furthermore, *in vivo* PET studies of $[^{18}\text{F}]\text{BO}$ ($[^{18}\text{F}]\text{15}$) have shown specificity for PARP-1 *via* correlated radiotracer uptake and PARP-1 expression, and reduced accumulation in the presence of olaparib (**1**) in ovarian, breast and pancreatic cancer models.^{64,88}

In 2015, Skrydstrup and co-workers synthesised a carbon-11 isotopologue of olaparib, $[^{11}\text{C}]\text{olaparib}$ ($[^{11}\text{C}]\text{1}$), *via* a three-component carbonylation of an aryl palladium precursor with $[^{11}\text{C}]\text{carbon monoxide}$ (Figure 9).⁹⁹ In addition, this procedure facilitated the repeated synthesis ($n = 3$) of $[^{11}\text{C}]\text{olaparib}$ ($[^{11}\text{C}]\text{1}$) in excellent radiochemical purity ($99 \pm 1\%$) and yield ($75 \pm 10\%$). However, the aryl

palladium precursor required for this preparation was found to be labile under an atmosphere of air and consequently, was impracticable for further pre-clinical development. To date, this remains the sole preparation of [¹¹C]olaparib (**[¹¹C]1**) to the best of our knowledge which may be due to the general preference for fluorine-18 radiotracers in this field or an absence of applicable carbon-11 radiolabelling methods.

Additionally, in 2015, Reiner and co-workers developed [¹⁸F]PARPi (**[¹⁸F]16a**) (IC₅₀ = 2.83 nM) in which the 4-*H*-piperazine moiety was substituted with a fluorine-18 radiolabelled benzamide moiety (Figure 9).⁸⁶ *Ex vivo* and *in vivo* pre-clinical studies in mouse models confirmed uptake and colocalisation of [¹⁸F]PARPi (**[¹⁸F]16a**) in orthotopic brain carcinomas, and facilitated delineation in oral and B-cell lymphoma tumour models *via* PET/CT and PET/MRI imaging.⁸⁷ Notably, [¹⁸F]PARPi (**[¹⁸F]16a**) is only the second PARP-1 inhibitor-derived nuclear imaging agent to reach clinical trials thus far. Phase I clinical trials are currently ongoing to investigate the application of this radiotracer for PET imaging of carcinomas of the brain (NCT04173104), and head and neck (NCT04173104).⁸⁸ One disadvantage of this imaging agent was the incorporation of fluorine-18 *via* a three-step labelling procedure which afforded [¹⁸F]PARPi (**[¹⁸F]16a**) in 10% radiochemical yield (non-decay corrected) in a total synthesis time of 90 minutes. In 2020, a more efficient one-pot, two-step radiolabelling procedure for the preparation of [¹⁸F]PARPi (**[¹⁸F]16a**) was developed. However, a low radiochemical yield of 9.6% (non-decay corrected) was afforded from this procedure which required 66 minutes.¹⁰⁰

Furthermore, in 2015, Reiner and co-workers also reported two equivalent radiotracers labelled with iodine radioisotopes suitable for PET and SPECT imaging, known as [^{124/131}I]I2-PARPi (**[^{124/131}I]16b**) (IC₅₀ = 9 nM) (Figure 9).¹⁰¹ *In vivo* PET and SPECT studies in orthotopic mouse models revealed that [^{124/131}I]I2-PARPi (**[^{124/131}I]16b**) was highly selective for PARP-1 in glioblastoma carcinomas and uptake was blocked by prior administration of olaparib (**1**). However, high levels of radioactivity were detected within thyroid tissue compared to tumour cells with a 1.82 ± 0.25 ratio. This may indicate a significant degree of deiodination *in vivo* and render [^{124/131}I]I2-PARPi (**[^{124/131}I]16b**) unsuitable for clinical application.

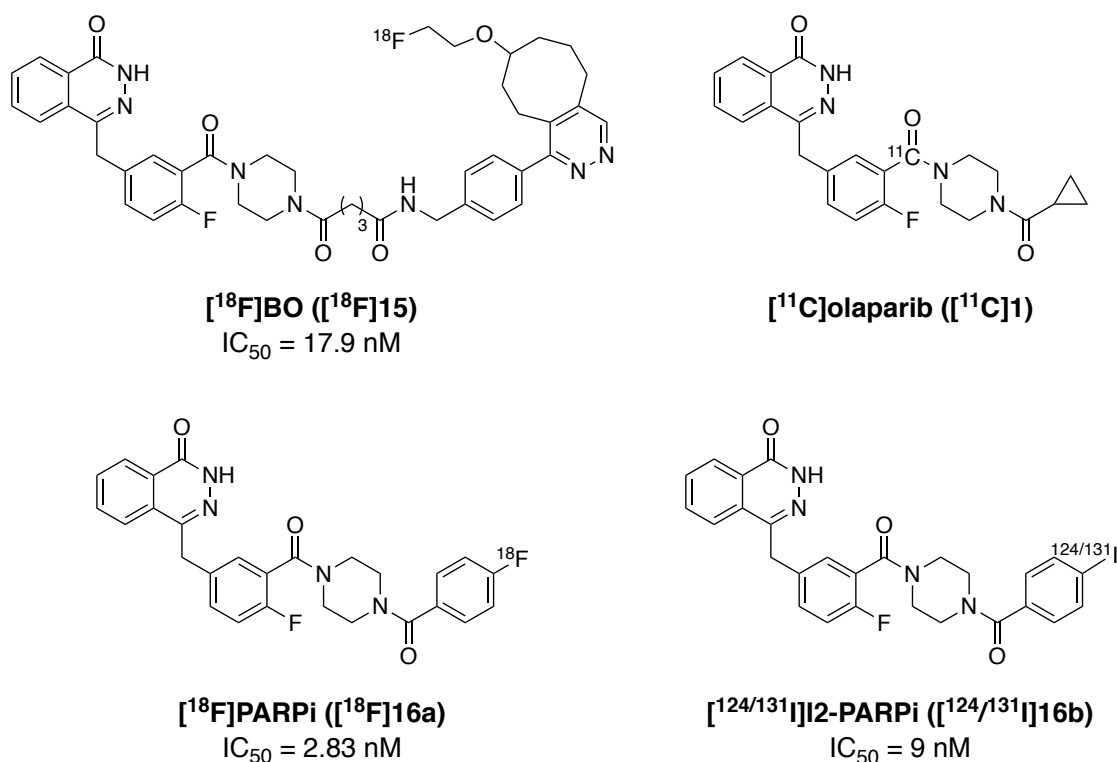


Figure 9 – Olaparib-derived nuclear imaging agents for PARP-1 from Reiner and co-workers and Skrydstrup and co-workers

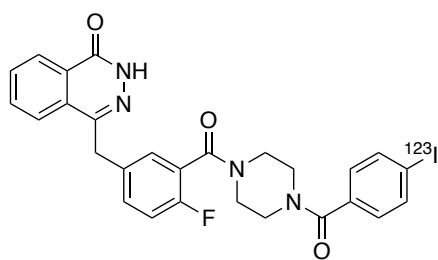
Concurrently, multiple olaparib-derived nuclear imaging agents were developed by Sutherland and co-workers, including Adele Blair, Filip Zmuda, and Kerry O'Rourke. The aim of this work was to develop novel olaparib-derived PET and SPECT imaging agents with the capacity to undergo late-stage radiolabelling with fluorine-18, carbon-11 or iodine-123/125. From a library of twenty-seven compounds, three were identified as lead candidates following physicochemical properties determination, *via* high-performance liquid chromatography (HPLC) methodology, and cell-free assessment of PARP-1 inhibition. Consequently, synthetic procedures were investigated for the preparation of [¹²³I]16b (also denoted as [^{*}I]I2-PARPi ([^{*}I]16b) by Reiner and co-workers), [¹⁸F]16a (also denoted as [¹⁸F]PARPi ([¹⁸F]16a) by Reiner and co-workers), and [¹⁸F]17 which exhibited cell-free PARP-1 inhibitory potency similar to that of olaparib (1) (Figure 10).^{102–105}

Firstly, a synthetic procedure was developed for the preparation of [^{123/125}I]16b *via* a solid state halogen exchange radioiodination reaction.¹⁰² Application of this method facilitated the synthesis of [¹²³I]16b in 36.5 ± 7.2% radiochemical yield (non-decay corrected, n = 6). Subsequently, [¹²³I]16b demonstrated high uptake and

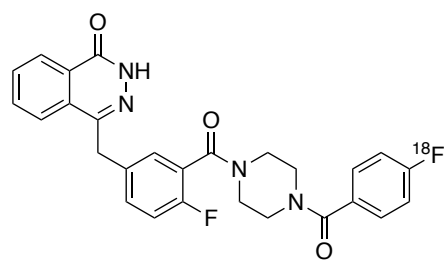
retention in an *ex vivo* subcutaneous xenograph mouse model of glioblastoma and was correlated with expression of PARP-1 and a biomarker of proliferation which indicated PARP-1 specificity. Notably, *ex vivo* biodistribution studies also revealed rapid hepatobiliary clearance of [¹²³I]**16b** as previously observed for olaparib (**1**).

Thereafter, the Sutherland group sought to develop a fluorine-18 radiolabelling procedure for the synthesis of [¹⁸F]**16a**.¹⁰⁵ However, despite optimisation efforts the nucleophilic aromatic substitution reaction investigated for the preparation of [¹⁸F]**16a** generated a maximum of 19% radiochemical conversion, observed *via* HPLC of the crude product. Consequently, the focus of this study was transferred to the optimisation of a synthetic procedure for the preparation of [¹⁸F]**17**. A two-step one-pot radiolabelling method was then developed and afforded [¹⁸F]**17** in 9 ± 2% radiochemical yield (non-decay corrected, n = 7) for *ex vivo* biodistribution studies in subcutaneous xenograph mouse model of glioblastoma. These studies showed that [¹⁸F]**17** was specific for PARP-1 and retained within tumours. However, PET imaging with [¹⁸F]**17** generated high levels of radioactivity within the skeletal system due to *in vivo* defluorination and subsequent accumulation of radiofluoride in bone.

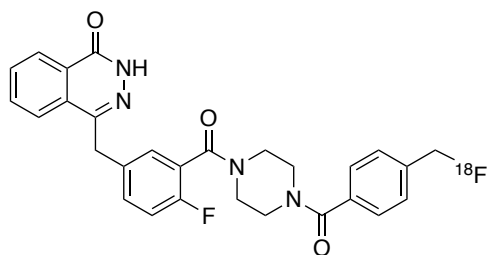
Finally, the Gouverneur and Cornelissen research groups have also been active in this research field. Notably, Wilson *et al.* published the radiosynthesis of a fluorine-18 isotopologue of olaparib in 2019, known as [¹⁸F]olaparib ([¹⁸F]**1**).¹⁰⁶ This isotopologue was prepared in 18 ± 3% radiochemical yield (non-decay corrected, n = 5) *via* copper-mediated radiofluorination of a boronic ester precursor, a methodology that was developed previously within the Gouverneur group.^{107,108} As expected, *in vitro* and *in vivo* studies conducted in xenograph mouse models of pancreatic ductal adenocarcinoma demonstrated high levels of [¹⁸F]olaparib ([¹⁸F]**1**) uptake that correlated with high PARP-1 expression and was blocked through prior administration of olaparib (**1**). Significantly, this work was the first successful production of an isotopologue for the globally approved PARP-1 inhibitor olaparib (**1**) and presents a novel opportunity to PET image PARP-1 and olaparib (**1**) biodistribution *in vivo* in the future.



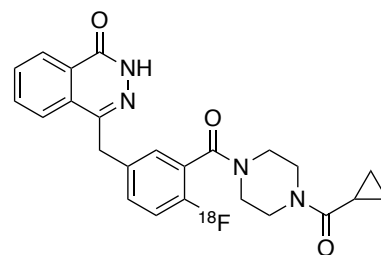
$[^{123}\text{I}]16$



$[^{18}\text{F}]16$



$[^{18}\text{F}]17$



$[^{18}\text{F}]olaparib$ ($[^{18}\text{F}]1$)

Figure 10 – Olaparib-derived nuclear imaging agents for PARP-1 from Sutherland and co-workers, and Gouverneur and co-workers

1.3 Synaptic Vesicle Glycoprotein 2A (SV2A)

1.3.1 Structure, Localisation and Proposed Functions of SV2A

First discovered by Buckley and Kelly in 1985, synaptic vesicle glycoprotein 2A (SV2A) is a twelve-transmembrane glycoprotein located in the membrane of secretory vesicles within neuronal and endocrine cells.¹⁰⁹ The SV2A glycoprotein consists of two transmembrane domains (TM domain 1 and 2, each of which contains six transmembrane helices), two intracellular domains (a cytoplasmic amino domain and loop between transmembrane helices 6 and 7), and one extracellular domain (an intravesicular loop between transmembrane helices 7 and 8) (Figure 11). Figure 11a below shows a two-dimensional protein topology of the SV2A glycoprotein structure. Furthermore, Figure 11b and 11c display three-dimensional models of the inward-open and outward-open conformations of the SV2A glycoprotein respectively.

The synaptic vesicle 2 (SV2) family of proteins, to which SV2A belongs, was one of the first synaptic vesicle protein families discovered in vertebrates and includes two additional paralogs, SV2B and SV2C.^{110,111} Notably, SV2A and SV2B are the major paralogs of the SV2 family whilst SV2C is commonly described as the minor paralog.¹¹² The SV2 glycoproteins possess highly conserved amino acid sequences with shared identities of 57–65%.^{112,113} Interestingly, the majority of conserved amino acid sequences are located within the transmembrane domains and the C-terminal region.^{112,114} Conversely, the N-terminal region is the least homologous within each SV2 paralog.¹¹² In addition, the intravesicular loop between transmembrane helices 7 and 8 present in each SV2 glycoprotein is the second least conserved region. However, the distinct intravesicular loop of each SV2 paralog consistently contains 3–5 *N*-glycosylated residues and repetitive hydrophobic residues, with preference for phenylalanine.¹¹² Consequently, it is thought that the *N*-glycosylated intravesicular loop is instrumental to differing localisation and functions of each SV2 paralog.¹¹⁴

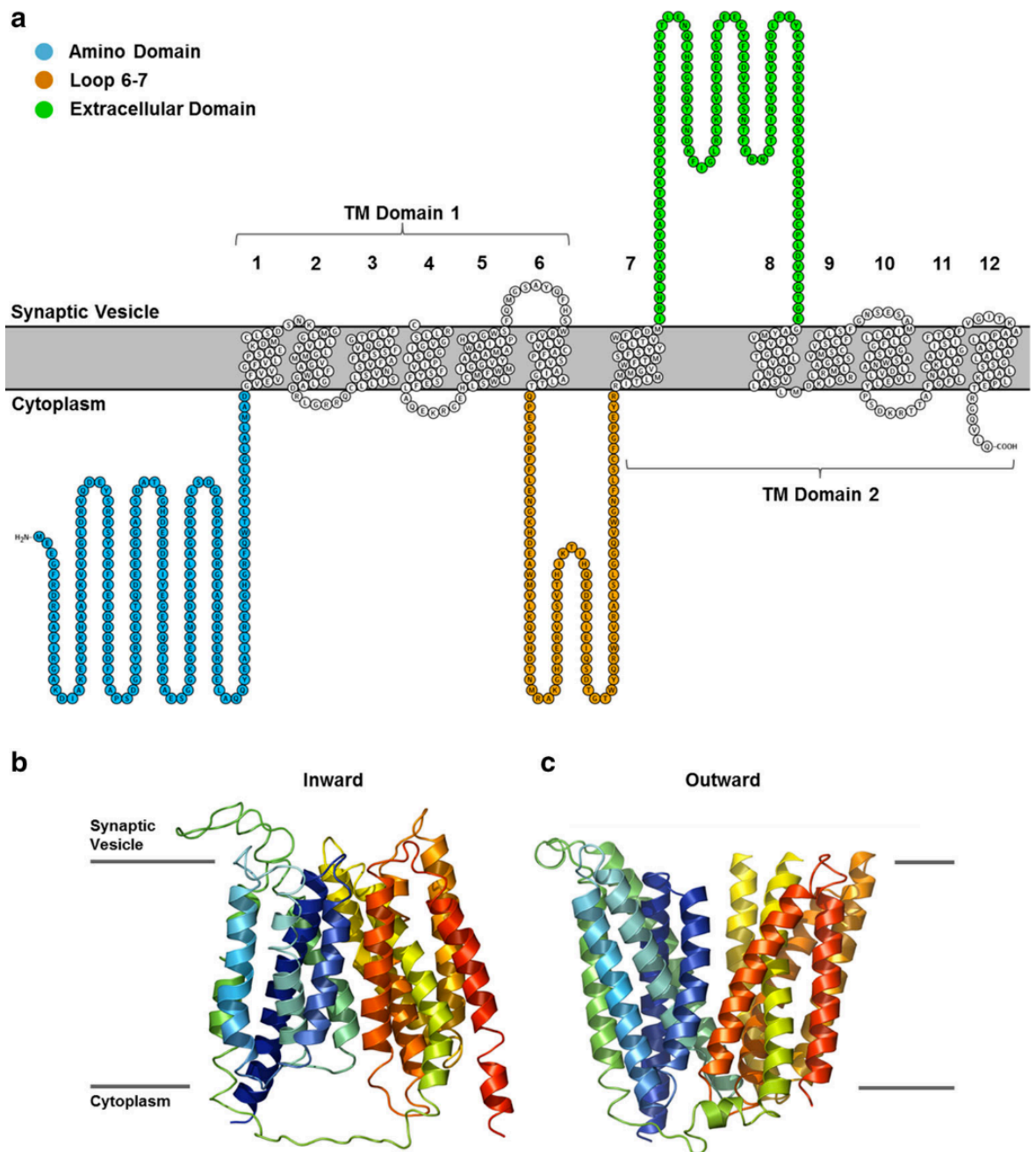


Figure 11 – Structure of the SV2A glycoprotein.¹¹⁰ (Reprinted from Figure 6 of W. Löscher *et al.*, *CNS Drugs*, 2016, **30**, 1055–1077, under the terms of the Creative Commons Attribution 4.0 International License.)

Despite the high degree of shared identity within the SV2 family of glycoproteins, each paralog exhibits differing localisation within the central nervous system. In the brain, SV2A is expressed in almost every region of the synaptome whilst SV2B exhibits substantial overlapping expression with SV2A but is present to a lesser degree.¹¹⁵ Conversely, SV2C has a significantly more limited regional expression with its presence detected in only a few areas of the brain.¹¹² Furthermore, SV2A is

present in both the glutamatergic and GABAergic neurons whereas it is thought that SV2B is limited to most glutamatergic neurons, and SV2C is restricted to GABAergic neurons.¹¹⁴ This varied distribution throughout the synaptome indicates that the SV2 glycoproteins are not employed for the transportation of specific neurotransmitters. Thus far, there is a lack of evidence to support the theory that the SV2 family are neurotransmitter transporters.¹¹⁶

In 1999, Janz *et al.* reported that SV2A- and SV2A/SV2B-knockout mice suffered from epileptic seizures and increased postnatal mortality. Notably, the absence of both SV2 paralogs resulted in presynaptic accumulation of calcium ions (Ca^{2+}) which in turn generated abnormal neurotransmitter release and induced epilepsy.¹¹⁷ To the best of our knowledge, this was the first report of a correlation between the expression of the SV2 family glycoproteins and epilepsy. It has since been proposed that SV2A plays a role in calcium ion-mediated exocytosis *via* the regulation of presynaptic calcium ion concentration or as a target for residual calcium ions.^{113,118}

Notably, the research field concerning the function of the SV2 family of glycoproteins has witnessed a marked increase since 2004 following the discovery that the anti-epileptic drug levetiracetam (UCB L059, Keppra[®]) (**18**) binds to SV2A. Consequently, numerous review articles regarding the possible functions of the SV2 family glycoproteins have been published in recent decades.^{113,114,116,118,119} To briefly summarise, it is currently widely accepted that SV2A performs a crucial function in neurotransmission, specifically vesicle trafficking and exocytosis in the presynaptic region. Furthermore, SV2A expression has been reported as a biomarker of multiple neurological diseases including epilepsy, Parkinson's disease, Alzheimer's disease, and schizophrenia. Nonetheless, the function of SV2A in neurological processes and diseases remains largely unknown and thus, is currently an active field of research.

1.3.2 SV2A as a Therapeutic Target for Epilepsy

Levetiracetam (**18**) was developed in a joint venture between UCB Pharma and Löscher *et al.* (Figure **12**).¹¹⁰ UCB Pharma discovered Levetiracetam (**18**), originally denoted as UCB L059, in 1977 whilst attempting to produce a second generation of nootropic pharmaceuticals. It was hoped that this novel generation would succeed

confirmation that SV2A was a viable target of novel therapeutic pharmaceuticals for the treatment of epilepsy. Subsequently, UCB Pharma developed a structural derivative of levetiracetam (**18**) known as brivaracetam (**20**) which exhibited selectivity for the SV2A glycoprotein with significantly higher affinity than levetiracetam (**18**).^{122–127} Brivaracetam (**20**) was approved by the EMA and FDA in 2016 as an adjunctive treatment for drug refractory partial-onset seizures in patients with epilepsy.^{110,128,129}

Moreover, UCB Pharma sought to develop novel SV2A ligands with increased affinity and anti-seizure potency compared to both levetiracetam (**18**) and brivaracetam (**20**). Ultimately, it was hoped that these ligands would be suitable for late-stage radiolabelling for application in PET imaging agent of the SV2A protein. A vast library of more than five hundred compounds was prepared and screened *in silico* via a three-dimensional pharmacophore model derived from six analogues of levetiracetam (**18**).¹³⁰ A selection of candidates was then assessed by *in vitro* determination of pharmacological, physicochemical, absorption, distribution, metabolism, and elimination (ADME), drug metabolism and pharmacokinetics properties.¹³⁰ Subsequently, three heterocyclic nonacetamide ligands with high affinity for SV2A and anti-seizure potency were identified. These SV2A ligands include UCB-A (**21**), UCB-H (**22**) and UCB-J (**23**) with each containing an acetamide moiety mimic in the form of a five or six-membered heterocycle-substituted pyrrolidinone core (Figure 13).¹³⁰

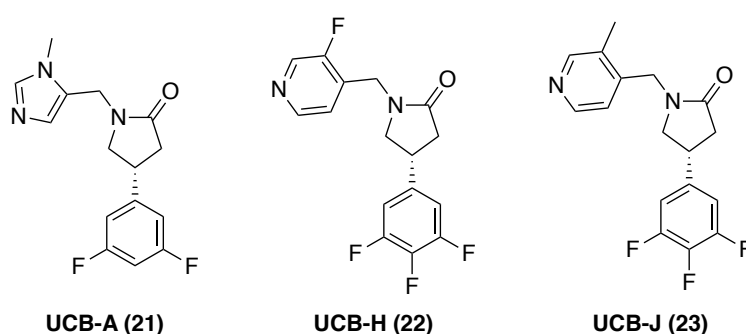


Figure 13 – Heterocyclic nonacetamide ligands UCB-A (**21**), UCB-H (**22**) and UCB-J (**23**)

1.3.3 PET and SPECT Imaging Agents for SV2A

The ubiquitous expression of SV2A within the glutamatergic and GABAergic neurons throughout almost every region of the brain renders this glycoprotein an attractive biomarker for nuclear imaging of synaptic density. Recently, synaptic density has been shown to decrease in multiple neurological disease states and therefore, the desire to quantitatively PET image the SV2A glycoprotein has significantly grown.^{116,118,131–133} [¹¹C] and [^{99m}Tc]Levetiracetam (**[¹¹C]18** and **[^{99m}Tc]18**) were developed by Cai *et al.*, Rashed *et al.*, and Sanad *et al.* for PET and SPECT imaging respectively (Figure 14).^{134–136} However, these imaging agents exhibit relatively low affinity for SV2A ($K_i = 2.5 \mu\text{M}$ for levetiracetam (**18**)) and slow brain penetration when compared with latterly discovered ligands and therefore, have not undergone further development.^{111,118,132}

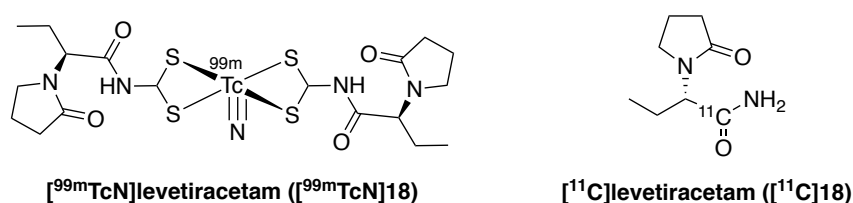


Figure 14 – Levetiracetam-derived PET and SPECT imaging agents

Additionally, a range of carbon-11 and fluorine-18 PET radiotracers for SV2A were developed in the last decade by UCB Pharma, in collaboration with Yale University, Uppsala University and University of Liège. Recently, these PET and SPECT radiotracer candidates have been described in detail by multiple review articles.^{116,118,131–133} To summarise, the SV2A ligands discovered by UCB Pharma have been further developed into PET radiotracers [¹¹C]UCB-A (**[¹¹C]21**)¹³⁷, [¹⁸F]UCB-H (**[¹⁸F]22**)^{138–140}, and [¹¹C]UCB-J (**[¹¹C]23**)¹⁴¹ (Figure 15).¹³¹ During pre-clinical *in vivo* testing, [¹¹C]UCB-J (**[¹¹C]23**) displayed efficient and reversible binding kinetics with high levels of uptake across the brain, relatively low nonspecific binding, and moderate metabolism in non-human primates.¹⁴¹ Notably, pre-administration of levetiracetam (**18**) resulted in a significant blocking effect of up to 89% occupancy indicating specific binding of [¹¹C]UCB-J (**[¹¹C]23**) to SV2A *in vivo*.¹⁴¹ Conversely, despite desirable nanomolar affinity for SV2A, [¹¹C]UCB-A (**[¹¹C]21**)¹³⁷ and [¹⁸F]UCB-H (**[¹⁸F]22**)^{138–140} exhibit slower binding and low specific binding to SV2A respectively.^{111,132}

Subsequently, [^{11}C]UCB-J (**[^{11}C]23**) was progressed into human clinical trials and was found to facilitate *in vivo* PET imaging of SV2A in a consistent manner to pre-clinical imaging studies.^{111,131} Of these PET radiotracers from UCB Pharma, [^{11}C]UCB-J (**[^{11}C]23**) has become the most frequently employed in this field of research due to the favourable properties it has displayed for *in vivo* PET imaging. Thus far, [^{11}C]UCB-J (**[^{11}C]23**) has been utilised for PET imaging studies to examined numerous conditions including Alzheimer’s disease, Parkinson’s disease, Lewy body dementia, Huntington’s disease, obesity, ischemic stroke, and human immunodeficiency virus.^{142–150} Furthermore, a fluorine-18 equivalent [^{18}F]UCB-J (**[^{18}F]23**) was subsequently developed due to the favourable properties of fluorine-18 relative to carbon-11 for nuclear imaging. As expected, [^{18}F]UCB-J (**[^{18}F]23**) produced promising results during pre-clinical *in vivo* studies of non-human primates, similar to [^{11}C]UCB-J (**[^{11}C]23**).¹⁵¹ However, [^{18}F]UCB-J (**[^{18}F]23**) was synthesised *via* nucleophilic aromatic substitution of an iodonium salt precursor which required very high temperatures (200 °C) and produced a very poor radiochemical yield of only 1–2%. Furthermore, chiral HPLC was required to facilitate separation of enantiomers as the final synthetic step which can be both costly and time consuming.¹¹¹

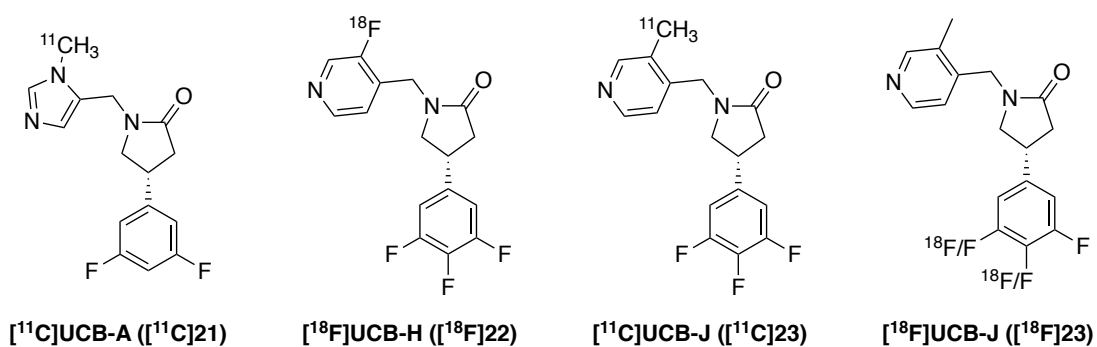


Figure 15 – PET Imaging agents [^{11}C]UCB-A (**[^{11}C]21**), [^{18}F]UCB-H (**[^{18}F]22**), [^{11}C]UCB-J (**[^{11}C]23**), and [^{18}F]UCB-J (**[^{18}F]23**)

Consequently, a second generation of nuclear imaging agents were derived from the structure of [^{11}C]UCB-A (**[^{11}C]21**) and [^{11}C]UCB-J (**[^{11}C]23**), namely [^{18}F]SynVesT-1 (**[^{18}F](*R*)-24**), [^{18}F]SynVesT-2 (**[^{18}F]25**) and [^{18}F]SDM-16 (**[^{18}F]26**) (Figure 16). Notably, this most recent series of SV2A radiotracers have been designed with consideration to late-stage facile incorporation of a fluorine-18 radionuclide. In 2019, [^{18}F]SynVesT-1 (**[^{18}F](*R*)-24**) was simultaneously synthesised

by Constantinescu *et al.*, and by Li *et al.* via similar approaches.^{152,153} The synthetic route employed by each group is discussed in greater detail in Section 2.2.1 of this thesis. Due to the parallel nature of research, this PET imaging agent was previously denoted in literature as [¹⁸F]MNI-1126 or [¹⁸F]SDM-8. However, a consensus was reached and the name [¹⁸F]SynVesT-1 (**[¹⁸F](R)-24**) is now widely utilised for clarity. Non-human primate pre-clinical studies have consistently shown that [¹⁸F]SynVesT-1 (**[¹⁸F](R)-24**) exhibits very favourable properties for *in vivo* PET imaging of SV2A.^{152–154} Moreover, as reported for [¹¹C]UCB-J (**[¹¹C]23**), [¹⁸F]SynVesT-1 (**[¹⁸F](R)-24**) has displayed high brain uptake, high binding affinity with specificity for SV2A, and suitable pharmacokinetics in a first-in-human study conducted by Naganawa and Li *et al.* in 2021.¹⁵⁵ Notably, [¹⁸F]SynVesT-1 (**[¹⁸F](R)-24**) was found to possess a higher binding potential than [¹¹C]UCB-J (**[¹¹C]23**) indicating excellent potential as a PET imaging agent for SV2A with increased synthetic accessibility.¹⁵⁵

Finally, concurrent to the work described in Section 2.2 of this thesis, two derivatives of [¹⁸F]SynVesT-1 (**[¹⁸F](R)-24**) have been developed, termed [¹⁸F]SynVesT-2 (**[¹⁸F]25**, previously [¹⁸F]SDM-2) and [¹⁸F]SDM-16 (**[¹⁸F]26**).^{156,157} Pre-clinical studies in non-human primates have found that [¹⁸F]SynVesT-2 (**[¹⁸F]25**) exhibits similar binding potential yet faster pharmacokinetics than [¹¹C]UCB-J (**[¹¹C]23**) and consequently, generates high quality PET images.¹⁵⁶ Furthermore, pre-clinical data indicates that [¹⁸F]SynVesT-2 (**[¹⁸F]25**) is suitable for quantitative kinetic modelling and translation into human clinical trials at Yale PET Centre is ongoing.¹⁵⁶ Notably, pre-clinical studies of [¹⁸F]SDM-16 (**[¹⁸F]26**) in non-human primates have shown that this SV2A ligand displays greater metabolic stability than any previous SV2A PET radiotracers and therefore, potential utility for the quantification of SV2A in the wider central nervous system.

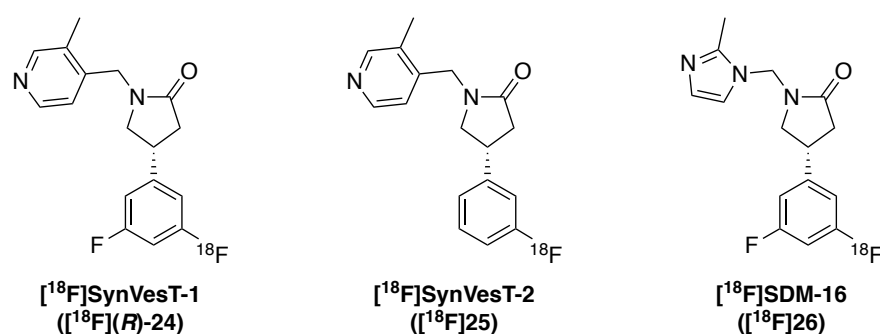


Figure 16 – PET Imaging agents [¹⁸F]SynVesT-1 (**[¹⁸F](R)-24**), [¹⁸F]SynVesT-2 (**[¹⁸F]25**), and [¹⁸F]SDM-16 (**[¹⁸F]26**)

1.4 Conclusion

In summary, through the innovation of modern healthcare a diverse toolkit of molecular imaging technologies has been produced which facilitates non-invasive imaging of numerous diseases and biological processes. Of these techniques, PET and SPECT offer superior sensitivity *via* the detection of nuclear imaging agents, and improved spacial resolution is attained when hybridised with CT. Thus far, PET and SPECT have been primarily utilised to diagnose and monitor oncological, cardiological and neurological diseases. However, in recent years, interest in the application of PET and SPECT imaging in drug development has grown; in the future, these imaging methods may become vital tools in the pharmaceutical research and approval process. Consequently, the demand for novel PET and SPECT imaging agents for a variety of biological targets continues to increase each year. Thus far, the use of carbon-11, fluorine-18, technetium-99m, and iodine-123 radionuclides has dominated this field, and numerous PET and SPECT radiotracers have proven very successful in clinical applications. However, there remains clear opportunity for innovation in this research area through the discovery of novel radiotracers. Furthermore, the development of superior radiolabelling methods will be crucial to the growth of these molecular imaging techniques.

In the field of oncology, nuclear imaging of the PARP-1 protein has garnered significant attention from both the academic and clinical research communities following the pioneering clinical success of PARP-1 inhibitor olaparib (**1**). PARP-1 inhibitors exploit synthetic lethality to induce cell death in tumours *via* inhibition of PARylation and subsequent DNA repair in patients with BRCA1/2-mutations. Multiple PARP-1 inhibitors have been found to produce remarkable clinical responses in a range of cancer types. PARP-1 presents an attractive biomarker for tumours and thus, PARP-1 inhibitors have become a structural basis for the development of novel nuclear imaging agents. Moreover, the majority of PET and SPECT imaging agents for PARP-1 developed thus far have been derived from olaparib (**1**). Despite significant advances in this field, multiple PARP-1 inhibitor-derived radiotracers have been deemed impracticable for further development due to challenging radiosynthesis procedures, poor radiochemical yields, or unsuitable *in vivo* properties. As such, additional research is required to identify a PARP-1 inhibitor-derived nuclear imaging agent that can be prepared in high radiochemical

yield and exhibits favourable *in vivo* properties for PET or SPECT imaging. Development of such a radiotracer could enable the investigation and greater understanding of the PARP-1 protein and various cancer types.

Furthermore, in the last decade, multiple nuclear imaging agents targeting the SV2A glycoprotein have emerged in the field of neurology. Ultimately, the development of anti-seizure drug levetiracetam (18) for the treatment of epilepsy lead to identification of SV2A as the binding site of the drug within the brain. Since this discovery, significant interest has grown regarding the role of SV2A in epilepsy and its overall function within the brain; thus, SV2A has become the subject of multiple research programmes. However, despite recent efforts, the function of SV2A has not been fully elucidated at this time and further research is required. Additionally, the presence of SV2A in the glutamatergic and GABAergic neurons throughout the synaptome presents this transmembrane glycoprotein as a potential biomarker for synaptic density. Synaptic density is known to change throughout the course of many neurological conditions including Alzheimer's disease, Parkinson's disease, schizophrenia, and epilepsy. Consequently, nuclear imaging of SV2A provides a valuable opportunity to quantitatively evaluate changes to synaptic density within the brain over the course of these neurological conditions. As this is an emerging field of research, the number of SV2A radiotracers currently available is very limited and the development of novel nuclear imaging agents is an ongoing process. Crucially, improved synthetic methods for the preparation of SV2A radiotracers currently in pre-clinical development or clinical trials would be extremely advantageous to this expanding research field.

2.0 Results and Discussion

2.1 Synthesis of Novel Olaparib-Derived PET Imaging Agents for PARP-1

2.1.1 Unpublished Previous Work in the Sutherland Group

Since 2012, the Sutherland group have worked to develop novel PET and SPECT imaging agents for PARP-1, for employment in the monitoring and treatment of various cancer types. The recurrent focus of this research has been specifically on small molecule PARP-1 inhibitors derived from olaparib (**1**), with an integral capacity for late-stage radiolabelling. Following on from the published work described in Section 1.2.3.2,^{102–105,158–161} the group sought to design and synthesise a novel library of PARP-1 inhibitor PET imaging agents with increased metabolic stability and that could undergo facile radiofluorination as the final synthetic step. It was proposed that this new series of compounds would largely conserve the structure of compound **16a**, shown in Figure 17 below, and incorporate alternative benzamide motifs for fluorine-18 radiolabelling, *via* a nucleophilic aromatic substitution (S_NAr) reaction.

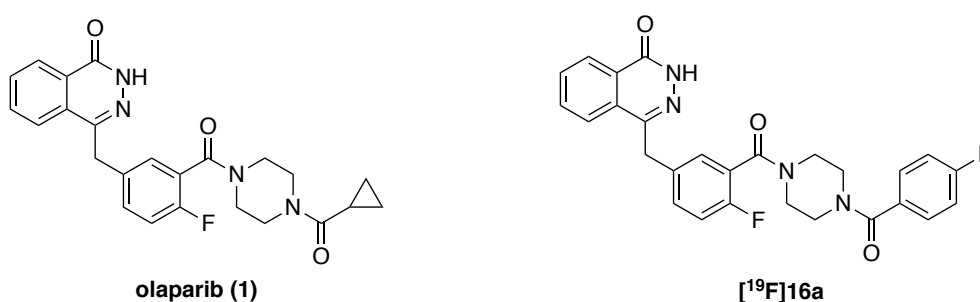
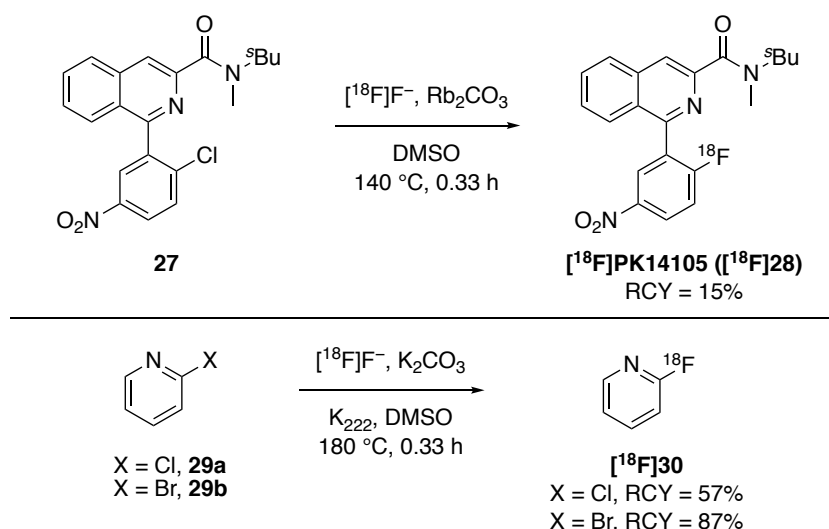


Figure 17 – Structure of olaparib (**1**) and Sutherland group compound **16a**

It is widely known that S_NAr reactions are promoted by the presence of electron-withdrawing substituents in the *ortho*- or *para*- positions, relative to the leaving group that is displaced, due to increased stability of the intermediate. In 2016, Gouverneur and co-workers published a review of fluorine-18 radiolabelling methods for haloarenes and haloheteroarenes with pertinence to PET radiotracer synthesis.²³ In this review, the authors highlighted that halide-displacing S_NAr reactions using

fluorine-18 have been widely and successfully facilitated by the presence of either electron-withdrawing substituents or heteroatoms, in the *ortho*- or *para*- positions. For example, Cremer and co-workers employed a *para*-nitro substituent in the synthesis of [¹⁸F]PK14105 ([¹⁸F]**28**), *via* an S_NAr reaction of chloride precursor **27**, for PET imaging of peripheral-type benzodiazepine binding sites (Scheme 2).¹⁶² Nitroarenes are frequently exploited as precursors for S_NAr radiofluorination reactions and generally provide higher radiochemical yields (RCY) than haloarene equivalents. Importantly, this work by Cremer and co-workers demonstrated that halides are favourably substituted for fluorine-18 in S_NAr reactions of halonitroarenes. Furthermore, research by Crouzel and co-workers shown below in Scheme 2 exemplifies fluorine-18 radiolabelling of *ortho*-substituted electron-deficient halopyridines **29a** and **29b** *via* S_NAr reactions, in high radiochemical yields.¹⁶³



Scheme 2 – Radiofluorination of electron-deficient arenes *via* S_NAr reactions

Consequently, Kerry O'Rourke of the Sutherland group synthesised a small library of novel PARP-1 inhibitors containing electron-deficient fluorobenzamide moieties, compounds **31**, **32**, **33** and **34**, herein referred to as the KO library (Figure 18).¹⁵⁸ This series of compounds was synthesised as fluorine-19 analogues for evaluation of physicochemical properties and *in vitro* PARP-1 inhibitory potency, since these attributes are presumed to be identical for the fluorine-18 equivalent compounds. Additionally, chloride or bromide analogues were synthesised for each compound in this library, to serve as appropriate precursors for radiofluorination *via* a S_NAr reaction.

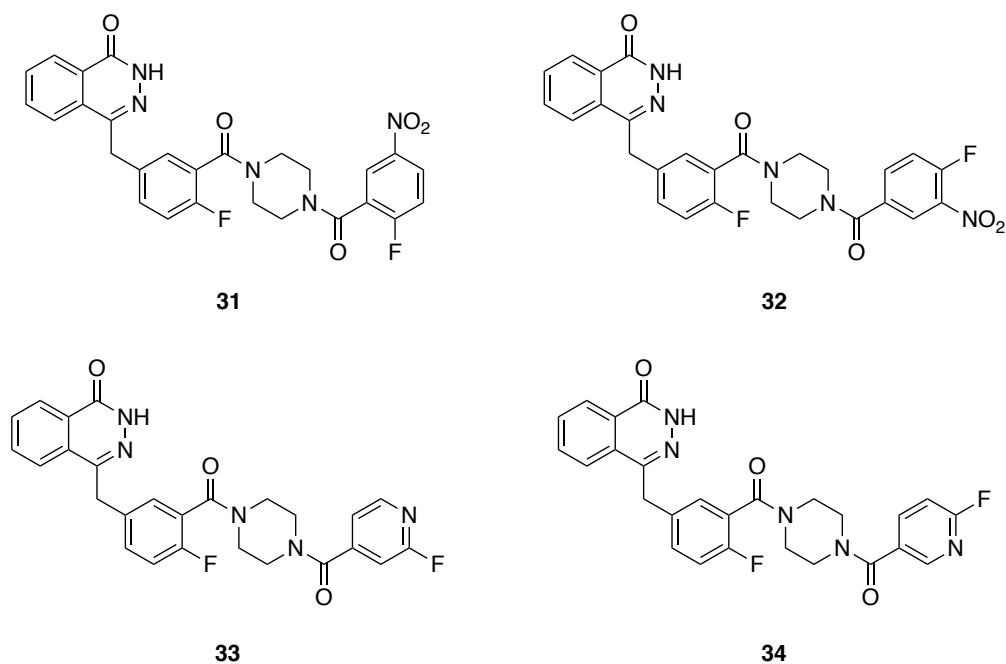
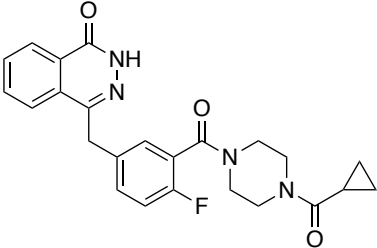
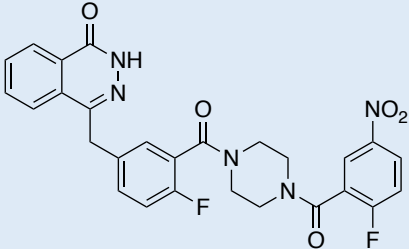
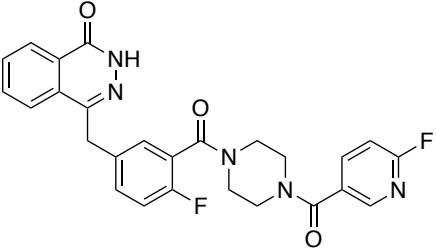


Figure 18 – Library of PARP-1 inhibitors synthesised by the Sutherland group

To determine which compounds in the KO library were suitable for further development as PET imaging agents, compounds **31**, **32**, **33** and **34** were subjected to physicochemical properties analysis using high performance liquid chromatography (HPLC) methodology.^{158,164} Full experimental detail, results and discussion of physicochemical properties testing for these compounds can be found in the PhD thesis of Kerry O'Rourke.¹⁵⁸ All four compounds exhibited satisfactory physicochemical properties and were consequently submitted to extensive *in vitro* studies of PARP-1 inhibitory potency and cytotoxicity.^{158,165} *In vitro* testing was performed using immunofluorescence-based assays of PARylation and colony formation assays in two glioblastoma cell lines, G7 and E2 stem cells. A selection of half-maximal inhibitory concentration (IC₅₀) values obtained from these PARylation inhibition assays are shown in Table 5 below. Full experimental detail, results and discussion of *in vitro* work performed can be found in the PhD thesis of Maria C. Liuzzi.¹⁶⁵ This analysis revealed that compounds **31** and **34** possess the necessary physicochemical properties to cross the blood-brain barrier (BBB) and are more potent and cytotoxic PARP-1 inhibitors than olaparib (**1**), under our experimental conditions. It was concluded that both compounds **31** and **34** were suitable for further development as PET imaging agents for PARP-1 and radiosynthesis of [¹⁸F]**31** would be investigated in future projects.

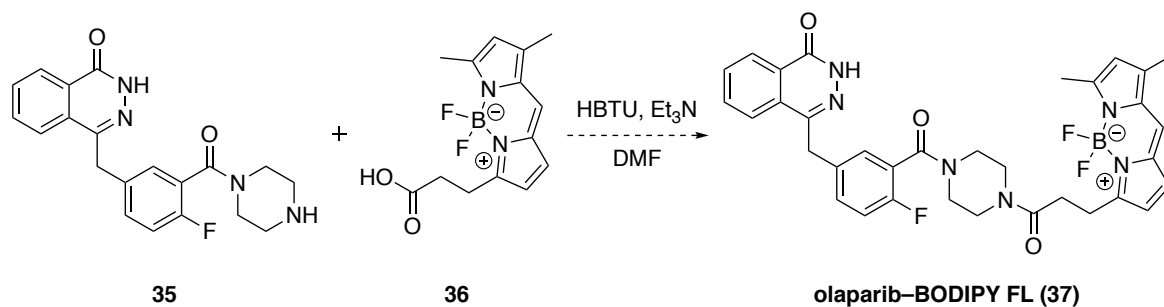
Table 5 – IC₅₀ values of olaparib (**1**) and compounds **31** and **34** in glioblastoma G7 and E2 stem cell lines

Compound	No.	PARylation Inhibition	
		IC ₅₀ (nM)	
		G7	E2
	1	4.92	4.17
	31	0.851	1.12
	34	0.319	0.552

2.1.2 Proposed Research

The overall objective of this research project was to expand upon the work previously carried out within the Sutherland group on new PARP-1 inhibitors for PET imaging, based on the structure of olaparib (**1**). The first aim of this project was to prepare the olaparib core **35** using the synthetic route previously published by the Sutherland group.¹⁰² Subsequently, the olaparib core **35** would be employed in a coupling reaction with BODIPY FL propionic acid **36** to obtain an established PARP-1 inhibitor with fluorescent properties, olaparib-BODIPY FL (**37**) (Scheme 3).^{166,167} Olaparib-BODIPY FL (**37**) would then be applied for the development of *in vitro* biological studies of PARP-1 inhibition by our project collaborators at the Institute of Cancer Sciences, University of Glasgow. Such studies include a competitive inhibitor displacement fluorescence assay, which would allow various binding

properties of novel olaparib analogues with PARP-1 to be assessed. Furthermore, our collaborators would employ olaparib-BODIPY FL (**37**) to investigate the uptake and retention of olaparib (**1**) in the nuclei of glioblastoma cell lines.



Scheme 3 – Proposed synthesis of olaparib-BODIPY FL (**37**)

The third aim, and key objective, of this project was to design and synthesise a library of novel olaparib-derived PARP-1 inhibitors with susceptibility to late-stage fluorine-18 radiolabelling methods, for use as PET radiotracers. It was proposed that this series of compounds, herein referred to as the HM library, would employ an alternative scaffold design and radiofluorination methodology to PARP-1 inhibitors previously investigated by the Sutherland group.

Prior to this project, multiple key interactions were identified between various PARP-1 inhibitors and the PARP-1 catalytic site.^{65,168–170} It had been suggested that olaparib (**1**) exhibits potent binding to PARP-1 due to these same interactions (Figure **19A**). The aryl ring of the phthalazinone system participates in non-polar π - π stacking with tyrosine-907, and the amide moiety participates in hydrogen bonding to serine-904 and glycine-863. Further hydrogen bonding interactions are present between the *meta*-benzyl carbonyl and methionine-890. Therefore, it was proposed that all compounds of the HM library would retain the olaparib core structure **35** and consequently exhibit high PARP-1 inhibitory potency.

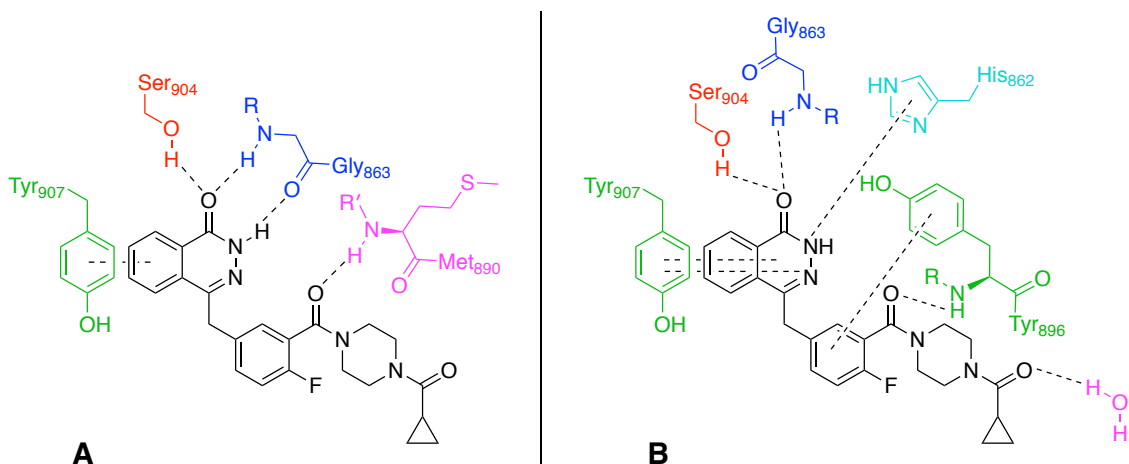


Figure 19 – Key binding interactions of olaparib (**1**) with PARP-1 catalytic site

In December 2020, Gajiwala and co-workers published a crystal structure of the human PARP-1 catalytic domain complexed with olaparib (**1**) (PDB ID: 7kk4).¹⁷¹ One month later in January 2021, Neuhaus and co-workers also reported a crystal structure of the human PARP-1 catalytic domain complexed with olaparib (**1**) (PDB ID: 7AAD).³⁵ All key interactions observed in these studies are in agreement (Figure **19B**), though differ from those previously proposed. The phthalazinone system participates in non-polar π - π stacking and cation- π interactions, through the 3-N atom, with tyrosine-907. The carbonyl of the phthalazinone participates in hydrogen bonding to serine-904 and glycine-863. Cation- π interactions were also observed between the phthalazinone, through the 2-N atom, and histidine-862. Additional non-polar π - π stacking was reported between the central fluorobenzyl ring and tyrosine-896, which also participates in hydrogen bonding to the *meta*-benzyl carbonyl. Finally, the carbonyl of the cyclopropylamide moiety was found to hydrogen bond to a conserved water molecule. No key interactions have been observed between the catalytic site of PARP-1 and the piperazine or cyclopropyl moieties of olaparib (**1**) to date. Notably, in 2004, Fujii and co-workers reported that a large hydrophobic pocket is formed adjacent to the PARP-1 catalytic site following binding of an inhibitor ligand.¹⁷² This pocket is found on the opposite side of the catalytic domain to the region in which the phthalazinone moiety of olaparib (**1**) is bound.

Reiner and co-workers have reported multiple olaparib-derived structures, such as compound [¹⁸F]**15**, in which the 4-NH-piperazine moiety is substituted with a long lipophilic hydrocarbon chain and coupled to a bulky terminal ring system (Figure

20).^{97,98,173} These compounds retain potency for PARP-1 despite significant structural modification and are applicable as fluorescent or PET imaging agents.

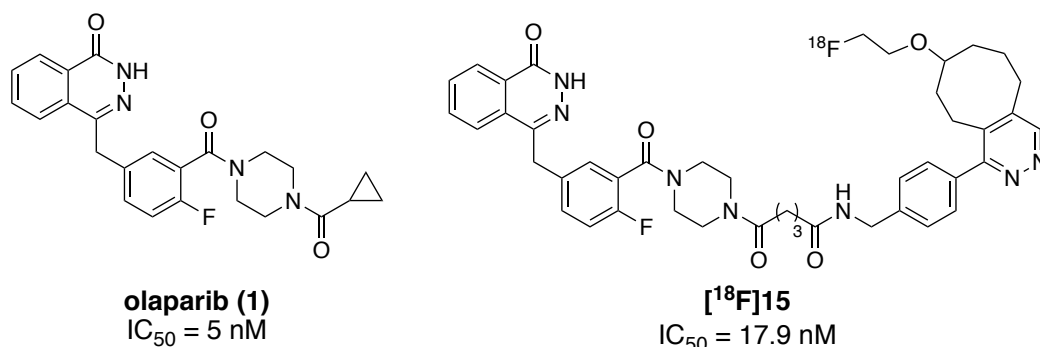
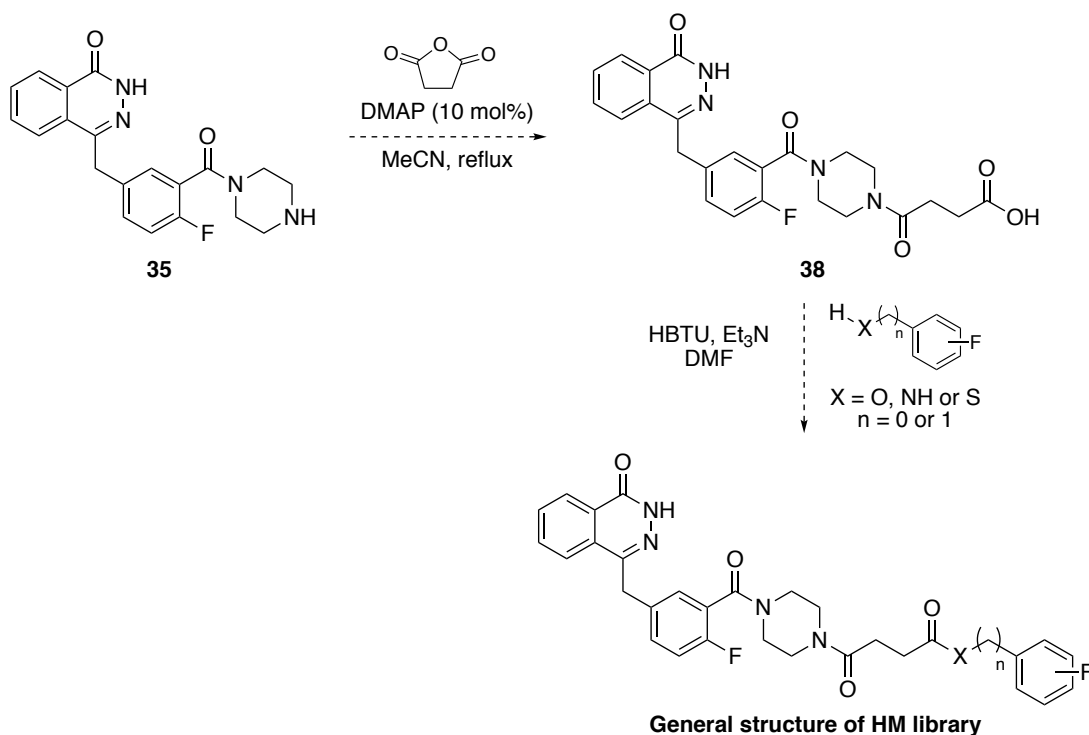


Figure 20 – Olaparib analogue [¹⁸F]15 synthesised by Reiner and co-workers

Evidently, this absence of key binding interactions outwith the core scaffold of olaparib **35** and the large adjacent hydrophobic pocket permit the PARP-1 catalytic site to tolerate a diverse range of modified olaparib-based ligands. As such, it was proposed the HM library compounds would be synthesised by acylation of the olaparib core **35** with succinic anhydride to introduce a lipophilic hydrocarbon linker to the scaffold (Scheme 4). Resulting intermediate **38** would provide a pendant carboxylic acid handle for coupling to a range of fluoroarene nucleophiles.



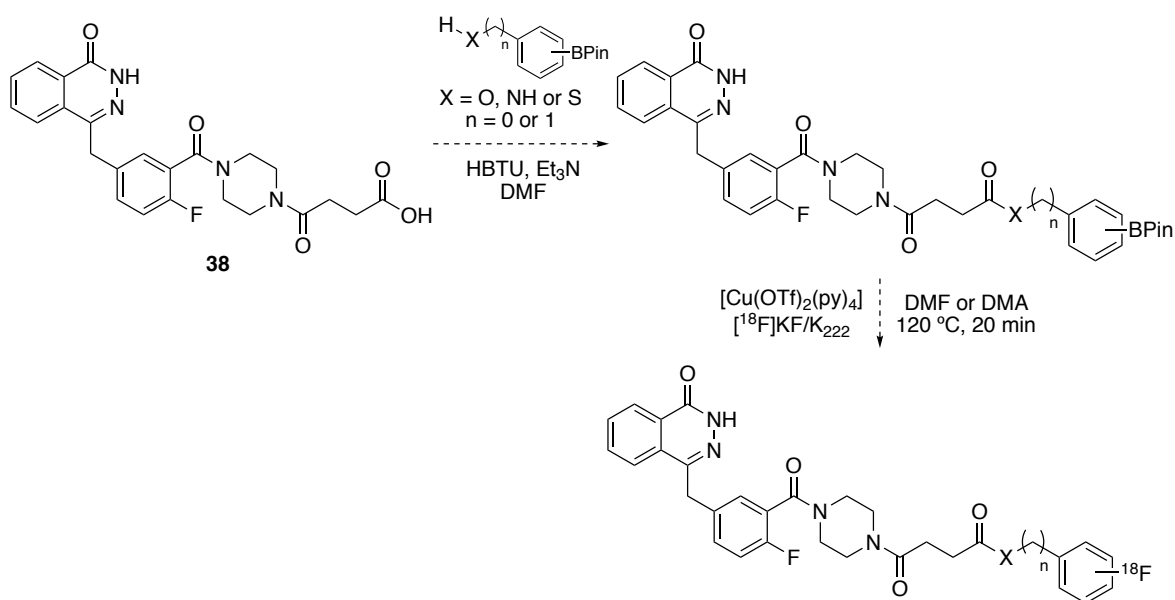
Scheme 4 – Proposed synthesis of novel PARP-1 inhibitors for PET imaging

As a result of this new scaffold, the HM library of PARP-1 inhibitors would have an elongated structure and increased degree of flexibility compared to previous Sutherland group compounds. It was proposed that these structural changes may result in alternative interactions within the PARP-1 catalytic site and influence inhibitory potency. Furthermore, it was hoped that a greater understanding of PARP-1 inhibitor SAR could be obtained. Fluorine-19 analogues would be synthesised exclusively at this stage of the project, as previously discussed for the KO library, to mimic the fluorine-18 equivalents in subsequent physicochemical properties analysis and *in vitro* biological studies.

Once synthesised, this small library of potential PET radiotracers would be subjected to physicochemical properties evaluation using high performance liquid chromatography (HPLC) techniques developed by Tavares *et al.*, to identify the compounds with optimal drug-like properties.¹⁶⁴ The properties to be determined include the partition coefficient ($\log P$), percentage plasma protein binding (%PPB), membrane partition coefficient (K_m) and membrane permeability (P_m). Those with favourable physicochemical properties would then be assessed for PARP-1 inhibitory potency by our collaborators at the Institute of Cancer Sciences, University of Glasgow, using a range of *in vitro* studies in two glioblastoma models. Should any of these compounds show scope for development as a PET imaging agent for PARP-1, a corresponding precursor would be synthesised and a fluorine-18 radiolabelling method investigated.

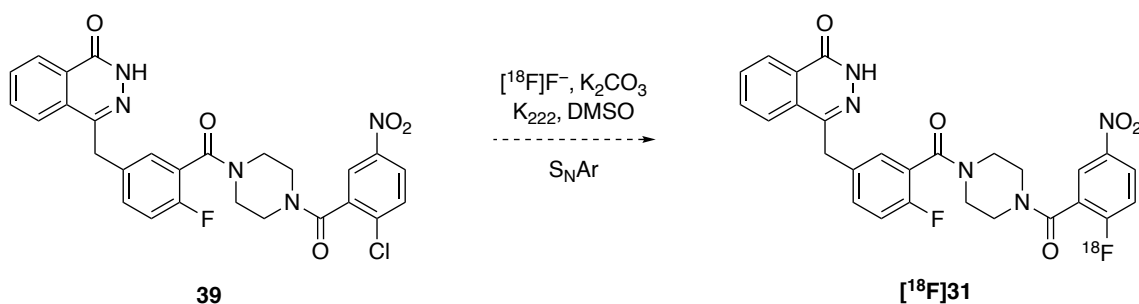
In 2014, Gouverneur and co-workers reported a novel radiolabelling procedure of aryl pinacol boronic ester precursors using [¹⁸F]fluoride and tetrakis(pyridine)copper(II) bis(trifluoromethanesulfonate), *via* a Chan-Lam-inspired radiofluorodeborylation reaction.¹⁰⁷ This method was applicable to a wide range of electron-deficient and electron-rich arenes with diverse functionality, and was employed in the radiosynthesis of three established PET imaging agents in high radiochemical yields. Additionally, Gouverneur and co-workers published an optimised procedure for this same radiofluorodeborylation reaction in 2016.¹⁰⁸ The authors proved this procedure to be both robust and reliable by successfully synthesising eight further PET radiotracers across three different laboratories and synthetic modules.

Therefore, it was proposed that this methodology would be used in the radiosynthesis of fluorine-18 analogues of the HM library compounds (Scheme 5). When required, aryl pinacol boronic ester precursors would be obtained by coupling carboxylic acid intermediate **38** with the appropriate commercially available aryl boronic ester nucleophiles.



Scheme 5 – Proposed radiofluorination procedure

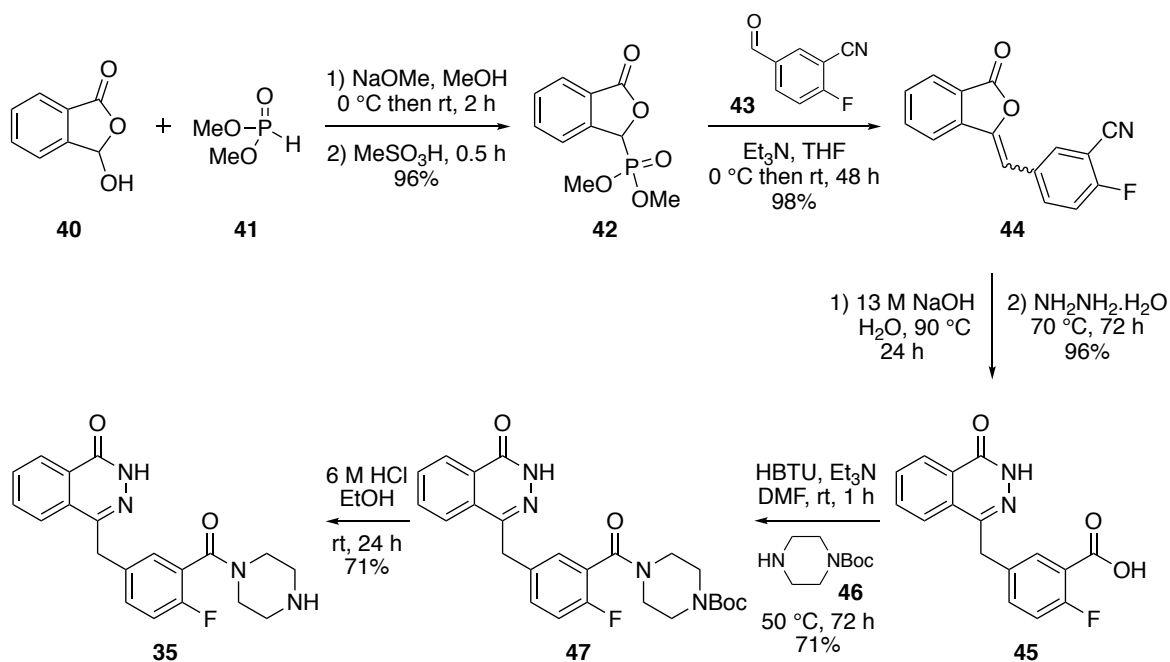
Finally, as discussed in Section 2.1.1, compound **31** was previously identified as a more potent PARP-1 inhibitor than olaparib (**1**) and selected for further development as a PET imaging agent. Therefore, an additional aim of this project was to investigate the radiosynthesis of [¹⁸F]**31** via a S_NAr reaction (Scheme 6).



Scheme 6 – Proposed radiosynthesis of [¹⁸F]**31**

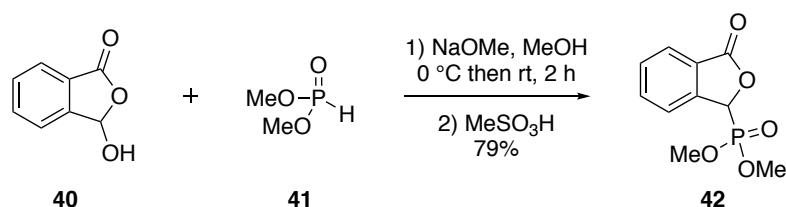
2.1.3 Synthesis of the Olaparib Core Structure

The first aim of this project was to synthesise the olaparib core structure **35**, as this is the key intermediate for the preparation of all subsequent olaparib (**1**) analogues. It was proposed that this would be achieved following the synthetic route to compound **35** previously published by the Sutherland group (Scheme 7).¹⁰² This method was adapted from synthetic procedures reported by Menear *et al.* in 2008 for the preparation of olaparib (**1**).^{74,174}



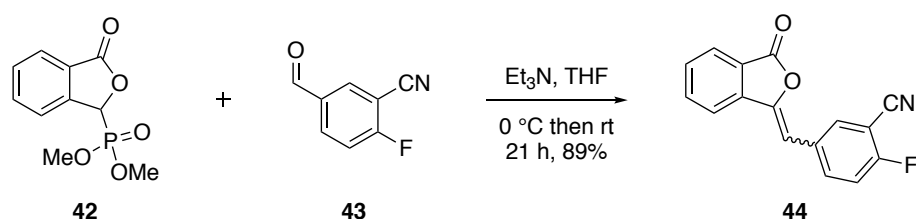
Scheme 7 –Synthetic route for preparation of the olaparib core (**35**) published by the Sutherland group

Firstly, phosphorylation of commercially available 2-carboxybenzaldehyde (**40**) was performed under basic conditions using dimethylphosphite (**41**) and sodium methoxide to afford benzofuran-1-one phosphonate ester **42** in 79% yield (Scheme 8). Notably, this reaction afforded **42** in a lower yield than previously reported by the Sutherland group.¹⁰² This was likely due to experimental variability commonly observed between distinct reactions, and is produced by differences in reaction scale, handling technique, and ambient conditions.



Scheme 8 – Synthesis of benzofuran-1-one phosphonate ester **42**

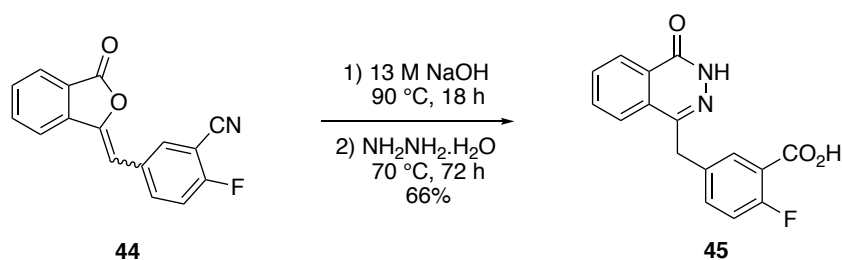
The phosphonate ester moiety of benzofuran-1-one **42** was then transformed through a Horner-Wadsworth-Emmons (HWE) reaction with 2-fluoro-5-formylbenzonitrile (**43**) in the presence of triethylamine to give alkene **44** in 89% yield (Scheme 9). The *E* and *Z* isomeric ratio of the isolated product **44** was determined by ^1H NMR spectroscopy to be 75:25, respectively. HWE reactions typically favour formation of *E*-alkenes, as observed here, and this selectivity can be rationalised through consideration of the reaction intermediates. Following nucleophilic attack of the phosphonate ester-stabilised anion at the benzaldehyde carbonyl, the *anti* oxaphosphetane is formed faster than the *syn* oxaphosphetane. The preceding betaine intermediate undergoes rotation to generate the *anti* oxaphosphetane faster as this reduces steric interactions. Subsequent elimination from the *anti* oxaphosphetane to form the *E*-alkene is also faster than the corresponding *Z*-alkene formation. No efforts were made to influence the *E/Z* selectivity of this step or to separate the isomers of alkene **44** as the alkene geometry was inconsequential to the succeeding synthetic step.



Scheme 9 – Synthesis of alkene **44** *via* a HWE reaction

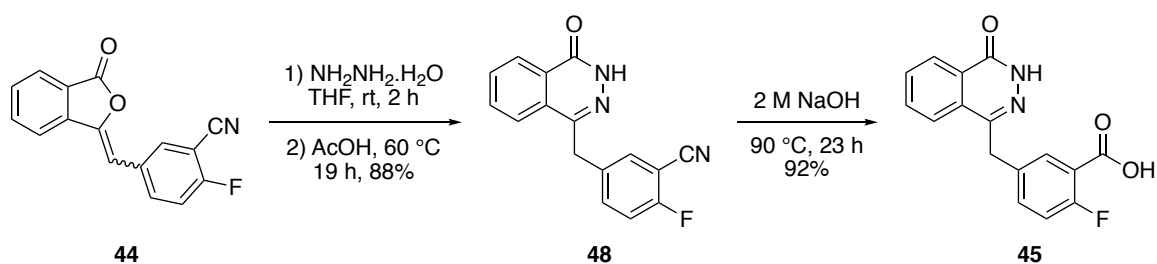
The next stage in the preparation of the olaparib core **35** was to introduce a carboxylic acid handle, for subsequent amide coupling, and the phthalazinone moiety, vital for PARP-1 binding interactions. Both transformations were achieved using a one-pot, two-step procedure (Scheme 10). Alkene **44** was treated with 13 M aqueous sodium hydroxide at 90 °C resulting in hydrolysis of the nitrile functionality to the corresponding carboxylic acid. This was followed by the addition

of hydrazine monohydrate at a lower temperature of 70 °C to facilitate a cyclocondensation reaction. Subsequent acidification of the crude reaction mixture using 6 M aqueous hydrochloric acid afforded phthalazinone **45** in 66% yield over two steps. Repetition of this one-pot procedure produced phthalazinone **45** in variable yields, therefore it was proposed that these transformations would be performed independently with the aim of improving reproducibility and overall yield.



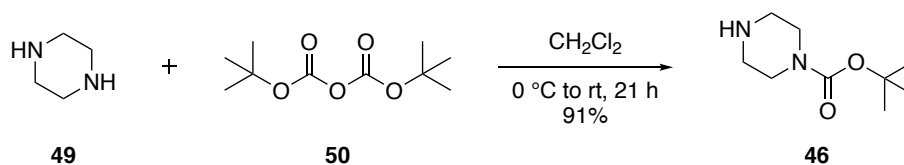
Scheme 10 – Synthesis of phthalazinone **45** *via* a one-pot, two-step procedure

Literature procedures reported by Menear *et al.* were employed for the synthesis of intermediates **48** and **45** in a stepwise manner from alkene **44** (Scheme 11).¹⁷⁵ Firstly, transformation of the benzofuran-1-one moiety was carried out using hydrazine monohydrate under acidic conditions to give phthalazinone **48** in 88% yield. Hydrolysis of the nitrile functionality in intermediate **48** was then achieved with 2 M sodium hydroxide and afforded phthalazinone **45** in excellent 92% yield. Employment of this alternative synthetic route overcame significant reproducibility issues of the previous one-pot procedure and phthalazinone **45** was isolated in high yields at both milligram and multigram scale. Additionally, phthalazinone **45** was prepared in a significantly shorter reaction time of 42 h, and higher yield of 81% over two steps. Furthermore, this sequential approach was more atom economical. In the one-pot method, 13 M aqueous sodium hydroxide, 14 equivalents of hydrazine monohydrate and 6 M aqueous hydrochloric acid were employed. The stepwise procedures required only 1.2 equivalents of hydrazine monohydrate, 25 mol% of acetic acid and 2 M aqueous sodium hydroxide.



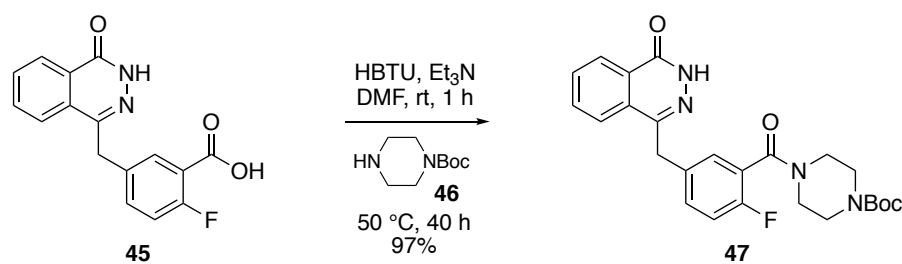
Scheme 11 – Synthesis of phthalazinone **45** via two sequential reactions

Following the preparation of phthalazinone **45**, the next objective was to introduce a piperazine ring to the scaffold through an amide coupling reaction. Under standard conditions, there is an inherent risk that piperazine (**49**) will undergo dimerisation with the carboxylic acid of **45**. Therefore, it was necessary to protect one of the nucleophilic nitrogen atoms of piperazine (**49**). A *tert*-butyloxycarbonyl (boc) protecting group was identified as a suitable choice since the reaction conditions required for both installation and deprotection do not interfere with any other functionality or synthetic steps in this route. Following a literature procedure, *N*-Boc piperazine (**46**) was prepared from piperazine (**49**) and di-*tert*-butyl dicarbonate (**50**) in 91% yield (Scheme 12).¹⁷⁶



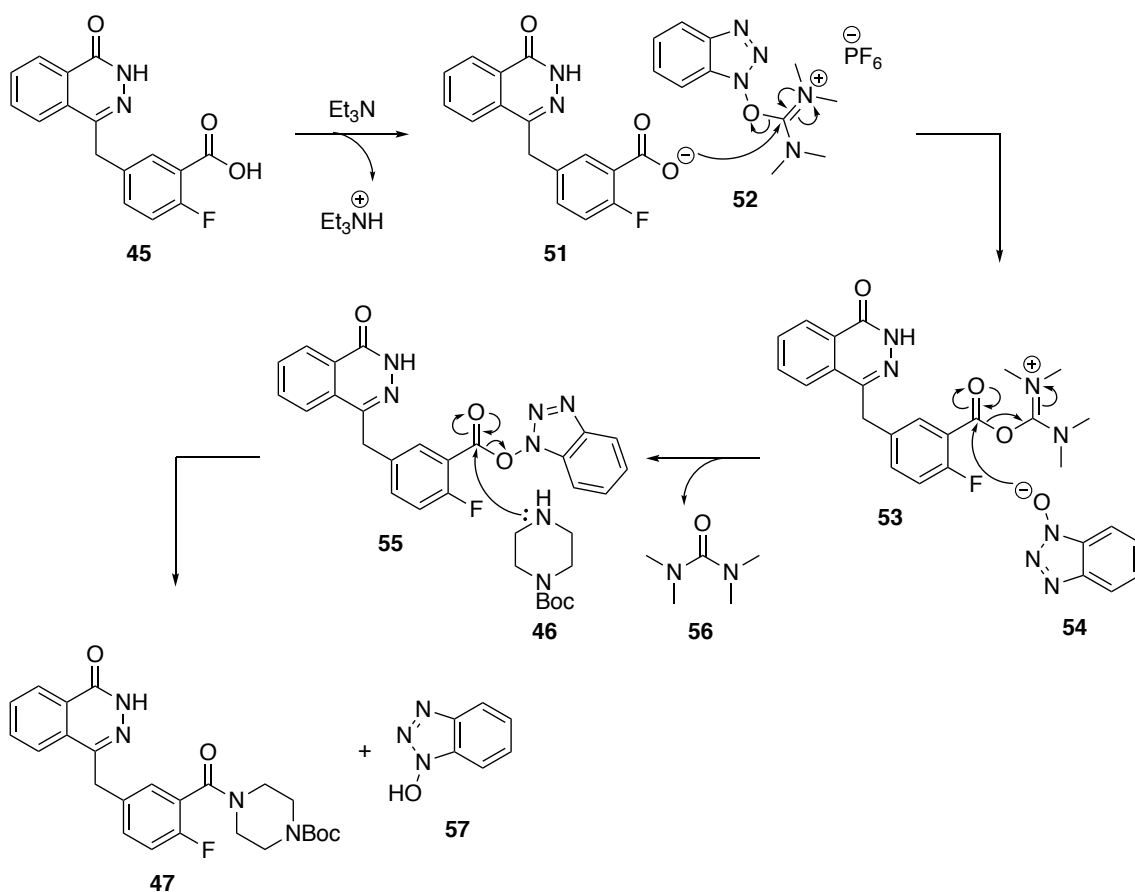
Scheme 12 – Mono *N*-Boc protection of piperazine **49**

Subsequently, the *N*-Boc-protected olaparib core **47** was prepared from carboxylic acid **45** and *N*-Boc piperazine (**46**), via an amide coupling reaction, in 97% yield (Scheme 13). This amide bond formation was achieved using *O*-benzotriazole-*N,N,N',N'*-tetramethyluroniumhexafluorophosphate (HBTU), a uronium-based coupling reagent, in the presence of triethylamine.

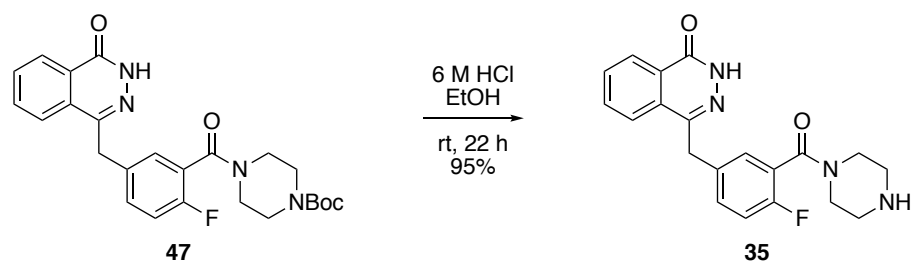


Scheme 13 – Synthesis of *N*-Boc-protected olaparib core **47**

The proposed mechanism for this HBTU-mediated synthesis of **47** is shown below in Scheme **14**.¹⁷⁷ Under basic conditions, carboxylic acid **45** undergoes deprotonation to form carboxylate anion **51**, which then attacks the electrophilic carbon of the uronium moiety within HBTU (**52**), *via* a nucleophilic substitution (S_N2) reaction. The resultant intermediate **53** is then attacked by the *O*-benzotriazole (OBt) anion **54**, in an additional S_N2 reaction, to give the OBt activated ester intermediate **55** and tetramethylurea (**56**). Subsequently, nucleophilic *N*-Boc piperazine (**46**) attacks intermediate **55**, in a final S_N2 reaction, to give hydroxybenzotriazole (HOBt) (**57**) and the desired amide **47**. When performing HBTU-mediated couplings, it is advantageous to add the nucleophilic amine, such as *N*-Boc piperazine **46**, to the reaction mixture following formation of intermediate **55**. This prevents nucleophilic attack of the amine into HBTU (**52**), which can lead to formation of a guanidylated-amine side-product.¹⁷⁷



Finally, the *N*-Boc-protected olaparib core **47** underwent deprotection using 6 M aqueous hydrochloric acid to afford the desired olaparib core **35** in 95% yield (Scheme 15). In conclusion, the seven-step synthetic route described above was scalable and employed to produce multi-gram quantities of **35** in good yield.



2.1.4 Synthesis of Olaparib-BODIPY FL (37)

Following the successful synthesis of the olaparib core **35**, the next project aim was to functionalise the 4-*NH*-piperazine ring with a pendant BODIPY fluorophore for the preparation of olaparib-BODIPY FL (**37**). Olaparib-BODIPY FL (**37**) was originally reported by Reiner and co-workers as a fluorescent probe applicable to *in vivo* imaging studies of PARP-1 inhibition.^{166,167} In a PARP-1 activity assay, olaparib-BODIPY FL (**37**) exhibited an IC₅₀ of 12.2 nM which, although less potent than olaparib (**1**) (IC₅₀ of 1.7 nM), indicates sufficient PARP-1 affinity for molecular imaging (Figure 21). Furthermore, olaparib-BODIPY FL (**37**) displayed selectivity for PARP-1 in murine models of ovarian and pancreatic cancer. Subsequently, Reiner and co-workers have demonstrated the multifaceted utility of olaparib-BODIPY FL (**37**) as a fluorescent PARP-1 imaging agent in glioblastoma cell lines.^{101,178,179} As of 2017, olaparib-BODIPY FL (**37**) is under investigation in a phase I/II clinical trial for application as a fluorescent PARP-1 binding imaging agent in oral squamous cell cancer.¹⁸⁰ As described in Section 2.1.2, this project sought to employ a fluorescent probe for molecular imaging of PARP-1 in glioblastoma cell lines. Based on the above literature precedent from Reiner and co-workers, olaparib-BODIPY FL (**37**) was selected as a suitable agent.

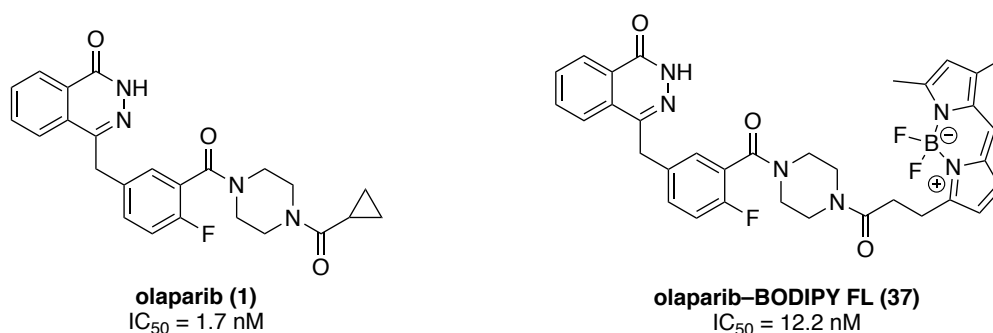
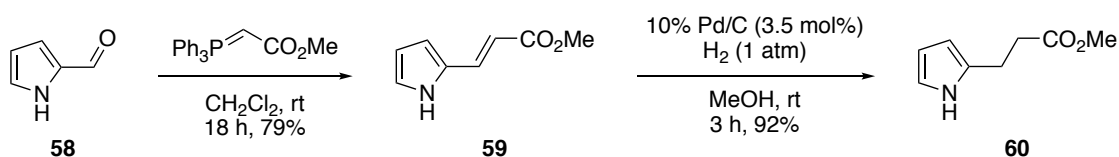


Figure 21 –IC₅₀ of olaparib (**1**) and olaparib-BODIPY FL (**37**)

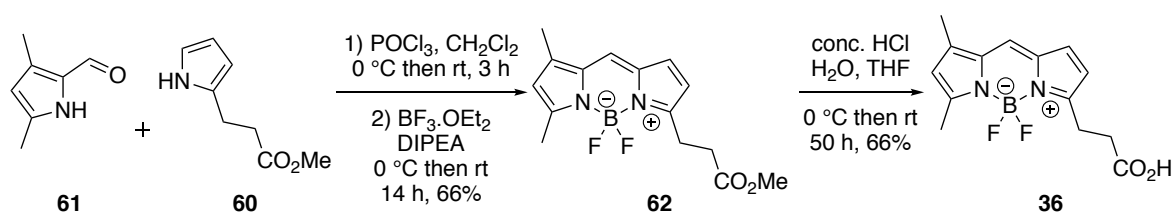
The preparation of olaparib-BODIPY FL (**37**) began with the synthesis of BODIPY FL propionic acid **36** using literature procedures.^{181,182} First, commercially available pyrrole-2-carboxyaldehyde (**58**) underwent a Wittig olefination under mild conditions with methyl (triphenylphosphoranylidene)acetate to give the desired *E*-alkene **59** in 79% yield (Scheme 16). The geometry of this alkene was confirmed by ¹H NMR spectroscopy of the isolated product, which showed two doublets between 6–8 ppm

with coupling constants indicative of a vicinal *trans* relationship. The *E*-alkene was produced selectively over the *Z*-isomer since the negative charge of the phosphonium ylide generated from methyl (triphenylphosphoranylidene)acetate is stabilised *via* delocalisation by the methyl ester moiety. Due to this stabilising effect, the reaction proceeds more slowly and affords a later *trans* oxaphosphetane transition state with a more planar structure with reduced steric repulsions. Furthermore, this delocalisation of the ylide negative charge onto the methyl ester carbonyl generates a strong dipole along the H₂C–CO₂Me bond. Adoption of the *trans* oxaphosphetane transition state produces a favourable antiparallel orientation of this dipole and the dipole which exists along the C=O bond of aldehyde **58**. Alkene **59** was subsequently reduced *via* hydrogenation with 10% wt. palladium on carbon. Full conversion to the corresponding alkane was observed by ¹H NMR spectroscopy after 3 h, which allowed for facile purification using a short plug of Celite® to afford methyl 3-(1'*H*-pyrrol-2'-yl)propanoate (**60**) in 92% yield (Scheme 16).



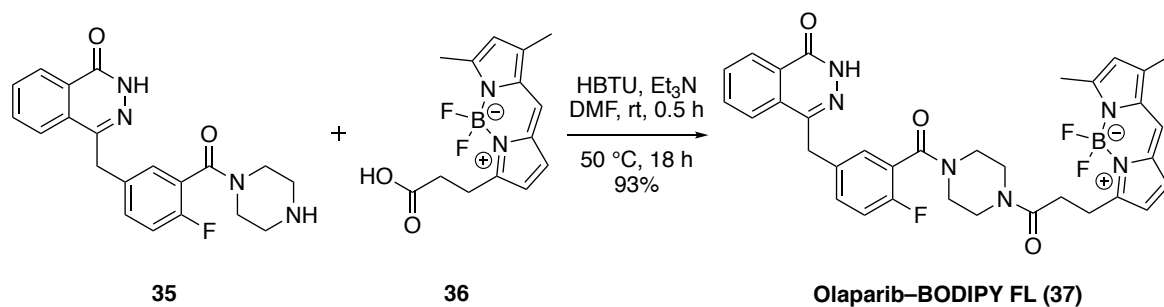
Scheme 16 – Synthesis of **60** *via* Wittig and hydrogenation reactions

Assembly of the BODIPY fluorophore was undertaken next. Methyl 3-(1'*H*-pyrrol-2'-yl)propanoate (**60**) was coupled with commercially available 3,5-dimethylpyrrole-2-carboxaldehyde (**61**) in the presence of phosphorous(V) oxychloride generating a dipyrin intermediate. Formation of this intermediate was evident by thin layer chromatography after 3 h, and subsequent addition of boron trifluoride diethyl etherate and Hünig's base provided BODIPY propionic ester **62** in 66% yield. Ester hydrolysis of BODIPY propionic ester **62** was then achieved using concentrated hydrochloric acid to give BODIPY propionic acid **36** in 66% yield (Scheme 17).



Scheme 17 – Synthesis of BODIPY propionic ester **62** and acid **36**

With both BODIPY propionic acid **36** and the olaparib core **35** in hand, an HBTU-mediated amide coupling reaction was performed in the presence of triethylamine to afford the desired olaparib-BODIPY FL (**37**) in 93% yield (Scheme 18).



Scheme 18 – Synthesis of olaparib-BODIPY FL (**37**)

Notably, formation of the *N,N'*-diacylated piperazine moiety resulted in the appearance of rotational isomers in the ^1H and ^{13}C NMR spectra of olaparib-BODIPY FL (**37**). It has been proposed that the amide functionalities of such substituted piperazine rings possess partial double bond character, and as such free rotation of the C–N bond of the amide is restricted.¹⁸³ Consequently, it was believed the rotamers observed in the NMR spectra of olaparib-BODIPY FL (**37**) were due to restricted rotation between *cis* and *trans* isomers (Figure 22).

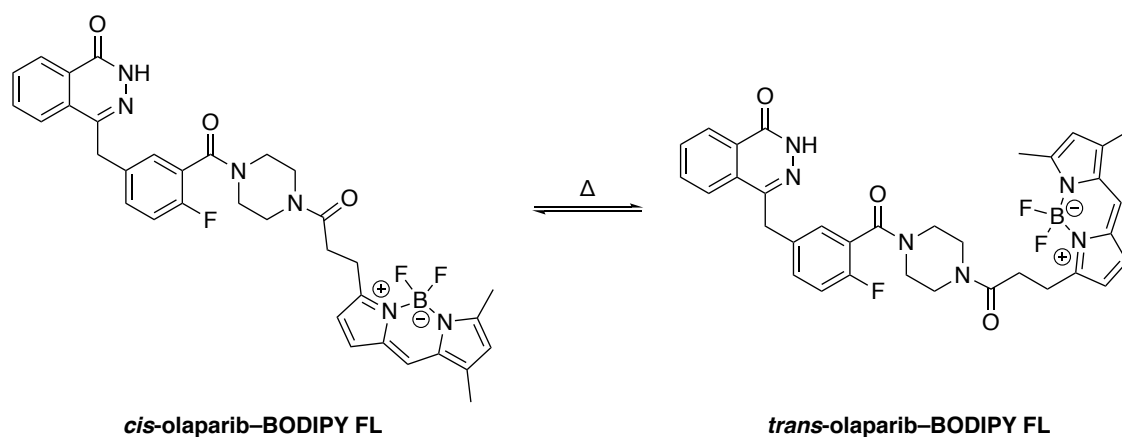


Figure 22 – Proposed *cis* and *trans* isomers of olaparib-BODIPY FL (**37**)

Rotational isomers were most clearly observed in the ^1H NMR spectrum, for signals relating to hydrogen atoms of the piperazine ring (which appeared as four signals, integrating to two protons each, between 3.10 ppm and 3.70 ppm), and the adjacent CH_2 (which appeared as two signals, integrating to one proton each, at 2.71 and

2.78 ppm). Upon heating the ^1H NMR sample to 100 °C, rotamer peaks underwent coalescence due to rapid interconversion of the *cis* and *trans* isomers (Figure 23). Furthermore, rotational isomers were observed for all compounds subsequently synthesised in this project which contain the *N,N'*-diacylated piperazine moiety.

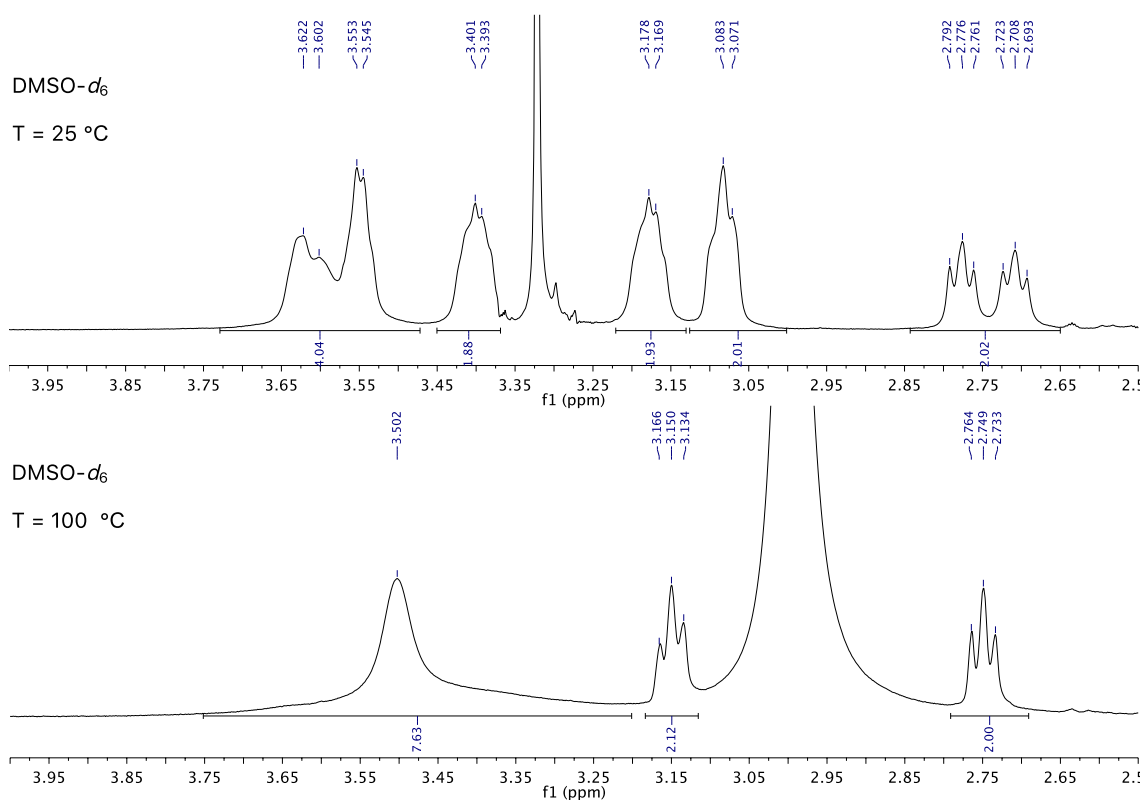


Figure 23 – Expansion of ^1H NMR spectra of olaparib-BODIPY FL (37)

The photophysical properties of olaparib-BODIPY FL (37) were then examined through measurement of absorption and emission spectra. The absorption spectrum was recorded in methanol at the varied concentrations of 1 μM , 5 μM , and 10 μM , and showed a maximum at 504 nm, with a molar extinction coefficient of $64779 \text{ M}^{-1} \text{ cm}^{-1}$ (Figure 24). The emission spectrum was also measured in methanol at a concentration of 1 μM , which displayed maximum emission at 511 nm (Figure 24). Emission spectra recorded at concentrations of 5 μM , and 10 μM in methanol displayed intense off-scale emission bands attesting to the highly fluorescent character of olaparib-BODIPY FL (37).

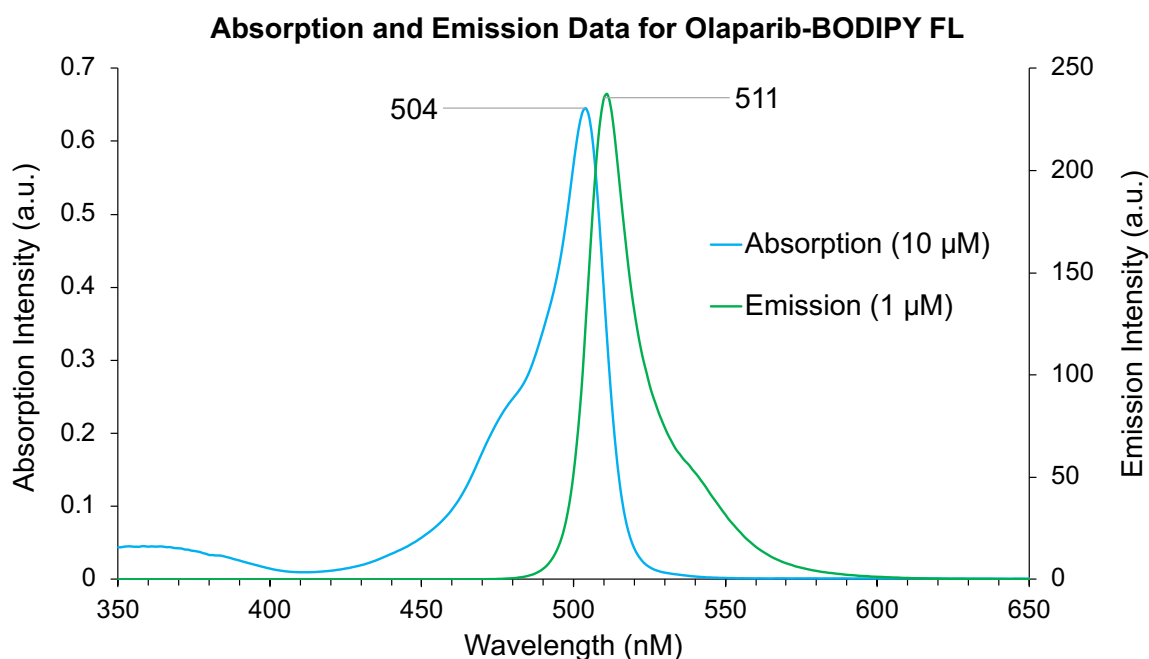


Figure 24 - Absorption and emission spectra for olaparib-BODIPY FL (**37**)

Investigations are currently underway at the Institute of Cancer Sciences, University of Glasgow, into the applications of olaparib-BODIPY FL (**37**) for *in vitro* biological studies of PARP-1. Development of an *in vitro* competitive displacement fluorescence assay of PARP-1 inhibition is ongoing. In the future, submission of novel olaparib analogues to this assay will facilitate evaluation of cellular uptake, distribution, PARP-1 affinity, and retention.

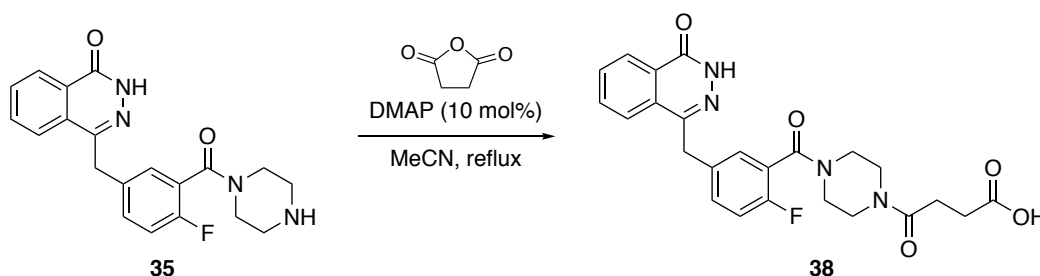
2.1.5 Synthesis of Novel Olaparib-Derived PARP-1 Inhibitors

Extension of the olaparib core structure **35** *via* coupling to succinic anhydride was then explored. Initially, *N*-acylation of the olaparib core **35** was attempted using 2 equivalents of succinic anhydride and catalytic amounts of 4-dimethylaminopyridine (10 mol%) (DMAP) under reflux (Table **6**, entry 1). Under these conditions, full conversion of the olaparib core **35** was observed within 24 h; however, purification of the carboxylic acid product **38** proved challenging. Following aqueous acid-base extraction, ¹H NMR spectroscopy of the product revealed a mixture of **38** and succinic acid in a 45 : 55 ratio. Separation of this mixture was previously attempted by flash column chromatography, employing an eluant system of 10% methanol and 0.1% acetic acid in dichloromethane. However, due to the polarity and acidic functionality of both compounds, co-elution of **38** and succinic acid was observed.

Subsequent attempts to isolate **38** by trituration or recrystallisation from a range of common organic solvents also proved unsuccessful. Consequently, the decision was made to employ an acid-base extraction as the sole method of purification, which necessitated optimisation of the reaction conditions to prevent formation of substantial quantities of succinic acid.

Under these initial reaction conditions, excess succinic anhydride in the crude reaction mixture was subjected to aqueous acidic and basic conditions, resulting in hydrolysis to succinic acid. It was therefore proposed that the equivalents of succinic anhydride used in this procedure would be adjusted. Employment of the olaparib core **35** and succinic anhydride in equal molar ratio was found to significantly reduce production of succinic acid, and gave **38** and succinic acid in an 85 : 15 ratio (entry 2). This prompted the decision to employ succinic anhydride as the limiting reagent, and the olaparib core **35** in a slight excess (entry 3). These optimised conditions afforded carboxylic acid intermediate **38** in 81% yield.

Table 6 – Optimisation of acylation conditions for the synthesis of **38**

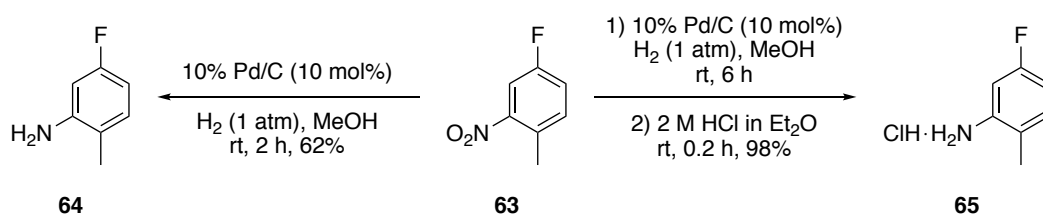


Entry	Equiv. of 35	Equiv. of succinic anhydride	Time (h)	Ratio of 38 : succinic acid ^a	Isolated Yield of 38 (%)
1	1	2	24	45 : 55	-
2	1	1	18	85 : 15	-
3	1.2	1	16	96 : 4	81

^aDetermined using ¹H NMR spectroscopy.

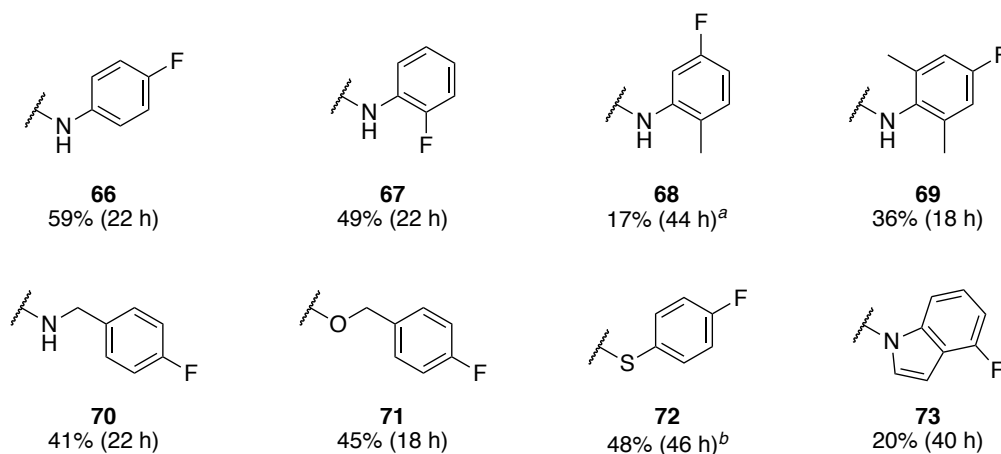
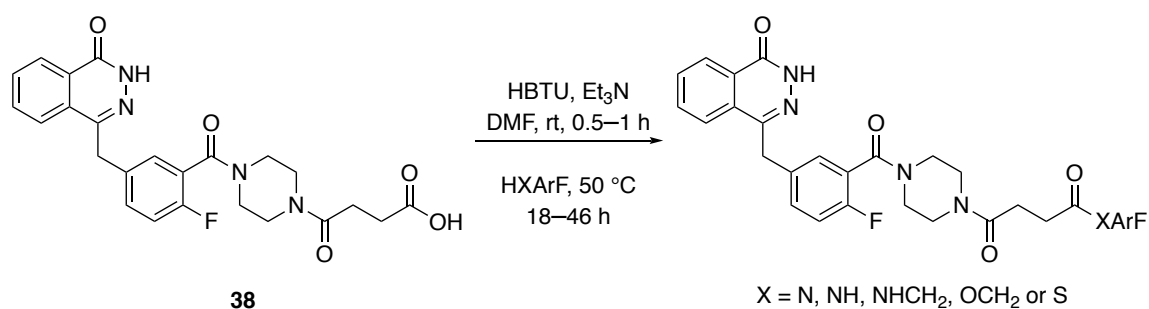
With a synthetic route now established for the synthesis of carboxylic acid intermediate **38**, the focus of the project was to couple **38** to a range of fluoroarene nucleophiles. Commercially available 2-nitro-4-fluorotoluene (**63**) underwent

hydrogenation using 10% wt. palladium on carbon to give 2-methyl-5-fluoroaniline (**64**) in 62% yield (Scheme 19). However, the volatility of aniline **64** when exposed to elevated temperatures (30–40 °C) *in vacuo* made handling impracticable. Consequently, reduction of 2-nitro-4-fluorotoluene (**63**) was repeated and the resultant aniline **64** was treated with 2 M hydrochloric acid to give 2-methyl-5-fluoroaniline hydrochloride (**65**) in 98% yield (Scheme 19).



Scheme 19 - Synthesis of anilines **64** and **65**

Carboxylic acid intermediate **38** was then submitted to coupling reactions with eight structurally diverse fluoroarene nucleophiles, including 2-methyl-5-fluoroaniline hydrochloride (**65**), *ortho*- and *para*-fluoroanilines, 4-fluorobenzyl amine, 4-fluorobenzyl alcohol, 4-fluorothiophenol and 4-fluoroindole (Scheme 20). HBTU was employed as the coupling agent in the presence of triethylamine to afford compounds **66–73** in adequate yields for this stage of the project. Optimisation of these coupling conditions was not explored, and accordingly moderate yields of **66–73** were obtained. It should be noted that these coupling conditions will require optimisation for the future syntheses of any compounds nominated for further development as PET imaging agents. It was proposed that this series of compounds would allow the impact of altering the fluorine labelling site (**66**, **67** and **68**), increasing lipophilicity and steric bulk (**68** and **69**), further extension and flexibility of the scaffold (**70** and **71**) and installation of alternative heteroatoms or heteroarenes (**71**, **72** and **73**) to be investigated. Furthermore, the range of fluoroarene nucleophiles selected for preparation of this library were chosen due to the commercial availability of the corresponding aryl boronic ester nucleophiles or their ease of synthesis.



Scheme 20 – Synthesis of novel PARP-1 inhibitors for PET imaging. ^aStirred at room temperature for 3 h. ^bStirred at room temperature for 2 h.

2.1.6 Physicochemical Properties Evaluation of Novel Olaparib-Derived PARP-1 Inhibitors

With this new generation of olaparib analogues at our disposal, the next objective was to identify which of these compounds possessed favourable physicochemical properties. As with therapeutic drug discovery, it is advantageous to assess the bioavailability of potential radiotracers during the preliminary stages of development. Ultimately, these compounds are intended for use as PET imaging agents for PARP-1 in various cancer types including glioblastoma which occurs within the brain. As such, it is imperative that these compounds penetrate the blood-brain barrier (BBB). Physicochemical properties which influence the partition of radiotracers across the BBB include the partition coefficient ($\log P$), percentage plasma protein binding (%PPB), membrane partition coefficient (K_m) and permeability coefficient (P_m).

2.1.6.1 Partition Coefficient

The lipophilicity of an organic compound is a quantitative expression of the affinity that compound possesses towards lipophilic environments.¹⁸⁴ The partition coefficient ($\log P$) is the most widely employed descriptor of lipophilicity. Traditionally, $\log P$ is determined experimentally through liquid/liquid extraction, also known as the “shake flask” method.¹⁸⁵ In this method, a compound is partitioned between two equilibrated immiscible phases, typically octanol and water.¹⁸⁶ The resultant concentration of compound measured in each of these phases provides a ratio, and the log of this ratio is defined as the partition coefficient ($\log P$) (Figure 25).

$$\log P = \log \left(\frac{[\text{Concentration}]_{\text{Octanol}}}{[\text{Concentration}]_{\text{Water}}} \right)$$

Figure 25 – Equation for $\log P$ calculation

However due to the time consuming nature of the “shake flask” method, alternative experimental and *in silico* methods to measure $\log P$ have since been developed, including HPLC methodology using a C18 column.^{164,185,187} Furthermore, lipophilicity is commonly exploited for prediction of absorption, distribution, metabolism, and elimination (ADME) properties, and BBB-permeability of therapeutic drugs.^{185,187} In addition, compounds with moderate $\log P$ values (1.5–4.5) are able to penetrate the BBB most effectively; compounds with low (< 0) or high (> 5) $\log P$ values are prone to rapid *in vivo* metabolic clearance and high percentage plasma-protein binding, respectively.

2.1.6.2 Plasma Protein Binding

Once a drug compound enters the bloodstream it participates in a wide variety of interactions with constituents of the plasma. Human serum albumin (HAS) and α_1 -acid glycoprotein (AGP) are two proteins found in high abundance within the plasma that bind to drug compounds with significant affinity.¹⁸⁸ As a result, only the unbound fraction of a drug is free to interact with the intended biological target and cause therapeutic effects. The percentage of a drug that is bound to the plasma protein

(%PPB) can be measured traditionally through equilibrium dialysis or ultrafiltration methods; however, HPLC techniques have been developed for more efficient evaluation of %PPB.^{164,189,190} These HPLC methods involve the use of columns in which the silica stationary phase has been bonded to immobilised HSA protein. Compounds with higher %PPB display poorer *in vivo* brain penetration and metabolic clearance, which in turn leads to bioaccumulation in off-target organs.^{164,185,189} In the context of radiotracers for applications in the brain, the effects of high %PPB would result in poor quality images from a poor signal-to-noise ratio.

2.1.6.3 Membrane Partition Coefficient and Permeability

To cross the BBB a drug compound will also be subject to interactions with cellular membranes which is often the rate-limiting factor of drug absorption.¹⁹¹ The membrane partition coefficient (K_m) and permeability (P_m) are two fundamental physicochemical properties used to describe such interactions. The membrane partition coefficient (K_m) is the equilibrium constant of partitioning of a compound between a cell membrane and an aqueous phase.^{191–193} As such, K_m provides a quantitative expression of all interactions between a drug and cellular membrane. Chromatography methods have been developed to measure K_m using immobilised artificial membranes (IAM).^{164,191–193} These techniques employ columns in which the silica stationary phase has been bonded to phosphatidyl choline to mimic a lipid bilayer. Additionally, permeability (P_m) is a quantitative expression of the permeation of a compound across a cellular membrane *via* passive diffusion. P_m is directly proportional to K_m with molecular weight (MW) as a proportionality constant (Figure 26).^{191–193}

$$P_m = \frac{K_m}{MW}$$

Figure 26 – Equation for P_m calculation

2.1.6.4 Physicochemical Properties of Novel PARP-1 Inhibitors

In the 2012 study by Tavares *et al.*, ten established imaging agents were submitted to physicochemical properties determination *via* HPLC methodology, and the results compared with *in vivo* brain distribution data.¹⁶⁴ From this analysis, the authors

reported an ideal value range for each of these physicochemical properties as criteria with which candidate radiotracers can be assessed (Table 7). Potential imaging agents with physicochemical properties values within these ranges are considered likely to permeate the BBB. Moreover, the authors proposed that this technique offers a reliable high-throughput system for screening and ranking of candidate radiotracers to aid with lead compound selection in future radiotracer development programmes.

Table 7 – Physicochemical properties criteria for potential imaging agents

Physicochemical Property	Ideal Value
$\log P$	<4.0
%PPB	<95%
K_m	<250
P_m	<0.5

All eight compounds synthesised in this project were submitted to physicochemical properties evaluation using these HPLC methods (Table 8, Section 3.3, Appendix I). Physicochemical properties listed for olaparib (**1**) were previously determined within the Sutherland group using this method.¹⁰² Due to technical issues, attempts to determine $\log P$ using HPLC methods proved impracticable. However, both calculated and experimental $\log P$ values for olaparib (**1**) were found to be similar. Consequently, the decision was made to use calculated $\log P$ (cLog P) values, obtained from ChemDraw Prime 17.1 software in this instance.

From this library, four compounds were selected for *in vitro* testing due to limited resources. In general, all the compounds tested possess physicochemical properties within the desirable criteria for a BBB-permeable radiotracer, except for compound **73** (shown in red). Compound **73** containing a 4-fluoroindole moiety was the only compound to demonstrate high %PPB outwith the ideal range, and exhibited the highest membrane partition coefficient, K_m , and permeability, P_m values of any compound tested. Additionally, compound **72** possessed the highest $\log P$ of this library and high %PPB extremely close to the upper limit of the ideal range (shown in red). These factors led to the decision that compounds **72** and **73** would be excluded from further development. Of the remaining analogues under

consideration, compound **71** possessed the highest %PPB, K_m and P_m values and thus was also excluded. No further differentiation could be made based on the HPLC measured values. Subsequently, compound **68** was excluded in favour of **69** based on contribution to SAR investigations. In conclusion, compounds **66**, **67**, **69** and **70** were nominated for *in vitro* assessment of PARP-1 inhibitory potency.

Table 8 – Physicochemical properties of novel olaparib-derived PARP-1 inhibitors for PET imaging

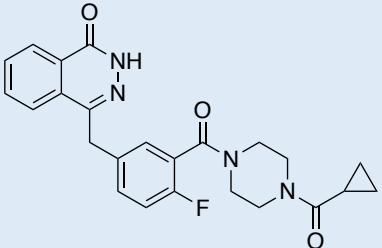
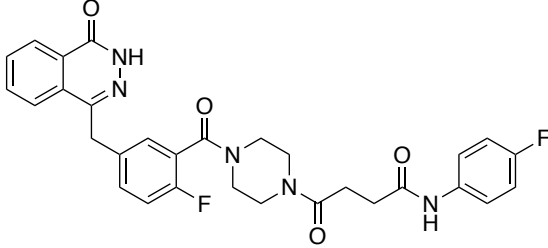
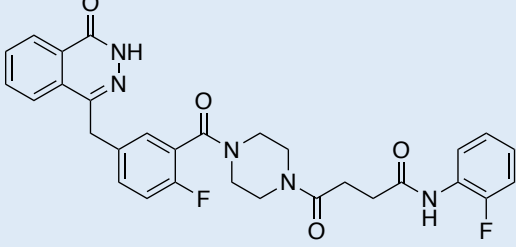
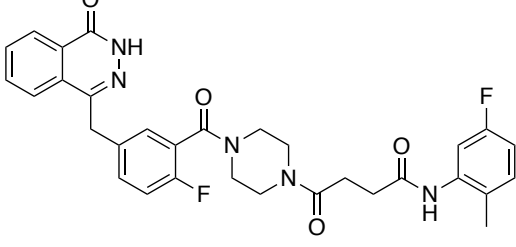
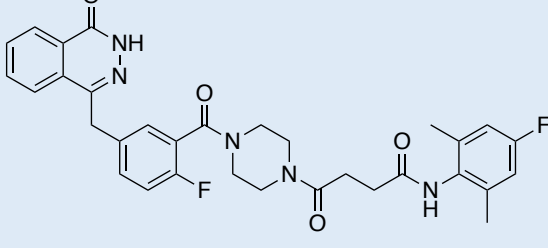
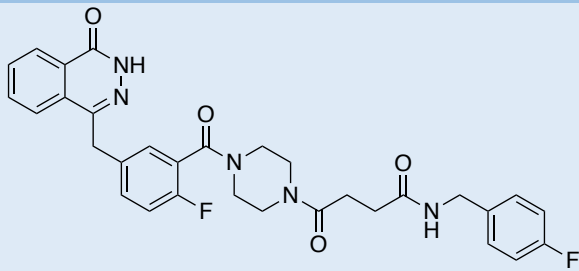
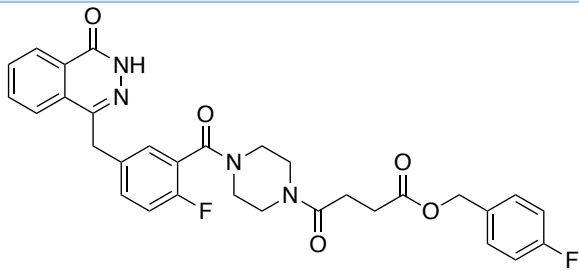
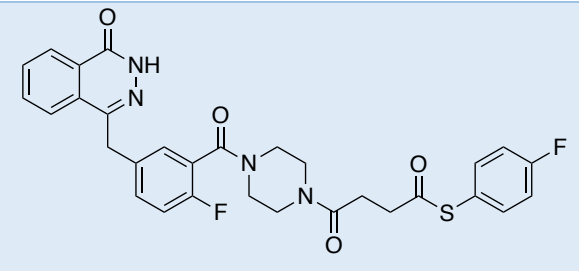
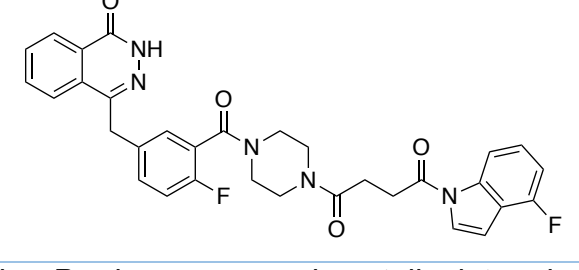
Compound	No.	cLog P	%PPB	K_m	P_m
	1	2.02 & 1.95*	75.9	-	-
	66	2.37	87.9	40.8	0.0730
	67	2.37	83.3	31.8	0.0568
	68	2.86	86.4	45.7	0.0798
	69	3.35	84.2	39.3	0.0670

Table 8 – Physicochemical properties of novel olaparib-derived PARP-1 inhibitors for PET imaging (continued)

Compound	No.	cLog <i>P</i>	%PPB	<i>K_m</i>	<i>P_m</i>
	70	2.44	83.8	31.3	0.0546
	71	3.12	90.3	60.3	0.105
	72	3.62	94.2	86.5	0.150
	73	2.72	98.5	142	0.244

*log *P* value was experimentally determined using HPLC methods.

2.1.7 *In Vitro* Biological Evaluation of Novel Olaparib-Derived PARP-1 Inhibitors

Olaparib (**1**) and compounds **66**, **67**, **69** and **70** were submitted to *in vitro* biological evaluation by Maria C. Liuzzi at the Institute of Cancer Sciences, University of Glasgow. All *in vitro* studies discussed herein were conducted in two glioblastoma models. Glioblastoma is a cancer type that overexpresses PARP-1 and is the biological target of oncology research carried out by our collaborators. It is common for glioblastoma cell lines from distinct patients to respond differently to identical therapeutic treatments. As such, two distinct cell lines were employed in this study, the G7 and E2 stem cell lines. Comprehensive experimental detail, results, and discussion of the *in vitro* studies discussed herein can be found in the PhD thesis of Maria C. Liuzzi.¹⁶⁵

PARP-1 inhibitory potency was assessed *via* immunofluorescence PARylation assays. As previously discussed in Section 1.2.1, PARP-1 facilitates and undergoes PARylation in a vital step of the repair pathway for DNA single-strand breaks. Therefore, the degree of PARylation is indicative of PARP-1 activity levels. For each assay, G7 or E2 cells were incubated with the compound of interest at eight distinct concentrations between 0.1–24 nM. Each compound was tested at these eight concentrations in triplicate wells. Furthermore, each assay was performed three times ($n = 3$). The quantity of PARylated protein within nuclei was measured *via* staining with fluorescent antibodies. The activity of PARP-1 was quantified as the ratio of PAR-positive nuclei to total nuclei (mean nuclear fluorescence) per cell per well, normalised to positive and negative controls, and then expressed as a percentage. Subsequently, the percentage of PARP-1 activity was plotted against concentration to afford a dose-response curve (Table **9**). Using GraphPad Prism 7.0 software, a four-parameter logistic model was fitted to the resultant curves to calculate an IC_{50} value for each compound (Table **9**, provided by Maria C. Liuzzi). For responses that generated a partial dose-response curve (i.e., did not reach 50% inhibition of PARP-1 activity between 0.1–24 nM), it was not possible to fit a logistic model. In such cases (e.g., compound **70** in E2 cells), the IC_{50} value was determined *via* extrapolation from the raw data. For responses that produced no dose-response curve (i.e., negligible or no inhibition of PARP-1 activity between 0.1–24 nM), the IC_{50} value could not be extrapolated from the raw data and was concluded to be

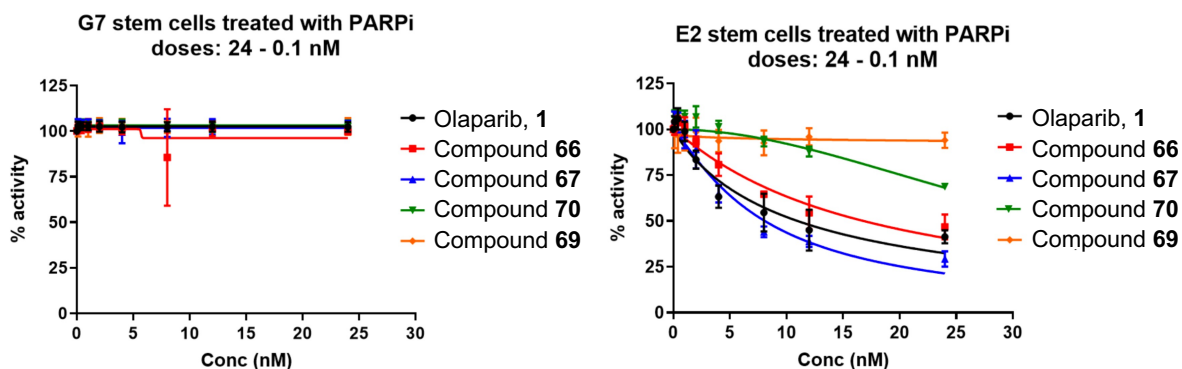
higher than the maximum concentration of compound tested in these assays (> 24 nM).

In the G7 stem cell line, no dose-response curve was observed for any of the compounds tested, including olaparib (**1**). However, this result does not indicate a complete absence of PARP-1 inhibitory potency. It can be concluded that, in this cell line, the IC₅₀ values for all compounds tested are greater than 24 nM. Repetition of this assay across a wider concentration range would be required to obtain accurate IC₅₀ values.

In the E2 stem cell line, compounds **66** and **67** were found to inhibit PARP-1 with similar dose-response to olaparib (**1**). The IC₅₀ value of compound **66** was found to be 16.9 nM, and as such **66** is only marginally less potent than olaparib (**1**), which exhibited an IC₅₀ value of 11.0 nM. For compound **67**, an IC₅₀ value of 8.11 nM was determined and was the only compound found to be a more potent PARP-1 inhibitor than olaparib (**1**). Evidently, the position of the fluorine atom on the pendant arene only moderately influences binding and potency. A dose-response curve was not produced from testing of compound **69** across this concentration range. As such, the IC₅₀ value of compound **69** could not be accurately determined and was concluded to be greater than 24 nM. This reduction in efficacy suggests that the increased lipophilicity and steric bulk of the pendent fluoroarene moiety are detrimental to binding. Compound **70**, with an IC₅₀ value of 35.5 nM, showed a threefold reduction in potency compared to olaparib (**1**), although it retained sufficient inhibitory effect at nanomolar concentrations. This drop in potency may be due to the structure elongation and increased flexibility of the pendent fluoroarene moiety.

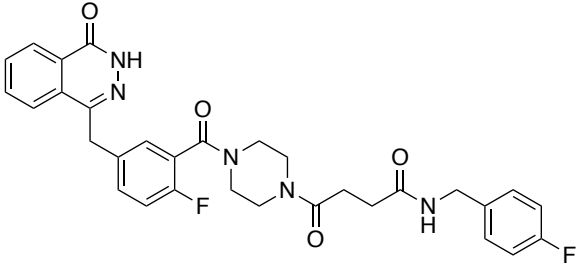
It can be concluded from these results that compounds **66**, **67** and **70** are potent PARP-1 inhibitors *in vitro* and would likely exhibit high affinity for PARP-1 *in vivo*. Of these compounds, **66** and **67** display the greatest similarity to olaparib (**1**) and scope for further development as PET radiotracers for PARP-1.

Table 9 – Dose-response curves and calculated IC₅₀ values of olaparib (1) and novel PARP-1 inhibitors in glioblastoma G7 and E2 cell lines



Compound	No.	PARylation Inhibition IC ₅₀ (nM) (n = 3)	
		G7 cells	E2 cells
	1	> 24.0	11.0
	66	> 24.0	16.9
	67	> 24.0	8.11
	69	> 24.0	> 24.0

Table 10 – Dose-response curves and calculated IC₅₀ values of olaparib (**1**) and novel PARP-1 inhibitors in glioblastoma G7 and E2 cell lines (continued)

	70	> 24.0	35.5
---	-----------	--------	------

2.1.8 Radiochemistry

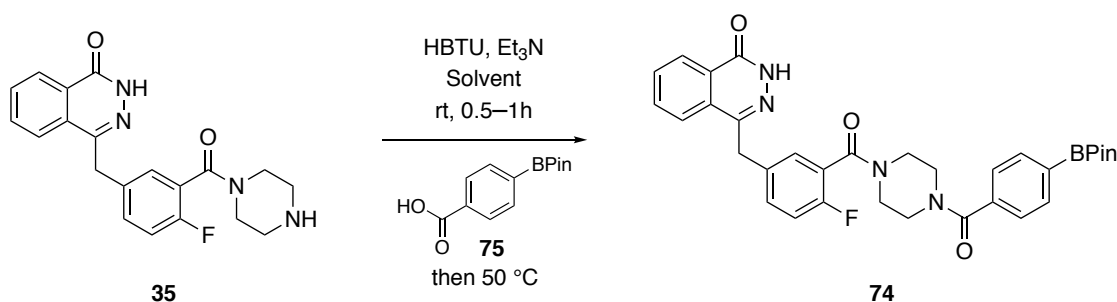
2.1.8.1 Synthesis of Aryl Pinacol Boronic Ester Precursor **74**

In parallel with the biological evaluation of the HM library of novel olaparib-analogues, an objective of this project was to prepare aryl pinacol boronic ester precursor **74**. It was proposed that precursor **74** would be a suitable substrate with which to adapt and optimise the copper-mediated radiofluorodeborylation procedure, published by Gouverneur and co-workers, for application with the FX_{FN} synthesiser at the West of Scotland PET centre.^{107,108}

Initially, the olaparib core (**35**) was submitted to an HBTU-mediated amide coupling reaction with commercially available 4-carboxylphenylboronic acid pinacol ester (**75**) in DMF (Table **10**, entry 1). Under these conditions, full conversion of the olaparib core (**35**) was observed within 16 h *via* TLC. However, purification of the boronic ester product proved problematic and **74** was isolated in only 18% yield. It was proposed that this low yield was due to retention or hydrolysis of **74** on the silica stationary phase during flash column chromatography. Subsequent repetition of this procedure without the use of chromatographic purification did not significantly improve the isolated yield of **74** (entry 2). Further investigation revealed that **74** exhibits poor solubility in most common organic solvents, with exception of chloroform. This led to the theory that liquid/liquid extraction using ethyl acetate was the cause of low product recovery thus far. Consequently, this coupling reaction was repeated employing acetonitrile as an alternative solvent that could be readily evaporated *in vacuo* prior to liquid/liquid extraction using chloroform (entry 3). Notably, changing the solvent to acetonitrile allowed for full reaction of the olaparib

core (**35**) within the same time frame as when DMF was employed. It is also worth noting that trituration was required to remove tetramethylurea (**56**), a by-product of HBTU-mediated coupling reactions (Scheme 14). Under these optimised conditions, aryl pinacol boronic ester precursor **74** was afforded in 75% yield. Moreover, in another attempt, by-product tetramethylurea (**56**) was removed through repetitive liquid/liquid extraction using chloroform and a saturated aqueous sodium bicarbonate solution but this was found to be detrimental to the yield of **74** (entry 4).

Table 11 – Optimisation of pinacol boronic ester **74** synthesis



Entry	Solvent	Time (h)	Purification	Yield of 74 (%)
1	DMF	16	LLE ^a , FCC and trituration	18
2	DMF	18	LLE ^a and trituration	23
3	MeCN	16	LLE ^b and trituration	75
4	MeCN	16	LLE ^b	55

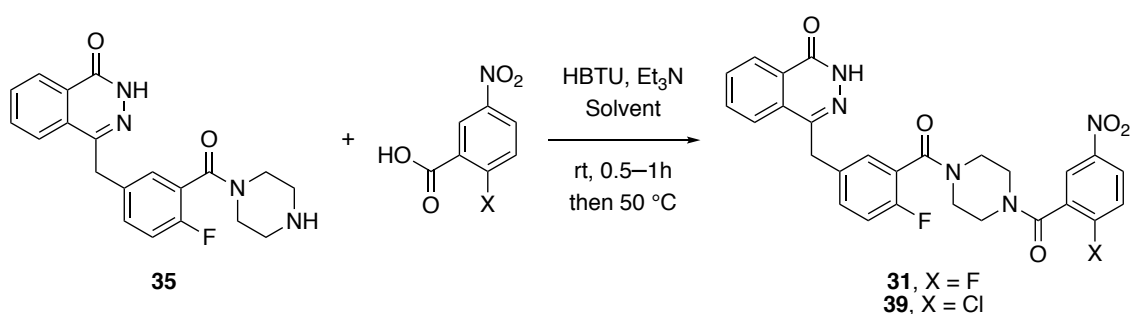
Note: LLE^a = liquid/liquid extraction using ethyl acetate, LLE^b = liquid/liquid extraction using chloroform, and FCC = flash column chromatography.

With an effective method for the preparation and purification of precursor **74** now established, development of the copper-mediated radiofluorodeborylation procedure could commence. However due to significant disruption from the covid-19 coronavirus pandemic, development of this radiosynthetic method was suspended and could not be undertaken within the time constraints of this project.

2.1.8.2 Synthesis of Analytical Standard **31** and Precursors **39** and **76**

Whilst the HM library of novel olaparib-analogues underwent biological evaluation, the focus of this project shifted to the radiosynthesis of [^{18}F]**31**. Previously in the Sutherland group, it was shown that fluorine-19 analogue **31** and chloride precursor **39** could be readily prepared from the olaparib core **35**, *via* HBTU-mediated amide bond formation with the appropriate halobenzoic acids, in moderate yields (Table 11, entries 1 and 2). As such, this procedure was adapted for the synthesis of compounds **31** and **39** in this project. Changing the reaction solvent from DMF to acetonitrile was found to afford the desired products in higher yields using shorter reaction times (entries 3 and 4).

Table 12 – Synthesis of **39** and **31** *via* HBTU-mediated amide coupling reactions



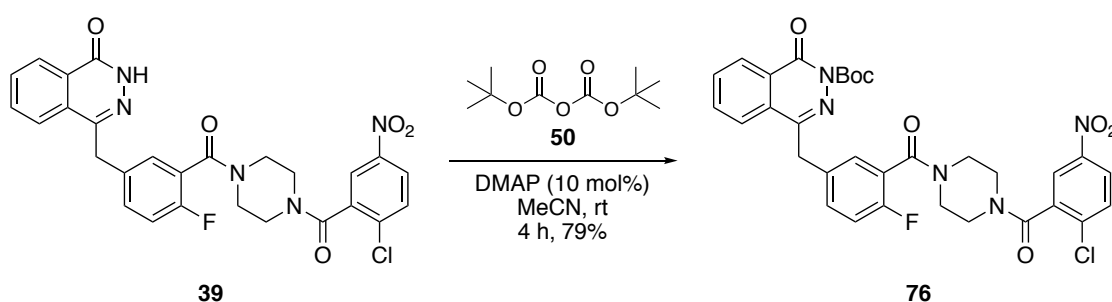
Entry	Product	Solvent	Time (h)	Isolated Yield (%)
1 ^a	31	DMF	48	55
2 ^a	39	DMF	48	42
3	31	MeCN	18	64
4	39	MeCN	16	84

^aSynthesis performed by Kerry O'Rourke.

However, following flash column chromatography chloride precursor **39** was found to contain 40% tetramethylurea (**56**). It was imperative that the tetramethylurea (**56**) impurity was removed so not to inhibit nucleophilic attack of [^{18}F]fluoride in the subsequent S_NAr radiolabelling reaction, since this would be employed as the limiting reagent. Purification was achieved by trituration using the minimal volume of chloroform and chilled hexane. Notably, these alternative conditions produced

chloride precursor **39** in 84% yield, a twofold increase when compared to the use of DMF (Table **11**, entries 2 and 4).

Additionally, it was proposed that the phthalazinone 2-*NH* moiety of chloride precursor **39** could participate in hydrogen bonding to the nucleophilic [¹⁸F]fluoride and impede the radiochemical yield of this reaction. Consequently, it was decided that the radiosynthesis of [¹⁸F]**31** would also be attempted using an analogous Boc-protected chloride precursor **76**. Following a Boc-protection procedure previously employed in the Sutherland group, precursor **76** was prepared in 79% yield from chloride precursor **39** using di-*tert*-butyl dicarbonate (**50**) and catalytic amounts of DMAP, under mild conditions (Scheme **21**).¹⁰⁵



Scheme 21 – Synthesis of Boc-protected chloride precursor **76**

2.1.8.3 Development of HPLC Conditions

Following any attempt to prepare [¹⁸F]**31**, it would be necessary to confirm the identity and purity of the isolated product through comparison of chromatographic retention time (*t_r*) with known analytical standards using analytical HPLC. As such, HPLC conditions were required for chromatographic separation of [¹⁸F]**31** and **39** or **76**. Development of this HPLC method was performed using **31** as a non-radioactive analytical standard. Initially, eluant systems comprising ethanol and water were explored since aqueous formulation of radiotracers is required for *in vivo* application. However, large percentages of ethanol were required for elution and so alternative solvent systems were investigated. It was found that elution with isocratic 35% acetonitrile in water at a flow rate of 1 mL min⁻¹ facilitated sufficient separation of chloride precursor **39** (*t_r* = 10.973 min) and standard **31** (*t_r* = 9.200 min) (Figure **27**).

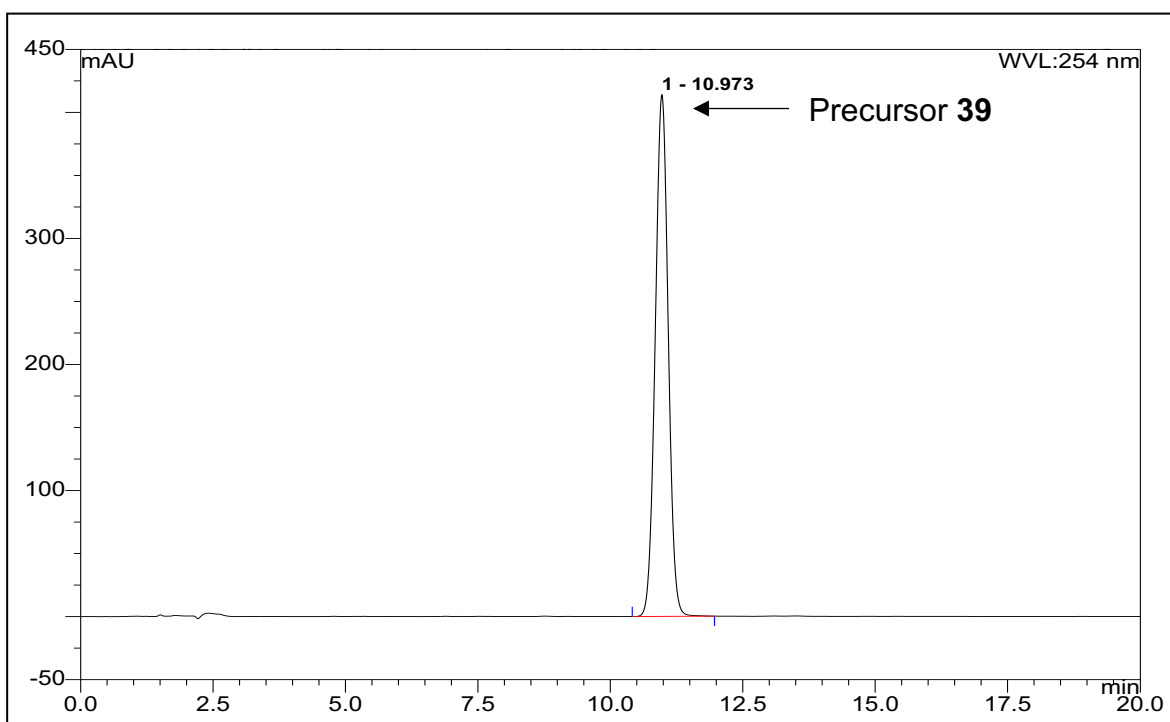
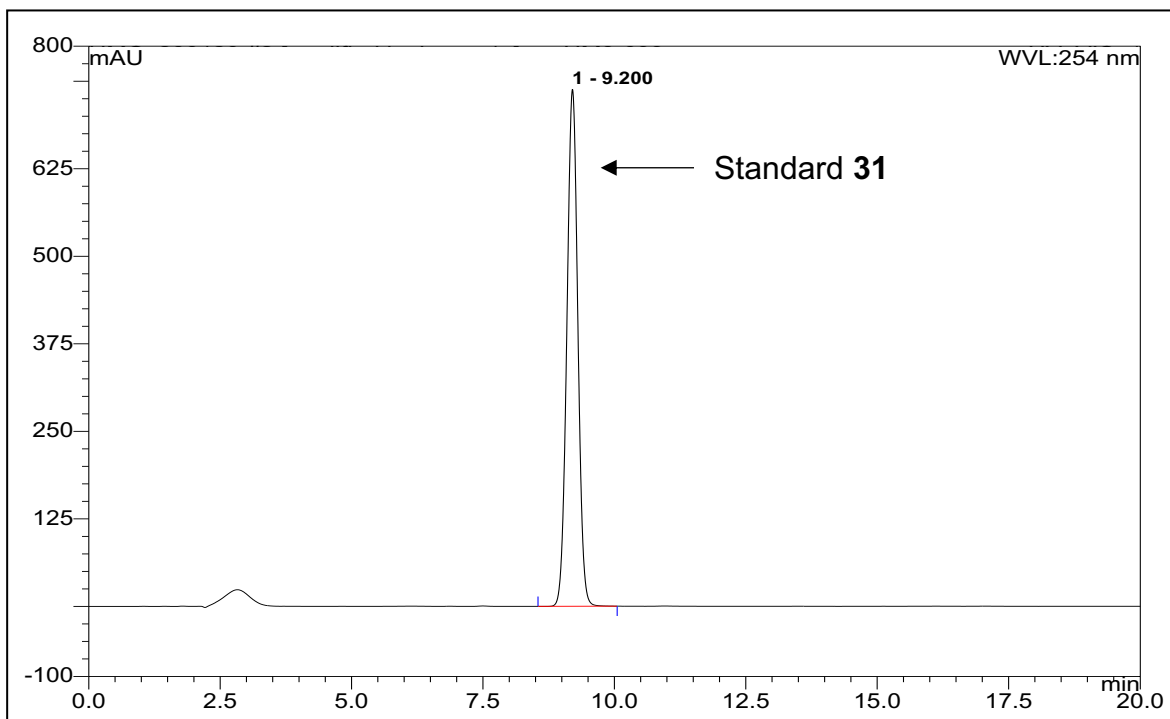


Figure 27 – Analytical HPLC UV chromatograms of standard **31** and chloride precursor **39**

Application of this isocratic method to analyse a sample containing both precursors **39** and **76**, and standard **31** resulted in complete retention of **76**. As such, alternative HPLC conditions were explored. It was found that elution with a gradient of 35–75% acetonitrile in water at a flow rate of 1 mL min⁻¹ facilitated optimal separation of chloride precursor **39** (t_r = 10.973 min), Boc-protected chloride precursor **76** (t_r = 17.940 min), and standard **31** (t_r = 9.193 min) (Figure 28).

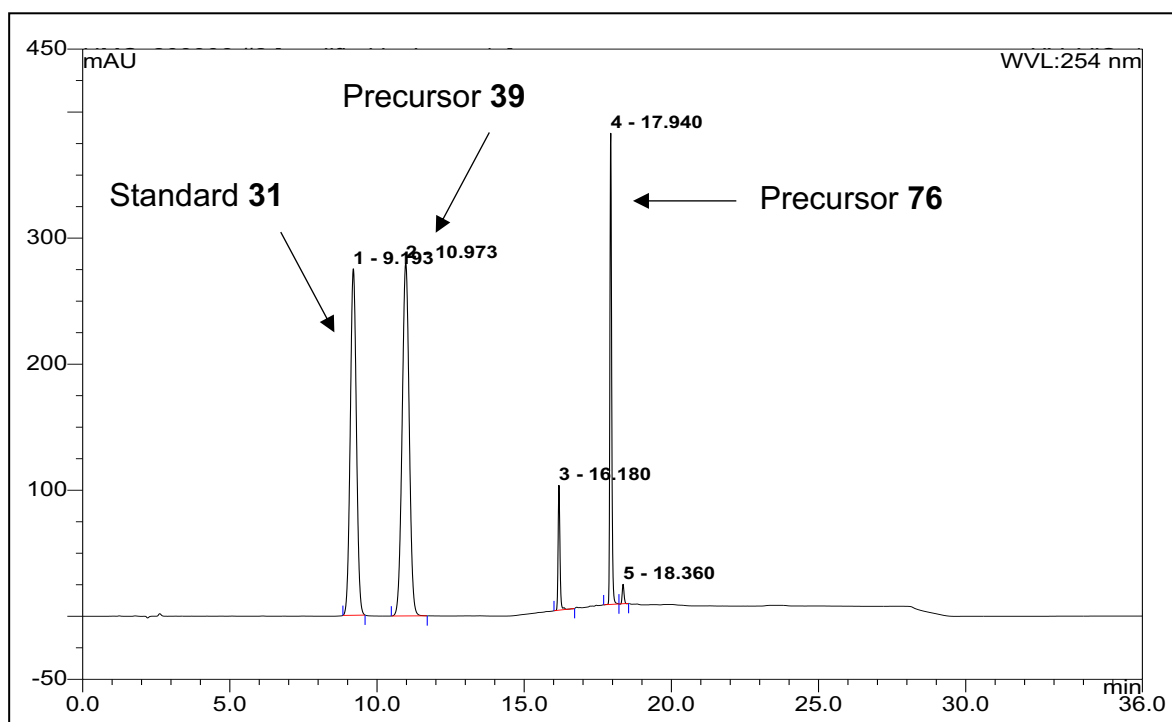


Figure 28 – Analytical HPLC UV chromatogram of chloride precursor **39**, Boc-protected chloride precursor **76** and standard **31**

The radiosynthesis of [¹⁸F]**31** would be performed at the West of Scotland PET centre using a fully automated GE TRACERlab™ FX_{FN} synthesiser with in-built semi-preparative HPLC capability for product purification. The schematic of this synthesiser can be found in Appendix II. Since [¹⁸F]fluoride would be used as the limiting reagent, excess precursor **39** or **76** would be present in the crude reaction mixtures. However when precursor **76** would be employed, it was expected that residual **76** would undergo deprotection to precursor **39** concurrently with a deprotection step to afford [¹⁸F]**31** from the Boc-protected equivalent. As such, development of semi-preparative HPLC conditions was required for chromatographic separation of [¹⁸F]**31** and **39** only. Due to the short half-life of [¹⁸F]fluoride (110 min) and consequent decay of [¹⁸F]**31** it would be advantageous

to the radiochemical yield for this HPLC method to be as short as practicable. Furthermore, the FX_{FN} synthesiser is capable of isocratic eluant flow only. It was found that elution with 35% acetonitrile in water at a flow rate of 3 mL min⁻¹ facilitated optimal separation of chloride precursor **39** ($t_r = 15.173$ min) and standard **31** ($t_r = 12.820$ min) (Figure 29).

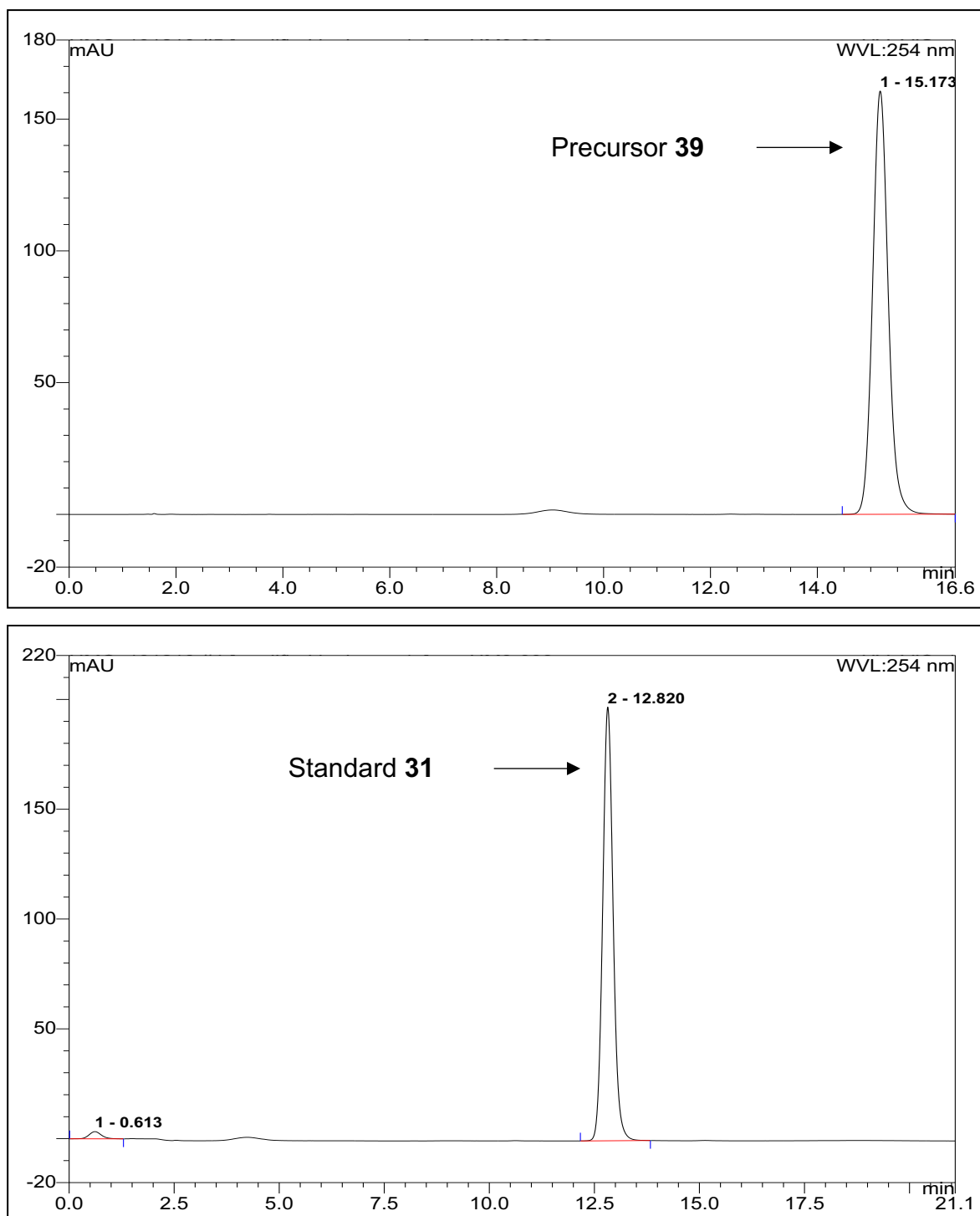
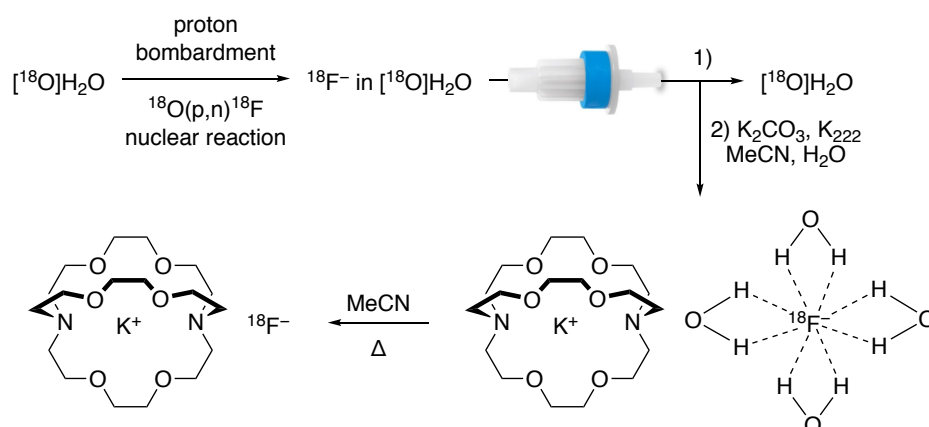


Figure 29 – Semi-preparative HPLC UV chromatograms of chloride precursor **39** and standard **31**

2.1.8.4 Production of [¹⁸F]Fluoride

[¹⁸F]Fluoride was produced by irradiation of 95–97 atom% [¹⁸O]enriched water in a niobium target chamber, *via* the ¹⁸O(p,n)¹⁸F nuclear reaction, in a GE Healthcare PETtrace 860 cyclotron at the West of Scotland PET Centre (Scheme 22). The resultant aqueous [¹⁸F]fluoride was transferred to the FX_{FN} synthesiser and passed through an ion exchange cartridge to trap the [¹⁸F]fluoride whilst allowing collection of valuable residual [¹⁸O]enriched water. The [¹⁸F]fluoride was then eluted from the ion exchange cartridge using a solution of 85% acetonitrile in water containing a potassium counterion and phase transfer catalyst, and then transferred to the reaction vessel. Potassium carbonate was selected to produce [¹⁸F]KF due to the non-nucleophilic and weakly basic carbonate anion.²³ Kryptofix[®] 222 (K₂₂₂), an aminopolyether cryptand, was chosen as the phase transfer catalyst to increase the solubility and nucleophilicity of [¹⁸F]fluoride in organic solvent *via* complexation of the potassium cation.²² In this resultant solution, [¹⁸F]fluoride is a weak nucleophile due to participation in hydrogen bonding with water molecules and as such must undergo dehydration to restore nucleophilic reactivity. Consequently, the [¹⁸F]fluoride solution was dried under vacuum *via* azeotropic distillation with acetonitrile at 110 °C to produce ‘naked’ [¹⁸F]fluoride as a [¹⁸F]KF/K₂₂₂ complex.



Scheme 22 – Production of [¹⁸F]fluoride as a [¹⁸F]KF/K₂₂₂ complex

2.1.8.5 Radiosynthesis of [¹⁸F]31 from Precursor 39

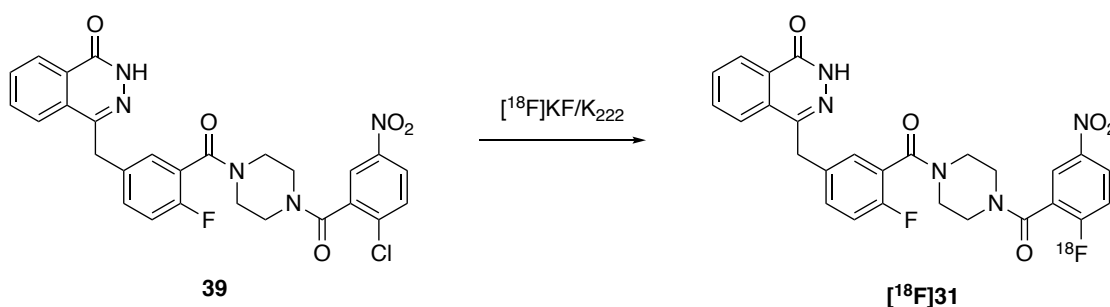
Having established suitable HPLC and [¹⁸F]fluoride production conditions, the next objective was to develop a procedure for the synthesis of [¹⁸F]31 from chloride precursor 39 via a S_NAr reaction. Polar aprotic solvents are favoured for nucleophilic radiofluorination reactions due to their inherent disinclination to participate in hydrogen bonding with [¹⁸F]fluoride.¹⁹⁴ As such, it was proposed that this radiolabelling reaction would be examined using acetonitrile and dimethyl sulfoxide (DMSO). In each instance, semi-preparative HPLC was employed to isolate the product, the radiochemical yield was measured in mega becquerels immediately following transfer of the product into a sample vial (as soon as practicable), and then an aliquot was submitted to analytical HPLC. Firstly, the purity of the product was evaluated by integration of all peaks in the UV and radio-HPLC chromatograms, and expressed as a ratio of [¹⁸F]31 to 'impurities'. The term 'impurities' denotes residual chloride precursor 39 and any other UV active side-products. Due to the small quantities of [¹⁸F]31 produced, the UV chromatogram was typically very weak. Subsequently, the aliquot was spiked with standard 31 and the resultant UV chromatogram overlaid with the radio-HPLC chromatogram for confirmation of the product identity by comparison of retention times. Notably, the sample was passed sequentially through the diode array detector and then the gamma detector which resulted in a small difference in retention times. Therefore, a single compound produced peaks in the UV and radio chromatograms with 0.2 minute separation.

An initial attempt was performed using acetonitrile at 90 °C for 5 minutes which afforded only trace quantities of [¹⁸F]31 (Table 12, entry 1). Due to the extremely small quantity of [¹⁸F]31 produced, HPLC purification proved challenging and a mixture of compounds was collected including [¹⁸F]fluoride and chloride precursor 39. Next the solvent was changed to DMSO and the reaction temperature was increased to 110 °C (entry 2). It was found that these conditions increased the radiochemical yield to 7%, and both the UV and radiochemical purity were significantly improved as a result. The radiochemical yield was increased further to 15% by extending the reaction time to 15 minutes (entry 3). Consequently, the increased radiochemical conversion led to greater chromatographic separation of [¹⁸F]31 and [¹⁸F]fluoride, and so [¹⁸F]31 was isolated in 93% radiochemical purity. Regrettably, a software malfunction resulted in collection of additional non-

radioactive impurities which were observed in the UV chromatogram (Figure 30). Finally, increasing the reaction time to 20 minutes was not conducive to improvement of the radiochemical yield (entry 4).

In conclusion, [¹⁸F]31 was afforded from precursor 39 in the highest radiochemical yield of 15% and 93% radiochemical purity using DMSO at 110 °C for 15 minutes. Moreover, it is reasonable to assume that the chemical purity of 23%, observed in the HPLC UV chromatogram, would be vastly improved in future syntheses of [¹⁸F]31 under these conditions.

Table 13 – Radiosynthesis of [¹⁸F]31 from precursor 39



Entry	Solvent	Temp. (°C)	Time (min)	^a Ratio of [¹⁸ F]31 : Impurities	^b Ratio of [¹⁸ F]31 : [¹⁸ F]F ⁻	Decay Corrected RCY (%)
1	MeCN	90	5	0.1 : 99.9	2 : 98	-
2	DMSO	110	5	83 : 17	57 : 43	7
3	DMSO	110	15	23 : 77 ^c	93 : 7	15
4	DMSO	110	20	68 : 32	100 : 0	10

^aDetermined from analytical HPLC UV spectra. ^bDetermined from analytical radio-HPLC spectra. ^cRatio could not be determined with accuracy due to shoulder peak impurity (UV peak 2, t_r = 8.853 min) (Figure 30).

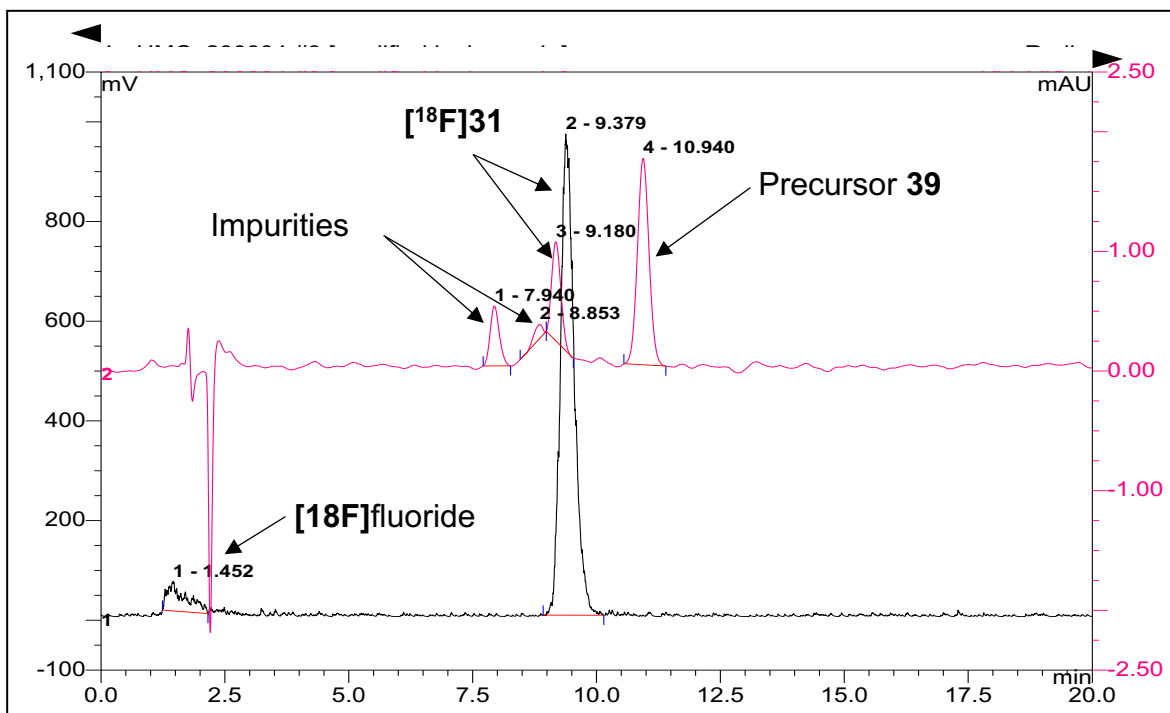
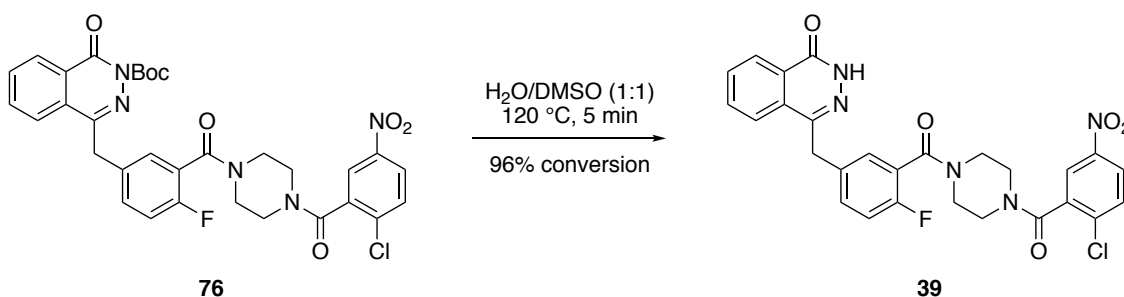


Figure 30 – Overlay of analytical HPLC non-spiked UV (shown in pink) and radio (shown in black) chromatograms relating to Table 12, entry 3.

2.1.8.6 Radiosynthesis of [¹⁸F]31 from Precursor 76

The radiosynthesis of [¹⁸F]31 was next attempted using Boc-protected chloride precursor 76. The first objective of this work was to determine suitable conditions for Boc-deprotection of the intermediate produced by the radiolabelling step. It was previously demonstrated by the Sutherland group, that water could be employed for Boc-deprotection of a similar olaparib-derived analogue.¹⁰⁵ This procedure was adapted and the reaction exemplified using precursor 76 as an appropriate mimetic. It was found that precursor 76 underwent rapid deprotection to precursor 39 using a 1 : 1 mixture of water and DMSO at 120 °C in only 5 minutes (Scheme 23). HPLC analysis of the crude reaction mixture showed 96% conversion to precursor 39 with 4% trace impurities.

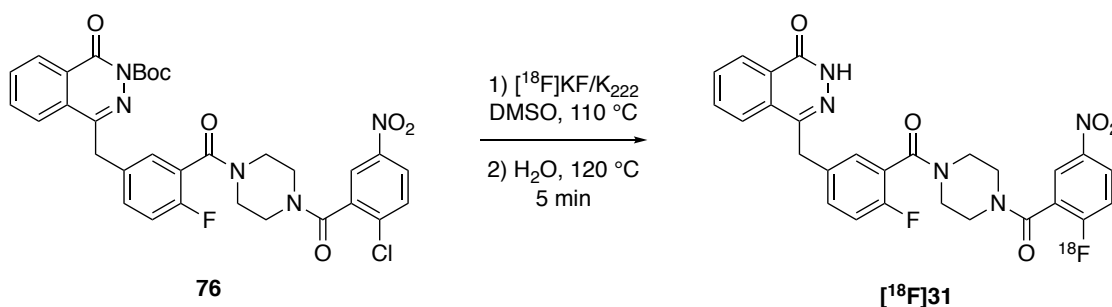


Scheme 23 – Water-mediated Boc-deprotection of precursor 76

With an efficient Boc-deprotection procedure established, conditions for radiolabelling of Boc-protected chloride precursor 76 were investigated. In the first instance, precursor 76 was submitted to a S_NAr reaction using [¹⁸F]fluoride and DMSO at 110 °C for 20 minutes. These conditions and subsequent deprotection produced [¹⁸F]31 in 5% radiochemical yield and 100% radiochemical purity (Table 13, entry 1). However, as reported for a previous radiolabelling reaction (Table 12, entry 3), a ‘shoulder peak’ impurity was observed in the UV chromatogram (t_r = 8.907 min) in significant quantity. This two-step procedure was then attempted using a shorter 15 minute radiolabelling step (entry 2). Under these conditions, [¹⁸F]31 was afforded in 6% radiochemical yield, 100% chemical purity and 88% radiochemical purity. Regrettably, 20% of the crude reaction mixture was sent to the waste stream due to a technical issue within the FX_{FN} synthesiser and so the true radiochemical yield of this process was likely 8%. It is reasonable to postulate that further attempts under these conditions would yield [¹⁸F]31 in slightly increased

radiochemical yields. Furthermore, additional measures could be taken to trap excess [^{18}F]fluoride following the radiolabelling step, such as incorporation of an aluminium oxide cartridge before semi-preparative HPLC purification.

Table 14 – Radiosynthesis of [^{18}F]31 from precursor 76



Entry	Step 1 Time (min)	^a Ratio of [^{18}F]31 : Impurities	^b Ratio of [^{18}F]31 : [^{18}F]F ⁻	Decay Corrected RCY (%)
1	20	41 : 59	100 : 0	5
2	15	100 : 0	88 : 12	6

^aDetermined from analytical HPLC UV spectra. ^bDetermined from analytical radio-HPLC spectra.

From this brief screening of reaction conditions, it was found that use of precursor 76 afforded [^{18}F]31 in lower radiochemical yield than precursor 39 when treated with identical radiofluorination conditions. Notably, no excess Boc-protected chloride precursor 76 was observed during semi-preparative HPLC purification. As such, it is reasonable to presume that deprotection of the radiolabelled intermediate to give [^{18}F]31 was also successful. Therefore, the overall longer synthesis duration due to the additional deprotection step was likely the cause of lower radiochemical yields when precursor 76 was employed. Due to significant disruption from the covid-19 coronavirus pandemic, further development of a radiosynthetic method for the preparation of [^{18}F]31 was suspended at this stage.

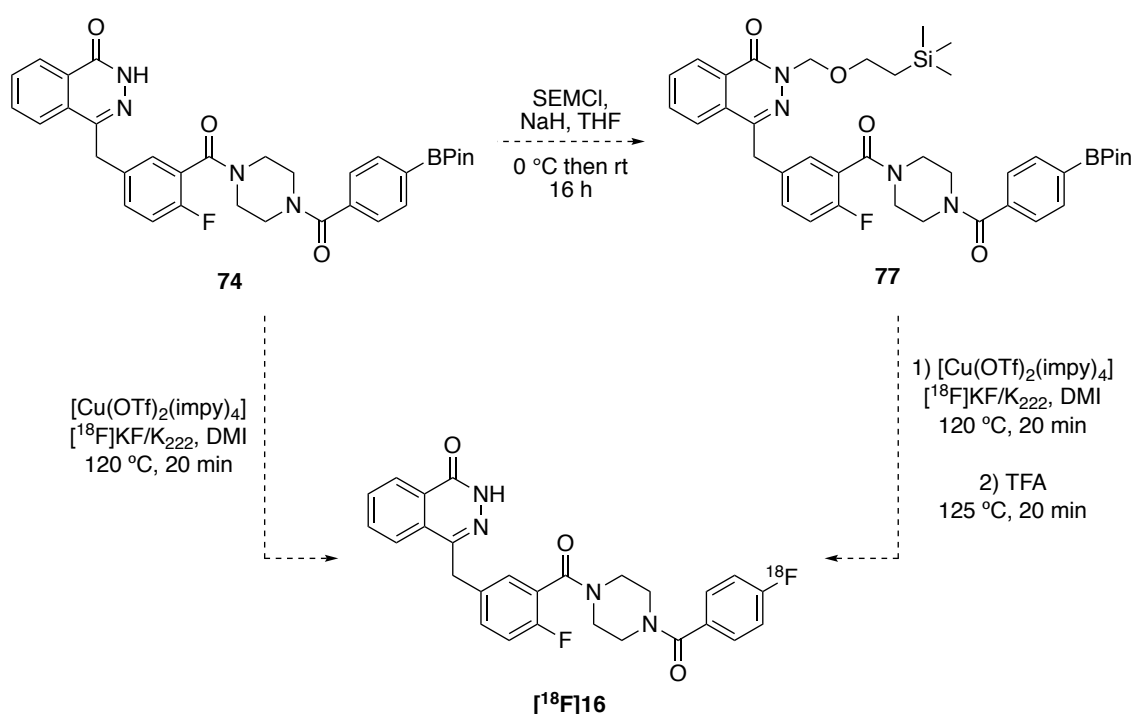
2.1.9 Conclusions and Future Work

In summary, the core structure of olaparib (**35**) was synthesised in multi-gram quantities *via* a seven-step synthetic route and subsequently derivatised. A fluorescent PARP-1 inhibitor, olaparib-BODIPY FL (**37**), was prepared from the core structure of olaparib (**35**) in five steps. Olaparib-BODIPY FL (**37**) is currently employed in the development of an *in vitro* competitive displacement fluorescence assay of PARP-1 inhibition and investigations of olaparib (**1**) cellular uptake and retention in glioblastoma models. Once optimisation of this *in vitro* assay is complete, it would be worthwhile to submit both the KO and HM libraries of novel olaparib-derived PARP-1 inhibitors for testing. This would allow for an evaluation of cellular uptake and distribution, PARP-1 affinity and retention for each analogue. Comparison of these attributes would facilitate a SAR analysis of the complimentary libraries.

A library of eight novel olaparib-derived PARP-1 inhibitors was prepared containing a lipophilic hydrocarbon chain linker and terminal fluoroarene system. This library of compounds was subjected to physicochemical properties determination *via* HPLC methodology. Assessment of this data facilitated the selection of four analogues that exhibit favourable drug-like properties for penetration of the BBB *in vivo*. Compounds **66**, **67**, **69** and **70** were then submitted to *in vitro* biological evaluation of PARP-1 inhibitory potency and cytotoxicity in two glioblastoma models. It was found that analogues **66**, **67** and **70** are potent PARP-1 inhibitors; of these compounds, **66** and **67** displayed similar potency to olaparib (**1**). Moreover, **67** (IC₅₀ value of 8.11 nM) was the only analogue found to be a more potent PARP-1 inhibitor than olaparib (**1**) (IC₅₀ value of 11.0 nM). Therefore, compounds **66** and **67** will likely exhibit high affinity for PARP-1 *in vivo* and demonstrate promise for further development as PET radiotracers for the PARP-1 protein.

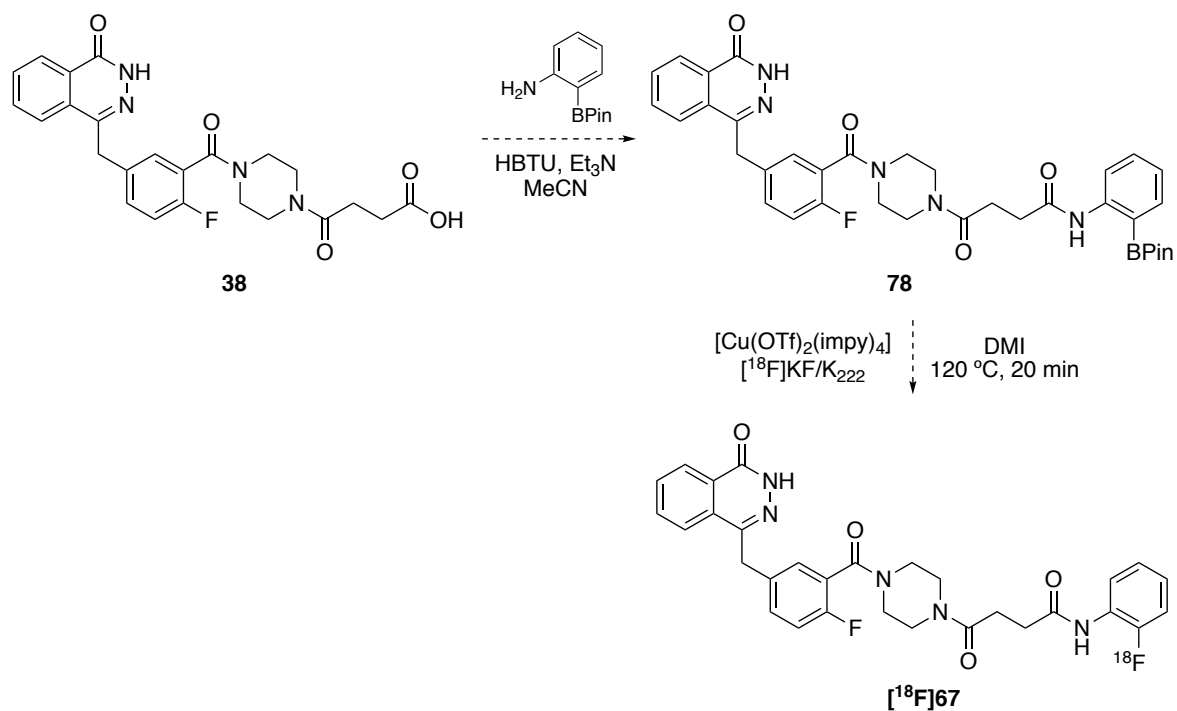
The next stage of this project will be the development of [¹⁸F]**67** as a PET imaging agent for PARP-1. This work has been initiated and an optimised procedure has been established for the synthesis of aryl pinacol boronic ester precursor **74** in 75% yield. Concurrent to this project Cornelissen, Gouverneur and co-workers reported extensive optimisation of the copper-mediated radiofluorodeborylation procedure that was intended for use in this project.^{106,195,196} In their efforts to produce

[¹⁸F]olaparib (**[¹⁸F]1**), the authors found that application of tetrakis(imidazo[1,2-b]pyridazine)copper(II) bis(trifluoromethanesulfonate), a novel copper(II) complex, in 1,3-dimethyl-2-imidazolidinone (DMI) at 120 °C for 20 minutes provided optimal radiochemical yields. Furthermore, it was reported that superior radiochemical yields were achieved when the phthalazinone 2-NH moiety of olaparib (**1**) was protected with a 2-(trimethylsilyl)ethoxymethyl (SEM) group. As such, initially precursor **74** will be treated under these optimised radiofluorodeborylation conditions (Scheme **24**). If insufficient radiochemical yields are obtained, it would be advisable to prepare the SEM-protected precursor **77** and employ this alternative precursor for the synthesis of [¹⁸F]**16a** (Scheme **24**).



Scheme 24 – Proposed synthetic routes for the preparation of [¹⁸F]**16a**

Following successful application of this radiofluorodeborylation method for the preparation of [¹⁸F]**16a**, this approach could also be used for the synthesis of [¹⁸F]**67**. The aryl pinacol boronic ester precursor **78** (or SEM protected equivalent) will be prepared *via* an HBTU-mediated coupling reaction of carboxylic acid **38** and 2-aminophenylboronic acid pinacol ester (Scheme **25**). Precursor **78** will then be employed in the radiosynthesis of [¹⁸F]**67**.



Scheme 25 – Proposed radiosynthesis of [^{18}F]67

Preliminary investigations have been conducted into the radiosynthesis of [^{18}F]31 via a $\text{S}_{\text{N}}\text{Ar}$ reaction with [^{18}F]fluoride using precursors **39** and **76**. It was found that use of precursor **76** afforded [^{18}F]31 in lower radiochemical yield than precursor **39** when treated with identical radiolabelling conditions. A procedure was developed for the preparation of [^{18}F]31 in 15% radiochemical yield and 93% radiochemical purity using precursor **39** in DMSO at 110 °C for 15 minutes. In addition, increased reaction times were not conducive to improved radiochemical yields. In the future, further optimisation is required for the radiosynthesis of [^{18}F]31. It would be reasonable to screen higher reaction temperatures and alternative fluoride chelating agents, such as tetra-*n*-butylammonium hydrogen carbonate (TBAHCO_3) which produces nucleophilic tetra-*n*-butylammonium [^{18}F]fluoride ($[\text{}^{18}\text{F}]\text{TBAF}$) *in situ*.¹⁹⁷ Previous work by the Sutherland group found that use of $[\text{}^{18}\text{F}]\text{TBAF}$ afforded higher radiochemical yields than use of a $[\text{}^{18}\text{F}]\text{KF}/\text{K}_{222}$ complex, in an aliphatic nucleophilic radiofluorination reaction.¹⁰⁵ Initially, it would be advisable to perform this optimisation without purification of the crude reaction mixture. Analytical HPLC of the crude reaction mixture will allow for evaluation of radiochemical conversion. Once the radiochemical conversion of this process has been optimised, alternative conditions for semi-preparative HPLC purification of [^{18}F]31 should be explored to improve chromatographic separation and chemical purity.

Once efficient procedures have been established for the radiosynthesis of [¹⁸F]67 and [¹⁸F]31, parallel *in vivo* PET imaging studies could be performed. Such studies would allow assessment and comparison of the *in vivo* distribution of these analogues. It was found that [¹⁸F]67 is a potent PARP-1 inhibitor that displays lower levels of cytotoxicity than [¹⁸F]31 which is a more potent inhibitor. Analysis of PARP-1 specific binding and off-target interactions may provide valuable insight into the variation of PARP-1 inhibitory potency and cytotoxicity exhibited by these distinct scaffolds.

Additionally, *in silico* methods could be exploited to gain a deeper understanding of the SAR of olaparib-derived PARP-1 inhibitors. The analogues produced in the KO and HM libraries could be subjected to computational molecular docking with the PARP-1 catalytic site to observe key binding interactions. This could be achieved employing the recently published crystal structures of the human PARP-1 catalytic domain complexed with olaparib (**1**) (PDB ID: 7kk4 and 7AAD).^{35,171} If successful, this may also provide justification for the variation of PARP-1 inhibitory potency and cytotoxicity exhibited by these distinct scaffolds.

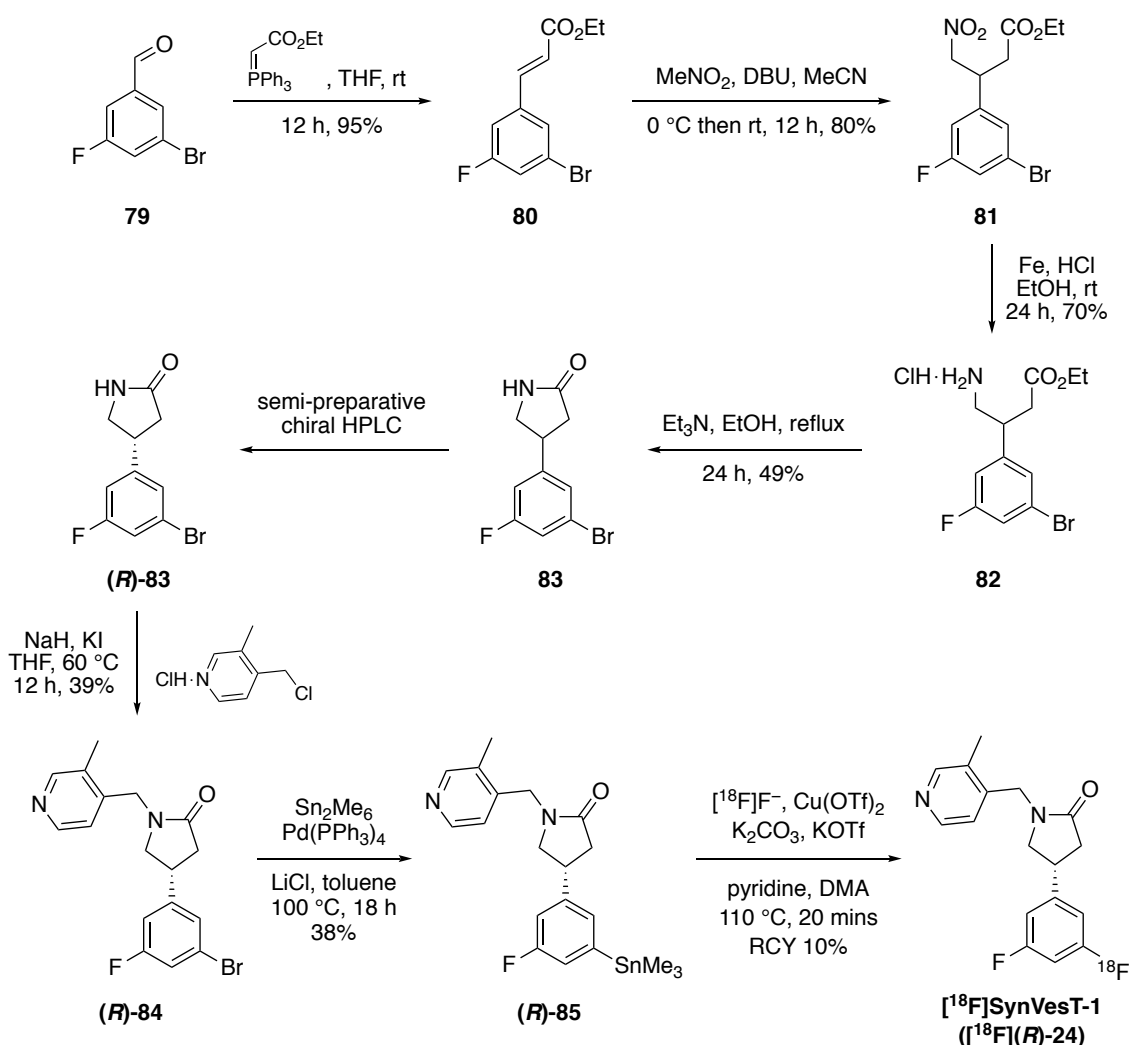
2.2 Novel Enantioselective Synthesis of [¹⁸F]SynVesT-1 ([¹⁸F](R)-24): A PET Imaging Agent for SV2A

2.2.1 Proposed Research

Although it is widely acknowledged that the synaptome undergoes significant alterations in numerous neurological conditions, thus far no techniques have been established for *in vivo* analysis of synaptic structure and function within clinical settings. In collaboration with Professor Seth Grant and Dr Adriana Tavares at the University of Edinburgh, the overall aim of this research project is to enable advance *in vivo* imaging of synaptic structure and function in living humans over the course of their lifespan using SV2A PET imaging and new synaptomics technology. It was proposed that this novel technique will have implications in neuropathology, diagnosis and monitoring of neurological conditions, development of therapeutic agents, and treatment of neurological diseases. As previously discussed in Section 1.3.3, [¹⁸F]SynVesT-1 ([¹⁸F](R)-24) has been identified as a lead candidate for development as a PET imaging agent for the SV2A protein, and was shown to possess optimal kinetic and binding properties for *in vivo* imaging during pre-clinical and clinical validation.^{152–155} It was proposed that [¹⁸F]SynVesT-1 ([¹⁸F](R)-24) would be employed in this work for *in vivo* quantitative PET imaging of the SV2A protein to measure synaptic density within the brain of murine animal models across the natural ageing and lifetime. The data generated from this *in vivo* imaging will then be validated at novel scale and resolution using pioneering single-synapse-resolution synaptome mapping developed by Grant and co-workers in 2018.¹⁹⁸

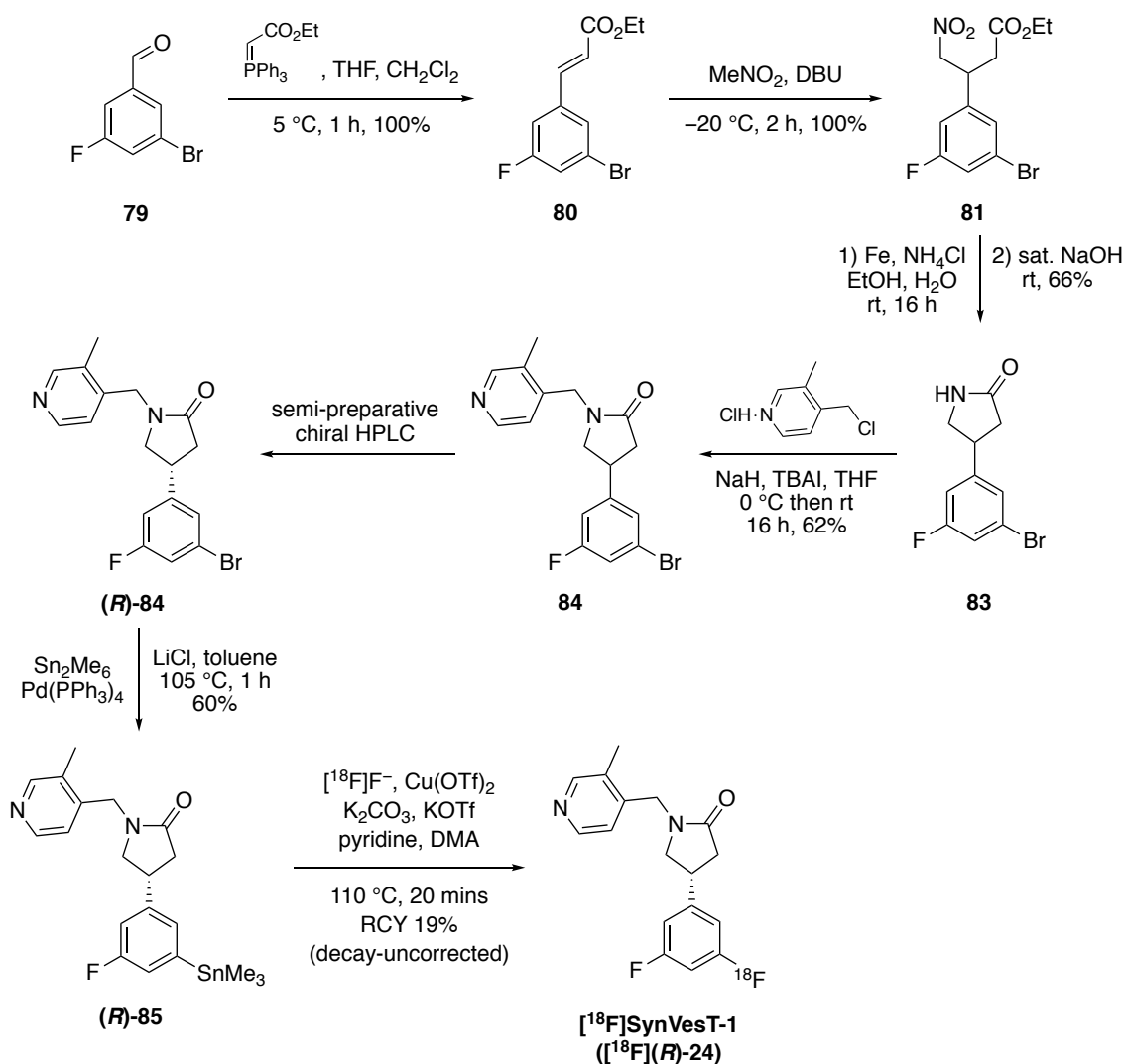
As such, it would be necessary to prepare significant quantities of [¹⁸F]SynVesT-1 ([¹⁸F](R)-24) and the corresponding racemate [¹⁸F]MNI-1038 ([¹⁸F]24) for utilisation in the optimisation of an *in vivo* quantitative SV2A PET imaging technique. As briefly highlighted in Section 1.3.3, prior to this project [¹⁸F]SynVesT-1 ([¹⁸F](R)-24) was synthesised by Constantinescu *et al.*, and concurrently by Li *et al.* employing similar approaches. Both synthetic strategies were derived from the original synthesis of SV2A ligand UCB-J (23) developed by Mercier *et al.* in 2014.¹³⁰ The synthetic route reported by Constantinescu *et al.* for the preparation of [¹⁸F]SynVesT-1 ([¹⁸F](R)-24) consisted of eight steps including chiral resolution *via* semi-preparative chiral HPLC as the fifth step (Scheme 26).¹⁵² To summarise, 3-bromo-5-

fluorobenzaldehyde (**79**) was submitted to a Wittig reaction with (carbethoxymethylene)triphenylphosphorane, a Michael addition with nitromethane, reduction under acidic conditions with iron, and base-mediated intramolecular cyclisation to produce pyrrolidin-2-one **83** as a racemic mixture. Semi-preparative chiral HPLC was subcontracted to a specialised purification company for the isolation of the desired *R*-enantiomer (**(R)**-**83**), which then underwent *N*-alkylation with 4-(chloromethyl)-3-methylpyridine hydrochloride, and a palladium-catalysed stannylation with hexamethylditin. Subsequently, the resultant organotin precursor (**(R)**-**85**) was subjected to copper-mediated nucleophilic radiofluorination conditions developed by Sanford, Scott and co-workers to afford [¹⁸F]SynVesT-1 ([¹⁸F]**(R)**-**24**) in 10% radiochemical yield.¹⁹⁹



Scheme 26 – Synthesis of [¹⁸F]SynVesT-1 ([¹⁸F]**(R)**-**24**) by Constantinescu *et al.*

In parallel, Li *et al.* prepared [^{18}F]SynVesT-1 ([^{18}F](*R*)-**24**) in seven steps including chiral resolution *via* semi-preparative chiral HPLC as the fifth step (Scheme 27).¹⁵³ Overall, 3-bromo-5-fluorobenzaldehyde (**79**) underwent sequential transformations identical to those reported by Constantinescu *et al.* using analogous reaction conditions. One key exception was that reduction of nitroalkane **81** and subsequent intramolecular cyclisation were performed using a one-pot, two step procedure to give pyrrolidin-2-one **83** in a significantly higher yield of 66%. Comparatively, lactam **83** was afforded from nitroalkane **81** in 34% yield over two individual steps by Constantinescu *et al.*¹⁵² Subsequently, racemate intermediate **84** was subjected to chiral resolution to isolate the required *R*-enantiomer (*R*)-**84**. Notably, [^{18}F]SynVesT-1 ([^{18}F](*R*)-**24**) was produced in a higher radiochemical yield of 19% (decay uncorrected) treating the same organotin precursor (*R*)-**85** with copper-mediated nucleophilic radiolabelling conditions using [^{18}F]fluoride.

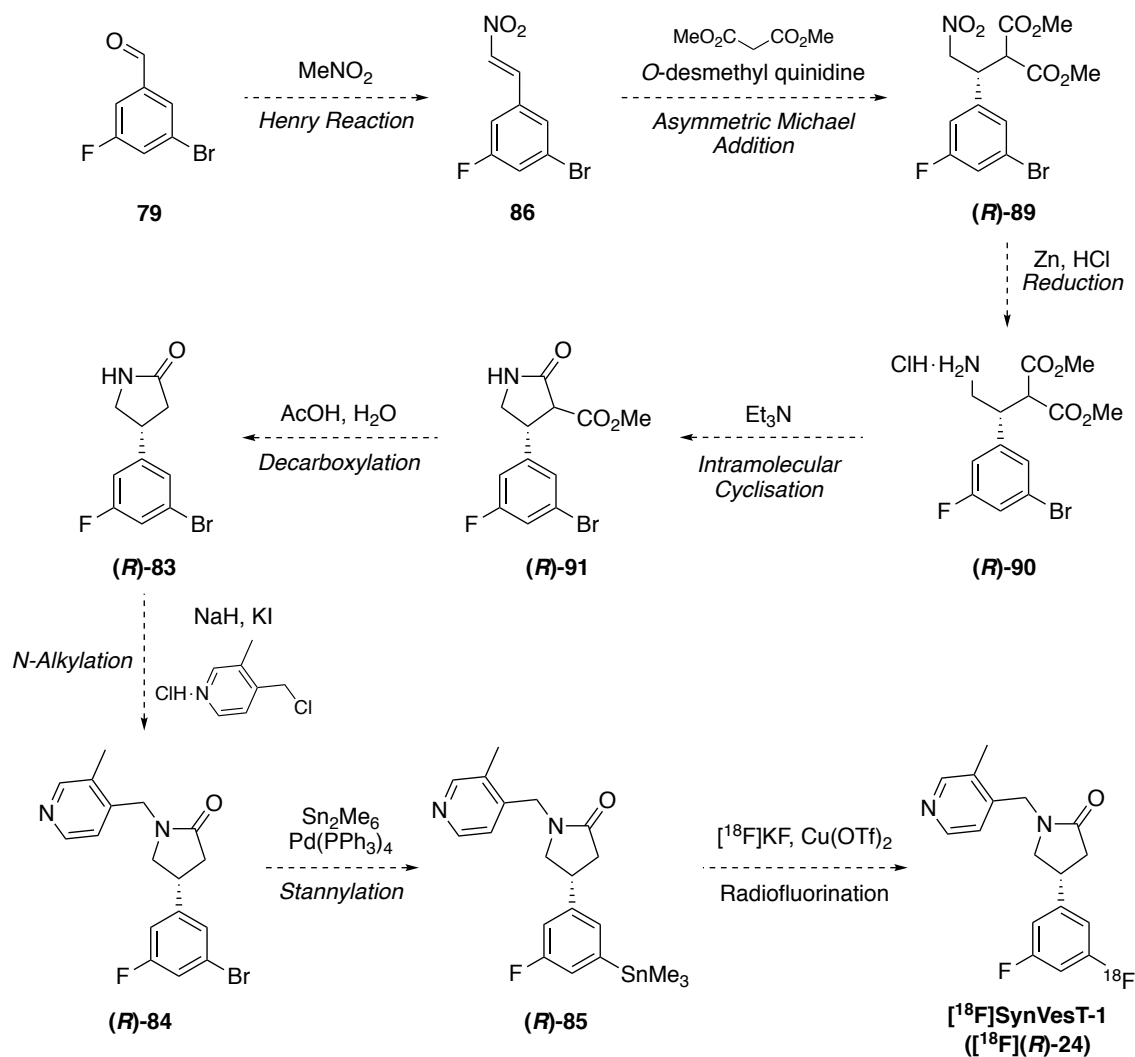


Scheme 27 – Synthesis of [^{18}F]SynVesT-1 ([^{18}F](*R*)-**24**) by Li *et al.*

Both aforementioned strategies for the production of [^{18}F]SynVesT-1 (**[^{18}F](R)-24**) utilise non-enantioselective procedures to synthesise racemic intermediates and exploit chiral HPLC to separate the *R*- and *S*-enantiomers at late stages. However, these approaches require costly chiral HPLC columns and necessitate large scale syntheses since 50% of the material is discarded following chiral resolution. Furthermore, semi-preparative HPLC introduces a troublesome production bottleneck as limited quantities of material can undergo chromatographic separation during each injection. Consequently, it was decided that the use of semi-preparative chiral HPLC would be circumvented during this project through employment of enantioselective reactions. Therefore, the key aim of this project was to develop a novel enantioselective synthetic route to [^{18}F]SynVesT-1 (**[^{18}F](R)-24**) in parallel with a complimentary route to the racemate compound [^{18}F]MNI-1038 (**[^{18}F]24**).

In 2016, Li *et al.* developed an asymmetric procedure for the synthesis of [^{11}C]UCB-J (**[^{11}C]23**) using an enantioselective Michael addition to implement the desired stereochemistry in an early synthetic stage.¹⁴¹ It was proposed that this literature route would be adapted and optimised for the synthesis of [^{18}F]SynVesT-1 (**[^{18}F](R)-24**) in this work (Scheme 28). Initially, benzaldehyde **79** would undergo a Henry reaction with nitromethane to give nitrostyrene **86**. The chiral organocatalyst *O*-desmethyl quinidine (**87**) would be prepared in one step from quinidine (**88**) *via* a desmethylation reaction. Submission of nitrostyrene **86** to an enantioselective Michael addition with dimethyl malonate using the quinidine-derived catalyst **87** would provide intermediate (**R**)-**89**. Additionally, nitrostyrene **86** would undergo coupling with dimethyl malonate in the absence of a chiral catalyst to afford the racemate intermediate **89**. Subsequently, compound **89** would be utilised as an analytical standard to determine the enantiomeric ratio of intermediate (**R**)-**89** *via* chiral HPLC analysis. Following optimisation of the key chiral step, intermediate (**R**)-**89** would undergo reduction of the nitro functionality and subsequent base-mediated intramolecular cyclisation of amine (**R**)-**90** to produce lactam (**R**)-**91**. Successive decarboxylation under acidic conditions, *N*-alkylation with 4-(chloromethyl)-3-methylpyridine hydrochloride, and palladium-catalysed stannylation with hexamethylditin would then be performed to obtain the desired organotin precursor (**R**)-**85**.

Previous investigations by Li *et al.* have examined the production of [¹⁸F]SynVesT-1 (**[¹⁸F](R)-24**) from various precursors analogous to organotin compound **(R)-85** including, but not limited to, an iodonium ylide precursor and pinacol boronic ester precursor.^{153,200} Notably, the authors concluded that organotin precursor **(R)-85** provided the highest radiochemical yield of [¹⁸F]SynVesT-1 (**[¹⁸F](R)-24**). As such, **(R)-85** was identified as an appropriate precursor for utility in this project. Following successful development of an enantioselective synthetic route, it was proposed that both the racemate **85** and **(R)-85** would be prepared on a large scale. The radiosynthesis of the racemate [¹⁸F]MNI-1038 (**[¹⁸F]24**) would then be optimised using the copper-mediated nucleophilic radiofluorination conditions from Sanford, Scott and co-workers by collaborators at the University of Edinburgh.¹⁹⁹ Subsequently, the optimised radiolabelling procedure would be utilised to prepare sufficient quantities of [¹⁸F]SynVesT-1 (**[¹⁸F](R)-24**) for application in the development of a quantitative *in vivo* PET imaging study.



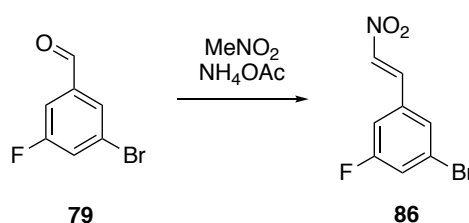
Scheme 28 – Proposed enantioselective synthesis of [¹⁸F]SynVesT-1 ([¹⁸F](R)-24)

2.2.2 Initial Enantioselective Synthetic Route to [¹⁸F]SynVesT-1 ([¹⁸F](R)-24)

Development of the proposed asymmetric synthetic route to [¹⁸F]SynVesT-1 ([¹⁸F](R)-24) began with optimisation of a Henry reaction between 3-bromo-5-fluorobenzaldehyde (**79**) and nitromethane. This reaction was mediated by ammonium acetate which deprotonates nitromethane to form a nitronate anion stabilised by resonance. The resultant nitronate then undergoes an aldol reaction with 3-bromo-5-fluorobenzaldehyde (**79**) to produce a β-nitroalcohol intermediate. Subsequently, acidic conditions facilitate dehydration of the β-nitroalcohol to afford nitrostyrene **86**. Following a procedure developed within the Sutherland group for the coupling of nitromethane with electron-rich benzaldehydes, an initial reaction was performed in toluene under reflux for 15 h (Table **14**, entry 1).²⁰¹ However,

application of these conditions with electron-poor benzaldehyde **79** produced a complex mixture of compounds that proved challenging to separate. Nitrostyrene **86** was successfully purified by flash column chromatography however, the product was isolated in only 26% yield and consequently, alternative reaction conditions were explored. It was found that the employment of acetic acid/nitromethane (2 : 1) as the reaction solvent under reflux for 16 h generated a complex mixture of compounds resulting from decomposition (entry 2).²⁰² Subsequently, decreasing the reaction temperature to 90 °C allowed for the preparation of nitrostyrene **86** in 74% yield (entry 3). The geometry of the isolated alkene **86** was confirmed by ¹H NMR spectroscopy, which showed two doublets with 13.6 Hz coupling constants indicative of a vicinal *trans* relationship.

Table 15 – Optimisation of Henry reaction conditions for the synthesis of **86**

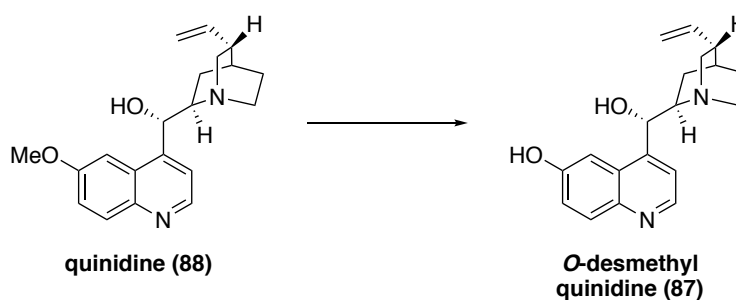


Entry	Solvent	Temp. (°C)	Time (h)	Yield of 86 (%)
1	toluene	reflux	15	26
2	acetic acid/MeNO ₂ (2 : 1)	reflux	16	-
3	acetic acid/MeNO ₂ (2 : 1)	90	5	74

Preparation of *O*-desmethyl quinidine (**87**) was undertaken next *via* a desmethylation reaction of the commercially available cinchona alkaloid quinidine (**88**). In the first instance, a reaction was performed using 3 equivalents of sodium ethanethiolate in DMF at 115 °C, as reported by Li *et al.* (Table 15, entry 1).¹⁴¹ Under these conditions desmethylation was slow and only 56% conversion to **87** was observed by ¹H NMR spectroscopy after 115 h. In an effort to promote efficient reactivity, the reaction was repeated at 130 °C which generated 64% conversion after only 16 h (entry 2). It was found that the addition of 2 equivalents of sodium ethanethiolate facilitated further reactivity and 83% conversion of quinidine (**88**) was observed by 20 h. However, no further significant progress was detected by 39 h with 88% conversion achieved and *O*-desmethyl quinidine (**87**) was subsequently

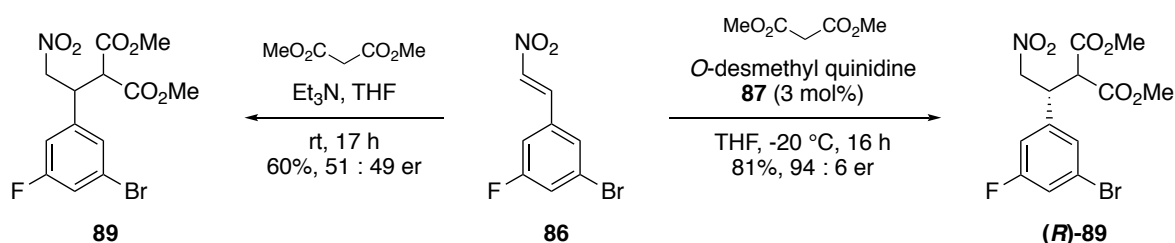
isolated in 32% yield. In one final attempt using sodium ethanethiolate, 3 equivalents were added at the start of the procedure followed by an additional 3 equivalents after 22 h (entry 3). Full reaction of quinidine (**88**) was observed by 44 h; however, *O*-desmethyl quinidine (**87**) was isolated in only 64% yield. In each attempt, employing sodium ethanethiolate for desmethylation of quinidine (**88**), flash column chromatography was required for isolation of **87** from the resultant by-products. It was proposed that due to the polarity and basic character of compound **87**, partial retention on the silica stationary phase may be responsible for the observed disparity between reaction conversion and isolated yields. Desmethylation mediated by boron tribromide is another commonly exploited method in the literature which generates gaseous methyl bromide and a dibromo(aryloxy)borane intermediate. Successive aqueous work-up facilitates hydrolysis of this intermediate to the desired phenolic product. Notably, the resultant boric acid and hydrobromic acid by-products are miscible with aqueous solutions and sufficient purification of the desmethylated product can be achieved without flash column chromatography. Subsequently, treatment of quinidine (**88**) with boron tribromide in dichloromethane under reflux for only 2 hours, followed by acid-base extraction afforded *O*-desmethyl quinidine (**87**) in 81% yield (entry 4).²⁰³

Table 16 – Synthesis of *O*-desmethyl quinidine (**87**)



Entry	Reagent (equiv.)	Solvent	Temp. (°C)	Time (h)	Yield of 87 (%)
1	EtSNa (3)	DMF	115	115	-
2	EtSNa (5)	DMF	130	39	32
3	EtSNa (6)	DMF	130	44	64
4	BBr ₃ (4)	CH ₂ Cl ₂	-78 °C then reflux	2	81

The next objectives undertaken were the preparation of intermediate (**R**)-**89** and assessment of enantioselectivity *via* chiral HPLC analysis of the enantiomeric ratio (*er*). Firstly, nitrostyrene **86** was subjected to conjugate addition with dimethyl malonate under basic conditions using triethylamine to provide intermediate **89** in 60% yield for utility as a HPLC calibrant (Scheme 29). An enantioselective Michael addition of dimethyl malonate to nitrostyrene **86** catalysed by *O*-desmethyl quinidine (**87**) was then performed. Cinchona alkaloid-derived compound **87** was developed by Deng and co-workers as a bifunctional organocatalyst for enantioselective conjugate additions.^{204–208} *O*-Desmethyl quinidine (**87**) is reported to adopt a *gauche*-open conformation and a network of hydrogen bonding interactions is formed between the quinuclidine moiety of **87** and the Michael donor, and between the phenolic hydroxy moiety of **87** and both the Michael donor and acceptor (Figure 31). These interactions orientate and stabilise the transition state facilitating enantioselectivity. In the first instance, nitrostyrene **86** was treated with dimethyl malonate and *O*-desmethyl quinidine (**87**) (5 mol%) in tetrahydrofuran at $-20\text{ }^{\circ}\text{C}$. However, ^1H NMR spectroscopy indicated that the reaction stopped at 74% conversion of **86** after 18 h. Addition of 5 mol% **87** produced only a marginal increase to 81% conversion by 42 h and the desired product (**R**)-**89** was subsequently isolated in 72% yield. Given the importance of hydrogen bonding to the transition state it was proposed that an elevated reaction mixture concentration would promote reactivity. As such, an additional reaction was performed using twenty-fold larger scale (4 mmol) and five-fold higher concentration (0.5 M) with a decreased catalyst loading of 3 mol% **87**. Under these conditions, full reaction of nitrostyrene **86** was observed after 16 h and intermediate (**R**)-**89** was afforded with a 94 : 6 enantiomeric ratio and in 81% yield (Scheme 29) (Appendix III).



Scheme 29 – Synthesis of intermediates (**R**)-**89** and **89**

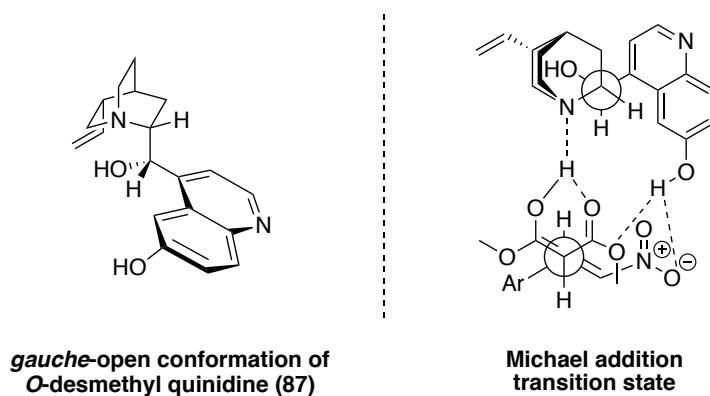
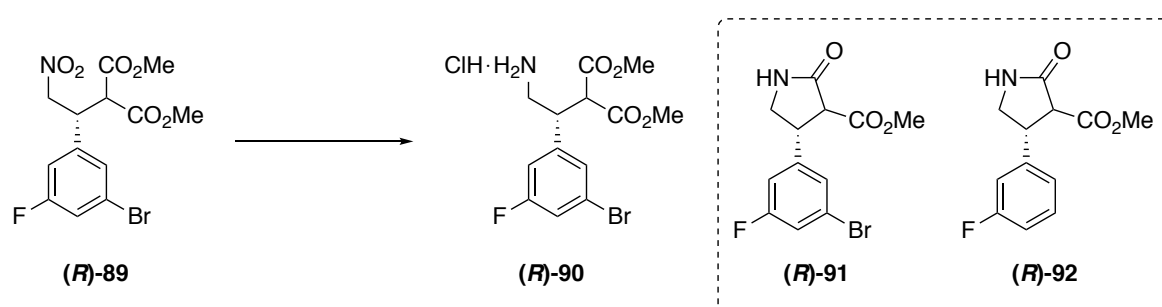


Figure 31 – Gauche-open conformer of O-desmethyl quinidine (**87**) and resultant transition state of enantioselective Michael addition

With a synthetic approach established for the preparation of intermediate (**R**)-**89** in good yield and high enantioselectivity, conditions for reduction of the nitro functionality were investigated (Table 16). Initially, intermediate (**R**)-**89** was treated with zinc and hydrochloric acid in ethanol at room temperature (entry 1). After 24 h, no reaction was observed and subsequent elevation of the reaction temperature to 60 °C produced a complex mixture of compounds which did not include starting material (**R**)-**89** or amine (**R**)-**90**. Switching the solvent to methanol allowed for a four-fold higher reaction mixture concentration (0.2 M) to be employed with zinc and hydrochloric acid (entry 2). However, again no reaction took place at room temperature and successive stirring under reflux afforded a complex mixture of unidentified compounds. Subsequent applications of zinc with acetic acid, and iron with hydrochloric acid also resulted in a mixture of unidentified compounds, likely formed *via* decomposition of the starting material (**R**)-**89** (entries 3 and 4). In addition to these conditions derived from the Béchamp reduction, an attempt to prepare amine (**R**)-**90** was carried out using tin(II) chloride in ethyl acetate under reflux (entry 5).^{209,210} Under these conditions, a complex mixture was again formed which did not contain the desired product. Only partial separation of the crude mixture was achieved by flash column chromatography, but this permitted tentative identification of lactam (**R**)-**91** as one of the major side-products. In work by Benaglia and co-workers, the use of trichlorosilane and Hünig's base was reported as a metal-free procedure applicable to the reduction of aliphatic nitro compounds.^{211,212} Submission of intermediate (**R**)-**89** to these conditions also generated an inseparable mixture of unidentified compounds (entry 6). Next, the decision was made to attempt hydrogenation of (**R**)-**89** with Raney nickel under 2 bar of pressure

using a Parr shaker apparatus however, no reaction was detected and only starting material was recovered after 4 h (entry 7). Further examination of the literature provided an alternative nickel-catalysed procedure, which was employed for the reduction of nitroalkanes analogous to **(R)**-89 in the synthesis of *(R)*-baclofen and *(R)*-rolipram.^{213,214} Consequently, **(R)**-89 underwent reduction using nickel boride and hydrogen formed *in situ* from reaction of nickel(II) chloride and sodium borohydride in methanol (entry 8). After stirring for only 0.5 h at room temperature, full reaction of **(R)**-89 was observed by TLC and ¹H NMR spectroscopy. Following flash column chromatography, ¹H NMR and mass spectroscopy revealed that the product contained a 1 : 2.3 ratio of lactams **(R)**-91 and **(R)**-92. Further chromatographic separation of these lactams was not possible due to similar retention on silica.

Table 17 – Attempted synthesis of amine intermediate **(R)**-90



Entry	Reagents (equiv.)	Solvent	Temp. and Time	Outcome
1	Zn (5), HCl (2)	EtOH	rt, 24 h then 60 °C, 46 h	complex mixture
2	Zn (5), HCl (2)	MeOH	rt, 20 h then reflux, 19 h	complex mixture
3	Zn (5), AcOH (5)	MeOH	60 °C, 20 h	complex mixture
4	Fe (5), HCl (2)	MeOH	rt, 24 h	complex mixture
5	SnCl ₂ ·2H ₂ O (5)	EtOAc	reflux, 20 h	complex mixture containing (R) -91
6	HSiCl ₃ (3.5), DIPEA (5)	CH ₂ Cl ₂	0 °C to rt, 16 h	complex mixture
7	H ₂ [2 bar], Raney Ni	MeOH	rt, 4 h	no reaction observed
8	NiCl ₂ ·6H ₂ O (2), NaBH ₄ (11)	MeOH	rt, 0.5 h	1 : 2.3 mixture of (R) -91 : (R) -92

After evaluation of the reaction conditions screened thus far, employment of nickel boride for the reduction of intermediate **(R)-89** displayed the most promise for further development. As such, it was proposed that lactam **(R)-91** would be prepared directly from **(R)-89** in a single synthetic procedure. Therefore, optimisation of the reaction conditions would be required to limit reduction of the C–Br bond within intermediate **(R)-89**. However, subsequent attempts carried out at lower temperatures of 0 °C and –20 °C produced complex mixtures and only partial reaction of starting material **(R)-89**.

This prompted a comparison of the attempts to reduce intermediate **(R)-89** described in this work with the reduction of analogous nitroalkane **81** in the distinct syntheses of [¹⁸F]SynVesT-1 ([¹⁸F]**(R)-24**) reported by Constantinescu and Huang.^{152,153} Under the reaction conditions employed by Constantinescu *et al.*, using iron and hydrochloric acid in ethanol, nitroalkane **81** underwent reduction to the desired amine **82** in 70% yield (Scheme **26**) whilst intermediate **(R)-89** generated a complex mixture of inseparable compounds. Following evaluation of the chemical structure of nitroalkanes **(R)-89** and **81**, it is not clear why these compounds react in such a different manner.

2.2.3 Revision of Synthetic Strategy

Given the difficulties encountered in attempts to prepare amine **(R)-90** and lactam **(R)-91** thus far, an alternative approach was sought for the enantioselective synthesis of [¹⁸F]SynVesT-1 ([¹⁸F]**(R)-24**) which would not involve the use of dimethyl malonate. It was proposed that asymmetric organocatalysis would be exploited once again in this secondary route due to the high degree of enantioselectivity than can be achieved using chiral organocatalysts, as exemplified in the first synthetic route. Notably, concurrent with production of this thesis, Benjamin List and David W.C. MacMillan were awarded the Nobel Prize in Chemistry 2021 for the development of asymmetric organocatalysis.²¹⁵ In 2000, seminal work by the independent research groups of List and MacMillan described the use of proline and chiral imidazolidinone organocatalysts, respectively for novel enantioselective transformations.^{216,217} These pioneering studies initiated the rapid growth and establishment of organocatalysis as the third field within asymmetric synthesis, alongside transition metal and enzymatic catalysis, over the last two

decades.^{218–220} Subsequently, numerous chiral amine organocatalysts have been developed including the diarylprolinol silyl ethers **(S)**-93 and **(S)**-94, first reported by the Jørgensen and Hayashi research groups simultaneously in 2005 (Figure 32).^{221,222} Since their discovery, the Jørgensen-Hayashi catalysts including **(R)**-93 and **(R)**-94, and numerous diarylprolinol silyl ether derivatives have been widely employed as versatile and highly enantioselective organocatalysts in the synthesis of complex natural products and pharmaceuticals.^{223–225}

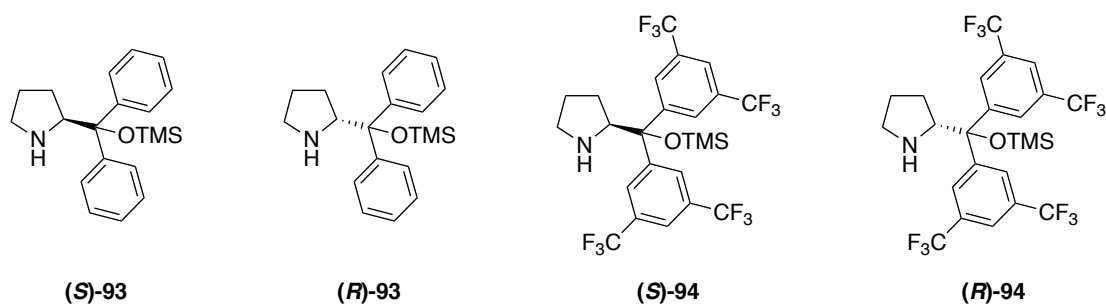
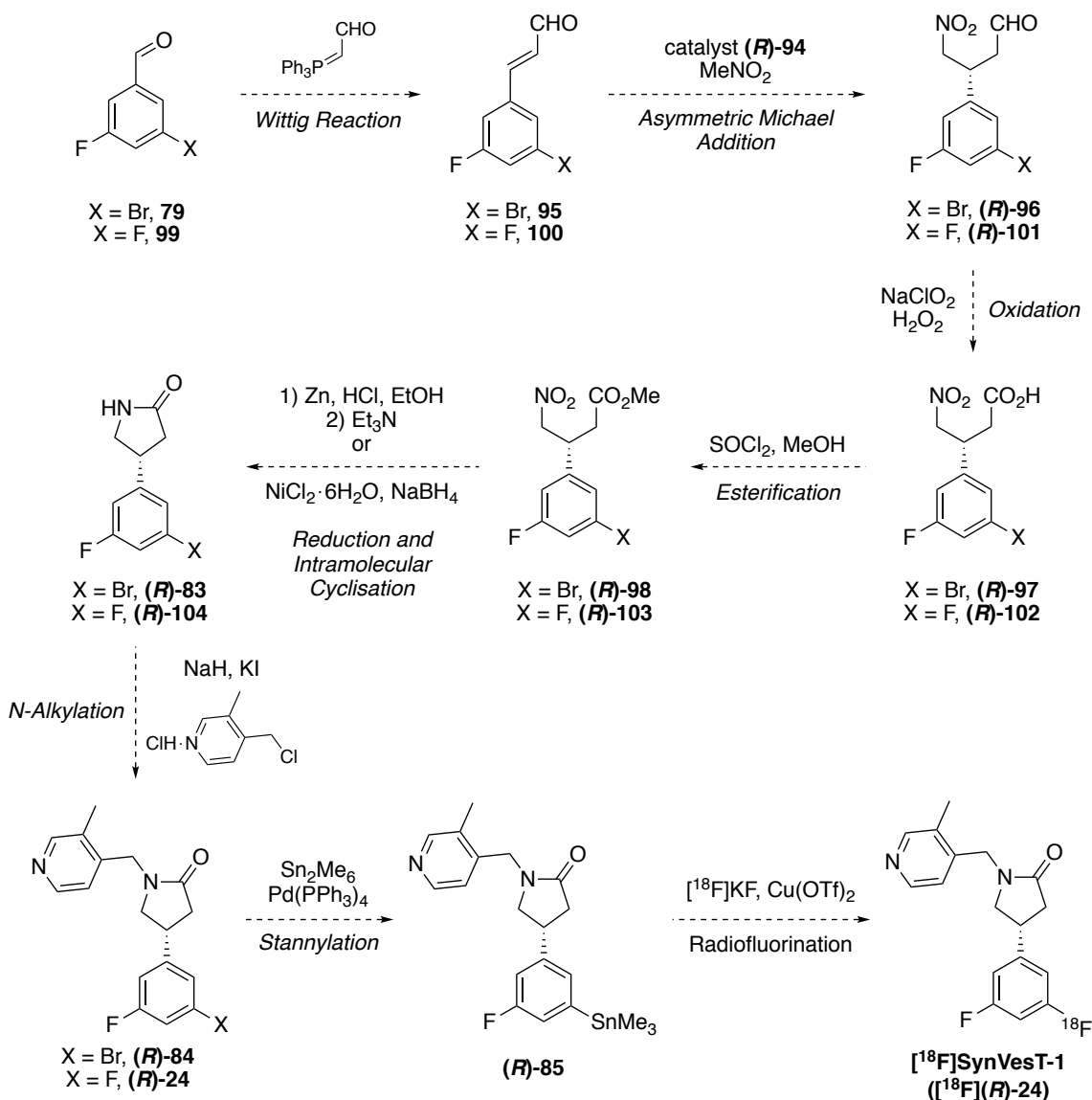


Figure 32 – Jørgensen-Hayashi diarylprolinol silyl ether organocatalysts

Based on literature precedent, a novel enantioselective synthetic route to [¹⁸F]SynVesT-1 ([¹⁸F]**(R)**-24) exploiting enantioselective aminocatalysis at an early-stage was designed (Scheme 30). Initially, a Wittig reaction would be performed with benzaldehyde **79** and (triphenylphosphoranylidene)acetaldehyde to produce cinnamaldehyde **95**. Subsequently, the Jørgensen-Hayashi organocatalyst **(R)**-94 would be employed to mediate an asymmetric Michael addition of nitromethane to give α,β -unsaturated aldehyde **95**. The resultant aldehyde **(R)**-96 would then undergo successive Pinnick oxidation to the corresponding carboxylic acid **(R)**-97 using sodium chlorite and hydrogen peroxide. Esterification with thionyl chloride in methanol would afford methyl ester **(R)**-98. Given the structural similarity of nitroalkanes **(R)**-98 and **81**, it was anticipated that treatment of **(R)**-98 with zinc under acidic conditions and subsequent base-mediated intramolecular cyclisation would generate pyrrolidin-2-one **(R)**-83, in a similar manner to the synthesis of **83** from **81** by Constantinescu *et al.*¹⁵² Furthermore, it was proposed that the preparation of pyrrolidin-2-one **(R)**-83 in a single step would be investigated through application of nickel(II) chloride and sodium borohydride. As previously described in Section 2.2.1, submission of pyrrolidin-2-one **(R)**-83 to *N*-alkylation with 4-(chloromethyl)-3-methylpyridine hydrochloride, and palladium-catalysed stannylation with hexamethylditin would subsequently afford the desired organotin

precursor **(R)**-85. Throughout development of a fluorine-18 radiolabelling procedure for the synthesis of [¹⁸F]SynVesT-1 (**[¹⁸F]**(**R**)-24), it would be necessary to confirm the identity and purity of the isolated product by comparison of chromatographic retention time (*t_r*) with the equivalent fluorine-19 analogue using analytical HPLC. Therefore, this synthetic route would also be performed starting with 3,5-difluorobenzaldehyde (**99**) for preparation of the non-radioactive HPLC standard SynVesT-1 (**(R)**-24) (Scheme 30).



Scheme 30 – Revised proposal for enantioselective synthesis of SynVesT-1 (**(R)**-24) and [¹⁸F]SynVesT-1 (**[¹⁸F]**(**R**)-24)

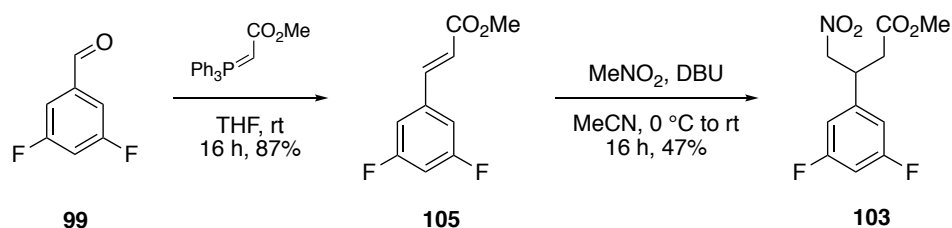
2.2.4 Racemic Synthetic Route to MNI-1038 (**24**) and [¹⁸F]MNI-1038 ([¹⁸F]**24**)

With a novel enantioselective strategy devised for the synthesis of SynVesT-1 ((*R*)-**24**), organotin precursor (*R*)-**85** and subsequently [¹⁸F]SynVesT-1 ([¹⁸F](*R*)-**24**), the decision was made to prioritise preparation of the corresponding racemates MNI-1038 (**24**), precursor **85** and [¹⁸F]MNI-1038 ([¹⁸F]**24**). The basis of this decision was multifaceted. Firstly, preparation of these racemic compounds *via* a complimentary route would facilitate optimisation of the synthetic procedures succeeding formation of nitroalkanes **98** and **103** without using valuable chiral material. In addition, this would generate racemic analytical standards for evaluation of enantioselectivity in the subsequent asymmetric synthetic route *via* chiral HPLC. Ultimately, *in vivo* kinetics studies of both [¹⁸F]SynVesT-1 ([¹⁸F](*R*)-**24**) and [¹⁸F]MNI-1038 ([¹⁸F]**24**) would be performed *via* dynamic PET imaging for development of a quantitative PET imaging technique for the SV2A protein. However, it would be preferable to perform optimisation of the copper-mediated nucleophilic radiofluorination reaction conditions using the racemate organotin precursor **85** generating [¹⁸F]MNI-1038 ([¹⁸F]**24**) before attempting the synthesis of [¹⁸F]SynVesT-1 ([¹⁸F](*R*)-**24**).

2.2.4.1 Synthesis of MNI-1038 (**24**)

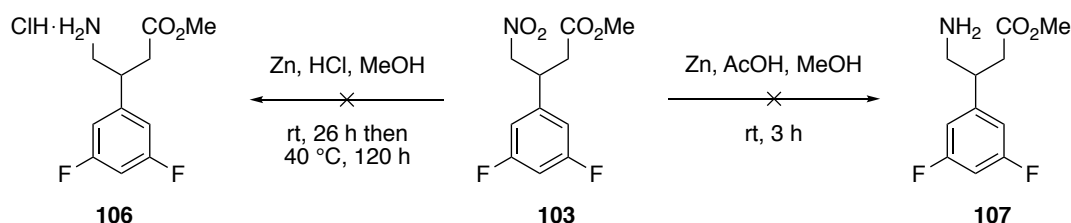
The synthesis of MNI-1038 (**24**) began with a Wittig olefination of commercially available 3,5-difluorobenzaldehyde (**99**) with methyl (triphenylphosphoranylidene)acetate under mild conditions to provide multigram quantities of methyl cinnamate **105** in 87% yield (Scheme **31**). As previously discussed in Section 2.1.4, the phosphonium ylide employed in this Wittig reaction is resonance stabilised and consequently gave **105** as the *E*-alkene. The geometry of the isolated alkene **105** was confirmed by ¹H NMR spectroscopy, which showed two doublets with vicinal *trans* coupling constants of 16.0 Hz. Notably, an initial attempt to prepare **105** using an elevated reaction temperature of 50 °C produced a complex mixture of unidentified side-products. Following a literature procedure from Constantinescu *et al.*, the α,β-unsaturated methyl ester functionality of methyl cinnamate **105** then underwent conjugate addition with nitromethane in the presence of a strong base, 1,8-diazabicyclo[5.4.0]undec-7-ene (DBU), to afford nitroalkane **103** (Scheme **31**).¹⁵² In the first instance, numerous side-products were generated and purification of **103** was attempted by flash column chromatography

using an eluant system comprised of ethyl acetate and petroleum ether (40–60). However, co-elution of nitroalkane **103** with an unknown side-product was observed by ^1H NMR spectroscopy of the isolated product. During a subsequent reaction under the same conditions, further investigation revealed that this impurity exhibited identical retention on silica to nitroalkane **103**, except when elution was performed with dichloromethane in hexane. Application of these conditions enabled isolation of nitroalkane **103** in 47% yield.



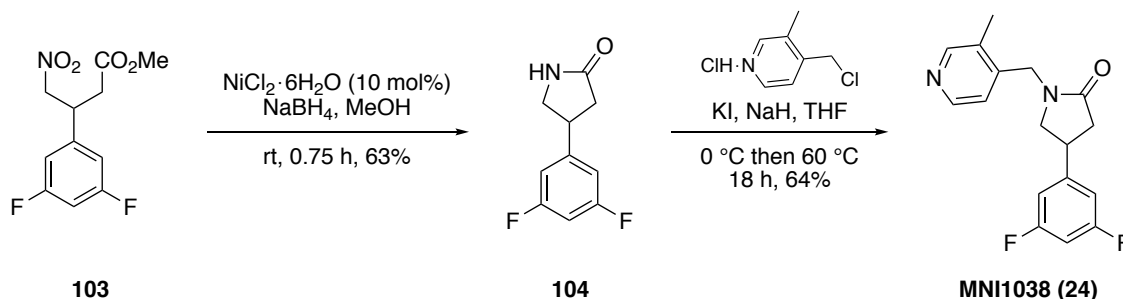
Scheme 31 – Synthesis of intermediates **105** and **103**

Following preparation of nitroalkane **103** at gram-scale, the next objective was to identify suitable reaction conditions for reduction of the nitro functionality. Initially, employment of zinc powder under acid conditions was examined (Scheme **32**). In the first instance, nitroalkane **103** was treated with zinc and hydrochloric acid at room temperature however, no reaction was observed by ^1H NMR spectroscopy after 26 h. Consequently, the reaction temperature was increased to 40 °C which produced a complex mixture of compounds after 120 h that did not include the desired amine **106**. In contrast, employment of zinc in the presence of acetic acid facilitated full reaction of nitroalkane **103** in 3 h at room temperature. Nonetheless, a complex mixture of compounds was also generated under these conditions and so an alternative procedure was sought.



Scheme 32 – Attempts to reduce nitroalkane **103** using zinc under acid conditions

With the previous attempts to reduce nitroalkane (**R**)-**89** (Table 16, Section 2.2.2) in mind, it was anticipated that pyrrolidin-2-one **104** could be prepared directly from nitroalkane **103** through a one-pot, two-step procedure catalysed by nickel boride. Given that this synthetic procedure would be subsequently employed for reduction of nitroalkane **98**, containing a C–Br bond liable to reduction, the decision was made to use catalytic quantities of nickel boride. Subsequent reaction of nickel(II) chloride (10 mol%) and sodium borohydride (5 equiv.) in methanol provided nickel boride and hydrogen gas, which in turn mediated efficient reduction and intramolecular cyclisation of nitroalkane **103** to afford pyrrolidin-2-one **104** in 63% yield (Scheme 33). The final stage in the synthesis of MNI-1038 (**24**) was the sodium hydride-mediated N-alkylation of pyrrolidin-2-one **104** with 4-(iodomethyl)-3-methylpyridine, which was formed *in situ* via a Finkelstein-type reaction of 4-(chloromethyl)-3-methylpyridine hydrochloride and potassium iodide.²²⁶ Generation of the weaker alkyl C–I bond, relative to the corresponding C–Cl bond, was exploited to promote nucleophilic attack of pyrrolidin-2-one **104** via an S_N2 reaction. After stirring in tetrahydrofuran at 60 °C for 18 h, MNI-1038 (**24**) was isolated in 64% yield and sufficient quantity for application as an analytical HPLC standard (Scheme 33).

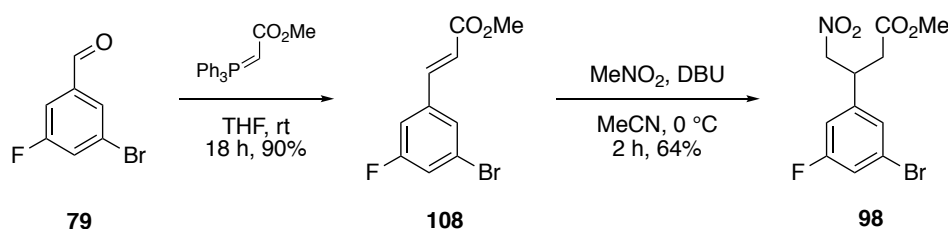


Scheme 33 – Synthesis of MNI-1038 (**24**) via pyrrolidin-2-one **104**

2.2.4.2 Synthesis of **85**: Precursor to [¹⁸F]MNI-1038 ([¹⁸F]**24**)

The synthetic route established for the preparation of MNI-1038 (**24**) was then employed for the synthesis of organotin precursor **85** as a racemic mixture. Firstly, a Wittig reaction of commercially available 3-bromo-5-fluorobenzaldehyde (**79**) and methyl (triphenylphosphoranylidene)acetate under the previously determined conditions gave *E*-alkene **108** in 82% yield. As expected, ¹H NMR spectroscopy of the isolated product showed two doublets with vicinal *trans* coupling constants of 16.0 Hz. In addition, this procedure was consistently high yielding and subsequent

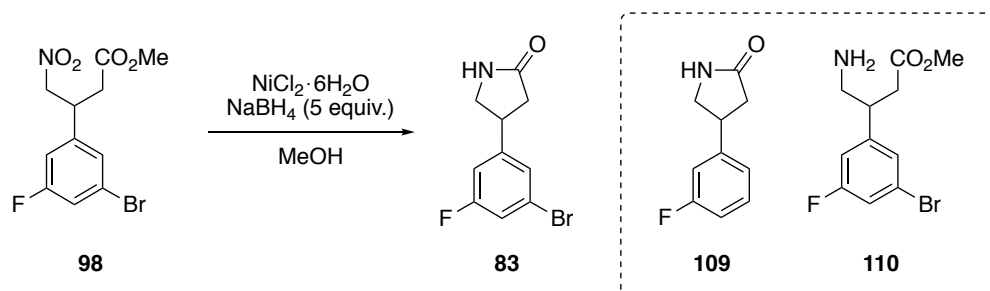
reactions performed at multigram scale under these conditions provided methyl cinnamate **108** in 90% yield (Scheme 34). Next, methyl cinnamate **108** underwent conjugate addition with nitromethane in the presence of DBU to give nitroalkane **98**. Given the side-products and moderate yields obtained during the analogous synthesis of nitroalkane **103**, it was proposed that additional control would be exerted over the addition of DBU and the reaction temperature in this instance. It was found that, on a small scale (1.48 mmol), the dropwise addition of DBU over 1 h at 0 °C, followed by a 2 h reaction facilitated full reaction of methyl cinnamate **108**, and preparation of nitroalkane **98** in 64% yield (Scheme 34). Subsequently, the reaction was performed on a twenty-fold larger scale (30.1 mmol), in which DBU was added dropwise over 1.5 h at 0 °C and then stirred for 2 h. The reaction mixture was then promptly warmed to room temperature and full reaction of **108** was observed after 3 h. Under these conditions modified for larger scale synthesis, multigram quantities of nitroalkane **98** were produced in 53% yield.



Scheme 34 – Synthesis of intermediates **108** and **98**

The next stage in the synthesis of precursor **85** was reduction and intramolecular cyclisation of **98** to give pyrrolidin-2-one **83** (Table 17). Following the previously devised procedure, nitroalkane **98** was treated with nickel(II) chloride (10 mol%) and sodium borohydride (5 equiv.) in methanol at room temperature. After only 0.25 h, starting material **98** was no longer observed by TLC and so the reaction was quenched to prevent production of side-product **109** *via* C–Br bond reduction. However, pyrrolidin-2-one **83** was subsequently isolated in only 39% yield which prompted the decision to attempt optimisation of this procedure (entry 1). Multiple side-products were detected by TLC under these initial conditions and so, it was proposed that a lower concentration reaction mixture could decrease the prevalence of undesired side-reactions. However, subsequent attempts carried out at lower concentrations of 0.02 M and 0.1 M resulted in no reaction or facilitated only partial reaction of nitroalkane **98** (entries 2 and 3). Following a literature procedure,

preparation of the active nickel boride catalyst prior to addition of nitroalkane **98** was also found to result in low levels of conversion to the desired product and led to a 1 : 0.15 mixture of **98** to **83** even after 18 h (entry 4).²²⁷ It was found that reducing the reaction mixture temperature to 0 °C for the duration of sodium borohydride addition followed by stirring at room temperature enabled full reaction of nitroalkane **98** after 0.25 h and fewer side-reactions were observed by TLC. Nonetheless, this method was not conducive to improvement of the yield and pyrrolidin-2-one **83** was afforded in only 23% yield (entry 5). Next, this two-step, one-pot reaction was performed employing alternative catalyst loadings of 5, 20 and 30 mol% (entries 6–8). Application of 5 mol% nickel(II) chloride produced a mixture of numerous compounds after 2 h from which pyrrolidin-2-one **83** was isolated in only 27% yield (entry 6). Employment of 20 and 30 mol% nickel(II) chloride facilitated full reaction of nitroalkane **98** after 0.25 h. However, ¹H NMR spectroscopy of the crude material revealed that pyrrolidin-2-one **83** was the minor product in each mixture. Notably, subsequent evaporation of the NMR solvent at 45 °C *in vacuo* for 1.5 h was found to facilitate production of pyrrolidin-2-one **83** as the major component. Therefore, it was suggested that the major product initially obtained under these conditions was the uncyclised amine **110**, which then underwent intramolecular cyclisation to give pyrrolidin-2-one **83** when heated to 45 °C *in vacuo*. Regrettably, the use of 20 and 30 mol% nickel(II) chloride afforded inseparable mixtures of pyrrolidin-2-one **83** and debrominated analogue **109** (entries 7 and 8). Given the insights gained, it was proposed that the isolated yields of pyrrolidin-2-one **83** described in entries 1 and 5 were lower than anticipated due to partial cyclisation of amine **110** following full reduction of nitroalkane **98**. Subsequently, nitroalkane **98** was treated with 10 mol% nickel(II) chloride and sodium borohydride at room temperature for 0.25 h on a sixteen-fold larger scale (3.19 mmol). The resultant amine intermediate **110** then underwent intramolecular cyclisation at 45 °C *in vacuo* for 1.5 h. Pyrrolidin-2-one **83** was subsequently isolated in approximately 52% yield, although contained 9% **109** which could not be removed *via* flash column chromatography (entry 9).

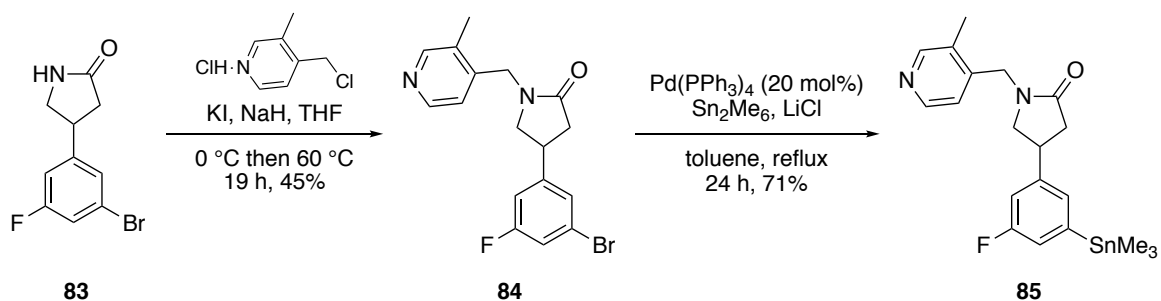
Table 18 – Synthesis of pyrrolidin-2-one **83**

Entry	Equiv. of $\text{NiCl}_2 \cdot 6\text{H}_2\text{O}$	Reaction Conc.	Temp. and Time	Outcome
1	10 mol%	0.2 M	rt, 0.25 h	39% yield
2	10 mol%	0.02 M	rt, 2 h	no reaction ^a
3	10 mol%	0.1 M	rt, 28 h	1 : 1 mixture of 98 : 83 ^a
4	10 mol% ^b	0.2 M	rt, 18 h	1 : 0.15 mixture of 98 : 83 ^a
5	10 mol%	0.2 M	0 °C then rt, 0.25 h	23% yield
6	5 mol%	0.2 M	rt, 2 h	27% yield
7	20 mol%	0.2 M	rt, 0.25 h ^c	1 : 0.13 mixture of 83 : 109 ^a
8	30 mol%	0.2 M	rt, 0.25 h ^c	1 : 0.17 mixture of 83 : 109 ^a
9	10 mol%	0.2 M	rt, 0.25 h ^c	52% yield (1 : 0.10 mixture of 83 : 109 ^a)

^aDetermined using ^1H NMR spectroscopy. ^bNickel(II) chloride (10 mol%) and sodium borohydride (1.5 equiv.) were stirred in methanol at rt for 0.5 h prior to addition of nitroalkane **98** and sodium borohydride (3.5 equiv.). ^cIntramolecular cyclisation of amine **110** achieved *via* heating to 45 °C *in vacuo* for 1.5 h.

Pyrrolidin-2-one **83** was then submitted to *N*-alkylation with 4-(chloromethyl)-3-methylpyridine hydrochloride using potassium iodide and sodium hydride as previously described. Employment of these conditions allowed for the preparation of intermediate **84** in 45% yield (Scheme 35). Subsequently, whilst performing this reaction on a multigram scale, liquid/liquid extraction of the reaction mixture proved challenging due to an emulsion, likely formed by residual mineral oil. Consequently, intermediate **84** was isolated in a slightly diminished yield of 37% and it was proposed that sodium hydride would be subjected to washing with hexane prior to

usage in all successive reactions at large scale. It is worth noting that intermediate **84** and the corresponding debrominated compound could not be fully separated by chromatographic purification at this stage. Intermediate **84** then underwent palladium-catalysed stannylation using hexamethylditin and tetrakis(triphenylphosphine)palladium(0) (20 mol%) in the presence of lithium chloride to give **85** in 37% yield at first attempt. Notably, a debrominated side-product was isolated in 30% yield which was significantly higher than anticipated. This indicated that following oxidative insertion of the palladium(0) catalyst to the C–Br bond, transmetalation with hexamethylditin proceeded slowly resulting in significant protodepalladation. Given that hexamethylditin is liable to oxidation in air, it was proposed that the distannane utilised for this reaction had undergone partial degradation in storage and an alternative supply was purchased.^{228,229} Repetition of this procedure employing an alternative batch of hexamethylditin was subsequently performed at an approximately three-fold larger scale (1.64 mmol) and resulted in the synthesis of organotin precursor **85** in 71% yield (Scheme 35). Under these conditions, sufficient quantities of **85** were prepared for subsequent development of a radiofluorination procedure for the synthesis of [¹⁸F]MNI-1038 ([¹⁸F]**24**).

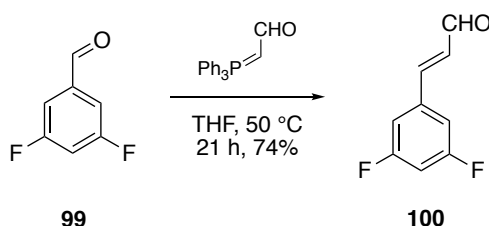


Scheme 35 – Synthesis of intermediate **84** and organotin precursor **85**

2.2.5 Revised Enantioselective Synthetic Route to SynVesT-1 ((*R*)-24) and [¹⁸F]SynVesT-1 ([¹⁸F](*R*)-24)

2.2.5.1 Enantioselective Synthesis of SynVesT-1 ((*R*)-24)

In parallel with the development of a radiofluorination procedure using racemates MNI-1038 (**24**) and organotin precursor **85**, the enantioselective synthesis of SynVesT-1 ((*R*)-24) and (*R*)-85 was investigated. The first objective in the synthesis of SynVesT-1 ((*R*)-24) was preparation of cinnamaldehyde **100** from commercially available 3,5-difluorobenzaldehyde (**99**) and (triphenylphosphoranylidene)acetaldehyde *via* a Wittig reaction. In the first instance, residual **99** was observed by TLC after stirring in tetrahydrofuran at room temperature for 16 h. To accelerate this Wittig olefination, the temperature of the reaction mixture was increased to 50 °C, which facilitated full conversion of **99** to **100** after an additional 26 h, and subsequent isolation of cinnamaldehyde **100** in 58% yield. Herein, this reaction was performed at 50 °C for 21 h to prepare multigram quantities of cinnamaldehyde **100** in 74% yield (Scheme 36). The phosphonium ylide employed in this Wittig reaction is resonance stabilised by the adjacent carbonyl and therefore selectively afforded **100** as the *E*-alkene. The geometry of **100** was confirmed by ¹H NMR spectroscopy, in which the α- and β-hydrogen atoms relative to the carbonyl share a vicinal *trans* coupling constant of 16.0 Hz.



Scheme 36 – Synthesis of cinnamaldehyde **100** *via* a Wittig reaction

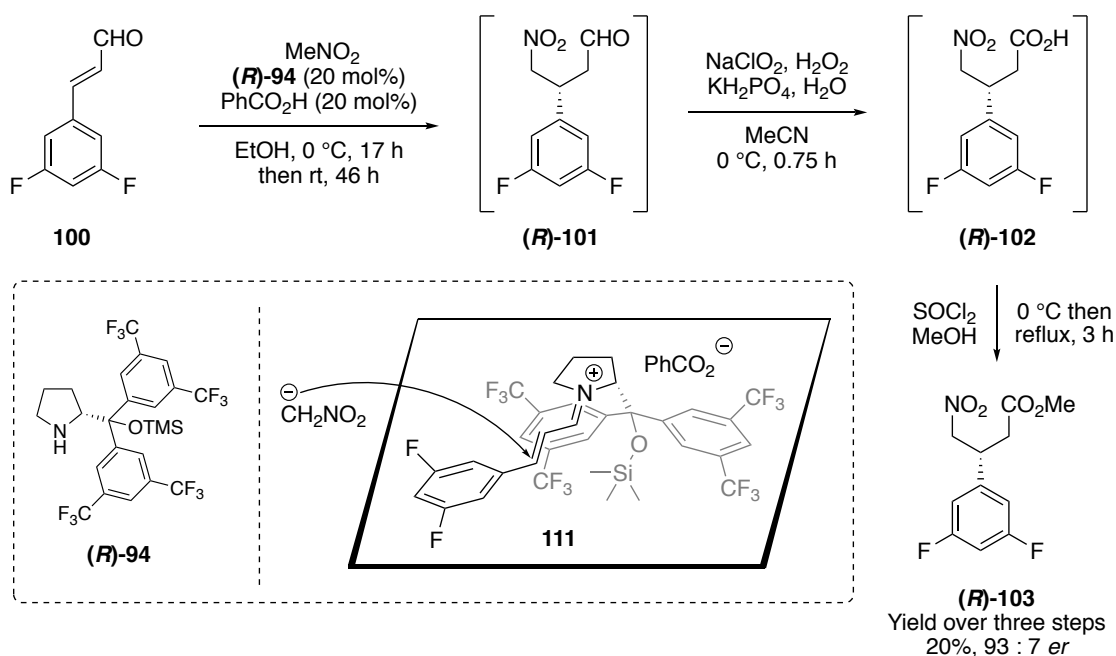
Conditions for the asymmetric Michael addition of nitromethane to cinnamaldehyde **100** exploiting Jørgensen-Hayashi organocatalyst (*R*)-94 were then explored. In this reaction, condensation of secondary amine organocatalyst (*R*)-94 with the carbonyl of cinnamaldehyde **100** generates an α,β-unsaturated iminium ion **111** in the presence of an acidic cocatalyst (Scheme 37 inset). Formation of this iminium

intermediate lowers the lowest unoccupied molecular orbital (LUMO) energy and increases the electrophilicity of the β -position, relative to α,β -unsaturated aldehyde **100**. Consequently, the decreased energy gap between the LUMO of iminium ion **111** and the highest occupied molecular orbital (HOMO) of nitromethane promotes the subsequent conjugate addition. The iminium ion **111** adopts an *E,E* configuration such that the difluorophenyl moiety points away from the bulky trimethylsilyl group to minimise unfavourable steric interactions. Furthermore, the pendant *meta*-trifluoromethyl-substituted phenyl moieties of catalyst **(R)-94** sterically hinder one diastereotopic face of the iminium ion **111**.^{223,230–234} Consequently, nucleophilic attack of nitromethane occurs at the β -position from the exposed *Re*-face to give the corresponding enamine intermediate. Subsequent hydrolysis regenerates catalyst **(R)-94** and affords the enantioenriched aldehyde **(R)-101**.

In 2007, Wang and co-workers reported a three-step asymmetric synthesis of (*R*)- and (*S*)-baclofen, a GABA_B receptor antagonist.²³⁵ Starting from 4-chlorocinnamaldehyde, the authors employed Jørgensen-Hayashi organocatalyst **(S)-93** (see Figure **32** for structure) to induce chirality in the first synthetic step *via* an enantioselective Michael addition of nitromethane. In this procedure, adapted from Hayashi's original method, Wang and co-workers used equal catalytic loadings of **(S)-93** (20 mol%) and cocatalyst benzoic acid (20 mol%) in ethanol at 0 °C to afford the corresponding conjugate addition product in 75% yield and 97% enantiomeric excess. It was proposed that this method would be suitable for the synthesis of aldehyde **(R)-101** using the alternative organocatalyst **(R)-94**, which was selected for utility in this work due to reports of increased reactivity and enantioselectivity compared with **(S)-93**.^{221,223}

However, application of these conditions using **(R)-94** (20 mol%) produced no reaction of cinnamaldehyde **100** after 17 h. Consequently, the reaction mixture was warmed to room temperature which facilitated full reaction of **100** after 46 h but resulted in significant side-reactions (Scheme **37**). Notably, in a preliminary attempt, aldehyde **(R)-101** was unstable when exposed to silica gel. Therefore, the decision was made to forgo chromatographic purification of **(R)-101** and the resultant carboxylic acid **(R)-102**, opting instead to purify the corresponding methyl ester **(R)-103**. As such, the reaction mixture underwent liquid/liquid extraction with acid and

then base, and the resultant intermediate **(R)-101** was submitted to a Pinnick oxidation without further purification. Oxidation of aldehyde **(R)-101** was achieved using sodium chlorite under mild acidic conditions and hydrogen peroxide, as a hypochlorous acid scavenger, after stirring at 0 °C for only 0.75 h.^{235,236} Following liquid/liquid extraction, carboxylic acid **(R)-102** was subjected to esterification with methanol and thionyl chloride under reflux for 3 h to afford nitroalkane **(R)-103** in 20% yield over three steps and with an enantiomeric ratio of 93 : 7, as determined by chiral HPLC (Appendix III). This reaction clearly exemplified that the Jørgensen-Hayashi organocatalyst **(R)-94** could be employed to produce aldehyde **(R)-101** in excellent enantiomeric purity however, alternative conditions were sought with the aim of diminishing side-reactions to increase the overall yield of nitroalkane **(R)-103**.

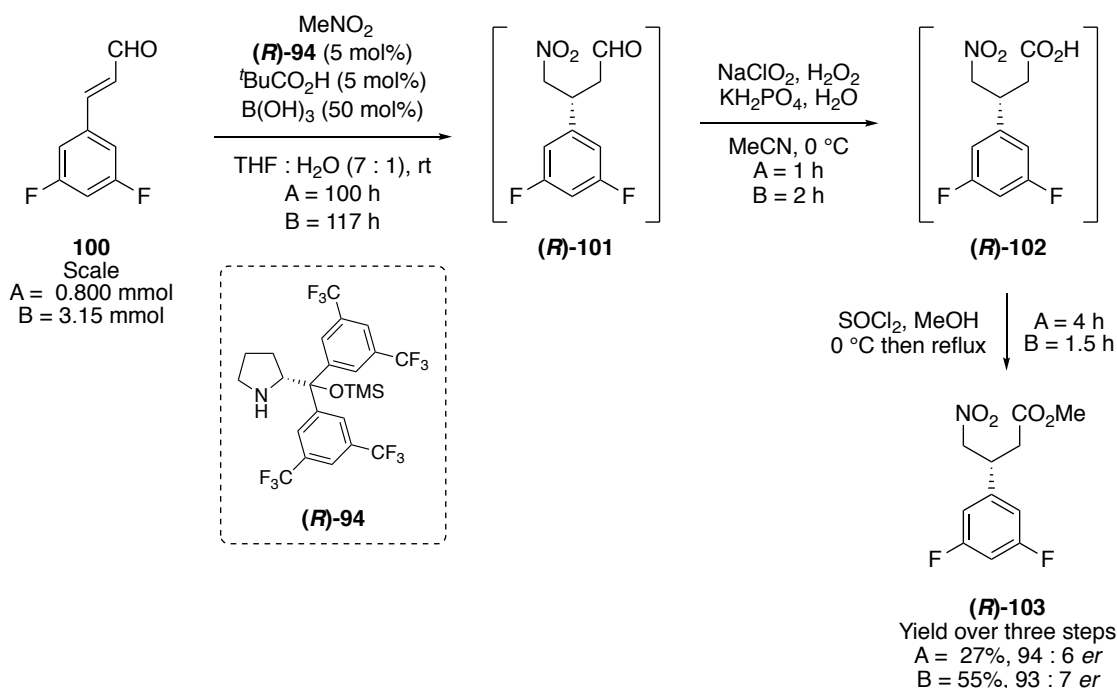


Scheme 37 – Initial enantioselective synthesis of nitroalkane **(R)-103** and stereochemical model of *Re*-face nucleophilic attack to iminium ion **111** (inset)

In 2010, Devine and co-workers at Merck developed an asymmetric synthesis of telcagepant, a CGRP receptor antagonist used for the treatment of migraine.²³⁷ A vital step in this synthetic route was enantioselective Michael addition of nitromethane to 2,3-difluorocinnamaldehyde, catalysed by Jørgensen-Hayashi organocatalyst **(S)-93** (see Figure 32 for structure). The authors reported that application of alcoholic solvents and benzoic acid cocatalyst as originally reported by Hayashi and co-workers resulted in significant side-reactions, and up to 24%

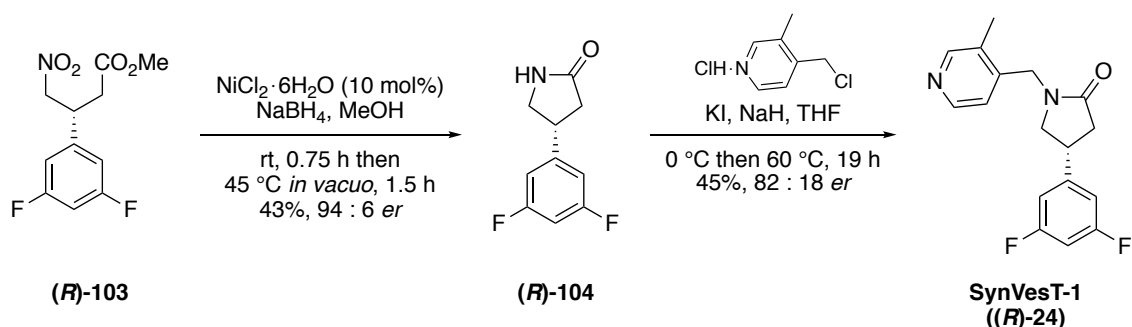
yield of side-products.²³⁸ In brief, detailed studies revealed that the use of pivalic and boric acids as dual-cocatalysts in aqueous tetrahydrofuran suppressed these side-reactions, and provided optimal reaction times and yields. Therefore, an attempt to prepare aldehyde **(R)-101** from cinnamaldehyde **100** was carried out using nitromethane (6 equiv.), organocatalyst **(R)-94** (5 mol%), pivalic acid (5 mol%) and boric acid (50 mol%) in a mixture of tetrahydrofuran and water (7 : 1) (Scheme **38**). On a 0.8 mmol scale, 95% conversion of **100** to **(R)-101** was observed by ¹H NMR spectroscopy after stirring at room temperature for 100 h. Crucially, no side-reactions were observed using ¹H NMR spectroscopy. As before, liquid/liquid extraction was employed to isolate intermediates **(R)-101** and **(R)-102** in sufficient purity for subsequent synthetic steps. Aldehyde **(R)-101** was then submitted to Pinnick oxidation with sodium chlorite and hydrogen peroxide at 0 °C for 1 h which facilitated 88% conversion to the corresponding carboxylic acid **(R)-102**. Subsequently, thionyl chloride-mediated esterification with methanol was performed and the desired nitroalkane **(R)-103** was isolated in 27% yield over three steps with a 94 : 6 *er* (Appendix III).

Given that these alternative conditions inhibited the production of side-products and afforded nitroalkane **(R)-103** in a slightly higher yield with excellent enantiomeric purity using a four-fold lower organocatalyst loading, this procedure was adopted for the subsequent synthesis of **(R)-103** (Scheme **38**). On an approximately four-fold larger scale, the enantioselective Michael addition of nitromethane to cinnamaldehyde **100** proceeded at a marginally slower rate and reached 83% conversion to aldehyde **(R)-101** after 100 h. However, no further significant progress was detected by 117 h with 85% conversion achieved. Subsequently, treatment of aldehyde **(R)-101** with Pinnick oxidation conditions provided full conversion to carboxylic acid **(R)-102** in 2 h, and esterification with methanol and thionyl chloride achieved 100% conversion after 1.5 h under reflux. Notably, these amended conditions allowed for the preparation of methyl ester **(R)-103** in an improved yield of 55% over three steps and excellent enantioselectivity (93 : 7 *er*) (Appendix III).



Scheme 38 – Alternate enantioselective synthesis of nitroalkane **(R)-103**

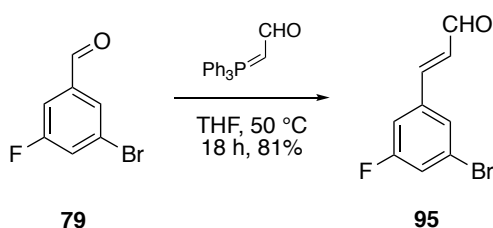
Pyrrolidin-2-one **(R)-104** was then prepared from nitroalkane **(R)-103** in 43% yield and 94 : 6 *er* via the nickel boride-catalysed one-pot, two-step procedure previously developed for nitro reduction and intramolecular cyclisation (Scheme 39). Next, *N*-alkylation of pyrrolidin-2-one **(R)-104** with 4-(chloromethyl)-3-methylpyridine hydrochloride was performed according to the previously described method to provide SynVesT-1 (**(R)-24**) in 45% yield however, a slight loss in enantiopurity was observed (82 : 18 *er*) (Appendix III). Nonetheless, SynVesT-1 (**(R)-24**) was prepared in sufficient quality and quantity for application as an analytical HPLC standard.



Scheme 39 – Synthesis of SynVesT-1 (**(R)-24**) via pyrrolidin-2-one **(R)-104**

2.2.5.2 Enantioselective Synthesis of (*R*)-85: Precursor to SynVesT-1 ((*R*)-24)

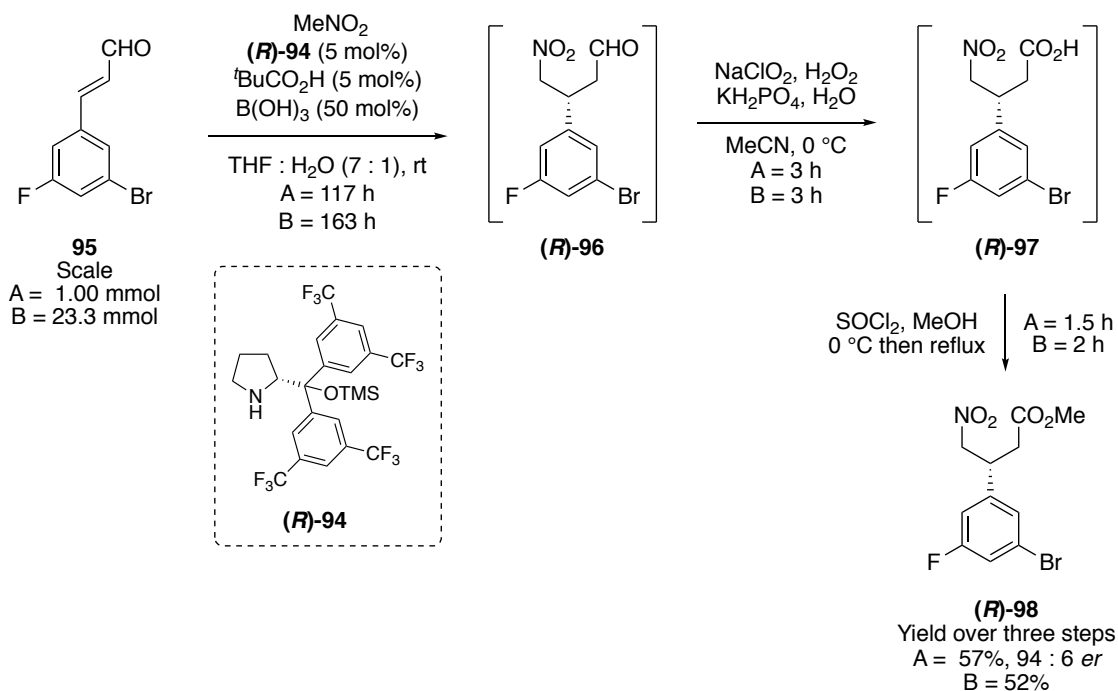
The novel asymmetric synthetic route developed for the preparation of SynVesT-1 ((*R*)-24) was then exploited for the final objective of this work, the enantioselective synthesis of organotin precursor (*R*)-85. Firstly, 3-bromo-5-fluorobenzaldehyde was reacted with (triphenylphosphoranylidene)acetaldehyde at 50 °C to afford multigram quantities of *E*-alkene **95** in 81% yield *via* a Wittig reaction (Scheme 40). As expected, ¹H NMR spectroscopy of **95** confirmed that the α- and β-hydrogen atoms relative to the carbonyl share a vicinal *trans* coupling constant of 16.0 Hz.



Scheme 40 – Synthesis of cinnamaldehyde **95** *via* a Wittig reaction

Cinnamaldehyde **95** then underwent enantioselective Michael addition of nitromethane using (*R*)-**94** (5 mol%), pivalic acid (5 mol%) and boric acid (50 mol%) in a mixture of tetrahydrofuran and water (7 : 1) (Scheme 41). On a 1 mmol scale, 100% conversion of **95** to aldehyde (*R*)-**96** was achieved after stirring at room temperature for 117 h and no side-products were observed by ¹H NMR spectroscopy. As before, liquid/liquid extraction was exploited to isolate intermediates (*R*)-**96** and (*R*)-**97** in sufficient purity for subsequent synthetic steps. Aldehyde (*R*)-**96** was then subjected to Pinnick oxidation using sodium chlorite and hydrogen peroxide at 0 °C for 3 h which facilitated 100% conversion to the corresponding carboxylic acid (*R*)-**97**. Finally, thionyl chloride-mediated esterification of (*R*)-**97** with methanol was performed under reflux which generated 100% conversion to methyl ester (*R*)-**98** after 1.5 h. Subsequently, nitroalkane (*R*)-**98** was isolated in 57% yield over three steps with an excellent enantiomeric ratio of 94 : 6 (Appendix III). Consequently, this procedure was repeated at a significantly larger scale (23.3 mmol) for the synthesis of nitroalkane (*R*)-**98** in multigram quantities. Notably, the enantioselective Michael addition of nitromethane to cinnamaldehyde **95** achieved 86% conversion to aldehyde (*R*)-**96** after 139 h but no further significant progress was detected by 163 h. Similarly, limited conversion was

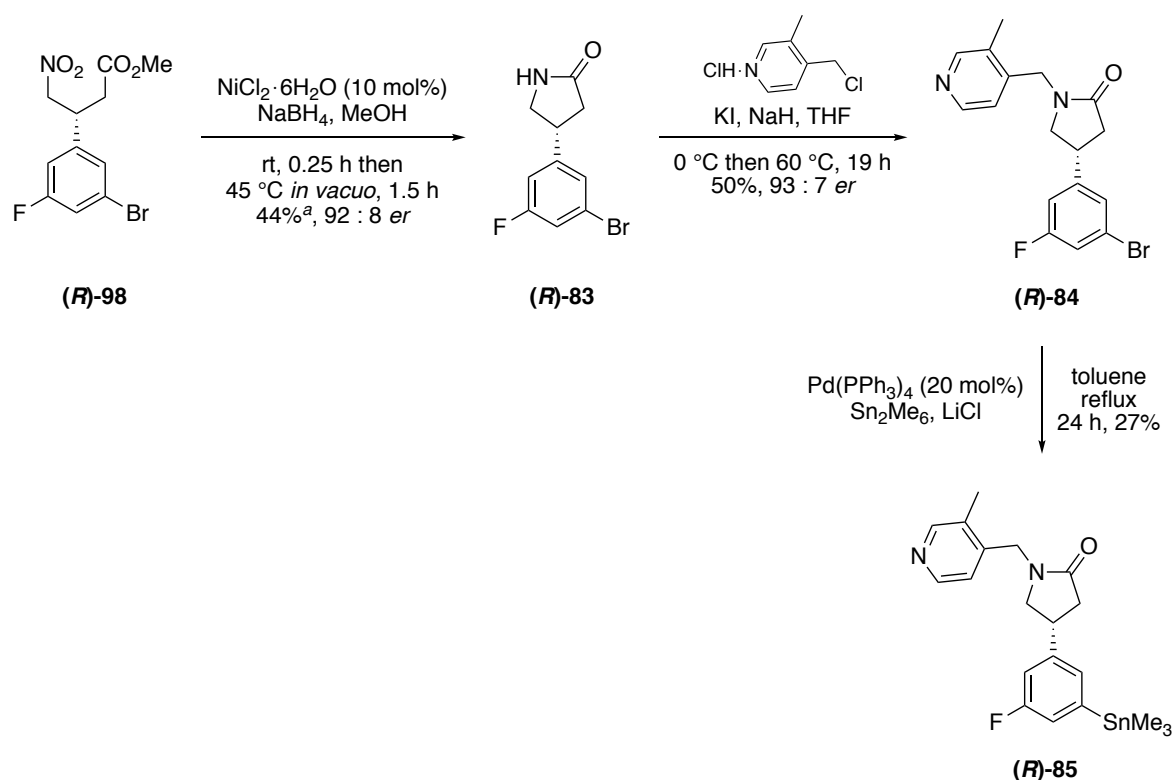
noted for the larger scale synthesis of aldehyde **(R)-101**. These results indicate that a slightly increased catalyst loading of **(R)-94** may be required to achieve full reaction of cinnamaldehydes **100** or **95** in subsequent enantioselective Michael additions performed at multigram scale. Nonetheless, successive treatment of aldehyde **(R)-96** with Pinnick oxidation and esterification conditions, as previously described, allowed for the preparation of nitroalkane **(R)-98** in 52% yield over three steps.



Scheme 41 – Enantioselective synthesis of nitroalkane **(R)-98**

Next, nitroalkane **(R)-98** was submitted to nickel boride-catalysed nitro reduction and intramolecular cyclisation *via* the one-pot, two-step procedure previously developed. The resultant pyrrolidin-2-one **(R)-83** was afforded in approximately 44% yield as a highly enantioenriched mixture (92 : 8 *er*) but also contained the debrominated equivalent **(R)-109** in a ratio of 1 : 0.18 (Scheme 42) (Appendix III). In this reaction, the addition of sodium borohydride was performed in four portions over ten minutes since nickel boride and hydrogen gas are produced in a vigorous exothermic reaction, as was the procedure at sub-molar scale. However, given the significantly larger scale of this reaction (12.2 mmol), this rate of addition generated a significant rise in temperature which may have promoted reduction of the C–Br bond resulting in a higher prevalence of the dehalogenated side-product **(R)-109**. Pyrrolidin-2-one **(R)-83** was then subjected to *N*-alkylation with 4-(chloromethyl)-3-

methylpyridine hydrochloride using potassium iodide and sodium hydride as previously described, except that the sodium hydride was washed with hexane prior to use, to circumvent the presence of mineral oil in subsequent purification. Under these conditions, intermediate **(R)-84** was prepared at gram scale in 50% yield with no detrimental impact on the enantiomeric ratio (93 : 7 *er*) (Appendix III). As before, it is worth noting that intermediate **(R)-84** and the corresponding debrominated compound could not be fully separated by chromatographic purification at this stage. Intermediate **(R)-84** then underwent palladium-catalysed stannylation using hexamethylditin and tetrakis(triphenylphosphine)palladium(0) (20 mol%) in the presence of lithium chloride to give organotin precursor **(R)-85**. Regrettably, the corresponding debrominated side-product formed *via* protodepalladation was isolated in a considerable 42% yield. Given that the conditions used in this instance were identical to those which gave racemate **85** in 71% yield, it was suggested that the alternative batch of hexamethylditin employed in this reaction was of lower purity potentially due to oxidative degradation in storage. Notwithstanding, the desired organotin precursor **(R)-85** was isolated in 27% yield. Furthermore, due to the nature of the chiral HPLC column it was deemed impracticable to determine the enantiomeric ratio of organotin precursor **(R)-85**.



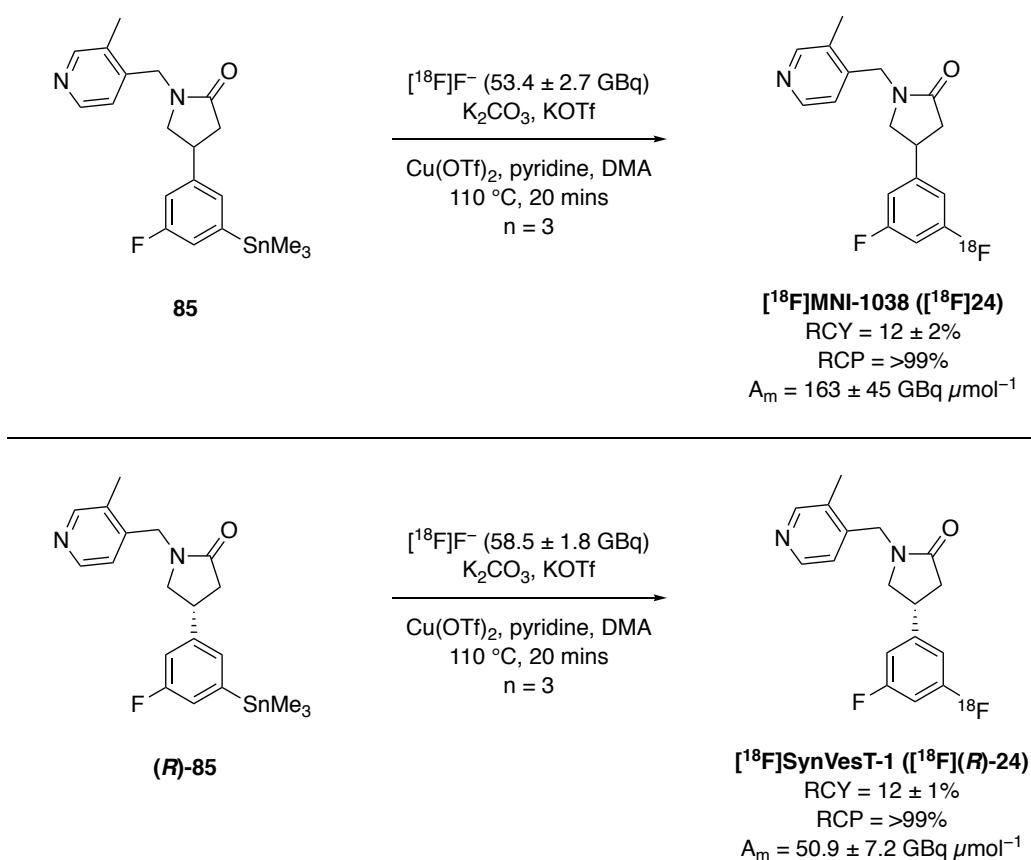
Scheme 42 – Enantioselective synthesis of organotin precursor **(R)-85**. ^aMixture of **(R)-83** and debrominated side-product **(R)-109** in a ratio of 1 : 0.18.

2.2.6 Radiosynthesis of [¹⁸F]MNI-1038 ([¹⁸F]24) and [¹⁸F]SynVesT-1 ([¹⁸F](R)-24)

Development of a radiofluorination procedure was then undertaken by Tim Morgan at the University of Edinburgh, using a GE TRACERlab™ FX_{FN} synthesiser with in-built semi-preparative HPLC capability for product purification. Initially, racemic organotin precursor **85** was submitted to copper-mediated nucleophilic radiolabelling originally developed by Sanford, Scott and co-workers, using the experimental conditions reported by Constantinescu *et al.*^{152,199} However, HPLC analysis of the reaction mixture displayed negligible conversion of [¹⁸F]fluoride to [¹⁸F]MNI-1038 ([¹⁸F]24) *via* comparison of chromatographic retention time with the MNI-1038 (**24**) standard. Next, a pre-dissolution step was incorporated in which the [¹⁸F]fluoride was stirred in DMA at 100 °C for 5 minutes prior to the addition of precursor **85**, copper(II) trifluoromethanesulfonate and pyridine.²³⁹ This approach was also found to produce negligible conversion of [¹⁸F]fluoride to [¹⁸F]24. Although the organotin precursor and other reagents were used in large excess to the [¹⁸F]fluoride, HPLC analysis of the reaction mixture showed that precursor **85** was fully consumed within the 20 minute reaction. As such, the decision was made to introduce precursor **85**, copper(II) trifluoromethanesulfonate and pyridine to the synthesiser without pre-mixing which led to a considerable increase in conversion. Screening the equivalents used of each reagent was subsequently performed and the highest conversion to [¹⁸F]24 was achieved using precursor **85** (5.00 mg, 11.2 μmol), copper(II) trifluoromethanesulfonate (8.00 mg, 22.1 μmol) and pyridine (20.0 μL, 248 μmol) in DMA (0.7 mL) at 110 °C for 20 minutes.

With radiolabelling conditions established, [¹⁸F]24 was subsequently purified by semi-preparative HPLC using an optimal isocratic mobile phase of 50% acetonitrile in 0.1 M aqueous ammonium acetate. Given that [¹⁸F]24 would be subsequently administered *in vivo* for PET imaging of the SV2A protein, it was necessary to reformulate the fluorine-18 radiolabelled product into a saline solution containing the minimum volume of ethanol *via* solid phase extraction (SPE). Initial reformulation attempts employed a Sep-Pak® tC18 vac or C18 plus short cartridge but were deemed impracticable due to incomplete retention of [¹⁸F]24 and produced lower isolated radiochemical yields. Subsequently, optimal reformulation of [¹⁸F]24 as a 10% ethanol in saline solution was achieved using an Oasis® HLB cartridge.

The optimised radiolabelling procedure was then applied to organotin precursor **85** for production of [¹⁸F]MNI-1038 (**[¹⁸F]24**) in triplicate. Starting from 53.4 ± 2.7 GBq of [¹⁸F]fluoride, this procedure allowed for the preparation of [¹⁸F]MNI-1038 (**[¹⁸F]24**) in 12 ± 2% radiochemical yield with a radiochemical purity of >99%, in a total synthesis time of 58 minutes (n = 3) (Scheme 43). Furthermore, the molar activity of **[¹⁸F]24** was calculated as 163 ± 45 GBq μmol⁻¹ through comparison of the analytical HPLC UV chromatograms of the product with those of the MNI-1038 (**24**) standard at known concentrations. Finally, the enantioenriched organotin precursor (**R**)-**85** was submitted to this procedure in triplicate. Starting from 58.5 ± 1.8 GBq of [¹⁸F]fluoride, [¹⁸F]SynVesT-1 (**[¹⁸F](R)-24**) was afforded in 12 ± 1% radiochemical yield with a radiochemical purity of >99%, in a total synthesis time of 57 minutes (n = 3). In addition, the molar activity of **[¹⁸F](R)-24** was calculated as previously described with the analytical HPLC standard SynVesT-1 (**(R)-24**) to be 50.9 ± 7.2 GBq μmol⁻¹. Thus far, the molar activity of [¹⁸F]MNI-1038 (**[¹⁸F]24**) and [¹⁸F]SynVesT-1 (**[¹⁸F](R)-24**) produced through this procedure has been variable due to a low number of experimental replicates (n = 3).



Scheme 43 – Radiosynthesis of [¹⁸F]MNI-1038 (**[¹⁸F]24**) and [¹⁸F]SynVesT-1 (**[¹⁸F](R)-24**)

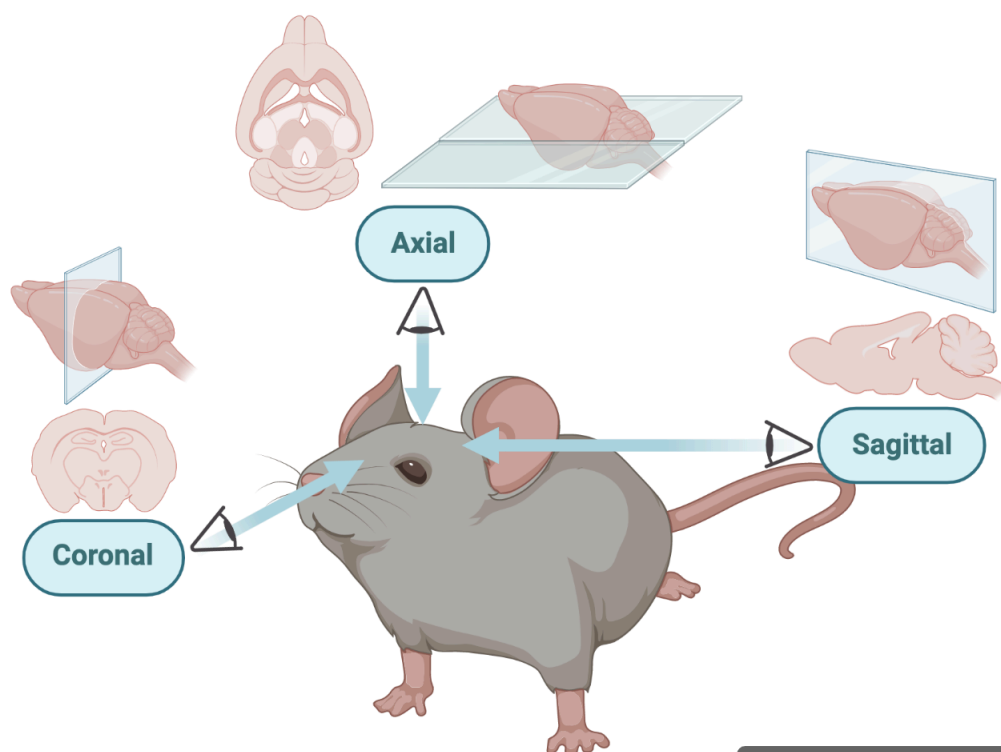
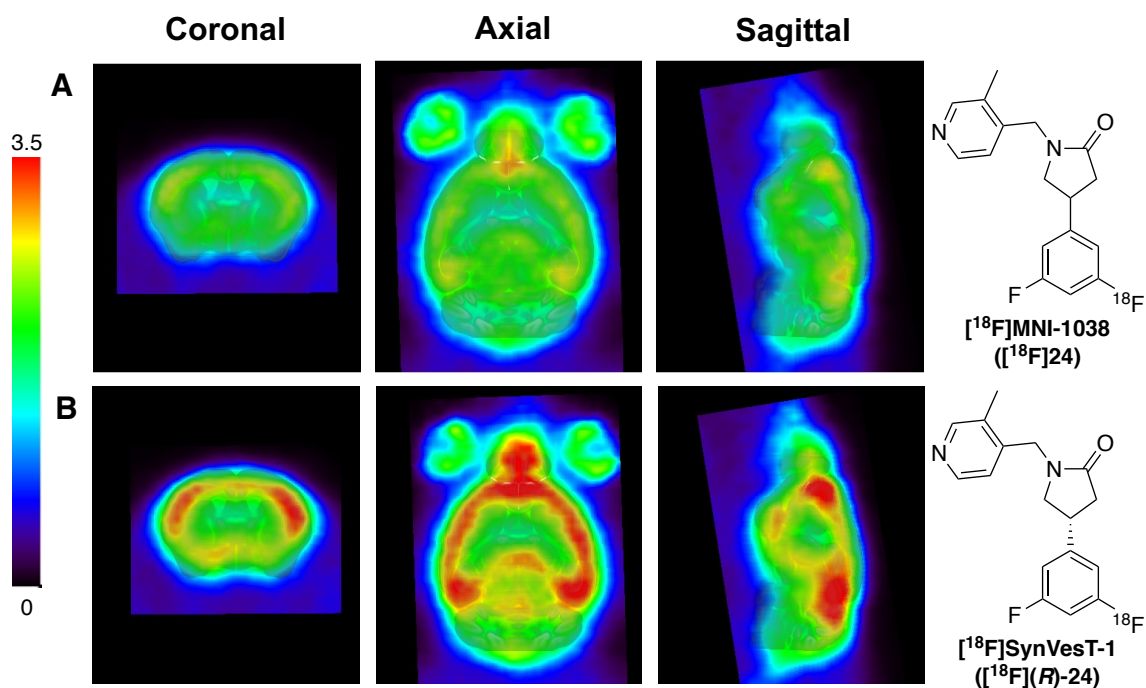
2.2.7 PET Imaging of SV2A with [¹⁸F]MNI-1038 ([¹⁸F]24) and [¹⁸F]SynVesT-1 ([¹⁸F](R)-24)

Following the development of optimised synthetic routes to radiotracers [¹⁸F]MNI-1038 ([¹⁸F]24) and [¹⁸F]SynVesT-1 ([¹⁸F](R)-24), the focus of the project transferred to the development of a quantitative *in vivo* PET imaging technique for the SV2A protein. It is vital to possess a thorough knowledge of the kinetic properties of a radiotracer to enable *in vivo* application in quantitative PET imaging studies. Whilst the kinetic properties of these imaging agents have been previously examined in both non-human primates and healthy humans, there has been no comparative kinetics assessment in murine models published thus far.^{152,153,155}

In work performed by Carlos J. Alcaide-Corral and Catriona Wimberley, at the University of Edinburgh both [¹⁸F]MNI-1038 ([¹⁸F]24) and [¹⁸F]SynVesT-1 ([¹⁸F](R)-24) underwent kinetic properties evaluation in the mouse brain *via* dynamic PET/CT imaging of eight naive male C57Bl6/J mice over 2 hours following administration of the chosen radiotracer. The resultant PET images were summed from 30 to 60 minutes and the standard uptake values (SUVs) produced were converted into SUV maps of the whole brain (Figure 33, A and B). SUV refers to the ratio of radioactivity concentration in tissue at a specific time to the injected dose of radioactivity per kilogram of body weight. Furthermore, the PET images were registered to a mouse brain atlas that had been obtained by MRI to determine regional SUVs. It was found that both [¹⁸F]MNI-1038 ([¹⁸F]24) and [¹⁸F]SynVesT-1 ([¹⁸F](R)-24) exhibit similar spatial distribution throughout the 53 regions of the brain that were analysed but with substantially different degrees of uptake. In Figure 33 A and B, the SUV maps are displayed in the coronal, axial, and sagittal planes using a colour scale in which regions of high uptake are shown in red and regions of low uptake or “spill over” are shown in blue. In Figure 33 A, moderate uptake of [¹⁸F]MNI-1038 ([¹⁸F]24) can be observed across the brain including in the cerebellum and optical nerves (two eyes clearly shown in the axial slice) (green regions). Furthermore, low uptake was observed in the striatum, hippocampus, and thalamus (blue regions). Conversely, the highest uptake of [¹⁸F]MNI-1038 ([¹⁸F]24) was recorded in the cortex and olfactory bulb (yellow/orange regions). In Figure 33 B, significantly higher uptake of [¹⁸F]SynVesT-1 ([¹⁸F](R)-24) was observed in all brain regions when compared to [¹⁸F]MNI-1038 ([¹⁸F]24). Moderate uptake of [¹⁸F]SynVesT-1 ([¹⁸F](R)-24) was

recorded in the striatum, hippocampus, thalamus, optical nerves, and medulla (green regions). Furthermore, high uptake was observed in the cortex and olfactory bulb (red/yellow regions) which are known to possess high synaptic density.

Additionally, the total SUVs of the whole brain were plotted against time to afford time activity curves for each radiotracer (Figure **33C**). These curves demonstrate that the enantioenriched [^{18}F]SynVesT-1 (**[^{18}F](R)-24**) (red line) underwent rapid and significantly higher uptake into brain tissue than the racemic mixture [^{18}F]MNI-1038 (**[^{18}F]**24**) (blue line). However, SUVs are a measure of the total uptake of a radiotracer including non-displaceable uptake such as non-specific binding and tissue perfusion. To perform a quantitative analysis of [^{18}F]SynVesT-1 (**[^{18}F](R)-24**) bound specifically to the SV2A protein, it is necessary to measure the proportion of radiotracer that partakes in non-displaceable uptake. Common methods employed for this measurement include arterial blood sampling and reference tissue regions. However, arterial blood sampling is challenging in murine models due the small animal size, and the wide-spread occurrence of the SV2A protein within the brain does not allow for identification of a reference tissue region without the presence of radiotracer. Consequently, studies are underway to investigate the use of dynamic PET imaging with factor analysis to quantify radiotracer in the blood *via* an image-derived input function. Subsequent estimation of the non-displaceable uptake of [^{18}F]SynVesT-1 (**[^{18}F](R)-24**) will facilitate quantitative measurement of specific binding of the radiotracer to the SV2A protein.**



Created in [BioRender.com](https://www.biorender.com)

Figure 33 – Average SUV maps of $[^{18}\text{F}]\text{MNI-1038}$ ($[^{18}\text{F}]\text{24}$) (A) (C, blue line) and $[^{18}\text{F}]\text{SynVesT-1}$ ($[^{18}\text{F}](R)\text{-24}$) (B) (C, red line) in whole mouse brain. Images A and B courtesy of Carlos J. Alcaide-Corral and Catriona Wimberley. Image of mouse was created using BioRender.com.

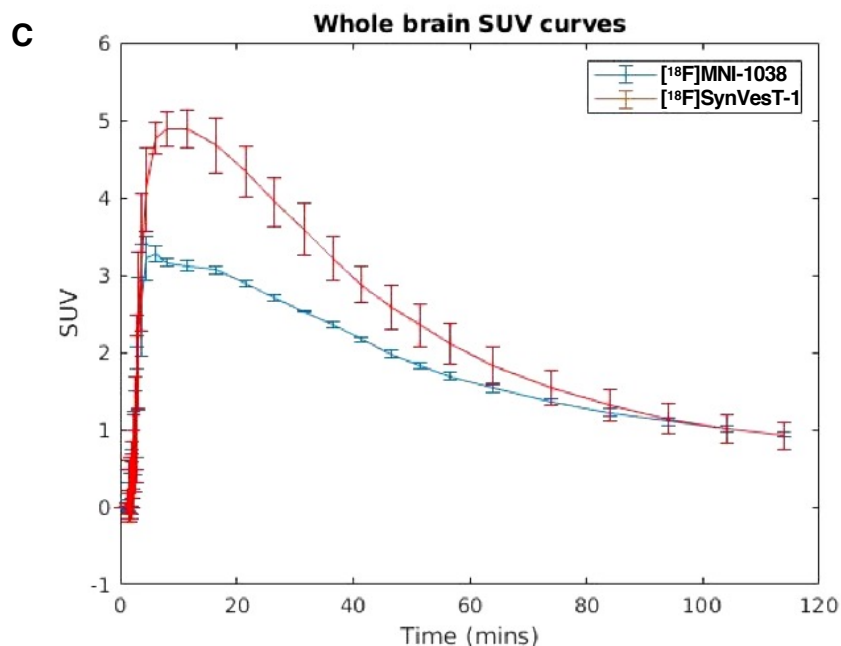


Figure 34 (continued) – SUV Time activity curves (C) of [¹⁸F]MNI-1038 (**[¹⁸F]24**) (A) (C, blue line) and [¹⁸F]SynVesT-1 (**[¹⁸F](R)-24**) (B) (C, red line) in whole mouse brain . Graph C courtesy of Carlos J. Alcaide-Corral and Catriona Wimberley.

2.2.8 Conclusions and Future Work

In summary, a synthetic route for the preparation of [¹⁸F]MNI-1038 (**[¹⁸F]24**) and two enantioselective synthetic routes toward [¹⁸F]SynVesT-1 (**[¹⁸F](R)-24**) were investigated. Both asymmetric routes to the organotin precursor (**(R)-85**) exploited organocatalysed enantioselective Michael addition reactions to induce chirality in early synthetic stages. The initial asymmetric route explored, which employed the bifunctional organocatalyst *O*-desmethyl quinidine (**87**), was ultimately deemed impracticable due to challenges encountered when various attempts were made to reduce the nitro functionality of the Michael addition product (**(R)-89**).

As such, an alternative enantioselective synthesis of [¹⁸F]SynVesT-1 (**[¹⁸F](R)-24**) and complimentary route to the racemate compound [¹⁸F]MNI-1038 (**[¹⁸F]24**) were designed. Firstly, a four-step synthetic route was developed for the preparation of the fluorine-19 analogue MNI-1038 (**24**). These synthetic procedures were then applied and further optimised for the synthesis of **85** the organotin precursor to [¹⁸F]MNI-1038 (**[¹⁸F]24**), in five steps. Racemic HPLC standard MNI-1038 (**24**) and precursor **85** were then utilised by our collaborators to develop a copper-mediated

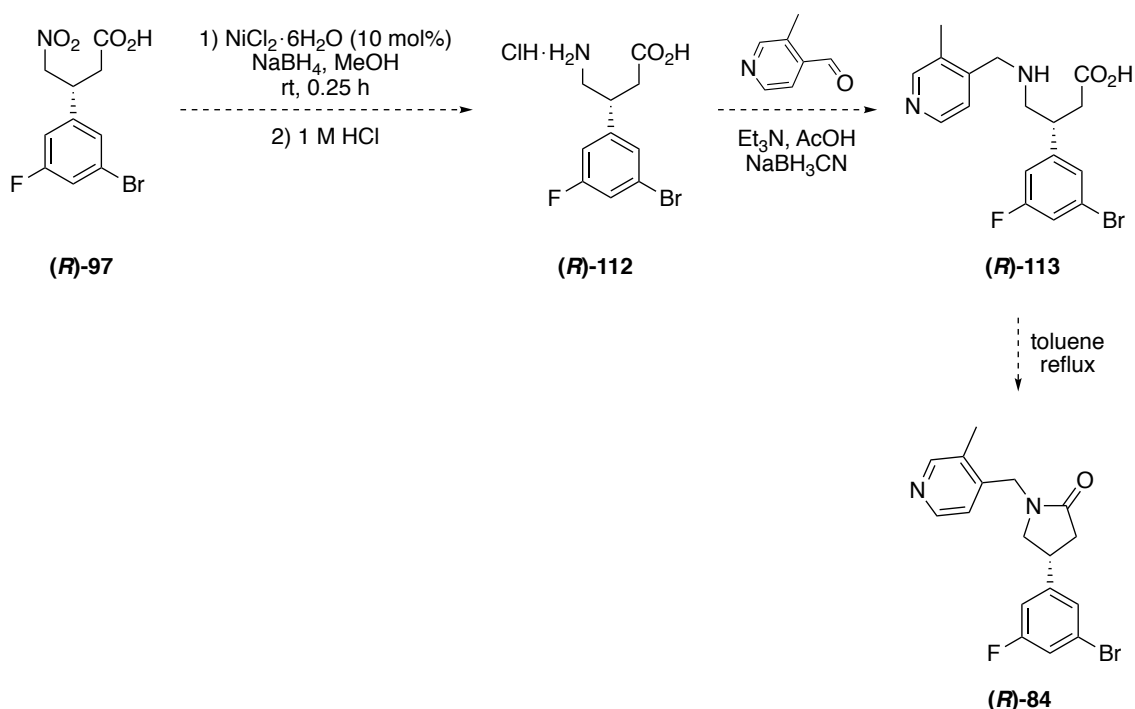
nucleophilic radiofluorination procedure for the preparation of [^{18}F]MNI-1038 (**[^{18}F]24**). The second asymmetric route, which utilised the Jørgensen-Hayashi diarylprolinol silyl ether organocatalyst (**(R)-94**), was first optimised and employed for the synthesis of fluorine-19 equivalent SynVesT-1 (**((R)-24**) in six synthetic steps. Finally, this enantioselective synthetic approach was applied for the synthesis of (**(R)-85** the organotin precursor to [^{18}F]SynVesT-1 (**[^{18}F](R)-24**), in seven steps. Crucially, this novel enantioselective synthetic route allowed for the preparation of both the HPLC standard SynVesT-1 (**((R)-24**) and precursor (**(R)-85** in excellent 93 : 7 enantiomeric ratios without application of costly chiral resolution techniques.

Organotin precursor (**(R)-85** was subsequently submitted to the optimised fluorine-18 radiolabelling conditions to afford [^{18}F]SynVesT-1 (**[^{18}F](R)-24**). Both radiotracers [^{18}F]MNI-1038 (**[^{18}F]24**) and [^{18}F]SynVesT-1 (**[^{18}F](R)-24**) were then subjected to preliminary *in vivo* kinetic properties evaluation in mouse brain and the total uptake was measured. The next stage of this project will be to determine the specific binding of [^{18}F]SynVesT-1 (**[^{18}F](R)-24**) to the SV2A protein to enable the development of a quantitative PET imaging technique.

Therefore, future synthetic work will focus on the synthesis of precursor (**(R)-85** in multigram quantities. The initial Wittig reaction, Michael addition, Pinnick oxidation and esterification steps of the novel enantioselective synthetic route described were consistently good yielding and generated products with high enantiopurity. However, one area which requires optimisation is the limited 85% conversion to aldehyde (**(R)-101** noted for the enantioselective Michael addition of nitromethane to cinnamaldehyde **95** when carried out at larger scales. It is reasonable to suggest that a slightly increased catalyst loading of 7.5 mol% (**(R)-94** will be sufficient to achieve full reaction of cinnamaldehyde **95** in subsequent syntheses performed at multigram scale. Notably, the three synthetic steps following nitroalkane (**(R)-98** formation gave moderate yields and further investigation of these reactions should be carried out to maximise the overall yield of this synthetic route. The nickel boride-catalysed reduction of nitroalkane (**(R)-98** proceeds efficiently in 100% conversion however, a significant degree of debromination was also observed. It is reasonable to suggest that the reaction temperature be maintained at 20 °C throughout the addition of sodium borohydride to limit this dehalogenation side-reaction. Furthermore, the subsequent intramolecular cyclisation to give pyrrolidin-2-one (**(R)-**

83 could be accelerated through addition of a base such as triethylamine, or possibly even promote cyclisation at room temperature. This may limit any dehalogenation formed during the intramolecular cyclisation reaction at 45 °C which may contain residual traces of nickel boride.

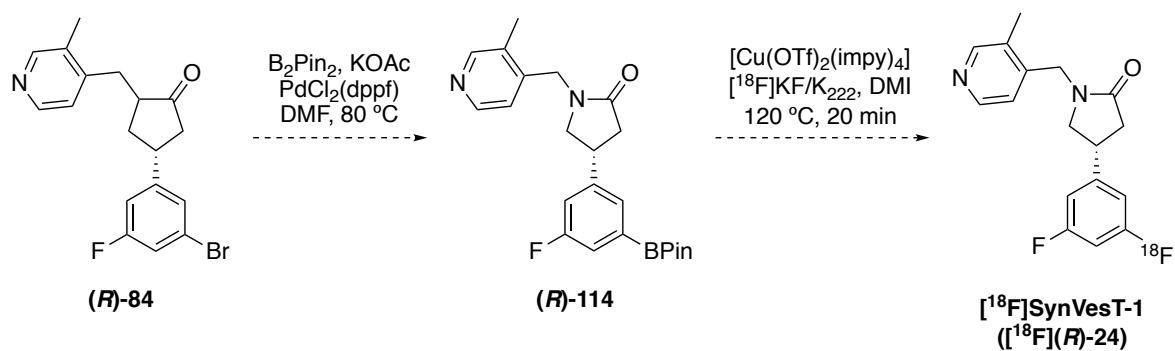
Moreover, the synthesis of intermediate **(R)-84** could be attempted using an alternative synthetic route (Scheme 44). Carboxylic acid intermediate **(R)-97** could be prepared from 3-bromo-5-fluorobenzaldehyde (**79**) in three steps as previously described, then treated with nickel(II) chloride and sodium borohydride followed by hydrochloric acid to afford amine **(R)-112**. Coupling of amine **(R)-112** and 3-methyl-4-pyridinecarboxaldehyde under standard reductive amination conditions could then be exploited to afford intermediate **(R)-113**. Subsequently, intramolecular cyclisation of this intermediate could be achieved through a condensation reaction performed under Dean-Stark conditions to afford pyrrolidin-2-one intermediate **(R)-84**.²⁴⁰



Scheme 44 – Alternative synthetic route to intermediate **(R)-84**

In addition, the palladium-catalysed stannylation reaction to afford organotin precursor **(R)-85** from **(R)-84** has shown variable yields which appears to be dependent on the purity of the hexamethylditin reagent. Future work could

investigate the use of a pinacol boronic ester precursor (**(R)**-114) and exploit a copper(II)-catalysed nucleophilic radiofluorination method developed by Gouverneur and co-workers for the synthesis of [¹⁸F]SynVesT-1 ([¹⁸F](**(R)**-24) (Scheme 45).^{106,153,195,196}



Scheme 45 – Proposed synthesis of [¹⁸F]SynVesT-1 ([¹⁸F](**(R)**-24) via pinacol boronic ester precursor (**(R)**-114

2.3 Transition Metal-Catalysed Reactions of Aryl Iodides

2.3.1 Introduction

Aryl and heteroaryl iodides are a fundamental class of organic compound, abundant in natural products, agrochemicals, and pharmaceutical drugs such as **115–119** (Figure 34).^{241–246} Iodoarenes, and haloarenes in general, are also crucially important synthetic intermediates that are commonly utilised for the preparation of organometallic reagents and free-radical intermediates, and transition metal-catalysed cross-coupling reactions to facilitate a wide-variety of chemical transformations *via* the formation of C–C, C–N, C–O and C–S bonds.^{247–254} Aryl iodides are particularly valuable intermediates as they possess increased reactivity relative to bromides, chlorides and fluorides, owing to the comparatively weak C–I bond.^{248,255}

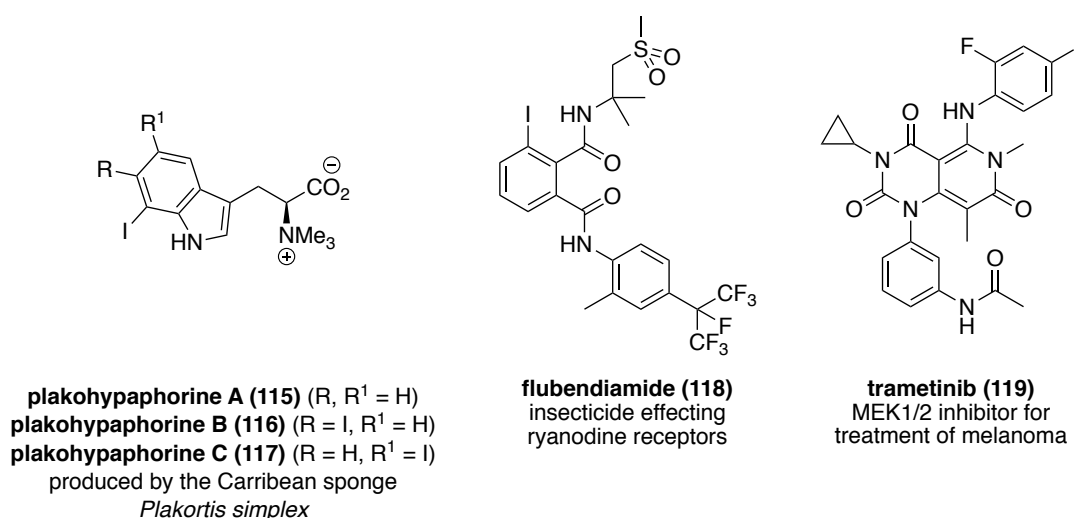


Figure 35 – Aryl iodides in natural products, agrochemicals, and pharmaceutical drugs

Due to the significant utility of aryl iodides, many general strategies have been developed for the synthesis of these haloarenes. Traditional methods include direct iodination of a C–H bond *via* electrophilic aromatic substitution using a strong oxidant or electrophilic iodine reagent, and the indirect iodination of aryl organolithium intermediates formed *via* directed lithiation, or aryl diazonium intermediates *via* the Sandmeyer reaction.^{247,256–262} However, these procedures typically require harsh reagents and conditions that are detrimental to functional

group tolerance, are limited to the iodination of activated aryl systems and suffer from poor regioselectivity or polyiodination.

Modern studies, including those performed by the Sutherland group, have therefore sought to develop mild procedures for the regioselective iodination of arenes that can be applied for the synthesis of complex target compounds. A range of metal-free conditions have been developed in recent years for oxidative, photo-induced or radical iodination of starting materials such as aryl halides, carboxylic and boronic acids, triflates and anilines or hydrazines *via* aryl diazonium salt intermediates.^{103,104,263–276} However, recent advances in the field of aryl iodination have been predominantly concentrated on transition metal-catalysed reactions including copper or nickel-catalysed halogen exchange, ruthenium-catalysed pseudo-halogen exchange, copper or gold-catalysed iododeboration, electrophilic aromatic substitution with an electrophilic iodine reagent facilitated by a gold, indium, iron or silver catalyst, and C–H activation catalysed by palladium, copper, rhodium, ruthenium or cobalt.^{103,248,255,277–281}

As previously discussed in Section 1.1.2, aryl and heteroaryl iodides containing radioactive nuclides of iodine, including iodine-123, iodine-124, iodine-125 and iodine-131, are indispensable within the discipline of molecular imaging.^{2,24,27,28,282} Traditionally, radioiodine has been incorporated into organic molecules *via* nucleophilic or electrophilic aromatic substitution.^{2,24,282,283} Iodine radioisotopes are produced as nucleophilic iodide and generally supplied as aqueous solutions of sodium iodide in the presence of sodium hydroxide.⁸ This is advantageous for employment in nucleophilic aromatic substitution reactions including the radioiodination of aryl iodides (containing iodine-127) *via* isotope exchange, and aryl bromides or chlorides *via* halogen exchange.^{2,24,282,284} However, the utility of isotope exchange reactions is limited due to competition between radioactive and non-radioactive iodide which generates an inseparable mixture of isotopic compounds with poor molar activity.²⁸² In addition, halogen exchange reactions of aryl bromides and chlorides commonly require high temperatures and long reaction times.^{2,284} Furthermore, the separation of aryl radioiodides from residual haloarene starting materials can prove challenging.²⁸² Extended purification times are especially detrimental to the preparation of radiopharmaceuticals since synthesis duration must be minimised as far as practicable to preserve radioactivity.

Alternatively, activated arenes can undergo direct radioiodination of C–H bonds *via* electrophilic aromatic substitution, following the oxidation of radioactive sodium iodide with an oxidant such as chloramine-T (**120**), Pierce™ iodination reagent (**121**) (formerly Iodo-Gen®), *N*-chlorosuccinimide (**122**) and peracetic acid (**123**) (Figure 35).^{2,24,282–284}

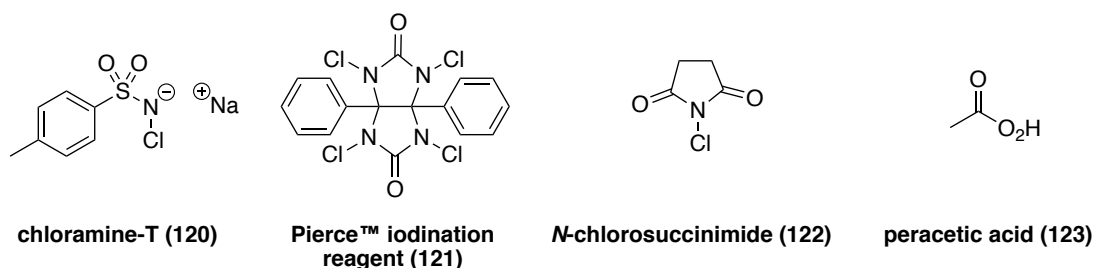
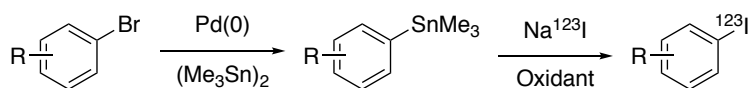


Figure 36 – Common reagents employed for oxidation of radioactive sodium iodide

For arenes that are not activated towards electrophilic aromatic substitution, organometallic intermediates such as aryl organostannanes are commonly prepared from the corresponding aryl bromides *via* palladium-catalysed stannylation (Scheme 46). Upon treatment with an electrophilic source of radioiodide, formed *in situ* using sodium radioiodide and an oxidant, the labile C–Sn bond present within these intermediates facilitates an *ipso*-electrophilic aromatic substitution reaction.^{2,24,28,282–284} This oxidative iododestannylation reaction is the most frequently employed method of radioiodination within the field of nuclear medicine and affords radioiodinated arenes in high yields with regioselectivity.^{28,282} The key limitations of this technique include the use of strong oxidising reagents which are intolerant of many functionalities, and the potential for residual tin residues within the radioiodinated imaging agents that would have *in vivo* toxicity implications.



Scheme 46 – Oxidative radioiododestannylation *via* an *ipso*-electrophilic aromatic substitution reaction

Over the last four decades the use of SPECT imaging agents has significantly increased and thus the demand for mild and efficient radioiodination methods that overcome the limitations of traditional methods as previously described has grown.

With respect to the radioiodination of arenes, the fields of nucleophilic and electrophilic aromatic substitution have witnessed the development of milder conditions that are suitable for application to a wider scope of substrates. Notably, the majority of novel radioiodination methods developed in recent years have been transition metal-catalysed reactions including nickel(0)-catalysed halogen exchange of aryl bromides, copper(I)-, copper(II)- or gold(I)-catalysed iododeboration, copper(II)-catalysed three-component cycloaddition *via* click chemistry, and *N*-acylsulfonamide directed C–H activation *via* palladacycle formation. A number of these recent advances were established within the Sutherland research group, and a summary of modern radioiodination methodologies was recently collated in a review article that was published collaboratively by the Sutherland and Cailly research groups.²⁸

From this range of established synthetic procedures for the preparation of aryl iodides and radioiodides, it can be observed that aryl halides and organometallic intermediates are the most frequently employed starting materials and precursors. However, as previously highlighted, the utility of these intermediates and associated procedures is intrinsically limited by harsh reaction conditions and challenging purification of the desired products. Phenol-derived aryl sulfonates such as methanesulfonates (mesylates, Ms, **124**), *p*-toluenesulfonates (tosylates, Ts, **125**), trifluoromethanesulfonates (triflates, Tf, **126**) and nonafluorobutanesulfonates (nonaflates, Nf, **127**) are commonly referred to as pseudo-halides due to their capability to mimic the electrophilic behaviour of aryl halides (Figure **36**).²⁸⁵ The inherent utility of these pseudo-halides is due to the more labile C–O bond and increased electrophilicity of the *ipso*-carbon, relative to the parent phenolic species, generated by the adjacent electron-withdrawing sulfonyl moiety, and that the sulfonate ion (RSO_3^-) is an excellent leaving group.^{286,287} Furthermore, triflates and nonaflates exhibit increased reactivity relative to mesylates and tosylates due to the strongly electron-withdrawing properties of their perfluoroalkyl moieties.^{286,287} Consequently, aryl sulfonates and perfluoroalkylsulfonates in particular have been employed as alternative starting materials in a wide-range of nucleophilic substitution reactions and cross-coupling reactions for the production of C–C, C–N, C–P and C–S bonds.^{287–301}

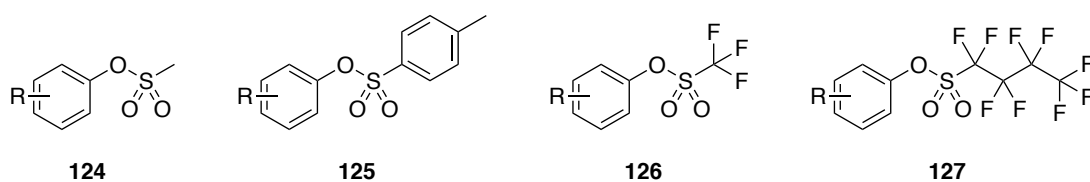
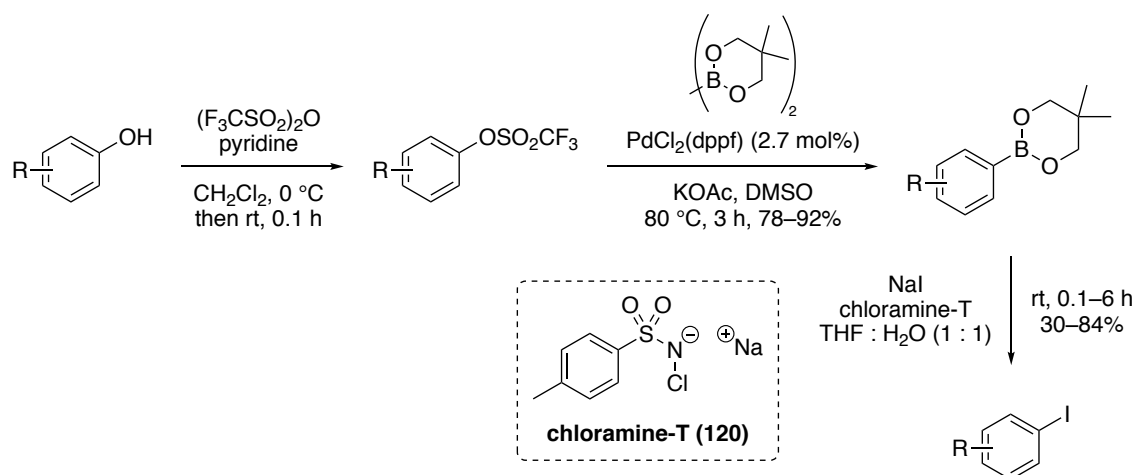


Figure 37 – Structures of phenol-derived aryl sulfonates

These aryl sulfonates are readily accessible from the corresponding phenols, of which there is a broad and generally inexpensive, commercially available scope. Furthermore, phenolic functionality is ubiquitous within bioactive compounds such as steroids, amino acids and numerous FDA approved pharmaceuticals.¹²⁹ Current synthetic methods to prepare aryl halides directly from phenols require harsh conditions which impedes their wide-spread application as substrates for iodination or radioiodination.^{302,303} Although the use of phenol-derived aryl sulfonates for transition metal-catalysed cross-coupling reactions has become increasingly common in recent years, there has been very limited reports of their utility for the production of aryl halides.

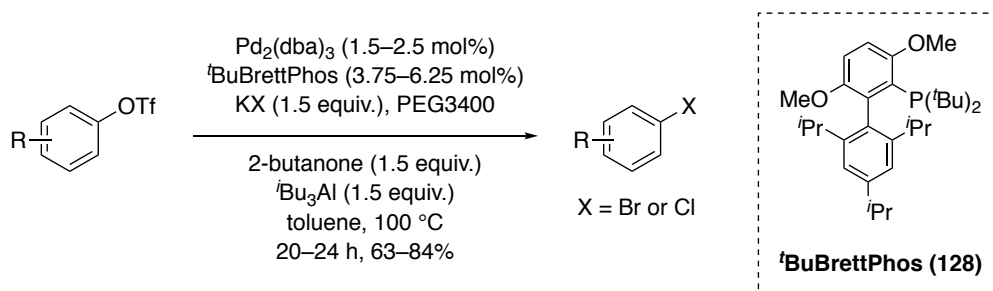
In 2005, Huffman and co-workers developed a three-step procedure for the synthesis of aryl bromides and iodides in which phenol substrates underwent successive transformation to aryl triflates, and then neopentylboronate esters *via* palladium(0)-catalysed borylation (Scheme 47).³⁰⁴ The resultant boronate intermediates were then subjected to iododeboration through treatment with oxidant chloramine-T (**120**) and sodium iodide to afford the corresponding aryl iodides *via* electrophilic aromatic substitution. Although effective for electron-rich arenes, this synthetic approach was not compatible with electron-deficient substrates. Ultimately, this synthetic approach was deemed too elaborate and inefficient for the preparation of aryl iodides from phenols.



Scheme 47 – Three-step synthesis of aryl iodides from phenols by Huffman and co-workers

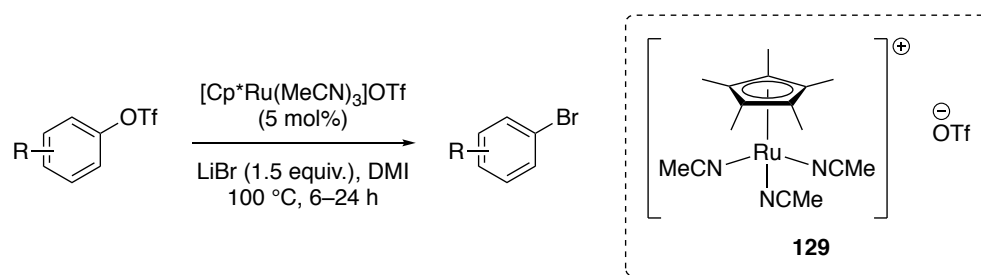
A more direct approach for the synthesis of aryl halides from phenols was later pioneered by Buchwald and co-workers, who developed the first transition metal-catalysed halogenation of aryl triflates *via* palladium(0)-catalysed pseudo-halogen exchange reactions. In 2009, the Buchwald research group reported the preparation of aryl fluorides and shortly thereafter in 2010, the complimentary synthesis of aryl bromides and chlorides directly from aryl triflates employing tris(dibenzylideneacetone)dipalladium(0) and the sterically hindered dialkybiarylphosphine ligand *t*-BuBrettPhos (**128**) (Scheme **48**).^{285,305} This procedure was shown to generate a diverse range of aryl bromides and chlorides in good yields of 63–84% after 20–24 h however, the use of multiple additives was required. The potassium halide sources exhibited poor solubility in toluene which necessitated the use of polyethylene glycol 3400 (PEG3400) as a phase transfer catalyst. In addition, the potassium triflate by-product was observed to inhibit the production of the desired aryl halides and prompted the addition of Lewis acid tri-*iso*-butylaluminium. However, a significant quantity of C–C cross-coupling between tri-*iso*-butylaluminium and the aryl substrate was then observed. Subsequently, the addition of 2-butanone was found to inhibit cross-coupling through the production of aluminium alkoxides and facilitated the preparation of aryl halides in good yields. Despite further optimisation for improved utility with a wider substrate scope, this palladium(0)-catalysed pseudo-halogen exchange has not been shown to be applicable for the synthesis of aryl iodides from aryl triflates, thus far.^{306–309} Notably, this seminal work by Buchwald and co-workers established that aryl sulfonates

could be successfully employed in lieu of aryl halides for transition metal-catalysed halogenation.



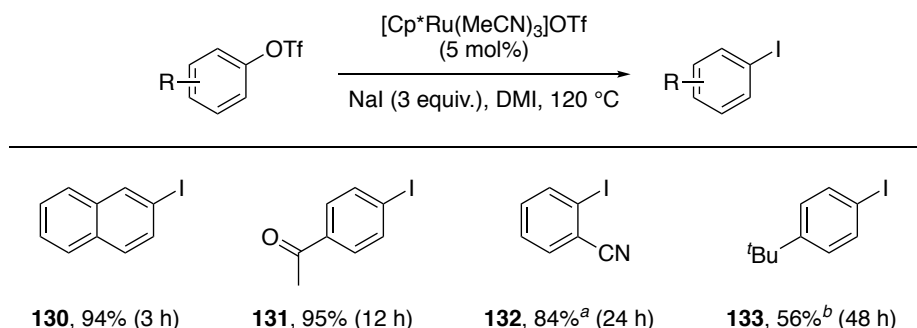
Scheme 48 – Palladium-catalysed synthesis of aryl bromides and chlorides from aryl triflates by Buchwald and co-workers

Subsequently in 2012, Hayashi and co-workers developed an alternative approach for the bromination of aryl triflates using an electron-rich ruthenium(II) catalyst, tris(acetonitrile)pentamethylcyclopentadienylruthenium(II) trifluoromethanesulfonate (**129**) (5 mol%), with lithium bromide in 1,3-dimethyl-2-imidazolidinone (DMI) (Scheme **49**).³¹⁰ This pseudo-halogen exchange reaction was found to proceed at a mild temperature of 100 °C in modest timescales and without the use of additives. A selection of electronically diverse aryl triflates was submitted to these conditions and the bromination of electron-deficient arenes was achieved in high yields of 83–97%. However, the synthesis of electron-rich aryl and heteroaryl bromides required elevated temperatures (120 °C), an increased loading of catalyst **129** (10 or 15 mol%) loading, or increased equivalents of lithium bromide (3 or 6 equiv.). Furthermore, significantly longer reaction times of up to 48 h were necessary to obtain yields of 70–93%. Notably, selective reactivity with the triflate functionality of 4-chloronaphthalen-1-yl trifluoromethanesulfonate was observed which demonstrates the utility of this method for the preparation of dihaloarenes with scope for subsequent orthogonal functionalisation.



Scheme 49 – Ruthenium-catalysed synthesis of aryl bromides from aryl triflates by Hayashi and co-workers

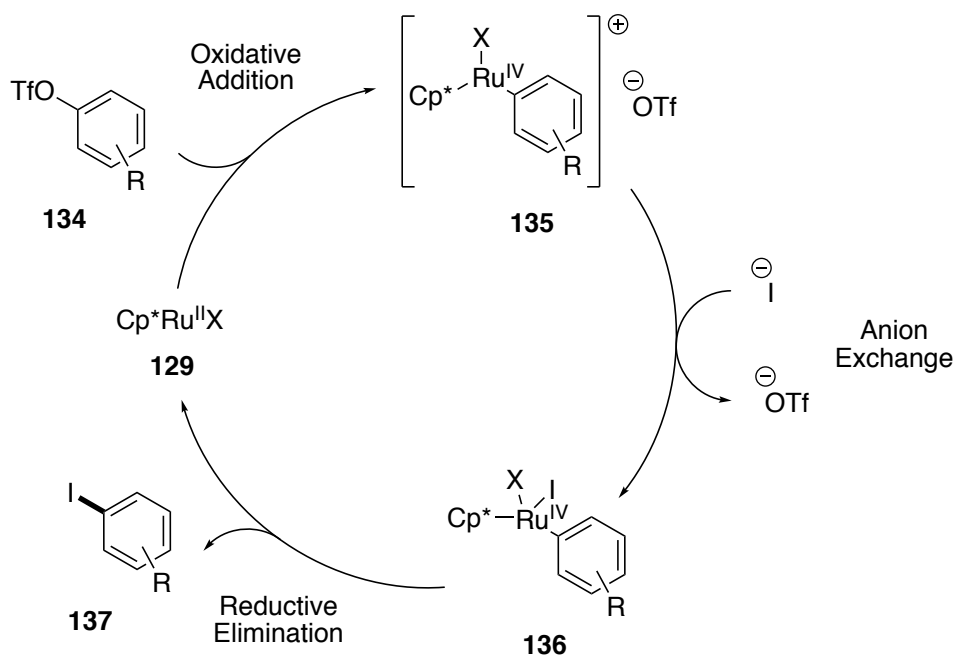
In the same study, Hayashi and co-workers also treated four aryl triflates with ruthenium(II) catalyst **129** (5 mol%) and sodium iodide (3 equiv.) in DMI to afford aryl iodides **130–133** (Scheme 50). The authors found that use of an elevated reaction temperature (120 °C) and equivalents of the halide source (3 equiv.) was essential for iodination of all four aryl triflates. Electron-deficient aryl iodides **130** and **131** were prepared readily in high yield; however, the synthesis of *ortho*-substituted **132** required an increased loading of catalyst **129** (10 mol%). In addition, the iodination of moderately electron-rich 4-*tert*-butylphenyl trifluoromethanesulfonate was achieved but required the use of 15 mol% of ruthenium(II) catalyst **129** and 6 equivalents of sodium iodide to afford **133** in only 56% yield after 48 h. Consequently, the authors concluded that this methodology was not widely applicable to the synthesis of electron-rich aryl iodides. To the best of our knowledge, this procedure from Hayashi and co-workers was the first transition metal-catalysed halogenation of phenols *via* aryl sulfonates that demonstrated scope for application to aryl iodination.



Scheme 50 – Ruthenium-catalysed synthesis of aryl iodides from aryl triflates.

^aReaction performed using [Cp*Ru(MeCN)₃]OTf (**129**) (10 mol%). ^bReaction performed using [Cp*Ru(MeCN)₃]OTf (**129**) (15 mol%) and NaI (6 equiv.).

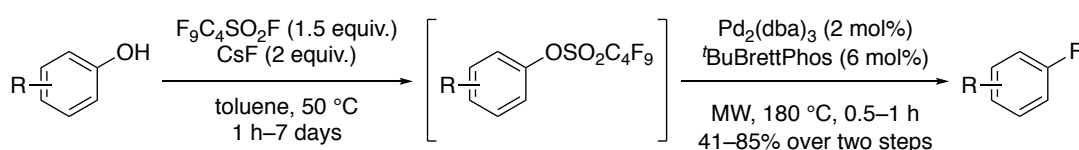
Hayashi and co-workers hypothesised that this reaction proceeds through a ruthenium(II)/ruthenium(IV) catalytic cycle (Scheme 51).³¹⁰ The authors concluded that the electron-donating nature of the pentamethylcyclopentadiene (Cp*) ligand was crucial to the observed reactivity following unsuccessful aryl halogenation attempts using a catalytic system developed three years previous for the halogenation of alkenyl triflates, comprised of ruthenium(III) acetylacetonate (Ru(acac)₃) (3 mol%), ethylmagnesium bromide (12 mol%) and 3,4,7,8,-tetramethyl-1,10-phenanthroline (3 mol%).³¹¹ The electron-donating nature of the Cp* ligand generates an electron-enriched ruthenium(II) catalyst **129**, which is activated for oxidative addition to the aryl triflate **134**. Oxidative addition of **134** produces a cationic η^1 -arylruthenium(IV) complex **135** which then undergoes anion exchange of the triflate group with a halide anion, and subsequent co-ordination of the halide produces the neutral ruthenium species **136**. Finally, reductive elimination affords the aryl halide product **137** and regeneration of the ruthenium(II) catalyst **129**.



Scheme 51 – Proposed catalytic cycle of ruthenium-catalysed halogenation

In addition to the aforementioned research on the utility of aryl triflates in pseudo-halogen exchange reactions, aryl nonaflates were also investigated by Larhed and co-workers in 2013.³¹² Derived from the palladium(0)-catalysed halogenation of aryl triflates reported by Buchwald and co-workers, Larhed and co-workers developed a one-pot, two-step, microwave-assisted palladium(0)-catalysed procedure for the

fluorination of phenols *via* aryl nonaflate intermediates (Scheme 52). In the first step of this procedure, a small series of phenols underwent conversion to aryl nonaflates using perfluoro-1-butanesulfonyl fluoride (nonaflyl fluoride) in the presence of caesium fluoride. The authors reported that reaction times varied significantly dependent upon the nucleophilicity and solubility of the phenol substrate. Subsequently, fluorination was performed using tris(dibenzylideneacetone)dipalladium(0) (2 mol%) with Buchwald ligand *t*BuBrettPhos (**128**) (6 mol%) and proceeded rapidly under microwave heating at 180 °C to afford aryl fluorides in 41–85% yield over two steps. Although tolerant of many functionalities, including tertiary amines, ethers, nitriles, ketones and esters, the authors found that this methodology was not compatible with electron-rich or protic substrates. Furthermore, a competitive reaction employing 1 equivalent of caesium fluoride, caesium chloride and caesium bromide underwent fluorination in greater than 90% conversion, with less than 10% of the aryl chloride and traces of the aryl bromide products observed. Notably, no attempts to prepare aryl chlorides, bromides, or iodides from phenols under these conditions were described.



Scheme 52 – One-pot, two-step palladium-catalysed synthesis of aryl fluorides from phenols *via* aryl nonaflates by Larhed and co-workers

2.3.2 Previous Work in the Sutherland Group

The deficit of mild yet robust methods for the synthesis of aryl iodides and radioiodides from ubiquitous phenols *via* transition metal-catalysed reactions, prompted investigations within the Sutherland group. To the best of our knowledge, the ruthenium(II)-catalysed iodination of aryl triflates reported by Hayashi and co-workers is the sole exemplar of this transformation but exhibits limited utility for application with electron-deficient arenes (Scheme 50).³¹⁰ It was proposed that this methodology would be adopted as a starting point from which to further develop a transition metal-catalysed synthesis of aryl iodides from phenols. However, it was envisaged that an alternative phenol-derived intermediate to the aryl triflate would

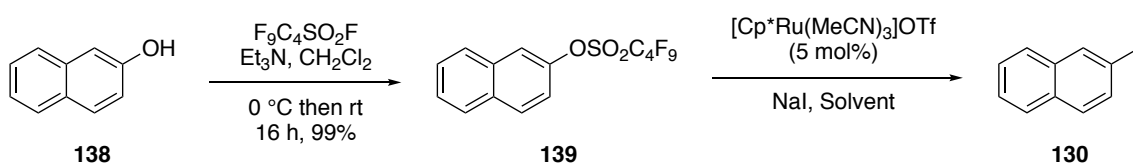
be required to promote this pseudo-halogen exchange reaction without the use of forcing conditions.

Notably, nonaflates possess multiple advantageous properties when compared to triflates.²⁸⁷ Aryl nonaflates can be readily prepared from the corresponding phenols under basic conditions with nonafluryl fluoride, a relatively inexpensive industrial by-product. Furthermore, this reagent is considerably less expensive than analogous reagents for the synthesis of aryl triflates such as triflic anhydride. In addition, nonaflates are significantly more stable than the equivalent triflates which are prone to hydrolysis, and can undergo purification *via* column chromatography and storage over prolonged periods of time.^{294,295} As such, there has been a significant increase in the application of nonaflates as alternatives to triflates in transition metal-catalysed cross-coupling reactions over the last two decades.^{287,290–292,294–296,298–301,312–314} Interestingly, nonaflates are more reactive than the analogous triflates in some palladium-catalysed cross-coupling reactions, and are less likely to undergo O–SO₂ bond cleavage during Stille reactions.^{287,313} This improved reactivity is likely due to the augmented electron-withdrawing properties of the nonafluorobutanesulfonate moiety due to the greater number of fluorine atoms compared with triflates.

Therefore, it was proposed that phenols would be converted to aryl nonaflates and then subjected to iodination *via* pseudo-halogen exchange catalysed by the ruthenium(II)-catalyst, tris(acetonitrile)pentamethylcyclopentadienylruthenium(II) trifluoromethanesulfonate (**129**). It was anticipated that the increased reactivity of aryl nonaflates, versus triflates, would also allow for a lower catalyst loading of ruthenium(II) catalyst **129** (5 mol%) than that used by Hayashi and co-workers (5–15 mol%). In preliminary work performed by Nikki Sloan, 2-naphthyl nonaflate (**139**) was prepared in 99% yield from 2-naphthol (**138**) and nonafluryl fluoride in the presence of triethylamine at room temperature (Table **18**). Subsequently, screening of iodination conditions was carried out using 2-naphthyl nonaflate (**139**) with 5 mol% of ruthenium(II) catalyst **129** and 1.5 equivalents of sodium iodide at 120 °C.¹⁶¹ Initially, the aprotic, high boiling point solvents DMF and *N*-methyl-2-pyrrolidone (NMP) were explored as less expensive alternatives to DMI (Table **18**, entries 1 and 2). Under these conditions, the use of NMP facilitated the preparation of iodide **130** in 47% yield, whilst DMF afforded **130** in only 10% yield. In subsequent

attempts that employed 3 equivalents of sodium iodide, the use of DMF was clearly superior and gave iodide **130** in 92% yield although no improvement of yield was observed for the reaction using NMP (entries 3 and 4). Next, a brief screen of temperatures revealed that the reaction temperature could be lowered to 100 °C with no detrimental impact on the efficiency of this iodination or the yield of iodide **130** (entries 5 and 6). Under the optimised conditions, treatment of nonaflate **139** with ruthenium(II) catalyst **129** (5 mol%) and sodium iodide (3 equiv.) in DMF, afforded iodide **130** in 93% yield after only 1 h at 100 °C (entry 5).

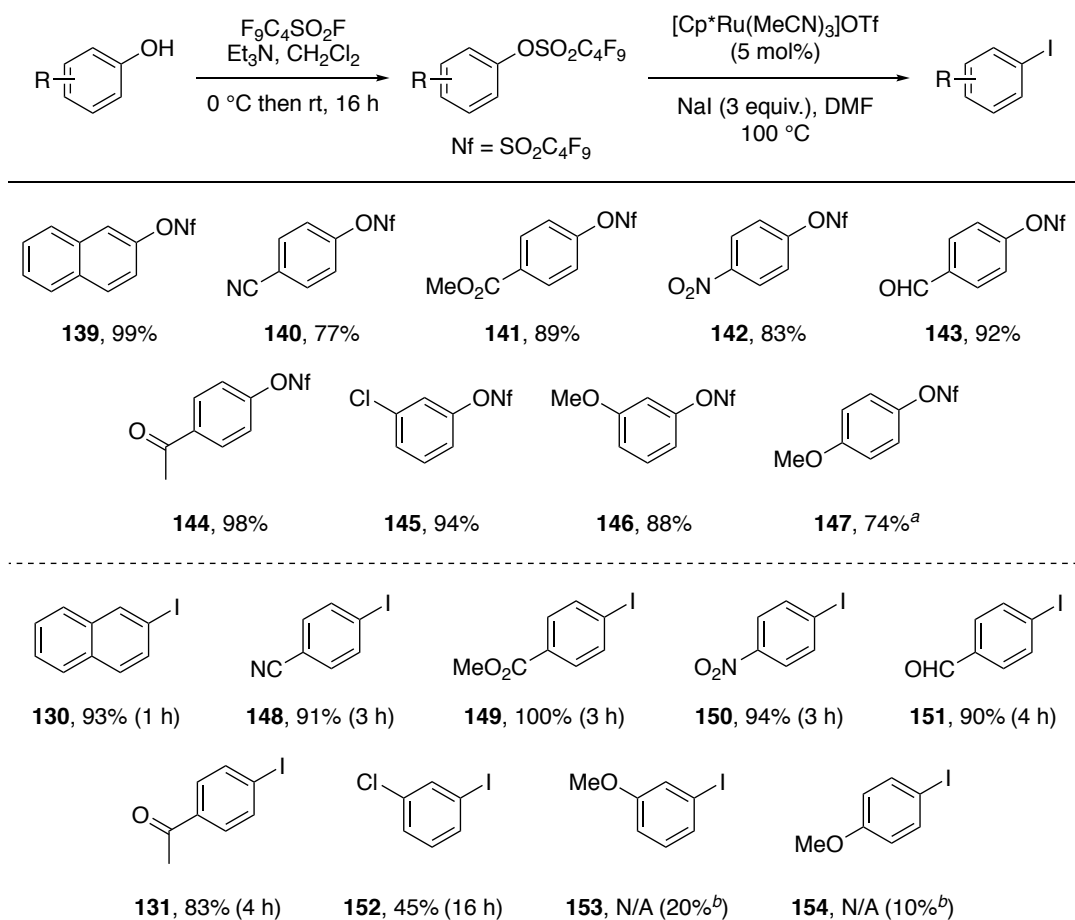
Table 19 – Initial screen of reaction conditions for the ruthenium-catalysed iodination of aryl nonaflates using 2-naphthyl nonaflate (**139**)



Entry	Solvent	Equiv. of NaI	Temp. (°C)	Time (h)	Yield of 130 (%)
1	NMP	1.5	120	3	47
2	DMF	1.5	120	3	10
3	NMP	3	120	2	47
4	DMF	3	120	2	92
5	DMF	3	100	1	93
6	DMF	3	80	4	88

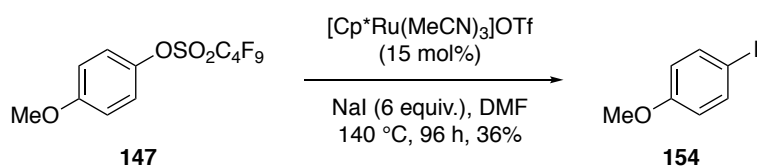
Next, a series of electronically diverse aryl nonaflates were prepared under mild conditions from the corresponding phenols in 74–99% yield, using nonaflyl fluoride in the presence of triethylamine at room temperature (Scheme **53**). These aryl nonaflates were then submitted to the optimised iodination conditions of ruthenium(II) catalyst **129** (5 mol%) and sodium iodide (3 equiv.) in DMF at 100 °C (Scheme **53**). As expected, the pseudo-halogen exchange of electron-deficient aryl nonaflates **140–144** proceeded efficiently to generate the corresponding iodides in 83–100% yield after only 3–4 h. However, the more electron-rich 3-chlorophenyl nonaflate (**145**) required an extended reaction time of 16 h to afford iodide **152** in a moderate yield of 45%. Furthermore, electron-rich anisole nonaflates **146** and **147**

were poorly converted, 20% and 10% conversion respectively, to the corresponding iodides even after prolonged reactions of 72 h.



Scheme 53 – Synthesis of aryl nonaflates from phenols and preliminary investigation of ruthenium-catalysed iodination. ^aReaction took 48 h. ^bConversion to iodide determined using ¹H NMR spectroscopy after 72 h.

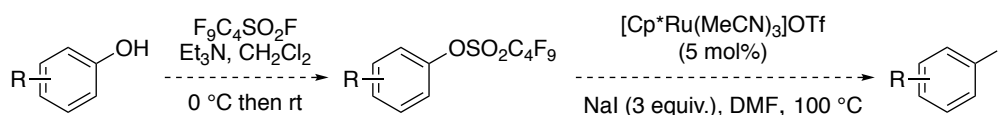
Subsequently, attempts were made to optimise the iodination of 4-methoxyphenyl nonaflate (**147**) to establish suitable conditions for application with a range of electron-rich nonaflates. However, a maximum yield of only 36% was achieved despite increasing the loading of ruthenium(II) catalyst **129**, equivalents of sodium iodide, temperature, and reaction duration (Scheme 54).



Scheme 54 – Highest yielding synthesis of 4-iodoanisole (**154**)

2.3.3 Proposed Research

The overall aim of this project was the continued development of transition metal-catalysed methods for the iodination of readily available phenols *via* aryl nonaflates, under relatively rapid and mild conditions. Following on from the work reported by Hayashi and co-workers³¹⁰ and the preliminary investigations carried out within the Sutherland group,¹⁶¹ it was proposed that a series of structurally and electronically diverse aryl nonaflates would be synthesised from the corresponding commercially available phenols (Scheme 55). These aryl nonaflates would then be subjected to iodination *via* a ruthenium(II) catalyst **129**-catalysed pseudo-halogen exchange reaction. Given the preliminary results of this project, it was proposed that further optimisation of this reaction would be necessary for application to electron-rich arenes. Once a general, mild, and efficient iodination procedure was established and the scope of this transformation was identified, the next aim of this project would be the synthesis of structurally complex aryl iodides. Finally, it was proposed that the methodology developed using iodine-127, would be subsequently adapted and applied to the preparation of SPECT imaging agents using radioactive isotopes of iodine and established as a novel radioiodination procedure.



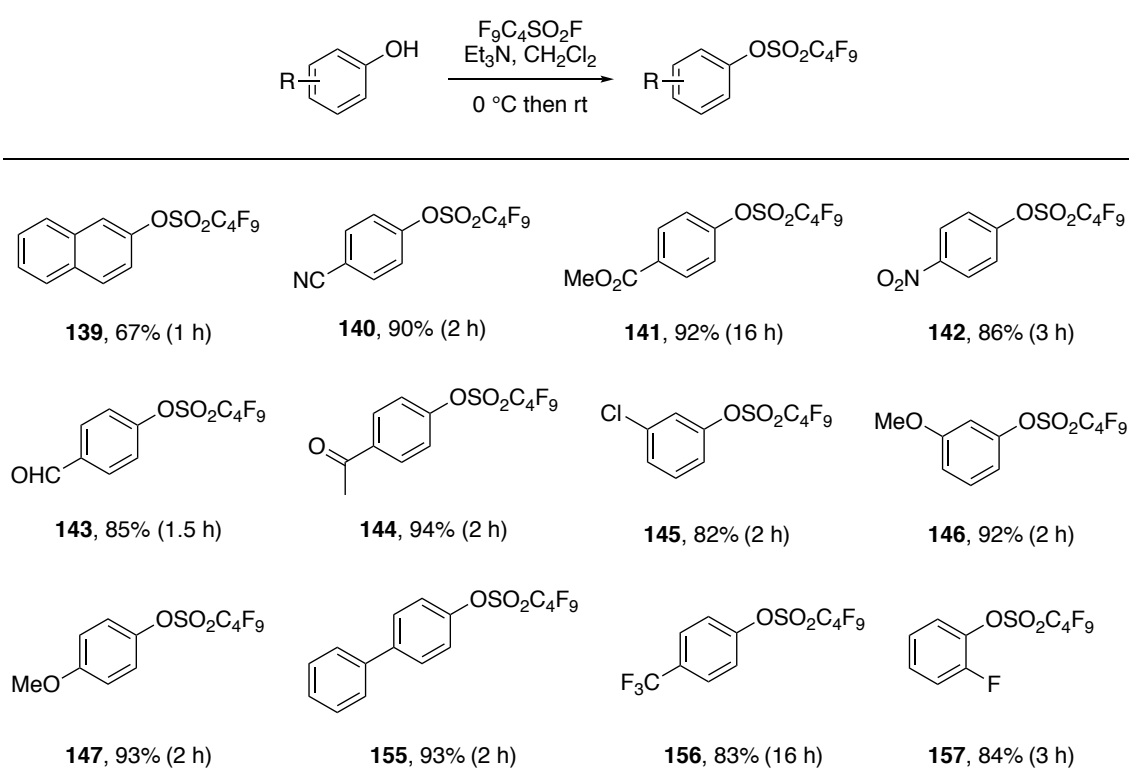
Scheme 55 – Proposed synthesis of aryl iodides from phenols *via* aryl nonaflates

2.3.4 Ruthenium-Catalysed Iodination of Aryl Nonaflates

2.3.4.1 Synthesis of Aryl Nonaflates

The first aim of this project was to prepare a library of aryl nonaflates which would subsequently be used to establish the scope and limitations of the ruthenium(II)-catalysed iodination reaction and perform further procedural optimisation where necessary. A selection of twelve commercially available phenols were treated with nonafluoride and triethylamine under mild conditions to afford the analogous aryl nonaflates **139–147** and **155–157** in 67–94% yield (Scheme 56). This procedure was generally very efficient with complete conversion of most phenol substrates to

the corresponding nonaflates observed by TLC after 1–3 h. It is worth noting that 2-naphthyl nonafluorobutanesulfonate (**139**) was afforded in 67% yield due to a handling error; however, nonaflate **139** was previously synthesised in 99% yield under equivalent conditions by Nikki Sloan. Furthermore, purification of the desired nonaflates *via* column chromatography was facile and performed using a very short length of silica gel. The substrate scope included nine nonaflates previously utilised within this project (**139–147**) and was expanded to include a moderately electron-rich biphenyl nonaflate (**155**) and electron-deficient fluorinated analogues (**156** and **157**). Notably, this library of aryl nonaflates was found to be stable in refrigerated storage for four years.



Scheme 56 – Synthesis of aryl nonaflates

In addition, it was envisaged that a more structurally complex aryl nonaflate would be synthesised to examine the utility of this iodination methodology for compounds with biological applications. As described in Section 1.2.3.2, an olaparib-derived SPECT imaging agent [¹²³I]**16b** was previously developed within the Sutherland group for visualisation of the PARP-1 protein.¹⁰² One limitation of the preparation of this radiotracer was the high temperature of 210 °C required to facilitate radioiodination of a bromide precursor *via* a solid state halogen exchange reaction.

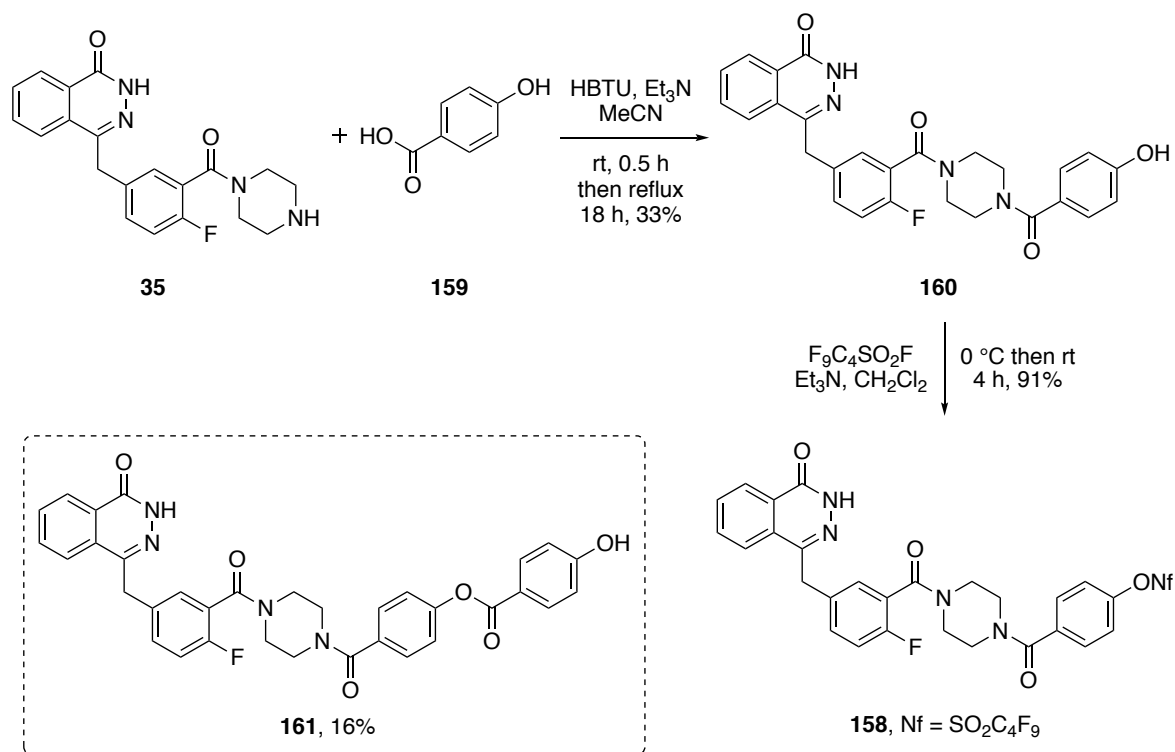
Therefore, it was proposed that radiotracer [^{123}I]**16b** could alternatively be prepared from the corresponding nonaflate analogue **158** under relatively mild conditions using this ruthenium(II)-catalysed pseudo-halogen exchange reaction. As is standard practice, this work would initially be performed using iodine-127 to minimise non-essential handling of radioactivity and afford **16b**, and then repeated with iodine-125 and iodine-123 to prepare [^{125}I]**16b** and [^{123}I]**16b** respectively (Scheme 57).



Scheme 57 – Proposed synthesis of SPECT imaging agent **16b**

Consequently, the olaparib core structure **35** (synthesis previously described in Section 2.1.3) was submitted to an HBTU-mediated coupling reaction with commercially available 4-hydroxybenzoic acid (**159**) in the presence of triethylamine (Scheme 58). Consultation of the literature provided precedent for DCC and EDCI-mediated amide bond forming reactions with 4-hydroxybenzoic acid (**159**) in good yields, without mitigation of its bifunctionality *via* installation of a protecting group.^{315,316} Notably, Wood and co-workers reported that the DCC-mediated amide coupling of acid **159** with methylpiperazine was favoured over a competitive side-reaction with the hydroxy functionality of **159** when performed at elevated temperatures.³¹⁵ As such, the decision was made to forgo the use of a protecting group on the hydroxy functionality of acid **159** in the interest of time, and this amide coupling reaction was performed in acetonitrile under reflux. Under these conditions, the desired phenolic intermediate **160** was afforded in a low yield of 33%, although in sufficient quantity for subsequent applications. Somewhat unsurprisingly, a side-product identified as compound **161** using NMR spectroscopy and mass spectrometry was isolated in 16% yield during the purification of **160** *via* column chromatography. This side-product may have formed *via* ester bond formation between intermediate **160** and 4-hydroxybenzoic acid (**159**) due to the

nucleophilicity of the hydroxy functionality within **160**. Additionally, an ester-linked dimer of 4-hydroxybenzoic acid (**159**) may have formed and underwent subsequent amide coupling with the olaparib core structure **35**. Finally, intermediate **160** was then treated with nonaflyl fluoride under the standard basic conditions used previously, to give nonaflate **158** in an excellent yield of 91% after only 4 h.



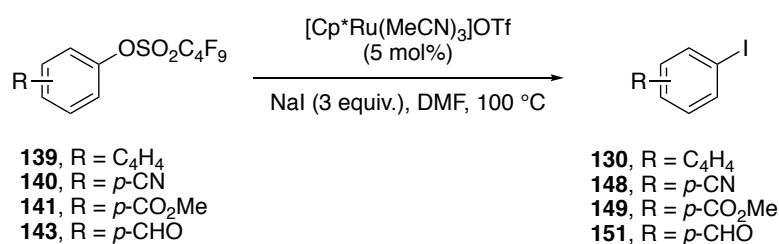
Scheme 58 – Synthesis of aryl nonaflate **158** via intermediate **160**

2.3.4.2 Investigation of Ruthenium-Catalysed Iodination

Following the synthesis of aryl nonaflates **139–147** and **155–158**, the next objective was to duplicate the preliminary results of the ruthenium(II)-catalysed pseudo-halogen exchange reaction reported within the Sutherland group (Scheme **53**).¹⁶¹ Initially, 2-naphthyl nonaflate (**139**) was treated with the optimal conditions established thus far, 5 mol% of ruthenium(II) catalyst **129** with 3 equivalents of sodium iodide in DMF at 100 °C (Table **19**, entry 1). Notably, the ruthenium(II) catalyst **129** employed in this reaction is highly sensitive to air and moisture. Nonetheless, our efforts were focussed on the development of this methodology without the use of glovebox or Schlenk techniques. As such, a dry, sealed reaction vessel containing sodium iodide was employed, and the ruthenium(II) catalyst **129** was added as a solution in anhydrous DMF under argon. However, ¹H NMR

spectroscopy of the reaction mixture after 24 h revealed only 19% conversion from nonaflate **139** to iodide **130**. The iodination of 2-naphthyl nonaflate (**139**) was then repeated using more stringent air handling techniques including rigorous drying of all materials prior to use, handling ruthenium(II) catalyst **129** under argon at all times including weighing, and use of 3 Å molecular sieves (entry 2). This adjustment in protocol resulted in full conversion of nonaflate **139** to the desired iodinated product after 19 h, and 2-iodonaphthalene (**130**) was isolated in an excellent yield of 92%. Consequently, the decision was made to adopt this method as the general ruthenium(II)-catalysed iodination procedure. Electron-deficient nonaflates **140**, **141** and **143** were also subjected to iodination using this general procedure (entries 3–5). Under these conditions, *p*-cyanophenyl nonaflate (**140**) was converted to the corresponding iodide in 70% conversion and 4-iodobenzonitrile (**148**) was afforded in 40% yield. However, nonaflates **141** and **143** underwent only 38% and 32% conversion respectively to the analogous iodides even after extended reaction times of 66 h.

Table 20 – Initial ruthenium-catalysed iodination of aryl nonaflates



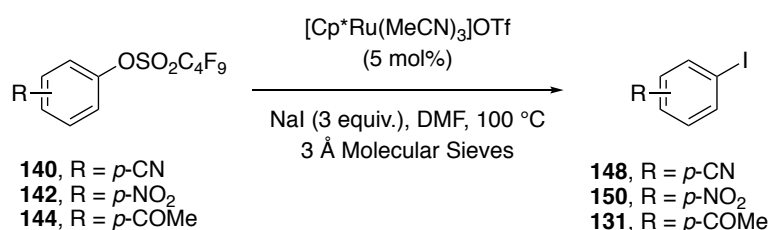
Entry	Nonaflate	Stringent Air Handling ^a	Time (h)	Conversion to Iodide (%) ^b	Isolated Yield of Iodide (%)
1	139	No	24	19	-
2	139	Yes	19	100	92
3	140	Yes	24	70	40
4	141	Yes	66	38	-
5	143	Yes	66	32	-

^aAs described in text above. ^bDetermined using ¹H NMR spectroscopy.

The incomplete conversion to the desired aryl iodides observed in these initial reactions, despite significantly longer reaction times compared to previous work in the Sutherland group, was deemed unsatisfactory. Furthermore, this procedure

would be inadequate for future application of this methodology to radioiodination for which reaction times must be minimised as far as practicable. After consideration of the sensitivity of the ruthenium(II) catalyst **129** to both air and moisture, it was decided that a new batch of catalyst would be investigated. The catalyst **129** batch in use at that time had been exposed to air and moisture on numerous occasions over a period of six months which would likely have had a detrimental impact on catalytic activity. Employing a newly sourced batch of catalyst **129** from the same supplier (Strem Chemicals), *p*-cyanophenyl nonaflate (**140**) was once again subjected to the general ruthenium(II)-catalysed iodination procedure and underwent 86% conversion to 4-iodobenzonitrile (**148**) after 18 h (Table **20**, entry 1). This increase in conversion of 16% was indicative that the older batch of ruthenium(II) catalyst **129** used previously had undergone degradation to some degree as hypothesised. Two additional electron-deficient nonaflates, *p*-nitrophenyl nonaflate (**142**) and *p*-acetylphenyl nonaflate (**144**) were submitted to this general procedure with the new batch of catalyst **129** (entries 2 and 3). Full reaction of nonaflate **142** was observed after 24 h and the corresponding iodide **150** was given in 63% yield. Furthermore, nonaflate **144** underwent 58% conversion to iodide **131** after 24 h and 4-iodoacetophenone (**131**) was subsequently isolated in a moderate yield of 46%. Consequently, this new batch of ruthenium(II) catalyst **129** was employed for all subsequent reactions.

Table 21 – Iodination using new batch of ruthenium(II) catalyst **129**



Entry	Nonaflate	Time (h)	Conversion to Iodide (%) ^a	Isolated Yield of Iodide (%)
1	140	18	86	-
2	142	24	100	63
3	144	24	58	46

^aDetermined using ¹H NMR spectroscopy.

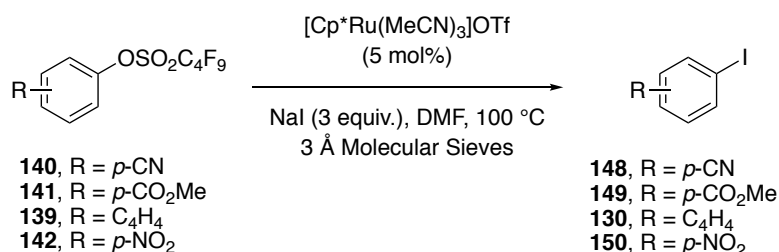
Although these results were encouraging, additional investigations were necessary to pursue reduced reaction times whilst maintaining or even improving conversion. Firstly, electron-deficient aryl nonaflates **140** and **141** were submitted to the general ruthenium(II)-catalysed pseudo-halogen exchange procedure (Table **21**, entries 1 and 2). These reactions underwent analysis *via* ¹H NMR spectroscopy after 3 h to facilitate comparison with the results previously reported within the Sutherland group. It was found *p*-cyanophenyl nonaflate (**140**) and methyl 4-nonafluorobutanesulfonyloxybenzoate (**141**) underwent 71% and 30% conversion respectively to the corresponding iodides **148** and **149**. Notably, these reactions produced similar conversion to equivalent experiments that employed the previous batch of catalyst **129** but were achieved after significantly shorter periods of time as desired (Table **19**). However, both reactions exhibited lesser reactivity than reported in the preliminary results of this project (Scheme **53**).

The efforts of this project were then directed towards the iodination of 2-naphthyl nonaflate (**139**) given that this substrate had provided the highest conversion to and yield of the corresponding iodide from the library of aryl nonaflates thus far (Table **21**). Initially, nonaflate **139** was subjected to the general ruthenium(II)-catalysed iodination procedure and underwent 90% conversion to 2-iodonaphthalene (**130**) after only 1 h (entry 3). In an attempt to promote complete iodination of nonaflate **139**, this reaction was then performed in duplicate except the reaction mixture was degassed under argon for five minutes prior to heating (entry 4). This was achieved by placing the reaction vessel into an ultrasonic bath and bubbling argon through the reaction mixture whilst on degas mode with a 23 gauge vent needle. Conversely, 86% conversion to iodide **130** was observed indicating that degassing had a very slight detrimental impact on the reaction efficiency. To substantiate this theory, the iodination of *p*-cyanophenyl nonaflate (**140**) was repeated and the reaction mixture was degassed in an identical manner (entry 5). Notably, only 53% conversion to 4-iodobenzonitrile (**148**) was achieved after 3 h compared to 71% conversion when performed without degassing (entry 1). As such, it was concluded that degassing of the reaction mixture negatively impacts the activity of catalyst **129** and this step was omitted from all subsequent applications of this methodology.

Next, the iodination of nonaflate **139** was performed at two millimolar scales in parallel, one identical to the preceding attempts and the other at two-fold larger scale

(entries 6 and 7). It was proposed that increasing the scale of this experiment and consequently the quantity of ruthenium(II) catalyst **129** employed from 3 milligrams to 6 milligrams would help to minimise any negative impact on productivity caused by inherent balance error or air/moisture sensitivity during handling. At the two-fold larger scale of 0.235 millimoles, nonaflate **139** underwent greater than 95% conversion to 2-iodonaphthalene (**130**) with only trace quantities of **139** observed by ¹H NMR spectroscopy after 1.5 h (entry 7). Furthermore, iodide **130** was isolated in a good yield of 78%. This was a satisfactory improvement upon the equivalent experiment performed at 0.117 millimoles in which 90% conversion to iodide **130** was observed and 2-iodonaphthalene (**130**) was isolated in 67% yield (entry 6). As such, electron-deficient nonaflates **140**, **141** and **142** were then subjected to the ruthenium(II)-catalysed iodination procedure at an increased scale (entries 8–10). Notably, these conditions facilitated the highest conversion of each aryl nonaflate to the corresponding iodide thus far and within a reduced reaction duration of only 3 h.

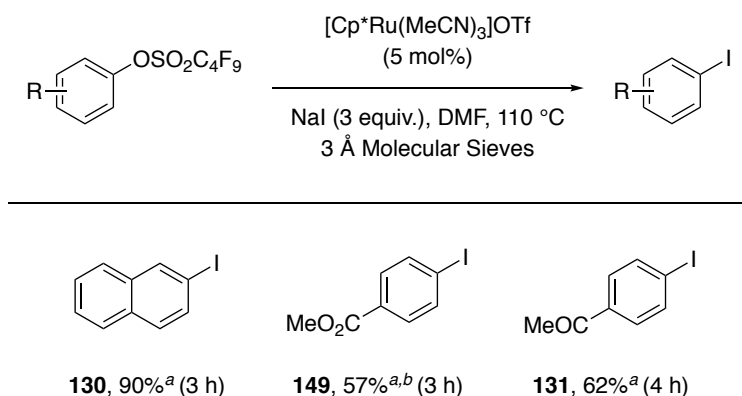
Table 22 – Reduction of reaction time for ruthenium-catalysed iodination



Entry	Nonaflate	Scale (mmol)	Degassed	Time (h)	Conversion to Iodide (%) ^a	Isolated Yield of Iodide (%)
1	140	0.125	No	3	71	-
2	141	0.115	No	3	30	-
3	139	0.117	No	1	90	-
4	139	0.117	Yes	1	86	-
5	140	0.125	Yes	3	53	-
6	139	0.117	No	1.5	90	67
7	139	0.235	No	1.5	>95	78
8	140	0.249	No	3	74	-
9	141	0.230	No	3	60	-
10	142	0.237	No	3	89	-

^aDetermined using ¹H NMR spectroscopy.

Despite the incremental improvements made to this methodology thus far, the reactivity and yields attained were consistently lesser than those reported in the preliminary results of this project (Scheme 53). In an attempt to promote reactivity, the temperature of this procedure was increased to 110 °C and screened using nonaflates **139**, **141**, and **144** (Scheme 59). Although moderate to good reactivity was observed with each nonaflate employed, the elevated reaction temperature did not facilitate a significant improvement in conversion to the resultant aryl iodides **130**, **149**, and **131**, relative to previous experiments performed at 100 °C (Tables 19–21).

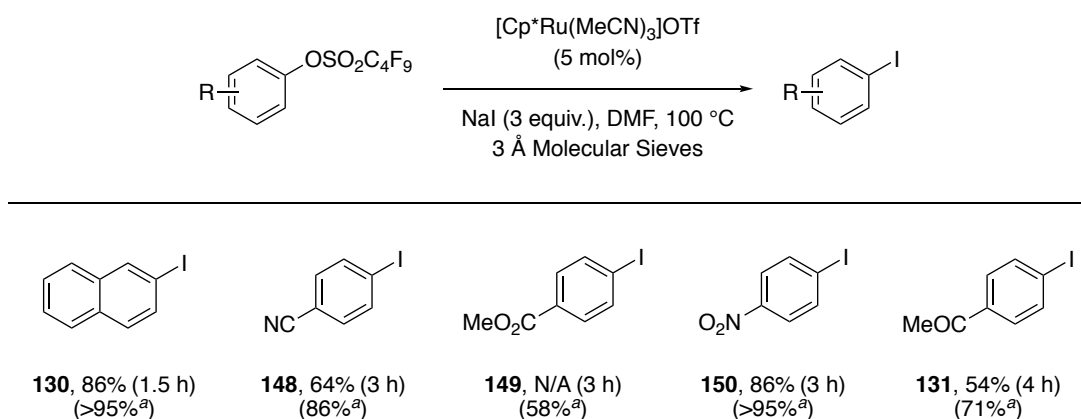


Scheme 59 – Elevation of temperature for ruthenium-catalysed iodination.

^aConversion to iodide determined using ¹H NMR spectroscopy. ^bIsolated yield of 41%.

The final variable investigated was the water content of the anhydrous DMF supply that had been used in all previous experiments within this project. Karl Fischer titration was performed on a sample of anhydrous DMF by a technician, Frank McGeoch and an average water content of 47 ppm was measured *via* six independent titrations. Although the water content was marginally within the manufacturer specifications of less than 50 ppm, it was proposed that the water traces present in the solvent were inhibiting the activity of ruthenium(II) catalyst **129**. Consequently, a new supply of anhydrous DMF was sourced and five aryl nonaflates were resubmitted to the general ruthenium(II)-catalysed iodination procedure (Scheme 60). It was found that four of these pseudo-halogen exchange reactions proceeded with the highest reactivity and efficiency observed thus far. The one exception to this was methyl 4-iodobenzoate (**149**) which was produced in 58% conversion and consequently, was not subjected to purification in this instance. In

addition, four of the five aryl iodides were isolated in good to excellent yields of 54–86% after sufficiently brief reaction durations of 1.5–4 h. As such, it was concluded that this reaction is sensitive to trace quantities of water within the reaction solvent and that anhydrous DMF should be dispensed from the most anhydrous source practicable for the successful application of this methodology.



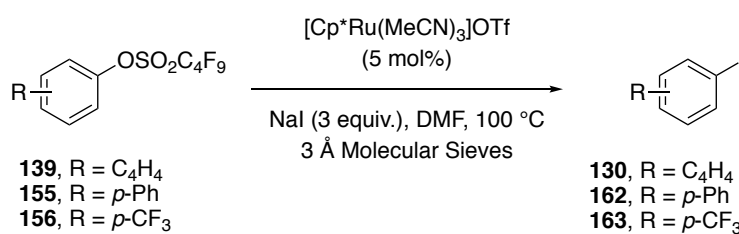
Scheme 60 – Improved ruthenium-catalysed iodination of aryl nonaflates.

^aConversion to iodide determined using ¹H NMR spectroscopy.

The next objective of the project was to determine the substrate scope of this methodology using the diverse library of aryl nonaflates synthesised previously. However due to significant disruption caused by the covid-19 coronavirus pandemic, this research project was suspended for a prolonged period. After access to the research laboratory had been restored, it was necessary to replace both the ruthenium(II) catalyst **129** and anhydrous DMF which had undergone degradation by air and moisture with new batches. Notably, catalyst **129** underwent a significant colour change from orange to black during this time. Upon receipt of a new batch of ruthenium(II) catalyst **129** from Strem Chemicals, visual inspection of the catalyst prompted the suspicion that this batch had undergone degradation prior to its arrival. As a quality control measure, this newly delivered batch of ruthenium(II) catalyst **129** was employed for the iodination of 2-naphthyl nonaflate (**139**) under the general iodination conditions developed in this project (Table **22**, entry 1). However, no reaction was observed by ¹H NMR spectroscopy and it was established that this batch of catalyst **129** was inactive. Consequently, a second new batch of catalyst **129** was then sourced from the same supplier and presented as a dark brown powder upon delivery. As such, this secondary batch of catalyst **129** was employed for the iodination of 2-naphthyl nonaflate (**139**) under the general conditions in

triplicate (entries 2–4). However, it was found that conversion of nonaflate **139** to 2-iodonaphthalene (**130**) was limited to 40–46% despite increased reaction times of up to 4 h. To confirm that this low reactivity was common to other substrates, this batch of catalyst **129** was then employed for the iodination of two additional aryl nonaflates, (1,1'-biphenyl)-4-yl nonaflate (**155**) and (4-trifluoromethyl)phenyl nonaflate (**156**) (entries 5 and 6). As expected, none or poor conversion to the analogous iodides was observed by ¹H NMR spectroscopy. Further investigation revealed that each batch of ruthenium(II) catalyst **129** received following the covid-19 coronavirus pandemic had originated from the same bulk production lot which had been manufactured three years earlier. As such, it was concluded that this supply of catalyst **129** was of unreliable quality due to prolonged storage.

Table 23 – Quality control of ruthenium(II) catalyst **129**



Entry	Nonaflate	Time (h)	Conversion to iodide (%) ^b
1	139	1	0
2	139	1.5	46
3	139	3	45
4	139	4	40
5	155	3	0
6	156	3	27

^aDetermined using ¹H NMR spectroscopy.

2.3.4.3 Investigation of an Alternative Ruthenium Catalyst

Following the supply issues relating to ruthenium(II) catalyst **129**, it was proposed that the triflate anion of catalyst **129** may be interchangeable with a complementary weakly coordinating anion. Crucially, this alternative catalyst would be sourced from a different supplier (Sigma-Aldrich) than catalyst **129**. The decision was made to explore the use of an analogous ruthenium(II) catalyst,

tris(acetonitrile)pentamethylcyclopentadienylruthenium(II) hexafluorophosphate (**164**) (Figure 37). Based on literature precedent by Hayashi and co-workers, it was envisaged that the hexafluorophosphate anion of ruthenium(II) catalyst **164** would be a suitable substitute given the desired application of the catalyst.³¹⁰

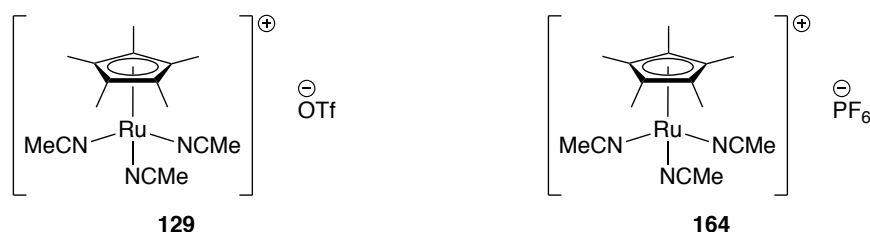
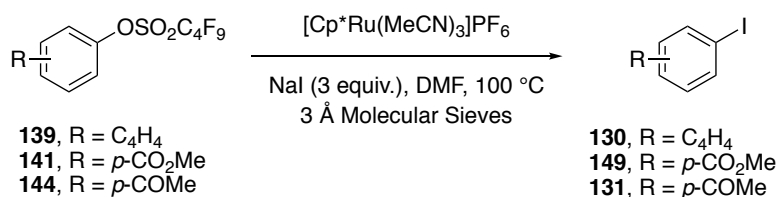


Figure 38 – Structure of ruthenium(II) catalysts **129** and **164**

As was now standard practice in this project, ruthenium(II) catalyst **164** was first investigated with 2-naphthyl nonaflate (**139**) due to the high conversion and yields obtained previously when this substrate was treated with ruthenium(II) catalyst **129**. Initially, 2-naphthyl nonaflate (**139**) was submitted to the general iodination procedure with ruthenium(II) catalyst **164** (4.5 mol%) and sodium iodide in DMF at 100 °C and monitored regularly by ¹H NMR spectroscopy (Table 23, entry 1). Under these conditions, 79% conversion to 2-iodonaphthalene (**130**) was observed after 5 h and allowed for the isolation of iodide **130** in 59% yield. Comparison of this result with a previous experiment using ruthenium(II) catalyst **129** established that the use of ruthenium(II) catalyst **164** resulted in a slower and less productive reaction. Therefore, it was concluded that **164** was a less reactive catalyst than **129**. Consequently, the reaction using **164** was repeated with an increased catalyst loading of 6.5 mol% which produced full conversion after 3 h, and 2-iodonaphthalene (**130**) was afforded in 75% yield (entry 2). Although this catalyst facilitated a more sluggish reaction, these conditions were deemed a suitable substitute for those previously developed with catalyst **129**. The attention of the project then shifted to investigate the scope of this pseudo-halogen exchange reaction mediated by ruthenium(II) catalyst **164**. Nonaflates **141** and **144** were submitted to these conditions and produced 59% and 54% conversion respectively after 3 h (entries 3 and 4). Notably, these reactions did not make substantial further progress after 6 h, at which point 64% and 60% conversion was observed correspondingly.

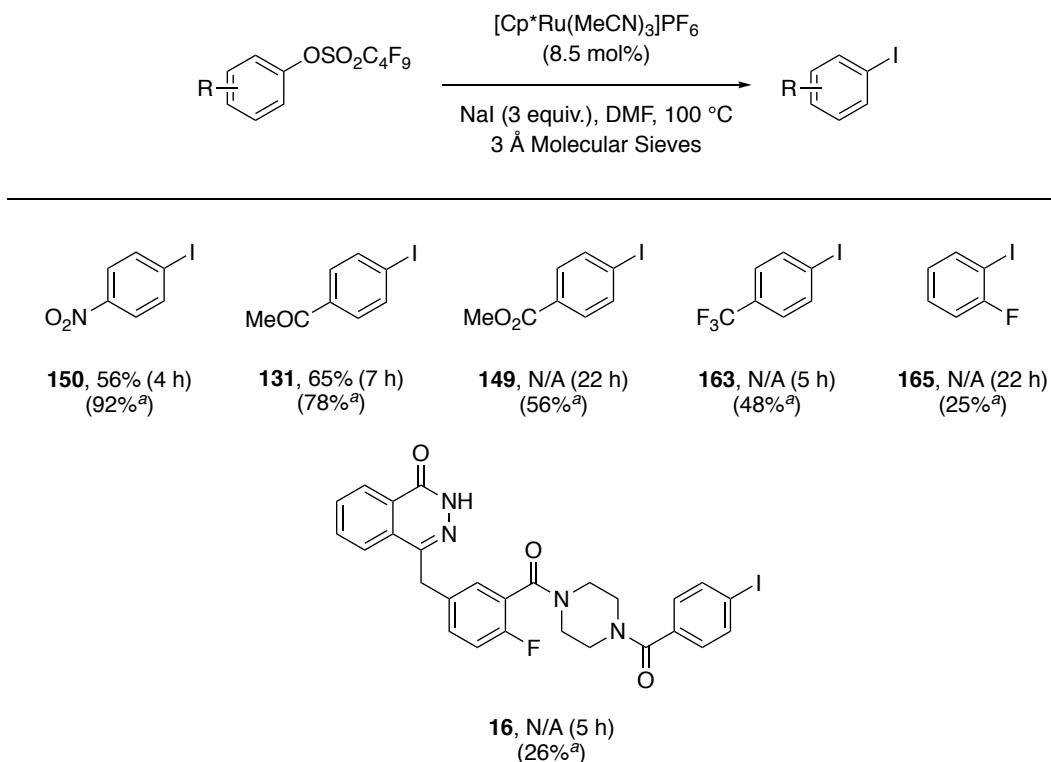
Table 24 – Iodination of aryl nonaflates using ruthenium(II) catalyst **164**

Entry	Nonaflate	[Cp [*] Ru(MeCN) ₃]PF ₆ (164) (mol%)	Time (h)	Conversion to Iodide (%) ^a	Isolated Yield of Iodide (%)
1	139	4.5	5	79	59
2	139	6.5	3	100	75
3	141	6.5	6	64	-
4	144	6.5	6	60	-

^aDetermined using ¹H NMR spectroscopy.

Consequently, the loading of ruthenium(II) catalyst **164** was further increased to 8.5 mol% and a series of five aryl nonaflates were submitted to this iodination procedure (Scheme **61**). Under these conditions, electron-deficient *p*-nitrophenyl nonaflate (**142**) and *p*-acetylphenyl nonaflate (**144**) underwent good conversion to the corresponding iodides after 4 and 7 h respectively. As envisaged, the elevated loading of catalyst **164** was found to facilitate a more efficient and productive iodination of nonaflate **144**. Subsequently, iodides **150** and **131** were isolated in good yields of 56% and 65%. Notably, the disparity between reaction conversion and isolated yield of iodide **150** was caused by repetitive purification *via* flash column chromatography and preparative thin layer chromatography. In addition, marginally less electron-deficient nonaflates **141**, **156** and **157** underwent low to moderate conversion to iodides **149**, **163** and **165** despite elongated reaction times of up to 22 h. Generally, very little (up to 13%) or no reaction progress was observed after the initial 5 h of these experiments, indicating a significant decline in the catalytic activity of **164** over time. Finally, the iodination of aryl nonaflate **158**, potential precursor to PARP-1 SPECT imaging agent [¹²³I]**16b**, was attempted using the same conditions. It was found that aryl nonaflate **158** underwent 26% conversion to the non-radioactive analogue **16b** after 5 h, and no further reaction progress was observed by ¹H NMR spectroscopy of the mixture after 24 h. Although the

conversion was relatively low, this reaction demonstrated that this novel methodology could be applied successfully to more complex organic compounds such as SPECT imaging agents. From this substrate screen it is evident that further optimisation will be required to utilise ruthenium(II) catalyst **164** for the iodination of aryl nonaflates *via* pseudo-halogen exchange.

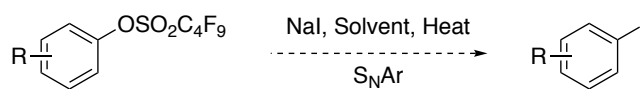


Scheme 61 – Iodination of aryl nonaflates using increased loading of ruthenium(II) catalyst **164**. ^aConversion to iodide determined using ¹H NMR spectroscopy.

2.3.5 Metal-Free Iodination of Aryl Nonaflates *via* an S_NAr Reaction

Concurrent with the development of a ruthenium(II)-catalysed pseudo-halogen exchange procedure, a metal-free iodination method was also briefly investigated given the possible environmental and economic benefits. Consultation of the literature provided multiple examples in which aryl iodides were prepared from aryl triflates *via* nucleophilic aromatic substitution (S_NAr) reactions.^{317–319} Typically in these studies, aryl triflates were treated with multiple equivalents of sodium iodide in high boiling point solvents at elevated temperatures. Since nonaflates contain a greater quantity of electronegative fluorine atoms compared with triflates, it was proposed that the nonaflate group may be a suitable or even superior leaving group

for displacement from an arene within an S_NAr reaction. As such, it was proposed that a series of aryl nonaflates would be submitted to iodination *via* an S_NAr reaction through facile treatment with sodium iodide at an elevated temperature (Scheme 62).



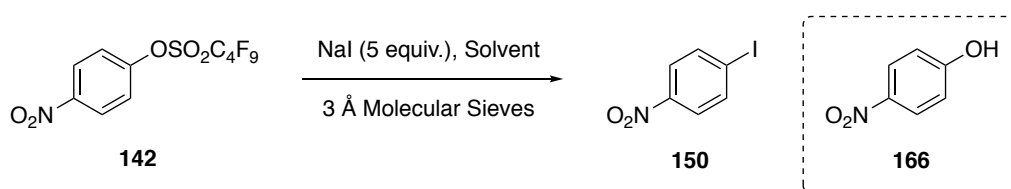
Scheme 62 – Proposed iodination of aryl nonaflates *via* an S_NAr reaction

Given that S_NAr reactions are promoted by the presence of electron-withdrawing substituents in the *ortho*- or *para*- positions relative to the leaving group, *p*-nitrophenyl nonaflate (**142**) was selected for screening of reaction conditions. Firstly, *p*-nitrophenyl nonaflate (**142**) was treated with 5 equivalents of sodium iodide in toluene under reflux and inert conditions (Table 24, entry 1). However, no reaction was observed by ¹H NMR spectroscopy after 5 h. To allow for elevation of the reaction temperature, DMF was employed as the solvent in a subsequent attempt (entry 2). Under these conditions, full conversion of nonaflate **142** to 4-iodonitrobenzene (**150**) was not achieved despite an extended reaction time of 91 h. A maximum conversion of 58% was observed, as were traces of decomposition likely caused by prolonged exposure to high temperatures. To increase the rate and reactivity of this procedure, two further attempts were made at higher temperatures of 140 °C and 160 °C. Elevation of the reaction temperature to 140 °C resulted in a substantially higher reaction rate and 48% conversion to iodide **150** was observed after 20 h (entry 3). However, 15% of the aryl nonaflate starting material remained and *p*-nitrophenol (**166**) was produced as a side-product in 37% conversion. Subsequently, the rate of this reaction was further accelerated when performed at 160 °C with only 27% of nonaflate **142** remaining after 3 h, and full consumption achieved by 20 h (entry 4). Moreover, this increased temperature of 160 °C was found to accelerate the rate at which *p*-nitrophenol (**166**) was produced with respect to iodide (**150**) and was given in 42% conversion.

Notably, *p*-nitrophenol (**166**) was not observed when this reaction was carried out at up to 120 °C and was produced in increasingly higher quantities with elevation of the reaction temperature. Notwithstanding, it was concluded from this series of experiments that a temperature of 160 °C would be required to facilitate this S_NAr

reaction in an appropriate timescale. Subsequently, NMP was employed as an alternative polar, aprotic solvent with a high boiling point at a reaction temperature of 160 °C to examine the impact of solvent on this reaction (entry 5). Although full consumption of nonaflate **142** was achieved after only 5 h, the production of *p*-nitrophenol (**166**) in 57% conversion was equally significant. Therefore, it was proposed that this side-product was formed *via* hydrolysis with water traces present within each solvent. Moreover, it was concluded that the production of *p*-nitrophenol (**166**) was greatly dependant on the reaction temperature and would not be inhibited by the employment of a particular solvent. Consequently, the decision was made to focus the efforts of this project on the synthesis of aryl iodides from aryl nonaflates *via* palladium-catalysed pseudo-halogen exchange reactions.

Table 25 – Screen of S_NAr reaction conditions with *p*-nitrophenyl nonaflate (**142**)



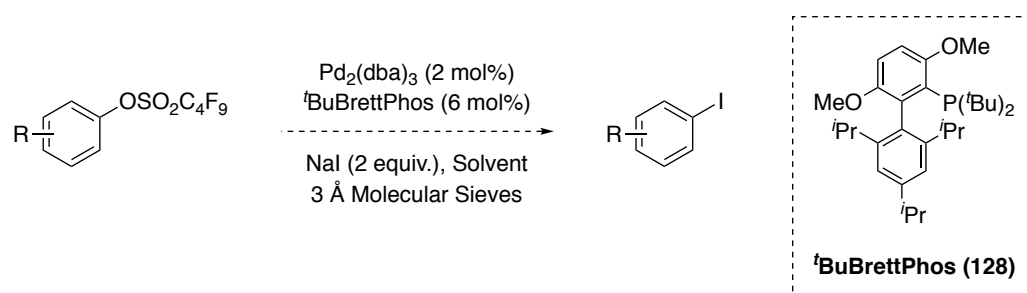
Entry	Solvent	Temp. (°C)	Time (h)	Ratio of 142 : 150 : 166 ^a		
1	toluene	reflux	5	100	0	0
2	DMF	120	91	42	58	0
3	DMF	140	20	15	48	37
4	DMF	160	20	0	58	42
5	NMP	160	5	0	43	57

^aDetermined using ¹H NMR spectroscopy.

2.3.6 Palladium-Catalysed Iodination of Aryl Nonaflates

As discussed in Section 2.3.1, Larhed and co-workers reported a microwave-assisted palladium(0)-catalysed method for the synthesis of aryl fluorides from aryl alcohols *via* aryl nonaflate intermediates.³¹² In summary, the authors established a one-pot, two-step method in which phenols were first converted to aryl nonaflates using nonafllyl fluoride with caesium fluoride, and then subjected to microwave-assisted fluorination catalysed by tris(dibenzylideneacetone)dipalladium(0)

(Pd₂(dba)₃) (2 mol%) and ^tBuBrettPhos (**128**) (6 mol%) in toluene at 180 °C. This one-pot procedure was exploited for the preparation of aryl fluorides in moderate to good yields over two steps. Furthermore, the authors identified that fluorination was substantially favoured over chlorination or bromination through a competitive experiment employing all three corresponding caesium salts in equal quantity. However, the scope of this methodology was not extended to include the synthesis of aryl chlorides, bromides, or iodides from phenols. Given that the facile iodination of arenes *via* aryl nonaflate intermediates was of interest to the Sutherland group, it was proposed that this methodology from Larhed and co-workers would be further investigated and adapted for the synthesis of aryl iodides using sodium iodide in lieu of a caesium halide salt (Scheme **63**). In addition, it was envisaged that this work would explore the use of lower reaction temperatures and the absence of microwave irradiation.

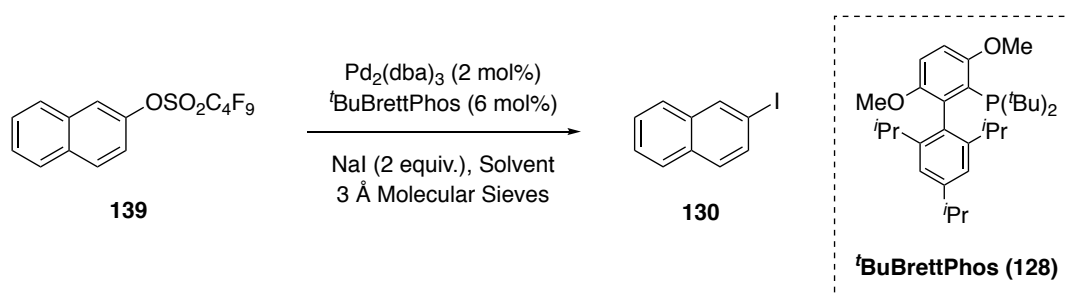


Scheme 63 – Proposed palladium-catalysed iodination of aryl nonaflates

2-Naphthyl nonaflate (**139**) was selected as the substrate for investigation of reaction conditions due to the high conversion and yields of the corresponding iodide **130** obtained within the aforementioned ruthenium(II)-catalysed project. Firstly, nonaflate **139** was treated with Pd₂(dba)₃ (2 mol%), ^tBuBrettPhos (**128**) (6 mol%) and sodium iodide in toluene at 140 °C (Table **25**, entry 1). These conditions facilitated a slow reaction with no iodide **130** observed by TLC after 4 h, and only 9% conversion observed by ¹H NMR spectroscopy after 22 h. In a subsequent attempt, Pd₂(dba)₃ and Buchwald ligand **128** were combined in half of the reaction solvent total volume and stirred at room temperature for 0.25 h before preparation of the reaction mixture (entry 2). This modification of the reaction procedure increased the initial reaction rate and 8% conversion to iodide **130** was produced after only 3 h. However, no further progress was observed up to 19 h and thus, iodide **130** was not given in a greater overall conversion. Elevation of the reaction

temperature from 140 °C to 160 °C was also found to accelerate the rate of iodination with a marginally higher conversion of 12% measured after 3 h (entry 3). Once more, no further reactivity was observed despite an elongated reaction time of 19 h. Given that pre-stirring Pd₂(dba)₃ with Buchwald ligand **128** and performance of this reaction at 160 °C produced the highest conversions thus far, all subsequent attempts employed these conditions. A brief screening of high boiling point solvents was then carried out (entries 4–6). The reaction performed in *p*-xylene produced iodide **130** in 12% conversion indicating equivalent reactivity to the employment of toluene (entry 4). However, no reactivity was observed in either attempt using DMF or NMP after 19 h (entries 5 and 6).

Table 26 – Initial screening of reaction conditions for palladium-catalysed iodination



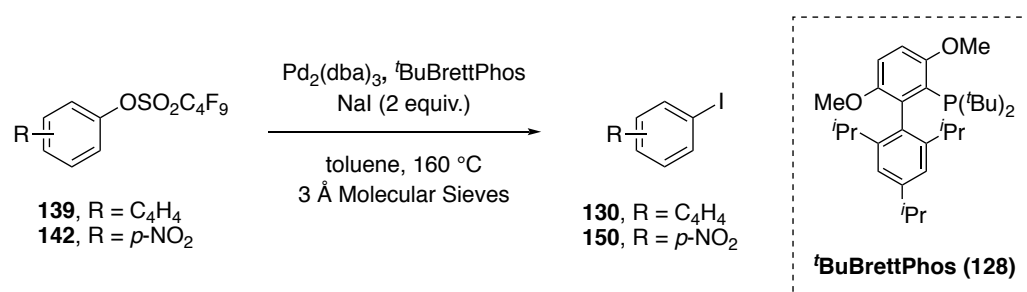
Entry	Pre-stir ^a	Solvent	Temp. (°C)	Time (h)	Conversion to Iodide (%) ^b
1	No	toluene	140	22	9
2	Yes	toluene	140	3	8
3	No	toluene	160	3	12
4	Yes	<i>p</i> -xylene	160	18	12
5	Yes	DMF	160	19	0
6	Yes	NMP	160	19	0

^aAs described in text above. ^bDetermined using ¹H NMR spectroscopy.

With poor conversion observed thus far, the loading of Pd₂(dba)₃ and Buchwald ligand **128** was increased to 4 mol% and 12 mol% respectively (Table **26**, entry 2). As expected, this promoted reactivity but the resultant 18% conversion of nonaflate **139** to iodide **130** was an insufficient development (entry 2). To substantiate this finding, *p*-nitrophenyl nonaflate (**142**) was also submitted to this procedure using 2 mol% Pd₂(dba)₃ and 6 mol% Buchwald ligand **128**, and then repeated with a two-

fold higher catalyst and ligand loading (entries 3 and 4). Overall, this substrate demonstrated lower reactivity than 2-naphthyl nonaflate (**139**) and a similar increase in reactivity with the use of higher catalyst and ligand loading. Following this screen of conditions, it was concluded that iodination of aryl nonaflates using catalytic quantities of Pd₂(dba)₃ and ^tBuBrettPhos (**128**) with sodium iodide was inefficient. Furthermore, it was concluded that application of both Pd₂(dba)₃ and Buchwald ligand **128** in higher catalytic loadings or one equivalent may facilitate the desired iodination; however, these conditions were deemed financially undesirable, and this methodology was not further investigated.

Table 27 – Screening of catalyst loading for palladium-catalysed iodination

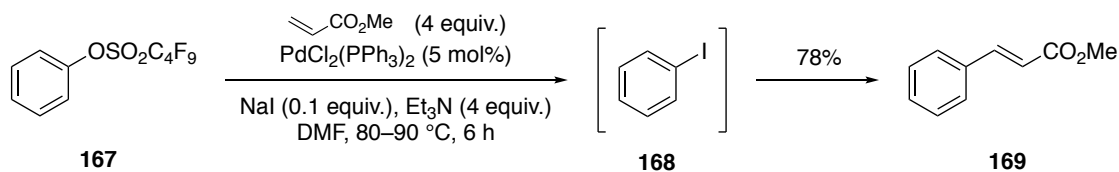


Entry	Nonaflate	Pd ₂ (dba) ₃ (mol%)	^t BuBrettPhos (128) (mol%)	Pre-stir ^a	Time (h)	Conversion to iodide (%) ^b
1	139	2	6	No	3	12
2	139	4	12	Yes	18	18
3	142	2	6	Yes	3	8
4	142	4	12	Yes	3	14

^aAs described in text above. ^bDetermined using ¹H NMR spectroscopy.

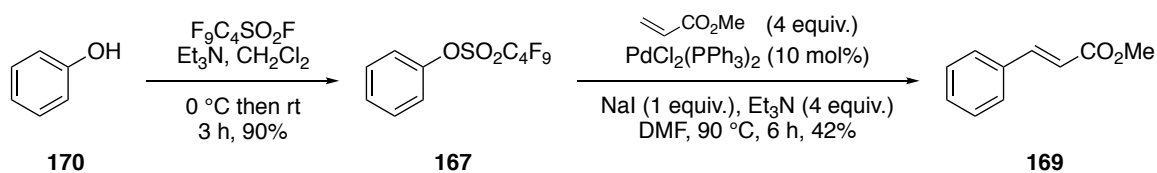
In 2011, Peng *et al.* reported a palladium(0)-catalysed Heck reaction of aryl nonaflates with various terminal alkenes mediated by iodide salts, albeit developed using a very limited substrate scope (Scheme **64**).²⁹⁸ The authors proposed that the aryl nonaflate first underwent a Finkelstein reaction with the substoichiometric iodide salt to produce the corresponding aryl iodide, followed by a Heck reaction with the terminal alkene catalysed by palladium(II)bis(triphenylphosphine) dichloride (PdCl₂(PPh₃)₂) (5 mol%). This hypothetical mechanism was based on a two-fold higher yield attained when a Heck reaction of *p*-chlorophenyl nonaflate and methyl acrylate was performed in the presence of an iodide salt. Furthermore, the authors

reasoned that this increased reactivity was due to improved oxidative addition of the aryl iodide intermediate to the palladium catalyst. However, no studies of the mechanism were performed to validate this claim.



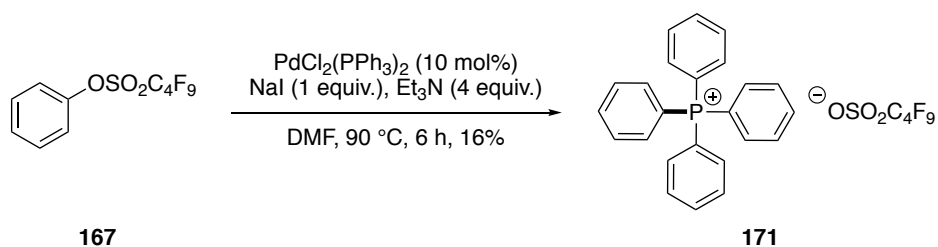
Scheme 64 – Pd/iodide salt mediated Heck reaction of phenyl nonaflate **167** by Peng *et al.*

It was proposed that if the hypothesis from Peng *et al.* was correct, preparation and isolation of the resultant aryl iodide from an aryl nonaflate would be possible simply through deprivation of the methyl acrylate from this reaction. The first objective of this work was to reproduce the Heck reaction of phenyl nonaflate (**167**) and methyl acrylate as described by Peng *et al.* before attempting to isolate iodobenzene (**168**) (Scheme **64**). Initially, phenyl nonaflate (**167**) was prepared from phenol (**170**) following the previously developed procedure with nonafllyl fluoride and triethylamine, in an excellent yield of 90% (Scheme **65**). Following the method described by Peng *et al.*, the palladium(0)/iodide salt-mediated Heck reaction of phenyl nonaflate (**167**) and methyl acrylate was then attempted at 90 °C. Under these conditions, a mixture of phenyl nonaflate (**167**) and methyl *trans*-cinnamate (**169**) was afforded in a ratio of 1 : 1 after 6 h, and an unidentified side-product was observed. Notably, this side-product was confirmed not to be iodobenzene *via* ¹H NMR spectroscopy. The Heck reaction was then attempted using 1 equivalent of sodium iodide at 90 °C and produced a 1 : 1 mixture of **167** and **169** after 6 h, which allowed for the isolation of **169** in only 31% yield. Furthermore, elevation of the reaction temperature to 110 °C also produced a mixture of **167** and **169** in a ratio of 1.2 : 1 after 6 h. Finally, the use of an increased PdCl₂(PPh₃)₂ loading of 10 mol% with 1 equivalent of sodium iodide at 90 °C gave a mixture of **167** and **169** in a ratio of 0.3 : 1 after 6 h. However, methyl *trans*-cinnamate (**169**) was then isolated in a significantly lower yield than expected of only 42% (Scheme **65**).



Scheme 65 – Optimised conditions for the synthesis of phenyl nonaflate (**167**) and methyl *trans*-cinnamate (**169**)

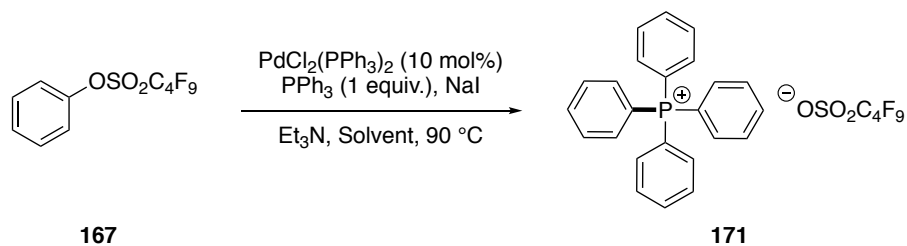
Notably, the production of iodobenzene (**168**) was not observed under these conditions. However, during each attempt to prepare methyl *trans*-cinnamate (**169**), in equivalent yield to that reported by Peng *et al.*, an unidentified side-product was observed by ^1H NMR spectroscopy of the reaction mixture. Given the poor conversion and yields obtained thus far, it was proposed that the identity of this side-product and the pathway by which it is formed would be investigated. Phenyl nonaflate (**167**) was treated with $\text{PdCl}_2(\text{PPh}_3)_2$ (10 mol%), sodium iodide and triethylamine in DMF at $90\text{ }^\circ\text{C}$ for 6 h (Scheme 66). However, methyl acrylate was withheld from this reaction to inhibit the synthesis of **169**. As envisaged, this facilitated production of the unidentified side-product which then underwent isolation and characterisation *via* NMR spectroscopy and mass spectrometry. Subsequently, the side-product was identified as a novel tetraarylphosphonium salt (TAPS), tetraphenylphosphonium nonaflate (**171**) and was isolated in 16% yield. Literature precedent for the palladium-catalysed synthesis of tetraphenylphosphonium bromide, tetraphenylphosphonium iodide and tetraphenylphosphonium triflate was consulted to substantiate this conclusion.³²⁰ In addition, it was proposed that TAPS **171** was formed *via* reductive elimination of phenyl and a triphenylphosphine ligand of $\text{PdCl}_2(\text{PPh}_3)_2$ from a palladium(II) intermediate.³²¹



Scheme 66 – Palladium-catalysed synthesis of TAPS **171**

Over the past two decades, interest in TAPSs has grown due to their utility as alternative cross-coupling reagents,^{322,323} superior thermally stable ionic liquids,^{324,325} catalysts for the synthesis of cyclic carbonates and oxazolidinones from epoxides,^{326–328} PET imaging agents for oncology and cardiology application,^{329–333} and solubility-control groups that are capable of supporting a variety of reagents, ligands and catalysts within small molecule and peptide synthesis.^{320,334–343} TAPSs were prepared from substituted aryl halides or triflates and triphenylphosphine using either a palladium- or nickel-catalysed procedure as reported by Marcoux and Charette in 2008.^{320,338} Although widely employed, these methods are intolerant of some functionalities and require elevated reaction temperatures of 145–180 °C. Furthermore, these procedures have not yet been applied for the synthesis of nonaflate TAPSs, to the best of our knowledge.

Given the observed propensity of aryl nonaflate **167** to undergo carbon–phosphorus bond formation with triphenylphosphine, the palladium-catalysed procedure for the synthesis of tetraphenylphosphonium nonaflate (**171**) was further optimised (Table **27**). The addition of triphenylphosphine in stoichiometric quantities (1 equiv.) allowed for the preparation of TAPS **171** in a significantly improved yield of 57% (entry 1). Next, the vital roles of both the additive sodium iodide and triethylamine in this process were demonstrated by withholding each from distinct reactions, which consequently failed to produce TAPS **171** within the timeframes observed (entries 2 and 3). Use of less than four equivalents of triethylamine was shown to be detrimental to the reaction rate, with significantly longer reaction times of up to 21 h required to achieve full conversion of phenyl nonaflate (**167**), and yield of TAPS **171** (entries 4 and 5). Furthermore, this C–P bond forming reaction was not facilitated when attempted using toluene, dioxane or acetonitrile (entries 6–8).

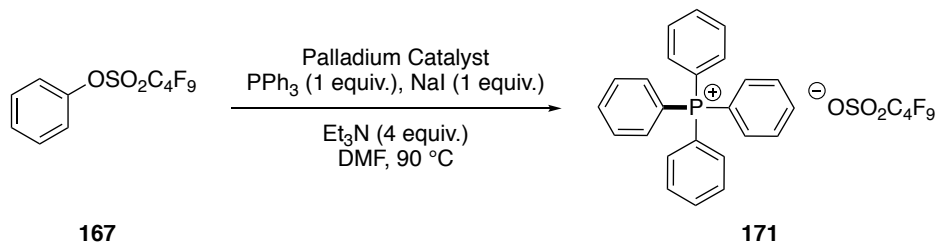
Table 28 – Optimisation of palladium-catalysed synthesis of TAPS **171**

Entry	Equiv. of NaI	Equiv. of Et ₃ N	Solvent	Time (h)	Isolated Yield of 171 (%)
1	1	4	DMF	6	57
2	0	4	DMF	3	-
3	1	0	DMF	22	-
4	1	1	DMF	21	39
5	1	2	DMF	6	45
6	1	4	toluene	4	-
7	1	4	acetonitrile	4	-
8	1	4	1,4-dioxane	4	-

As such, a subsequent screening of palladium catalysts was performed using 1 equivalent of triphenylphosphine and sodium iodide, with 4 equivalents of triethylamine in DMF at 90 °C (Table **28**). Firstly, the use of PdCl₂(PPh₃)₂ was examined at alternative loadings of 5 mol% and 15 mol% (entries 1 and 2). Neither catalyst loading was beneficial to the yield of TAPS **171** however, an increase in reaction rate was observed when 15 mol% PdCl₂(PPh₃)₂ was employed and full conversion of phenyl nonaflate (**167**) was achieved after only 4 h. Subsequently, a screen of catalysts including Pd₂(dba)₃, Pd(PPh₃)₄, Pd(dppf)Cl₂ and Pd(OAc)₂ was performed (entries 3–6). Each palladium catalyst facilitated full conversion of nonaflate **167** after 4 h and produced tetraphenylphosphonium nonaflate (**171**) in moderate to good yield. It was found that Pd₂(dba)₃, Pd(PPh₃)₄ and Pd(dppf)Cl₂ were less productive than PdCl₂(PPh₃)₂ at equivalent loading of 10 mol%, whilst Pd(OAc)₂ offered superior reactivity and gave TAPS **171** in a good yield of 68%. This optimised method allowed for the synthesis of tetraphenylphosphonium nonaflate (**171**) in good yield under milder conditions than those previously described in the literature for analogous halide and triflate TAPSs. As such, following a delay caused by the covid-19 coronavirus pandemic, the decision was made to

investigate the application of this methodology for additional C–P bond forming reactions of aryl nonaflates.

Table 29 – Screening of palladium catalysts for the synthesis of TAPS **171**

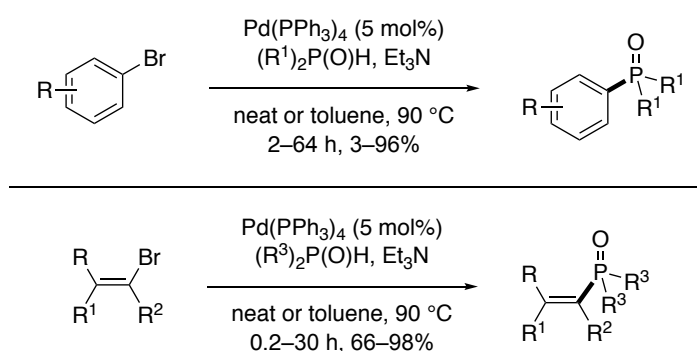


Entry	Catalyst (mol%)	Time (h)	Isolated Yield of 171 (%)
1	PdCl ₂ (PPh ₃) ₂ (5 mol%)	6	41
2	PdCl ₂ (PPh ₃) ₂ (15 mol%)	4	54
3	Pd ₂ (dba) ₃ (10 mol%)	4	40
4	Pd(PPh ₃) ₄ (10 mol%)	4	40
5	Pd(dppf)Cl ₂ (10 mol%)	4	54
6	Pd(OAc) ₂ (10 mol%)	4	68

2.3.7 Iodide-Accelerated, Palladium-Catalysed Phosphorylation Reactions of Aryl Nonaflates

2.3.7.1 Background of Metal-Catalysed Aryl Phosphorylation

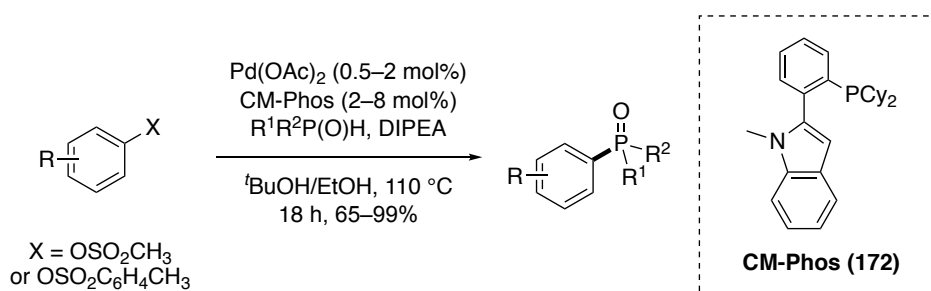
Aryl phosphorus compounds are readily utilised in a range of disciplines including organic synthesis,^{344–347} materials chemistry,^{348–355} and medicinal chemistry.^{356–365} The value of these compounds has provoked significant interest in the field of organophosphorus chemistry. Over the past five decades, a substantial quantity of research has been conducted to improve traditional procedures and establish novel methodology for the construction of aryl carbon–phosphorus bonds. The most commonly exploited method for aryl phosphorylation was once the reaction of aryl organometallic reagents, such as Grignard or organolithium species, with electrophilic chlorophosphorus reagents.^{345,366–368} However in 1981, Hirao and co-workers established a milder aryl C–P bond-forming process *via* palladium-catalysed cross-coupling of electrophilic aryl bromides with various dialkyl phosphite reagents under basic conditions (Scheme 67).^{369,370} Furthermore, the authors subsequently demonstrated that this method could also be readily adopted for the preparation of vinylphosphonates *via* cross-coupling of vinyl bromides with dialkyl phosphite reagents.^{370,371}



Scheme 67 – Palladium-catalysed C–P cross-coupling by Hirao and co-workers

This seminal work by Hirao and co-workers has inspired numerous derivative studies of metal-catalysed aryl C–P bond-formation, with focus on the use of palladium, nickel and copper catalysts, which have been reviewed periodically.^{372–377} In addition, much of this research has sought to further optimise the palladium-catalysed Hirao reaction, expand its application to a wider scope of electrophilic

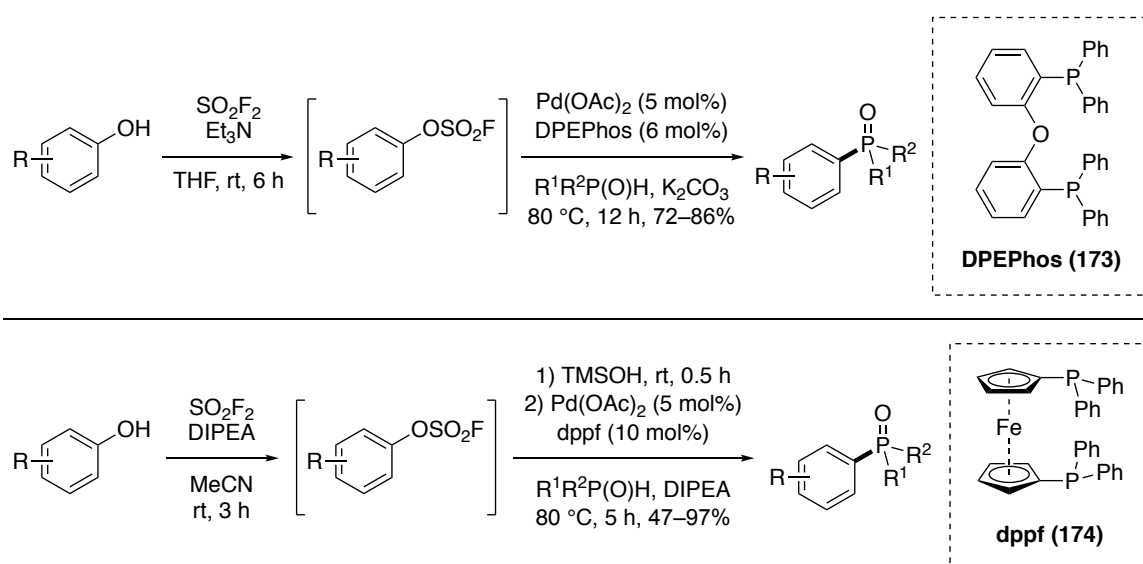
arenes and organophosphorus P(O)–H substrates, and elucidate the mechanism by which aryl C–P bond-formation proceeds.^{378–386} Aryl halides are frequently employed as the electrophilic aryl substrate of the Hirao reaction and derived methods however, phenols are ubiquitous within biologically active compounds such as steroids, amino acids and numerous FDA approved pharmaceuticals.¹²⁹ Consequently, there is considerable interest in the phosphorylation of phenol-derived aryl sulfonates *via* Hirao-type reactions. As previously discussed in Section 2.3.1, phenol-derived aryl sulfonates such as mesylates, tosylates, triflates and nonaflates are commonly exploited intermediates due to their increased reactivity relative to the corresponding phenol. Aryl mesylates and tosylates have been shown to undergo cross-coupling with P(O)–H compounds including dialkyl phosphites, alkyl arylphosphinates, and secondary phosphine oxides *via* palladium, nickel, and dual nickel/photoredox catalysis.^{387–389} In 2015, Kwong and co-workers reported the first palladium-catalysed cross-coupling of aryl mesylates and tosylates with dialkyl phosphites and alkyl arylphosphinates (Scheme 68).³⁸⁷ The authors employed a catalytic system of Pd(OAc)₂ (0.5–2 mol%) and sterically hindered dialkybiarylphosphine ligand CM-Phos (**172**) (2–8 mol%) under basic conditions to prepare a diverse library of tertiary phosphine oxides in high yields of 65–99% after 18 h reactions at 110 °C. Furthermore, this method was successfully employed for the phosphorylation of biologically active phenols 17β-estradiol, a sex steroid hormone,³⁹⁰ and 6-hydroxyflavone, a flavonoid neutralising modulator of GABA_A receptors,³⁹¹ in good yields *via* mesylate intermediates.



Scheme 68 – Palladium-catalysed C–P cross-coupling by Kwong and co-workers

In 2021, concurrent with the work described herein, the research groups of Ding and Xu independently reported one-pot procedures for the palladium-catalysed phosphorylation of phenols *via* aryl fluorosulfonate intermediates (Scheme 69).^{392,393} Both groups treated a range of phenols with gaseous sulfur fluoride

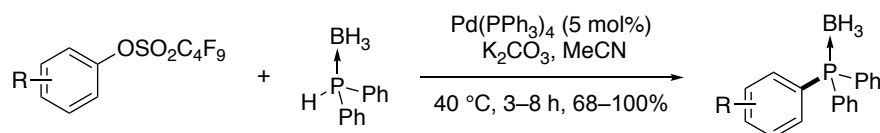
under basic conditions to afford aryl fluorosulfonates *in situ*, which were then submitted to phosphorylation with a range of dialkyl phosphites, alkyl arylphosphinates, and secondary phosphine oxides. In each case, C–P cross-coupling was achieved using Pd(OAc)₂ (5 mol%) with a bidentate bisphosphine ligand, either DPEPhos (**173**) or 1,1'-bis(diphenylphosphine)ferrocene (dppf) (**174**), in the presence of base at 80 °C. These methods were tolerant of a broad range of functionality and allowed for the preparation of diverse tertiary phosphine oxides in good yields after short reaction times. In addition, Xu and co-workers demonstrated the utility of their one-pot protocol with a selection of more structurally complex compounds including a naturally occurring flavone apigenin, a steroid 17β-estradiol and an olaparib-derived PARP inhibitor.



Scheme 69 – One-pot palladium-catalysed phosphorylation of phenols *via* aryl fluorosulfonates by independent groups of Ding and Xu

Furthermore, aryl triflates have also been commonly investigated as fluorosulfonate intermediates to facilitate the phosphorylation of phenols.^{320,372–374,377,382,394–397} However, as previously discussed in Section 2.3.2, aryl nonaflates offer a less expensive alternative with increased reactivity despite improved stability in storage. Notably, there are very limited reports of metal-catalysed C–P bond-forming reactions that employ aryl nonaflate intermediates. Generally, those reported in the literature are singular examples provided for comparison purposes within studies that are primarily focussed on the use of aryl halides or triflates.^{398–401} In 1999, Lipshutz and co-workers reported the first and only study of C–P bond-forming

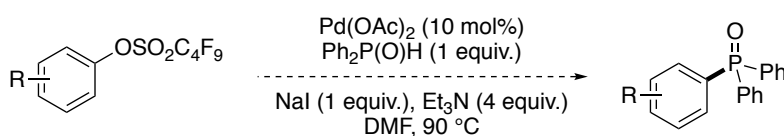
reactions specifically for application with aryl nonaflates, to the best of our knowledge (Scheme 70).⁴⁰² In this work, the authors submitted a small library of aryl nonaflates albeit limited in structural or electronic diversity to C–P cross-coupling with diphenylphosphine borane using Pd(PPh₃)₄ (5 mol%) under basic conditions. The corresponding library of triarylphosphine boranes was afforded in high yields of 68–100% after short reaction times of only 3–8 h at a mild temperature of 40 °C.



Scheme 70 – Palladium-catalysed C–P cross-coupling by Lipshutz and co-workers

2.3.7.2 Proposed Research

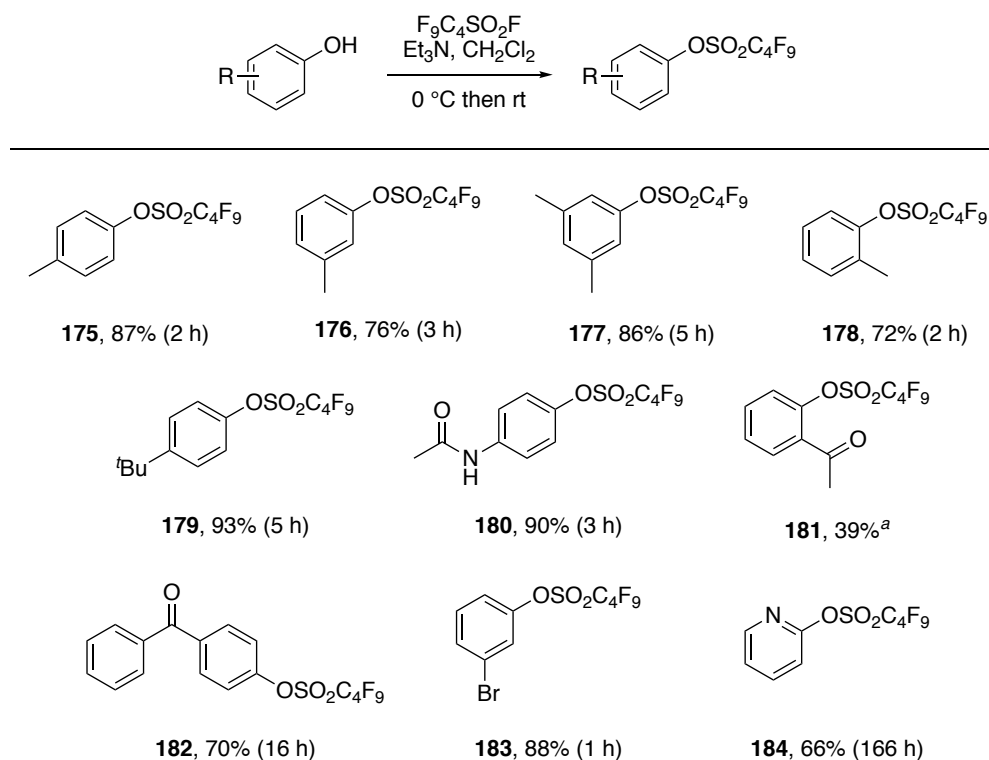
Given the advances in metal-catalysed C–P bond-forming reactions made since the discovery of the Hirao reaction and the improved reactivity of aryl nonaflates versus triflates or halides, the decision was made to develop a palladium-catalysed procedure for the cross-coupling of phenol-derived aryl nonaflates with secondary P(O)–H compounds. Moreover, it was envisaged that this methodology would circumvent the use of additional phosphine ligands or toxic gaseous reagents required for existing procedures and would allow for the preparation of tertiary P(O)–H compounds in short reaction times. The conditions previously optimised for the synthesis of TAPS **171**, the use of palladium acetate (Pd(OAc)₂) (10 mol%), sodium iodide and triethylamine, would initially be explored for the cross-coupling of aryl nonaflates with diphenylphosphine oxide to afford functionalised triphenylphosphine oxides (Scheme 71). Subsequently, the scope of the optimised procedure would be further investigated through cross-coupling of an aryl nonaflate with a range of secondary P(O)–H reagents. Furthermore, it was proposed that the utility of this methodology would be shown through the synthesis of aryl phosphorus compounds with established applications in materials and medicinal chemistry.



Scheme 71 – Proposed synthesis of triarylphosphine oxides from aryl nonaflates

2.3.7.3 Synthesis of Supplementary Aryl Nonaflates

The first objective of this project was to prepare a supplementary library of aryl nonaflates which would be used to optimise the palladium-catalysed phosphorylation reaction and subsequently investigate the scope and limitations of this methodology. A series of ten commercially available phenols which possess diverse substitution and electronic properties were treated with nonaflyl fluoride and triethylamine under mild conditions to afford the analogous aryl nonaflates **175–184** in 39–93% yield (Scheme **72**). Generally, this procedure was very efficient with complete reaction of most phenol substrates observed within 1–5 h by TLC and the resultant aryl nonaflates were subsequently isolated in high yields of 70–93%. However, two exceptions to this were 2'-hydroxyacetophenone and 2-hydroxypyridine. These substrates did not achieve full conversion despite forcing conditions, including the use of DMAP (10 mol%) and elevated temperatures, or significantly longer reaction times of up to 166 h. The poorer reactivity shown by these substrates was likely due to the inductive effect of the electron-withdrawing acetyl group and heteroatom located at the *ortho* position of each phenol starting material. Consequently, 2-acetylphenyl nonaflate (**181**) and pyridin-2-yl nonaflate (**184**) were afforded in moderate yields of 39% and 66% respectively.

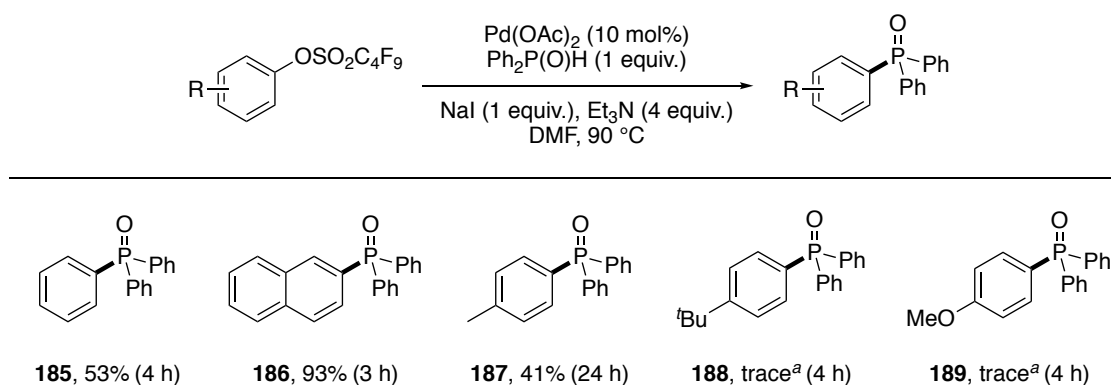


Scheme 72 – Preparation of a second library of aryl nonaflates. ^aReaction was performed at room temperature for 4 h, in the presence of DMAP (10 mol%) for 18 h, and then under reflux for 21 h.

2.3.7.4 Optimisation and Investigation of Mechanism

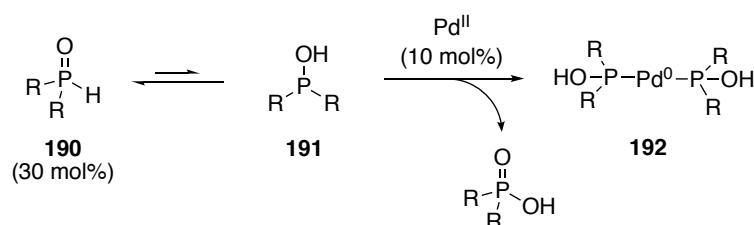
Initially, five aryl nonaflates were submitted to C–P cross-coupling with diphenylphosphine oxide using Pd(OAc)₂ (10 mol%), sodium iodide (1 equiv.), and triethylamine (4 equiv.) in DMF at 90 °C (Scheme 73). The selection of Pd(OAc)₂, triethylamine and DMF at 90 °C was substantiated by previous procedural optimisation for the synthesis of TAPS **171** and literature examples of their applications in C–P bond formation.^{369–371,378–386} Under these conditions, ¹H NMR spectroscopy showed that phenyl nonaflate (**167**) and 2-naphthyl nonaflate (**139**) underwent full conversion to the corresponding triarylphosphine oxides **185** and **186** after short reaction times of 4 and 3 h, respectively. Furthermore, the phosphorylated products **185** and **186** were isolated in yields of 53% and 93%. However, the phosphorylation of *p*-substituted aryl nonaflates **175**, **179**, and **147** proved challenging and only traces of the desired C–P coupled products **187**, **188**, and **189** were observed after 4 h. The reaction of *p*-tolyl nonaflate (**175**) was allowed to continue but achieved only 70% conversion despite an extended reaction time of 24 h. Notably, no residual diphenylphosphine oxide was observed in the reaction

mixture by ^{31}P NMR spectroscopy and subsequently, (*p*-tolyl)diphenylphosphine oxide (**187**) was isolated in 41% yield. Repetition of this reaction at an elevated temperature of 120 °C was found to increase the reaction rate and facilitated 70% conversion after only 6 h. However, the diphenylphosphine oxide cross-coupling partner was fully consumed within this period preventing any further progress.



Scheme 73 – Initial screening of aryl nonaflates for the palladium-catalysed C–P bond-forming reaction. ^aDetermined using ^1H NMR spectroscopy.

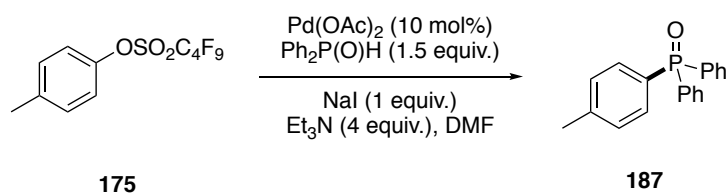
Therefore, optimisation studies were required and *p*-tolyl nonaflate (**175**) was deemed a suitable model substrate for this work due to the weak inductive effect of the methyl substituent. The results obtained thus far indicated that diphenylphosphine oxide was consumed as the phosphorus cross-coupling partner through an additional route. Mechanistic studies by the groups of Ackermann, Stawinski, Montchamp and Keglevich have shown that secondary P(O)–H compounds **190** exist in equilibrium with the phosphinous acid P–OH form **191** and that this tautomer performs multiple roles in metal-catalysed C–P bond-forming reactions (Scheme **74**).^{378,380,383–386,403} These groups have established that the P–OH tautomer **191** performs reduction of the palladium(II) pre-catalyst to the active palladium(0) species, acts as a ligand, and participates as the nucleophilic cross-coupling partner. Consequently, 30 mol% of the secondary P(O)–H compound **190** is required to prepare 10 mol% of the ligated active palladium(0) species **192** from Pd(OAc)₂. Given that 1 equivalent of the secondary P(O)–H compound **190** is consumed as the cross-coupling partner, a minimum of 1.3 equivalents is required to facilitate total conversion of the aryl substrate.



Scheme 74 – Reduction and ligation of palladium(II) pre-catalyst by tautomeric phosphinous acid form of secondary P(O)–H compound

p-Tolyl nonaflate (**175**) was next treated with 1.5 equivalents of diphenylphosphine oxide and the standard conditions of Pd(OAc)₂ (10 mol%), sodium iodide, and triethylamine in DMF at 90 °C (Table 29, entry 1). These conditions facilitated an improved conversion of 84% after 72 h. However, diphenylphosphine oxide was fully consumed after 72 h preventing full conversion of nonaflate **175**. Consequently, a screening of reaction temperatures up to 120 °C was performed with 1.5 equivalents of diphenylphosphine oxide (entries 2–4). It was found that a minimum temperature of 110 °C was required to achieve full conversion of nonaflate **175** and (*p*-tolyl)diphenylphosphine oxide (**187**) was afforded in 58% yield after 24 h. Further elevation of the reaction temperature to 120 °C provided a significant acceleration in reaction rate with full conversion of nonaflate **175** observed after only 4 h. Furthermore, phosphorylated product **187** was isolated in 78% yield.

Table 30 – Screening of reaction temperature for the palladium-catalysed C–P bond-forming reaction

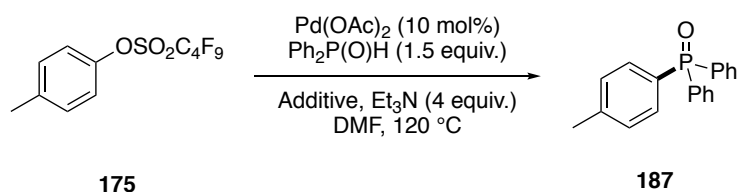


Entry	Temp. (°C)	Time (h)	Conversion to 187 (%) ^a	Isolated Yield of 187 (%)
1	90	72	84	-
2	100	24	80	-
3	110	24	100	58
4	120	4	100	78

^aDetermined using ¹H NMR spectroscopy.

Having established a set of improved conditions for the palladium-catalysed C–P cross-coupling of *p*-tolyl nonaflate (**175**) and diphenylphosphine oxide in a short reaction time and high yield, the next objective undertaken was an investigation of the impact of additives on reaction rate and outcome. Thus far, sodium iodide had been employed as an additive. However, ionic additives such as salts of acetate and chloride are frequently employed to promote palladium-catalysed cross-coupling reactions, including the Hirao reaction and its derivatives.^{378,380,382,404–407} Therefore, a screening of sodium acetate and sodium chloride was performed using *p*-tolyl nonaflate (**175**) with Pd(OAc)₂ (10 mol%), diphenylphosphine oxide and triethylamine in DMF at 120 °C (Table 30, entries 1 and 2). Notably, both alternative additives facilitated phosphorylation of **175** albeit at significantly slower rates than sodium iodide (entry 3), and reaction times of 22 h and 32 h were required to achieve full conversion of aryl nonaflate **175**. Furthermore, (*p*-tolyl)diphenylphosphine oxide (**187**) was afforded in lower yields of 55% and 64%.

Table 31 – Screening of additives for the palladium-catalysed C–P bond-forming reaction



Entry	Additive (equiv.)	Time (h)	Isolated Yield of 187 (%)
1	NaOAc (1)	22	55
2	NaCl (1)	32	64
3	NaI (1)	4	78
4	NaI (0.1)	8	76
5	None	24	79

Given that the application of sodium iodide facilitated the most efficient and high yielding phosphorylation reaction, the role of iodide in this palladium-catalysed C–P cross-coupling reaction was further explored. The cross-coupling of *p*-tolyl nonaflate (**175**) and diphenylphosphine oxide was performed in triplicate, with each reaction using either 0, 0.1 or 1 equivalents of sodium iodide (Figure 38). Dimethyl terephthalate (0.31 equiv.) was included in each experiment as an internal standard

to measure the reaction conversion at time intervals *via* ^1H NMR spectroscopy. The integrals of the signals corresponding to the methyl moiety present in **175** and **187** were calibrated to that of the methyl ester moieties of dimethyl terephthalate. The data obtained from this screening is presented in Figure 38, a conversion graph of **175** to **187**. As previously observed, the reaction that employed 1 equivalent of sodium iodide was complete after 4 h (~95% conversion). In contrast, only 51% conversion was observed after the same period when 0.1 equivalents of sodium iodide were used. Furthermore, a total reaction time of 8 h facilitated complete reaction of **175** (~95% conversion) which indicated that the action of iodide was indeed catalytic in nature. Moreover, the absence of sodium iodide clearly demonstrated the significant acceleration of reaction rate generated by this additive. Without sodium iodide present, only 12% conversion was observed after 4 h and a prolonged reaction time of 24 h was required to attain completion (~96% conversion).

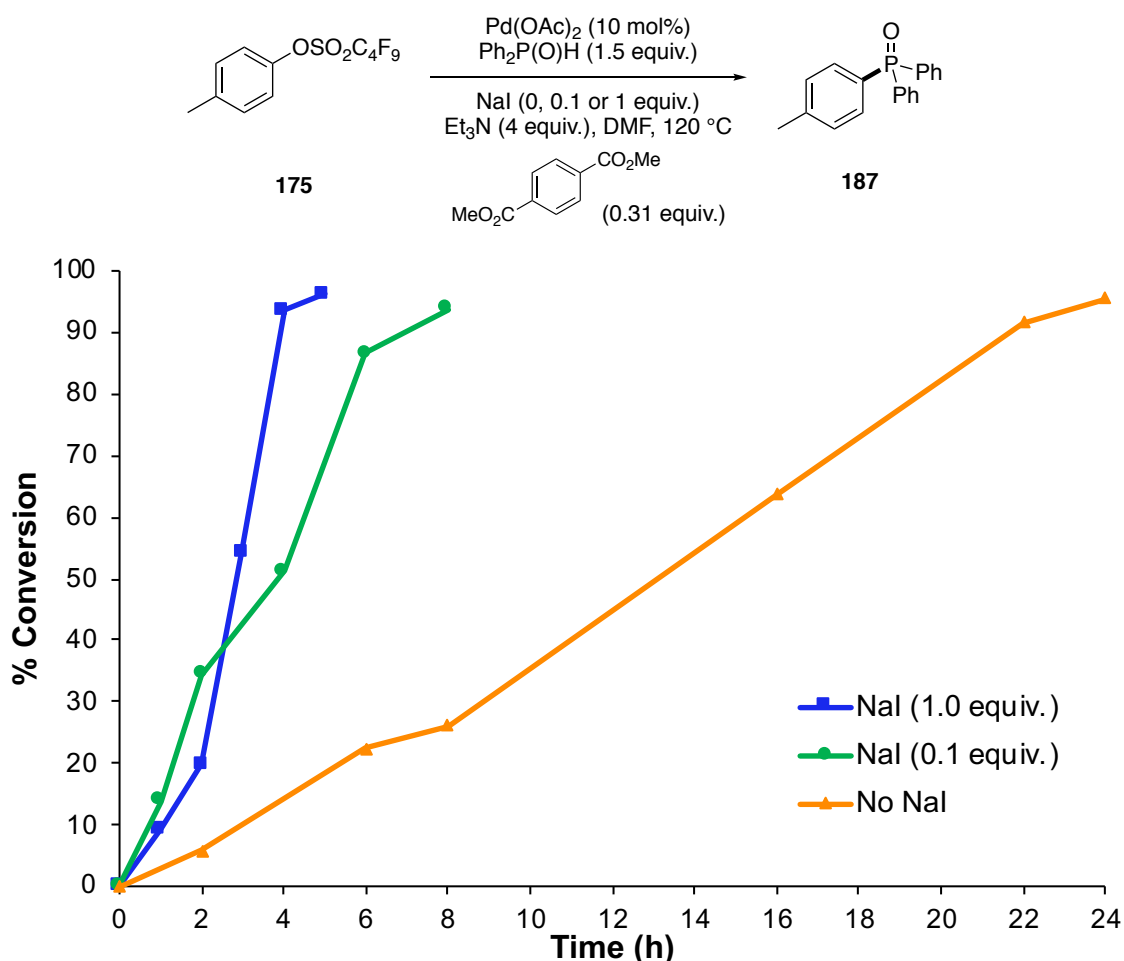
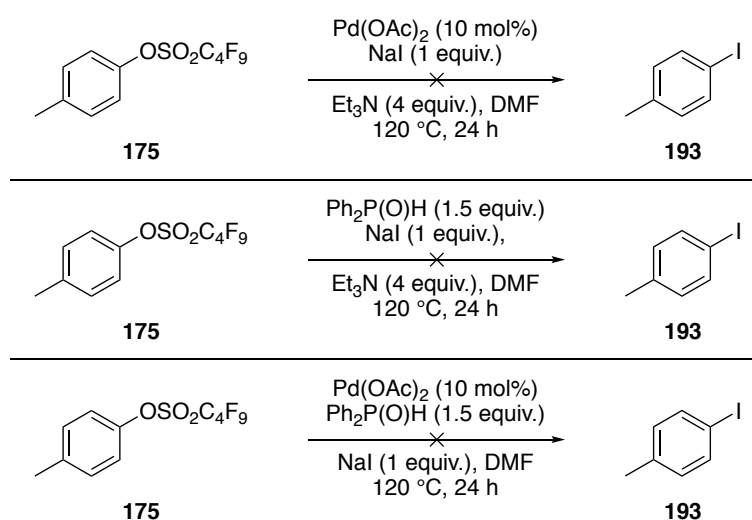


Figure 39 – Graph of conversion versus time for the synthesis of (*p*-tolyl)diphenylphosphine oxide (**187**) to examine additive effects

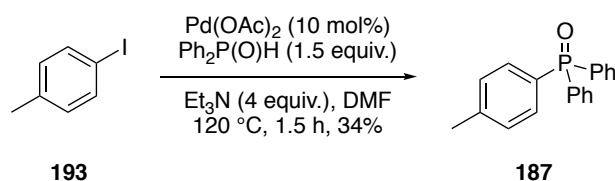
These reactions were then repeated without dimethyl terephthalate present for the length of time needed to facilitate full conversion of **175** (entries 3–5). Notably, the phosphorylated product **187** was afforded in similar yields for all three procedures (76–79%), and the efficient phosphorylation reaction facilitated by stoichiometric sodium iodide was deemed most favourable. As such, the conditions described by Table **30**, entry 3 were herein referred to as the optimised conditions for the iodide-accelerated, palladium-catalysed C–P bond-forming reaction of aryl nonaflates.

Within the literature, it has been suggested that additives such as sodium iodide accelerate palladium-catalysed cross-coupling reactions due to the formation of aryl iodide intermediates *via* the Finkelstein reaction.^{298,408,409} These intermediates possess labile C–I bonds which undergo oxidative addition with palladium at an accelerated rate relative to the original aryl substrate. For example, the palladium(0)-catalysed Heck reaction of aryl nonaflates with terminal alkenes mediated by iodide salts as reported by Peng *et al.*, discussed previously in Section 2.3.6. Consequently, the decision was made to investigate whether 4-iodotoluene (**193**) was generated as an intermediate during the cross-coupling of *p*-tolyl nonaflate (**175**) and diphenylphosphine oxide. A series of control reactions were performed employing the optimised conditions except in the absence of one reagent to prevent the production of (*p*-tolyl)diphenylphosphine oxide (**187**). Control reactions without diphenylphosphine oxide, Pd(OAc)₂ and triethylamine were monitored by ¹H NMR spectroscopy over 24 h however, no reactivity was observed under these conditions (Scheme **75**).



Scheme 75 – Investigation of 4-iodotoluene (**193**) as an intermediate

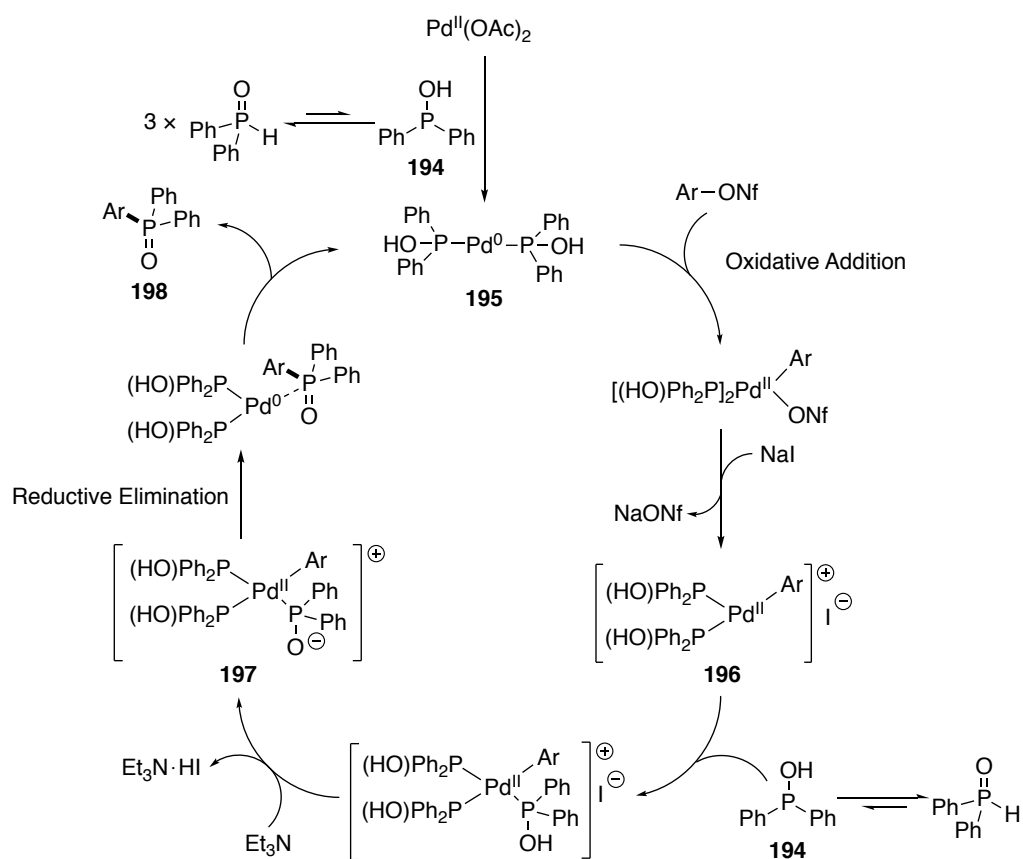
Furthermore, the use of 4-iodotoluene (**193**) as the aryl substrate for C–P cross-coupling with diphenylphosphine oxide was explored by Leanne Riley of the Sutherland group. 4-Iodotoluene (**193**) was treated with the optimised reaction conditions in the absence of sodium iodide (Scheme 76). Notably, full conversion of **193** was observed after only 1.5 h but the phosphorylated product **187** was isolated in a low yield of 34%. When compared to the equivalent reaction that employed *p*-tolyl nonaflate (**175**) with sodium iodide (1 equiv.), which required a 4 h reaction to afford **187** in 78% yield, this transformation was slightly faster but significantly lower yielding. Given the results of these investigations, it was concluded that aryl iodide intermediates such as 4-iodotoluene (**193**) are not generated during the iodide-accelerated, palladium-catalysed C–P bond-forming reaction.



Scheme 76 – Palladium-catalysed cross-coupling of 4-iodotoluene (**193**) with diphenylphosphine oxide

Based on these mechanistic experiments and the existing literature in this field, a mechanism for the iodide-accelerated, palladium-catalysed C–P bond-forming reaction of aryl nonaflates was proposed (Scheme 77). As previously discussed, the groups of Ackermann, Stawinski, Montchamp and Keglevich have shown that the tautomeric P–OH form of a secondary P(O)–H compound can reduce a palladium(II) pre-catalyst and then coordinate to afford a palladium(0) species, and subsequently act as a nucleophilic cross-coupling partner.^{378,380,383–386} Consequently, diphenylphosphine oxide exists in equilibrium with the tautomer phosphinous acid **194**. Initially, tautomer **194** (10 mol%) performs the reduction of Pd(OAc)₂ (10 mol%) and coordination with **194** (20 mol%) affords the active palladium(0) species **195**. In the presence of sodium iodide, oxidative addition of the aryl nonaflate to **195** may then be followed by loss of the nonaflate ligand to afford sodium nonaflate. This would generate the palladium(II) complex **196** which remains coordinatively unsaturated with the iodide anion only weakly coordinated. Furthermore, it is proposed that the coordinatively unsaturated nature of **196** may accelerate the rate at which the nucleophilic coupling partner phosphinous acid **194** coordinates to the

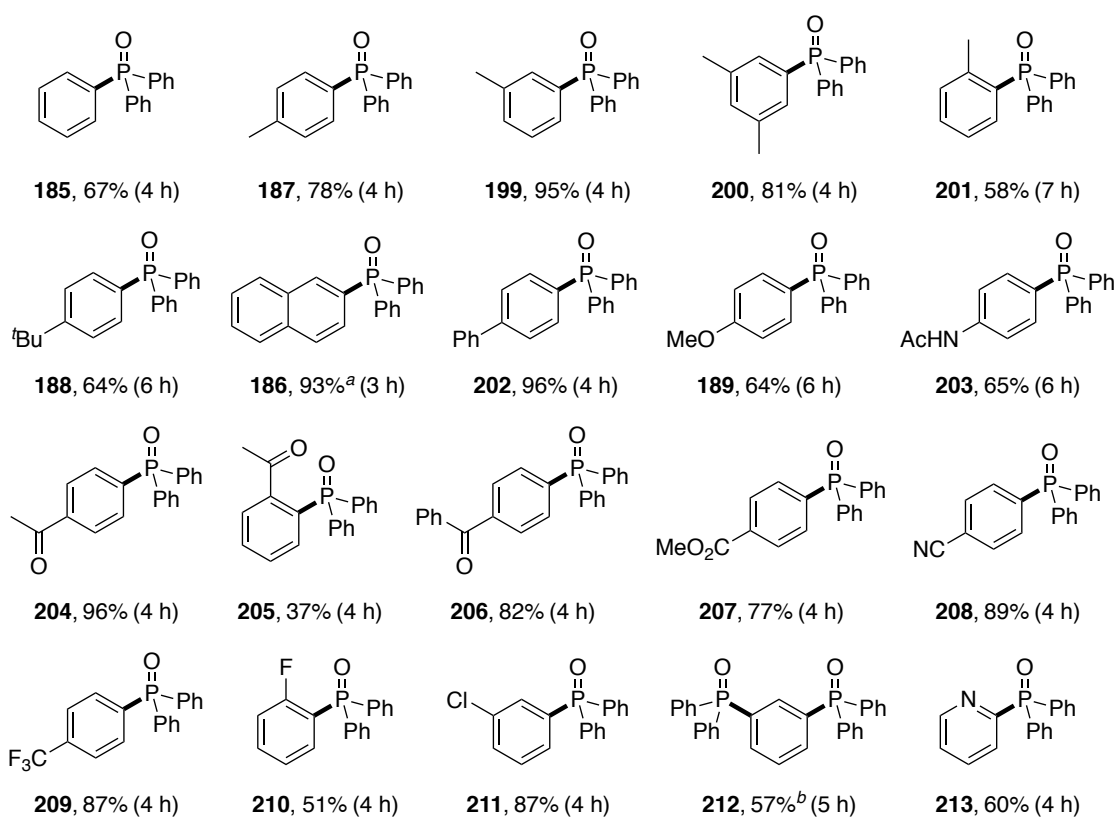
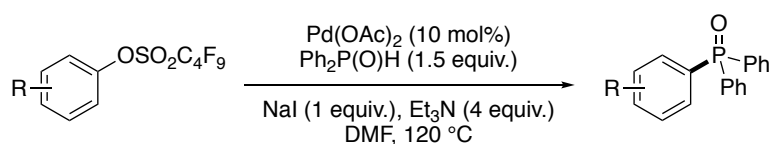
palladium(II) complex.⁴¹⁰ Subsequent deprotonation performed by triethylamine affords palladium(II) complex **197** from which the desired phosphorylated product **198** is formed *via* reductive elimination. Alternatively, iodide is known to impose a larger *trans* effect than other anions when complexed to palladium.⁴⁰⁶ Iodide is a strong σ -donating ligand which weakens the coordination between the metal and the ligand in the *trans* position relative to the iodide. Consequently, substitution reactions of the ligand *trans* to iodide are accelerated in comparison with other anions. It is reasonable to suggest that this may also be responsible for the acceleration of this palladium-catalysed C–P cross-coupling reaction by sodium iodide.



Scheme 77 – Proposed mechanism for the iodide-accelerated, palladium-catalysed C–P bond-forming reaction of aryl nonaflates

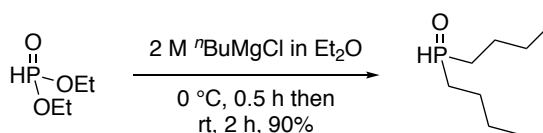
2.3.7.5 Substrate Scope

Using the optimised conditions established with *p*-tolyl nonaflate (**175**), the scope of the iodide-accelerated, palladium-catalysed phosphorylation reaction was investigated with diphenylphosphine oxide and a range of aryl nonaflates (Scheme **78**). This methodology was shown to be widely applicable to a library of twenty aryl nonaflates that possess a variety of structures and different electronic properties. Furthermore, the majority of triarylphosphine oxides were produced in high yields after short reaction times of only 4 h. Only one substrate from the library of aryl nonaflates screened was found to be incompatible with this procedure. Submission of *p*-nitrophenyl nonaflate (**142**) failed to produce the corresponding triarylphosphine oxide and ¹H NMR spectroscopy of the reaction mixture showed full decomposition of **142**. Comparison of methyl-substituted tertiary phosphine oxides **187**, **199**, **200**, and **201** showed that substitution in the *ortho* position necessitated a slightly longer reaction time and was detrimental to yield, relative to equivalent substitution at the *meta* and *para* positions. This *ortho*-substitution effect was more pronounced for electron-withdrawing substituents as shown by tertiary phosphine oxides **204** versus **205**. Biaryl nonaflates such as 2-naphthyl nonaflate (**139**) and (1,1'-biphenyl)-4-yl nonaflate (**155**) were particularly reactive and afforded **186** and **202** in high yields of 93% and 96%, respectively. Aryl nonaflates bearing an electron-donating substituent also required slightly longer reaction times as evidenced by the production of **189** in 64% yield after 6 h. In contrast, electron-deficient aryl nonaflates underwent full conversion to triarylphosphine oxides in 4 h and were isolated in high yields. In addition, aryl nonaflates that possess halide substituents including fluoride and chloride were also compatible. However, submission of 3-bromophenyl nonaflate (**183**) to this procedure afforded a mixture of products. Following flash column chromatography, analysis *via* ¹H and ³¹P NMR spectroscopy revealed that bis-phosphine oxide **212** was given as the major product, whilst the desired triarylphosphine oxide was a minor product. Consequently, this reaction was repeated using 3 equivalents of diphenylphosphine oxide to promote bis-coupling and **212** was afforded in 57% yield after 5 h. Furthermore, this procedure was also compatible with heterocyclic nonaflates such as pyridin-2-yl nonaflate (**184**) for the preparation of **213** in 60% yield.



Scheme 78 – Scope of aryl nonaflates employed in the iodide-accelerated, palladium-catalysed C–P bond-forming reaction. ^aReaction performed with $\text{Ph}_2\text{P(O)H}$ (1 equiv.) at 90 °C. ^bReaction performed with 3-bromophenyl nonaflate (**183**) and $\text{Ph}_2\text{P(O)H}$ (3 equiv.).

Next, the focus of this work was to investigate the scope of nucleophilic phosphorus coupling partners that could be employed for C–P cross-coupling with aryl nonaflates. This study was performed using *p*-tolyl nonaflate (**175**) as a model aryl substrate due to its utility in previous optimisation work. Initially, *p*-tolyl nonaflate (**175**) would be reacted with bis(*p*-tolyl)phosphine oxide, di(*n*-butyl)phosphine oxide (**214**), diethyl phosphite and ethyl phenylphosphinate under the conditions optimised for biaryl P(O)–H compounds. Of these organophosphorus compounds, only di(*n*-butyl)phosphine oxide (**214**) was not commercially available. Following a literature procedure from Busacca and co-workers, **214** was efficiently prepared from diethyl phosphite and 2 M *n*-butylmagnesium chloride in diethyl ether solution in 90% yield (Scheme 79).⁴¹¹

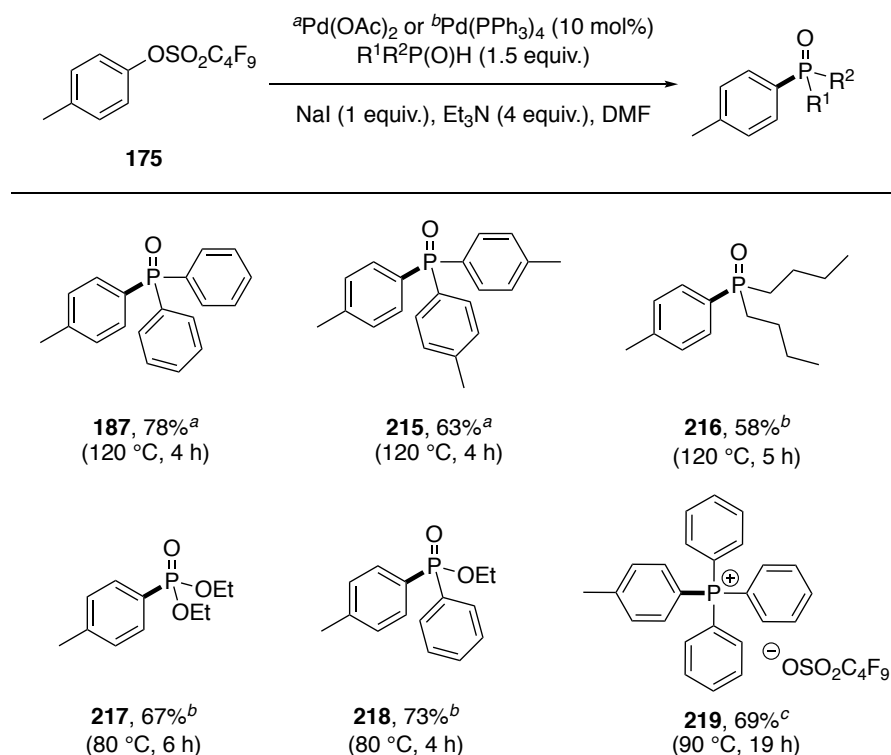


Scheme 79 – Synthesis of di(*n*-butyl)phosphine oxide (**214**)

As expected, the cross-coupling of nonaflate **175** with bis(*p*-tolyl)phosphine oxide proceeded efficiently under the optimised conditions for the synthesis of (*p*-tolyl)diphenylphosphine oxide (**187**), and tris(*p*-tolyl)phosphine oxide (**215**) was isolated in 63% yield after 4 h (Scheme **80**). In contrast, the attempted phosphorylation reactions with di(*n*-butyl)phosphine oxide (**214**) and diethyl phosphite generated no reaction or only trace quantities of the desired product **217** even after extended reaction times of 24 h. Resultant attempts performed at an elevated temperature of 150 °C failed to promote phosphorylation and enabled partial degradation of nonaflate **175** to *p*-cresol after 24 h. Furthermore, the reaction of nonaflate **175** with ethyl phenylphosphinate produced an inseparable complex mixture of products when performed at 120 °C and subsequently at 90 °C.

For this reason, the use of Pd(PPh₃)₄ (10 mol%) was then explored given its historic application in the Hirao reaction.^{369–371} The iodide-accelerated phosphorylation reaction of nonaflate **175** with di(*n*-butyl)phosphine oxide (**214**) was repeated except using Pd(PPh₃)₄ (10 mol%) and produced dialkylphosphine oxide **216** in 58% yield after only 5 h at 120 °C. Under identical conditions, the cross-coupling of nonaflate **175** and diethyl phosphite produced the desired phosphonate ester **217** and an unknown side-product in a ratio of 2 : 1 respectively. A brief screening of reaction temperatures between 60–90 °C was then performed for the reactions of nonaflate **175** with diethyl phosphite and ethyl phenylphosphinate. It was found that when using more reactive phosphorus coupling partners such as these a reaction temperature of 80 °C afforded 100% conversion to the desired C–P coupled products efficiently with minimal side-reactions. Using Pd(PPh₃)₄ (10 mol%) at this optimal temperature, phosphonate **217** and phosphinate **218** were given in 67% and 73% yield after 6 h and 4 h, respectively. Notably, triphenylphosphine oxide was commonly observed as a by-product when Pd(PPh₃)₄ was employed as the catalyst for this methodology. However, this impurity was successfully removed *via* flash column chromatography, trituration, or a successive combination of both techniques. Finally, C–P coupling of *p*-tolyl nonaflate (**175**) and triphenylphosphine

was attempted to exemplify the utility of this method for the synthesis of substituted TAPSs such as **219**. An initial reaction performed using the same conditions as for the synthesis of TAPS **171** produced an inseparable mixture of compounds after only 4 h. A larger excess of the coupling partner triphenylphosphine (4 equiv.) was subsequently proven to be advantageous to limiting the formation of side-products albeit to the detriment of the reaction rate. This modified procedure facilitated the preparation of (*p*-tolyl)triphenylphosphonium nonaflate (**219**) in a good yield of 69%.

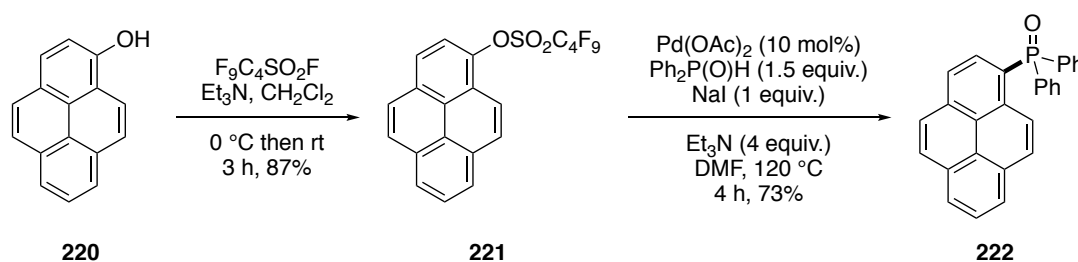


Scheme 80 – Scope of phosphorus coupling partners employed in the iodide-accelerated, palladium-catalysed C–P bond-forming reaction. ^cReaction performed using Pd(OAc)₂ (10 mol%) with coupling partner PPh₃ (4 equiv.).

2.3.7.6 Synthesis of Aryl Phosphorus Compounds with Functionality

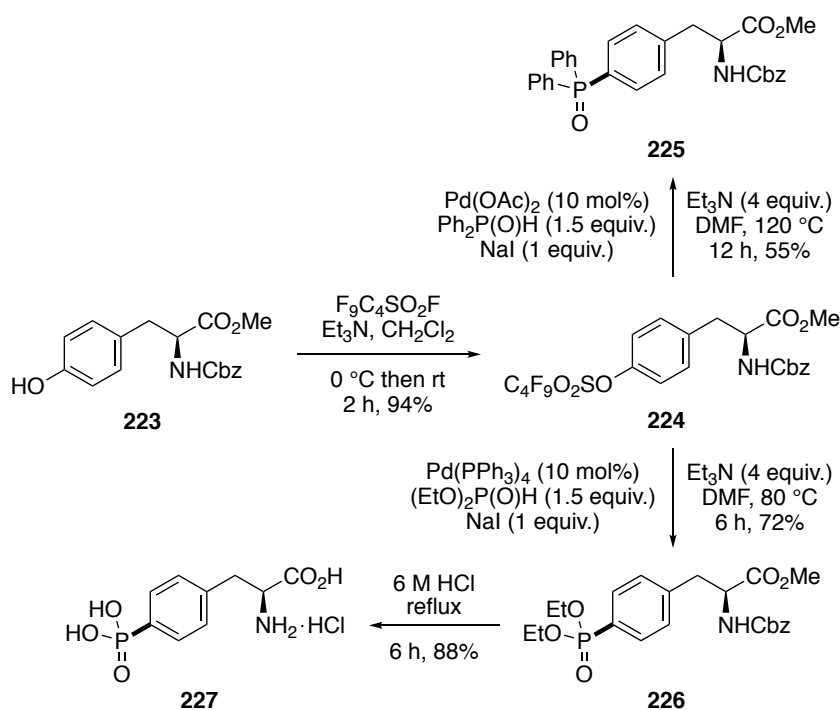
Having explored the mechanism and scope of the iodide-accelerated, palladium-catalysed C–P bond-forming reaction, the next aim of this project was to exploit this methodology to transform phenols into aryl phosphorus compounds with applications in various fields of chemistry. The first target compound selected was (1-pyrenyl)diphenylphosphine oxide (**222**), an electron transporting blue-light-emitter for use in organic light emitting diodes (OLEDs).⁴¹² In the first step, pyren-1-

ol (**220**) was treated with nonafllyl fluoride and triethylamine under mild conditions to afford 1-pyrenyl nonaflate (**221**) in 87% yield (Scheme **81**). Using the conditions optimised for cross-coupling of biaryl P(O)–H compounds, nonaflate **221** underwent phosphorylation with diphenylphosphine oxide to give (1-pyrenyl)diphenylphosphine oxide (**222**) in a good yield of 73%. Previous synthesis of this compound started from 1-bromopyrene and required three steps, lithiation, phosphorylation and oxidation.^{412–414} Notably, this novel methodology facilitated the synthesis of **222** from commercially available material in only two steps and circumvented the use of organolithium reagents such as *n*-butyl lithium.



Scheme 81 – Synthesis of (1-pyrenyl)diphenylphosphine oxide (**222**)

Next, a commercially available L-tyrosine derivative bearing benzyloxycarbonyl and methyl ester protecting groups (**223**) was converted to the corresponding aryl nonaflate **224** under the standard conditions previously described and was isolated in 94% yield (Scheme **82**). To explore the use of this method with structurally complex compounds, the cross-coupling of nonaflate **224** and diphenylphosphine oxide was performed under the conditions optimised for biaryl P(O)–H compounds. The resultant triarylphosphine oxide **225** was isolated in 55% yield after a reaction time of 12 h. Notably, **225** was shown to be unstable at high temperatures when left stirring for longer. For example, a reaction time of 22 h returned only a 42% yield. L-Tyrosine-derived nonaflate **224** was also submitted to iodide-accelerated phosphorylation with diethyl phosphite using Pd(PPh₃)₄ (10 mol%) at 80 °C for 6 h to give phosphonate **226** in 72% yield at 1 mmol scale. Global deprotection of **226** was then achieved using 6 M hydrochloric acid under reflux to afford 4-phosphono-L-phenylalanine hydrochloride (**227**) in 88% yield after 6 h. This phosphorylated amino acid has been employed in numerous medicinal chemistry studies including the development of novel thrombin inhibitors and as competitive *N*-methyl-D-aspartic acid antagonists.^{394,415–418}



Scheme 82 – Synthesis of phosphorylated phenylalanine analogues **225** and **227**

2.3.8 Conclusions and Future Work

In summary, a large library of aryl nonafluorobutanesulfonates was efficiently prepared from the corresponding phenols in excellent yields under mild conditions and was submitted to investigations of novel transition metal-catalysed iodination and phosphorylation reactions. Initially, the iodination of aryl nonaflates was investigated with an electron-rich ruthenium(II) catalyst, tris(acetonitrile)pentamethylcyclopentadienylruthenium(II) trifluoromethanesulfonate (5 mol%) (**129**), in the presence of sodium iodide. Due to the air and moisture sensitivity of **129**, the handling procedure of this reaction required optimisation and was then exploited for the preparation of a small series of aryl iodides. However, subsequent issues with the supply of **129** prevented further exploration of this procedure. Consequently, the analogous ruthenium(II) catalyst, tris(acetonitrile)pentamethylcyclopentadienylruthenium(II) hexafluorophosphate (**164**), was sourced from an alternative manufacturer and an equivalent study was performed. Further optimisation revealed that an increased catalytic loading of **164** (8.5 mol%) was necessary to achieve comparable conversion to catalyst **129** (5 mol%) and required longer reaction times.

In the future, an increased 10–15 mol% loading of ruthenium(II) catalyst **164** could be explored to attain higher levels of iodination in reduced reaction times. Alternatively, the ruthenium(III) catalyst, dichloro(pentamethylcyclopentadienyl)ruthenium(III) polymer, could be investigated. This catalyst has been shown by Butkevich *et al.* to exhibit equivalent reactivity to catalyst **129** for the iodination of aryl triflates when employed at a loading of only 5 mol% and is less expensive.⁴¹⁹ Furthermore, ruthenium(II) catalyst **129** could be further explored if prepared in-house. Following a two-step procedure reported by Fagan *et al.*, **129** could be produced through treatment of dichloro(pentamethylcyclopentadienyl)ruthenium(III) polymer with 1 M lithium triethylborohydride, followed by acetonitrile under reflux and then silver triflate.⁴²⁰ Regardless of the specific ruthenium(II) catalyst chosen to proceed with, these initial findings suggest that further procedural optimisation will be required for application with electron-rich aryl nonaflates. Finally, it is proposed that this methodology will ultimately be adapted for the radioiodination of aryl nonaflate precursors to SPECT imaging agents such as PARP-1 inhibitor [¹²³I]**16b**.

A brief investigation of a metal-free procedure for the iodination of aryl nonaflates *via* an S_NAr reaction was also carried out. This study explored conditions for a pseudo-halogen exchange of the electron-deficient *p*-nitrophenyl nonaflate (**142**) with an excess of sodium iodide at elevated temperatures. Ultimately, this method was deemed impracticable due to the high temperatures (140 or 160 °C) required for efficient conversion. Furthermore, these temperatures resulted in significant thermal decomposition of aryl nonaflate **142** to the corresponding *p*-nitrophenol (**166**) starting material. Notably, the desired aryl iodide was achieved with a maximum conversion of only 58% and also produced the corresponding phenol (42%) as a significant by-product.

The project then explored a pseudo-halogen exchange reaction for the iodination of aryl nonaflates catalysed by tris(dibenzylideneacetone)dipalladium(0) and the sterically hindered dialkybiarylphosphine ligand ^tBuBrettPhos (**128**). However, screening of reaction conditions including temperature, solvent, and catalytic loading of Pd₂(dba)₃ and ^tBuBrettPhos (**128**) failed to produce the desired aryl iodides in conversions greater than just 18%. Therefore, this method was also

regarded as impracticable, and an alternative palladium-catalysed strategy was sought.

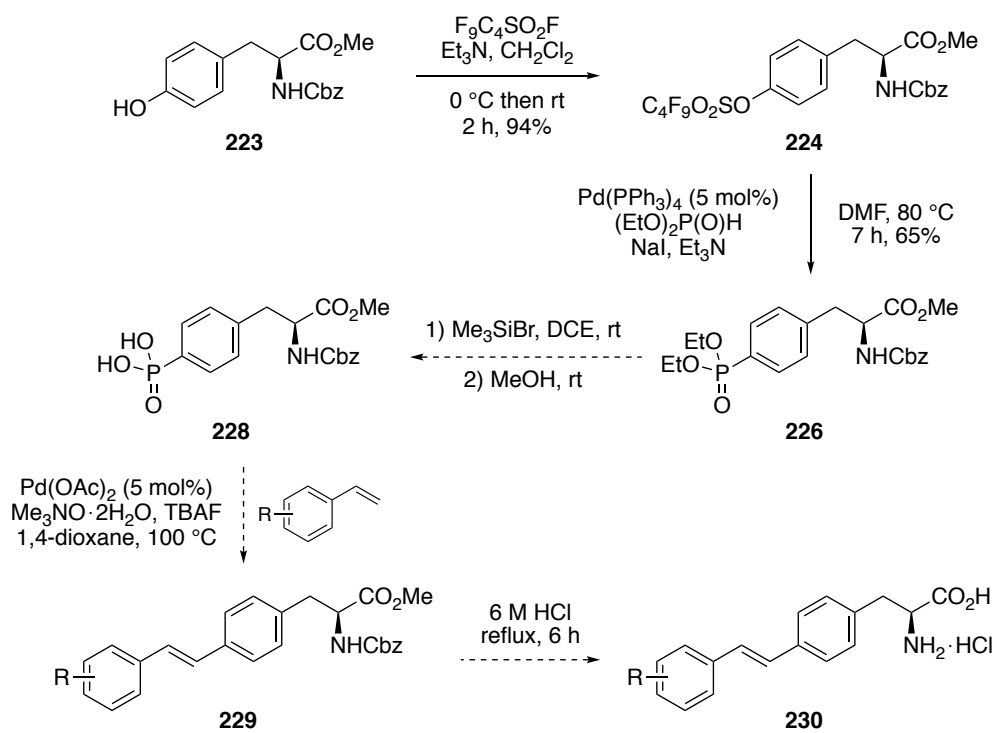
An iodide mediated, palladium-catalysed Heck reaction of aryl nonaflates and terminal alkenes using sodium iodide and palladium(II)bis(triphenylphosphine) dichloride (5 mol%) was investigated. However, attempts to isolate an aryl iodide intermediate, which this reaction was proposed to proceed through were unsuccessful. Moreover, no evidence of an aryl iodide intermediate was observed under the various reaction conditions employed. Notably, a side-product subsequently identified as tetraphenylphosphonium nonaflate (**171**) revealed the propensity of aryl nonaflates to participate in C–P bond-forming reactions with phosphorus ligands in the presence of sodium iodide and a palladium catalyst. The palladium-catalysed C–P cross-coupling reaction was then optimised to prepare TAPS **171** in good yield under milder conditions than literature preparations of analogous halide and triflate TAPSs.

The conditions developed for the synthesis of TAPS **171** were then investigated for cross-coupling of aryl nonaflates with secondary aryl P(O)–H compounds. After further optimisation and preliminary mechanistic studies, it was found that sodium iodide significantly accelerated the rate of palladium-catalysed C–P bond-formation (six-fold increase) and a mechanism was proposed. It was suggested that this acceleratory effect occurs due to formation of a coordinatively unsaturated palladium(0) complex or the *trans* effect of iodide when complexed to a palladium intermediate. The broad scope of this optimised, iodide-accelerated, palladium-catalysed C–P bond forming reaction was exemplified with a range of structurally and electronically diverse aryl nonaflates to afford tertiary arylphosphine oxides in high yields after short reaction times. Additional optimisation extended the scope of nucleophilic secondary phosphorus P(O)–H coupling partners that were applicable with this methodology to include substituted phosphine oxides, dialkyl phosphine oxides, dialkyl phosphites and alkyl arylphosphinates.

Finally, the synthetic utility of this methodology was shown through the synthesis of organophosphorus compounds with established applications in materials and medicinal chemistry. A blue-light-emitter (1-pyrenyl)diphenylphosphine oxide (**222**) for OLEDs was prepared from commercially available pyren-1-ol in 64% yield over

two steps. Furthermore, biologically active 4-phosphono-L-phenylalanine hydrochloride (**227**) was prepared from a commercially available L-tyrosine derivative in 60% yield over three steps.

Within the Sutherland group, a focus of significant research efforts is the development of novel fluorescent amino acids for molecular imaging.^{421–426} In the future, the iodide-accelerated, palladium-catalysed C–P bond-forming reactions developed in this work could be employed for the synthesis of L-tyrosine-derived fluorescent amino acids (Scheme **83**). Concurrent with the composition of this thesis, a 5 mol% loading of Pd(PPh₃)₄ was investigated for the synthesis of phosphonate **226** from L-tyrosine-derived nonaflate **224** by Leanne Riley. Under these conditions, phosphonate **226** was afforded in only a slightly lower yield of 65% and a reaction time of 7 h was required. Moving forward, phosphonate **226** could undergo selective deprotection of the ethyl phosphonate ester using bromotrimethylsilane followed by treatment with methanol to afford phosphonic acid **228**.⁴²⁷ Subsequently, a library of stilbene-type amino acids could be prepared from phosphonic acid **228** through oxidative palladium-catalysed Heck-inspired cross-coupling with a range of functionalised styrenes, and subsequent global deprotection with 6 M hydrochloric acid.⁴²⁸ Notably, this synthetic approach would allow for rapid late-stage structural diversification from the common intermediate **228** and facilitate an investigation of the relationship between structure and fluorescent properties of this amino acid scaffold.



Scheme 83 – Proposed synthesis of novel stilbene-type fluorescent amino acids via phosphonate and phosphonic acid intermediates

3.0 Experimental

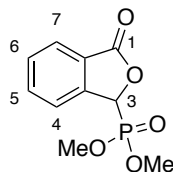
3.1 General Experimental

All reagents and starting materials were obtained from commercial sources and used as received unless otherwise stated. Dry solvents (acetonitrile, dichloromethane, THF, toluene) were purified using a PureSolv 500 MD solvent purification system. All reactions were performed under an atmosphere of air unless otherwise stated. Dry glassware was oven-dried at 140 °C for a minimum of 16 h, cooled to room temperature *in vacuo* and then purged with argon. Brine is defined as a saturated aqueous solution of sodium chloride. Merck aluminium-backed plates pre-coated with silica gel 60 (UV₂₅₄) were used for thin layer chromatography and were visualised under UV light (254/365 nm) then stained with iodine, potassium permanganate, vanillin or ninhydrin solution. Flash column chromatography was carried out using Merck Geduran Si 60 (40–63 μm). ¹H and ¹³C NMR spectra were recorded on Bruker DPX 400, Bruker AVI 400, Bruker AVIII 400 (¹H 400 MHz; ¹³C 101 MHz) spectrometers or a Bruker AVIII 500 (¹H 500 MHz; ¹³C 126 MHz) spectrometer with chemical shift values reported in ppm relative to tetramethylsilane (δ_{H} 0.00 and δ_{C} 0.0), CDCl₃ (δ_{H} 7.26 and δ_{C} 77.2), CD₃OD (δ_{H} 3.31 and δ_{C} 49.0), DMSO-*d*₆ (δ_{H} 2.50 and δ_{C} 39.5) or 3-(trimethylsilyl)propionic-2,2,3,3-*d*₄ acid sodium salt in D₂O (δ_{H} 0.00 and δ_{C} 0.0). Assignments of ¹H and ¹³C NMR signals are based on COSY, DEPT, HSQC and HMBC experiments. Mass spectra were obtained using a JEOL JMS-700 spectrometer or a Bruker microTOFq high resolution mass spectrometer. Melting points were determined on a Gallenkamp melting point apparatus and are uncorrected. Infrared spectra were recorded neat on a Shimadzu FTIR-84005 spectrometer. Optical rotations were determined as solutions irradiating with the sodium D line (λ = 598 nm) using an Autopol V polarimeter. $[\alpha]_{\text{D}}$ values are reported in units 10⁻¹ deg cm² g⁻¹. UV-Vis spectra were recorded on a Perkin Elmer Lambda 25 instrument and fluorescence spectra were recorded on a Shimadzu RF-5301PC spectrofluorophotometer. Emission data were measured using an excitation slit width of 3 nm and emission slit width of 5 nm. Chiral HPLC spectra were recorded on Shimadzu LC-20AD prominence liquid chromatograph with a CBM-20A prominence communications bus module, DGU-20A5 prominence degasser, SPD-M20A prominence diode array detector (210 or 254 nm) and a Shimadzu CTO-20AC prominence column oven (25 °C). Analysis was performed

using 20 μL sample injections and methods were calibrated with the corresponding racemic mixtures. Data acquisition and processing was performed using LabSolutions 1.21 SP1 chromatography software.

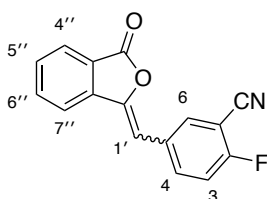
3.2 PARP-1 Experimental

(\pm)-3-Dimethoxyphosphoryl-3*H*-2-benzofuran-1-one (**42**)¹⁰²



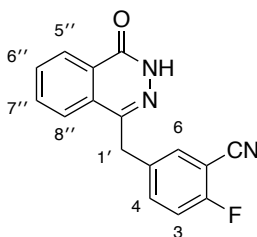
In an oven-dried flask under argon, a stirred solution of sodium methoxide (25% wt. in methanol) (12.2 mL, 53.3 mmol) in methanol (76 mL) was cooled to 0 °C and dimethyl phosphite (**41**) (4.59 mL, 50.0 mmol) was added dropwise. 2-Carboxybenzaldehyde (**40**) (5.00 g, 33.3 mmol) was added portionwise to the reaction mixture, which was then warmed to room temperature and stirred for 2 h. Methanesulfonic acid (3.89 mL, 59.9 mmol) was then added dropwise to the reaction mixture and a white suspension was formed. The reaction mixture was concentrated *in vacuo*, the resulting residue suspended in water (50 mL) and the crude product extracted with dichloromethane (3 \times 50 mL). The combined organic layers were dried (MgSO_4), filtered and concentrated *in vacuo*. The crude material was purified by trituration with diethyl ether to give (\pm)-3-dimethoxyphosphoryl-3*H*-2-benzofuran-1-one (**42**) as a white solid (6.37 g, 79%). Mp 90–91 °C (lit.¹⁰² 90–91 °C); δ_{H} (400 MHz, CD_3OD) 3.72 (3H, d, J 10.8 Hz, CH_3), 3.91 (3H, d, J 10.8 Hz, CH_3), 6.10 (1H, d, J 10.8 Hz, 3-H), 7.68 (1H, t, J 7.5 Hz, 5-H), 7.75 (1H, d, J 7.5 Hz, 4-H), 7.83 (1H, t, J 7.5 Hz, 6-H), 7.94 (1H, d, J 7.5 Hz, 7-H); δ_{C} (101 MHz, CD_3OD) 54.9 (d, $^2J_{\text{CP}}$ 6.8 Hz, CH_3), 55.3 (d, $^2J_{\text{CP}}$ 7.4 Hz, CH_3), 76.4 (d, $^1J_{\text{CP}}$ 167.0 Hz, CH), 124.7 (d, $^3J_{\text{CP}}$ 3.0 Hz, CH), 126.2 (d, $^2J_{\text{CP}}$ 4.1 Hz, C), 126.8 (d, $^5J_{\text{CP}}$ 1.9 Hz, CH), 131.2 (d, $^4J_{\text{CP}}$ 2.9 Hz, CH), 135.9 (d, $^4J_{\text{CP}}$ 2.8 Hz, CH), 145.2 (d, $^3J_{\text{CP}}$ 4.0 Hz, C), 171.3 (d, $^3J_{\text{CP}}$ 2.7 Hz, C); m/z (EI) 242 (M^+ , 37%), 213 (10), 199 (9), 133 (100), 105 (13), 77 (17), 51 (5).

2-Fluoro-5-[(*Z/E*)-(3''-oxo-2''-benzofuran-1''-ylidene)methyl]benzonitrile (**44**)¹⁰²



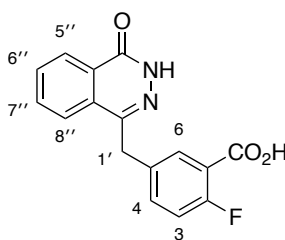
In an oven-dried flask under argon, (\pm)-3-dimethoxyphosphoryl-3*H*-2-benzofuran-1-one (**42**) (6.30 g, 26.0 mmol) and 2-fluoro-5-formylbenzonitrile (**43**) (3.52 g, 23.6 mmol) were dissolved in anhydrous tetrahydrofuran (95 mL) and cooled to 0 °C. Triethylamine (3.62 mL, 26.0 mmol) was added dropwise to the reaction mixture, which was then warmed to room temperature and stirred for 21 h. The resultant suspension was concentrated *in vacuo* and the crude residue suspended in water (80 mL). The product was collected by vacuum filtration and washed with water (2 \times 80 mL), hexane (2 \times 80 mL) and diethyl ether (2 \times 80 mL) to give 2-fluoro-5-[(*Z/E*)-(3''-oxo-2''-benzofuran-1''-ylidene)methyl]benzonitrile (**44**) as a white solid (5.54 g, 89%). NMR spectra showed a 3:1 mixture of *E* and *Z* isomers. Only signals for the major isomer are recorded. The product was used in subsequent synthesis without separation of the major and minor isomers. Mp 164–167 °C (lit.¹⁰² 164–167 °C); δ_{H} (400 MHz, DMSO-*d*₆) 6.98 (1H, s, 1'-H), 7.65 (1H, t, *J* 9.0 Hz, ArH), 7.67–7.75 (1H, m, ArH), 7.92 (1H, td, *J* 7.6, 1.0 Hz, ArH), 7.97–8.00 (1H, m, ArH), 8.08 (1H, dt, *J* 8.0, 1.0 Hz, ArH), 8.12–8.21 (2H, m, 2 \times ArH); δ_{C} (101 MHz, DMSO-*d*₆) 100.8 (d, ²*J*_{CF} 15.8 Hz, C), 103.4 (CH), 113.8 (C), 117.4 (d, ²*J*_{CF} 20.0 Hz, CH), 121.0 (CH), 122.6 (C), 125.4 (CH), 130.9 (CH), 131.0 (d, ⁴*J*_{CF} 3.7 Hz, C), 134.2 (CH), 135.4 (CH), 136.7 (d, ³*J*_{CF} 9.0 Hz, CH), 139.5 (C), 145.4 (C), 161.5 (d, ¹*J*_{CF} 258.1 Hz, C), 165.9 (C); *m/z* (EI) 265 (M⁺, 100%), 237 (12), 208 (64), 182 (10), 133 (13), 104 (14), 63 (29), 45 (8).

2-Fluoro-5-[(4''-oxo-3''H-phthalazin-1''-yl)methyl]benzonitrile (**48**)¹⁷⁵



In an oven-dried flask under argon, 2-fluoro-5-[(*Z/E*)-(3''-oxo-2''-benzofuran-1''-ylidene)methyl]benzonitrile (**44**) (5.43 g, 20.5 mmol) was suspended in anhydrous tetrahydrofuran (55 mL) and degassed for 0.5 h. To the degassed solution was added hydrazine monohydrate (1.19 mL, 24.6 mmol). The reaction mixture was stirred at room temperature for 2 h. Acetic acid (0.300 mL, 5.24 mmol) was added, and the reaction mixture was heated to 60 °C for 19 h. The reaction mixture was cooled to 50 °C and water (55 mL) was added slowly, resulting in the formation of a white precipitate. The reaction mixture was cooled to room temperature and the precipitate was collected by vacuum filtration. This was washed with a solution of tetrahydrofuran and water (1:1) (20 mL) and then diethyl ether (3 × 20 mL) to give 2-fluoro-5-[(4''-oxo-3''H-phthalazin-1''-yl)methyl]benzonitrile (**48**) as a white solid (5.03 g, 88%). Mp 213–215 °C. Spectroscopic data were consistent with the literature.¹⁷⁵ δ_{H} (400 MHz, DMSO-*d*₆) 4.37 (2H, s, 1'-H₂), 7.46 (1H, t, *J* 9.0 Hz, 3-H), 7.71 (1H, ddd, *J* 9.0, 5.3, 2.3 Hz, 4-H), 7.84 (1H, dd, *J* 7.9, 7.5 Hz, 6''-H), 7.88–7.94 (2H, m, 6-H and 7''-H), 7.98 (1H, d, *J* 7.9 Hz, 8''-H), 8.26 (1H, d, *J* 7.9 Hz, 5''-H), 12.57 (1H, s, NH); δ_{C} (101 MHz, DMSO-*d*₆) 36.0 (CH₂), 99.9 (d, ²*J*_{CF} 15.3 Hz, C), 114.0 (C), 116.5 (d, ²*J*_{CF} 19.5 Hz, CH), 125.3 (CH), 126.1 (CH), 127.9 (C), 129.0 (C), 131.6 (CH), 133.6 (CH), 134.0 (CH), 135.7 (d, ⁴*J*_{CF} 3.6 Hz, C), 136.6 (d, ³*J*_{CF} 8.6 Hz, CH), 144.4 (C), 159.3 (C), 161.2 (d, ¹*J*_{CF} 254.4 Hz, C); *m/z* (ESI) 581 (2MNa⁺, 100%).

2-Fluoro-5-[(4''-oxo-3''H-phthalazin-1''-yl)methyl]benzoic acid (**45**)¹⁰²

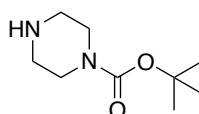


Method A: To a stirred suspension of 2-fluoro-5-[(*Z/E*)-(3''-oxo-2''-benzofuran-1''-ylidene)methyl]benzotrile (**44**) (5.53 g, 20.8 mmol) in water (210 mL) was added 13 M aqueous sodium hydroxide solution (31.5 mL, 410 mmol). The reaction mixture was heated to 90 °C and stirred for 18 h. After cooling to 70 °C, hydrazine monohydrate (14.1 mL, 291 mmol) was added to the reaction mixture slowly then stirred for a further 72 h. The reaction mixture was then cooled to room temperature, acidified with 6 M aqueous hydrochloric acid solution to pH 2 and stirred at room temperature for 1 h, which produced a red precipitate. The resultant precipitate was collected by vacuum filtration. This was washed with water (3 × 150 mL) and diethyl ether (3 × 150 mL). The crude material was purified by trituration with acetone to give 2-fluoro-5-[(4''-oxo-3''H-phthalazin-1''-yl)methyl]benzoic acid (**45**) as a pale pink solid (4.09 g, 66%). Mp >300 °C. Spectroscopic data were consistent with the literature.¹⁰² δ_{H} (400 MHz, DMSO-*d*₆) 4.36 (2H, s, 1'-H₂), 7.24 (1H, dd, *J* 10.8, 8.5 Hz, 3-H), 7.54–7.62 (1H, m, 4-H), 7.79–7.87 (2H, m, 6-H and 6''-H), 7.90 (1H, td, *J* 7.5, 1.3 Hz, 7''-H), 7.98 (1H, d, *J* 7.5 Hz, 8''-H), 8.26 (1H, dd, *J* 7.8, 1.3 Hz, 5''-H), 12.60 (1H, s, NH), 13.24 (1H, br s, OH); δ_{C} (101 MHz, DMSO-*d*₆) 36.3 (CH₂), 117.0 (d, ²*J*_{CF} 22.8 Hz, CH), 119.1 (d, ²*J*_{CF} 10.7 Hz, C), 125.5 (CH), 126.1 (CH), 127.9 (C), 129.1 (C), 131.6 (CH), 131.9 (CH), 133.6 (CH), 134.3 (d, ⁴*J*_{CF} 3.4 Hz, C), 134.9 (d, ³*J*_{CF} 8.7 Hz, CH), 144.9 (C), 159.4 (C), 160.3 (d, ¹*J*_{CF} 255.5 Hz, C), 165.0 (d, ³*J*_{CF} 2.8 Hz, C); *m/z* (ESI) 297 ((M-H)⁻. 100%).

Method B: To a stirred suspension of 2-fluoro-5-[(4''-oxo-3''H-phthalazin-1''-yl)methyl] benzonitrile (**48**) (5.03 g, 18.0 mmol) in water (21 mL) was added 2 M aqueous sodium hydroxide solution (18.9 mL, 37.8 mmol). The reaction mixture was heated to 90 °C and stirred for 23 h. After cooling to room temperature, the reaction mixture was filtered *in vacuo* and the sinter funnel was washed with water (5 mL).

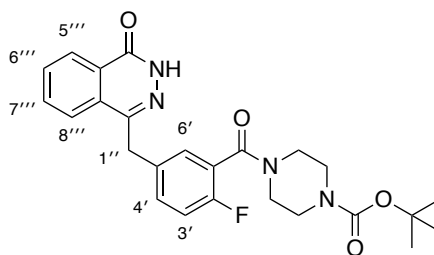
The filtrate was then heated to 60 °C and 2 M aqueous hydrochloric acid solution (30 mL) was added dropwise, which produced a white precipitate. The crude mixture was cooled to 50 °C and the product collected by vacuum filtration. This was washed with water (30 mL) and diethyl ether (3 × 30 mL) to give 2-fluoro-5-[(4''-oxo-3''H-phthalazin-1''-yl)methyl]benzoic acid (**45**) as a white solid (4.93 g, 92%). Spectroscopic data were consistent with that described above.

***tert*-Butyl piperazine-1-carboxylate (**46**)**¹⁰²



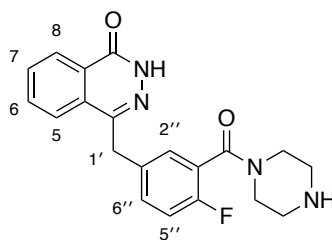
A stirred solution of piperazine (**49**) (0.500 g, 5.80 mmol) in dichloromethane (12 mL) was cooled to 0 °C, and to this was added a solution of di-*tert*-butyl dicarbonate (0.633 g, 2.90 mmol) in dichloromethane (6 mL) dropwise over 0.5 h. The reaction mixture was left stirring in an ice bath at 0 °C and allowed to slowly reach room temperature for 21 h. The crude mixture was washed with water (20 mL), the organic and aqueous layers were separated, and the aqueous layer extracted with dichloromethane (3 × 20 mL). The combined organic layers were dried (MgSO₄), filtered and concentrated *in vacuo* to give *tert*-butyl piperazine-1-carboxylate (**46**) as a white solid (0.490 g, 91%). Mp 46–48 °C (lit.¹⁰² 46–48 °C); δ_H (400 MHz, CD₃OD) 1.46 (9H, s, ^tBu), 2.75 (4H, t, *J* 5.0 Hz, 4 × NCH₂), 3.38 (4H, t, *J* 5.0 Hz, 4 × NCH₂); δ_C (101 MHz, CD₃OD) 28.7 (3 × CH₃), 44.8 (2 × CH₂), 46.3 (2 × CH₂), 81.1 (C), 156.4 (C); *m/z* (CI) 187 (MH⁺, 78%), 175 (5), 131 (100), 87 (20), 73 (10).

***tert*-Butyl 4-{2'-fluoro-5'-[(4'''-oxo-3'''*H*-phthalazin-1'''-yl)methyl]benzoyl}piperazine-1-carboxylate (**47**)¹⁰²**



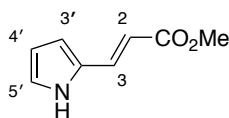
To a stirred solution of 2-fluoro-5-[(4'''-oxo-3'''*H*-phthalazin-1'''-yl)methyl]benzoic acid (**45**) (4.91 g, 16.5 mmol) and *O*-benzotriazole-*N,N,N',N'*-tetramethyluroniumhexafluorophosphate (6.87 g, 18.1 mmol) in anhydrous *N,N'*-dimethylformamide (82 mL), under argon, was added triethylamine (3.44 mL, 24.7 mmol). The reaction mixture was stirred at room temperature for 1 h. *tert*-Butyl piperazine-1-carboxylate (**46**) (3.37 g, 18.1 mmol) was added to the reaction mixture, which was then heated to 50 °C and stirred for 40 h. The reaction mixture was cooled to room temperature, diluted with ethyl acetate (240 mL) and washed with water (3 × 80 mL). The organic layer was dried (MgSO₄), filtered and concentrated *in vacuo*. The crude material was purified by flash column chromatography eluting with 4% methanol in dichloromethane to give *tert*-butyl 4-{2'-fluoro-5'-[(4'''-oxo-3'''*H*-phthalazin-1'''-yl)methyl]benzoyl}piperazine-1-carboxylate (**47**) as an off-white solid (7.47 g, 97%). Mp 214–216 °C (lit.¹⁰² 214–216 °C); δ_{H} (400 MHz, CDCl₃) 1.46 (9H, s, ^tBu), 3.27 (2H, br s, NCH₂), 3.38 (2H, t, *J* 5.1 Hz, 2 × NCH), 3.51 (2H, br s, 2 × NCH), 3.75 (2H, br s, 2 × NCH), 4.28 (2H, s, 1''-H₂), 7.03 (1H, t, *J* 8.8 Hz, 3'-H), 7.27–7.36 (2H, m, 4'-H and 6'-H), 7.68–7.80 (3H, m, 6'''-H, 7'''-H and 8'''-H), 8.44–8.50 (1H, m, 5'''-H), 10.52 (1H, s, NH); δ_{C} (101 MHz, CDCl₃) 28.5 (3 × CH₃), 37.9 (CH₂), 42.1 (2 × CH₂), 47.0 (2 × CH₂), 80.5 (C), 116.3 (d, ²*J*_{CF} 22.2 Hz, CH), 124.1 (d, ²*J*_{CF} 17.9 Hz, C), 125.2 (CH), 127.3 (CH), 128.5 (C), 129.3 (d, ³*J*_{CF} 3.7 Hz, CH), 129.7 (C), 131.7 (d, ³*J*_{CF} 8.1 Hz, CH), 131.8 (CH), 133.8 (CH), 134.5 (d, ⁴*J*_{CF} 3.0 Hz, C), 145.7 (C), 154.6 (C), 157.1 (d, ¹*J*_{CF} 246.1 Hz, C), 160.6 (C), 165.2 (C); *m/z* (EI) 466 (M⁺, 17%), 365 (40), 311 (30), 281 (100), 254 (30), 196 (12), 178 (42), 165 (10), 85 (16), 57 (57).

4-[4''-Fluoro-3''-(piperazine-1'''-carbonyl)benzyl]-2H-phthalazin-1-one (35)¹⁰²



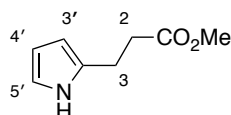
To a stirred suspension of *tert*-butyl 4-{2'-fluoro-5'-[(4'''-oxo-3'''*H*-phthalazin-1'''-yl)methyl]benzoyl}piperazine-1-carboxylate (**47**) (3.73 g, 8.00 mmol) in ethanol (100 mL) was added 6 M aqueous hydrochloric acid solution (200 mL). The suspension was stirred at room temperature for 22 h. The reaction mixture was concentrated *in vacuo* and the resultant residue partitioned between 6 M aqueous sodium hydroxide solution (100 mL) and ethyl acetate (100 mL). The organic and aqueous layers were then separated, and the aqueous layer was extracted with ethyl acetate (2 × 100 mL). The combined organic layers were dried (MgSO₄), filtered and concentrated *in vacuo*. The crude material was purified by flash column chromatography eluting with 10% methanol in dichloromethane to give 4-[4''-fluoro-3''-(piperazine-1'''-carbonyl)benzyl]-2H-phthalazin-1-one (**35**) as a white solid (2.78 g, 95%). Mp 193–195 °C. Spectroscopic data were consistent with the literature.¹⁰² δ_{H} (400 MHz, CDCl₃) 2.25–3.15 (4H, m, 4 × NCH), 3.16–3.96 (4H, m, 4 × NCH), 4.25 (2H, s, 1'-H₂), 5.99 (1H, br s, NH), 6.97 (1H, t, *J* 8.8 Hz, 5''-H), 7.24–7.35 (2H, m, 2''-H and 6''-H), 7.64–7.76 (3H, m, 5-H, 6-H and 7-H), 8.38–8.46 (1H, m, 8-H), 12.01 (1H, br s, CONHN); δ_{C} (101 MHz, CDCl₃) 37.9 (CH₂), 43.3 (CH₂), 45.9 (CH₂), 46.4 (CH₂), 48.4 (CH₂), 116.1 (d, ²*J*_{CF} 22.1 Hz, CH), 124.4 (d, ²*J*_{CF} 18.4 Hz, C), 125.2 (CH), 127.3 (CH), 128.4 (C), 129.2 (d, ³*J*_{CF} 3.8 Hz, CH), 129.7 (C), 131.3 (d, ³*J*_{CF} 8.0 Hz, CH), 131.7 (CH), 133.8 (CH), 134.3 (d, ⁴*J*_{CF} 3.0 Hz, C), 145.7 (C), 157.2 (d, ¹*J*_{CF} 247.7 Hz, C), 160.8 (C), 165.0 (C); *m/z* (ESI) 367 (MH⁺, 100%).

Methyl (*E*)-3-(1'*H*-pyrrol-2'-yl)acrylate (**59**)⁴²⁹



To a stirred solution of methyl (triphenylphosphoranylidene)acetate (3.51 g, 10.5 mmol) in anhydrous dichloromethane (15 mL) in an oven-dried flask under argon, was added a solution of pyrrole-2-carboxaldehyde (**58**) (0.500 g, 5.26 mmol) in anhydrous dichloromethane (10 mL). The reaction mixture was stirred at room temperature for 18 h and then concentrated *in vacuo*. The crude material was purified by flash column chromatography eluting with 20% ethyl acetate in hexane to give methyl (*E*)-3-(1'*H*-pyrrol-2'-yl)acrylate (**59**) as a pale beige solid (0.627 g, 79%). Mp 80–82 °C (lit.⁴²⁹ 86–88 °C); δ_{H} (400 MHz, CDCl₃) 3.78 (3H, s, CH₃), 6.03 (1H, d, *J* 15.9 Hz, 2-H), 6.26–6.30 (1H, m, 4'-H), 6.55–6.59 (1H, m, 3'-H), 6.91–6.95 (1H, m, 5'-H), 7.58 (1H, d, *J* 15.9 Hz, 3-H), 8.70–9.09 (1H, br s, NH); δ_{C} (101 MHz, CDCl₃) 51.7 (CH₃), 110.9 (CH), 111.1 (CH), 114.6 (CH), 122.6 (CH), 128.5 (C), 134.7 (CH), 168.3 (C); *m/z* (ESI) 174 (MNa⁺, 100%).

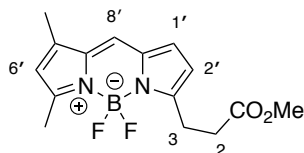
Methyl 3-(1'*H*-pyrrol-2'-yl)propanoate (**60**)⁴²⁹



A stirred solution of methyl (*E*)-3-(1'*H*-pyrrol-2'-yl)acrylate (**59**) (0.618 g, 4.09 mmol) and 10% palladium on carbon (0.152 g, 0.143 mmol) in methanol (6 mL) was degassed with hydrogen for 1 h. The reaction mixture was stirred under an atmosphere of hydrogen for a further 2 h. The crude reaction mixture was purified through a short pad of Celite[®] eluting with methanol to give methyl 3-(1'*H*-pyrrol-2'-yl)propanoate (**60**) as a light brown oil (0.576 g, 92%). Spectroscopic data were consistent with the literature.⁴²⁹ δ_{H} (400 MHz, CDCl₃) 2.65 (2H, t, *J* 6.8 Hz, 2-H₂), 2.92 (2H, t, *J* 6.8 Hz, 3-H₂), 3.71 (3H, s, CH₃), 5.93 (1H, br s, 3'-H), 6.08–6.14 (1H, m, 4'-H), 6.64–6.71 (1H, m, 5'-H), 8.53 (1H, br s, NH); δ_{C} (101 MHz, CDCl₃) 22.7

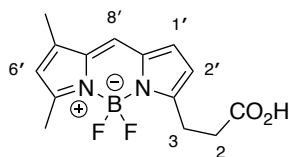
(CH₂), 34.5 (CH₂), 51.9 (CH₃), 105.6 (CH), 108.1 (CH), 116.9 (CH), 131.1 (C), 174.7 (C); *m/z* (ESI) 176 (MNa⁺. 100%).

Methyl 3-[4',4'-difluoro-5',7'-dimethyl-4'-bora-3'a,4'a-diaza-s-indacene- 3'-yl]propionate (62)⁴³⁰



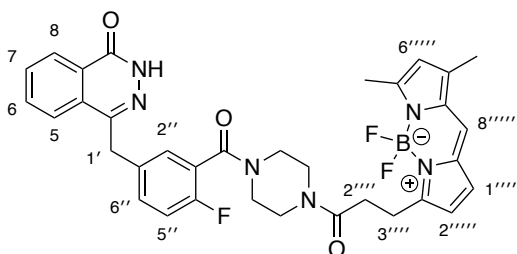
In an oven-dried flask under argon, methyl 3-(1*H*-pyrrol-2'-yl)propanoate (**60**) (0.250 g, 1.63 mmol) and 3,5-dimethylpyrrole-2-carboxaldehyde (**61**) (0.220 g, 1.79 mmol) were dissolved in anhydrous dichloromethane (16 mL) and cooled to 0 °C. Phosphorous(V) oxychloride (0.167 mL, 1.79 mmol) was added dropwise to the reaction mixture, which was then warmed to room temperature and stirred for 3 h. The reaction mixture was cooled to 0 °C, and *N,N*-diisopropylethylamine (1.28 mL, 7.34 mmol) and boron trifluoride diethyl etherate (0.810 mL, 6.56 mmol) were added. The reaction mixture was warmed to room temperature and stirred for 14 h. The crude reaction mixture was then diluted with brine (30 mL) and filtered through a short pad of Celite[®], which was then washed with dichloromethane (16 mL). The organic and aqueous layers were separated, and the aqueous layer was extracted with dichloromethane (4 × 30 mL). The combined organic layers were dried (MgSO₄), filtered and concentrated *in vacuo*. The crude material was purified by flash column chromatography eluting with 100% dichloromethane to give methyl 3-[4',4'-difluoro-5',7'-dimethyl-4'-bora-3'a,4'a-diaza-s-indacene-3'-yl]propionate (**62**) as a dark red solid (0.331 g, 66%). Mp 74–76 °C (lit.⁴³⁰ 76–78 °C); δ_H (400 MHz, CDCl₃) 2.24 (3H, s, ArCH₃), 2.56 (3H, s, ArCH₃), 2.77 (2H, t, *J* 7.6 Hz, 2-H₂), 3.29 (2H, t, *J* 7.6 Hz, 3-H₂), 3.69 (3H, s, CH₃), 6.10 (1H, s, 6'-H), 6.26 (1H, d, *J* 4.0 Hz, 2'-H), 6.87 (1H, d, *J* 4.0 Hz, 1'-H), 7.07 (1H, s, 8'-H); δ_C (101 MHz, CDCl₃) 11.4 (CH₃), 15.1 (CH₃), 24.1 (CH₂), 33.4 (CH₂), 51.9 (CH₃), 116.8 (CH), 120.6 (CH), 124.0 (CH), 128.2 (CH), 133.4 (C), 135.4 (C), 144.0 (C), 157.2 (C), 160.6 (C), 173.1 (C); *m/z* (ESI) 329 (MNa⁺. 100%).

3-[4',4'-Difluoro-5',7'-dimethyl-4'-bora-3'a,4'a-diaza-s-indacene-3'-yl]propionic acid (36)⁴³⁰



A stirred solution of methyl 3-[4',4'-difluoro-5',7'-dimethyl-4'-bora-3'a,4'a-diaza-s-indacene-3'-yl]propionate (**62**) (0.0650 g, 0.212 mmol) in tetrahydrofuran (1.5 mL) and water (1 mL) was cooled to 0 °C. Concentrated hydrochloric acid (0.450 mL, 5.40 mmol) was added to the reaction mixture, which was then warmed to room temperature and stirred for 50 h. The reaction mixture was concentrated *in vacuo* and the crude residue was purified by flash column chromatography eluting with 4% methanol in dichloromethane to give 3-[4',4'-difluoro-5',7'-dimethyl-4'-bora-3'a,4'a-diaza-s-indacene-3'-yl]propionic acid (**36**) as a dark red solid (0.0407 g, 66%). Mp 192–195 °C (lit.⁴³⁰ 194–196 °C); δ_{H} (400 MHz, DMSO-*d*₆) 2.26 (3H, s, ArCH₃), 2.47 (3H, s, ArCH₃), 2.60–2.67 (2H, m, 2-H₂), 3.04–3.11 (2H, m, 3-H₂), 6.31 (1H, s, 6'-H), 6.38 (1H, d, *J* 4.0 Hz, 2'-H), 7.09 (1H, d, *J* 4.0 Hz, 1'-H), 7.70 (1H, s, 8'-H), 12.30 (1H, br s, OH); δ_{C} (101 MHz, DMSO-*d*₆) 11.0 (CH₃), 14.5 (CH₃), 23.5 (CH₂), 32.4 (CH₂), 116.5 (CH), 120.4 (CH), 125.4 (CH), 128.8 (CH), 133.0 (C), 134.6 (C), 144.3 (C), 156.9 (C), 159.5 (C), 173.4 (C); *m/z* (ESI) 315 (MNa⁺, 100%).

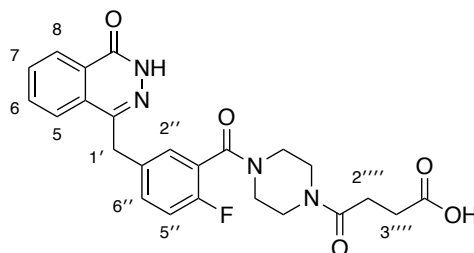
4-{3'-[4''-(1''''-oxo-3''''-{4''''',4'''''-difluoro-5''''',7'''''-dimethyl-4'''''-bora-3''''''a,4''''''a-diaza-s-indacene-3''''''-yl]propyl)piperazine-1''''-carbonyl]-4''-fluorobenzyl}-2*H*-phthalazin-1-one (37)¹⁶⁶



To a stirred solution of 3-[4',4'-difluoro-5',7'-dimethyl-4'-bora-3'a,4'a-diaza-s-indacene-3'-yl]propionic acid (**36**) (0.0500 g, 0.171 mmol) and *O*-benzotriazole-*N,N,N',N'*-tetramethyluroniumhexafluorophosphate (0.0710 g, 0.188 mmol) in

anhydrous *N,N'*-dimethylformamide (2 mL), under argon, was added triethylamine (0.0360 mL, 0.257 mmol). The reaction mixture was stirred at room temperature for 0.5 h. 4-[4''-Fluoro-3'''-(piperazine-1'''-carbonyl)benzyl]-2*H*-phthalazin-1-one (**35**) (0.0630 g, 0.171 mmol) was added to the reaction mixture, which was then heated to 50 °C and stirred for 18 h. The reaction mixture was cooled to room temperature, diluted with ethyl acetate (5 mL) and washed with water (5 mL). The organic layer was dried (MgSO₄), filtered and concentrated *in vacuo*. The crude material was purified by flash column chromatography eluting with 0–4% gradient of methanol in dichloromethane to give 4-{3''-[4'''-(1'''-oxo-3''''-{4''''',4'''''-difluoro-5''''',7''''''-dimethyl-4''''''-bora-3''''''a, 4''''''a-diaza-s-indacene-3''''''-yl)propyl)piperazine-1'''-carbonyl]-4''-fluorobenzyl}-2*H*-phthalazin-1-one (**37**) as a red foam (0.102 g, 93%). UV/Vis (methanol) λ_{max} (ϵ , M⁻¹ cm⁻¹) = 504 nm (64779) measured at concentrations of 1 μ M, 5 μ M, and 10 μ M and λ_{Em} = 511 nm. Spectroscopic data were consistent with the literature.¹⁶⁶ δ_{H} (500 MHz, DMSO-*d*₆, T = 100 °C) 2.27 (3H, s, CH₃), 2.49 (3H, s, CH₃), 2.75 (2H, t, *J* 7.8 Hz, 2''''-H₂), 3.15 (2H, t, *J* 7.8 Hz, 3''''-H₂), 3.50 (8H, br s, 4 × NCH₂), 4.33 (2H, s, 1'-H₂), 6.27 (1H, s, 6''''''-H), 6.40 (1H, d, *J* 4.0 Hz, 2''''''-H), 7.08 (1H, d, *J* 4.0 Hz, 1''''''-H), 7.18 (1H, t, *J* 9.0 Hz, 5''-H), 7.34 (1H, dd, *J* 6.5, 2.2 Hz, 2''-H), 7.39–7.44 (1H, m, 6''-H), 7.58 (1H, s, 8''''''-H), 7.81 (1H, t, *J* 7.6 Hz, 7-H), 7.87 (1H, t, *J* 7.6 Hz, 6-H), 7.93 (1H, d, *J* 7.6 Hz, 5-H), 8.29 (1H, d, *J* 7.6 Hz, 8-H), 12.25 (1H, br s, NH); δ_{C} (126 MHz, DMSO-*d*₆, T = 100 °C) 10.3 (CH₃), 13.8 (CH₃), 23.4 (CH₂), 30.9 (CH₂), 36.0 (CH₂), 115.3 (d, ²*J*_{CF} 21.5 Hz, CH), 116.5 (CH), 119.7 (CH), 123.4 (d, ²*J*_{CF} 18.3 Hz, C), 124.4 (CH), 124.7 (CH), 125.6 (CH), 127.7 (C), 128.2 (CH), 128.4 (d, ³*J*_{CF} 3.9 Hz, CH), 128.8 (C), 130.8 (CH), 131.1 (d, ³*J*_{CF} 8.1 Hz, CH), 132.7 (CH), 134.1 (C), 134.3 (d, ⁴*J*_{CF} 3.3 Hz, C), 143.4 (C), 144.1 (C), 156.1 (d, ¹*J*_{CF} 245.4 Hz, C), 157.5 (C), 158.6 (C), 158.8 (C), 163.8 (C), 169.4 (C), (signals of the piperazine ring (4 × CH₂) and a quaternary carbon from BODIPY moiety were not observed); *m/z* (ESI) 663 (MNa⁺. 100%).

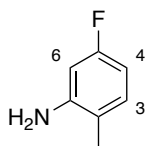
4-{3''-[4'''-(1''''-Oxo-4''''-butanoic acid)-piperazine-1'''-carbonyl]-4''-fluorobenzyl}-2*H*-phthalazin-1-one (38)



In an oven-dried flask under argon, 4-[4''-fluoro-3''-(piperazine-1'''-carbonyl)benzyl]-2*H*-phthalazin-1-one (**35**) (0.0660 g, 0.180 mmol), succinic anhydride (0.0150 g, 0.150 mmol) and 4-(dimethylamino)pyridine (0.00180 g, 0.0150 mmol) were dissolved in anhydrous acetonitrile (3 mL). The reaction mixture was stirred under reflux for 16 h and then concentrated *in vacuo*. The resultant residue was partitioned between saturated aqueous sodium bicarbonate solution (15 mL) and ethyl acetate (15 mL). The organic and aqueous layers were then separated. The aqueous layer was acidified to pH 2 with 1 M aqueous hydrochloric acid solution and extracted with ethyl acetate (3 × 15 mL). The combined organic layers were dried (MgSO₄), filtered and concentrated *in vacuo* to give 4-{3''-[4'''-(1''''-oxo-4''''-butanoic acid)-piperazine-1'''-carbonyl]-4''-fluorobenzyl}-2*H*-phthalazin-1-one (**38**) as a white solid (0.0567 g, 81%). Mp 200–205 °C; $\nu_{\max}/\text{cm}^{-1}$ (neat) 3169 (NH/OH), 2922 (CH), 1782 (C=O), 1636 (C=O), 1439, 1247, 842. NMR spectra showed a 1:1 mixture of rotational isomers. Signals for both rotational isomers are recorded. δ_{H} (400 MHz, CD₃OD) 2.55–2.73 (8H, m, 2 × 2''''-H₂ and 2 × 3''''-H₂), 3.28 (2H, br s, 2 × NCH), 3.35 (2H, br s, 2 × NCH), 3.47–3.53 (4H, m, 4 × NCH), 3.62–3.75 (6H, m, 6 × NCH), 3.77–3.83 (2H, m, 2 × NCH), 4.36 (4H, s, 2 × 1'-H₂), 7.14 (2H, t, *J* 9.0 Hz, 2 × 5''-H), 7.35–7.41 (2H, m, 2 × 2''-H), 7.43–7.49 (2H, m, 2 × 6''-H), 7.77–7.88 (4H, m, 2 × 6-H and 2 × 7-H), 7.92 (2H, dd, *J* 7.4, 3.4 Hz, 2 × 5-H), 8.34 (2H, d, *J* 7.6 Hz, 2 × 8-H); δ_{C} (101 MHz, CD₃OD) 28.8 (2 × CH₂), 30.1 (2 × CH₂), 38.1 (2 × CH₂), 42.4 (CH₂), 42.9 (CH₂), 43.0 (CH₂), 43.2 (CH₂), 46.0 (CH₂), 46.5 (CH₂), 47.9 (CH₂), 48.1 (CH₂), 117.1 (d, ²*J*_{CF} 21.9 Hz, 2 × CH), 124.6 (d, ²*J*_{CF} 18.2 Hz, C), 124.6 (d, ²*J*_{CF} 18.2 Hz, C), 126.7 (2 × CH), 127.5 (2 × CH), 129.1 (2 × C), 130.1 (d, ³*J*_{CF} 3.8 Hz, CH), 130.1 (d, ³*J*_{CF} 3.8 Hz, CH), 130.8 (2 × C), 132.8 (2 × CH), 133.3 (d, ³*J*_{CF} 8.1 Hz, 2 × CH), 135.0 (2 × CH), 136.4 (d, ⁴*J*_{CF} 3.4 Hz, 2 × C), 147.6 (2 × C), 158.3 (d, ¹*J*_{CF} 247.0 Hz,

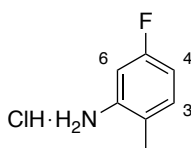
2 × C), 162.2 (2 × C), 167.2 (C), 167.3 (C), 172.8 (C), 172.8 (C), 176.6 (2 × C); *m/z* (ESI) 489.1563 (MNa⁺. C₂₄H₂₃FN₄NaO₅ requires 489.1545).

2-Methyl-5-fluoroaniline (**64**)⁴³¹



A stirred solution of 2-nitro-4-fluorotoluene (**63**) (0.123 mL, 1.00 mmol) and 10% palladium on carbon (0.106 g, 0.100 mmol) in methanol (10 mL) was degassed with hydrogen for 0.5 h. The reaction mixture was stirred under an atmosphere of hydrogen for a further 2 h. The reaction mixture was passed through a short pad of Celite[®] eluting with methanol and concentrated *in vacuo*. The crude material was purified by flash column chromatography eluting with 10% diethyl ether in petroleum ether (40–60) to give 2-methyl-5-fluoroaniline (**64**) as a light brown oil (0.0780 g, 62%). Spectroscopic data were consistent with the literature.⁴³¹ δ_{H} (500 MHz, CDCl₃) 2.11 (3H, s, CH₃), 3.68 (2H, br s, NH₂), 6.33–6.43 (2H, m, 4-H and 6-H), 6.92–7.00 (1H, m, 3-H); δ_{C} (126 MHz, CDCl₃) 16.8 (CH₃), 101.7 (d, ²*J*_{CF} 24.6 Hz, CH), 104.9 (d, ²*J*_{CF} 21.0 Hz, CH), 117.8 (d, ⁴*J*_{CF} 2.6 Hz, C), 131.3 (d, ³*J*_{CF} 9.6 Hz, CH), 145.9 (d, ³*J*_{CF} 10.6 Hz, C), 162.4 (d, ¹*J*_{CF} 241.4 Hz, C); *m/z* (EI) 125 (M⁺, 82%), 124 (100), 108 (8), 97 (10), 84 (15), 77 (11), 57 (16).

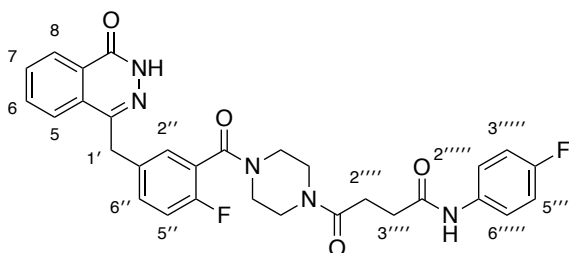
2-Methyl-5-fluoroaniline hydrochloride (**65**)



A stirred solution of 2-nitro-4-fluorotoluene (**63**) (0.397 mL, 3.22 mmol) and 10% palladium on carbon (0.343 g, 0.322 mmol) in methanol (32 mL) was degassed with hydrogen for 0.5 h. The reaction mixture was stirred under an atmosphere of hydrogen for a further 6 h. The reaction mixture was passed through a short pad of Celite[®] eluting with diethyl ether and concentrated *in vacuo*. The crude material was

dissolved in diethyl ether (3.22 mL) and 2 M hydrochloric acid in anhydrous diethyl ether solution (3.22 mL) was added, which formed a white precipitate. The suspension was stirred at room temperature for 10 minutes. The precipitate was collected by vacuum filtration and washed with diethyl ether (3 × 10 mL) to give 2-methyl-5-fluoroaniline hydrochloride (**65**) as a white solid (0.513 g, 98%). Decomposition >140 °C; $\nu_{\max}/\text{cm}^{-1}$ (neat) 2822 (NH), 2598 (CH), 1562, 1535, 1503, 1256, 868, 824; δ_{H} (400 MHz, CD₃OD) 2.38 (3H, s, CH₃), 7.09–7.22 (2H, m, 4-H and 6-H), 7.41 (1H, dd, *J* 8.6, 5.8 Hz, 3-H); δ_{C} (101 MHz, CD₃OD) 16.4 (CH₃), 111.6 (d, ²*J*_{CF} 25.9 Hz, CH), 116.8 (d, ²*J*_{CF} 21.0 Hz, CH), 129.1 (d, ⁴*J*_{CF} 3.6 Hz, C), 132.0 (d, ³*J*_{CF} 9.8 Hz, C), 134.4 (d, ³*J*_{CF} 8.6 Hz, CH) 162.5 (d, ¹*J*_{CF} 246.2 Hz, C); *m/z* (EI) 125.0646 (M⁺. C₇H₈FN requires 125.0641), 251 (26%), 159 (5), 124 (100), 107 (8), 97 (10), 77 (11), 56 (13).

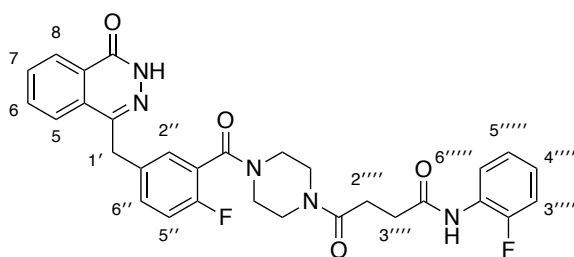
4-{3''-[4'''-(1''''-Oxo-4''''-{N-[4''''-fluorophenyl]butanamide})]-piperazine-1''''-carbonyl]-4''-fluorobenzyl}-2*H*-phthalazin-1-one (66)



To a stirred solution of 4-{3''-[4'''-(1''''-oxo-4''''-butanoic acid)-piperazine-1''''-carbonyl]-4''-fluorobenzyl}-2*H*-phthalazin-1-one (**38**) (0.0720 g, 0.154 mmol) and *O*-benzotriazole-*N,N,N',N'*-tetramethyluroniumhexafluorophosphate (0.0641 g, 0.169 mmol) in anhydrous *N,N*-dimethylformamide (1.5 mL), under argon, was added triethylamine (0.0320 mL, 0.230 mmol). The reaction mixture was stirred at room temperature for 1 h. 4-Fluoroaniline (0.0146 mL, 0.154 mmol) was added to the reaction mixture, which was then heated to 50 °C and stirred for 22 h. The reaction mixture was cooled to room temperature, diluted with ethyl acetate (5 mL) and washed with water (5 × 5 mL). The organic layer was dried (MgSO₄), filtered and concentrated *in vacuo*. The crude material was purified by flash column chromatography eluting with 4% methanol in dichloromethane to give 4-{3''-[4'''-(1''''-oxo-4''''-{N-[4''''-fluorophenyl]butanamide})]-piperazine-1''''-carbonyl]-4''-fluorobenzyl}-2*H*-phthalazin-1-one (**66**) as a white solid (0.0505 g, 59%). Mp 180–

182 °C; $\nu_{\max}/\text{cm}^{-1}$ (neat) 3271 (NH), 3210 (NH), 3071 (CH), 2978 (CH), 2916 (CH), 1620 (C=O), 1550, 1504, 1435, 1358, 1211, 1165, 1010, 833. NMR spectra showed a 1:1 mixture of rotational isomers. Signals for both rotational isomers are recorded. δ_{H} (400 MHz, CDCl_3) 2.67–2.84 (8H, m, $2 \times 2''''\text{-H}_2$ and $2 \times 3''''\text{-H}_2$), 3.19–3.86 (16H, m, $16 \times \text{NCH}$), 4.27 (4H, s, $2 \times 1'\text{-H}_2$), 6.92 (4H, t, J 8.4 Hz, $2 \times 3''''\text{-H}$ and $2 \times 5''''\text{-H}$), 7.02 (2H, t, J 9.2 Hz, $2 \times 5''\text{-H}$), 7.28–7.35 (4H, m, $2 \times 2''\text{-H}$ and $2 \times 6''\text{-H}$), 7.42–7.49 (4H, m, $2 \times 2''''\text{-H}$ and $2 \times 6''''\text{-H}$), 7.67–7.80 (6H, m, $2 \times 5\text{-H}$, $2 \times 6\text{-H}$ and $2 \times 7\text{-H}$), 8.42–8.49 (2H, m, $2 \times 8\text{-H}$), 8.68 (1H, br s, CONHPh), 8.72 (1H, br s, CONHPh), 11.34 (1H, br s, CONHN), 11.36 (1H, br s, CONHN); δ_{C} (101 MHz, CDCl_3) 28.7 ($2 \times \text{CH}_2$), 32.3 (CH_2), 32.4 (CH_2), 37.7 ($2 \times \text{CH}_2$), 41.6 (CH_2), 42.0 (CH_2), 42.1 ($2 \times \text{CH}_2$), 45.1 (CH_2), 45.7 (CH_2), 46.8 (CH_2), 47.0 (CH_2), 115.5 (d, ${}^2J_{\text{CF}}$ 22.4 Hz, $4 \times \text{CH}$), 116.3 (d, ${}^2J_{\text{CF}}$ 22.0 Hz, CH), 116.3 (d, ${}^2J_{\text{CF}}$ 22.0 Hz, CH), 121.4 (d, ${}^3J_{\text{CF}}$ 7.4 Hz, $2 \times \text{CH}$), 121.5 (d, ${}^3J_{\text{CF}}$ 7.4 Hz, $2 \times \text{CH}$), 123.6 (d, ${}^2J_{\text{CF}}$ 18.0 Hz, C), 123.7 (d, ${}^2J_{\text{CF}}$ 18.0 Hz, C), 125.1 ($2 \times \text{CH}$), 127.2 ($2 \times \text{CH}$), 128.4 ($2 \times \text{C}$), 129.3 (d, ${}^3J_{\text{CF}}$ 3.2 Hz, CH), 129.5 (d, ${}^3J_{\text{CF}}$ 3.2 Hz, CH), 129.6 ($2 \times \text{C}$), 131.8 ($2 \times \text{CH}$), 131.9 (d, ${}^3J_{\text{CF}}$ 7.5 Hz, CH), 131.9 (d, ${}^3J_{\text{CF}}$ 7.5 Hz, CH), 133.8 ($2 \times \text{CH}$), 134.5 (d, ${}^4J_{\text{CF}}$ 3.9 Hz, $2 \times \text{C}$), 134.6 (d, ${}^4J_{\text{CF}}$ 3.2 Hz, $2 \times \text{C}$), 145.6 (C), 145.6 (C), 157.1 (d, ${}^1J_{\text{CF}}$ 249.3 Hz, $2 \times \text{C}$), 159.1 (d, ${}^1J_{\text{CF}}$ 243.5 Hz, $2 \times \text{C}$), 160.8 ($2 \times \text{C}$), 165.2 (C), 165.4 (C), 170.7 ($2 \times \text{C}$), 171.0 (C), 171.1 (C); m/z (ESI) 582.1909 (MNa^+ . $\text{C}_{30}\text{H}_{27}\text{F}_2\text{N}_5\text{NaO}_4$ requires 582.1923).

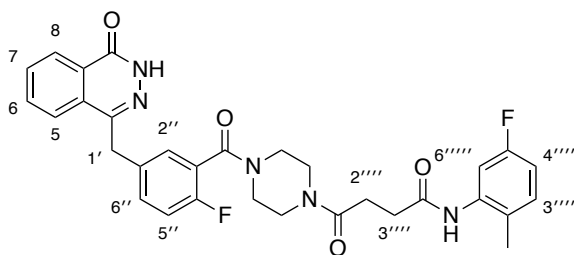
4-{3''-[4''''-(1''''-Oxo-4''''-{N-[2''''-fluorophenyl]butanamide})-piperazine-1''''-carbonyl]-4''-fluorobenzyl}-2H-phthalazin-1-one (67)



The reaction was carried out according to the previously described procedure for compound **66**, using 4-{3''-[4''''-(1''''-oxo-4''''-butanoic acid)-piperazine-1''''-carbonyl]-4''-fluorobenzyl}-2H-phthalazin-1-one (**38**) (0.0650 g, 0.139 mmol), O-benzotriazole-*N,N,N',N'*-tetramethyluroniumhexafluorophosphate (0.0580 g, 0.153 mmol), anhydrous *N,N'*-dimethylformamide (1.5 mL), triethylamine (0.0290 mL,

0.208 mmol) and 2-fluoroaniline (0.0134 mL, 0.139 mmol). The crude material was purified by flash column chromatography eluting with 3% methanol in dichloromethane to give 4-{3''-[4'''-(1''''-oxo-4''''-{N-[2''''-fluorophenyl]butanamide})-piperazine-1'''-carbonyl]-4''-fluorobenzyl}-2H-phthalazin-1-one (**67**) as a white solid (0.0382 g, 49%). Mp 125–127 °C; $\nu_{\max}/\text{cm}^{-1}$ (neat) 3252 (NH), 3188 (NH), 3009 (CH), 2916 (CH), 1616 (C=O), 1533, 1433, 1354, 1222, 1169, 1011. NMR spectra showed a 1:1 mixture of rotational isomers. Signals for both rotational isomers are recorded. δ_{H} (400 MHz, CDCl_3) 2.67–2.84 (8H, m, $2 \times 2''''\text{-H}_2$ and $2 \times 3''''\text{-H}_2$), 3.19–3.87 (16H, m, $16 \times \text{NCH}$), 4.28 (4H, s, $2 \times 1'\text{-H}_2$), 6.95–7.11 (8H, m, $2 \times 3''''\text{-H}$, $2 \times 5''''\text{-H}$, $2 \times \text{ArH}$ and $2 \times 5''\text{-H}$), 7.28–7.37 (4H, m, $2 \times 2''\text{-H}$ and $2 \times 6''\text{-H}$), 7.65–7.80 (6H, m, $2 \times 5\text{-H}$, $2 \times 6\text{-H}$ and $2 \times 7\text{-H}$), 8.16–8.31 (4H, m, $2 \times \text{ArH}$ and $2 \times \text{CONHPh}$), 8.43–8.50 (2H, m, $2 \times 8\text{-H}$), 11.20–11.41 (2H, m, $2 \times \text{CONHN}$); δ_{C} (101 MHz, CDCl_3) 28.7 ($2 \times \text{CH}_2$), 32.5 ($2 \times \text{CH}_2$), 37.8 ($2 \times \text{CH}_2$), 41.6 (CH_2), 42.0 (CH_2), 42.1 ($2 \times \text{CH}_2$), 45.1 (CH_2), 45.6 (CH_2), 46.8 (CH_2), 47.0 (CH_2), 114.9 (d, ${}^2J_{\text{CF}}$ 19.1 Hz, CH), 114.9 (d, ${}^2J_{\text{CF}}$ 19.1 Hz, CH), 116.3 (d, ${}^2J_{\text{CF}}$ 21.9 Hz, CH), 116.3 (d, ${}^2J_{\text{CF}}$ 21.9 Hz, CH), 122.0 (d, ${}^3J_{\text{CF}}$ 5.7 Hz, $2 \times \text{CH}$), 123.7 (d, ${}^2J_{\text{CF}}$ 17.4 Hz, C), 123.7 (d, ${}^2J_{\text{CF}}$ 17.4 Hz, C), 124.3 (d, ${}^3J_{\text{CF}}$ 7.3 Hz, CH), 124.4 (d, ${}^3J_{\text{CF}}$ 7.3 Hz, CH), 124.5 (d, ${}^4J_{\text{CF}}$ 3.1 Hz, $2 \times \text{CH}$), 125.1 ($2 \times \text{CH}$), 126.5 ($2 \times \text{C}$), 127.3 ($2 \times \text{CH}$), 128.4 ($2 \times \text{C}$), 129.3 (d, ${}^3J_{\text{CF}}$ 3.0 Hz, CH), 129.5 (d, ${}^3J_{\text{CF}}$ 3.0 Hz, CH), 129.6 ($2 \times \text{C}$), 131.7 ($2 \times \text{CH}$), 131.9 (d, ${}^3J_{\text{CF}}$ 8.0 Hz, $2 \times \text{CH}$), 133.7 ($2 \times \text{CH}$), 134.6 (d, ${}^4J_{\text{CF}}$ 3.3 Hz, $2 \times \text{C}$), 145.6 ($2 \times \text{C}$), 152.6 (d, ${}^1J_{\text{CF}}$ 243.0 Hz, $2 \times \text{C}$), 157.1 (d, ${}^1J_{\text{CF}}$ 248.4 Hz, $2 \times \text{C}$), 160.8 ($2 \times \text{C}$), 165.2 (C), 165.3 (C), 170.6 (C), 170.7 (C), 170.8 ($2 \times \text{C}$); m/z (ESI) 582.1909 (MNa^+ , $\text{C}_{30}\text{H}_{27}\text{F}_2\text{N}_5\text{NaO}_4$ requires 582.1923).

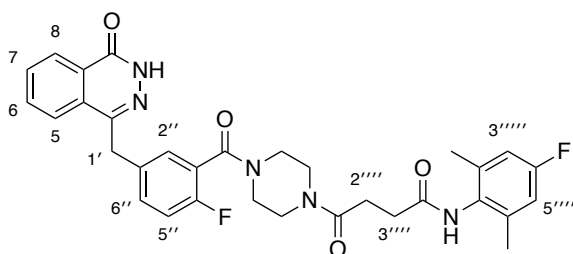
4-{3''-[4'''-(1''''-Oxo-4''''-{N-[2''''-methyl-5''''-fluorophenyl]butanamide)}]-piperazine-1'''-carbonyl]-4''-fluorobenzyl}-2H-phthalazin-1-one (68)



The reaction was carried out according to the previously described procedure for compound **66**, using 4-{3''-[4'''-(1''''-oxo-4''''-butanoic acid)-piperazine-1'''-carbonyl]-4''-fluorobenzyl}-2H-phthalazin-1-one (**38**) (0.150 g, 0.322 mmol), O-benzotriazole-*N,N,N',N'*-tetramethyluroniumhexafluorophosphate (0.134 g, 0.354 mmol), anhydrous *N,N'*-dimethylformamide (3 mL), triethylamine (0.135 mL, 0.966 mmol) and 2-methyl-5-fluoroaniline hydrochloride (**65**) (0.0520 g, 0.322 mmol). The reaction mixture was initially stirred at room temperature for 3 h and then at 50 °C for 44 h. The reaction mixture was cooled to room temperature, diluted with ethyl acetate (20 mL) and washed with saturated aqueous sodium bicarbonate solution (10 mL), water (10 mL) and 2 M aqueous lithium chloride solution (10 mL). The organic layer was dried (MgSO₄), filtered and concentrated *in vacuo*. The crude material was purified by flash column chromatography eluting with 0–4% gradient of methanol in dichloromethane to give 4-{3''-[4'''-(1''''-oxo-4''''-{N-[2''''-methyl-5''''-fluorophenyl]butanamide)}]-piperazine-1'''-carbonyl]-4''-fluorobenzyl}-2H-phthalazin-1-one (**68**) as a white solid (0.0314 g, 17%). Mp 133–135 °C; $\nu_{\max}/\text{cm}^{-1}$ (neat) 3264 (NH), 3210 (NH), 3055 (CH), 2924 (CH), 1636 (C=O), 1535, 1435, 1350, 1281, 1227, 1173, 1011, 910. NMR spectra showed a 1:1 mixture of rotational isomers. Signals for both rotational isomers are recorded. δ_{H} (400 MHz, CDCl₃) 2.20 (3H, s, CH₃), 2.22 (3H, s, CH₃), 2.65–2.85 (8H, m, 2 × 2''''-H₂ and 2 × 3''''-H₂), 3.22–3.88 (16H, m, 16 × NCH), 4.28 (4H, s, 2 × 1'-H₂), 6.70 (2H, t, *J* 8.2 Hz, 2 × 4''''-H), 6.98–7.09 (4H, m, 2 × 5''-H and 2 × 3''''-H), 7.28–7.37 (4H, m, 2 × 2''-H and 2 × 6''-H), 7.67–7.84 (8H, m, 2 × 5-H, 2 × 6-H, 2 × 7-H and 2 × 6''''-H), 8.20 (1H, br s, CONHPh), 8.25 (1H, br s, CONHPh), 8.41–8.50 (2H, m, 2 × 8-H), 11.20 (1H, br s, CONHN), 11.25 (1H, br s, CONHN); δ_{C} (101 MHz, CDCl₃) 17.3 (2 × CH₃), 29.2 (2 × CH₂), 32.7 (CH₂), 32.7 (CH₂), 37.8 (2 × CH₂), 41.6 (CH₂), 42.0 (CH₂), 42.1 (CH₂), 42.1 (CH₂), 45.1 (CH₂), 45.6 (CH₂), 46.8 (CH₂), 47.0 (CH₂), 109.1 (d, ²*J*_{CF} 26.1 Hz,

2 × CH), 110.9 (d, $^2J_{CF}$ 21.5 Hz, 2 × CH), 116.3 (d, $^2J_{CF}$ 22.1 Hz, 2 × CH), 123.0–123.2 (m, 2 × C), 123.5 (d, $^2J_{CF}$ 17.9 Hz, C), 123.7 (d, $^2J_{CF}$ 17.9 Hz, C), 125.1 (2 × CH), 127.3 (2 × CH), 128.4 (2 × C), 129.4 (d, $^3J_{CF}$ 2.9 Hz, CH), 129.5 (d, $^3J_{CF}$ 2.9 Hz, CH), 129.6 (2 × C), 131.0 (d, $^3J_{CF}$ 3.8 Hz, CH), 131.1 (d, $^3J_{CF}$ 3.8 Hz, CH), 131.7 (2 × CH), 131.9 (d, $^3J_{CF}$ 7.9 Hz, 2 × CH), 133.8 (2 × CH), 134.6 (d, $^4J_{CF}$ 3.4 Hz, 2 × C), 137.2 (d, $^3J_{CF}$ 11.2 Hz, 2 × C), 145.6 (2 × C), 157.1 (d, $^1J_{CF}$ 248.7 Hz, 2 × C), 160.8 (C), 160.8 (C), 161.4 (d, $^1J_{CF}$ 242.8 Hz, 2 × C), 165.2 (C), 165.3 (C), 170.8 (C), 170.9 (C), 170.9 (2 × C); m/z (ESI) 596.2075 (MNa⁺. C₃₁H₂₉F₂N₅NaO₄ requires 596.2080).

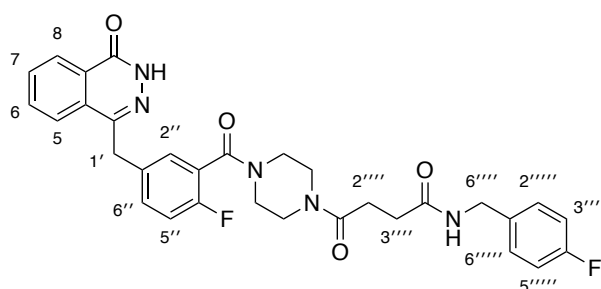
4-{3''-[4'''-(1''''-Oxo-4''''-{N-[2''''',6'''''-dimethyl-4'''''-fluorophenyl]butanamide))-piperazine-1'''-carbonyl]-4''-fluorobenzyl}-2*H*-phthalazin-1-one (69)



The reaction was carried out according to the previously described procedure for compound **66**, using 4-{3''-[4'''-(1''''-oxo-4''''-butanoic acid)-piperazine-1'''-carbonyl]-4''-fluorobenzyl}-2*H*-phthalazin-1-one (**38**) (0.100 g, 0.214 mmol), *O*-benzotriazole-*N,N,N',N'*-tetramethyluroniumhexafluorophosphate (0.0891 g, 0.235 mmol), anhydrous *N,N'*-dimethylformamide (2 mL), triethylamine (0.0450 mL, 0.323 mmol) and 2,6-dimethyl-4-fluoroaniline (0.0275 mL, 0.214 mmol). The reaction mixture was initially stirred at room temperature for 0.5 h and then at 50 °C for 18 h. The crude material was purified by flash column chromatography eluting with 4% methanol in dichloromethane to give 4-{3''-[4'''-(1''''-oxo-4''''-{N-[2''''',6'''''-dimethyl-4'''''-fluorophenyl]butanamide))-piperazine-1'''-carbonyl]-4''-fluorobenzyl}-2*H*-phthalazin-1-one (**69**) as a white solid (0.0446 g, 36%). Mp 136–138 °C; ν_{max}/cm^{-1} (neat) 3221 (NH), 2978 (CH), 2907 (CH), 1632 (C=O), 1466, 1433, 1223, 1128, 1011, 746. NMR spectra showed a 1:1 mixture of rotational isomers. Signals for all rotational isomers are recorded. δ_H (500 MHz, CDCl₃) 2.12–2.32 (12H, m, 4 × CH₃), 2.52–2.89 (8H, m, 2 × 2''''-H₂ and 2 × 3''''-H₂), 3.17–3.88 (16H, m, 16 × NCH), 4.27 (4H, s, 2 × 1'-H₂), 6.67–8.84 (4H, m, 2 × 3''''-H and 2 × 5''''-H), 7.02 (2H, t, J 9.0 Hz, 2 × 5''-H), 7.28–

7.37 (4H, m, 2 × 2''-H and 2 × 6''-H), 7.64–7.81 (8H, m, 2 × 5-H, 2 × 6-H and 2 × 7-H and 2 × CONHPh), 8.41–8.48 (2H, m, 2 × 8-H), 11.17–11.86 (2H, m, 2 × CONHN); δ_C (126 MHz, CDCl₃) 18.6–18.9 (m, 4 × CH₃), 28.8 (CH₂), 28.9 (CH₂), 31.3 (CH₂), 31.3 (CH₂), 37.8 (2 × CH₂), 41.6 (CH₂), 42.0 (CH₂), 42.1 (CH₂), 42.2 (CH₂), 45.1 (CH₂), 45.7 (CH₂), 46.8 (CH₂), 47.1 (CH₂), 114.4–115.4 (m, 4 × CH), 116.3 (d, ²J_{CF} 21.8 Hz, CH), 116.3 (d, ²J_{CF} 21.8 Hz, CH), 123.7 (d, ²J_{CF} 17.9 Hz, C), 123.7 (d, ²J_{CF} 17.9 Hz, C), 125.1 (2 × CH), 127.3 (2 × CH), 128.4 (2 × C), 129.3 (d, ³J_{CF} 2.6 Hz, CH), 129.4 (d, ³J_{CF} 2.6 Hz, CH), 129.6 (2 × C), 130.0 (2 × C), 131.7 (2 × CH), 131.9 (d, ³J_{CF} 7.8 Hz, 2 × CH), 133.8 (2 × CH), 134.6 (2 × C), 137.9 (d, ³J_{CF} 8.8 Hz, 4 × C), 145.6 (2 × C), 157.1 (d, ¹J_{CF} 248.2 Hz, C), 157.1 (d, ¹J_{CF} 248.2 Hz, C), 160.8 (2 × C), 161.2 (d, ¹J_{CF} 245.3 Hz, 2 × C), 165.2 (C), 165.3 (C), 170.8 (C), 170.9 (C), 171.2 (C), 171.2 (C); *m/z* (ESI) 610.2216 (MNa⁺. C₃₂H₃₁F₂N₅NaO₄ requires 610.2236).

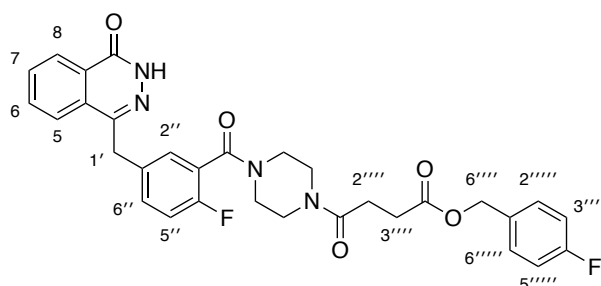
4-{3''-[4'''-(1''''-Oxo-4''''-{N-[4''''-fluorobenzyl]butanamide})-piperazine-1'''-carbonyl]-4''-fluorobenzyl]-2*H*-phthalazin-1-one (70)



The reaction was carried out according to the previously described procedure for compound **66**, using 4-{3''-[4'''-(1''''-oxo-4''''-butanoic acid)-piperazine-1'''-carbonyl]-4''-fluorobenzyl]-2*H*-phthalazin-1-one (**38**) (0.0650 g, 0.139 mmol), *O*-benzotriazole-*N,N,N',N'*-tetramethyluroniumhexafluorophosphate (0.0580 g, 0.153 mmol), anhydrous *N,N'*-dimethylformamide (1.5 mL), triethylamine (0.0290 mL, 0.208 mmol) and 4-fluorobenzylamine (0.0159 mL, 0.139 mmol). The reaction mixture was cooled to room temperature, diluted with ethyl acetate (5 mL) and washed with brine (5 × 5 mL). The organic layer was dried (MgSO₄), filtered and concentrated *in vacuo*. The crude material was purified by flash column chromatography eluting with 4% methanol in dichloromethane to give 4-{3''-[4'''-(1''''-oxo-4''''-{N-[4''''-fluorobenzyl]butanamide})-piperazine-1'''-carbonyl]-4''-

fluorobenzyl]-2*H*-phthalazin-1-one (**70**) as a white solid (0.0326 g, 41%). Mp 135–137 °C; $\nu_{\max}/\text{cm}^{-1}$ (neat) 3281 (NH), 3188 (NH), 3064 (CH), 2904 (CH), 1628 (C=O), 1549, 1508, 1433, 1354, 1282, 1219, 1009. NMR spectra showed a 1:1 mixture of rotational isomers. Signals for both rotational isomers are recorded. δ_{H} (400 MHz, CDCl_3) 2.53–2.77 (8H, m, $2 \times 2''''\text{-H}_2$ and $2 \times 3''''\text{-H}_2$), 3.17–3.86 (16H, m, $16 \times \text{NCH}$), 4.27 (4H, s, $2 \times 1'\text{-H}_2$), 4.35 (4H, d, J 5.8 Hz, $2 \times 6''''\text{-H}_2$), 6.66 (1H, t, J 5.8 Hz, CONHC), 6.71 (1H, t, J 5.8 Hz, CONHC), 6.92 (4H, t, J 8.2 Hz, $2 \times 3''''\text{-H}$ and $2 \times 5''''\text{-H}$), 7.02 (2H, t, J 8.8 Hz, $2 \times 5''\text{-H}$), 7.20 (4H, dd, J 8.2, 5.6 Hz, $2 \times 2''''\text{-H}$ and $2 \times 6''''\text{-H}$), 7.28–7.36 (4H, m, $2 \times 2''\text{-H}$ and $2 \times 6''\text{-H}$), 7.66–7.80 (6H, m, $2 \times 5\text{-H}$, $2 \times 6\text{-H}$ and $2 \times 7\text{-H}$), 8.43 (2H, d, J 6.8 Hz, $2 \times 8\text{-H}$), 11.34 (1H, br s, CONHN), 11.37 (1H, br s, CONHN); δ_{C} (101 MHz, CDCl_3) 28.6 ($2 \times \text{CH}_2$), 31.3 (CH_2), 31.4 (CH_2), 37.8 ($2 \times \text{CH}_2$), 41.5 (CH_2), 42.0 ($2 \times \text{CH}_2$), 42.1 (CH_2), 42.9 ($2 \times \text{CH}_2$), 45.1 (CH_2), 45.7 (CH_2), 46.8 (CH_2), 47.1 (CH_2), 115.4 (d, $^2J_{\text{CF}}$ 21.5 Hz, $4 \times \text{CH}$), 116.3 (d, $^2J_{\text{CF}}$ 22.0 Hz, $2 \times \text{CH}$), 123.7 (d, $^2J_{\text{CF}}$ 17.8 Hz, C), 123.7 (d, $^2J_{\text{CF}}$ 17.8 Hz, C), 125.1 ($2 \times \text{CH}$), 127.2 ($2 \times \text{CH}$), 128.4 ($2 \times \text{C}$), 129.3 ($2 \times \text{CH}$), 129.4 (d, $^3J_{\text{CF}}$ 7.8 Hz, $4 \times \text{CH}$), 129.6 ($2 \times \text{C}$), 131.7 ($2 \times \text{CH}$), 131.8 (d, $^3J_{\text{CF}}$ 7.8 Hz, $2 \times \text{CH}$), 133.7 ($2 \times \text{CH}$), 134.3 (d, $^4J_{\text{CF}}$ 3.2 Hz, C), 134.4 (d, $^4J_{\text{CF}}$ 3.2 Hz, C), 134.6 (d, $^4J_{\text{CF}}$ 3.4 Hz, $2 \times \text{C}$), 145.5 ($2 \times \text{C}$), 157.1 (d, $^1J_{\text{CF}}$ 248.4 Hz, $2 \times \text{C}$), 160.8 ($2 \times \text{C}$), 162.1 (d, $^1J_{\text{CF}}$ 246.3 Hz, $2 \times \text{C}$), 165.2 (C), 165.3 (C), 170.8 (C), 170.9 (C), 172.2 ($2 \times \text{C}$); m/z (ESI) 596.2063 (MNa^+ . $\text{C}_{31}\text{H}_{29}\text{F}_2\text{N}_5\text{NaO}_4$ requires 596.2080).

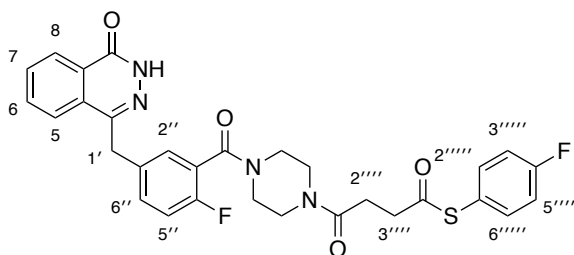
4-{3''-[4''''-(1''''-Oxo-4''''-{*N*-[4''''-fluorobenzyl]butanoate})-piperazine-1''''-carbonyl]-4''-fluorobenzyl]-2*H*-phthalazin-1-one (71**)**



The reaction was carried out according to the previously described procedure for compound **66**, using 4-{3''-[4''''-(1''''-oxo-4''''-butanoic acid)-piperazine-1''''-carbonyl]-4''-fluorobenzyl]-2*H*-phthalazin-1-one (**38**) (0.100 g, 0.214 mmol), *O*-benzotriazole-*N,N,N',N'*-tetramethyluroniumhexafluorophosphate (0.0891 g, 0.235 mmol),

anhydrous *N,N'*-dimethylformamide (2 mL), triethylamine (0.0450 mL, 0.323 mmol) and 4-fluorobenzyl alcohol (0.0233 mL, 0.214 mmol). The reaction mixture was initially stirred at room temperature for 0.5 h and then at 50 °C for 18 h. The crude material was purified by flash column chromatography eluting with 3% methanol in dichloromethane to give 4-{3''-[4'''-(1''''-oxo-4''''-{*N*-[4''''-fluorobenzyl]butanoate)}]-piperazine-1'''-carbonyl]-4''-fluorobenzyl}-2*H*-phthalazin-1-one (**71**) as a white solid (0.0550 g, 45%). Mp 83–85 °C; $\nu_{\max}/\text{cm}^{-1}$ (neat) 3179 (NH), 3001 (CH), 2901 (CH), 1732 (C=O), 1638 (C=O), 1510, 1466, 1433, 1354, 1221, 1153, 1011, 829. NMR spectra showed a 1:1 mixture of rotational isomers. Signals for both rotational isomers are recorded. δ_{H} (500 MHz, CDCl_3) 2.53–2.75 (8H, m, 2 × 2''''-H₂ and 2 × 3''''-H₂), 3.20–3.87 (16H, m, 16 × NCH), 4.29 (4H, s, 2 × 1'-H₂), 5.08 (4H, s, 2 × 6''''-H₂), 6.94–7.08 (6H, m, 2 × 5''-H, 2 × 3''''-H and 2 × 5''''-H), 7.27–7.41 (8H, m, 2 × 2''-H, 2 × 6''-H, 2 × 2''''-H and 2 × 6''''-H), 7.66–7.79 (6H, m, 2 × 5-H, 2 × 6-H and 2 × 7-H), 8.47 (2H, d, *J* 5.6 Hz, 2 × 8-H), 11.29–11.65 (2H, m, 2 × CONHN); δ_{C} (126 MHz, CDCl_3) 27.9 (2 × CH₂), 29.3 (2 × CH), 37.7 (CH₂), 37.8 (CH₂), 41.5 (CH₂), 42.0 (2 × CH₂), 42.1 (CH₂), 45.0 (CH₂), 45.6 (CH₂), 46.8 (CH₂), 47.0 (CH₂), 65.8 (2 × CH₂), 115.5 (d, $^2J_{\text{CF}}$ 21.5 Hz, 4 × CH), 116.2 (d, $^2J_{\text{CF}}$ 22.1 Hz, CH), 116.3 (d, $^2J_{\text{CF}}$ 22.1 Hz, CH), 123.6 (d, $^2J_{\text{CF}}$ 17.8 Hz, C), 123.7 (d, $^2J_{\text{CF}}$ 17.8 Hz, C), 125.1 (2 × CH), 127.2 (2 × CH), 128.4 (2 × C), 129.3 (d, $^3J_{\text{CF}}$ 2.9 Hz, CH), 129.5 (d, $^3J_{\text{CF}}$ 2.9 Hz, CH), 129.6 (2 × C), 130.2 (d, $^3J_{\text{CF}}$ 8.4 Hz, 4 × CH), 131.7 (2 × CH), 131.8 (2 × C), 131.8 (d, $^3J_{\text{CF}}$ 8.2 Hz, 2 × CH), 133.7 (2 × CH), 134.6 (d, $^4J_{\text{CF}}$ 3.5 Hz, 2 × C), 145.6 (2 × C), 157.0 (d, $^1J_{\text{CF}}$ 247.7 Hz, 2 × C), 160.9 (2 × C), 162.7 (d, $^1J_{\text{CF}}$ 247.3 Hz, 2 × C), 165.1 (C), 165.3 (C), 169.9 (C), 170.0 (C), 172.8 (2 × C); *m/z* (ESI) 597.1901 (MNa⁺. C₃₁H₂₈F₂N₄NaO₅ requires 597.1920).

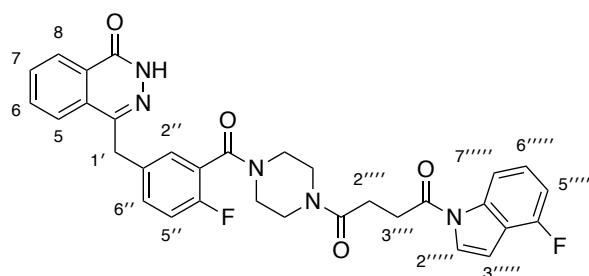
4-{3''-[4'''-(1''''-Oxo-4''''-{N-[4''''-fluorophenyl]butanethioate})-piperazine-1'''-carbonyl]-4''-fluorobenzyl}-2*H*-phthalazin-1-one (72)



The reaction was carried out according to the previously described procedure for compound **66**, using 4-{3''-[4'''-(1''''-oxo-4''''-butanoic acid)-piperazine-1'''-carbonyl]-4''-fluorobenzyl}-2*H*-phthalazin-1-one (**38**) (0.150 g, 0.322 mmol), O-benzotriazole-*N,N,N',N'*-tetramethyluroniumhexafluorophosphate (0.134 g, 0.354 mmol), anhydrous *N,N'*-dimethylformamide (3 mL), triethylamine (0.0670 mL, 0.481 mmol) and 4-fluorothiophenol (0.0343 mL, 0.322 mmol). The reaction mixture was initially stirred at room temperature for 2 h and then at 50 °C for 46 h. The reaction mixture was cooled to room temperature, diluted with ethyl acetate (20 mL) and washed with a saturated aqueous sodium bicarbonate solution (10 mL), water (10 mL) and 2 M aqueous lithium chloride solution (10 mL). The organic layer was dried (MgSO₄), filtered and concentrated *in vacuo*. The crude material was purified by flash column chromatography eluting with 0–3% gradient of methanol in dichloromethane to give 4-{3''-[4'''-(1''''-oxo-4''''-{N-[4''''-fluorophenyl]butanethioate})-piperazine-1'''-carbonyl]-4''-fluorobenzyl}-2*H*-phthalazin-1-one (**72**) as a white solid (0.0893 g, 48%). Mp 108–110 °C; $\nu_{\max}/\text{cm}^{-1}$ (neat) 3194 (NH), 2994 (CH), 2909 (CH), 1705 (C=O), 1643 (C=O), 1489, 1466, 1435, 1227, 1011, 733. NMR spectra showed a 1:1 mixture of rotational isomers. Signals for both rotational isomers are recorded. δ_{H} (400 MHz, CDCl₃) 2.64 (2H, t, *J* 6.4 Hz, 2''''-H₂), 2.72 (2H, t, *J* 6.4 Hz, 2''''-H₂), 3.04 (4H, t, *J* 6.4 Hz, 2 × 3''''-H₂), 3.22–3.86 (16H, m, 16 × NCH), 4.28 (4H, s, 2 × 1'-H₂), 7.03 (2H, t, *J* 8.8 Hz, 2 × 5''-H), 7.08 (4H, t, *J* 8.8 Hz, 2 × 3''''-H and 2 × 5''''-H), 7.29–7.42 (8H, m, 2 × 2''-H, 2 × 6''-H, 2 × 2''''-H and 2 × 6''''-H), 7.67–7.80 (6H, m, 2 × 5-H, 2 × 6-H and 2 × 7-H), 8.43–8.51 (2H, m, 2 × 8-H), 11.04 (1H, br s, CONHN), 11.09 (1H, br s, CONHN); δ_{C} (101 MHz, CDCl₃) 28.0 (CH₂), 28.1 (CH₂), 37.8 (CH₂), 37.8 (CH₂), 38.3 (CH₂), 38.3 (CH₂), 41.6 (CH₂), 42.0 (CH₂), 42.1 (CH₂), 42.1 (CH₂), 45.1 (CH₂), 45.6 (CH₂), 46.8 (CH₂), 47.0 (CH₂), 116.3 (d, ²*J*_{CF} 21.5 Hz, CH), 116.4 (d, ²*J*_{CF} 21.5 Hz, CH), 116.6 (d, ²*J*_{CF} 22.2 Hz, 4 × CH), 122.9 (d, ⁴*J*_{CF} 3.4

Hz, 2 × C), 123.7 (d, $^2J_{CF}$ 17.9 Hz, C), 123.8 (d, $^2J_{CF}$ 17.9 Hz, C), 125.1 (2 × CH), 127.3 (2 × CH), 128.4 (2 × C), 129.3 (d, $^3J_{CF}$ 3.4 Hz, CH), 129.5 (d, $^3J_{CF}$ 3.4 Hz, CH), 129.6 (2 × C), 131.7 (2 × CH), 131.9 (d, $^3J_{CF}$ 8.1 Hz, 2 × CH), 133.8 (2 × CH), 134.6 (d, $^4J_{CF}$ 3.4 Hz, 2 × C), 136.7 (d, $^3J_{CF}$ 8.6 Hz, 4 × CH), 145.6 (2 × C), 157.1 (d, $^1J_{CF}$ 248.3 Hz, 2 × C), 160.7 (2 × C), 163.6 (d, $^1J_{CF}$ 251.1 Hz, 2 × C), 165.1 (C), 165.3 (C), 169.4 (C), 169.5 (C), 197.1 (C), 197.2 (C); m/z (ESI) 599.1531 (MNa⁺. C₃₀H₂₆F₂N₄NaO₄S requires 599.1535).

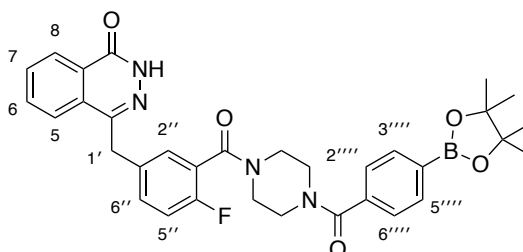
4-{3''-[4'''-(1''''-Oxo-4''''-{N-[4''''-fluoroindole]butanamide)}-piperazine-1'''-carbonyl]-4''-fluorobenzyl}-2H-phthalazin-1-one (73)



The reaction was carried out according to the previously described procedure for compound **66**, using 4-{3''-[4'''-(1''''-oxo-4''''-butanoic acid)-piperazine-1'''-carbonyl]-4''-fluorobenzyl}-2H-phthalazin-1-one (**38**) (0.150 g, 0.322 mmol), O-benzotriazole-*N,N,N',N'*-tetramethyluroniumhexafluorophosphate (0.134 g, 0.354 mmol), anhydrous *N,N'*-dimethylformamide (3 mL), triethylamine (0.0670 mL, 0.481 mmol) and 4-fluoroindole (0.0435 g, 0.322 mmol). The reaction mixture was initially stirred at room temperature for 0.5 h and then at 50 °C for 40 h. The crude material was purified by flash column chromatography eluting with 0–4% gradient of methanol in dichloromethane to give 4-{3''-[4'''-(1''''-oxo-4''''-{N-[4''''-fluoroindole]butanamide)}-piperazine-1'''-carbonyl]-4''-fluorobenzyl}-2H-phthalazin-1-one (**73**) as a white solid (0.0375 g, 20%). Mp 141–143 °C; ν_{max}/cm^{-1} (neat) 3161 (NH), 3007 (CH), 2899 (CH), 1716 (C=O), 1639 (C=O), 1622 (C=O), 1487, 1464, 1433, 1354, 1288, 1197, 1153, 1012, 925. NMR spectra showed a 1:1 mixture of rotational isomers. Signals for both rotational isomers are recorded. δ_H (400 MHz, CDCl₃) 2.81 (2H, t, J 6.4 Hz, 2''''-H₂), 2.89 (2H, t, J 6.4 Hz, 2''''-H₂), 3.24–3.47 (8H, m, 2 × 3''''-H₂, 4 × NCH), 3.53–3.93 (12H, m, 12 × NCH), 4.28 (4H, s, 2 × 1'-H₂), 6.74 (2H, d, J 3.8 Hz, 2 × 3''''-H), 6.94 (2H, dd, J 9.4, 8.2 Hz, 2 × 5''''-H), 7.04 (2H, t, J 8.6 Hz, 2 × 5''-H), 7.21–7.28 (2H, m, 2 × 6''''-H), 7.29–7.40 (4H, m, 2 × 2''-H and 2 × 6''-H), 7.53 (2H, d, J 3.8 Hz,

2 × 2''''-H), 7.65–7.81 (6H, m, 2 × 5-H, 2 × 6-H and 2 × 7-H), 8.16 (1H, d, *J* 8.4 Hz, 7''''-H), 8.19 (1H, d, *J* 8.4 Hz, 7''''-H), 8.43–8.50 (2H, m, 2 × 8-H), 11.07 (1H, br s, CONHN), 11.15 (1H, br s, CONHN); δ_{C} (101 MHz, CDCl₃) 27.4 (2 × CH₂), 31.0 (CH₂), 31.1 (CH₂), 37.8 (2 × CH₂), 41.7 (CH₂), 42.1 (CH₂), 42.2 (2 × CH₂), 45.2 (CH₂), 45.7 (CH₂), 46.9 (CH₂), 47.1 (CH₂), 105.0 (2 × CH), 109.2 (d, ²*J*_{CF} 18.5 Hz, 2 × CH), 112.7 (2 × CH), 116.3 (d, ²*J*_{CF} 22.0 Hz, CH), 116.3 (d, ²*J*_{CF} 22.0 Hz, CH), 119.3 (d, ²*J*_{CF} 21.9 Hz, 2 × C), 123.7 (d, ²*J*_{CF} 17.5 Hz, C), 123.8 (d, ²*J*_{CF} 17.5 Hz, C), 124.7 (2 × CH), 125.1 (2 × CH), 126.1 (d, ³*J*_{CF} 7.4 Hz, 2 × CH), 127.3 (2 × CH), 128.4 (2 × C), 129.3 (d, ³*J*_{CF} 3.4 Hz, CH), 129.6 (d, ³*J*_{CF} 3.4 Hz, CH), 129.6 (2 × C), 131.7 (2 × CH), 131.9 (d, ³*J*_{CF} 8.1 Hz, 2 × CH), 133.8 (2 × CH), 134.6 (d, ⁴*J*_{CF} 3.5 Hz, 2 × C), 137.8 (d, ³*J*_{CF} 9.2 Hz, 2 × C), 145.6 (2 × C), 155.7 (d, ¹*J*_{CF} 249.0 Hz, 2 × C), 157.1 (d, ¹*J*_{CF} 248.5 Hz, 2 × C), 160.7 (C), 160.8 (C), 165.2 (C), 165.4 (C), 169.9 (C), 170.0 (C), 170.8 (2 × C); *m/z* (ESI) 606.1924 (MNa⁺. C₃₂H₂₇F₂N₅NaO₄ requires 606.1923).

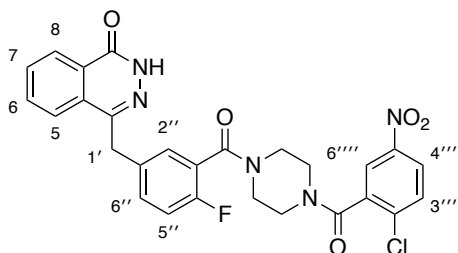
4-{3''-[4''''-(Benzoyl-4''''-boronic acid pinacol ester)piperazine-1''''-carbonyl]-4''-fluorobenzyl}-2*H*-phthalazin-1-one (74)⁴³²



To a stirred solution of 4-carboxylphenylboronic acid pinacol ester (**75**) (0.337 g, 1.36 mmol) and *O*-benzotriazole-*N,N,N',N'*-tetramethyluroniumhexafluorophosphate (0.569 g, 1.50 mmol) in anhydrous acetonitrile (14 mL), under argon, was added triethylamine (0.290 mL, 2.08 mmol). The reaction mixture was stirred at room temperature for 1 h. 4-[4''-Fluoro-3''-(piperazine-1''''-carbonyl)benzyl]-2*H*-phthalazin-1-one (**35**) (0.500 g, 1.36 mmol) was added to the reaction mixture, which was then heated to 50 °C and stirred for 16 h. The reaction mixture was cooled to room temperature and concentrated *in vacuo*. The resultant residue was dissolved in chloroform (80 mL) and washed with a saturated aqueous sodium bicarbonate solution (6 × 80 mL). The organic layer was dried (MgSO₄), filtered and concentrated *in vacuo*. The crude material was

purified by trituration from a mixture of chloroform and hexane to give 4-{3''-[4''''-(benzoyl-4''''-boronic acid pinacol ester)piperazine-1'''-carbonyl]-4''-fluorobenzyl}-2*H*-phthalazin-1-one (**74**) as a white solid (0.608 g, 75%). Mp 284–286 °C (lit.⁴³² 288–291 °C); δ_{H} (400 MHz, CDCl₃) 1.34 (12H, s, 4 × CH₃), 3.10–4.00 (8H, m, 8 × NCH), 4.28 (2H, s, 1'-H₂), 7.02 (1H, br s, 5''-H), 7.28–7.44 (4H, m, 2''-H, 6''-H, 2''''-H and 6''''-H), 7.65–7.90 (5H, m, 5-H, 6-H, 7-H, 3''''-H and 5''''-H), 8.42–8.52 (1H, m, 8-H), 11.20 (1H, br s, NH); δ_{C} (101 MHz, CDCl₃) 25.0 (4 × CH₃), 37.8 (CH₂), 42.4 (2 × CH₂), 47.3 (2 × CH₂), 84.2 (2 × C), 116.3 (d, ²J_{CF} 21.7 Hz, CH), 123.7 (d, ²J_{CF} 17.9 Hz, C), 125.1 (CH), 126.3 (2 × CH), 127.3 (CH), 128.4 (C), 129.3 (d, ³J_{CF} 3.5 Hz, CH), 129.6 (C), 131.7 (CH), 131.8 (d, ³J_{CF} 8.0 Hz, CH), 133.8 (CH), 134.6 (d, ⁴J_{CF} 3.4 Hz, C), 135.1 (2 × CH), 137.6 (C), 145.6 (C), 157.1 (d, ¹J_{CF} 249.0 Hz, C), 160.8 (C), 160.8 (C), 165.3 (C), 170.6 (C); *m/z* (ESI) 619 (MNa⁺. 100%).

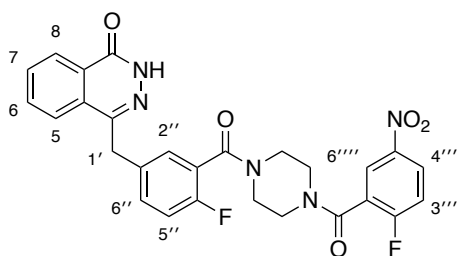
4-{3''-[4''''-(2''''-Chloro-5''''-nitrobenzoyl)piperazine-1'''-carbonyl]-4''-fluorobenzyl}-2*H*-phthalazin-1-one (39**)**



Method A: To a stirred solution of 2-chloro-5-nitrobenzoic acid (**231**) (0.121 g, 0.600 mmol) and *O*-benzotriazole-*N,N,N',N'*-tetramethyluroniumhexafluorophosphate (0.250 g, 0.660 mmol) in anhydrous acetonitrile (3 mL), under argon, was added triethylamine (0.125 mL, 0.900 mmol). The reaction mixture was stirred at room temperature for 0.5 h. 4-[4''-Fluoro-3''-(piperazine-1'''-carbonyl)benzyl]-2*H*-phthalazin-1-one (**35**) (0.220 g, 0.600 mmol) was added to the reaction mixture, which was then heated to 50 °C and stirred for 16 h. The reaction mixture was cooled to room temperature and concentrated *in vacuo*. The resultant residue was dissolved in chloroform (20 mL) and washed with a saturated aqueous sodium bicarbonate solution (3 × 20 mL). The organic layer was dried (MgSO₄), filtered and concentrated *in vacuo*. The crude material was purified by flash column chromatography eluting with 2% methanol in dichloromethane. Further purification by trituration from chloroform and hexane gave 4-{3''-[4''''-(2''''-chloro-5''''-

nitrobenzoyl)piperazine-1'''-carbonyl]-4''-fluorobenzyl]-2*H*-phthalazin-1-one (**39**) as an off-white solid (0.277 g, 84%). Mp 139–141 °C; $\nu_{\max}/\text{cm}^{-1}$ (neat) 3457 (NH), 2970 (CH), 1728 (C=O), 1636 (C=O), 1437, 1229, 909, 806. NMR spectra showed a 1.2:1 mixture of rotational isomers. Signals for both rotational isomers are recorded. δ_{H} (400 MHz, CDCl_3) 3.10–3.58 (8H, m, 8 × NCH), 3.59–4.18 (8H, m, 8 × NCH), 4.26 (2H, s, 1'-H₂), 4.31 (2H, s, 1'-H₂), 6.99 (1H, t, *J* 8.8 Hz, 5''-H), 7.08 (1H, t, *J* 8.8 Hz, 5''-H), 7.27–7.40 (4H, m, 2 × 2''-H and 2 × 6''-H), 7.56 (1H, d, *J* 8.8 Hz, 3'''-H), 7.63 (1H, d, *J* 8.8 Hz, 3'''-H), 7.68–7.82 (6H, m, 2 × 5-H, 2 × 6-H, 2 × 7-H), 8.11–8.26 (4H, m, 2 × 4'''-H and 2 × 6'''-H), 8.42–8.50 (2H, m, 2 × 8-H), 10.99 (1H, br s, NH), 11.03 (1H, br s, NH); δ_{C} (101 MHz, CDCl_3) 37.7 (CH₂), 37.8 (CH₂), 41.8 (CH₂), 41.9 (CH₂), 42.2 (CH₂), 42.2 (CH₂), 46.6 (CH₂), 46.7 (CH₂), 47.1 (CH₂), 47.3 (CH₂), 116.2 (d, ²*J*_{CF} 22.6 Hz, CH), 116.4 (d, ²*J*_{CF} 22.6 Hz, CH), 123.3–123.7 (m, 2 × CH, 2 × C), 125.1 (CH), 125.1 (CH), 125.3 (CH), 125.4 (CH), 127.3 (CH), 127.4 (CH), 128.4 (C), 128.5 (C), 129.5 (d, ³*J*_{CF} 3.2 Hz, CH), 129.6 (d, ³*J*_{CF} 3.2 Hz, CH), 129.7 (2 × C), 131.0 (CH), 131.2 (CH), 131.8 (CH), 131.8 (CH), 132.0 (d, ³*J*_{CF} 8.7 Hz, CH), 132.1 (d, ³*J*_{CF} 8.7 Hz, CH), 133.8 (2 × CH), 134.6 (d, ⁴*J*_{CF} 3.4 Hz, C), 134.7 (d, ⁴*J*_{CF} 3.4 Hz, C), 136.6 (C), 136.7 (C), 137.4 (2 × C), 145.6 (2 × C), 146.8 (C), 147.0 (C), 157.0 (d, ¹*J*_{CF} 248.3 Hz, C), 157.2 (d, ¹*J*_{CF} 248.3 Hz, C), 160.6 (2 × C), 164.7 (C), 164.8 (C), 165.2 (C), 165.4 (C); *m/z* (ESI) 572.1083 (MNa⁺. C₂₇H₂₁³⁵ClFN₅NaO₅ requires 572.1107).

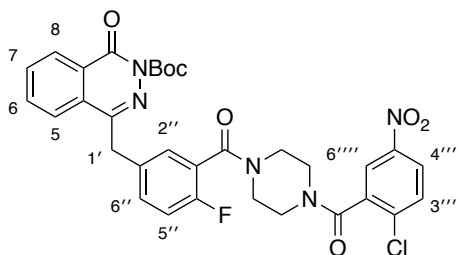
4-{3''-[4'''-(2''''-Fluoro-5''''-nitrobenzoyl)piperazine-1'''-carbonyl]-4''-fluorobenzyl]-2*H*-phthalazin-1-one (31**)**



The reaction was carried out according to the previously described procedure for compound **39**, using 2-fluoro-5-nitrobenzoic acid (**232**) (0.0555 g, 0.300 mmol), *O*-benzotriazole-*N,N,N',N'*-tetramethyluroniumhexafluorophosphate (0.125 g, 0.330 mmol), anhydrous acetonitrile (3 mL), triethylamine (0.0630 mL, 0.450 mmol) and 4-[4''-fluoro-3''-(piperazine-1'''-carbonyl)benzyl]-2*H*-phthalazin-1-one (**35**) (0.110 g,

0.300 mmol). The reaction mixture was initially stirred at room temperature for 1 h and then at 50 °C for 18 h. The crude material was purified by flash column chromatography eluting with 0–2% gradient of methanol in dichloromethane to give 4-{3'-[4'''-(2''''-fluoro-5''''-nitrobenzoyl)piperazine-1'''-carbonyl]-4''-fluorobenzyl}-2*H*-phthalazin-1-one (**31**) as a pale yellow solid (0.103 g, 64%). Mp 140–142 °C; $\nu_{\text{max}}/\text{cm}^{-1}$ (neat) 3400 (NH), 2980 (CH), 1782 (C=O), 1643 (C=O), 1437, 1259, 1170, 1008. NMR spectra showed a 1.1:1 mixture of rotational isomers. Signals for both rotational isomers are recorded. δ_{H} (400 MHz, DMSO-*d*₆) 3.07–3.46 (8H, m, 8 × NCH), 3.50–3.87 (8H, m, 8 × NCH), 4.30 (2H, s, 1'-H₂), 4.35 (2H, s, 1'-H₂), 7.20 (1H, t, *J* 9.0 Hz, 5''-H), 7.26 (1H, t, *J* 9.0 Hz, 5''-H), 7.32–7.50 (4H, m, 2 × 2''-H and 2 × 6''-H), 7.62 (1H, dd, *J* 8.8 Hz, 3''''-H), 7.64 (1H, dd, *J* 8.8 Hz, 3''''-H), 7.73–8.01 (6H, m, 2 × 5-H, 2 × 6-H, 2 × 7-H), 8.20–8.30 (2H, m, 2 × 8-H), 8.32–8.46 (4H, m, 2 × 4''''-H and 2 × 6''''-H), 12.56 (1H, br s, NH), 12.61 (1H, br s, NH); δ_{C} (101 MHz, DMSO-*d*₆) 36.4 (2 × CH₂), 40.8 (CH₂), 41.2 (CH₂), 41.4 (CH₂), 41.7 (CH₂), 45.9 (CH₂), 46.1 (CH₂), 46.5 (2 × CH₂), 115.8 (d, ²*J*_{CF} 21.8 Hz, CH), 115.9 (d, ²*J*_{CF} 21.8 Hz, CH), 117.7 (d, ²*J*_{CF} 24.4 Hz, CH), 117.7 (d, ²*J*_{CF} 24.4 Hz, CH), 123.4 (d, ²*J*_{CF} 18.2 Hz, 2 × C), 124.8–125.2 (m, 2 × CH, 2 × C), 125.4 (2 × CH), 126.0 (2 × CH), 127.2 (d, ³*J*_{CF} 10.9 Hz, CH), 127.2 (d, ³*J*_{CF} 10.9 Hz, CH), 127.9 (2 × C), 128.9 (d, ³*J*_{CF} 11.9 Hz, CH), 129.0 (d, ³*J*_{CF} 11.9 Hz, CH), 129.0 (C), 129.1 (C), 131.4 (CH), 131.5 (CH), 131.8 (d, ³*J*_{CF} 7.1 Hz, CH), 131.8 (d, ³*J*_{CF} 7.1 Hz, CH), 133.4 (CH), 133.5 (CH), 134.8 (d, ⁴*J*_{CF} 3.1 Hz, 2 × C), 144.1–144.4 (m, 2 × C), 144.7 (C), 144.8 (C), 156.3 (d, ¹*J*_{CF} 245.7 Hz, C), 156.4 (d, ¹*J*_{CF} 245.7 Hz, C), 159.3 (C), 159.4 (C), 161.0 (d, ¹*J*_{CF} 255.9 Hz, 2 × C), 161.9 (C), 162.0 (C), 164.0 (C), 164.1 (C); *m/z* (ESI) 556.1393 (MNa⁺. C₂₇H₂₁F₂N₅NaO₅ requires 556.1403).

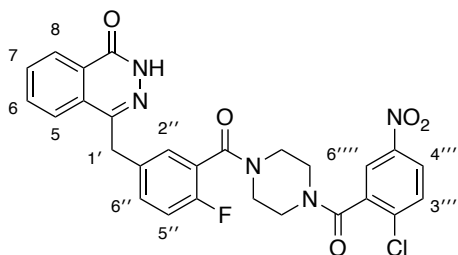
4-{3''-[4''''-(2''''-Chloro-5''''-nitrobenzoyl)piperazine-1''''-carbonyl]-4''-fluorobenzyl}-2-(tert-butyloxycarbonyl)phthalazin-1-one (76)



To a stirred solution of 4-{3''-[4''''-(2''''-chloro-5''''-nitrobenzoyl)piperazine-1''''-carbonyl]-4''-fluorobenzyl}-2*H*-phthalazin-1-one (**39**) (0.257 g, 0.467 mmol) in anhydrous acetonitrile (2.5 mL) in an oven-dried flask under argon, was added di-*tert*-butyl dicarbonate (0.122 g, 0.560 mmol) and 4-(dimethylamino)pyridine (0.00570 g, 0.0467 mmol). The reaction mixture was stirred at room temperature for 4 h and then concentrated *in vacuo*. The residue was dissolved in chloroform (30 mL) and washed with water (3 × 20 mL). The organic layer was dried (MgSO₄), filtered and concentrated *in vacuo*. The crude material was purified by flash column chromatography eluting with 2% methanol in dichloromethane to give 4-{3''-[4''''-(2''''-chloro-5''''-nitrobenzoyl)piperazine-1''''-carbonyl]-4''-fluorobenzyl}-2-(*tert*-butyloxycarbonyl)phthalazin-1-one (**76**) as a pale yellow solid (0.240 g, 79%). Mp 171–173 °C; $\nu_{\max}/\text{cm}^{-1}$ (neat) 3002 (CH), 2861 (CH), 2715, 1765 (C=O), 1638 (C=O), 1433, 1346, 1246, 1145, 1005, 743. NMR spectra showed a 1.1:1 mixture of rotational isomers. Signals for both rotational isomers are recorded. δ_{H} (400 MHz, CDCl₃) 1.64 (9H, s, ^tBu), 1.67 (9H, s, ^tBu), 3.15–3.50 (8H, m, 8 × NCH), 3.64–4.12 (8H, m, 8 × NCH), 4.28 (2H, s, 1'-H₂), 4.32 (2H, s, 1'-H₂), 6.98 (1H, t, *J* 8.8 Hz, 5''-H), 7.08 (1H, t, *J* 8.8 Hz, 5''-H), 7.28–7.42 (4H, m, 2 × 2''-H and 2 × 6''-H), 7.54–7.67 (4H, m, 2 × 5-H and 2 × 3''''-H), 7.68–7.78 (4H, m, 2 × 6-H and 2 × 7-H), 8.14–8.27 (4H, m, 2 × 4''''-H and 2 × 6''''-H), 8.40–8.50 (2H, m, 2 × 8-H); δ_{C} (101 MHz, CDCl₃) 27.9 (3 × CH₃), 28.0 (3 × CH₃), 38.0 (CH₂), 38.2 (CH₂), 41.8 (CH₂), 41.8 (CH₂), 42.1 (CH₂), 42.2 (CH₂), 46.5 (CH₂), 46.7 (CH₂), 47.1 (CH₂), 47.3 (CH₂), 86.0 (2 × C), 116.2 (d, ²*J*_{CF} 21.9 Hz, CH), 116.4 (d, ²*J*_{CF} 21.9 Hz, CH), 123.3–123.7 (m, 2 × CH, 2 × C), 125.3 (2 × CH), 125.3 (CH), 125.4 (CH), 128.2 (CH), 128.2 (CH), 128.9 (2 × C), 129.1 (C), 129.2 (C), 129.3 (d, ³*J*_{CF} 3.3 Hz, CH), 129.4 (d, ³*J*_{CF} 3.3 Hz, CH), 131.0 (CH), 131.2 (CH), 132.0 (d, ³*J*_{CF} 7.8 Hz, CH), 132.1 (d, ³*J*_{CF} 7.8 Hz, CH), 132.1 (2 × CH), 134.1 (2 × CH), 134.2 (d, ⁴*J*_{CF} 3.3 Hz, C), 134.3 (d, ⁴*J*_{CF} 3.3 Hz, C), 136.6

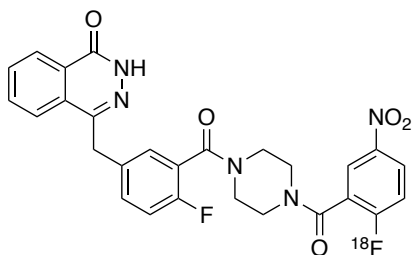
(C), 136.7 (C), 137.3 (2 × C), 145.4 (2 × C), 146.9 (C), 146.9 (C), 151.2 (C), 151.2 (C), 157.1 (d, $^1J_{CF}$ 249.1 Hz, C), 157.2 (d, $^1J_{CF}$ 249.1 Hz, C), 158.3 (2 × C), 164.6 (C), 164.8 (C), 165.1 (C), 165.3 (C); m/z (ESI) 672.1623 (MNa^+ . $C_{32}H_{29}^{35}ClFN_5NaO_7$ requires 672.1632).

4-{3''-[4'''-(2''''-Chloro-5''''-nitrobenzoyl)piperazine-1'''-carbonyl]-4''-fluorobenzyl}-2*H*-phthalazin-1-one (39)



Method B: To a 5.0 mL v-vial was added 4-{3''-[4'''-(2''''-chloro-5''''-nitrobenzoyl)piperazine-1'''-carbonyl]-4''-fluorobenzyl}-2-(*tert*-butyloxycarbonyl)phthalazin-1-one (**76**) (1.0 mg, 0.0015 mmol), dimethyl sulfoxide (0.25 mL) and water (0.25 mL). The reaction mixture was heated to 120 °C for 5 min then cooled to room temperature. An aliquot of the crude reaction mixture (0.050 mL) was diluted with acetonitrile (0.10 mL) and water (0.10 mL). The identity of the product was confirmed by HPLC analysis. The crude product solution (0.010 mL) was loaded onto a C18 Phenomenex Synergi™ 4 μm Hydro-RP 80 Å (150 mm × 4.60 mm) LC column using a Dionex™ UltiMate™ 3000 HPLC system. A flow rate of 1.0 mL min⁻¹ was used with mobile phase conditions: 0.0–13.0 min 35% acetonitrile in water, 13.0–14.0 min 45% acetonitrile in water, 14.0–15.0 min 55% acetonitrile in water, 15.0–16.0 min 65% acetonitrile in water, 16.0–26.0 min 75% acetonitrile in water, 26.0–36.0 min 35% acetonitrile in water. Detection was achieved using a UV variable wavelength detector at 254 nm. HPLC data collection and analysis were performed using Chromeleon 6.8 chromatography software and analytical methods were calibrated with standard solutions of **39** and **76**. 4-{3''-[4'''-(2''''-Chloro-5''''-nitrobenzoyl)piperazine-1'''-carbonyl]-4''-fluorobenzyl}-2*H*-phthalazin-1-one (**39**) eluted at 10.9 min and was afforded in 96% conversion.

4-{3''-[4'''-(2''''-[¹⁸F]Fluoro-5''''-nitrobenzoyl)piperazine-1'''-carbonyl]-4''-fluorobenzyl}-2*H*-phthalazin-1-one ([¹⁸F]31)



Method A: No-carrier-added aqueous [¹⁸F]fluoride (444 MBq at the end of cyclotron target irradiation) was produced by irradiation of 95–97 atom % [¹⁸O]enriched water in a niobium target chamber (2.7 mL target volume), via the ¹⁸O(p,n)¹⁸F nuclear reaction, in a GE Healthcare PETtrace 860 cyclotron at the West of Scotland PET Centre. The aqueous [¹⁸F]fluoride was transferred to a GE TRACERlab™ FX_{FN} synthesiser and trapped on a Waters Sep-Pak® Light QMA cartridge. [¹⁸F]Fluoride was eluted into the reaction vessel using a solution of Kryptofix® 222 (8.00 mg) and potassium carbonate (1.45 mg) in acetonitrile (0.85 mL) and water (0.15 mL). This solution was heated to 85 °C and dried under vacuum for 5 min. Anhydrous acetonitrile (1.0 mL) was added to the reaction vessel. The reaction mixture was then heated to 110 °C and dried under vacuum for 2 min. The reaction vessel was cooled to 70 °C and a solution of 4-{3''-[4'''-(2''''-chloro-5''''-nitrobenzoyl)piperazine-1'''-carbonyl]-4''-fluorobenzyl}-2*H*-phthalazin-1-one (**39**) (4.00 mg) in anhydrous dimethyl sulfoxide (1.00 mL) was added under nitrogen. The reaction mixture was heated to 110 °C and stirred for 0.25 h. The crude reaction mixture was then cooled to 50 °C, diluted with 35% acetonitrile in water (3.0 mL) and loaded onto a C18 Phenomenex Synergi™ 4 μm Hydro-RP 80 Å (150 mm × 10.0 mm) LC column. The crude material was purified by semi-preparative HPLC eluting with 35% acetonitrile in water at a flow rate of 3 mL min⁻¹. The radiolabelled product was detected by a gamma detector at a retention time of approximately 12.0 min and was collected in approximately 6.0 mL of 35% acetonitrile in water. The identity and purity of the radiolabelled product were confirmed by performing analytical radio-HPLC. A sample of the radiolabelled product was loaded onto a C18 Phenomenex Synergi™ 4 μm Hydro-RP 80 Å (150 mm × 4.60 mm) LC column using a Dionex™ UltiMate™ 3000 HPLC system. Isocratic mobile phase conditions of 35% acetonitrile in water at a flow rate of 1.0 mL min⁻¹ for 0.0–20.0 min was used. Detection was achieved

using a UV variable wavelength detector at 254 nm and an Eckert & Ziegler photo-multiplier tube FlowCount gamma radio-detector. HPLC data collection and analysis were performed using Chromeleon 6.8 chromatography software and analytical methods were calibrated with standard solutions of **39** and **31**. 4-{3'-[4'''-(2''''-[¹⁸F]Fluoro-5''''-nitrobenzoyl)piperazine-1'''-carbonyl]-4''-fluorobenzyl}-2*H*-phthalazin-1-one (**[¹⁸F]31**) was afforded in 15% decay corrected radiochemical yield (42.2 MBq at the end of product isolation) with a radiochemical purity of 93%. The total synthesis time from delivery of [¹⁸F]fluoride into the reaction vessel to isolation of product was approximately 46 min.

Method B: No-carrier-added aqueous [¹⁸F]fluoride (555 MBq at the end of cyclotron target irradiation) was produced and transferred to the reaction vessel of a GE TRACERlab™ FX_{FN} synthesiser as previously described for method A. This solution was heated to 85 °C and dried under vacuum for 5 min. Anhydrous acetonitrile (1.0 mL) was added to the reaction vessel then heated to 110 °C and dried under vacuum for 2 min. The reaction vessel was cooled to 70 °C and a solution of 4-{3'-[4'''-(2''''-chloro-5''''-nitrobenzoyl)piperazine-1'''-carbonyl]-4''-fluorobenzyl}-2-(*tert*-butyloxycarbonyl)phthalazin-1-one (**76**) (4.00 mg) in anhydrous dimethyl sulfoxide (1.0 mL) was added under nitrogen. The reaction mixture was heated to 110 °C and stirred for 15 min. The reaction vessel was cooled to 50 °C and water (1.0 mL) was added. The reaction mixture was heated to 120 °C and stirred for 5 min. The crude reaction mixture was then cooled to 50 °C, diluted with 35% acetonitrile in water (3.0 mL) and purified as previously described for method A. The radiolabelled product was detected by a gamma detector at a retention time of approximately 11.5 min and was collected in approximately 4.0 mL of 35% acetonitrile in water. The identity and purity of the radiolabelled product were confirmed by performing analytical HPLC as previously described for method A, except calibrated with standard solutions of **39**, **31** and **76**. 4-{3'-[4'''-(2''''-[¹⁸F]Fluoro-5''''-nitrobenzoyl)piperazine-1'''-carbonyl]-4''-fluorobenzyl}-2*H*-phthalazin-1-one (**[¹⁸F]31**) was afforded in 6% decay corrected radiochemical yield (18.3 MBq at the end of product isolation) with a radiochemical purity of 88%. The total synthesis time from delivery of [¹⁸F]fluoride into the reaction vessel to isolation of product was 51 min.

3.3 HPLC Methods for Physicochemical Properties Analysis

All physicochemical analyses were performed using a Dionex™ UltiMate™ 3000 series, and data acquisition and processing performed using Chromeleon 6.8 chromatography software. Standard and novel compounds were dissolved in 1:1 organic and aqueous phase mixture, prepared to a concentration of 0.5 mg/mL. The HPLC system oven was set to 25 °C, and UV detection achieved using a diode array detector (190–800 nm). Analysis was performed using 5 µL sample injections.

C18 Chromatography for Determination of Lipophilicity (Log *P*)¹⁶⁴

Log *P* values were determined using a Phenomenex Luna® 5 µm C18 100 Å (50 × 3 mm) column. The retention time for each compound of interest was measured using filtered acetonitrile and 0.01 mM phosphate buffered saline as the mobile phase at pH 4.0, pH 7.4 and pH 10.0. The pH was adjusted by the addition of concentrated hydrochloric acid or 0.05 M sodium hydroxide solution. The mobile phase flow rate was set at 1.0 mL min⁻¹. The chromatographic hydrophobicity index (CHI) value for all compounds was determined by measuring the retention time of each compound under the following mobile phase conditions: 0–10.5 min, 0–100% acetonitrile; 10.5–11.5 min, 100% acetonitrile; 11.5–12.0 min, 100–0% acetonitrile; 12.0–15.0 min, 0% acetonitrile. System calibration was achieved using the following compounds and plotting their mean CHI values against the measured retention time under all three pH conditions: theophylline (CHI = 15.76), phenyltetrazole (CHI = 20.18), benzimidazole (CHI = 30.71), colchicine (CHI = 41.37), acetophenone (CHI = 64.90), indole (CHI = 69.15), butyrophenone (CHI = 88.49) and valerophenone (CHI = 97.67). Using the calibration curves obtained and the following equations from a validated study, the log *P* of the compounds was calculated using Excel 2019 Software.

$$\text{CHI Log } D = 0.054\text{CHI} - 1.467$$

Where CHI Log *D* is the CHI value projected to the logarithmic scale.

$$\log P = 0.047\text{CHIN} + 0.36\text{HBC} - 1.10$$

Where CHIN is the gradient chromatographic hydrophobicity index of the non-ionised compound and HBC is hydrogen bond donor count.

Immobilised Artificial Membrane (IAM) Chromatography for Determination of Membrane Permeability (P_m) and Membrane Partition Coefficient (K_m)¹⁶⁴

P_m and K_m values were determined using previously developed methodology on a Registech IAM.PC.DD2 (150 × 4.6 mm) column. Acetonitrile and 0.01 mM phosphate buffered saline at pH 7.4 was used as the mobile phase, with a flow rate of 1.0 mL min⁻¹. The retention time of each compound of interest was measured under an isocratic mobile phase with the percentage acetonitrile ranging from 30–70%. The retention time of citric acid, as an unretained compound, under an isocratic mobile phase of 100% phosphate buffered saline was used for system corrections. The following equations were used to calculate P_m and K_m of the compounds of interest using Excel 2019 Software.

$$k_{IAM} = \frac{(t_r - t_0)}{t_0}$$

Where k_{IAM} = solute capacity factor on the IAM column, t_r = retention time of compound and t_0 = retention time of unretained compound.

$$k_{IAM} = \left(\frac{V_s}{V_m}\right) \times K_m$$

Where V_s = volume of the IAM interphase created by the immobilised phospholipids, V_m = total volume of the solvent within the IAM column and K_m = membrane partition coefficient.

$$V_m = \frac{W_{PhC}}{\delta_{PhC}} + \frac{W_{C10}}{\delta_{C10}} + \frac{W_{C3}}{\delta_{C3}}$$

Where the specific weight of PhC (δ_{PhC}) = 1.01779 g mL⁻¹ and C₁₀/C₃ ($\delta_{C10/C3}$) = 0.86 g mL⁻¹; W_{PhC} = 133 mg, W_{C10} = 12.73 mg and W_{C3} = 2.28 mg.

$$V_m = f_r \times t_0$$

Where f_r = flow rate.

$$P_m = \frac{K_m}{MW}$$

Where P_m = permeability and MW = molecular weight.

Human Serum Albumin (HSA) Chromatography for Determination of Percentage of Plasma Protein Binding (%PPB)¹⁶⁴

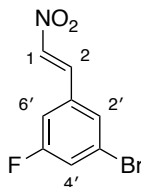
%PPB values were determined using previously developed methodology on a ChromTech HSA 5 μm (3.0 \times 50 mm) column. Isopropanol and 0.01 mM phosphate buffered saline at pH 7.4 was used as the mobile phase, with a flow rate of 1.8 mL min^{-1} . The retention time of each compound of interest was measured under the following mobile phase conditions: 0–3 min, 0–30% isopropanol; 3–10 min, 30% isopropanol; 10.5–11.0 min, 30–0% isopropanol; 11.0–15.0 min, 0% isopropanol. System calibration was achieved using the following reference compounds: warfarin (%PPB = 98.0), nizatidine (%PPB = 35.0), bromazepam (%PPB = 60.0), carbamazepine (%PPB = 75.0), nicardipine (%PPB = 95.0), ketoprofen (%PPB = 98.7), indomethacin (%PPB = 99.0) and diclofenac (%PPB = 99.8). The %PPB for the reference compounds were converted to the linear free energy related log K value, which when plotted against retention time on the HSA column, afforded a line equation from which the log K value of the unknown compounds could be extracted. The log K values of the unknown compounds could then be converted to %PPB. Log K and subsequent %PPB calculations for the compounds of interest were performed using Excel 2019 Software.

$$\log K = \log \left[\frac{\%PPB}{101 - \%PPB} \right]$$

$$\%PPB = \left[\frac{(101 - 10^{\log K})}{(1 + 10^{\log K})} \right]$$

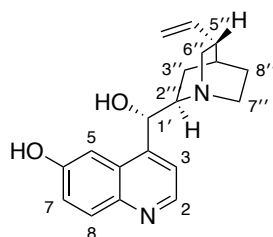
3.4 SV2A Experimental

(*E*)-2-(3'-Bromo-5'-fluorophenyl)nitroethene (**86**)



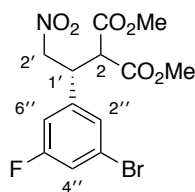
In an oven-dried flask under argon, 3-bromo-5-fluorobenzaldehyde (**79**) (0.500 g, 2.46 mmol), ammonium acetate (0.455 g, 5.90 mmol) and nitromethane (4.93 mL, 91.0 mmol) were dissolved in acetic acid (10 mL). The reaction mixture was heated to 90 °C and stirred for 5 h. The reaction mixture was cooled to room temperature, diluted with ethyl acetate (30 mL) and washed with water (3 × 30 mL). The organic layer was dried (MgSO₄), filtered and concentrated *in vacuo*. The crude material was purified by flash column chromatography eluting with 20% dichloromethane in hexane to give (*E*)-2-(3'-bromo-5'-fluorophenyl)nitroethene (**86**) as a pale yellow solid (0.447 g, 74%). Mp 89–91 °C; $\nu_{\text{max}}/\text{cm}^{-1}$ (neat) 3103 (CH), 3080 (CH), 1641 (C=C), 1574, 1512, 1423, 1346, 1279, 974, 845; δ_{H} (400 MHz, CDCl₃) 7.20 (1H, ddd, *J* 8.8, 2.4, 1.6 Hz, 4'-H), 7.38 (1H, ddd, *J* 7.6, 2.4, 1.6 Hz, 6'-H), 7.49 (1H, t, *J* 1.6 Hz, 2'-H), 7.53 (1H, d, *J* 13.6 Hz, 1-H), 7.88 (1H, d, *J* 13.6 Hz, 2-H); δ_{C} (101 MHz, CDCl₃) 114.6 (d, ²*J*_{CF} 22.5 Hz, CH), 122.5 (d, ²*J*_{CF} 24.5 Hz, CH), 123.9 (d, ³*J*_{CF} 9.8 Hz, C), 128.1 (d, ⁴*J*_{CF} 3.3 Hz, CH), 133.6 (d, ³*J*_{CF} 8.6 Hz, C), 136.2 (d, ⁴*J*_{CF} 2.9 Hz, CH), 139.2 (CH), 162.9 (d, ¹*J*_{CF} 253.3 Hz, C); *m/z* (ESI) 267.9371 (MNa⁺. C₈H₅⁷⁹BrFNNaO₂ requires 267.9380).

4-((1'S)-[(2''R,4''S,5''R)-5''-Ethenyl-1''-azabicyclo[2.2.2]octan-2''-yl]hydroxymethyl}quinolin-6-ol (87)²⁰⁴



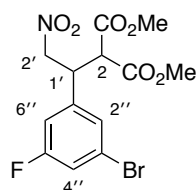
In an oven-dried flask under argon, a stirred solution of quinidine (**88**) (0.162 g, 0.500 mmol) in anhydrous dichloromethane (17 mL) was cooled to $-78\text{ }^{\circ}\text{C}$, and to this was added dropwise, 1 M boron tribromide in dichloromethane (2.00 mL, 2.00 mmol). The reaction mixture was warmed to room temperature and stirred under reflux for 2 h. The reaction mixture was cooled to $5\text{ }^{\circ}\text{C}$ and quenched with 2.5 M aqueous sodium hydroxide solution (10 mL). The organic and aqueous layers were separated, and the aqueous layer was extracted with dichloromethane ($2 \times 10\text{ mL}$). The aqueous layer was acidified with 1 M aqueous hydrochloric acid to pH 8, and the resulting white suspension was extracted with dichloromethane ($5 \times 10\text{ mL}$). The combined organic layers from this part of the work-up were dried (MgSO_4), filtered and concentrated *in vacuo* to give 4-((1'S)-[(2''R,4''S,5''R)-5''-ethenyl-1''-azabicyclo[2.2.2]octan-2''-yl]hydroxymethyl}quinolin-6-ol (**87**) as a pale yellow solid (0.125 g, 81%). Mp $>140\text{ }^{\circ}\text{C}$ (decomposition); $[\alpha]_{\text{D}}^{22} +253.7$ ($c\ 1.0$, EtOH). Spectroscopic data were consistent with the literature.²⁰⁴ δ_{H} (400 MHz, CD_3OD) 1.00–1.10 (1H, m, 3''-HH), 1.47–1.65 (2H, m, 8''-H₂), 1.73 (1H, br s, 4''-H), 2.15–2.26 (1H, m, 3''-HH), 2.27–2.37 (1H, m, 5''-H), 2.74–2.85 (1H, m, 7''-HH), 2.87–2.98 (2H, m, 6''-HH and 7''-HH), 3.07 (1H, td, $J\ 9.2, 2.4\text{ Hz}$, 2''-H), 3.64 (1H, ddd, $J\ 13.4, 7.8, 2.2\text{ Hz}$, 6''-HH), 5.03–5.15 (2H, m, H_2CCHC), 5.58–5.68 (1H, m, 1'-H), 6.15 (1H, ddd, $J\ 17.2, 10.2, 7.8\text{ Hz}$, H_2CCHC), 7.28 (1H, d, $J\ 2.4\text{ Hz}$, 5-H), 7.29–7.35 (1H, m, 7-H), 7.63 (1H, d, $J\ 4.6\text{ Hz}$, 3-H), 7.89 (1H, d, $J\ 8.8\text{ Hz}$, 8-H), 8.58 (1H, d, $J\ 4.6\text{ Hz}$, 2-H); δ_{C} (101 MHz, CD_3OD) 21.1 (CH_2), 26.9 (CH_2), 29.6 (CH), 41.1 (CH), 50.4 (CH_2), 50.8 (CH_2), 60.6 (CH), 72.1 (CH), 105.1 (CH), 115.3 (CH_2), 119.7 (CH), 123.3 (CH), 128.3 (C), 131.4 (CH), 141.4 (CH), 143.9 (C), 147.4 (CH), 149.5 (C), 158.0 (C); m/z (ESI) 311 (MH^+ .100%).

Dimethyl (1'*R*)-2-[1'-(3'',5''-difluorophenyl)-2'-nitroethyl]malonate ((*R*)-**89**)



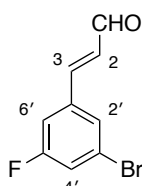
To a stirred solution of (*E*)-2-(3'-bromo-5'-fluorophenyl)nitroethene (**86**) (0.984 g, 4.00 mmol) in anhydrous tetrahydrofuran (4 mL) in an oven-dried flask under argon, was added dimethyl malonate (0.600 mL, 5.25 mmol). The reaction was cooled to $-20\text{ }^{\circ}\text{C}$ and a solution of 4-((1'*S*)-[(2''*R*,4''*S*,5''*R*)-5''-ethenyl-1''-azabicyclo[2.2.2]octan-2''-yl]hydroxymethyl)quinolin-6-ol (**87**) (0.0380 g, 0.122 mmol) in anhydrous tetrahydrofuran (4 mL) was added dropwise. The reaction mixture was stirred at $-20\text{ }^{\circ}\text{C}$ for 16 h. The mixture was warmed to room temperature and concentrated *in vacuo*. The crude material was purified by flash column chromatography eluting with 20% diethyl ether in hexane. Further purification by dissolution in a minimum amount of warm diethyl ether and triturated with cold hexane gave dimethyl (1'*R*)-2-[1'-(3'',5''-difluorophenyl)-2'-nitroethyl]malonate ((*R*)-**89**) as a white solid (1.22 g, 81%). Mp $71\text{--}73\text{ }^{\circ}\text{C}$; $\nu_{\text{max}}/\text{cm}^{-1}$ (neat) 2963 (CH), 1743 (C=O), 1724 (C=O), 1551, 1435, 1366, 1273, 1250, 1153, 864; $[\alpha]_{\text{D}}^{21} -2.9$ (*c* 1.0, CHCl₃); δ_{H} (500 MHz, CDCl₃) 3.65 (3H, s, CH₃), 3.78 (3H, s, CH₃), 3.80 (1H, d, *J* 8.5 Hz, 2-H), 4.21 (1H, ddd, *J* 9.3, 8.5, 4.8 Hz, 1'-H), 4.86 (1H, dd, *J* 13.8, 9.3 Hz, 2'-HH), 4.91 (1H, dd, *J* 13.8, 4.8 Hz, 2'-HH), 6.94 (1H, dt, *J* 9.0, 2.0 Hz, 4''-H), 7.17–7.21 (2H, m, 2''-H and 6''-H); δ_{C} (126 MHz, CDCl₃) 42.3 (d, $^4J_{\text{CF}}$ 1.8 Hz, CH), 53.3 (CH₃), 53.4 (CH₃), 54.4 (CH), 76.7 (CH₂), 114.4 (d, $^2J_{\text{CF}}$ 22.4 Hz, CH), 119.5 (d, $^2J_{\text{CF}}$ 24.2 Hz, CH), 123.4 (d, $^3J_{\text{CF}}$ 10.0 Hz, C), 127.2 (d, $^4J_{\text{CF}}$ 3.2 Hz, CH), 140.4 (d, $^3J_{\text{CF}}$ 7.8 Hz, C), 162.7 (d, $^1J_{\text{CF}}$ 252.6 Hz, C), 167.0 (C), 167.5 (C); *m/z* (ESI) 399.9809 (MNa⁺. C₁₃H₁₃⁷⁹BrFNNaO₆ requires 399.9802). The enantiomeric ratio was determined by HPLC analysis with a CHIRALCEL[®] OD-H column (95:5, hexane:*i*PrOH, flow rate of 1.0 mL/min): $t_{\text{major}} = 24.04\text{ min}$, $t_{\text{minor}} = 20.97\text{ min}$; 96:4 er.

Dimethyl (\pm)-2-[1'-(3'',5''-difluorophenyl)-2'-nitroethyl]malonate (**89**)



To a stirred solution of (*E*)-2-(3'-bromo-5'-fluorophenyl)nitroethene (**86**) (0.100 g, 0.406 mmol) in anhydrous tetrahydrofuran (2 mL) in an oven-dried flask under argon, was added dimethyl malonate (0.0603 mL, 0.528 mmol) and triethylamine (0.0736 mL, 0.528 mmol). The reaction mixture was stirred at room temperature for 17 h and then concentrated *in vacuo*. The crude material was purified by flash column chromatography eluting with 20% diethyl ether in hexane to give dimethyl (\pm)-2-[1'-(3'',5''-difluorophenyl)-2'-nitroethyl]malonate (**89**) as a colourless oil, which solidified upon standing (0.0923 g, 60%). Spectroscopic data as for (**R**)-**89**. The enantiomeric ratio was determined by HPLC analysis with a CHIRALCEL[®] OD-H column (95:5, hexane:*i*PrOH, flow rate of 1.0 mL/min): $t_{\text{major}} = 20.89$ min, $t_{\text{minor}} = 24.06$ min; 51:49 er.

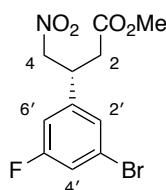
(*E*)-3-(3'-Bromo-5'-fluorophenyl)prop-2-enal (**95**)



3-Bromo-5-fluorobenzaldehyde (**79**) (6.09 g, 30.0 mmol) and (triphenylphosphoranylidene)acetaldehyde (10.0 g, 33.0 mmol) were dissolved in anhydrous tetrahydrofuran (300 mL), under argon. The reaction mixture was heated to 50 °C and stirred for 18 h. The reaction mixture was cooled to room temperature and concentrated *in vacuo*. The crude material was purified by flash column chromatography eluting with 10% diethyl ether in hexane to give (*E*)-3-(3'-bromo-5'-fluorophenyl)prop-2-enal (**95**) as a pale yellow solid (5.57 g, 81%). Mp 65–67 °C; $\nu_{\text{max}}/\text{cm}^{-1}$ (neat) 3071 (CH), 2862 (CH), 1659 (C=O), 1628 (C=C), 1574, 1427, 1269, 1126, 976, 849; δ_{H} (400 MHz, CDCl₃) 6.68 (1H, dd, *J* 16.0, 7.6 Hz, 2-H), 7.20 (1H,

dt, J 8.9, 2.0 Hz, 6'-H), 7.32 (1H, dt, J 7.8, 2.0 Hz, 4'-H), 7.36 (1H, d, J 16.0 Hz, 3-H), 7.48–7.51 (1H, m, 2'-H), 9.72 (1H, d, J 7.6 Hz, 1-H); δ_{C} (101 MHz, CDCl_3) 113.8 (d, $^2J_{\text{CF}}$ 22.2 Hz, CH), 121.5 (d, $^2J_{\text{CF}}$ 24.6 Hz, CH), 123.5 (d, $^3J_{\text{CF}}$ 9.9 Hz, C), 127.5 (d, $^4J_{\text{CF}}$ 3.2 Hz, CH), 130.8 (CH), 137.6 (d, $^3J_{\text{CF}}$ 8.3 Hz, C), 149.1 (d, $^4J_{\text{CF}}$ 2.7 Hz, CH), 162.9 (d, $^1J_{\text{CF}}$ 253.2 Hz, C), 192.9 (CH); m/z (ESI) 250.9469 (MNa^+ , $\text{C}_9\text{H}_6^{79}\text{BrFNaO}$ requires 250.9478).

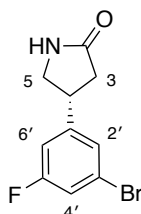
Methyl (3*R*)-3-(3'-bromo-5'-fluorophenyl)-4-nitrobutanoate ((*R*)-98)



To a stirred solution of (*E*)-3-(3'-bromo-5'-fluorophenyl)prop-2-enal (**95**) (0.229 g, 1.00 mmol) in tetrahydrofuran (3 mL) and water (0.4 mL), was added pivalic acid (0.00510 g, 0.0500 mmol), boric acid (0.0310 g, 0.500 mmol), nitromethane (0.330 mL, 6.00 mmol) and (*R*)- α,α -bis[3,5-bis(trifluoromethyl)phenyl]-2-pyrrolidinemethanol trimethylsilyl ether ((*R*)-**94**) (0.0300 g, 0.0500 mmol). The reaction mixture was stirred at room temperature for 117 h and concentrated *in vacuo*. The resultant residue was dissolved in ethyl acetate (20 mL) and washed with 1 M aqueous hydrochloric acid (20 mL), saturated aqueous sodium bicarbonate (20 mL) and brine (20 mL). The organic layer was dried (MgSO_4), filtered and concentrated *in vacuo* to give (3*R*)-3-(3'-bromo-5'-fluorophenyl)-4-nitrobutanal ((*R*)-**96**) as a yellow oil, which was used without further purification. (3*R*)-3-(3'-Bromo-5'-fluorophenyl)-4-nitrobutanal ((*R*)-**96**) was dissolved in acetonitrile (5 mL) and cooled to 0 °C. To this was added a solution of potassium dihydrogen phosphate (0.104 g, 0.764 mmol) in water (2.5 mL), hydrogen peroxide (0.140 mL, 1.37 mmol, 30% w/w in water) and a solution of sodium chlorite (0.271 g, 3.00 mmol) in water (5 mL). The reaction mixture was stirred at 0 °C for 3 h and quenched with sodium sulfite (0.378 g, 3.00 mmol). The mixture was stirred at room temperature for 0.5 h. The reaction mixture was then acidified with 1 M aqueous potassium bisulfate (4 mL) and extracted with ethyl acetate (3 \times 15 mL). The combined organic layers were dried (MgSO_4), filtered and concentrated *in vacuo* to give (3*R*)-3-(3'-bromo-5'-fluorophenyl)-4-nitrobutanoic acid ((*R*)-**97**) as a yellow oil, which was used without

further purification. To a stirred solution of (3*R*)-3-(3'-bromo-5'-fluorophenyl)-4-nitrobutanoic acid ((**R**)-**97**) in methanol (3 mL) at 0 °C, was added thionyl chloride (0.110 mL, 1.50 mmol). The reaction mixture was warmed to room temperature and then stirred under reflux for 1.5 h. The reaction mixture was cooled to room temperature and concentrated *in vacuo*. The resultant residue was dissolved in ethyl acetate (20 mL) and washed with water (20 mL). The aqueous layer was extracted with ethyl acetate (2 × 20 mL). The combined organic layers were dried (MgSO₄), filtered and concentrated *in vacuo*. The crude material was purified by flash column chromatography eluting with 60% dichloromethane in hexane to give methyl (3*R*)-3-(3'-bromo-5'-fluorophenyl)-4-nitrobutanoate ((**R**)-**98**) as a colourless oil, which solidified upon standing (0.181 g, 57% over three steps). Mp 39–40 °C; $\nu_{\max}/\text{cm}^{-1}$ (neat) 3082 (CH), 2955 (CH), 1724 (C=O), 1547, 1435, 1373, 1354, 1269, 1219, 1173, 914, 864; $[\alpha]_{\text{D}}^{19} +7.6$ (c 0.1, CHCl₃); δ_{H} (400 MHz, CDCl₃) 2.74 (1H, d, *J* 7.6 Hz, 2-*HH*), 2.74 (1H, d, *J* 7.2 Hz, 2-*HH*), 3.66 (3H, s, CH₃), 3.91–4.00 (1H, m, 3-H), 4.61 (1H, dd, *J* 13.2, 8.2 Hz, 4-*HH*), 4.72 (1H, dd, *J* 13.2, 6.4 Hz, 4-*HH*), 6.91 (1H, dt, *J* 8.9, 1.9 Hz, 6'-H), 7.15–7.21 (2H, m, 2'-H and 4'-H); δ_{C} (101 MHz, CDCl₃) 37.2 (CH₂), 39.6 (d, ⁴*J*_{CF} 1.8 Hz, CH), 52.3 (CH₃), 78.7 (CH₂), 113.8 (d, ²*J*_{CF} 22.1 Hz, CH), 119.1 (d, ²*J*_{CF} 24.3 Hz, CH), 123.4 (d, ³*J*_{CF} 9.9 Hz, C), 126.6 (d, ⁴*J*_{CF} 3.2 Hz, CH), 142.5 (d, ³*J*_{CF} 7.7 Hz, C), 162.8 (d, ¹*J*_{CF} 253.2 Hz, C), 170.6 (C); *m/z* (ESI) 341.9742 (MNa⁺. C₁₁H₁₁⁷⁹BrFNNaO₄ requires 341.9748). The enantiomeric ratio was determined by HPLC analysis with a CHIRALCEL® AD-H column (98:2, hexane:*i*PrOH, flow rate of 1.0 mL/min): *t*_{major} = 22.35 min, *t*_{minor} = 20.30 min; 94:6 er.

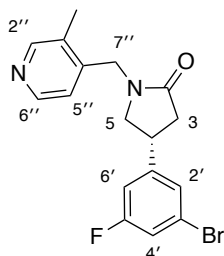
(4*R*)-4-(3'-Bromo-5'-fluorophenyl)pyrrolidin-2-one ((R**)-**83**)**¹⁵²



To a stirred solution of (3*R*)-3-(3'-bromo-5'-fluorophenyl)-4-nitrobutanoate ((**R**)-**98**) (3.91 g, 12.2 mmol) in methanol (61 mL), was added nickel(II) chloride hexahydrate (0.290 g, 1.22 mmol). Sodium borohydride (2.31 g, 61.0 mmol) was added in four portions over 0.2 h, producing a black precipitate and the evolution of gas. The

reaction mixture was stirred at room temperature for 0.25 h and then filtered through a short pad of Celite[®] with dichloromethane (300 mL). The filtrate was concentrated *in vacuo* at 45 °C for 1.5 h. The resultant residue was dissolved in chloroform (100 mL) and washed with water (100 mL). The organic and aqueous layers were separated, and the aqueous layer was extracted with chloroform (2 × 100 mL). The combined organic layers were dried (MgSO₄), filtered and concentrated *in vacuo*. The crude material was purified by flash column chromatography eluting with 5% methanol in diethyl ether to give (4*R*)-4-(3'-bromo-5'-fluorophenyl)pyrrolidin-2-one ((*R*)-**83**) and (4*R*)-4-(3'-fluorophenyl)pyrrolidin-2-one ((*R*)-**109**) in a ratio of 1 : 0.18 as a white solid (1.38 g, 44%). Mp 110–111 °C; [α]_D²⁰ -18.5 (c 0.1, CHCl₃). Spectroscopic data were consistent with the literature.¹⁵² Signals for ((*R*)-**83**) are recorded. δ_H (400 MHz, CDCl₃) 2.43 (1H, dd, *J* 16.8, 8.4 Hz, 3-*HH*), 2.74 (1H, dd, *J* 16.8, 8.8 Hz, 3-*HH*), 3.39 (1H, dd, *J* 9.6, 6.8 Hz, 5-*HH*), 3.59–3.71 (1H, m, 4-H), 3.75–3.83 (1H, m, 5-*HH*), 6.67 (1H, br s, NH), 6.91 (1H, dt, *J* 9.2, 2.0 Hz, 6'-H), 7.15 (1H, dt, *J* 8.0, 2.0 Hz, 4'-H), 7.18–7.21 (1H, m, 2'-H); δ_C (101 MHz, CDCl₃) 37.7 (CH₂), 39.8 (d, ⁴*J*_{CF} 1.8 Hz, CH), 49.1 (CH₂), 113.0 (d, ²*J*_{CF} 21.7 Hz, CH), 118.1 (d, ²*J*_{CF} 24.4 Hz, CH), 123.2 (d, ³*J*_{CF} 10.0 Hz, C), 126.0 (d, ⁴*J*_{CF} 3.1 Hz, CH), 146.4 (d, ³*J*_{CF} 7.7 Hz, C), 163.0 (d, ¹*J*_{CF} 252.5 Hz, C), 177.0 (C); *m/z* (ESI) 280 (MNa⁺. 100%). The enantiomeric ratio was determined by HPLC analysis with a CHIRALCEL[®] AD-H column (97:3, hexane: *i*-PrOH, flow rate of 1.0 mL/min): *t*_{major} = 27.78 min, *t*_{minor} = 37.31 min; 92:8 er.

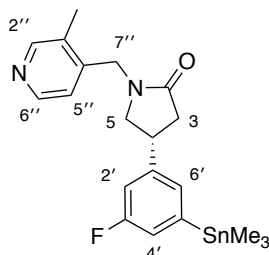
(4*R*)-4-(3'-Bromo-5'-fluorophenyl)-1-[(3''-methylpyridin-4''-yl)methyl]pyrrolidin-2-one ((*R*)-84**)¹⁵²**



Sodium hydride (0.857 g, 21.4 mmol, 60% dispersion in mineral oil) was added to an oven-dried flask under argon and cooled to 0 °C. This was washed with hexane (50 mL) and then dried *in vacuo* at room temperature for 1 h. The flask was cooled to 0 °C, and anhydrous tetrahydrofuran (27 mL) was added. To this solution was

added (4*R*)-4-(3'-bromo-5'-fluorophenyl)pyrrolidin-2-one ((**R**)-**83**) (1.38 g, 5.35 mmol), 4-(chloromethyl)-3-methylpyridine hydrochloride (1.11 g, 6.23 mmol) and potassium iodide (0.888 g, 5.35 mmol). The reaction mixture was warmed to room temperature and then stirred at 60 °C for 19 h. After cooling to 0 °C, the reaction was quenched with water (50 mL) and concentrated *in vacuo*. The resultant residue was dissolved in ethyl acetate (80 mL) and washed with water (80 mL). The aqueous layer was extracted with ethyl acetate (2 × 80 mL). The combined organic layers were dried (MgSO₄), filtered and concentrated *in vacuo*. The crude material was purified by flash column chromatography eluting with 10% methanol in diethyl ether to give (4*R*)-4-(3'-bromo-5'-fluorophenyl)-1-[(3''-methylpyridin-4''-yl)methyl]pyrrolidin-2-one ((**R**)-**84**) as a pale yellow solid (0.968 g, 50%). Mp 113–115 °C; [α]_D¹⁸ +28.9 (*c* 0.1, CHCl₃). Spectroscopic data were consistent with the literature.¹⁵² δ_H (400 MHz, CDCl₃) 2.31 (3H, s, CH₃), 2.59 (1H, dd, *J* 17.0, 7.8 Hz, 3-*HH*), 2.91 (1H, dd, *J* 17.0, 8.6 Hz, 3-*HH*), 3.23 (1H, dd, *J* 9.2, 6.0 Hz, 5-*HH*), 3.51–3.66 (2H, m, 4-*H* and 5-*HH*), 4.43 (1H, d, *J* 15.4 Hz, 7''-*HH*), 4.59 (1H, d, *J* 15.4 Hz, 7''-*HH*), 6.84 (1H, dt, *J* 9.2, 2.0 Hz, 6'-*H*), 7.04 (1H, d, *J* 4.8 Hz, 5''-*H*), 7.11 (1H, br t, *J* 2.0 Hz, 2'-*H*), 7.15 (1H, dt, *J* 8.0, 2.0 Hz, 4'-*H*), 8.38–8.46 (2H, m, 2''-*H* and 6''-*H*); δ_C (101 MHz, CDCl₃) 16.1 (CH₃), 36.9 (d, ⁴*J*_{CF} 1.9 Hz, CH), 38.2 (CH₂), 43.7 (CH₂), 53.5 (CH₂), 113.0 (d, ²*J*_{CF} 21.8 Hz, CH), 118.2 (d, ²*J*_{CF} 24.4 Hz, CH), 122.6 (CH), 123.3 (d, ³*J*_{CF} 10.0 Hz, C), 125.9 (d, ⁴*J*_{CF} 3.2 Hz, CH), 131.7 (C), 142.7 (C), 146.0 (d, ³*J*_{CF} 7.6 Hz, C), 148.2 (CH), 151.6 (CH), 162.9 (d, ¹*J*_{CF} 252.8 Hz, C), 173.1 (C); *m/z* (ESI) 363 (MH⁺, 100%). The enantiomeric ratio was determined by HPLC analysis with a CHIRALCEL[®] AD-H column (92:8, hexane:*i*PrOH, flow rate of 1.5 mL/min): *t*_{major} = 39.05 min, *t*_{minor} = 31.28 min; 93:7 er.

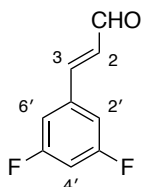
(4R)-4-[3'-Fluoro-5'-(trimethylstannyl)phenyl]-1-[(3''-methylpyridin-4''-yl)methyl]pyrrolidin-2-one ((R)-85)¹⁵³



Lithium chloride (0.265 g, 6.25 mmol) was added to a flask and dried in an oven at 140 °C overnight. (4R)-4-(3'-bromo-5'-fluorophenyl)-1-[(3''-methylpyridin-4''-yl)methyl]pyrrolidin-2-one ((R)-84) (0.454 g, 1.25 mmol) was dried under high vacuum for 1 h, purged with argon and dissolved in anhydrous toluene (13 mL). The oven-dried flask was cooled to room temperature *in vacuo* and then purged with argon. The (4R)-4-(3'-bromo-5'-fluorophenyl)-1-[(3''-methylpyridin-4''-yl)methyl]pyrrolidin-2-one ((R)-84) solution was added to the flask and degassed under argon for 0.33 h. Tetrakis(triphenylphosphine)palladium(0) (0.289 g, 0.250 mmol) was added and the mixture degassed under argon for a further 0.2 h. Hexamethylditin (0.520 mL, 2.51 mmol) was added and the reaction mixture was stirred under reflux for 24 h. After cooling to room temperature, the reaction was quenched with aqueous potassium fluoride (3 mL, 30% w/w) and stirred for 1 h. The crude mixture was filtered through a short pad of Celite[®] with ethyl acetate (300 mL) and concentrated *in vacuo*. The crude material was purified by flash column chromatography eluting with 5% methanol in diethyl ether to give (4R)-4-[3'-fluoro-5'-(trimethylstannyl)phenyl]-1-[(3''-methylpyridin-4''-yl)methyl] pyrrolidin-2-one ((R)-85) as a white solid (0.152 g, 27%). Mp 106–108 °C; $[\alpha]_{\text{D}}^{20} +25.1$ (c 0.1, CHCl₃). Spectroscopic data were consistent with the literature.¹⁵³ δ_{H} (400 MHz, CDCl₃) 0.29 (9H, s, 3 × CH₃), 2.31 (3H, s, CH₃), 2.65 (1H, dd, *J* 17.0, 8.2 Hz, 3-*HH*), 2.92 (1H, dd, *J* 17.0, 9.0 Hz, 3-*HH*), 3.21–3.33 (1H, m, 5-*HH*), 3.54–3.67 (2H, m, 4-H and 5-*HH*), 4.41 (1H, d, *J* 15.6 Hz, 7''-*HH*), 4.63 (1H, d, *J* 15.6 Hz, 7''-*HH*), 6.82 (1H, dt, *J* 10.0, 2.0 Hz, 2'-H), 7.01–7.11 (3H, m, 4'-H, 6'-H and 5''-H), 8.39–8.44 (2H, m, 2''-H and 6''-H); δ_{C} (101 MHz, CDCl₃) -9.3 (3 × CH₃), 16.1 (CH₃), 37.1 (d, ⁴*J*_{CF} 1.6 Hz, CH), 38.5 (CH₂), 43.7 (CH₂), 54.1 (CH₂), 113.4 (d, ²*J*_{CF} 21.8 Hz, CH), 121.0 (d, ²*J*_{CF} 17.5 Hz, CH), 122.4 (CH), 129.7 (d, ⁴*J*_{CF} 2.8 Hz, CH), 131.7 (C), 143.0 (C), 143.8

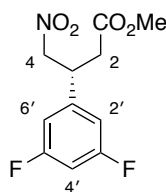
(d, $^3J_{CF}$ 5.6 Hz, C), 146.4 (d, $^3J_{CF}$ 2.8 Hz, C), 148.1 (CH), 151.4 (CH), 162.9 (d, $^1J_{CF}$ 252.8 Hz, C), 173.8 (C); m/z (ESI) 449 (MH⁺. 100%).

(E)-3-(3',5'-Difluorophenyl)prop-2-enal (100)



3,5-Difluorobenzaldehyde (**99**) (3.00 g, 21.1 mmol) and (triphenylphosphoranylidene)acetaldehyde (7.06 g, 23.2 mmol) were dissolved in anhydrous tetrahydrofuran (300 mL), under argon. The reaction mixture was heated to 50 °C and stirred for 21 h. The crude mixture was cooled to room temperature and concentrated *in vacuo*. The resultant residue was dissolved in ethyl acetate (100 mL) and washed with water (100 mL). The aqueous layer was extracted with ethyl acetate (2 × 100 mL). The combined organic layers were dried (MgSO₄), filtered and concentrated *in vacuo*. The crude material was purified by flash column chromatography eluting with 10% diethyl ether in petroleum ether (40–60) to give (*E*)-3-(3',5'-difluorophenyl)prop-2-enal (**100**) as a pale yellow solid (2.63 g, 74%). Mp 94–96 °C; ν_{max}/cm^{-1} (neat) 3094 (CH), 2970 (CH), 1690, 1670 (C=O), 1609 (C=C), 1589, 1450, 1323, 1115, 980, 837; δ_H (500 MHz, CDCl₃) 6.68 (1H, dd, J 16.0, 7.5 Hz, 2-H), 6.89 (1H, tt, J 8.5, 2.3 Hz, 4'-H), 7.05–7.11 (2H, m, 2'-H and 6'-H), 7.38 (1H, d, J 16.0 Hz, 3-H), 9.73 (1H, d, J 7.5 Hz, 1-H); δ_C (126 MHz, CDCl₃) 106.4 (t, $^2J_{CF}$ 25.4 Hz, CH), 111.2 (dd, $^2J_{CF}$ 19.8 Hz, $^4J_{CF}$ 6.3 Hz, 2 × CH), 130.7 (CH), 137.3 (t, $^3J_{CF}$ 9.5 Hz, C), 149.5 (t, $^4J_{CF}$ 3.0 Hz, CH), 163.4 (dd, $^1J_{CF}$ 250.2 Hz, $^3J_{CF}$ 12.6 Hz, 2 × C), 193.0 (CH); m/z (ESI) 191.0278 (MNa⁺. C₉H₆F₂NaO requires 191.0279).

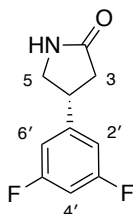
Methyl (3*R*)-3-(3',5'-difluorophenyl)-4-nitrobutanoate ((*R*)-103)



The reaction was carried out according to the previously described procedure for methyl (3*R*)-3-(3'-bromo-5'-fluorophenyl)-4-nitrobutanoate ((*R*)-98) using (*E*)-3-(3',5'-difluorophenyl)prop-2-enal (**100**) (0.530 g, 3.15 mmol), tetrahydrofuran (7 mL), water (1 mL), pivalic acid (0.0161 g, 0.158 mmol), boric acid (0.0977 g, 1.58 mmol), nitromethane (1.02 mL, 18.9 mmol) and (*R*)- α,α -bis[3,5-bis(trifluoromethyl)phenyl]-2-pyrrolidinemethanol trimethylsilyl ether ((*R*)-94) (0.0944 g, 0.158 mmol). (3*R*)-3-(3',5'-Difluorophenyl)-4-nitrobutanal ((*R*)-101) was afforded as a yellow oil, which was used without further purification. The subsequent reaction was carried out using (3*R*)-3-(3',5'-difluorophenyl)-4-nitrobutanal ((*R*)-101), acetonitrile (16 mL), potassium dihydrogen phosphate (0.320 g, 2.35 mmol) in water (8 mL), hydrogen peroxide (0.420 mL, 4.10 mmol, 30% w/w in water) and sodium chlorite (0.855 g, 9.45 mmol) in water (16 mL). The reaction mixture was stirred at 0 °C for 2 h then quenched with sodium sulfite (1.19 g, 9.45 mmol) and stirred at room temperature for 0.5 h. (3*R*)-3-(3',5'-Difluorophenyl)-4-nitrobutanoic acid ((*R*)-102) was afforded as a yellow oil, which was used without further purification. The subsequent reaction was carried out using (3*R*)-3-(3',5'-difluorophenyl)-4-nitrobutanoic acid ((*R*)-102), methanol (11 mL) and thionyl chloride (0.350 mL, 4.80 mmol). The crude material was purified by flash column chromatography eluting with 60% dichloromethane in hexane to give methyl (3*R*)-3-(3',5'-difluorophenyl)-4-nitrobutanoate ((*R*)-103) as a colourless oil, which solidified upon standing (0.449 g, 55% over three steps). Mp 51–53 °C; $\nu_{\max}/\text{cm}^{-1}$ (neat) 3094 (CH), 2959 (CH), 1732 (C=O), 1624, 1597, 1551, 1439, 1373, 1119, 980, 856; $[\alpha]_{\text{D}}^{19} +9.6$ (*c* 0.1, CHCl₃); δ_{H} (400 MHz, CDCl₃) 2.75 (1H, d, *J* 7.6 Hz, 2-*HH*), 2.75 (1H, d, *J* 7.2 Hz, 2-*HH*), 3.67 (3H, s, CH₃), 3.93–4.03 (1H, m, 3-*H*), 4.62 (1H, dd, *J* 13.0, 8.2 Hz, 4-*HH*), 4.73 (1H, dd, *J* 13.0, 6.6 Hz, 4-*HH*), 6.74 (1H, tt, *J* 8.6, 2.2 Hz, 4'-*H*), 6.75–6.82 (2H, m, 2'-*H* and 6'-*H*); δ_{C} (101 MHz, CDCl₃) 37.2 (CH₂), 39.9 (t, $^4J_{\text{CF}}$ 2.1 Hz, CH), 52.3 (CH₃), 78.8 (CH₂), 103.9 (t, $^2J_{\text{CF}}$ 25.3 Hz, CH), 110.7 (dd, $^2J_{\text{CF}}$ 18.8 Hz, $^4J_{\text{CF}}$ 7.3 Hz, 2 × CH), 142.3 (t, $^3J_{\text{CF}}$ 8.9 Hz, C), 163.4 (dd, $^1J_{\text{CF}}$ 251.1 Hz, $^3J_{\text{CF}}$ 12.9 Hz, 2 × C), 170.6 (C); *m/z* (ESI) 282.0547

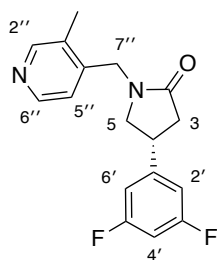
(MNa⁺. C₁₁H₁₁F₂NNaO₄ requires 282.0548). The enantiomeric ratio was determined by HPLC analysis with a CHIRALCEL[®] AD-H column (95:5, hexane: *i*-PrOH, flow rate of 1.0 mL/min): *t*_{major} = 14.84 min, *t*_{minor} = 12.30 min; 93:7 er.

(4*R*)-4-(3',5'-Difluorophenyl)pyrrolidin-2-one ((*R*)-104)



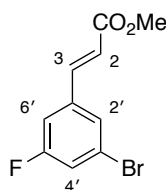
The reaction was carried out according to the previously described procedure for (4*R*)-4-(3'-bromo-5'-fluorophenyl)pyrrolidin-2-one ((*R*)-83) using methyl (3*R*)-3-(3',5'-difluorophenyl)-4-nitrobutanoate ((*R*)-103) (0.418 g, 1.61 mmol), methanol (8 mL), nickel(II) chloride hexahydrate (0.0383 g, 0.161 mmol) and sodium borohydride (0.305 g, 8.05 mmol). The reaction mixture was stirred at room temperature for 0.75 h and then filtered through a short pad of Celite[®] with dichloromethane (50 mL). The filtrate was concentrated *in vacuo* at 45 °C for 1.5 h. The resultant residue was dissolved in chloroform (20 mL) and washed with water (20 mL). The organic and aqueous layers were separated, and the aqueous layer was extracted with chloroform (2 × 20 mL). The combined organic layers were dried (MgSO₄), filtered and concentrated *in vacuo*. The crude material was purified by flash column chromatography eluting with 5% methanol in diethyl ether to give (4*R*)-4-(3',5'-difluorophenyl)pyrrolidin-2-one ((*R*)-104) as a white solid (0.138 g, 43%). Mp 94–96 °C; $\nu_{\text{max}}/\text{cm}^{-1}$ (neat) 3314 (NH), 3186 (CH), 2924 (CH), 1694 (C=O), 1659, 1624, 1597, 1447, 1304, 1115, 980, 856; $[\alpha]_{\text{D}}^{19}$ -25.9 (*c* 0.1, CHCl₃); δ_{H} (400 MHz, CDCl₃) 2.44 (1H, dd, *J* 16.9, 8.2 Hz, 3-*HH*), 2.74 (1H, dd, *J* 16.9, 9.0 Hz, 3-*HH*), 3.39 (1H, dd, *J* 9.6, 6.8 Hz, 5-*HH*), 3.61–3.72 (1H, m, 4-*H*), 3.75–3.83 (1H, m, 5-*HH*), 6.67–6.74 (1H, br s, NH), 6.71 (1H, tt, *J* 8.8, 2.4 Hz, 4'-*H*), 6.75–6.81 (2H, m, 2'-*H* and 6'-*H*); δ_{C} (101 MHz, CDCl₃) 37.7 (CH₂), 40.0 (t, ⁴*J*_{CF} 2.1 Hz, CH), 49.1 (CH₂), 102.8 (t, ²*J*_{CF} 25.2 Hz, CH), 109.9 (dd, ²*J*_{CF} 18.5 Hz, ⁴*J*_{CF} 7.0 Hz, 2 × CH), 146.2 (t, ³*J*_{CF} 8.8 Hz, C), 163.4 (dd, ¹*J*_{CF} 250.1 Hz, ³*J*_{CF} 12.9 Hz, 2 × C), 177.1 (C); *m/z* (ESI) 220.0539 (MNa⁺. C₁₀H₉F₂NNaO requires 220.0544). The enantiomeric ratio was determined by HPLC analysis with a CHIRALCEL[®] AD-H column (95:5, hexane: *i*-PrOH, flow rate of 1.0 mL/min): *t*_{major} = 18.85 min, *t*_{minor} = 26.08 min; 94:6 er.

(4*R*)-4-(3',5'-Difluorophenyl)-1-[(3''-methylpyridin-4''-yl)methyl]pyrrolidin-2-one ((*R*)-24)¹⁵³



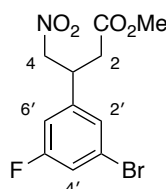
In an oven-dried flask under argon, (4*R*)-4-(3',5'-difluorophenyl)pyrrolidin-2-one ((*R*)-104) (0.120 g, 0.608 mmol), 4-(chloromethyl)-3-methylpyridine hydrochloride (0.141 g, 0.791 mmol) and potassium iodide (0.101 g, 0.608 mmol) were dissolved in anhydrous tetrahydrofuran (3 mL) and cooled to 0 °C. Sodium hydride (0.0980 g, 2.43 mmol, 60% dispersion in mineral oil) was added and the solution was warmed to room temperature and then to 60 °C. The reaction mixture was stirred at 60 °C for 19 h. After cooling to 0 °C, the reaction was quenched with water (20 mL) and concentrated *in vacuo*. The resultant residue was dissolved in ethyl acetate (20 mL) and washed with water (20 mL). The aqueous layer was extracted with ethyl acetate (2 × 20 mL). The combined organic layers were dried (MgSO₄), filtered and concentrated *in vacuo*. The crude material was purified by flash column chromatography eluting with 10% methanol in diethyl ether to give (4*R*)-4-(3',5'-difluorophenyl)-1-[(3''-methylpyridin-4''-yl)methyl]pyrrolidin-2-one ((*R*)-24) as a white solid (0.0830 g, 45%). Mp 106–108 °C; [α]_D¹⁹ +21.9 (*c* 0.1, CHCl₃). Spectroscopic data were consistent with previously published data.¹⁵³ δ_H (400 MHz, CDCl₃) 2.31 (3H, s, CH₃), 2.60 (1H, dd, *J* 17.0, 8.2 Hz, 3-*HH*), 2.91 (1H, dd, *J* 17.0, 8.6 Hz, 3-*HH*), 3.24 (1H, dd, *J* 8.0, 5.6 Hz, 5-*HH*), 3.53–3.66 (2H, m, 4-*H* and 5-*HH*), 4.42 (1H, d, *J* 15.6 Hz, 7''-*HH*), 4.62 (1H, d, *J* 15.6 Hz, 7''-*HH*), 6.66–6.76 (3H, m, 2'-*H*, 4'-*H* and 6'-*H*), 7.04 (1H, d, *J* 5.2 Hz, 5''-*H*), 8.39–8.45 (2H, m, 2''-*H* and 6''-*H*); δ_C (101 MHz, CDCl₃) 16.1 (CH₃), 37.1 (t, ⁴*J*_{CF} 2.1 Hz, CH), 38.2 (CH₂), 43.7 (CH₂), 53.5 (CH₂), 102.9 (t, ²*J*_{CF} 25.4 Hz, CH), 109.8 (dd, ²*J*_{CF} 18.6 Hz, ⁴*J*_{CF} 7.0 Hz, 2 × CH), 122.5 (CH), 131.7 (C), 142.8 (C), 145.8 (t, ³*J*_{CF} 8.8 Hz, C), 148.1 (CH), 151.5 (CH), 163.4 (dd, ¹*J*_{CF} 250.4 Hz, ³*J*_{CF} 12.8 Hz, 2 × C), 173.2 (C); *m/z* (ESI) 303 (MH⁺, 100%). The enantiomeric ratio was determined by HPLC analysis with a CHIRALCEL® AD-H column (90:10, hexane:*i*PrOH, flow rate of 1.5 mL/min): *t*_{major} = 27.60 min, *t*_{minor} = 22.20 min; 82:18 er.

(*E*)-Methyl 3-(3'-bromo-5'-fluorophenyl)prop-2-enoate (**108**)



3-Bromo-5-fluorobenzaldehyde (**79**) (6.80 g, 33.5 mmol) and methyl (triphenylphosphoranylidene)acetate (12.3 g, 36.9 mmol) were dissolved in anhydrous tetrahydrofuran (335 mL), under argon. The reaction mixture was stirred at room temperature for 18 h and then concentrated *in vacuo*. The crude material was purified by flash column chromatography eluting with 5% diethyl ether in petroleum ether (40–60) to give (*E*)-methyl 3-(3'-bromo-5'-fluorophenyl)prop-2-enoate (**108**) as a white solid (7.79 g, 90%). Mp 98–100 °C; $\nu_{\max}/\text{cm}^{-1}$ (neat) 3075 (CH), 2951 (CH), 1709 (C=O), 1639 (C=C), 1570, 1261, 1234, 1177, 999, 841; δ_{H} (500 MHz, CDCl_3) 3.82 (3H, s, CH_3), 6.42 (1H, d, J 16.0 Hz, 2-H), 7.15 (1H, dt, J 9.0, 2.0 Hz, 4'-H), 7.26 (1H, dt J 7.8, 2.0 Hz, 6'-H), 7.44 (1H, t, J 2.0 Hz, 2'-H), 7.56 (1H, d, J 16.0 Hz, 3-H); δ_{C} (126 MHz, CDCl_3) 52.1 (CH_3), 113.5 (d, $^2J_{\text{CF}}$ 22.2 Hz, CH), 120.7 (d, $^2J_{\text{CF}}$ 24.7 Hz, CH), 120.8 (CH), 123.3 (d, $^3J_{\text{CF}}$ 10.0 Hz, C), 127.1 (d, $^4J_{\text{CF}}$ 3.2 Hz, CH), 138.0 (d, $^3J_{\text{CF}}$ 8.4 Hz, C), 142.0 (d, $^4J_{\text{CF}}$ 2.7 Hz, CH), 162.9 (d, $^1J_{\text{CF}}$ 251.6 Hz, C), 166.7 (C); m/z (EI) 257.9690 (M^+ , $\text{C}_{10}\text{H}_8^{79}\text{BrFO}_2$ requires 257.9692), 227 (100%), 120 (100), 94 (17), 86 (31), 84 (49).

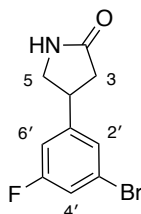
Methyl (\pm)-3-(3'-bromo-5'-fluorophenyl)-4-nitrobutanoate (**98**)



To a stirred solution of (*E*)-methyl 3-(3'-bromo-5'-fluorophenyl)prop-2-enoate (**108**) (0.383 g, 1.48 mmol) in anhydrous acetonitrile (7 mL), under argon, was added nitromethane (0.400 mL, 7.40 mmol). The reaction mixture was cooled to 0 °C and 1,8-diazabicyclo[5.4.0]undec-7-ene (0.230 mL, 1.54 mmol) was added dropwise over 1 h and stirred for a further 2 h. The crude mixture was concentrated *in vacuo*

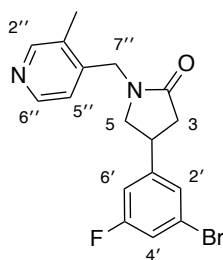
and the resulting residue was partitioned between ethyl acetate (15 mL) and water (15 mL). The aqueous layer was extracted with ethyl acetate (2 × 15 mL). The combined organic layers were dried (MgSO₄), filtered and concentrated *in vacuo*. The crude material was purified by flash column chromatography eluting with 60% dichloromethane in hexane to give methyl (±)-3-(3'-bromo-5'-fluorophenyl)-4-nitrobutanoate (**98**) as a colourless oil, which solidified upon standing (0.305 g, 64%). Spectroscopic data as for ((**R**)-**98**). The enantiomeric ratio was determined by HPLC analysis with a CHIRALCEL[®] AD-H column (98:2, hexane:*i*PrOH, flow rate of 1.0 mL/min): t_{Peak1} = 20.30 min, t_{Peak2} = 22.50 min; 50:50 er.

(±)-4-(3'-Bromo-5'-fluorophenyl)pyrrolidin-2-one (83)¹⁵²



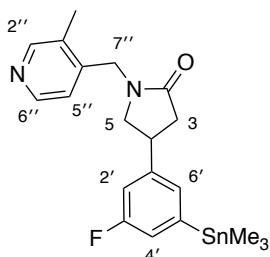
The reaction was carried out according to the previously described procedure for (4*R*)-4-(3'-bromo-5'-fluorophenyl)pyrrolidin-2-one ((**R**)-**83**) using methyl (±)-3-(3'-bromo-5'-fluorophenyl)-4-nitrobutanoate (**98**) (1.02 g, 3.19 mmol), methanol (16 mL), nickel(II) chloride hexahydrate (0.0758 g, 0.319 mmol) and sodium borohydride (0.605 g, 16.0 mmol). The crude material was purified by flash column chromatography eluting with 4% methanol in dichloromethane to give (±)-4-(3'-bromo-5'-fluorophenyl)pyrrolidin-2-one (**83**) and (±)-4-(3'-fluorophenyl)pyrrolidin-2-one (**109**) in a ratio of 1 : 0.10 as a colourless oil, which solidified upon standing (0.428 g, 52%). Spectroscopic data as for ((**R**)-**83**). The enantiomeric ratio was determined by HPLC analysis with a CHIRALCEL[®] AD-H column (97:3, hexane:*i*PrOH, flow rate of 1.0 mL/min): t_{Peak1} = 27.62 min, t_{Peak2} = 36.91 min; 50:50 er.

(±)-4-(3'-Bromo-5'-fluorophenyl)-1-[(3''-methylpyridin-4''-yl)methyl]pyrrolidin-2-one (84**)**¹⁵³



The reaction was carried out according to the previously described procedure for (4*R*)-4-(3',5'-difluorophenyl)-1-[(3''-methylpyridin-4''-yl)methyl]pyrrolidin-2-one ((*R*)-**24**) using (±)-4-(3'-bromo-5'-fluorophenyl)pyrrolidin-2-one (**83**) (0.350 g, 1.36 mmol), 4-(chloromethyl)-3-methylpyridine hydrochloride (0.315 g, 1.77 mmol), potassium iodide (0.226 g, 1.36 mmol), anhydrous tetrahydrofuran (7 mL) and sodium hydride (0.218 g, 5.44 mmol, 60% dispersion in mineral oil). The crude material was purified by flash column chromatography eluting with a 5–10% gradient of methanol in diethyl ether to give (±)-4-(3'-bromo-5'-fluorophenyl)-1-[(3''-methylpyridin-4''-yl)methyl]pyrrolidin-2-one (**84**) as a colourless oil, which solidified upon standing (0.220 g, 45%). Spectroscopic data as for ((*R*)-**84**). The enantiomeric ratio was determined by HPLC analysis with a CHIRALCEL® AD-H column (92:8, hexane:*i*PrOH, flow rate of 1.5 mL/min): $t_{Peak1} = 30.95$ min, $t_{Peak2} = 39.23$ min; 49:51 er.

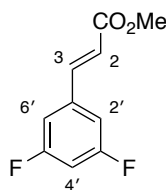
(±)-4-[3'-Fluoro-5'-(trimethylstannyl)phenyl]-1-[(3''-methylpyridin-4''-yl)methyl]pyrrolidin-2-one (85**)**¹⁵³



The reaction was carried out according to the previously described procedure for (4*R*)-4-[3'-fluoro-5'-(trimethylstannyl)phenyl]-1-[(3''-methylpyridin-4''-yl)methyl]pyrrolidin-2-one ((*R*)-**85**) using lithium chloride (0.348 g, 8.20 mmol), (±)-

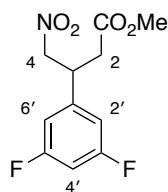
4-(3'-bromo-5'-fluorophenyl)-1-[(3''-methylpyridin-4''-yl)methyl]pyrrolidin-2-one (**84**) (0.596 g, 1.64 mmol), anhydrous toluene (16 mL), tetrakis(triphenylphosphine)palladium(0) (0.379 g, 0.328 mmol) and hexamethylditin (0.700 mL, 3.39 mmol). The crude material was purified by flash column chromatography eluting with 5% methanol in diethyl ether to give (±)-4-[3'-fluoro-5'-(trimethylstannyl)phenyl]-1-[(3''-methylpyridin-4''-yl)methyl]pyrrolidin-2-one (**85**) as a white solid (0.524 g, 71%). Spectroscopic data as for ((**R**)-**85**).

(E)-Methyl 3-(3',5'-difluorophenyl)prop-2-enoate (105)



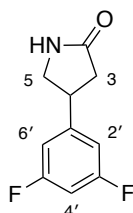
The reaction was carried out according to the previously described procedure for (*E*)-methyl 3-(3'-bromo-5'-fluorophenyl)prop-2-enoate (**108**) using 3,5-difluorobenzaldehyde (**99**) (1.42 g, 10.0 mmol), methyl (triphenylphosphoranylidene)acetate (3.68 g, 11.0 mmol) and anhydrous tetrahydrofuran (200 mL). The reaction mixture was stirred at room temperature for 16 h. The crude material was purified by flash column chromatography eluting with 5% diethyl ether in petroleum ether (40–60) to give (*E*)-methyl 3-(3',5'-difluorophenyl)prop-2-enoate (**105**) as a white solid (1.73 g, 87%). Mp 93–95 °C; $\nu_{\text{max}}/\text{cm}^{-1}$ (neat) 3090 (CH), 2959 (CH), 1724 (C=O), 1639 (C=C), 1620, 1589, 1431, 1281, 1172, 1119, 980, 845; δ_{H} (500 MHz, CDCl_3) 3.82 (3H, s, CH_3), 6.42 (1H, d, J 16.0 Hz, 2-H), 6.83 (1H, tt, J 8.5, 2.3 Hz, 4'-H), 6.99–7.06 (2H, m, 2'-H and 6'-H), 7.58 (1H, d, J 16.0 Hz, 3-H); δ_{C} (126 MHz, CDCl_3) 52.1 (CH_3), 105.6 (t, $^2J_{\text{CF}}$ 25.5 Hz, CH), 110.8 (dd, $^2J_{\text{CF}}$ 19.8 Hz, $^4J_{\text{CF}}$ 6.2 Hz, 2 × CH), 120.7 (CH), 137.8 (t, $^3J_{\text{CF}}$ 9.6 Hz, C), 142.4 (t, $^4J_{\text{CF}}$ 3.0 Hz, CH), 163.4 (dd, $^1J_{\text{CF}}$ 249.3 Hz, $^3J_{\text{CF}}$ 12.7 Hz, 2 × C), 166.8 (C); m/z (EI) 198.0501 (M^+ . $\text{C}_{10}\text{H}_8\text{F}_2\text{O}_2$ requires 198.0492), 167 (100%), 139 (38), 119 (31), 78 (18), 63 (25).

Methyl (\pm)-3-(3',5'-difluorophenyl)-4-nitrobutanoate (**103**)⁴³³



To a stirred solution of (*E*)-methyl 3-(3',5'-difluorophenyl)prop-2-enoate (**105**) (1.71 g, 8.65 mmol) in anhydrous acetonitrile (40 mL) under argon, was added nitromethane (2.35 mL, 43.3 mmol). The reaction mixture was cooled to 0 °C and 1,8-diazabicyclo[5.4.0]undec-7-ene (1.29 mL, 8.65 mmol) was added dropwise over 0.5 h. The reaction mixture was left stirring in an ice bath at 0 °C and allowed to slowly reach room temperature over 16 h. The reaction mixture was concentrated *in vacuo* and the resulting residue was partitioned between ethyl acetate (20 mL) and water (20 mL). The aqueous layer was extracted with ethyl acetate (2 × 20 mL). The combined organic layers were dried (MgSO₄), filtered and concentrated *in vacuo*. The crude material was purified by flash column chromatography eluting with 60% dichloromethane in hexane to give methyl (\pm)-3-(3',5'-difluorophenyl)-4-nitrobutanoate (**103**) as a colourless oil, which solidified upon standing (1.05 g, 47%). Spectroscopic data as for (*R*)-**103**. The enantiomeric ratio was determined by HPLC analysis with a CHIRALCEL[®] AD-H column (95:5, hexane:*i*PrOH, flow rate of 1.0 mL/min): t_{Peak1} = 12.42 min, t_{Peak2} = 14.98 min; 50:50 er.

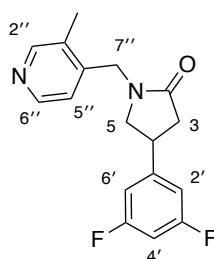
(\pm)-4-(3',5'-Difluorophenyl)pyrrolidin-2-one (**104**)¹⁵³



The reaction was carried out according to the previously described procedure for (4*R*)-4-(3'-bromo-5'-fluorophenyl)pyrrolidin-2-one (*(R)*-**83**) using methyl (\pm)-3-(3',5'-difluorophenyl)-4-nitrobutanoate (**103**) (0.078 g, 0.30 mmol), methanol (1.5 mL), nickel(II) chloride hexahydrate (0.0071 g, 0.030 mmol) and sodium borohydride (0.057 g, 1.5 mmol). The reaction mixture was stirred at room temperature for 0.75

h and then diluted with dichloromethane (14 mL). The resulting solution was filtered through a short pad of silica with 10% methanol in dichloromethane (100 mL) and concentrated *in vacuo* at 45 °C. The crude residue was dissolved in chloroform (30 mL) and washed with water (20 mL). The aqueous layer was extracted with chloroform (2 × 20 mL). The combined organic layers were dried (MgSO₄), filtered and concentrated *in vacuo*. The crude material was purified by flash column chromatography eluting with 4% methanol in dichloromethane to give (±)-4-(3',5'-difluorophenyl)pyrrolidin-2-one (**104**) as a white solid (0.037 g, 63%). Spectroscopic data as for ((**R**)-**104**). The enantiomeric ratio was determined by HPLC analysis with a CHIRALCEL[®] AD-H column (95:5, hexane:PrOH, flow rate of 1.0 mL/min): t_{Peak1} = 18.62 min, t_{Peak2} = 25.85 min; 50:50 er.

(±)-4-(3',5'-Difluorophenyl)-1-[(3''-methylpyridin-4''-yl)methyl]pyrrolidin-2-one (24**)**¹⁵³



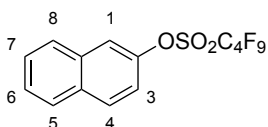
The reaction was carried out according to the previously described procedure for (4*R*)-4-(3',5'-difluorophenyl)-1-[(3''-methylpyridin-4''-yl)methyl]pyrrolidin-2-one ((**R**)-**24**) using (±)-4-(3',5'-difluorophenyl)pyrrolidin-2-one (**104**) (0.100 g, 0.507 mmol), 4-(chloromethyl)-3-methylpyridine hydrochloride (0.117 g, 0.659 mmol), potassium iodide (0.0842 g, 0.507 mmol), anhydrous tetrahydrofuran (3 mL) and sodium hydride (0.0812 g, 2.03 mmol, 60% dispersion in mineral oil). The reaction mixture was stirred at 60 °C for 18 h. After cooling to room temperature, the reaction was quenched with water (30 mL) and the mixture was extracted with ethyl acetate (3 × 30 mL). The combined organic layers were dried (MgSO₄), filtered and concentrated *in vacuo*. The crude material was purified by flash column chromatography eluting with 0–3% gradient of methanol in dichloromethane to give (±)-4-(3',5'-difluorophenyl)-1-[(3''-methylpyridin-4''-yl)methyl]pyrrolidin-2-one (**24**) as a white solid (0.0980 g, 64%). Spectroscopic data as for ((**R**)-**24**). The enantiomeric ratio was determined by HPLC analysis with a CHIRALCEL[®] AD-H column (90:10,

hexane:PrOH, flow rate of 1.5 mL/min): $t_{major} = 27.66$ min, $t_{minor} = 22.09$ min; 51:49
er.

3.5 Transition Metal-Catalysed Reactions of Aryl Nonaflates

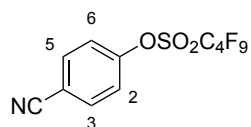
Experimental

2-Naphthyl nonafluorobutanesulfonate (**139**)⁴³⁴



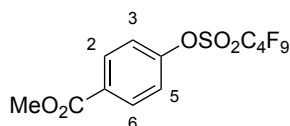
In an oven-dried flask under argon, 2-naphthol (1.00 g, 6.94 mmol) was dissolved in anhydrous dichloromethane (15 mL) and cooled to 0 °C. Triethylamine (2.42 mL, 17.4 mmol) was then added followed by perfluoro-1-butanesulfonyl fluoride (1.87 mL, 10.4 mmol). The reaction mixture was warmed to room temperature and stirred for 1 h. The crude mixture was then diluted with dichloromethane (50 mL) and washed with water (3 × 50 mL). The organic layer was dried (MgSO₄), filtered and concentrated *in vacuo*. The crude material was purified by flash column chromatography eluting with 5% ethyl acetate in petroleum ether (40–60) to give 2-naphthyl nonafluorobutanesulfonate (**139**) as a colourless oil (1.97 g, 67%). Spectroscopic data were consistent with the literature.⁴³⁴ δ_H (400 MHz, CDCl₃) 7.39 (1H, dd, J 9.0, 2.5 Hz, 3-H), 7.54–7.63 (2H, m, 2 × ArH), 7.77 (1H, d, J 2.5 Hz, 1-H), 7.84–7.92 (2H, m, 2 × ArH), 7.93 (1H, d, J 9.0 Hz, 4-H); δ_C (101 MHz, CDCl₃) 119.4 (CH), 119.7 (CH), 127.3 (CH), 127.7 (CH), 128.1 (CH), 128.2 (CH), 130.7 (CH), 132.5 (C), 133.5 (C), 147.5 (C); m/z (ESI) 425 ((M-H)⁻, 100%).

4-Cyanophenyl nonafluorobutanesulfonate (**140**)²⁹⁵



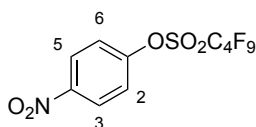
The reaction was carried out according to the previously described procedure for 2-naphthyl nonafluorobutanesulfonate (**139**) using 4-cyanophenol (0.200 g, 1.68 mmol), anhydrous dichloromethane (5 mL), triethylamine (0.590 mL, 4.23 mmol) and perfluoro-1-butanesulfonyl fluoride (0.460 mL, 2.56 mmol). The reaction mixture was stirred at room temperature for 2 h. The crude material was purified by flash column chromatography eluting with 20% ethyl acetate in petroleum ether (40–60) to give 4-cyanophenyl nonafluorobutanesulfonate (**140**) as a white solid (0.609 g, 90%). Mp 109–110 °C (lit.²⁹⁵ 111–112 °C); δ_{H} (500 MHz, CDCl_3) 7.44 (2H, d, J 9.0 Hz, 2-H and 6-H), 7.79 (2H, d, J 9.0 Hz, 3-H and 5-H); δ_{C} (101 MHz, CDCl_3) 113.0 (C), 117.2 (C), 122.8 (2 \times CH), 134.6 (2 \times CH), 152.4 (C); m/z (EI) 401 (M^+ , 38%), 337 (33), 219 (12), 118 (47), 102 (100), 90 (71), 77 (41), 69 (99).

Methyl 4-nonafluorobutanesulfonyloxybenzoate (**141**)²⁹⁵



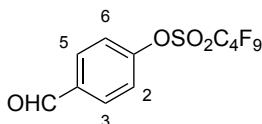
The reaction was carried out according to the previously described procedure for 2-naphthyl nonafluorobutanesulfonate (**139**) using methyl 4-hydroxybenzoate (0.200 g, 1.32 mmol), anhydrous dichloromethane (5 mL), triethylamine (0.460 mL, 3.30 mmol) and perfluoro-1-butanesulfonyl fluoride (0.360 mL, 2.00 mmol). The reaction mixture was stirred at room temperature for 16 h. The crude material was purified by flash column chromatography eluting with 15% ethyl acetate in petroleum ether (40–60) to give methyl 4-nonafluorobutanesulfonyloxybenzoate (**141**) as a colourless oil (0.526 g, 92%). Spectroscopic data were consistent with the literature.²⁹⁵ δ_{H} (400 MHz, CDCl_3) 3.94 (3H, s, OCH_3), 7.36 (2H, d, J 8.9 Hz, 3-H and 5-H), 8.14 (2H, d, J 8.9 Hz, 2-H and 6-H); δ_{C} (101 MHz, CDCl_3) 52.7 (CH_3), 121.6 (2 \times CH), 130.5 (C), 132.0 (2 \times CH), 152.9 (C), 165.6 (C); m/z (EI) 434 (M^+ , 70%), 403 (40), 339 (100), 151 (38), 123 (42).

4-Nitrophenyl nonafluorobutanesulfonate (**142**)²⁹⁹



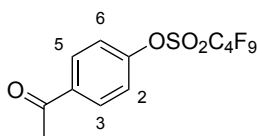
The reaction was carried out according to the previously described procedure for 2-naphthyl nonafluorobutanesulfonate (**139**) using 4-nitrophenol (0.200 g, 1.44 mmol), anhydrous dichloromethane (5 mL), triethylamine (0.500 mL, 3.59 mmol) and perfluoro-1-butanesulfonyl fluoride (0.390 mL, 2.17 mmol). The reaction mixture was stirred at room temperature for 3 h. The crude material was purified by flash column chromatography eluting with 10% ethyl acetate in hexane to give 4-nitrophenyl nonafluorobutanesulfonate (**142**) as a white solid (0.521 g, 86%). Mp 67–68 °C (lit.²⁹⁹ 68–70 °C); δ_{H} (400 MHz, CDCl_3) 7.49 (2H, d, J 9.2 Hz, 2-H and 6-H), 8.36 (2H, d, J 9.2 Hz, 3-H and 5-H); δ_{C} (101 MHz, CDCl_3) 122.6 (2 \times CH), 126.1 (2 \times CH), 147.3 (C), 153.5 (C); m/z (EI) 421 (M^+ , 30%), 327 (29), 219 (12), 131 (40), 77 (99), 69 (100).

4-Formylphenyl nonafluorobutanesulfonate (**143**)²⁹⁹



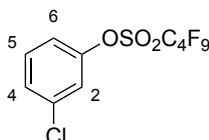
The reaction was carried out according to the previously described procedure for 2-naphthyl nonafluorobutanesulfonate (**139**) using 4-hydroxybenzaldehyde (0.100 g, 0.819 mmol), anhydrous dichloromethane (3 mL), triethylamine (0.290 mL, 2.08 mmol) and perfluoro-1-butanesulfonyl fluoride (0.220 mL, 1.22 mmol). The reaction mixture was stirred at room temperature for 1.5 h. The crude material was purified by flash column chromatography eluting with 30% ethyl acetate in petroleum ether (40–60) to give 4-formylphenyl nonafluorobutanesulfonate (**143**) as a viscous oil (0.280 g, 85%). Spectroscopic data were consistent with the literature.²⁹⁹ δ_{H} (500 MHz, CDCl_3) 7.48 (2H, d, J 8.7 Hz, 2-H and 6-H), 8.01 (2H, d, J 8.7 Hz, 3-H and 5-H), 10.05 (1H, s, CHO); δ_{C} (101 MHz, CDCl_3) 122.4 (2 \times CH), 131.9 (2 \times CH), 136.0 (C), 153.6 (C), 190.2 (CH); m/z (EI) 404 (M^+ , 40%), 339 (100), 219 (8), 121 (15), 93 (25), 65 (43).

4-Acetylphenyl nonafluorobutanesulfonate (**144**)²⁹⁵



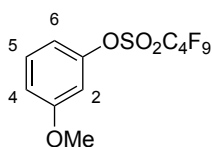
The reaction was carried out according to the previously described procedure for 2-naphthyl nonafluorobutanesulfonate (**139**) using 4-hydroxyacetophenone (0.272 g, 2.00 mmol), anhydrous dichloromethane (6 mL), triethylamine (0.700 mL, 5.02 mmol) and perfluoro-1-butanesulfonyl fluoride (0.540 mL, 3.01 mmol). The reaction mixture was stirred at room temperature for 2 h. The crude material was purified by flash column chromatography eluting with 50% diethyl ether in hexane to give 4-acetylphenyl nonafluorobutanesulfonate (**144**) as a white solid (0.786 g, 94%). Mp 38–40 °C (lit.²⁹⁵ 38–40 °C); δ_{H} (500 MHz, CDCl_3) 2.63 (3H, s, CH_3), 7.39 (2H, d, J 8.9 Hz, 2-H and 6-H), 8.06 (2H, d, J 8.9 Hz, 3-H and 5-H); δ_{C} (126 MHz, CDCl_3) 26.8 (CH_3), 121.8 (2 \times CH), 130.7 (2 \times CH), 137.0 (C), 152.9 (C), 196.3 (C); m/z (EI) 418 (M^+ , 30%), 403 (100), 339 (38), 219 (8), 131 (11), 120 (37), 107 (38).

3-Chlorophenyl nonafluorobutanesulfonate (**145**)⁴³⁵



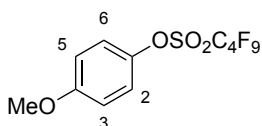
The reaction was carried out according to the previously described procedure for 2-naphthyl nonafluorobutanesulfonate (**139**) using 3-chlorophenol (0.257 g, 2.00 mmol), anhydrous dichloromethane (6 mL), triethylamine (0.700 mL, 5.02 mmol) and perfluoro-1-butanesulfonyl fluoride (0.540 mL, 3.01 mmol). The reaction mixture was stirred at room temperature for 2 h. The crude material was purified by flash column chromatography eluting with 100% hexane to give 3-chlorophenyl nonafluorobutanesulfonate (**145**) as a colourless oil (0.672 g, 82%). Spectroscopic data were consistent with the literature.⁴³⁵ δ_{H} (400 MHz, CDCl_3) 7.18–7.24 (1H, m, ArH), 7.30–7.33 (1H, m, ArH), 7.37–7.43 (2H, m, 2 \times ArH); δ_{C} (101 MHz, CDCl_3) 119.9 (CH), 122.2 (CH), 129.0 (CH), 131.1 (CH), 135.8 (C), 149.9 (C); m/z (EI) 410 (M^+ , 33%), 348 (9), 346 (27), 127 (28), 111 (44), 99 (34), 84 (100).

3-Methoxyphenyl nonafluorobutanesulfonate (**146**)²⁸⁹



The reaction was carried out according to the previously described procedure for 2-naphthyl nonafluorobutanesulfonate (**139**) using 3-methoxyphenol (0.219 mL, 2.00 mmol), anhydrous dichloromethane (6 mL), triethylamine (0.700 mL, 5.02 mmol) and perfluoro-1-butanesulfonyl fluoride (0.540 mL, 3.01 mmol). The reaction mixture was stirred at room temperature for 2 h. The crude material was purified by flash column chromatography eluting with 20% diethyl ether in hexane to give 3-methoxyphenyl nonafluorobutanesulfonate (**146**) as a colourless oil (0.747 g, 92%). Spectroscopic data were consistent with the literature.²⁸⁹ δ_{H} (400 MHz, CDCl_3) 3.83 (3H, s, OCH_3), 6.82 (1H, t, J 2.4 Hz, 2-H), 6.89 (1H, ddd, J 8.4, 2.4, 0.8 Hz, 4-H), 6.93 (1H, ddd, J 8.4, 2.4, 0.8 Hz, 6-H), 7.34 (1H, t, J 8.4 Hz, 5-H); δ_{C} (101 MHz, CDCl_3) 55.8 (CH_3), 107.7 (CH), 113.4 (CH), 114.2 (CH), 130.7 (CH), 150.6 (C), 161.0 (C); m/z (ESI) 429 (MNa^+ , 100%).

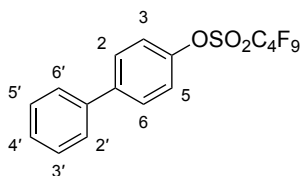
4-Methoxyphenyl nonafluorobutanesulfonate (**147**)²⁹⁵



The reaction was carried out according to the previously described procedure for 2-naphthyl nonafluorobutanesulfonate (**139**) using 4-methoxyphenol (0.372 g, 3.00 mmol), anhydrous dichloromethane (10 mL), triethylamine (1.05 mL, 7.50 mmol) and perfluoro-1-butanesulfonyl fluoride (0.810 mL, 4.50 mmol). The reaction mixture was stirred at room temperature for 2 h. The crude material was purified by flash column chromatography eluting with 10% diethyl ether in petroleum ether (40–60) to give 4-methoxyphenyl nonafluorobutanesulfonate (**147**) as a colourless oil (1.13 g, 93%). Spectroscopic data were consistent with the literature.²⁹⁵ δ_{H} (500 MHz, CDCl_3) 3.82 (3H, s, CH_3), 6.92 (2H, d, J 9.2 Hz, 3-H and 5-H), 7.21 (2H, d, J 9.2 Hz,

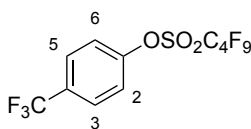
2-H and 6-H); δ_{C} (126 MHz, CDCl_3) 55.8 (CH_3), 115.2 (2 \times CH), 122.5 (2 \times CH), 143.4 (C), 159.2 (C); m/z (EI) 406 (M^+ , 12%), 219 (5), 123 (100), 95 (14), 69 (11).

(1,1'-Biphenyl)-4-yl nonafluorobutanesulfonate (**155**)⁴³⁶



The reaction was carried out according to the previously described procedure for 2-naphthyl nonafluorobutanesulfonate (**139**) using 4-phenylphenol (0.340 g, 2.00 mmol), anhydrous dichloromethane (6 mL), triethylamine (0.700 mL, 5.02 mmol) and perfluoro-1-butanesulfonyl fluoride (0.540 mL, 3.01 mmol). The reaction mixture was stirred at room temperature for 2 h. The crude material was purified by flash column chromatography eluting with 10% diethyl ether in hexane to give (1,1'-biphenyl)-4-yl nonafluorobutanesulfonate (**155**) as a white solid (0.838 g, 93%). Mp 45–47 °C (lit.⁴³⁶ 45.5–46.7 °C); δ_{H} (400 MHz, CDCl_3) 7.36 (2H, d, J 8.8 Hz, 3-H and 5-H), 7.38–7.42 (1H, m, 4'-H), 7.44–7.49 (2H, m, 3'-H and 5'-H), 7.54–7.58 (2H, m, 2'-H and 6'-H), 7.65 (2H, d, J 8.8 Hz, 2-H and 6-H); δ_{C} (101 MHz, CDCl_3) 121.8 (2 \times CH), 127.3 (2 \times CH), 128.2 (CH), 129.0 (2 \times CH), 129.1 (2 \times CH), 139.5 (C), 141.8 (C), 149.3 (C); m/z (ESI) 475 (MNa^+ , 100%).

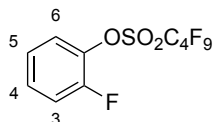
4-(Trifluoromethyl)phenyl nonafluorobutanesulfonate (**156**)²⁹⁰



The reaction was carried out according to the previously described procedure for 2-naphthyl nonafluorobutanesulfonate (**139**) using 4-hydroxybenzotrifluoride (0.200 g, 1.23 mmol), anhydrous dichloromethane (5 mL), triethylamine (0.430 mL, 3.09 mmol) and perfluoro-1-butanesulfonyl fluoride (0.330 mL, 1.84 mmol). The reaction mixture was stirred at room temperature for 16 h. The crude material was purified by flash column chromatography eluting with 20% ethyl acetate in petroleum ether (40–60) to give 4-(trifluoromethyl)phenyl nonafluorobutanesulfonate (**156**) as a

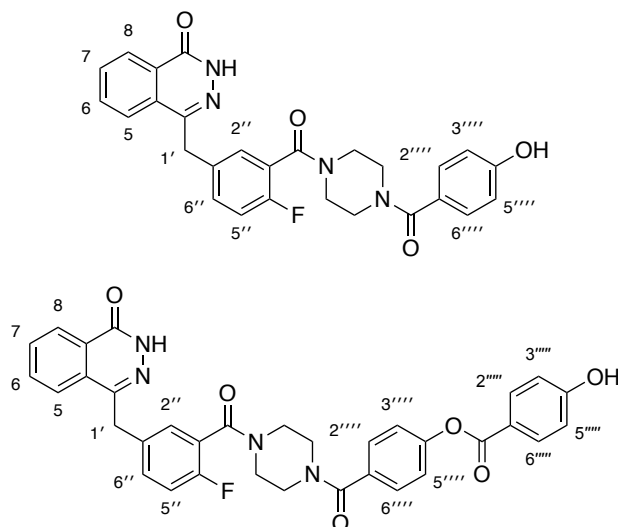
colourless oil (0.454 g, 83%). Spectroscopic data were consistent with the literature.²⁹⁰ δ_{H} (400 MHz, CDCl_3) 7.43 (2H, d, J 8.8 Hz, 2-H and 6-H), 7.75 (2H, d, J 8.8 Hz, 3-H and 5-H); δ_{C} (101 MHz, CDCl_3) 122.2 (2 \times CH), 123.4 (q, $^1J_{\text{CF}}$ 273.4 Hz, CF_3), 127.9 (q, $^3J_{\text{CF}}$ 3.6 Hz, 2 \times CH), 131.0 (q, $^2J_{\text{CF}}$ 33.4 Hz, C), 152.0 (C); m/z (EI) 444 (M^+ , 44%), 145 (100), 133 (36), 78 (32), 69 (41).

2-Fluorophenyl nonafluorobutanesulfonate (**157**)



The reaction was carried out according to the previously described procedure for 2-naphthyl nonafluorobutanesulfonate (**139**) using 2-fluorophenol (0.178 mL, 2.00 mmol), anhydrous dichloromethane (6 mL), triethylamine (0.700 mL, 5.02 mmol) and perfluoro-1-butanesulfonyl fluoride (0.540 mL, 3.01 mmol). The reaction mixture was stirred at room temperature for 3 h. The crude material was purified by flash column chromatography eluting with 10% diethyl ether in hexane to give 2-fluorophenyl nonafluorobutanesulfonate (**157**) as a colourless oil (0.661 g, 84%). $\nu_{\text{max}}/\text{cm}^{-1}$ (neat) 1612 (C=C), 1501 (C=C), 1431, 1227, 1200, 1142, 1096, 895, 760; δ_{H} (400 MHz, CDCl_3) 7.19–7.24 (1H, m, 6-H), 7.27 (1H, ddd, J 9.8, 8.4, 1.4 Hz, 3-H), 7.33–7.41 (2H, m, 4-H and 5-H); δ_{C} (101 MHz, CDCl_3) 117.8 (d, $^2J_{\text{CF}}$ 18.2 Hz, CH), 123.6 (CH), 125.2 (d, $^3J_{\text{CF}}$ 4.1 Hz, CH), 129.8 (d, $^3J_{\text{CF}}$ 7.1 Hz, CH), 137.3 (d, $^2J_{\text{CF}}$ 13.4 Hz, C), 153.9 (d, $^1J_{\text{CF}}$ 254.6 Hz, C); m/z (ESI) 416.9614 (MNa^+ . $\text{C}_{10}\text{H}_4\text{F}_{10}\text{NaO}_3\text{S}$ requires 416.9614).

4-{3''-[4'''-(4''''-hydroxybenzoyl)piperazine-1'''-carbonyl]-4''-fluorobenzyl}-2H-phthalazin-1-one (**160**) and 4-{3''-[4'''-(4''''-{4'''''-hydroxybenzoyloxy}benzoyl)piperazine-1'''-carbonyl]-4''-fluorobenzyl}-2H-phthalazin-1-one (**161**)



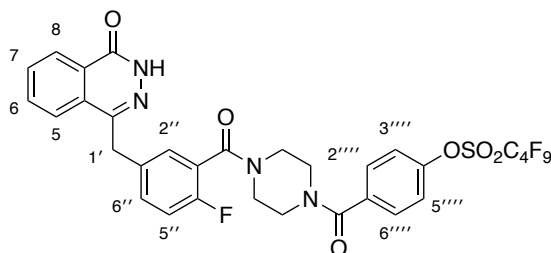
To a stirred solution of 4-hydroxybenzoic acid (**233**) (0.345 g, 2.50 mmol) and *O*-benzotriazole-*N,N,N',N'*-tetramethyluroniumhexafluorophosphate (1.04 g, 2.75 mmol) in anhydrous acetonitrile (13 mL), under argon, was added triethylamine (0.520 mL, 3.75 mmol). The reaction mixture was stirred at room temperature for 0.5 h. 4-[4''-Fluoro-3''-(piperazine-1'''-carbonyl)benzyl]-2H-phthalazin-1-one (**35**) (0.916 g, 2.50 mmol) was added and the reaction mixture was then stirred under reflux for 18 h. The reaction mixture was cooled to room temperature and concentrated *in vacuo*. The resultant residue was dissolved in 20% isopropanol in chloroform (100 mL) and washed with water (100 mL). The organic and aqueous layers were then separated, and the aqueous layer was extracted with 20% isopropanol in chloroform (100 mL). The combined organic layers were dried (MgSO₄), filtered and concentrated *in vacuo*. The crude material was purified by flash column chromatography eluting with 5% methanol in dichloromethane to give 4-{3''-[4'''-(4''''-hydroxybenzoyl)piperazine-1'''-carbonyl]-4''-fluorobenzyl}-2H-phthalazin-1-one (**160**) as an off-white solid (0.403 g, 33%) and 4-{3''-[4'''-(4''''-{4'''''-hydroxybenzoyloxy}benzoyl)piperazine-1'''-carbonyl]-4''-fluorobenzyl}-2H-phthalazin-1-one (**161**) as a white solid (0.241 g, 16%).

Data for **160**: Mp 165–167 °C; $\nu_{\max}/\text{cm}^{-1}$ (neat) 3379 (OH), 3163 (NH), 3009 (CH), 2906 (CH), 1647 (C=O), 1606 (C=O), 1429, 1232, 1168, 1004, 842, 790, 748; δ_{H}

(500 MHz, DMSO- d_6) 3.22 (2H, br s, 2 × NCH), 3.37–3.80 (6H, m, 6 × NCH), 4.33 (2H, s, 1'-H₂), 6.80 (2H, d, J 8.2 Hz, 3''''-H and 5''''-H), 7.23 (1H, t, J 9.0 Hz, 5''-H), 7.28 (2H, d, J 8.2 Hz, 2''''-H and 6''''-H), 7.36 (1H, dd, J 6.5, 2.5 Hz, 2''-H), 7.44 (1H, ddd, J 9.0, 5.0, 2.5 Hz, 6''-H), 7.81 (1H, dd, J 8.0, 7.0 Hz, 7-H), 7.87 (1H, dd, J 8.0, 7.0 Hz, 6-H), 7.95 (1H, d, J 8.0 Hz, 5-H), 8.26 (1H, d, J 8.0 Hz, 8-H), 9.90 (1H, br s, OH), 12.60 (1H, s, NH); δ_C (126 MHz, DMSO- d_6) 36.4 (CH₂), 41.3–41.6 (m, 2 × CH₂), 46.4–46.6 (m, 2 × CH₂), 114.9 (2 × CH), 116.0 (d, $^2J_{CF}$ 21.5 Hz, CH), 123.5 (d, $^2J_{CF}$ 18.4 Hz, C), 125.5 (CH), 125.6 (C), 126.1 (CH), 127.9 (C), 128.9 (d, $^3J_{CF}$ 3.5 Hz, CH), 129.1 (C), 129.4 (2 × CH), 131.5 (CH), 131.8 (d, $^3J_{CF}$ 8.1 Hz, CH), 133.5 (CH), 134.8 (d, $^4J_{CF}$ 3.2 Hz, C), 144.8 (C), 156.4 (d, $^1J_{CF}$ 245.1 Hz, C), 158.9 (C), 159.4 (C), 164.0 (C), 169.5 (C); m/z (ESI) 509.1600 (MNa⁺. C₂₇H₂₃FN₄NaO₄ requires 509.1596).

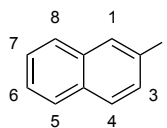
Data for **161**: Mp 258–260 °C; ν_{max}/cm^{-1} (neat) 3186(NH/OH), 2835 (CH), 1720 (C=O), 1646 (C=O), 1623(C=O), 1607 (C=O), 1434, 1263, 1231, 1196, 1157, 1061, 1000, 844, 762; δ_H (500 MHz, DMSO- d_6) 3.06–3.88 (8H, m, 8 × NCH), 4.33 (2H, s, 1'-H₂), 6.93 (2H, d, J 8.7 Hz, 3''''-H and 5''''-H), 7.24 (1H, t, J 8.5 Hz, 5''-H), 7.33 (2H, d, J 8.0 Hz, 3''''-H and 5''''-H), 7.35–7.40 (1H, m, 2''-H), 7.41–7.47 (1H, m, 6''-H), 7.51 (2H, d, J 8.0 Hz, 2''''-H and 6''''-H), 7.72–7.97 (3H, m, 5-H, 6-H and 7-H), 7.99 (2H, d, J 8.7 Hz, 2''''-H and 6''''-H), 8.25 (1H, d, J 8.0 Hz, 8-H), 10.58 (1H, br s, OH), 12.60 (1H, s, NH); δ_C (126 MHz, DMSO- d_6) 36.5 (CH₂), 41.1–41.6 (m, 2 × CH₂), 46.0–46.5 (m, 2 × CH₂), 115.7 (2 × CH), 116.0 (d, $^2J_{CF}$ 21.4 Hz, CH), 119.0 (C), 122.1 (2 × CH), 123.5 (d, $^2J_{CF}$ 18.3 Hz, C), 125.5 (CH), 126.1 (CH), 127.9 (C), 128.6 (2 × CH), 128.9 (d, $^3J_{CF}$ 2.6 Hz, CH), 129.1 (C), 131.6 (CH), 131.8 (d, $^3J_{CF}$ 8.9 Hz, CH), 132.3 (2 × CH), 132.9 (C), 133.5 (CH), 134.8 (d, $^4J_{CF}$ 2.3 Hz, C), 144.8 (C), 151.6 (C), 156.4 (d, $^1J_{CF}$ 245.4 Hz, C), 159.4 (C), 162.9 (C), 164.1 (C), 164.2 (C), 168.6 (C); m/z (ESI) 629.1790 (MNa⁺. C₃₄H₂₇FN₄NaO₆ requires 629.1807).

4-{3''-[4'''-(4''''-Nonafluorobutanesulfonyloxybenzoyl)piperazine-1'''-carbonyl]-4''-fluorobenzyl}-2H-phthalazin-1-one (158)



The reaction was carried out according to the previously described procedure for 2-naphthyl nonafluorobutanesulfonate (**139**) using 4-{3''-[4'''-(4''''-hydroxybenzoyl)piperazine-1'''-carbonyl]-4''-fluorobenzyl}-2H-phthalazin-1-one (**160**) (0.341 g, 0.700 mmol), anhydrous dichloromethane (4 mL), triethylamine (0.250 mL, 1.79 mmol) and perfluoro-1-butanesulfonyl fluoride (0.190 mL, 1.06 mmol). The reaction mixture was stirred at room temperature for 4 h. The crude material was purified by flash column chromatography eluting with 5% methanol in dichloromethane to give 4-{3''-[4'''-(4''''-nonafluorobutanesulfonyloxybenzoyl)piperazine-1'''-carbonyl]-4''-fluorobenzyl}-2H-phthalazin-1-one (**158**) as an off-white solid (0.490 g, 91%). Mp 116–118 °C; $\nu_{\max}/\text{cm}^{-1}$ (neat) 3200 (NH), 2894 (CH), 1634 (C=O), 1424, 1227, 1200, 1138, 1005, 888, 766; δ_{H} (400 MHz, CDCl_3) 3.00–4.07 (8H, m, 8 × NCH), 4.29 (2H, s, 1'-H₂), 7.03 (1H, br s, 5''-H), 7.28–7.43 (4H, m, 2''-H, 6''-H, 3'''-H and 5'''-H), 7.51 (2H, d, J 8.0 Hz, 2'''-H and 6'''-H), 7.64–7.83 (3H, m, 5-H, 6-H and 7-H), 8.38–8.56 (1H, m, 8-H), 11.50 (1H, br s, NH); δ_{C} (101 MHz, CDCl_3) 37.8 (CH₂), 41.5–42.9 (m, 2 × CH₂), 46.2–48.5 (m, 2 × CH₂), 116.3 (d, $^2J_{\text{CF}}$ 22.1 Hz, CH), 122.0 (2 × CH), 123.6 (d, $^2J_{\text{CF}}$ 17.9 Hz, C), 125.1 (CH), 127.3 (CH), 128.4 (C), 129.4 (d, $^3J_{\text{CF}}$ 3.6 Hz, CH), 129.5 (2 × CH), 129.6 (C), 131.7 (CH), 132.0 (d, $^3J_{\text{CF}}$ 8.2 Hz, CH), 133.8 (CH), 134.7 (d, $^4J_{\text{CF}}$ 3.3 Hz, C), 135.4 (C), 145.6 (C), 150.6 (C), 157.1 (d, $^1J_{\text{CF}}$ 248.1 Hz, C), 160.9 (C), 165.3 (C), 168.8 (C); m/z (ESI) 791.1001 (MNa⁺. C₃₁H₂₂F₁₀N₄NaO₆S requires 791.0993).

2-Iodonaphthalene (**130**)⁴³⁷

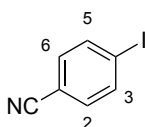


Method A: A stirrer bar, 3 Å molecular sieves and sodium iodide (0.106 g, 0.705 mmol) were added to a microwave tube and dried in an oven at 140 °C overnight. 2-Naphthyl nonafluorobutanesulfonate (**139**) (0.100 g, 0.235 mmol) was dried under high vacuum for 1 h, purged with argon and dissolved in anhydrous *N,N'*-dimethylformamide (1.0 mL). The oven-dried microwave tube was cooled to room temperature *in vacuo* and then purged with argon. Tris(acetonitrile)pentamethylcyclopentadienylruthenium(II) trifluoromethanesulfonate (0.00600 g, 0.0118 mmol) was weighed into an oven-dried vial under argon and added to the microwave tube. The 2-naphthyl nonafluorobutanesulfonate (**139**) solution was added to the microwave tube. The tube was sealed, heated to 100 °C and stirred for 1.5 h. The reaction mixture was cooled to room temperature and partitioned between ethyl acetate (10 mL) and water (10 mL). The aqueous layer was extracted with ethyl acetate (3 × 10 mL) and the combined organic layers were dried (MgSO₄), filtered and concentrated *in vacuo*. The crude material was purified through a short pad of silica, eluting with 100% petroleum ether (40–60) to give 2-iodonaphthalene (**130**) as a white solid (0.0510 g, 86%). Mp 50–52 °C (lit.⁴³⁷ 53–55 °C). δ_{H} (400 MHz, CDCl₃) 7.47–7.52 (2H, m, 2 × ArH), 7.58 (1H, d, *J* 8.7 Hz, 4-H), 7.70–7.74 (2H, m, 2 × ArH), 7.79–7.82 (1H, m, ArH), 8.25 (1H, br d, *J* 1.2 Hz, 1-H); δ_{C} (101 MHz, CDCl₃) 91.7 (C), 126.7 (CH), 126.9 (CH), 127.0 (CH), 128.0 (CH), 129.7 (CH), 132.3 (C), 134.6 (CH), 135.2 (C), 136.8 (CH); *m/z* (EI) 254 (M⁺, 100%), 127 (93), 126 (21), 77 (13).

Method B: The reaction was performed as described in method A above, except using sodium iodide (0.135 g, 0.900 mmol), 2-naphthyl nonafluorobutanesulfonate (**139**) (0.128 g, 0.300 mmol), anhydrous *N,N'*-dimethylformamide (1.2 mL) and tris(acetonitrile)pentamethylcyclopentadienylruthenium(II) hexafluorophosphate (0.00980 g, 0.0194 mmol). The reaction mixture was heated to 100 °C and stirred for 3 h. The reaction mixture was cooled to room temperature, diluted with ethyl acetate (15 mL) and washed with water (3 × 15 mL). The organic layer was dried

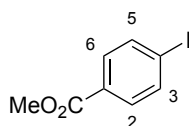
(MgSO₄), filtered and concentrated *in vacuo*. The crude material was purified through a short pad of silica, eluting with 100% hexane to give 2-iodonaphthalene (**130**) as a white solid (0.0568 g, 75%). Spectroscopic data were consistent with that described above.

4-Iodobenzonitrile (**148**)⁴³⁸



The reaction was carried out according to the previously described method A procedure for 2-iodonaphthalene (**130**) using sodium iodide (0.112 g, 0.747 mmol), tris(acetonitrile)pentamethylcyclopentadienylruthenium(II) trifluoromethanesulfonate (0.00640 g, 0.0125 mmol), 4-cyanophenyl nonafluorobutanesulfonate (**140**) (0.100 g, 0.249 mmol) and anhydrous *N,N'*-dimethylformamide (1.0 mL). The reaction mixture was stirred at 100 °C for 3 h. The crude material was purified by flash column chromatography, eluting with 5% diethyl ether in petroleum ether (40–60) to give 4-iodobenzonitrile (**148**) as a white solid (0.0365 g, 64%). Mp 122–124 °C (lit.⁴³⁸ 120–121 °C). δ_{H} (400 MHz, CDCl₃) 7.36 (2H, d, *J* 8.6 Hz, 3-H and 5-H), 7.84 (2H, d, *J* 8.6 Hz, 2-H and 6-H); δ_{C} (101 MHz, CDCl₃) 100.4 (C), 111.9 (C), 118.3 (C), 133.3 (2 × CH), 138.6 (2 × CH); *m/z* (EI) 229 (M⁺, 80%), 102 (100), 84 (95), 69 (31), 49 (38).

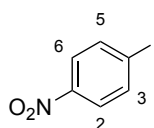
Methyl 4-iodobenzoate (**149**)⁴³⁷



The reaction was carried out according to the previously described method A procedure for 2-iodonaphthalene (**130**) using sodium iodide (0.104 g, 0.694 mmol), tris(acetonitrile)pentamethylcyclopentadienylruthenium(II) trifluoromethanesulfonate (0.00590 g, 0.0116 mmol), methyl 4-nonafluorobutanesulfonyloxybenzoate (**141**) (0.100 g, 0.230 mmol) and anhydrous *N,N'*-dimethylformamide (1.0 mL). The reaction mixture was stirred at 110 °C for 3

h. The crude material was purified by flash column chromatography eluting with 10% ethyl acetate in petroleum ether (40–60) to give methyl 4-iodobenzoate (**149**) as a white solid (0.0247 g, 41%). Mp 114–116 °C (lit.⁴³⁷ 119–120 °C). δ_{H} (400 MHz, CDCl_3) 3.91 (3H, s, CH_3), 7.74 (2H, d, J 8.7 Hz, 3-H and 5-H), 7.80 (2H, d, J 8.7 Hz, 2-H and 6-H); δ_{C} (101 MHz, CDCl_3) 52.4 (CH_3), 100.8 (C), 129.7 (C), 131.2 (2 \times CH), 137.8 (2 \times CH), 166.7 (C); m/z (EI) 262 (M^+ , 93%), 231 (100), 203 (38), 76 (67).

4-Iodonitrobenzene (**150**)⁴³⁹

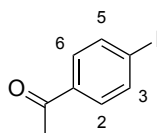


Method A: The reaction was carried out according to the previously described method A procedure for 2-iodonaphthalene (**130**) using sodium iodide (0.107 g, 0.711 mmol), tris(acetonitrile)pentamethylcyclopentadienylruthenium(II) trifluoromethanesulfonate (0.00610 g, 0.0119 mmol), 4-nitrophenyl nonafluorobutanesulfonate (**142**) (0.100 g, 0.237 mmol) and anhydrous *N,N'*-dimethylformamide (1.0 mL). The reaction mixture was stirred at 100 °C for 3 h. The crude material was purified through a short pad of silica, eluting with 20% ethyl acetate in petroleum ether (40–60) to give 4-iodonitrobenzene (**150**) as a white solid (0.0505 g, 86%). Mp 170–172 °C (lit.⁴³⁹ 171–173 °C). δ_{H} (400 MHz, CDCl_3) 7.91 (2H, d, J 8.0 Hz, 3-H and 5-H), 7.94 (2H, d, J 8.0 Hz, 2-H and 6-H); δ_{C} (101 MHz, CDCl_3) 102.8 (C), 125.0 (2 \times CH), 138.8 (2 \times CH), 148.0 (C); m/z (CI) 250 (MH^+ , 60%), 209 (12), 193 (15), 124 (30), 113 (22), 85 (78), 69 (100).

Method B: The reaction was carried out according to the previously described method B procedure for 2-iodonaphthalene (**130**) using sodium iodide (0.112 g, 0.750 mmol), tris(acetonitrile)pentamethylcyclopentadienylruthenium(II) hexafluorophosphate (0.0109 g, 0.0216 mmol), 4-nitrophenyl nonafluorobutanesulfonate (**142**) (0.105 g, 0.250 mmol) and anhydrous *N,N'*-dimethylformamide (1.0 mL). The reaction mixture was stirred at 100 °C for 4 h. The crude material was purified by preparative layer chromatography, eluting with 2%

diethyl ether in hexane to give 4-iodonitrobenzene (**150**) as a white solid (0.0345 g, 56%). Spectroscopic data were consistent with that described above.

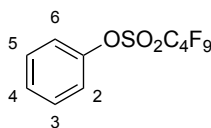
4-Iodoacetophenone (**131**)⁴³⁹



Method A: The reaction was carried out according to the previously described method A procedure for 2-iodonaphthalene (**130**) using sodium iodide (0.107 g, 0.717 mmol), tris(acetonitrile)pentamethylcyclopentadienylruthenium(II) trifluoromethanesulfonate (0.00610 g, 0.0120 mmol), 4-acetylphenyl nonafluorobutanesulfonate (**144**) (0.100 g, 0.239 mmol) and anhydrous *N,N'*-dimethylformamide (1.0 mL). The reaction mixture was stirred at 100 °C for 4 h. The crude material was purified by flash column chromatography eluting with 5% diethyl ether in petroleum ether (40–60) to give 4-iodoacetophenone (**131**) as a white solid (0.03160 g, 54%). Mp 84–85 °C (lit.⁴³⁹ 82–84 °C). δ_{H} (400 MHz, CDCl_3) 2.57 (3H, s, COCH_3), 7.66 (2H, d, J 8.6 Hz, 3-H and 5-H), 7.83 (2H, d, J 8.6 Hz, 2-H and 6-H); δ_{C} (101 MHz, CDCl_3) 26.6 (CH_3), 101.2 (C), 129.9 (2 \times CH), 136.5 (C), 138.1 (2 \times CH), 197.5 (C); m/z (ESI) 269 (MNa^+ , 100%).

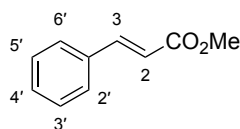
Method B: The reaction was carried out according to the previously described method B procedure for 2-iodonaphthalene (**130**) using sodium iodide (0.135 g, 0.900 mmol), tris(acetonitrile)pentamethylcyclopentadienylruthenium(II) hexafluorophosphate (0.01300 g, 0.0258 mmol), 4-acetylphenyl nonafluorobutanesulfonate (**144**) (0.125 g, 0.300 mmol) and anhydrous *N,N'*-dimethylformamide (1.2 mL). The reaction mixture was stirred at 100 °C for 7 h. The crude material was purified by flash column chromatography eluting with 5% diethyl ether in hexane to give 4-iodoacetophenone (**131**) as a white solid (0.04800 g, 65%). Spectroscopic data were consistent with that described above.

Phenyl nonafluorobutanesulfonate (**167**)⁴⁴⁰



The reaction was carried out according to the previously described procedure for 2-naphthyl nonafluorobutanesulfonate (**139**) using phenol (0.200 g, 2.12 mmol), anhydrous dichloromethane (7 mL), triethylamine (0.740 mL, 5.31 mmol) and perfluoro-1-butanesulfonyl fluoride (0.570 mL, 3.17 mmol). The reaction mixture was stirred at room temperature for 3 h. The crude material was purified by flash column chromatography eluting with 10% diethyl ether in petroleum ether (40–60) to give phenyl nonafluorobutanesulfonate (**167**) as a colourless oil (0.720 g, 90%). Spectroscopic data were consistent with the literature.⁴⁴⁰ δ_{H} (400 MHz, CDCl_3) 7.27–7.33 (2H, m, 2-H and 6-H), 7.37–7.42 (1H, m, 4-H), 7.43–7.50 (2H, m, 3-H and 5-H); δ_{C} (101 MHz, CDCl_3) 121.5 (2 \times CH), 128.5 (CH), 130.4 (2 \times CH), 150.0 (C); m/z (EI) 376 (M^+ , 42%), 312 (13), 219 (4), 143 (10), 93 (73), 84 (35), 77 (94), 69 (35), 65 (100).

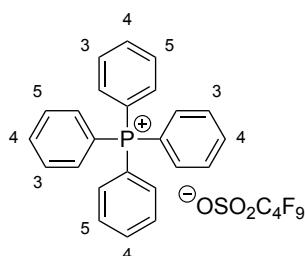
Methyl (2*E*)-3-phenylprop-2-enoate (**169**)⁴⁴¹



A stirrer bar and sodium iodide (0.0225 g, 0.150 mmol) were added to a microwave tube and dried in an oven at 140 °C overnight. The oven-dried microwave tube was then cooled to room temperature *in vacuo* and purged with argon. To the microwave tube was added palladium(II) bis(triphenylphosphine) dichloride (0.0105 g, 0.0150 mmol) and a solution of phenyl nonafluorobutanesulfonate (**167**) (0.0564 g, 0.150 mmol) in anhydrous *N,N'*-dimethylformamide (0.9 mL), followed by triethylamine (0.0840 mL, 0.600 mmol). Methyl acrylate (0.0540 mL, 0.600 mmol) was added dropwise to the microwave tube, which was then sealed, heated to 90 °C and stirred for 6 h. The reaction mixture was cooled to room temperature, diluted with ethyl acetate (10 mL) and washed with water (3 \times 10 mL). The organic layer was dried

(MgSO₄), filtered and concentrated *in vacuo*. The crude material was purified by flash column chromatography eluting with 10% diethyl ether in petroleum ether (40–60) to give methyl (2*E*)-3-phenylprop-2-enoate (**169**) as a white solid (0.0102 g, 42%). Mp 35–37 °C (lit.⁴⁴¹ 33–35 °C). δ_{H} (500 MHz, CDCl₃) 3.81 (3H, s, CH₃), 6.45 (1H, d, *J* 16.0 Hz, 2-H), 7.35–7.42 (3H, m, 4'-H and 2 × ArH), 7.50–7.56 (2H, m, 2 × ArH), 7.70 (1H, d, *J* 16.0 Hz, 3-H); δ_{C} (126 MHz, CDCl₃) 51.9 (CH₃), 118.0 (CH), 128.2 (2 × CH), 129.0 (2 × CH), 130.4 (CH), 134.5 (C), 145.0 (CH), 167.6 (C); *m/z* (ESI) 185 (MNa⁺. 100%).

Tetraphenylphosphonium nonafluorobutanesulfonate (**171**)



Method A: A stirrer bar and sodium iodide (0.0225 g, 0.150 mmol) were added to a microwave tube and dried in an oven at 140 °C overnight. Phenyl nonafluorobutanesulfonate (**167**) (0.0564 g, 0.150 mmol) was dried under high vacuum for 1 h, purged with argon and dissolved in anhydrous *N,N'*-dimethylformamide (0.9 mL). The oven-dried microwave tube was cooled to room temperature *in vacuo* and then purged with argon. To the tube was added triphenylphosphine (0.0393 g, 0.150 mmol) and palladium(II) bis(triphenylphosphine) dichloride (0.0105 g, 0.0150 mmol), followed by the phenyl nonafluorobutanesulfonate (**167**) solution and triethylamine (0.0850 mL, 0.610 mmol). The tube was then sealed, heated to 90 °C and stirred for 6 h. The reaction mixture was cooled to room temperature, diluted with ethyl acetate (10 mL), and washed with water (5 × 10 mL). The organic layer was dried (MgSO₄), filtered and concentrated *in vacuo*. The crude material was purified by trituration with diethyl ether to give tetraphenylphosphonium nonafluorobutanesulfonate (**171**) as an off-white solid (0.0550 g, 57%). Mp 147–149 °C; $\nu_{\text{max}}/\text{cm}^{-1}$ (neat) 3068 (CH), 1439, 1266, 1192, 1107, 1050, 999, 723; δ_{H} (400 MHz, CDCl₃) 7.57–7.67 [8H, m, 4 × (2-H and 6-H)], 7.72–7.81 [8H, m, 4 × (3-H and 5-H)], 7.89 (4H, tdt, *J* 7.6, 2.1, 1.3 Hz, 4 × 4-H); δ_{C} (101 MHz, CDCl₃) 117.7 (d, ¹*J*_{CP} 89.8 Hz, 4 × C), 130.9 (d, ³*J*_{CP} 12.9

Hz, 8 × CH), 134.6 (d, $^2J_{CP}$ 10.4 Hz, 8 × CH), 135.9 (d, $^4J_{CP}$ 3.1 Hz, 4 × CH); m/z (ESI) 339.1289 (M^+ . $C_{24}H_{20}P$ requires 339.1297); m/z (ESI) 298.9434 (M^- . $C_4F_9O_3S$ requires 298.9430).

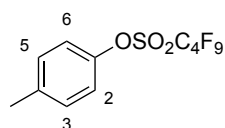
Method B: The reaction was performed as described in method A above, except using sodium iodide (0.0225 g, 0.150 mmol), phenyl nonafluorobutanesulfonate (**167**) (0.0564 g, 0.150 mmol), anhydrous *N,N'*-dimethylformamide (0.9 mL), triphenylphosphine (0.0393 g, 0.150 mmol), tris(dibenzylideneacetone)dipalladium(0) (0.0137 g, 0.0150 mmol) and triethylamine (0.0850 mL, 0.610 mmol). The reaction mixture was stirred at 90 °C for 4 h. The crude material was purified by trituration with diethyl ether to give tetraphenylphosphonium nonafluorobutanesulfonate (**171**) as an off-white solid (0.0379 g, 40%). Spectroscopic data were consistent as described above.

Method C: The reaction was performed as described in method A above, except using sodium iodide (0.0225 g, 0.150 mmol), phenyl nonafluorobutanesulfonate (**167**) (0.0564 g, 0.150 mmol), anhydrous *N,N'*-dimethylformamide (0.9 mL), triphenylphosphine (0.0393 g, 0.150 mmol), tetrakis(triphenylphosphine)palladium(0) (0.0173 g, 0.0150 mmol) and triethylamine (0.0850 mL, 0.610 mmol). The reaction mixture was stirred at 90 °C for 4 h. The crude material was purified by trituration with diethyl ether to give tetraphenylphosphonium nonafluorobutanesulfonate (**171**) as an off-white solid (0.0386 g, 40%). Spectroscopic data were consistent as described above.

Method D: The reaction was performed as described in method A above, except using sodium iodide (0.0225 g, 0.150 mmol), phenyl nonafluorobutanesulfonate (**167**) (0.0564 g, 0.150 mmol), anhydrous *N,N'*-dimethylformamide (0.9 mL), triphenylphosphine (0.0393 g, 0.150 mmol), [1,1'-bis(diphenylphosphino)ferrocene]dichloropalladium(II) complex with dichloromethane (0.0122 g, 0.0150 mmol) and triethylamine (0.0850 mL, 0.610 mmol). The reaction mixture was stirred at 90 °C for 4 h. The crude material was purified by trituration with diethyl ether to give tetraphenylphosphonium nonafluorobutanesulfonate (**171**) as an off-white solid (0.0521 g, 54%). Spectroscopic data were consistent as described above.

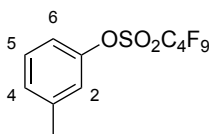
Method E: The reaction was performed as described in method A above, except using sodium iodide (0.0600 g, 0.400 mmol), phenyl nonafluorobutanesulfonate (**167**) (0.150 g, 0.400 mmol), anhydrous *N,N'*-dimethylformamide (2.4 mL), triphenylphosphine (0.105 g, 0.400 mmol), palladium(II) acetate (0.00900 g, 0.0400 mmol), and triethylamine (0.220 mL, 1.58 mmol). The reaction mixture was stirred at 90 °C for 4 h. The crude reaction mixture was cooled to room temperature, diluted with ethyl acetate (15 mL) and washed with water (5 × 15 mL). The organic layer was dried (MgSO₄), filtered and concentrated *in vacuo*. The crude material was purified by trituration with diethyl ether to give tetraphenylphosphonium nonafluorobutanesulfonate (**171**) as an off-white solid (0.173 g, 68%). Spectroscopic data were consistent as described above.

4-Methylphenyl nonafluorobutanesulfonate (**175**)²⁹⁹



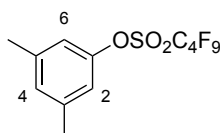
The reaction was carried out according to the previously described procedure for 2-naphthyl nonafluorobutanesulfonate (**139**) using *p*-cresol (1.08 g, 10.0 mmol), anhydrous dichloromethane (33 mL), triethylamine (3.48 mL, 25.0 mmol) and perfluoro-1-butanesulfonyl fluoride (2.70 mL, 15.0 mmol). The reaction mixture was stirred at room temperature for 2 h. The crude material was purified by flash column chromatography eluting with 5% diethyl ether in petroleum ether (40–60) to give 4-methylphenyl nonafluorobutanesulfonate (**175**) as a colourless oil (3.40 g, 87%). Spectroscopic data were consistent with the literature.²⁹⁹ δ_{H} (400 MHz, CDCl₃) 2.38 (3H, s, CH₃), 7.16 (2H, d, *J* 8.6 Hz, 3-H and 5-H), 7.24 (2H, d, *J* 8.6 Hz, 2-H and 6-H); δ_{C} (101 MHz, CDCl₃) 21.0 (CH₃), 121.2 (2 × CH), 130.8 (2 × CH), 138.6 (C), 148.0 (C); *m/z* (ESI) 413 (MNa⁺, 100%).

3-Methylphenyl nonafluorobutanesulfonate (**176**)



The reaction was carried out according to the previously described procedure for 2-naphthyl nonafluorobutanesulfonate (**139**) using *m*-cresol (0.209 mL, 2.00 mmol), anhydrous dichloromethane (5 mL), triethylamine (0.700 mL, 5.02 mmol) and perfluoro-1-butanesulfonyl fluoride (0.540 mL, 3.00 mmol). The reaction mixture was stirred at room temperature for 3 h. The crude material was purified by flash column chromatography eluting with 100% petroleum ether (40–60) to give 3-methylphenyl nonafluorobutanesulfonate (**176**) as a colourless oil (0.588 g, 76%). $\nu_{\text{max}}/\text{cm}^{-1}$ (neat) 2970 (CH), 1740, 1425, 1354, 1231, 1198, 1142, 1117, 930; δ_{H} (400 MHz, CDCl_3) 2.41 (3H, s, CH_3), 7.06–7.12 (2H, m, 2-H and 6-H), 7.17–7.22 (1H, m, 4-H), 7.29–7.36 (1H, m, 5-H); δ_{C} (101 MHz, CDCl_3) 21.5 (CH_3), 118.4 (CH), 122.0 (CH), 129.3 (CH), 130.0 (CH), 141.0 (C), 149.9 (C); m/z (EI) 389.9953 (M^+ . $\text{C}_{11}\text{H}_7\text{F}_9\text{O}_3\text{S}$ requires 389.9972), 326 (24), 151 (38), 107 (100), 91 (38), 77 (49).

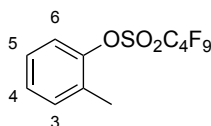
3,5-Dimethylphenyl nonafluorobutanesulfonate (**177**)⁴³⁵



The reaction was carried out according to the previously described procedure for 2-naphthyl nonafluorobutanesulfonate (**139**) using 3,5-dimethylphenol (0.244 g, 2.00 mmol), anhydrous dichloromethane (6 mL), triethylamine (0.700 mL, 5.02 mmol) and perfluoro-1-butanesulfonyl fluoride (0.540 mL, 3.01 mmol). The reaction mixture was stirred at room temperature for 5 h. The crude material was purified by flash column chromatography eluting with 5% diethyl ether in hexane to give 3,5-dimethylphenyl nonafluorobutanesulfonate (**177**) as a colourless oil (0.691 g, 86%). Spectroscopic data were consistent with the literature.⁴³⁵ δ_{H} (400 MHz, CDCl_3) 2.35 (6H, s, 2 × CH_3), 6.89 (2H, br s, 2-H and 6-H), 7.01 (1H, br s, 4-H); δ_{C} (101 MHz,

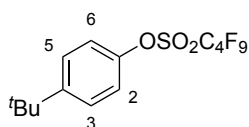
CDCl₃) 21.4 (2 × CH₃), 118.9 (2 × CH), 130.1 (CH), 140.5 (2 × C), 149.9 (C); *m/z* (ESI) 427 (MNa⁺. 100%).

2-Methylphenyl nonafluorobutanesulfonate (**178**)²⁹⁹



The reaction was carried out according to the previously described procedure for 2-naphthyl nonafluorobutanesulfonate (**139**) using *o*-cresol (0.270 g, 2.50 mmol), anhydrous dichloromethane (8 mL), triethylamine (0.870 mL, 6.25 mmol) and perfluoro-1-butanesulfonyl fluoride (0.680 mL, 3.77 mmol). The reaction mixture was stirred at room temperature for 2 h. The crude material was purified by flash column chromatography eluting with 5% diethyl ether in hexane to give 2-methylphenyl nonafluorobutanesulfonate (**178**) as a colourless oil (0.708 g, 72%). Spectroscopic data were consistent with the literature.²⁹⁹ δ_{H} (400 MHz, CDCl₃) 2.40 (3H, s, CH₃), 7.23–7.34 (4H, m, 3-H, 4-H, 5-H and 6-H); δ_{C} (126 MHz, CDCl₃) 16.6 (CH₃), 121.4 (CH), 127.8 (CH), 128.4 (CH), 131.1 (C), 132.3 (CH), 148.8 (C); *m/z* (ESI) 413 (MNa⁺. 100%).

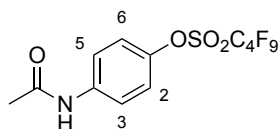
4-*tert*-Butylphenyl nonafluorobutanesulfonate (**179**)²⁹⁵



The reaction was carried out according to the previously described procedure for 2-naphthyl nonafluorobutanesulfonate (**139**) using 4-*tert*-butylphenol (0.300 g, 2.00 mmol), anhydrous dichloromethane (6 mL), triethylamine (0.700 mL, 5.02 mmol) and perfluoro-1-butanesulfonyl fluoride (0.540 mL, 3.01 mmol). The reaction mixture was stirred at room temperature for 5 h. The crude material was purified by flash column chromatography eluting with 100% hexane to give 4-*tert*-butylphenyl nonafluorobutanesulfonate (**179**) as a colourless oil (0.802 g, 93%). Spectroscopic data were consistent with the literature.²⁹⁵ δ_{H} (400 MHz, CDCl₃) 1.33 (9H, s, *t*-Bu), 7.20 (2H, d, *J* 9.0 Hz, 3-H and 5-H), 7.45 (2H, d, *J* 9.0 Hz, 2-H and 6-H); δ_{C} (101

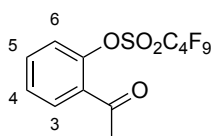
MHz, CDCl₃) 31.4 (3 × CH₃), 34.9 (C), 120.9 (2 × CH), 127.3 (2 × CH), 147.8 (C), 151.8 (C); *m/z* (ESI) 455 (MNa⁺. 100%).

4-Acetamidophenyl nonafluorobutanesulfonate (**180**)⁴⁴²



The reaction was carried out according to the previously described procedure for 2-naphthyl nonafluorobutanesulfonate (**139**) using 4-acetamidophenol (0.302 g, 2.00 mmol), anhydrous dichloromethane (6 mL), triethylamine (0.700 mL, 5.02 mmol) and perfluoro-1-butanesulfonyl fluoride (0.540 mL, 3.01 mmol). The reaction mixture was stirred at room temperature for 3 h. The crude material was purified by flash column chromatography eluting with 100% diethyl ether to give 4-acetamidophenyl nonafluorobutanesulfonate (**180**) as a white solid (0.781 g, 90%). Mp 102–103 °C. Spectroscopic data were consistent with the literature.⁴⁴² δ_{H} (400 MHz, CDCl₃) 2.19 (3H, s, CH₃), 7.23 (2H, d, *J* 9.0 Hz, 2-H and 6-H), 7.41 (1H, br s, NH), 7.60 (2H, d, *J* 9.0 Hz, 3-H and 5-H); δ_{C} (101 MHz, CDCl₃) 24.7 (CH₃), 121.1 (2 × CH), 122.1 (2 × CH), 138.0 (C), 145.7 (C), 168.6 (C); *m/z* (ESI) 456 (MNa⁺. 100%).

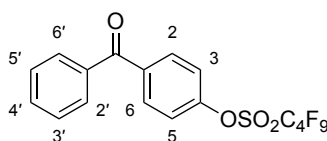
2-Acetylphenyl nonafluorobutanesulfonate (**181**)



The reaction was carried out according to the previously described procedure for 2-naphthyl nonafluorobutanesulfonate (**139**) using 2-hydroxyacetophenone (0.240 mL, 2.00 mmol), anhydrous dichloromethane (6 mL), triethylamine (0.700 mL, 5.02 mmol) and perfluoro-1-butanesulfonyl fluoride (0.540 mL, 3.01 mmol). The reaction mixture was stirred at room temperature for 4 h. 4-(Dimethylamino)pyridine (0.0240 g, 0.200 mmol) was then added and the reaction mixture was stirred at room temperature for 18 h before heating under reflux for 21 h. The crude material was purified by flash column chromatography eluting with 20% diethyl ether in hexane to give 2-acetylphenyl nonafluorobutanesulfonate (**181**) as a colourless oil (0.322 g,

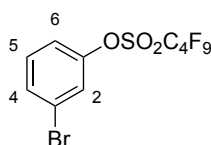
39%). $\nu_{\max}/\text{cm}^{-1}$ (neat) 1697 (C=O), 1604 (C=C), 1423, 1227, 1200, 1142, 891, 775; δ_{H} (400 MHz, CDCl_3) 2.64 (3H, s, CH_3), 7.36 (1H, dd, J 8.4, 1.2 Hz, 6-H), 7.48 (1H, td, J 7.6, 1.2 Hz, 4-H), 7.60 (1H, ddd, J 8.4, 7.6, 2.0 Hz, 5-H), 7.81 (1H, dd, J 7.6, 2.0 Hz, 3-H); δ_{C} (101 MHz, CDCl_3) 29.7 (CH_3), 122.9 (t, ${}^6J_{\text{CF}}$ 1.8 Hz, CH), 128.7 (CH), 130.8 (CH), 132.5 (C), 133.8 (CH), 147.1 (C), 196.8 (C); m/z (ESI) 440.9820 (MNa^+ . $\text{C}_{12}\text{H}_7\text{F}_9\text{NaO}_4\text{S}$ requires 440.9814).

4-Nonafluorobutanesulfonyloxybenzophenone (**182**)



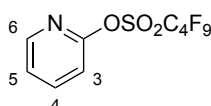
The reaction was carried out according to the previously described procedure for 2-naphthyl nonafluorobutanesulfonate (**139**) using 4-hydroxybenzophenone (0.200 g, 1.01 mmol), anhydrous dichloromethane (5 mL), triethylamine (0.350 mL, 2.51 mmol) and perfluoro-1-butanesulfonyl fluoride (0.270 mL, 1.50 mmol). The reaction mixture was stirred at room temperature for 16 h. The crude material was purified by flash column chromatography eluting with 20% ethyl acetate in petroleum ether (40–60) to give 4-nonafluorobutanesulfonyloxybenzophenone (**182**) as a beige solid (0.341 g, 70%). Mp 42–43 °C; $\nu_{\max}/\text{cm}^{-1}$ (neat) 2980 (CH), 1740 (C=O), 1651 (C=C), 1424, 1227, 1202, 1138, 889, 797, 731; δ_{H} (400 MHz, CDCl_3) 7.42 (2H, d, J 8.6 Hz, 3-H and 5-H), 7.52 (2H, t, J 7.6 Hz, 3'-H and 5'-H), 7.63 (1H, t, J 7.6 Hz, 4'-H), 7.80 (2H, d, J 7.6 Hz, 2'-H and 6'-H), 7.91 (2H, d, J 8.6 Hz, 2-H and 6-H); δ_{C} (101 MHz, CDCl_3) 121.5 (2 × CH), 128.7 (2 × CH), 130.1 (2 × CH), 132.3 (2 × CH), 133.2 (CH), 136.9 (C), 137.7 (C), 152.3 (C), 194.9 (C); m/z (EI) 480.0083 (M^+ . $\text{C}_{17}\text{H}_9\text{F}_9\text{O}_4\text{S}$ requires 480.0078), 169 (89), 105 (84), 84 (93), 63 (81).

3-Bromophenyl nonafluorobutanesulfonate (**183**)



The reaction was carried out according to the previously described procedure for 2-naphthyl nonafluorobutanesulfonate (**139**) using 3-bromophenol (0.356 g, 2.06 mmol), anhydrous dichloromethane (5 mL), triethylamine (0.720 mL, 5.17 mmol) and perfluoro-1-butanesulfonyl fluoride (0.560 mL, 3.11 mmol). The reaction mixture was stirred at room temperature for 1 h. The crude material was purified by flash column chromatography eluting with 100% petroleum ether (40–60) to give 3-bromophenyl nonafluorobutanesulfonate (**183**) as a colourless oil (0.830 g, 88%). $\nu_{\max}/\text{cm}^{-1}$ (neat) 1582 (C=C), 1468, 1425, 1354, 1227, 1200, 1142, 1034, 897, 785; δ_{H} (400 MHz, CDCl_3) 7.26 (1H, ddd, J 8.2, 2.0, 0.8 Hz, 6-H), 7.34 (1H, t, J 8.2 Hz, 5-H), 7.47 (1H, t, J 2.0 Hz, 2-H), 7.55 (1H, ddd, J 8.2, 2.0, 0.8 Hz, 4-H); δ_{C} (101 MHz, CDCl_3) 120.3 (CH), 123.2 (C), 125.0 (CH), 131.4 (CH), 131.9 (CH), 149.9 (C); m/z (EI) 453.8920 (M^+ , $\text{C}_{10}\text{H}_4^{79}\text{BrF}_9\text{O}_3\text{S}$ requires 453.8921), 392 (21), 390 (22), 173 (20), 171 (20), 157 (27), 155 (28), 83 (100), 78 (50), 63 (59).

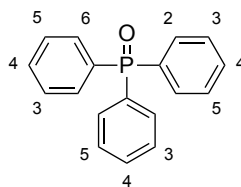
Pyridin-2-yl nonafluorobutanesulfonate (**184**)²⁹¹



The reaction was carried out according to the previously described procedure for 2-naphthyl nonafluorobutanesulfonate (**139**) using pyridin-2-ol (0.190 g, 2.00 mmol), anhydrous dichloromethane (6 mL), triethylamine (0.700 mL, 5.02 mmol) and perfluoro-1-butanesulfonyl fluoride (0.540 mL, 3.01 mmol). The reaction mixture was stirred at room temperature for 166 h. The crude material was purified by flash column chromatography eluting with 30% diethyl ether in hexane to give pyridin-2-yl nonafluorobutanesulfonate (**184**) as a colourless oil (0.495 g, 66%). Spectroscopic data were consistent with the literature.²⁹¹ δ_{H} (400 MHz, CDCl_3) 7.19 (1H, br d, J 8.2 Hz, 3-H), 7.40 (1H, ddd, J 7.4, 4.8, 0.4 Hz, 5-H), 7.90 (1H, ddd, J

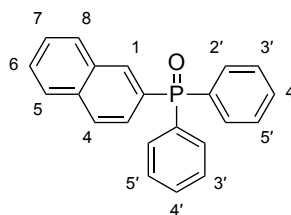
8.2, 7.4, 2.0 Hz, 4-H), 8.42 (1H, dd, J 4.8, 2.0 Hz, 6-H); δ_{C} (101 MHz, CDCl_3) 115.4 (CH), 124.4 (CH), 141.1 (CH), 148.9 (CH), 156.1 (C); m/z (ESI) 400 (MNa^+ , 100%).

Triphenylphosphine oxide (**185**)⁴⁰⁹



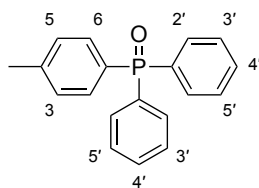
A stirrer bar and sodium iodide (0.0600 g, 0.400 mmol) were added to a microwave tube and dried in an oven at 140 °C overnight. Phenyl nonafluorobutanesulfonate (**167**) (0.150 g, 0.400 mmol) was dried under high vacuum for 1 h, purged with argon and dissolved in anhydrous N,N' -dimethylformamide (2.4 mL). Diphenylphosphine oxide (0.121 g, 0.600 mmol) was dried *in vacuo* for 1 h. The oven-dried microwave tube was cooled to room temperature *in vacuo* and then purged with argon. To the tube was added diphenylphosphine oxide and palladium(II) acetate (0.00900 g, 0.0400 mmol), followed by the phenyl nonafluorobutanesulfonate (**167**) solution and triethylamine (0.220 mL, 1.58 mmol). The tube was sealed, heated to 120 °C and stirred for 4 h. The reaction mixture was cooled to room temperature, diluted with ethyl acetate (15 mL) and washed with 2 M aqueous lithium chloride solution (3 \times 15 mL). The organic layer was dried (MgSO_4), filtered and concentrated *in vacuo*. The crude material was purified by flash column chromatography eluting with 2% methanol in diethyl ether to give triphenylphosphine oxide (**185**) as a white solid (0.0740 g, 67%). Mp 144–146 °C (lit.⁴⁰⁹ 148–149 °C); δ_{H} (400 MHz, CDCl_3) 7.42–7.50 [6H, m, 3 \times (3-H and 5-H)], 7.55 (3H, ttd, J 7.5, 1.6, 1.6 Hz, 3 \times 4-H), 7.62–7.72 [6H, m, 3 \times (2-H and 6-H)]; δ_{C} (101 MHz, CDCl_3) 128.6 (d, $^3J_{\text{CP}}$ 12.1 Hz, 6 \times CH), 132.1 (d, $^4J_{\text{CP}}$ 2.8 Hz, 3 \times CH), 132.2 (d, $^2J_{\text{CP}}$ 10.0 Hz, 6 \times CH), 132.7 (d, $^1J_{\text{CP}}$ 104.5 Hz, 3 \times C); m/z (ESI) 301 (MNa^+ , 100%).

(2-Naphthyl)diphenylphosphine oxide (**186**)⁴⁴³



The reaction was carried out according to the previously described procedure for triphenylphosphine oxide (**185**) using sodium iodide (0.0600 g, 0.400 mmol), 2-naphthyl nonafluorobutanesulfonate (**139**) (0.171 g, 0.400 mmol), anhydrous *N,N'*-dimethylformamide (2.4 mL), diphenylphosphine oxide (0.0809 g, 0.400 mmol), palladium(II) acetate (0.00900 g, 0.0400 mmol) and triethylamine (0.220 mL, 1.58 mmol). The reaction mixture was stirred at 90 °C for 3 h. The crude material was purified by flash column chromatography eluting with 30% ethyl acetate in dichloromethane to give (2-naphthyl)diphenylphosphine oxide (**186**) as a pale yellow solid (0.122 g, 93%). Mp 106–108 °C. Spectroscopic data were consistent with previously published data.⁴⁴³ δ_{H} (400 MHz, CDCl_3) 7.44–7.51 [4H, m, 2 \times (3'-H and 5'-H)], 7.52–7.67 (5H, m, 5 \times ArH), 7.68–7.77 [4H, m, 3 \times (2'-H and 6'-H)], 7.85–7.94 (3H, m, 3 \times ArH), 8.29 (1H, d, J 13.6 Hz, 1-H); δ_{C} (101 MHz, CDCl_3) 127.0 (d, $^3J_{\text{CP}}$ 10.8 Hz, CH), 127.1 (d, $^5J_{\text{CP}}$ 0.6 Hz, CH), 128.0 (d, $^5J_{\text{CP}}$ 0.8 Hz, CH), 128.3 (d, $^4J_{\text{CP}}$ 2.2 Hz, CH), 128.4 (d, $^2J_{\text{CP}}$ 9.8 Hz, CH), 128.7 (d, $^3J_{\text{CP}}$ 12.1 Hz, 4 \times CH), 129.1 (CH), 129.8 (d, $^1J_{\text{CP}}$ 104.6 Hz, C), 132.1 (d, $^4J_{\text{CP}}$ 2.6 Hz, 2 \times CH), 132.3 (d, $^2J_{\text{CP}}$ 10.1 Hz, 4 \times CH), 132.6 (d, $^3J_{\text{CP}}$ 13.2 Hz, C), 132.8 (d, $^1J_{\text{CP}}$ 103.9 Hz, 2 \times C), 134.2 (d, $^2J_{\text{CP}}$ 9.4 Hz, CH), 134.9 (d, $^4J_{\text{CP}}$ 2.4 Hz, C); m/z (ESI) 351 (MNa^+ , 100%).

(4-Methylphenyl)diphenylphosphine oxide (**187**)⁴⁴⁴



Method A: The reaction was carried out according to the previously described procedure for triphenylphosphine oxide (**185**) using sodium iodide (0.0600 g, 0.400 mmol), 4-methylphenyl nonafluorobutanesulfonate (**175**) (0.156 g, 0.400 mmol), anhydrous *N,N'*-dimethylformamide (2.4 mL), diphenylphosphine oxide (0.121 g, 0.600 mmol), palladium(II) acetate (0.00900 g, 0.0400 mmol) and triethylamine (0.220 mL, 1.58 mmol). The reaction mixture was stirred at 120 °C for 4 h. The crude material was purified by flash column chromatography eluting with 30% ethyl acetate in dichloromethane to give (4-methylphenyl)diphenylphosphine oxide (**187**) as a white solid (0.0905 g, 78%). Mp 118–120 °C. Spectroscopic data were consistent with previously published data.⁴⁴⁴ δ_{H} (400 MHz, CDCl_3) 2.40 (3H, s, CH_3), 7.27 (2H, dd, J 8.0, 2.8 Hz, 3-H and 5-H), 7.41–7.49 [4H, m, 2 \times (3'-H and 5'-H)], 7.50–7.59 (4H, m, 2-H, 6-H, 2 \times 4'-H), 7.62–7.71 [4H, m, 2 \times (2'-H and 6'-H)]; δ_{C} (101 MHz, CDCl_3) 21.8 (d, $^5J_{\text{CP}}$ 1.3 Hz, CH_3), 128.6 (d, $^3J_{\text{CP}}$ 12.1 Hz, 4 \times CH), 129.3 (d, $^1J_{\text{CP}}$ 107.0 Hz, C), 129.4 (d, $^3J_{\text{CP}}$ 12.5 Hz, 2 \times CH), 131.9 (d, $^4J_{\text{CP}}$ 2.7 Hz, 2 \times CH), 132.2 (d, $^2J_{\text{CP}}$ 9.8 Hz, 4 \times CH), 132.3 (d, $^2J_{\text{CP}}$ 10.3 Hz, 2 \times CH), 133.0 (d, $^1J_{\text{CP}}$ 104.3 Hz, 2 \times C), 142.6 (d, $^4J_{\text{CP}}$ 2.7 Hz, C); m/z (ESI) 315 (MNa^+ , 100%).

Method B: The reaction was carried out according to the previously described procedure for triphenylphosphine oxide (**185**) using sodium iodide (0.00300 g, 0.0200 mmol), 4-methylphenyl nonafluorobutanesulfonate (**175**) (0.0780 g, 0.200 mmol), anhydrous *N,N'*-dimethylformamide (1.2 mL), diphenylphosphine oxide (0.0610 g, 0.302 mmol), palladium(II) acetate (0.00450 g, 0.0200 mmol) and triethylamine (0.110 mL, 0.790 mmol). The reaction mixture was stirred at 120 °C for 8 h. The crude material was purified by flash column chromatography eluting with 2% methanol in diethyl ether to give (4-methylphenyl)diphenylphosphine oxide (**187**) as a white solid (0.0441 g, 76%). Spectroscopic data were consistent as described above.

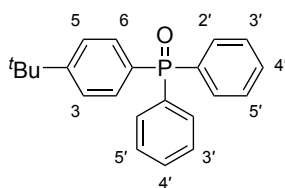
Method C: To an oven-dried microwave tube under argon, was added diphenylphosphine oxide (0.0610 g, 0.302 mmol) and palladium(II) acetate (0.00450 g, 0.0200 mmol), followed by a solution of 4-methylphenyl nonafluorobutanesulfonate (**175**) (0.0780 g, 0.200 mmol) in anhydrous *N,N'*-dimethylformamide (1.2 mL). Triethylamine (0.110 mL, 0.790 mmol) was then added and the tube was sealed. The reaction mixture was heated to 120 °C and stirred for 24 h. The reaction mixture was cooled to room temperature, diluted with ethyl acetate (15 mL) and washed with 2 M aqueous lithium chloride solution (3 × 15 mL). The organic layer was dried (MgSO₄), filtered and concentrated *in vacuo*. The crude material was purified by flash column chromatography eluting with 2% methanol in diethyl ether to give (4-methylphenyl)diphenylphosphine oxide (**187**) as a white solid (0.0461 g, 79%). Spectroscopic data were consistent as described above.

Method D: A stirrer bar and sodium acetate (0.0328 g, 0.400 mmol) were added to a microwave tube and dried in an oven at 140 °C overnight. 4-Methylphenyl nonafluorobutanesulfonate (**175**) (0.156 g, 0.400 mmol) was dried under high vacuum for 1 h, purged with argon and dissolved in anhydrous *N,N'*-dimethylformamide (2.4 mL). Diphenylphosphine oxide (**234**) (0.121 g, 0.600 mmol) was dried *in vacuo* for 1 h. The oven-dried microwave tube was cooled to room temperature *in vacuo* and then purged with argon. To the tube was added diphenylphosphine oxide (**234**) and palladium(II) acetate (0.00900 g, 0.0400 mmol), followed by the 4-methylphenyl nonafluorobutanesulfonate (**175**) solution and triethylamine (0.220 mL, 1.58 mmol). The tube was sealed, heated to 120 °C and stirred for 22 h. The reaction mixture was cooled to room temperature, diluted with ethyl acetate (15 mL) and washed with 2 M aqueous lithium chloride solution (3 × 15 mL). The organic layer was dried (MgSO₄), filtered and concentrated *in vacuo*. The crude material was purified by flash column chromatography eluting with 2% methanol in diethyl ether to give (4-methylphenyl)diphenylphosphine oxide (**187**) as a white solid (0.0642 g, 55%). Spectroscopic data were consistent as described above.

Method E: A stirrer bar and sodium chloride (0.0234 g, 0.400 mmol) were added to a microwave tube and dried in an oven at 140 °C overnight. 4-Methylphenyl nonafluorobutanesulfonate (**175**) (0.156 g, 0.400 mmol) was dried under high vacuum for 1 h, purged with argon and dissolved in anhydrous *N,N'*-

dimethylformamide (2.4 mL). Diphenylphosphine oxide (**234**) (0.121 g, 0.600 mmol) was dried *in vacuo* for 1 h. The oven-dried microwave tube was cooled to room temperature *in vacuo* and then purged with argon. To the tube was added diphenylphosphine oxide (**234**) and palladium(II) acetate (0.00900 g, 0.0400 mmol), followed by the 4-methylphenyl nonafluorobutanesulfonate (**175**) solution and triethylamine (0.220 mL, 1.58 mmol). The tube was sealed, heated to 120 °C and stirred for 32 h. The reaction mixture was cooled to room temperature, diluted with ethyl acetate (15 mL) and washed with 2 M aqueous lithium chloride solution (3 × 15 mL). The organic layer was dried (MgSO₄), filtered and concentrated *in vacuo*. The crude material was purified by flash column chromatography eluting with 2% methanol in diethyl ether to give (4-methylphenyl)diphenylphosphine oxide (**187**) as a white solid (0.0745 g, 64%). Spectroscopic data were consistent as described above.

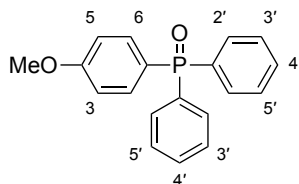
(4-*tert*-Butylphenyl)diphenylphosphine oxide (**188**)⁴⁴⁵



The reaction was carried out according to the previously described procedure for triphenylphosphine oxide (**185**) using sodium iodide (0.0600 g, 0.400 mmol), 4-*tert*-butylphenyl nonafluorobutanesulfonate (**179**) (0.173 g, 0.400 mmol), anhydrous *N,N'*-dimethylformamide (2.4 mL), diphenylphosphine oxide (0.121 g, 0.600 mmol), palladium(II) acetate (0.00900 g, 0.0400 mmol) and triethylamine (0.220 mL, 1.58 mmol). The reaction mixture was stirred at 120 °C for 6 h. The crude material was purified by flash column chromatography eluting with 2% methanol in dichloromethane to give (4-*tert*-butylphenyl)diphenylphosphine oxide (**188**) as an orange solid (0.0857 g, 64%). Mp 113–115 °C. Spectroscopic data were consistent with previously published data.⁴⁴⁵ δ_{H} (400 MHz, CDCl₃) 1.32 (9H, s, 3 × CH₃), 7.41–7.49 (6H, m, 6 × ArH), 7.50–7.56 (2H, m, 2 × 4'-H), 7.58 (2H, dd, *J* 11.8, 8.6 Hz, 2-H and 6-H), 7.63–7.72 [4H, m, 2 × (2'-H and 6'-H)]; δ_{C} (101 MHz, CDCl₃) 31.2 (3 × CH₃), 35.2 (C), 125.7 (d, ³*J*_{CP} 12.4 Hz, 2 × CH), 128.6 (d, ³*J*_{CP} 12.1 Hz, 4 × CH), 129.2 (d, ¹*J*_{CP} 106.9 Hz, C), 131.9 (d, ⁴*J*_{CP} 2.8 Hz, 2 × CH), 132.1 (d, ²*J*_{CP} 10.3 Hz,

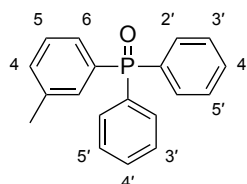
2 × CH), 132.2 (d, $^2J_{CP}$ 9.9 Hz, 4 × CH), 133.0 (d, $^1J_{CP}$ 104.3 Hz, 2 × C), 155.5 (d, $^4J_{CP}$ 2.8 Hz, C); m/z (ESI) 357 (MNa⁺. 100%).

(4-Methoxyphenyl)diphenylphosphine oxide (**189**)⁴⁰⁹



The reaction was carried out according to the previously described procedure for triphenylphosphine oxide (**185**) using sodium iodide (0.0600 g, 0.400 mmol), 4-methoxyphenyl nonafluorobutanesulfonate (**147**) (0.162 g, 0.400 mmol), anhydrous *N,N'*-dimethylformamide (2.4 mL), diphenylphosphine oxide (0.121 g, 0.600 mmol), palladium(II) acetate (0.00900 g, 0.0400 mmol) and triethylamine (0.220 mL, 1.58 mmol). The reaction mixture was stirred at 120 °C for 6 h. The crude material was purified by flash column chromatography eluting with 2% methanol in diethyl ether to give (4-methoxyphenyl)diphenylphosphine oxide (**189**) as a pale yellow solid (0.0784 g, 64%). Mp 103–105 °C (lit.⁴⁰⁹ 106–108 °C); δ_H (400 MHz, CDCl₃) 3.84 (3H, s, CH₃), 6.96 (2H, dd, J 8.8, 2.4 Hz, 3-H and 5-H), 7.40–7.55 (6H, m, 6 × ArH), 7.58 (2H, dd, J 11.2, 8.8 Hz, 2-H and 6-H), 7.62–7.71 [4H, m, 2 × (2'-H and 6'-H)]; δ_C (101 MHz, CDCl₃) 55.5 (CH₃), 114.2 (d, $^3J_{CP}$ 13.1 Hz, 2 × CH), 123.8 (d, $^1J_{CP}$ 110.8 Hz, C), 128.6 (d, $^3J_{CP}$ 12.1 Hz, 4 × CH), 131.9 (d, $^4J_{CP}$ 2.7 Hz, 2 × CH), 132.2 (d, $^2J_{CP}$ 10.0 Hz, 4 × CH), 133.2 (d, $^1J_{CP}$ 104.7 Hz, 2 × C), 134.1 (d, $^2J_{CP}$ 11.2 Hz, 2 × CH), 162.6 (d, $^4J_{CP}$ 2.8 Hz, C); m/z (ESI) 331 (MNa⁺. 100%).

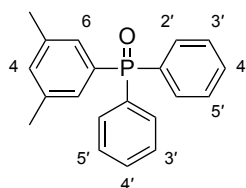
(3-Methylphenyl)diphenylphosphine oxide (**199**)⁴⁴⁶



The reaction was carried out according to the previously described procedure for triphenylphosphine oxide (**185**) using sodium iodide (0.0600 g, 0.400 mmol), 3-methylphenyl nonafluorobutanesulfonate (**176**) (0.156 g, 0.400 mmol), anhydrous

N,N'-dimethylformamide (2.4 mL), diphenylphosphine oxide (0.121 g, 0.600 mmol), palladium(II) acetate (0.00900 g, 0.0400 mmol) and triethylamine (0.220 mL, 1.58 mmol). The reaction mixture was stirred at 120 °C for 4 h. The crude material was purified by flash column chromatography eluting with 2% methanol in diethyl ether to give (3-methylphenyl)diphenylphosphine oxide (**199**) as a pale orange solid (0.111 g, 95%). Mp 112–114 °C. Spectroscopic data were consistent with previously published data.⁴⁴⁶ δ_{H} (400 MHz, CDCl₃) 2.36 (3H, s, CH₃), 7.29–7.41 (3H, m, 4-H, 5-H, and 6-H), 7.42–7.49 [4H, m, 2 × (3'-H and 5'-H)], 7.54 (2H, ttd, *J* 7.3, 1.7, 1.6 Hz, 2 × 4'-H), 7.58 (1H, br d, *J* 12.4 Hz, 2-H), 7.62–7.71 [4H, m, 2 × (2'-H and 6'-H)]; δ_{C} (101 MHz, CDCl₃) 21.6 (CH₃), 128.4 (d, ³*J*_{CP} 12.9 Hz, CH), 128.6 (d, ³*J*_{CP} 12.1 Hz, 4 × CH), 129.3 (d, ²*J*_{CP} 10.3 Hz, CH), 132.0 (d, ⁴*J*_{CP} 2.7 Hz, 2 × CH), 132.2 (d, ²*J*_{CP} 9.9 Hz, 4 × CH), 132.5 (d, ¹*J*_{CP} 104.5 Hz, C), 132.6 (d, ²*J*_{CP} 9.5 Hz, CH), 132.8 (d, ⁴*J*_{CP} 2.8 Hz, CH), 132.9 (d, ¹*J*_{CP} 104.2 Hz, 2 × C), 138.6 (d, ³*J*_{CP} 12.1 Hz, C); *m/z* (ESI) 315 (MNa⁺. 100%).

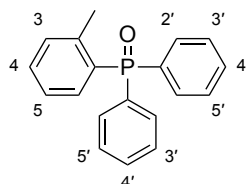
(3,5-Dimethylphenyl)diphenylphosphine oxide (**200**)⁴⁰⁹



The reaction was carried out according to the previously described procedure for triphenylphosphine oxide (**185**) using sodium iodide (0.0300 g, 0.200 mmol), 3,5-dimethylphenyl nonafluorobutanesulfonate (**177**) (0.0810 g, 0.200 mmol), anhydrous *N,N'*-dimethylformamide (1.2 mL), diphenylphosphine oxide (0.0610 g, 0.302 mmol), palladium(II) acetate (0.00450 g, 0.0200 mmol) and triethylamine (0.110 mL, 0.790 mmol). The reaction mixture was stirred at 120 °C for 4 h. The crude material was purified by flash column chromatography eluting with 1–2% gradient of methanol in diethyl ether to give (3,5-dimethylphenyl)diphenylphosphine oxide (**200**) as a pale yellow solid (0.0493 g, 81%). Mp 118–120 °C. Spectroscopic data were consistent with previously published data.⁴⁰⁹ δ_{H} (400 MHz, CDCl₃) 2.31 (6H, s, 2 × CH₃), 7.16 (1H, br s, 4-H), 7.27 (2H, br d, *J* 12.0 Hz, 2-H and 6-H), 7.42–7.49 [4H, m, 2 × (3'-H and 5'-H)], 7.54 (2H, tdt, *J* 7.4, 1.7, 1.6 Hz, 2 × 4'-H), 7.62–7.71 [4H, m, 2 × (2'-H and 6'-H)]; δ_{C} (101 MHz, CDCl₃) 21.4 (2 × CH₃), 128.6 (d, ³*J*_{CP}

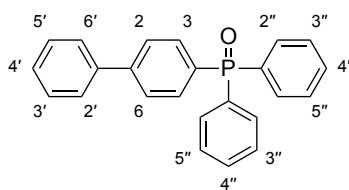
12.1 Hz, 4 × CH), 129.8 (d, $^2J_{CP}$ 9.9 Hz, 2 × CH), 131.9 (d, $^4J_{CP}$ 2.8 Hz, 2 × CH), 132.2 (d, $^1J_{CP}$ 104.1 Hz, C), 132.2 (d, $^2J_{CP}$ 9.9 Hz, 4 × CH), 132.9 (d, $^1J_{CP}$ 103.9 Hz, 2 × C), 133.8 (d, $^4J_{CP}$ 2.9 Hz, CH), 138.3 (d, $^3J_{CP}$ 12.9 Hz, 2 × C); m/z (ESI) 329 (MNa⁺. 100%).

(2-Methylphenyl)diphenylphosphine oxide (**201**)⁴⁴⁴



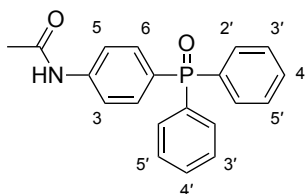
The reaction was carried out according to the previously described procedure for triphenylphosphine oxide (**185**) using sodium iodide (0.0600 g, 0.400 mmol), 2-methylphenyl nonafluorobutanesulfonate (**178**) (0.156 g, 0.400 mmol), anhydrous *N,N'*-dimethylformamide (2.4 mL), diphenylphosphine oxide (0.121 g, 0.600 mmol), palladium(II) acetate (0.00900 g, 0.0400 mmol) and triethylamine (0.220 mL, 1.58 mmol). The reaction mixture was stirred at 120 °C for 7 h. The crude material was purified by flash column chromatography eluting with 2% methanol in diethyl ether to give (2-methylphenyl)diphenylphosphine oxide (**201**) as an off-white solid (0.0679 g, 58%). Mp 119–121 °C (lit.⁴⁴⁴ 121.5–122.9 °C); δ_H (400 MHz, CDCl₃) 2.45 (3H, s, CH₃), 7.03 (1H, ddd, J 14.0, 7.5, 1.3 Hz, 6-H), 7.13 (1H, br td, J 7.5, 2.0 Hz, 5-H), 7.28 (1H, br dd, J 7.5, 4.0 Hz, 3-H), 7.41 (1H, tt, J 7.5, 1.3 Hz, 4-H), 7.44–7.50 [4H, m, 2 × (3'-H and 5'-H)], 7.55 (2H, ttd, J 7.4, 1.8, 1.6 Hz, 2 × 4'-H), 7.61–7.70 [4H, m, 2 × (2'-H and 6'-H)]; δ_C (101 MHz, CDCl₃) 21.8 (d, $^3J_{CP}$ 4.6 Hz, CH₃), 125.3 (d, $^3J_{CP}$ 12.9 Hz, CH), 128.7 (d, $^3J_{CP}$ 12.1 Hz, 4 × CH), 131.0 (d, $^1J_{CP}$ 103.5 Hz, C), 131.9 (d, $^4J_{CP}$ 2.8 Hz, 2 × CH), 132.0 (d, $^3J_{CP}$ 10.5 Hz, CH), 132.1 (d, $^2J_{CP}$ 9.9 Hz, 4 × CH), 132.2 (d, $^4J_{CP}$ 2.6 Hz, CH), 133.0 (d, $^1J_{CP}$ 103.7 Hz, 2 × C), 133.6 (d, $^2J_{CP}$ 12.8 Hz, CH), 143.5 (d, $^2J_{CP}$ 8.1 Hz, C); m/z (ESI) 315 (MNa⁺. 100%).

(1,1'-Biphenyl)-4-yl diphenylphosphine oxide (**202**)⁴⁴³



The reaction was carried out according to the previously described procedure for triphenylphosphine oxide (**185**) using sodium iodide (0.0300 g, 0.200 mmol), (1,1'-biphenyl)-4-yl nonafluorobutanesulfonate (**155**) (0.0905 g, 0.200 mmol), anhydrous *N,N'*-dimethylformamide (1.2 mL), diphenylphosphine oxide (0.0610 g, 0.302 mmol), palladium(II) acetate (0.00450 g, 0.0200 mmol) and triethylamine (0.110 mL, 0.790 mmol). The reaction mixture was stirred at 120 °C for 4 h. The crude material was purified by flash column chromatography eluting with 1% methanol in diethyl ether to give (1,1'-biphenyl)-4-yl diphenylphosphine oxide (**202**) as a pale brown oil (0.0680 g, 96%). Spectroscopic data were consistent with previously published data.⁴⁴³ δ_{H} (400 MHz, CDCl_3) 7.39 (1H, tt, J 7.3, 1.7 Hz, 4'-H), 7.43–7.52 (6H, m, 6 \times ArH), 7.53–7.63 (4H, m, 4 \times ArH), 7.66–7.78 (8H, m, 8 \times ArH); δ_{C} (101 MHz, CDCl_3) 127.3 (d, $^3J_{\text{CP}}$ 12.5 Hz, 2 \times CH), 127.4 (2 \times CH), 128.3 (CH), 128.7 (d, $^3J_{\text{CP}}$ 12.2 Hz, 4 \times CH), 129.1 (2 \times CH), 131.2 (d, $^1J_{\text{CP}}$ 105.6 Hz, C), 132.1 (d, $^4J_{\text{CP}}$ 2.7 Hz, 2 \times CH), 132.2 (d, $^2J_{\text{CP}}$ 10.0 Hz, 4 \times CH), 132.7 (d, $^2J_{\text{CP}}$ 10.3 Hz, 2 \times CH), 132.7 (d, $^1J_{\text{CP}}$ 104.8 Hz, 2 \times C), 140.0 (d, $^5J_{\text{CP}}$ 0.7 Hz, C), 144.8 (d, $^4J_{\text{CP}}$ 2.8 Hz, C); m/z (ESI) 377 (MNa^+ , 100%).

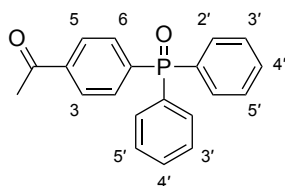
(4-Acetamidophenyl) diphenylphosphine oxide (**203**)⁴⁴⁷



The reaction was carried out according to the previously described procedure for triphenylphosphine oxide (**185**) using sodium iodide (0.0300 g, 0.200 mmol), 4-acetamidophenyl nonafluorobutanesulfonate (**180**) (0.0866 g, 0.200 mmol), anhydrous *N,N'*-dimethylformamide (1.2 mL), diphenylphosphine oxide (0.0610 g,

0.302 mmol), palladium(II) acetate (0.00450 g, 0.0200 mmol) and triethylamine (0.110 mL, 0.790 mmol). The reaction mixture was heated to 120 °C and stirred for 6 h. The reaction mixture was cooled to room temperature, diluted with ethyl acetate (15 mL) and washed with water (3 × 15 mL). The organic layer was dried (MgSO₄), filtered and concentrated *in vacuo*. The crude material was purified by flash column chromatography eluting with 8% methanol in diethyl ether to give (4-acetamidophenyl)diphenylphosphine oxide (**203**) as a brown solid (0.0431 g, 65%). Mp 144–146 °C (lit.⁴⁴⁷ 150–152 °C); δ_{H} (400 MHz, CDCl₃) 2.14 (3H, s, CH₃), 7.40–7.50 (6H, m, 6 × ArH), 7.54 (2H, ttd, *J* 7.4, 1.7, 1.6 Hz, 2 × 4'-H), 7.58–7.69 (6H, m, 6 × ArH), 9.28 (1H, br s, NH); δ_{C} (101 MHz, CDCl₃) 24.6 (CH₃), 119.7 (d, ³*J*_{CP} 12.6 Hz, 2 × CH), 126.3 (d, ¹*J*_{CP} 108.7 Hz, C), 128.7 (d, ³*J*_{CP} 12.2 Hz, 4 × CH), 132.1 (d, ²*J*_{CP} 10.0 Hz, 4 × CH), 132.2 (d, ⁴*J*_{CP} 2.6 Hz, 2 × CH), 132.4 (d, ¹*J*_{CP} 105.2 Hz, 2 × C), 133.1 (d, ²*J*_{CP} 10.9 Hz, 2 × CH), 142.4 (d, ⁴*J*_{CP} 3.0 Hz, C), 169.6 (C); *m/z* (ESI) 358 (MNa⁺. 100%).

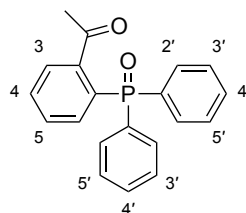
(4-Acetylphenyl)diphenylphosphine oxide (**204**)⁴⁴⁸



The reaction was carried out according to the previously described procedure for triphenylphosphine oxide (**185**) using sodium iodide (0.0300 g, 0.200 mmol), 4-acetylphenyl nonafluorobutanesulfonate (**144**) (0.0836 g, 0.200 mmol), anhydrous *N,N'*-dimethylformamide (1.2 mL), diphenylphosphine oxide (0.0610 g, 0.302 mmol), palladium(II) acetate (0.00450 g, 0.0200 mmol) and triethylamine (0.110 mL, 0.790 mmol). The reaction mixture was stirred at 120 °C for 4 h. The crude material was purified by flash column chromatography eluting with 2% methanol in diethyl ether to give (4-acetylphenyl)diphenylphosphine oxide (**204**) as a pale yellow solid (0.0615 g, 96%). Mp 116–118 °C (lit.⁴⁴⁸ 120.0–120.5 °C); δ_{H} (400 MHz, CDCl₃) 2.63 (3H, s, CH₃), 7.42–7.52 [4H, m, 2 × (3'-H and 5'-H)], 7.53–7.60 (2H, m, 2 × 4'-H), 7.61–7.71 [4H, m, 2 × (2'-H and 6'-H)], 7.79 (2H, dd, *J* 10.8, 8.4 Hz, 2-H and 6-H), 8.02 (2H, dd, *J* 8.4, 2.0 Hz, 3-H and 5-H); δ_{C} (101 MHz, CDCl₃) 27.0 (CH₃), 128.2 (d, ³*J*_{CP} 12.1 Hz, 2 × CH), 128.8 (d, ³*J*_{CP} 12.3 Hz, 4 × CH), 132.0 (d, ¹*J*_{CP} 105.2 Hz,

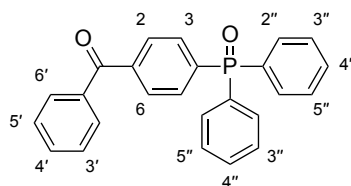
2 × C), 132.2 (d, $^2J_{CP}$ 10.0 Hz, 4 × CH), 132.4 (d, $^4J_{CP}$ 2.7 Hz, 2 × CH), 132.6 (d, $^2J_{CP}$ 10.1 Hz, 2 × CH), 137.9 (d, $^1J_{CP}$ 101.0 Hz, C), 139.6 (d, $^4J_{CP}$ 2.7 Hz, C), 197.7 (d, $^5J_{CP}$ 0.8 Hz, C); m/z (ESI) 343 (MNa⁺. 100%).

(2-Acetylphenyl)diphenylphosphine oxide (**205**)



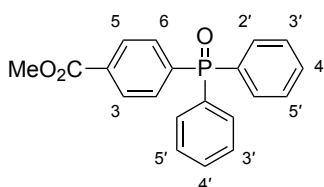
The reaction was carried out according to the previously described procedure for triphenylphosphine oxide (**185**) using sodium iodide (0.0300 g, 0.200 mmol), 2-acetylphenyl nonafluorobutanesulfonate (**181**) (0.0836 g, 0.200 mmol), anhydrous *N,N'*-dimethylformamide (1.2 mL), diphenylphosphine oxide (0.0610 g, 0.302 mmol), palladium(II) acetate (0.00450 g, 0.0200 mmol) and triethylamine (0.110 mL, 0.790 mmol). The reaction mixture was stirred at 120 °C for 4 h. The crude material was purified by flash column chromatography eluting with 6% methanol in diethyl ether to give (2-acetylphenyl)diphenylphosphine oxide (**205**) as a yellow solid (0.0236 g, 37%). Mp 119–121 °C; ν_{max}/cm^{-1} (neat) 3055 (CH), 1694 (C=O), 1435, 1246, 1188, 1107, 721; δ_H (400 MHz, CDCl₃) 2.45 (3H, s, CH₃), 7.41–7.55 (7H, m, 7 × ArH), 7.58–7.69 (7H, m, 7 × ArH); δ_C (101 MHz, CDCl₃) 29.6 (CH₃), 128.3 (d, $^3J_{CP}$ 9.2 Hz, CH), 128.4 (d, $^3J_{CP}$ 12.5 Hz, 4 × CH), 130.3 (d, $^3J_{CP}$ 11.9 Hz, CH), 131.3 (d, $^1J_{CP}$ 99.4 Hz, C), 131.7 (d, $^4J_{CP}$ 2.8 Hz, 2 × CH), 131.9 (d, $^4J_{CP}$ 3.7 Hz, CH), 132.0 (d, $^2J_{CP}$ 10.1 Hz, 4 × CH), 133.4 (d, $^1J_{CP}$ 108.2 Hz, 2 × C), 135.0 (d, $^2J_{CP}$ 10.5 Hz, CH), 144.6 (d, $^2J_{CP}$ 6.9 Hz, C), 201.6 (d, $^3J_{CP}$ 2.7 Hz, C); m/z (ESI) 343.0858 (MNa⁺. C₂₀H₁₇NaO₂P requires 343.0858).

4-(Diphenylphosphoryl)benzophenone (**206**)



The reaction was carried out according to the previously described procedure for triphenylphosphine oxide (**185**) using sodium iodide (0.0300 g, 0.200 mmol), 4-nonafluorobutanesulfonyloxybenzophenone (**182**) (0.0960 g, 0.200 mmol), anhydrous *N,N'*-dimethylformamide (1.2 mL), diphenylphosphine oxide (0.0610 g, 0.302 mmol), palladium(II) acetate (0.00450 g, 0.0200 mmol) and triethylamine (0.110 mL, 0.790 mmol). The reaction mixture was stirred at 120 °C for 4 h. The crude material was purified by flash column chromatography eluting with 2% methanol in diethyl ether to give 4-(diphenylphosphoryl)benzophenone (**206**) as a pale yellow solid (0.0624 g, 82%). Mp 138–140 °C; $\nu_{\max}/\text{cm}^{-1}$ (neat) 3028 (CH), 1659 (C=O), 1435, 1285, 1196, 1111, 926, 717; δ_{H} (400 MHz, CDCl_3) 7.45–7.54 (6H, m, 6 × ArH), 7.55–7.64 (3H, m, 3 × ArH), 7.65–7.74 [4H, m, 2 × (2''-H and 6''-H)], 7.76–7.89 (6H, m, 6 × ArH); δ_{C} (101 MHz, CDCl_3) 128.6 (2 × CH), 128.8 (d, $^3J_{\text{CP}}$ 12.2 Hz, 4 × CH), 129.8 (d, $^3J_{\text{CP}}$ 12.1 Hz, 2 × CH), 130.3 (2 × CH), 132.0 (d, $^1J_{\text{CP}}$ 105.1 Hz, 2 × C), 132.2 (d, $^2J_{\text{CP}}$ 10.0 Hz, 6 × CH), 132.4 (d, $^4J_{\text{CP}}$ 2.8 Hz, 2 × CH), 133.2 (CH), 136.9 (C), 137.1 (d, $^1J_{\text{CP}}$ 101.3 Hz, C), 140.7 (d, $^4J_{\text{CP}}$ 2.8 Hz, C), 196.2 (d, $^5J_{\text{CP}}$ 0.8 Hz, C); m/z (ESI) 405.1017 (MNa^+ . $\text{C}_{25}\text{H}_{19}\text{NaO}_2\text{P}$ requires 405.1015).

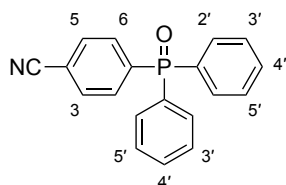
(4-Methoxycarbonylphenyl)diphenylphosphine oxide (**207**)⁴⁴⁹



The reaction was carried out according to the previously described procedure for triphenylphosphine oxide (**185**) using sodium iodide (0.0300 g, 0.200 mmol), methyl 4-nonafluorobutanesulfonyloxybenzoate (**141**) (0.0870 g, 0.200 mmol), anhydrous *N,N'*-dimethylformamide (1.2 mL), diphenylphosphine oxide (0.0610 g, 0.302 mmol), palladium(II) acetate (0.00450 g, 0.0200 mmol) and triethylamine (0.110 mL,

0.790 mmol). The reaction mixture was stirred at 120 °C for 4 h. The reaction mixture was cooled to room temperature and diluted with ethyl acetate (10 mL). The organic layer was washed with 2 M aqueous lithium chloride solution (3 × 10 mL) and then water (2 × 10 mL). The organic layer was dried (MgSO₄), filtered and concentrated *in vacuo*. The crude material was purified by flash column chromatography eluting with 2% methanol in diethyl ether to give (4-methoxycarbonylphenyl)diphenylphosphine oxide (**207**) as an off-white solid (0.0518 g, 77%). Mp 101–103 °C (lit.⁴⁴⁹ 104–105 °C); δ_{H} (400 MHz, CDCl₃) 3.93 (3H, s, CH₃), 7.42–7.51 [4H, m, 2 × (3'-H and 5'-H)], 7.56 (2H, ttd, *J* 7.5, 1.6, 1.5 Hz, 2 × 4'-H), 7.61–7.70 [4H, m, 2 × (2'-H and 6'-H)], 7.76 (2H, dd, *J* 11.6, 8.4 Hz, 2-H and 6-H), 8.11 (2H, dd, *J* 8.4, 2.4 Hz, 3-H and 5-H); δ_{C} (101 MHz, CDCl₃) 52.6 (CH₃), 128.8 (d, ³*J*_{CP} 12.2 Hz, 4 × CH), 129.5 (d, ³*J*_{CP} 12.1 Hz, 2 × CH), 132.0 (d, ¹*J*_{CP} 105.1 Hz, 2 × C), 132.2 (d, ²*J*_{CP} 10.2 Hz, 4 × CH), 132.3 (d, ²*J*_{CP} 10.8 Hz, 2 × CH), 132.3 (d, ⁴*J*_{CP} 2.7 Hz, 2 × CH), 133.3 (d, ⁴*J*_{CP} 2.7 Hz, C), 137.8 (d, ¹*J*_{CP} 101.2 Hz, C), 166.4 (d, ⁵*J*_{CP} 0.8 Hz, C); *m/z* (ESI) 359 (MNa⁺, 100%).

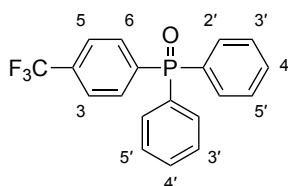
(4-Cyanophenyl)diphenylphosphine oxide (**208**)⁴⁴⁸



The reaction was carried out according to the previously described procedure for triphenylphosphine oxide (**185**) using sodium iodide (0.0300 g, 0.200 mmol), 4-cyanophenyl nonafluorobutanesulfonate (**140**) (0.0802 g, 0.200 mmol), anhydrous *N,N'*-dimethylformamide (1.2 mL), diphenylphosphine oxide (0.0610 g, 0.302 mmol), palladium(II) acetate (0.00450 g, 0.0200 mmol) and triethylamine (0.110 mL, 0.790 mmol). The reaction mixture was stirred at 120 °C for 4 h. The reaction mixture was cooled to room temperature and diluted with ethyl acetate (10 mL). The organic layer was washed with 2 M aqueous lithium chloride solution (3 × 10 mL) and then water (2 × 10 mL). The organic layer was dried (MgSO₄), filtered and concentrated *in vacuo*. The crude material was purified by flash column chromatography eluting with 2% methanol in diethyl ether to give (4-cyanophenyl)diphenylphosphine oxide (**208**) as a pale brown oil (0.0536 g, 89%). Spectroscopic data were consistent with

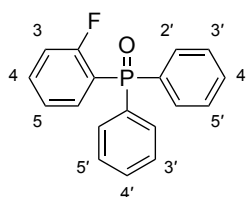
previously published data.⁴⁴⁸ δ_{H} (400 MHz, CDCl_3) 7.44–7.54 [4H, m, 2 \times (3'-H and 5'-H)], 7.59 (2H, ttd, J 7.5, 1.7, 1.6 Hz, 2 \times 4'-H), 7.61–7.70 [4H, m, 2 \times (2'-H and 6'-H)], 7.71–7.84 (4H, m, 2-H, 3-H, 5-H and 6-H); δ_{C} (101 MHz, CDCl_3) 115.7 (d, $^4J_{\text{CP}}$ 3.2 Hz, C), 118.0 (d, $^5J_{\text{CP}}$ 1.6 Hz, C), 128.9 (d, $^3J_{\text{CP}}$ 12.4 Hz, 4 \times CH), 131.3 (d, $^1J_{\text{CP}}$ 105.7 Hz, 2 \times C), 132.1 (d, $^3J_{\text{CP}}$ 11.4 Hz, 2 \times CH), 132.1 (d, $^2J_{\text{CP}}$ 10.3 Hz, 4 \times CH), 132.7 (d, $^4J_{\text{CP}}$ 3.1 Hz, 2 \times CH), 132.7 (d, $^2J_{\text{CP}}$ 10.1 Hz, 2 \times CH), 138.6 (d, $^1J_{\text{CP}}$ 99.5 Hz, C); m/z (ESI) 326 (MNa^+ , 100%).

[4-(Trifluoromethyl)phenyl]diphenylphosphine oxide (**209**)⁴⁴⁸



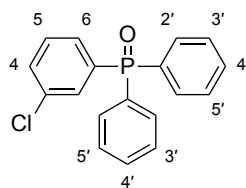
The reaction was carried out according to the previously described procedure for triphenylphosphine oxide (**185**) using sodium iodide (0.0300 g, 0.200 mmol), 4-(trifluoromethyl)phenyl nonafluorobutanesulfonate (**156**) (0.0890 g, 0.200 mmol), anhydrous N,N' -dimethylformamide (1.2 mL), diphenylphosphine oxide (0.0610 g, 0.302 mmol), palladium(II) acetate (0.00450 g, 0.0200 mmol) and triethylamine (0.110 mL, 0.790 mmol). The reaction mixture was stirred at 120 °C for 4 h. The reaction mixture was cooled to room temperature and diluted with ethyl acetate (10 mL). The organic layer was washed with 2 M aqueous lithium chloride solution (3 \times 10 mL) and then water (2 \times 10 mL). The organic layer was dried (MgSO_4), filtered and concentrated *in vacuo*. The crude material was purified by flash column chromatography eluting with 1% methanol in diethyl ether to give [4-(trifluoromethyl)phenyl]diphenylphosphine oxide (**209**) as a pale brown oil (0.0604 g, 87%). Spectroscopic data were consistent with previously published data.⁴⁴⁸ δ_{H} (400 MHz, CDCl_3) 7.49 [4H, td, J 7.4, 2.4 Hz, 2 \times (3'-H and 5'-H)], 7.58 (2H, t, J 7.4 Hz, 2 \times 4'-H), 7.66 [4H, dd, J 12.4, 7.4 Hz, 2 \times (2'-H and 6'-H)], 7.72 (2H, dd, J 8.4, 2.4 Hz, 3-H and 5-H), 7.82 (2H, dd, J 11.2, 8.4 Hz, 2-H and 6-H); δ_{C} (101 MHz, CDCl_3) 123.7 (q, $^1J_{\text{CF}}$ 273.6 Hz, CF_3), 125.5 (dq, $^3J_{\text{CP}}$ 12.0 Hz, $^3J_{\text{CF}}$ 3.8 Hz, 2 \times CH), 128.9 (d, $^3J_{\text{CP}}$ 12.3 Hz, 4 \times CH), 131.8 (d, $^1J_{\text{CP}}$ 105.4 Hz, 2 \times C), 132.2 (d, $^2J_{\text{CP}}$ 10.1 Hz, 4 \times CH), 132.5 (d, $^4J_{\text{CP}}$ 2.8 Hz, 2 \times CH), 132.7 (d, $^2J_{\text{CP}}$ 10.1 Hz, 2 \times CH), 133.8 (qd, $^2J_{\text{CF}}$ 32.9 Hz, $^4J_{\text{CP}}$ 2.9 Hz, C), 137.3 (d, $^1J_{\text{CP}}$ 101.2 Hz, C); m/z (ESI) 369 (MNa^+ , 100%).

(2-Fluorophenyl)diphenylphosphine oxide (**210**)



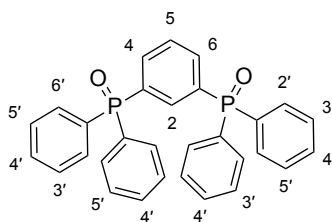
The reaction was carried out according to the previously described procedure for triphenylphosphine oxide (**185**) using sodium iodide (0.0300 g, 0.200 mmol), 2-fluorophenyl nonafluorobutanesulfonate (**157**) (0.0790 g, 0.200 mmol), anhydrous *N,N'*-dimethylformamide (1.2 mL), diphenylphosphine oxide (0.0610 g, 0.302 mmol), palladium(II) acetate (0.00450 g, 0.0200 mmol) and triethylamine (0.110 mL, 0.790 mmol). The reaction mixture was stirred at 120 °C for 4 h. The reaction mixture was cooled to room temperature and diluted with ethyl acetate (10 mL). The organic layer was washed with 2 M aqueous lithium chloride solution (3 × 10 mL) and then water (2 × 10 mL). The organic layer was dried (MgSO₄), filtered and concentrated *in vacuo*. The crude material was purified by flash column chromatography eluting with 2% methanol in diethyl ether to give (2-fluorophenyl)diphenylphosphine oxide (**210**) as a pale yellow solid (0.0303 g, 51%). Mp 119–121 °C; $\nu_{\max}/\text{cm}^{-1}$ (neat) 3010 (CH), 1601, 1437, 1273, 1191, 1119, 823, 757; δ_{H} (400 MHz, CDCl₃) 7.05–7.13 (1H, m, 3-H), 7.31 (1H, br t, *J* 7.6 Hz, 5-H), 7.47 [4H, td, *J* 7.4, 3.2 Hz, 2 × (3'-H and 5'-H)], 7.52–7.61 (3H, m, 4-H and 2 × 4'-H), 7.73 [4H, dd, *J* 12.6, 7.4 Hz, 2 × (2'-H and 6'-H)], 7.83–7.93 (1H, m, 6-H); δ_{C} (101 MHz, CDCl₃) 116.2 (dd, ²*J*_{CF} 22.8 Hz, ³*J*_{CP} 5.6 Hz, CH), 120.4 (dd, ¹*J*_{CP} 100.6 Hz, ²*J*_{CF} 18.6 Hz, C), 124.7 (dd, ³*J*_{CP} 10.6, ⁴*J*_{CF} 3.4 Hz, CH), 128.6 (d, ³*J*_{CP} 12.6 Hz, 4 × CH), 131.9 (dd, ²*J*_{CP} 10.6 Hz, ⁵*J*_{CF} 2.0 Hz, 4 × CH), 132.2 (d, ⁴*J*_{CP} 2.9 Hz, 2 × CH), 132.3 (d, ¹*J*_{CP} 108.6 Hz, 2 × C), 134.8–135.0 (m, 2 × CH), 163.1 (dd, ¹*J*_{CF} 251.3 Hz, ²*J*_{CP} 2.1 Hz, C); *m/z* (ESI) 319.0654 (MNa⁺. C₁₈H₁₄FNaOP requires 319.0659).

(3-Chlorophenyl)diphenylphosphine oxide (**211**)



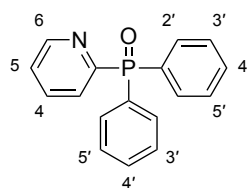
The reaction was carried out according to the previously described procedure for triphenylphosphine oxide (**185**) using sodium iodide (0.0300 g, 0.200 mmol), 3-chlorophenyl nonafluorobutanesulfonate (**145**) (0.0820 g, 0.200 mmol), anhydrous *N,N'*-dimethylformamide (1.2 mL), diphenylphosphine oxide (0.0610 g, 0.302 mmol), palladium(II) acetate (0.00450 g, 0.0200 mmol) and triethylamine (0.110 mL, 0.790 mmol). The reaction mixture was stirred at 120 °C for 4 h. The reaction mixture was cooled to room temperature and diluted with ethyl acetate (10 mL). The organic layer was washed with 2 M aqueous lithium chloride solution (3 × 10 mL) and then water (2 × 10 mL). The organic layer was dried (MgSO₄), filtered and concentrated *in vacuo*. The crude material was purified by flash column chromatography eluting with 2% methanol in diethyl ether to give (3-chlorophenyl)diphenylphosphine oxide (**211**) as an off-white solid (0.0544 g, 87%). Mp 99–101 °C; $\nu_{\max}/\text{cm}^{-1}$ (neat) 3055 (CH), 1439, 1400, 1188, 1119, 1076, 795, 752, 721; δ_{H} (400 MHz, CDCl₃) 7.40 (1H, td, *J* 7.8, 3.3 Hz, 5-H), 7.44–7.60 (8H, m, 8 × ArH), 7.61–7.71 (5H, m, 5 × ArH); δ_{C} (101 MHz, CDCl₃) 128.8 (d, $^3J_{\text{CP}}$ 12.3 Hz, 4 × CH), 130.1 (d, $^3J_{\text{CP}}$ 13.0 Hz, CH), 130.3 (d, $^2J_{\text{CP}}$ 9.4 Hz, CH), 132.0 (d, $^1J_{\text{CP}}$ 105.4 Hz, 2 × C), 132.0 (d, $^2J_{\text{CP}}$ 10.7 Hz, CH), 132.2 (d, $^2J_{\text{CP}}$ 10.0 Hz, 4 × CH), 132.2 (d, $^4J_{\text{CP}}$ 1.8 Hz, CH), 132.4 (d, $^4J_{\text{CP}}$ 2.9 Hz, 2 × CH), 135.1 (d, $^3J_{\text{CP}}$ 15.7 Hz, C), 135.3 (d, $^1J_{\text{CP}}$ 101.6 Hz, C); *m/z* (ESI) 335.0365 (MNa⁺. C₁₈H₁₄³⁵ClNaOP requires 335.0363).

1,3-Bis(diphenylphosphoryl)benzene (**212**)⁴⁵⁰



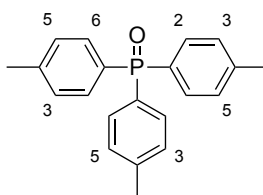
The reaction was carried out according to the previously described procedure for triphenylphosphine oxide (**185**) using sodium iodide (0.0300 g, 0.200 mmol), 3-bromophenyl nonafluorobutanesulfonate (**183**) (0.0910 g, 0.200 mmol), anhydrous *N,N'*-dimethylformamide (1.2 mL), diphenylphosphine oxide (0.121 g, 0.600 mmol), palladium(II) acetate (0.00450 g, 0.0200 mmol) and triethylamine (0.110 mL, 0.790 mmol). The reaction mixture was stirred at 120 °C for 5 h. The reaction mixture was cooled to room temperature and diluted with ethyl acetate (10 mL). The organic layer was washed with 2 M aqueous lithium chloride solution (3 × 10 mL) and then water (2 × 10 mL). The organic layer was dried (MgSO₄), filtered and concentrated *in vacuo*. The crude material was purified by flash column chromatography eluting with 3% methanol in dichloromethane to give 1,3-bis(diphenylphosphoryl)benzene (**212**) as a colourless oil (0.0545 g, 57%). Spectroscopic data were consistent with previously published data.⁴⁵⁰ δ_{H} (400 MHz, CDCl₃) 7.40 [8H, td, *J* 7.6, 2.8 Hz, 4 × (3'-H and 5'-H)], 7.52 (4H, ttd, *J* 7.4, 1.5, 1.3 Hz, 4 × 4'-H), 7.53–7.60 [8H, m, 4 × (2'-H and 6'-H)], 7.61 (1H, t, *J* 7.6 Hz, 5-H), 7.68 (1H, tt, *J* 11.7, 1.2 Hz, 2-H), 7.90–8.00 (2H, m, 4-H and 6-H); δ_{C} (101 MHz, CDCl₃) 128.7 (d, ³*J*_{CP} 12.7 Hz, 8 × CH), 129.1 (t, ³*J*_{CP} 11.3 Hz, CH), 131.8 (d, ¹*J*_{CP} 105.3 Hz, 4 × C), 132.1 (d, ²*J*_{CP} 10.1 Hz, 8 × CH), 132.3 (d, ⁴*J*_{CP} 2.8 Hz, 4 × CH), 133.8 (dd, ¹*J*_{CP} 102.1 Hz, ³*J*_{CP} 10.9 Hz, 2 × C), 135.5 (t, ²*J*_{CP} 11.2 Hz, CH), 135.6 (dd, ²*J*_{CP} 10.2 Hz, ⁴*J*_{CP} 3.3 Hz, 2 × CH); *m/z* (ESI) 501 (MNa⁺. 100%).

Pyridin-2-yl diphenylphosphine oxide (**213**)⁴⁵¹



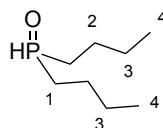
The reaction was carried out according to the previously described procedure for triphenylphosphine oxide (**185**) using sodium iodide (0.0600 g, 0.400 mmol), pyridin-2-yl nonafluorobutanesulfonate (**184**) (0.151 g, 0.400 mmol), anhydrous *N,N'*-dimethylformamide (2.4 mL), diphenylphosphine oxide (0.121 g, 0.600 mmol), palladium(II) acetate (0.00900 g, 0.0400 mmol) and triethylamine (0.220 mL, 1.58 mmol). The reaction mixture was stirred at 120 °C for 4 h. The reaction mixture was cooled to room temperature and diluted with ethyl acetate (10 mL). The organic layer was washed with 2 M aqueous lithium chloride solution (3 × 10 mL) and then water (2 × 10 mL). The organic layer was dried (MgSO₄), filtered and concentrated *in vacuo*. The crude material was purified by flash column chromatography eluting with 2% methanol in diethyl ether to give pyridin-2-yl diphenylphosphine oxide (**213**) as a white solid (0.0673 g, 60%). Mp 101–103 °C (lit.⁴⁵¹ 106–107 °C); δ_{H} (400 MHz, CDCl₃) 7.34–7.55 (7H, m, 7 × ArH), 7.80–7.86 (1H, m, 3-H), 7.88 [4H, dd, *J* 12.0, 8.0 Hz, 2 × (2'-H and 6'-H)], 8.30 (1H, t, *J* 6.8 Hz, 4-H), 8.72–8.81 (1H, m, 6-H); δ_{C} (101 MHz, CDCl₃) 125.4 (d, ⁴*J*_{CP} 3.2 Hz, CH), 128.5 (d, ³*J*_{CP} 12.3 Hz, 4 × CH), 128.5 (d, ³*J*_{CP} 19.0 Hz, CH), 132.0 (d, ⁴*J*_{CP} 2.9 Hz, 2 × CH), 132.2 (d, ²*J*_{CP} 9.5 Hz, 4 × CH), 132.3 (d, ¹*J*_{CP} 104.5 Hz, 2 × C), 136.3 (d, ²*J*_{CP} 9.2 Hz, CH), 150.3 (d, ³*J*_{CP} 19.2 Hz, CH), 156.5 (d, ¹*J*_{CP} 132.2 Hz, C); *m/z* (ESI) 302 (MNa⁺. 100%).

Tris(*p*-tolyl)phosphine oxide (**215**)⁴⁵²



A stirrer bar and sodium iodide (0.0600 g, 0.400 mmol) were added to a microwave tube and dried in an oven at 140 °C overnight. 4-Methylphenyl nonafluorobutanesulfonate (**175**) (0.156 g, 0.400 mmol) was dried under high vacuum for 1 h, purged with argon and dissolved in anhydrous *N,N'*-dimethylformamide (2.4 mL). The oven-dried microwave tube was cooled to room temperature *in vacuo* and then purged with argon. To the tube was added bis(*p*-tolyl)phosphine oxide (0.138 g, 0.600 mmol) and palladium(II) acetate (0.00900 g, 0.0400 mmol), followed by the 4-methylphenyl nonafluorobutanesulfonate (**175**) solution and triethylamine (0.220 mL, 1.58 mmol). The tube was sealed, heated to 120 °C and stirred for 4 h. The reaction mixture was cooled to room temperature, diluted with ethyl acetate (15 mL) and washed with 2 M aqueous lithium chloride solution (3 × 15 mL). The organic layer was dried (MgSO₄), filtered and concentrated *in vacuo*. The crude material was purified by flash column chromatography eluting with 2% methanol in diethyl ether to give tris(*p*-tolyl)phosphine oxide (**215**) as a white solid (0.0810 g, 63%). Mp 135–137 °C (lit.⁴⁵² 140 °C); δ_{H} (400 MHz, CDCl₃) 2.39 (9H, s, 3 × CH₃), 7.24 [6H, dd, *J* 8.0, 2.4 Hz, 3 × (3-H and 5-H)], 7.54 [6H, dd, *J* 12.0, 8.0 Hz, 3 × (2-H and 6-H)]; δ_{C} (101 MHz, CDCl₃) 21.7 (d, ⁵*J*_{CP} 1.4 Hz, 3 × CH₃), 129.3 (d, ³*J*_{CP} 12.4 Hz, 6 × CH), 129.9 (d, ¹*J*_{CP} 106.7 Hz, 3 × C), 132.2 (d, ²*J*_{CP} 10.3 Hz, 6 × CH), 142.3 (d, ⁴*J*_{CP} 2.8 Hz, 3 × C); *m/z* (ESI) 343 (MNa⁺. 100%).

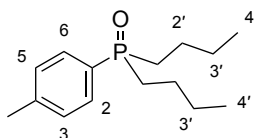
Di(*n*-butyl)phosphine oxide (**214**)⁴¹¹



In an oven-dried flask under argon, a stirred solution of 2 M *n*-butylmagnesium chloride in diethyl ether (5.00 mL, 10.0 mmol) was cooled to 0 °C. To this flask was added dropwise, a solution of diethyl phosphite (0.390 mL, 3.03 mmol) in anhydrous

diethyl ether (1.0 mL) over 0.25 h. The reaction mixture was stirred for 0.25 h and then warmed to room temperature. The mixture was stirred for a further 2 h. The reaction mixture was cooled to 0 °C and 0.1 M aqueous hydrochloric acid solution (8 mL) was added dropwise, followed by *tert*-butyl methyl ether (8 mL). The resultant biphasic mixture was stirred vigorously for 0.1 h and then allowed to stand for 0.1 h. The organic layer was decanted from the viscous gel and retained. Dichloromethane (10 mL) was added to the viscous gel and stirred vigorously for 0.1 h. The resultant biphasic mixture was filtered through a short pad of Celite[®] with dichloromethane (30 mL), and the organic and aqueous layers of the filtrate were separated. The combined organic layers were dried (MgSO₄), filtered and concentrated *in vacuo*. The crude material was azeotroped with hexane (10 mL) to give di(*n*-butyl)phosphine oxide (**214**) as a white solid (0.445 g, 90%). Mp 55–57 °C (lit.⁴¹¹ 55–56 °C). δ_{H} (400 MHz, CDCl₃) 0.94 (6H, t, *J* 7.4 Hz, 2 × 4-H₃), 1.38–1.51 (4H, m, 2 × 3-H₂), 1.52–1.69 (4H, m, 2 × 2-H₂), 1.70–1.90 (4H, m, 2 × 1-H₂), 6.86 (1H, dtt, *J* 445.2, 4.4, 2.8 Hz, *HP*); δ_{C} (101 MHz, CDCl₃) 13.7 (2 × CH₃), 23.9 (d, ²*J*_{CP} 8.4 Hz, 2 × CH₂), 24.0 (d, ³*J*_{CP} 9.6 Hz, 2 × CH₂), 28.1 (d, ¹*J*_{CP} 65.4 Hz, 2 × CH₂); *m/z* (ESI) 185 (MNa⁺. 100%).

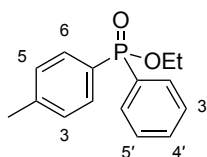
(4-Methylphenyl)di(*n*-butyl)phosphine oxide (**216**)



A stirrer bar and sodium iodide (0.0600 g, 0.400 mmol) were added to a microwave tube and dried in an oven at 140 °C overnight. 4-Methylphenyl nonafluorobutanesulfonate (**175**) (0.156 g, 0.400 mmol) was dried under high vacuum for 1 h, purged with argon and dissolved in anhydrous *N,N'*-dimethylformamide (2.4 mL). Di(*n*-butyl)phosphine oxide (**214**) (0.0973 g, 0.600 mmol) was dried *in vacuo* for 1 h. The oven-dried microwave tube was cooled to room temperature *in vacuo* and then purged with argon. To the tube was added di(*n*-butyl)phosphine oxide (**214**) followed by the 4-methylphenyl nonafluorobutanesulfonate (**175**) solution, and the mixture was degassed under argon for 0.1 h. Tetrakis(triphenylphosphine)palladium(0) (0.0462 g, 0.0400 mmol) and triethylamine (0.220 mL, 1.58 mmol) were added and the tube was sealed. The

reaction mixture was heated to 120 °C and stirred for 5 h. The reaction mixture was cooled to room temperature, diluted with ethyl acetate (30 mL) and washed with water (3 × 30 mL). The organic layer was dried (MgSO₄), filtered and concentrated *in vacuo*. The crude material was purified by flash column chromatography eluting with 0–2% gradient of methanol in diethyl ether to give (4-methylphenyl)di(*n*-butyl)phosphine oxide (**216**) as a white solid (0.0587 g, 58%). Mp 51–53 °C; $\nu_{\max}/\text{cm}^{-1}$ (neat) 2926 (CH), 2865 (CH), 1462, 1163, 1109, 1054, 900, 808, 757; δ_{H} (400 MHz, CDCl₃) 0.85 (6H, t, *J* 7.2 Hz, 2 × 4'-H₃), 1.30–1.65 [8H, m, 2 × (2'-H₂ and 3'-H₂)], 1.75–2.00 (4H, m, 2 × 1'-H₂), 2.39 (3H, s, 4-CH₃), 7.27 (2H, dd, *J* 8.2, 2.4 Hz, 3-H and 5-H), 7.56 (2H, dd, *J* 10.6, 8.2 Hz, 2-H and 6-H); δ_{C} (101 MHz, CDCl₃) 13.7 (2 × CH₃), 21.6 (d, ⁵*J*_{CP} 1.2 Hz, CH₃), 23.7 (d, ²*J*_{CP} 4.1 Hz, 2 × CH₂), 24.2 (d, ³*J*_{CP} 14.4 Hz, 2 × CH₂), 29.9 (d, ¹*J*_{CP} 68.9 Hz, 2 × CH₂), 129.4 (d, ³*J*_{CP} 11.4 Hz, 2 × CH), 129.5 (d, ¹*J*_{CP} 94.5 Hz, C), 130.5 (d, ²*J*_{CP} 9.0 Hz, 2 × CH), 141.8 (d, ⁴*J*_{CP} 2.6 Hz, C); *m/z* (ESI) 275.1534 (MNa⁺. C₁₅H₂₅NaOP requires 275.1535).

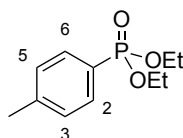
Ethyl (4-methylphenyl)phenylphosphinate (**218**)⁴⁵³



A stirrer bar and sodium iodide (0.0300 g, 0.200 mmol) were added to a microwave tube and dried in an oven at 140 °C overnight. 4-Methylphenyl nonafluorobutanesulfonate (**175**) (0.0780 g, 0.200 mmol) was dried under high vacuum for 1 h, purged with argon and dissolved in anhydrous *N,N'*-dimethylformamide (1.2 mL). The oven-dried microwave tube was cooled to room temperature *in vacuo* and then purged with argon. To the tube was added tetrakis(triphenylphosphine)palladium(0) (0.0231 g, 0.0200 mmol) and the 4-methylphenyl nonafluorobutanesulfonate (**175**) solution, followed by ethyl phenylphosphinate (0.0450 mL, 0.299 mmol) and triethylamine (0.110 mL, 0.790 mmol). The tube was sealed, heated to 80 °C and stirred for 4 h. The reaction mixture was cooled to room temperature, diluted with ethyl acetate (15 mL) and washed with water (3 × 15 mL). The organic layer was dried (MgSO₄), filtered and concentrated *in vacuo*. The crude material was purified by flash column chromatography eluting with 1% methanol in diethyl ether to give ethyl (4-

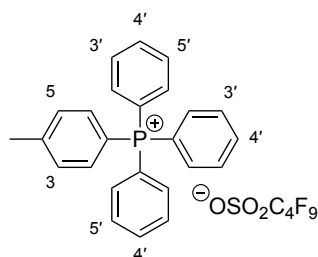
methylphenyl)phenylphosphinate (**218**) as a colourless oil (0.0381 g, 73%). Spectroscopic data were consistent with previously published data.⁴⁵³ δ_{H} (400 MHz, CDCl_3) 1.36 (3H, t, J 7.2 Hz, OCH_2CH_3), 2.38 (3H, s, 4- CH_3), 4.09 (2H, quin., J 7.2 Hz, OCH_2CH_3), 7.25 (2H, dd, J 8.0, 3.2 Hz, 3-H and 5-H), 7.39–7.47 (2H, m, 3'-H and 5'-H), 7.50 (1H, ttd, J 7.4, 1.9, 1.3 Hz, 4'-H), 7.70 (2H, dd, J 12.0, 8.0 Hz, 2-H and 6-H), 7.76–7.84 (2H, m, 2'-H and 6'-H); δ_{C} (101 MHz, CDCl_3) 16.7 (d, $^3J_{\text{CP}}$ 6.7 Hz, CH_3), 21.8 (d, $^5J_{\text{CP}}$ 1.3 Hz, CH_3), 61.1 (d, $^2J_{\text{CP}}$ 5.9 Hz, CH_2), 128.6 (d, $^1J_{\text{CP}}$ 139.8 Hz, C), 128.6 (d, $^3J_{\text{CP}}$ 13.2 Hz, 2 \times CH), 129.4 (d, $^3J_{\text{CP}}$ 13.5 Hz, 2 \times CH), 131.7 (d, $^2J_{\text{CP}}$ 10.0 Hz, 2 \times CH), 131.9 (d, $^2J_{\text{CP}}$ 10.6 Hz, 2 \times CH), 132.1 (d, $^4J_{\text{CP}}$ 2.8 Hz, CH), 132.2 (d, $^1J_{\text{CP}}$ 137.6 Hz, C), 142.7 (d, $^4J_{\text{CP}}$ 2.9 Hz, C); m/z (ESI) 283 (MNa^+ , 100%).

Diethyl (4-methylphenyl)phosphonate (**217**)⁴⁵³



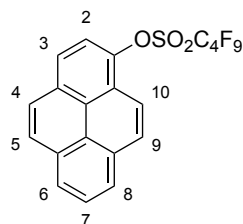
The reaction was carried out according to the previously described procedure for ethyl (4-methylphenyl)phenylphosphinate (**218**) using sodium iodide (0.105 g, 0.700 mmol), 4-methylphenyl nonafluorobutanesulfonate (**175**) (0.273 g, 0.700 mmol), anhydrous N,N' -dimethylformamide (4 mL), tetrakis(triphenylphosphine)palladium(0) (0.0809 g, 0.0700 mmol), diethyl phosphite (0.136 mL, 1.06 mmol) and triethylamine (0.390 mL, 2.80 mmol). The reaction mixture was stirred at 80 °C for 6 h. The crude material was purified by flash column chromatography eluting with 1% methanol in diethyl ether to give diethyl (4-methylphenyl)phosphonate (**217**) as a yellow oil (0.107 g, 67%). Spectroscopic data were consistent with previously published data.⁴⁵³ δ_{H} (400 MHz, CDCl_3) 1.31 (6H, t, J 7.2 Hz, 2 \times OCH_2CH_3), 2.39 (3H, s, 4- CH_3), 3.99–4.18 (4H, m, 2 \times OCH_2CH_3), 7.26 (2H, ddd, J 8.0, 4.0, 0.4 Hz, 3-H and 5-H), 7.69 (2H, dd, J 13.2, 8.0 Hz, 2-H and 6-H); δ_{C} (101 MHz, CDCl_3) 16.5 (d, $^3J_{\text{CP}}$ 6.6 Hz, 2 \times CH_3), 21.8 (d, $^5J_{\text{CP}}$ 1.4 Hz, CH_3), 62.1 (d, $^2J_{\text{CP}}$ 5.4 Hz, 2 \times CH_2), 125.2 (d, $^1J_{\text{CP}}$ 190.8 Hz, C), 129.3 (d, $^3J_{\text{CP}}$ 15.5 Hz, 2 \times CH), 132.0 (d, $^2J_{\text{CP}}$ 10.4 Hz, 2 \times CH), 143.0 (d, $^4J_{\text{CP}}$ 3.1 Hz, C); m/z (ESI) 251 (MNa^+ , 100%).

(4-Methylphenyl)triphenylphosphonium nonafluorobutanesulfonate (**219**)



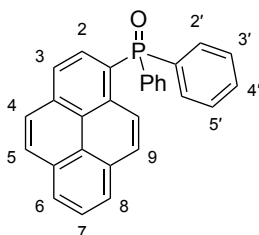
The reaction was carried out according to the previously described procedure for tris(*p*-tolyl)phosphine oxide (**215**) using sodium iodide (0.0450 g, 0.300 mmol), 4-methylphenyl nonafluorobutanesulfonate (**175**) (0.117 g, 0.300 mmol), anhydrous *N,N'*-dimethylformamide (1.8 mL), triphenylphosphine (0.315 g, 1.20 mmol), palladium(II) acetate (0.00670 g, 0.0300 mmol) and triethylamine (0.170 mL, 1.22 mmol). The reaction mixture was stirred at 90 °C for 19 h. The reaction mixture was cooled to room temperature, diluted with ethyl acetate (20 mL), and washed with water (3 × 20 mL). The organic layer was dried (MgSO₄), filtered and concentrated *in vacuo*. The crude material was purified by trituration with diethyl ether to give (4-methylphenyl)triphenylphosphonium nonafluorobutanesulfonate (**219**) as a yellow solid (0.136 g, 69%). Mp 118–120 °C; $\nu_{\max}/\text{cm}^{-1}$ (neat) 3059 (CH), 1437, 1265, 1200, 1106, 1050, 726; δ_{H} (400 MHz, CDCl₃) 2.52 (3H, s, ArCH₃), 7.48 (2H, dd, *J* 12.4, 8.4 Hz, 2-H and 6-H), 7.55 (2H, dd, *J* 8.4, 3.6 Hz, 3-H and 5-H), 7.57–7.65 [6H, m, 3 × (2'-H and 6'-H)], 7.75 [6H, td, *J* 7.6, 3.6 Hz, 3 × (3'-H and 5'-H)], 7.88 (3H, tdt, *J* 7.6, 1.9, 1.2 Hz, 3 × 4'-H); δ_{C} (101 MHz, CDCl₃) 22.0 (d, $^5J_{\text{CP}}$ 1.6 Hz, CH₃), 113.8 (d, $^1J_{\text{CP}}$ 92.4 Hz, C), 118.0 (d, $^1J_{\text{CP}}$ 90.0 Hz, 3 × C), 130.8 (d, $^3J_{\text{CP}}$ 12.9 Hz, 6 × CH), 131.6 (d, $^3J_{\text{CP}}$ 13.4 Hz, 2 × CH), 134.5 (d, $^2J_{\text{CP}}$ 10.3 Hz, 6 × CH), 134.5 (d, $^2J_{\text{CP}}$ 10.8 Hz, 2 × CH), 135.8 (d, $^4J_{\text{CP}}$ 3.0 Hz, 3 × CH), 147.5 (d, $^4J_{\text{CP}}$ 3.1 Hz, C); *m/z* (ESI) 353.1451 (M⁺. C₂₅H₂₂P requires 353.1454); *m/z* (ESI) 298.9430 (M⁻. C₄F₉O₃S requires 298.9430).

1-Pyrenyl nonafluorobutanesulfonate (**221**)



The reaction was carried out according to the previously described procedure for 2-naphthyl nonafluorobutanesulfonate (**139**) using pyren-1-ol (**220**) (0.327 g, 1.50 mmol), anhydrous dichloromethane (5 mL), triethylamine (0.530 mL, 3.80 mmol) and perfluoro-1-butanesulfonyl fluoride (0.410 mL, 2.28 mmol). The reaction mixture was stirred at room temperature for 3 h. The crude material was purified by flash column chromatography eluting with 5% diethyl ether in hexane to give 1-pyrenyl nonafluorobutanesulfonate (**221**) as a white solid (0.654 g, 87%). Mp 122–124 °C; $\nu_{\max}/\text{cm}^{-1}$ (neat) 3049 (CH), 1598 (C=C), 1416, 1236, 1193, 1135, 1031, 904, 844; δ_{H} (400 MHz, CDCl_3) 7.96 (1H, d, J 8.4 Hz, 2-H), 8.01–8.12 (3H, m, 3 × ArH), 8.15 (1H, d, J 8.4 Hz, 3-H), 8.19–8.30 (4H, m, 4 × ArH); δ_{C} (101 MHz, CDCl_3) 118.7 (CH), 119.5 (CH), 123.9 (C), 124.1 (C), 125.1 (CH), 125.8 (C), 126.3 (CH), 126.6 (CH), 126.8 (CH), 127.0 (CH), 128.6 (CH), 129.9 (CH), 130.8 (C), 131.0 (C), 131.1 (C), 142.9 (C); m/z (ESI) 523.0024 (MNa^+ . $\text{C}_{20}\text{H}_9\text{F}_9\text{NaO}_3\text{S}$ requires 523.0021).

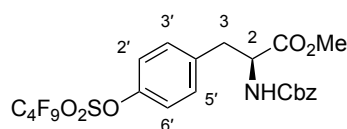
(1-Pyrenyl)diphenylphosphine oxide (**222**)⁴¹²



A stirrer bar and sodium iodide (0.0300 g, 0.200 mmol) were added to a microwave tube and dried in an oven at 140 °C overnight. 1-Pyrenyl nonafluorobutanesulfonate (**221**) (0.100 g, 0.200 mmol) and diphenylphosphine oxide (0.0610 g, 0.302 mmol) were dried under high vacuum for 1 h. The oven-dried microwave tube was cooled to room temperature *in vacuo* and then purged with argon. To the tube was added 1-pyrenyl nonafluorobutanesulfonate (**221**), diphenylphosphine oxide and

palladium(II) acetate (0.00450 g, 0.0200 mmol). Anhydrous *N,N'*-dimethylformamide (1.2 mL) and triethylamine (0.110 mL, 0.790 mmol) were then added, and the tube was sealed. The reaction mixture was heated to 120 °C and stirred for 4 h. The reaction mixture was cooled to room temperature, diluted with ethyl acetate (15 mL) and washed with water (3 × 15 mL). The organic layer was dried (MgSO₄), filtered and concentrated *in vacuo*. The crude material was purified by flash column chromatography eluting with 2% methanol in diethyl ether to give (1-pyrenyl)diphenylphosphine oxide (**222**) as an off-white solid (0.0588 g, 73%). Mp 233–235 °C. Spectroscopic data were consistent with previously published data.⁴¹² δ_{H} (400 MHz, CDCl₃) 7.47 [4H, td, *J* 7.4, 2.9 Hz, 2 × (3'-H and 5'-H)], 7.57 (2H, ttd, *J* 7.4, 1.7, 1.3 Hz, 2 × 4'-H), 7.68–7.80 (5H, m, 5 × ArH), 8.00–8.11 (4H, m, 4 × ArH), 8.19 (1H, d, *J* 9.2 Hz, ArH), 8.24 (2H, t, *J* 7.6 Hz, 2 × ArH), 8.94 (1H, d, *J* 9.2 Hz, ArH); δ_{C} (101 MHz, CDCl₃) 123.7 (d, ³*J*_{CP} 13.7 Hz, CH), 124.3 (d, ⁵*J*_{CP} 0.9 Hz, C), 125.3 (d, ¹*J*_{CP} 103.6 Hz, C), 125.3 (d, ³*J*_{CP} 10.3 Hz, C), 126.3 (CH), 126.5 (d, ²*J*_{CP} 6.5 Hz, CH), 126.6 (2 × CH), 127.3 (d, ⁵*J*_{CP} 0.8 Hz, CH), 128.8 (d, ³*J*_{CP} 12.2 Hz, 4 × CH), 129.0 (CH), 130.0 (CH), 130.6 (C), 131.2 (d, ⁵*J*_{CP} 0.8 Hz, C), 131.3 (d, ³*J*_{CP} 12.2 Hz, CH), 132.0 (d, ⁴*J*_{CP} 2.8 Hz, 2 × CH), 132.4 (d, ²*J*_{CP} 9.9 Hz, 4 × CH), 133.5 (d, ¹*J*_{CP} 104.7 Hz, 2 × C), 134.3 (d, ²*J*_{CP} 8.2 Hz, C), 134.4 (d, ⁴*J*_{CP} 2.6 Hz, C); *m/z* (ESI) 425 (MNa⁺. 100%).

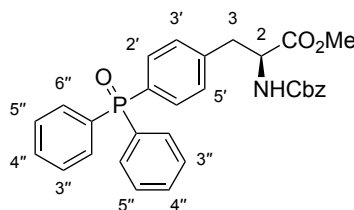
Methyl (2S)-2-[(benzyloxycarbonyl)amino]-3-[(phenylnonafluorobutanesulfonate)-4'-yl]propanoate (224)



The reaction was carried out according to the previously described procedure for 2-naphthyl nonafluorobutanesulfonate (**139**) using methyl (2S)-2-[(benzyloxycarbonyl) amino]-3-(4-hydroxyphenyl)propanoate (**223**) (0.988 g, 3.00 mmol), anhydrous dichloromethane (10 mL), triethylamine (1.05 mL, 7.53 mmol) and perfluoro-1-butanesulfonyl fluoride (0.810 mL, 4.50 mmol). The reaction mixture was stirred at room temperature for 2 h. The crude material was purified by flash column chromatography eluting with 50% diethyl ether in hexane to give methyl (2S)-2-[(benzyloxycarbonyl)amino]-3-[(phenylnonafluorobutanesulfonate)-4'-

yl]propanoate (**224**) as a colourless oil which solidified upon standing (1.72 g, 94%). Mp 46–48 °C; $\nu_{\max}/\text{cm}^{-1}$ (neat) 3341 (NH), 2959 (CH), 1717 (C=O), 1501 (C=C), 1423, 1200, 1142, 1015, 891; $[\alpha]_{\text{D}}^{17} -14.6$ (*c* 0.5, MeOH); δ_{H} (400 MHz, CDCl_3) 3.09 (1H, dd, *J* 14.0, 6.4 Hz, 3-*HH*), 3.19 (1H, dd, *J* 14.0, 5.6 Hz, 3-*HH*), 3.72 (3H, s, OCH_3), 4.60–4.72 (1H, m, 2-H), 5.07 (1H, d, *J* 12.2 Hz, *OCHHP*h), 5.12 (1H, d, *J* 12.2 Hz, *OCHHP*h), 5.26 (1H, d, *J* 8.0 Hz, NH), 7.18 (4H, br s, 2'-H, 3'-H, 5'-H and 6'-H), 7.28–7.42 (5H, m, Ph); δ_{C} (101 MHz, CDCl_3) 37.8 (CH_2), 52.6 (CH_3), 54.8 (CH), 67.3 (CH_2), 121.6 (2 × CH), 128.3 (2 × CH), 128.5 (CH), 128.7 (2 × CH), 131.2 (2 × CH), 136.2 (C), 136.7 (C), 149.0 (C), 155.6 (C), 171.6 (C); *m/z* (ESI) 634.0549 (MNa^+ . $\text{C}_{22}\text{H}_{18}\text{F}_9\text{NNaO}_7\text{S}$ requires 634.0552).

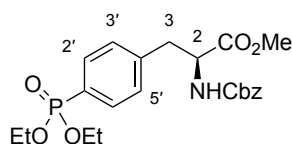
Methyl (2*S*)-2-[(benzyloxycarbonyl)amino]-3-[(triphenylphosphine oxide)-4'-yl]propanoate (**225**)



The reaction was carried out according to the previously described procedure for triphenylphosphine oxide (**185**) using sodium iodide (0.0300 g, 0.200 mmol), methyl (2*S*)-2-[(benzyloxycarbonyl)amino]-3-[(phenylnonafluorobutanesulfonate)-4'-yl]propanoate (**224**) (0.122 g, 0.200 mmol), anhydrous *N,N'*-dimethylformamide (1.2 mL), diphenylphosphine oxide (0.0610 g, 0.302 mmol), palladium(II) acetate (0.00450 g, 0.0200 mmol) and triethylamine (0.110 mL, 0.790 mmol). The reaction mixture was stirred at 120 °C for 12 h. The reaction mixture was cooled to room temperature, diluted with ethyl acetate (15 mL), and washed with water (3 × 15 mL). The organic layer was dried (MgSO_4), filtered and concentrated *in vacuo*. The crude material was purified by flash column chromatography eluting with 3–4% gradient of methanol in dichloromethane to give methyl (2*S*)-2-[(benzyloxycarbonyl)amino]-3-[(triphenylphosphine oxide)-4'-yl]propanoate (**225**) as a pale yellow oil (0.0561 g, 55%). $\nu_{\max}/\text{cm}^{-1}$ (neat) 3206 (NH), 3032 (CH), 1709 (C=O), 1534, 1436, 1175, 1115, 1053, 746; $[\alpha]_{\text{D}}^{23} +41.8$ (*c* 0.1, CHCl_3); δ_{H} (400 MHz, CDCl_3) 3.12 (1H, dd, *J* 13.6, 6.0 Hz, 3-*HH*), 3.21 (1H, dd, *J* 13.6, 5.6 Hz, 3-*HH*), 3.70 (3H, s, CH_3), 4.60–4.75 (1H, m, 2-H), 5.08 (2H, s, CH_2Ph), 5.30 (1H, d, *J* 7.6 Hz, NH), 7.19 (2H, dd, *J* 8.4,

2.4 Hz, 3'-H and 5'-H), 7.27–7.35 (5H, m, Ph), 7.45 [4H, td, J 7.1, 2.9 Hz, 2 × (3''-H and 5''-H)], 7.50–7.60 (4H, m, 2'-H, 6'-H and 2 × 4''-H), 7.61–7.69 [4H, m, 2 × (2''-H and 6''-H)]; δ_C (101 MHz, CDCl₃) 38.3 (CH₂), 52.6 (CH₃), 54.7 (CH), 67.2 (CH₂), 128.2 (2 × CH), 128.4 (CH), 128.6 (d, $^3J_{CP}$ 12.2 Hz, 4 × CH), 128.7 (2 × CH), 129.6 (d, $^3J_{CP}$ 12.5 Hz, 2 × CH), 131.5 (d, $^1J_{CP}$ 105.3 Hz, C), 132.1 (d, $^4J_{CP}$ 2.9 Hz, 2 × CH), 132.2 (d, $^2J_{CP}$ 9.9 Hz, 4 × CH), 132.5 (d, $^2J_{CP}$ 10.3 Hz, 2 × CH), 132.6 (d, $^1J_{CP}$ 105.1 Hz, 2 × C), 136.2 (C), 140.4 (d, $^4J_{CP}$ 1.8 Hz, C), 155.7 (C), 171.7 (C); m/z (ESI) 536.1596 (MNa⁺. C₃₀H₂₈NNaO₅P requires 536.1597).

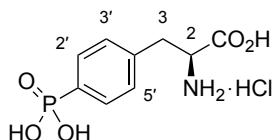
Methyl (2S)-2-[(benzyloxycarbonyl)amino]-3-[(diethylphenylphosphonate)-4'-yl]propanoate (226)



A stirrer bar and sodium iodide (0.105 g, 0.700 mmol) were added to a microwave tube and dried in an oven at 140 °C overnight. Methyl (2S)-2-[(benzyloxycarbonyl)amino]-3-[(phenylnonafluorobutanesulfonate)-4'-yl]propanoate (**224**) (0.428 g, 0.700 mmol) was dried under high vacuum for 1 h. The oven-dried microwave tube was cooled to room temperature *in vacuo* and then purged with argon. To the tube was added methyl (2S)-2-[(benzyloxycarbonyl)amino]-3-[(phenylnonafluorobutanesulfonate)-4'-yl]propanoate (**224**), anhydrous *N,N*-dimethylformamide (4 mL) and diethyl phosphite (0.135 mL, 1.05 mmol). The mixture was degassed under argon for 0.1 h. Tetrakis(triphenylphosphine)palladium(0) (0.0809 g, 0.0700 mmol) and triethylamine (0.390 mL, 2.80 mmol) were added, and the tube was sealed. The reaction mixture was heated to 80 °C and stirred for 6 h. The reaction mixture was cooled to room temperature, diluted with ethyl acetate (50 mL) and washed with water (3 × 50 mL). The organic layer was dried (MgSO₄), filtered and concentrated *in vacuo*. The crude material was purified by flash column chromatography eluting with 2% methanol and 2% toluene in diethyl ether to give methyl (2S)-2-[(benzyloxycarbonyl)amino]-3-[(diethylphenylphosphonate)-4'-yl]propanoate (**226**) as a colourless oil (0.228 g, 72%). ν_{max}/cm^{-1} (neat) 3248 (NH), 2983 (CH), 1714 (C=O), 1533, 1225, 1017, 961, 745; $[\alpha]_D^{23} +50.1$ (c 0.1, CHCl₃); δ_H (400 MHz, CDCl₃)

1.31 (6H, t, J 7.0 Hz, $2 \times \text{OCH}_2\text{CH}_3$), 3.11 (1H, dd, J 14.0, 6.0 Hz, 3-*HH*), 3.20 (1H, dd, J 14.0, 5.6 Hz, 3-*HH*), 3.71 (3H, s, CH_3), 4.00–4.20 (4H, m, $2 \times \text{OCH}_2\text{CH}_3$), 4.61–4.75 (1H, m, 2-H), 5.07 (1H, d, J 12.4 Hz, *OCHHP*Ph), 5.11 (1H, d, J 12.4 Hz, *OCHHP*Ph), 5.28 (1H, d, J 8.0 Hz, NH), 7.20 (2H, dd, J 8.2, 3.6 Hz, 3'-H and 5'-H), 7.27–7.42 (5H, m, Ph), 7.71 (2H, dd, J 13.2, 8.2 Hz, 2'-H and 6'-H); δ_{C} (101 MHz, CDCl_3) 16.5 (d, $^3J_{\text{CP}}$ 6.6 Hz, $2 \times \text{CH}_3$), 38.3 (CH_2), 52.6 (CH_3), 54.7 (CH), 62.2 (d, $^2J_{\text{CP}}$ 5.6 Hz, $2 \times \text{CH}_2$), 67.2 (CH_2), 127.3 (d, $^1J_{\text{CP}}$ 190.3 Hz, C), 128.2 ($2 \times \text{CH}$), 128.4 (CH), 128.7 ($2 \times \text{CH}$), 129.6 (d, $^3J_{\text{CP}}$ 15.4 Hz, $2 \times \text{CH}$), 132.1 (d, $^2J_{\text{CP}}$ 10.3 Hz, $2 \times \text{CH}$), 136.2 (C), 140.7 (d, $^4J_{\text{CP}}$ 2.8 Hz, C), 155.7 (C), 171.7 (C); m/z (ESI) 472.1498 (MNa^+ . $\text{C}_{22}\text{H}_{28}\text{NNaO}_7\text{P}$ requires 472.1496).

(2*S*)-2-Amino-3-[(phenylphosphonate)-4'-yl]propanoic hydrochloride (227)



Methyl (2*S*)-2-[(benzyloxycarbonyl)amino]-3-[(diethylphenylphosphonate)-4'-yl]propanoate (**226**) (0.209 g, 0.465 mmol) was suspended in 6 M aqueous hydrochloric acid solution (1.70 mL, 10.2 mmol) and stirred under reflux for 6 h. The reaction mixture was cooled to room temperature and concentrated *in vacuo*. The crude material was purified by trituration with diethyl ether to give (2*S*)-2-amino-3-[(phenylphosphonate)-4'-yl]propanoic hydrochloride (**227**) as a white solid (0.115 g, 88%). Mp 218–220 °C; $\nu_{\text{max}}/\text{cm}^{-1}$ (neat) 2745 (OH), 1729 (C=O), 1605, 1501, 1407, 1135, 921; $[\alpha]_{\text{D}}^{25} +3.5$ (c 0.1, H_2O); δ_{H} (400 MHz, D_2O) 3.25 (1H, dd, J 14.6, 7.6 Hz, 3-*HH*), 3.41 (1H, dd, J 14.6, 5.6 Hz, 3-*HH*), 4.32 (1H, dd, J 7.6, 5.6 Hz, 2-H), 7.43 (2H, dd, J 8.0, 3.2 Hz, 3'-H and 5'-H), 7.71 (2H, dd, J 12.8, 8.0 Hz, 2'-H and 6'-H); δ_{C} (101 MHz, D_2O) 38.6 (CH_2), 57.3 (CH), 132.3 (d, $^3J_{\text{CP}}$ 14.5 Hz, $2 \times \text{CH}$), 134.0 (d, $^2J_{\text{CP}}$ 10.2 Hz, $2 \times \text{CH}$), 136.2 (d, $^1J_{\text{CP}}$ 180.5 Hz, C), 140.3 (d, $^4J_{\text{CP}}$ 3.1 Hz, C), 174.7 (C); m/z (ESI) 246.0527 (MH^+ . $\text{C}_9\text{H}_{13}\text{NO}_5\text{P}$ requires 246.0526).

4.0 References

- 1 M. L. James and S. S. Gambhir, *Physiol. Rev.*, 2012, **92**, 897–965.
- 2 S. L. Pimlott and A. Sutherland, *Chem. Soc. Rev.*, 2011, **40**, 149–162.
- 3 P. W. Miller, N. J. Long, R. Vilar and A. D. Gee, *Angew. Chem. Int. Ed.*, 2008, **47**, 8998–9033.
- 4 M. E. Phelps, *Proc. Natl. Acad. Sci.*, 2000, **97**, 9226–9233.
- 5 A. Paans, A. Van Waarde, P. H. Elsinga, A. T. M. Willemsen and W. Vaalburg, *Methods*, 2002, **27**, 195–207.
- 6 S. M. Ametamey, M. Honer and P. A. Schubiger, *Chem. Rev.*, 2008, **108**, 1501–1516.
- 7 D. A. Mankoff, *J. Nucl. Med.*, 2007, **48**, 18N–21N.
- 8 A. Sutherland, *Synthesis*, 2019, **51**, 4368–4373.
- 9 F. Lu and Z. Yuan, *Quant. Imaging Med. Surg.*, 2015, **5**, 433–447.
- 10 K. A. Kurdziel, L. Lindenberg, E. Mena, B. Turkbey and P. Choyke, *Curr. Mol. Imaging*, 2013, **2**, 42–52.
- 11 L. Zhu, K. Ploessl and H. F. Kung, *Chem. Soc. Rev.*, 2014, **43**, 6683–6691.
- 12 V. M. Petriev, V. K. Tishchenko and R. N. Krasikova, *Pharm. Chem. J.*, 2016, **50**, 209–220.
- 13 R. L. Wahl, J. M. Herman and E. Ford, *Semin. Radiat. Oncol.*, 2011, **21**, 88–100.
- 14 N. George, E. G. Gean, A. Nandi, B. Frolov, E. Zaidi, H. Lee, J. R. Brašić and D. F. Wong, *CNS Drugs*, 2015, **29**, 313–330.
- 15 W. Wei, E. B. Ehlerding, X. Lan, Q. Luo and W. Cai, *Eur. J. Nucl. Med. Mol. Imaging*, 2018, **45**, 132–150.
- 16 J.-C. Janssen, S. Meißner, N. Woythal, V. Prasad, W. Brenner, G. Diederichs, B. Hamm and M. R. Makowski, *Eur. Radiol.*, 2018, **28**, 610–619.
- 17 M. R. Kilbourn and P. J. H. Scott, *Handbook of radiopharmaceuticals: methodology and applications*, John Wiley & Sons, Ltd., 2nd edn., 2021, vol. 30.
- 18 P. W. Miller, N. J. Long, R. Vilar and A. D. Gee, *Angew. Chem. Int. Ed.*, 2008, **47**, 8998–9033.
- 19 J. S. Fowler and A. P. Wolf, *Acc. Chem. Res.*, 1997, **30**, 181–188.
- 20 C. Uprimny, *Wien. Med. Wochenschr*, 2019, **169**, 3–11.
- 21 R. Halder and T. Ritter, *J. Org. Chem.*, 2021, **86**, 13873–13884.

- 22 O. Jacobson, D. O. Kiesewetter and X. Chen, *Bioconjug. Chem.*, 2015, **26**, 1–18.
- 23 S. Preshlock, M. Tredwell and V. Gouverneur, *Chem. Rev.*, 2016, **116**, 719–766.
- 24 M. J. Adam and D. S. Wilbur, *Chem. Soc. Rev.*, 2005, **34**, 153–163.
- 25 A. Duatti, *Nucl. Med. Biol.*, 2021, **92**, 202–216.
- 26 A. Nikjou and M. Sadeghi, *Appl. Radiat. Isot.*, 2018, **136**, 45–58.
- 27 T. Ferris, L. Carroll, S. Jenner and E. O. Aboagye, *J. Label. Compd. Radiopharm.*, 2021, **64**, 92–108.
- 28 E. Dubost, H. McErlain, V. Babin, A. Sutherland and T. Cailly, *J. Org. Chem.*, 2020, **85**, 8300–8310.
- 29 M. Di Girolamo and G. Fabrizio, *Challenges*, 2018, **9**, 1–24.
- 30 J. D. Steffen, M. M. McCauley and J. M. Pascal, *Nucleic Acids Res.*, 2016, **44**, 9771–9783.
- 31 C. J. Lord and A. Ashworth, *Science*, 2017, **355**, 1152–1158.
- 32 E. E. Alessova and O. I. Lavrik, *Nucleic Acids Res.*, 2019, **47**, 3811–3827.
- 33 J. O. Spiegel, B. Van Houten and J. D. Durrant, *DNA Repair*, 2021, **103**, 103125.
- 34 L. van Beek, É. McClay, S. Patel, M. Schimpl, L. Spagnolo and T. Maia de Oliveira, *Int. J. Mol. Sci.*, 2021, **22**, 5112.
- 35 T. E. H. Ogden, J. C. Yang, M. Schimpl, L. E. Easton, E. Underwood, P. B. Rawlins, M. M. McCauley, M. F. Langelier, J. M. Pascal, K. J. Embrey and D. Neuhaus, *Nucleic Acids Res.*, 2021, **49**, 2266–2288.
- 36 J. C. Amé, C. Spenlehauer and G. De Murcia, *BioEssays*, 2004, **26**, 882–893.
- 37 P. Chambon, J. D. Weill and P. Mandel, *Biochem. Biophys. Res. Commun.*, 1963, **11**, 39–43.
- 38 P. Chambon, J. D. Weill, J. Doly, M. T. Strosser and P. Mandel, *Biochem. Biophys. Res. Commun.*, 1966, **25**, 638–643.
- 39 Y. Nishizuka, K. Ueda, K. Nakazawa and O. Hayaishi, *J. Biol. Chem.*, 1967, **242**, 3164–3171.
- 40 R. H. Reeder, K. Ueda, T. Honjo, Y. Nishizuka and O. Hayaishi, *J. Biol. Chem.*, 1967, **242**, 3172–3179.
- 41 T. Sugimura, S. Fujimura, S. Hasegawa and Y. Kawamura, *Biochim. Biophys. Acta - Nucleic Acids Protein Synth.*, 1967, **138**, 438–441.
- 42 S. Fujimura, S. Hasegawa, Y. Shimizu and T. Sugimura, *Biochim. Biophys.*

- Acta - Nucleic Acids Protein Synth.*, 1967, **145**, 247–259.
- 43 S. Hasegawa, S. Fujimura, Y. Shimizu and T. Sugimura, *Biochim. Biophys. Acta - Nucleic Acids Protein Synth.*, 1967, **149**, 369–376.
- 44 W. L. Kraus, *Mol. Cell*, 2015, **58**, 902–910.
- 45 P. Bai, *Mol. Cell*, 2015, **58**, 947–958.
- 46 D. V. Ferraris, *J. Med. Chem.*, 2010, **53**, 4561–4584.
- 47 M. O. Hottiger, *Mol. Cell*, 2015, **58**, 1134.
- 48 I. A. Richard, J. T. Burgess, K. J. O’Byrne and E. Bolderson, *Front. Cell Dev. Biol.*, 2022, **9**, 801200.
- 49 Z. Wang, F. Wang, T. Tang and C. Guo, *Front. Med.*, 2012, **6**, 156–164.
- 50 A. N. Weaver and E. S. Yang, *Front. Oncol.*, 2013, **3**, 290.
- 51 S. Vyas, I. Matic, L. Uchima, J. Rood, R. Zaja, R. T. Hay, I. Ahel and P. Chang, *Nat. Commun.*, 2014, **5**, 4426.
- 52 M. O. Hottiger, P. O. Hassa, B. Lüscher, H. Schüler and F. Koch-Nolte, *Trends Biochem. Sci.*, 2010, **35**, 208–219.
- 53 J. Gros Lambert, E. Prokhorova and I. Ahel, *DNA Repair*, 2021, **105**, 103144.
- 54 A. Sonnenblick, E. de Azambuja, H. A. Azim and M. Piccart, *Nat. Rev. Clin. Oncol.*, 2015, **12**, 27–41.
- 55 N. Chatterjee and G. C. Walker, *Environ. Mol. Mutagen.*, 2017, **58**, 235–263.
- 56 A. Padella, A. Ghelli Luserna Di Rorà, G. Marconi, M. Ghetti, G. Martinelli and G. Simonetti, *J. Hematol. Oncol.*, 2022, **15**, 1–21.
- 57 A. Toss and C. Laura, *J. Cancer Sci. Ther.*, 2013, **5**, 409–416.
- 58 M.-C. Caron, A. K. Sharma, J. O’Sullivan, L. R. Myler, M. T. Ferreira, A. Rodrigue, Y. Coulombe, C. Ethier, J.-P. Gagné, M.-F. Langelier, J. M. Pascal, I. J. Finkelstein, M. J. Hendzel, G. G. Poirier and J.-Y. Masson, *Nat. Commun.*, 2019, **10**, 2954.
- 59 J. Rudolph, J. Mahadevan, P. Dyer and K. Luger, *Elife*, 2018, **7**, 1–23.
- 60 W. H. Hou, S. H. Chen and X. Yu, *Mutat. Res. - Rev. Mutat. Res.*, 2019, **780**, 82–91.
- 61 Cancer Research UK, Cancer Statistics for the UK, <https://www.cancerresearchuk.org/health-professional/cancer-statistics-for-the-uk#heading-Three>, (accessed 9 May 2022).
- 62 F. Rojo, J. García-Parra, S. Zazo, I. Tusquets, J. Ferrer-Lozano, S. Menendez, P. Eroles, C. Chamizo, S. Servitja, N. Ramírez-Merino, F. Lobo, B. Bellosillo, J. M. Corominas, J. Yelamos, S. Serrano, A. Lluch, A. Rovira

- and J. Albanell, *Ann. Oncol.*, 2012, **23**, 1156–1164.
- 63 A. Galia, A. E. Calogero, R. A. Condorelli, F. Fraggetta, C. La Corte, F. Ridolfo, P. Bosco, R. Castiglione and M. Salemi, *Eur. J. Histochem.*, 2012, **56**, 45–48.
- 64 J. C. Knight, S. Koustoulidou and B. Cornelissen, *Eur. J. Nucl. Med. Mol. Imaging*, 2017, **44**, 1065–1078.
- 65 A. Ruf, G. De Murcia and G. E. Schulz, *Biochemistry*, 1998, **37**, 3893–3900.
- 66 L. Zandarashvili, M.-F. Langelier, U. K. Velagapudi, M. A. Hancock, J. D. Steffen, R. Billur, Z. M. Hannan, A. J. Wicks, D. B. Krastev, S. J. Pettitt, C. J. Lord, T. T. Talele, J. M. Pascal and B. E. Black, *Science*, 2020, **368**, eaax6367.
- 67 X. Jiang, W. Li, X. Li, H. Bai and Z. Zhang, *Cancer Manag. Res.*, 2019, **11**, 4371–4390.
- 68 A. A. Turk and K. B. Wisinski, *Cancer*, 2018, **124**, 2498–2506.
- 69 Y. Pommier, M. J. O'Connor and J. De Bono, *Sci. Transl. Med.*, 2016, **8**, 362ps17.
- 70 Y. Zhao, L.-X. Zhang, T. Jiang, J. Long, Z.-Y. Ma, A.-P. Lu, Y. Cheng and D.-S. Cao, *Eur. J. Med. Chem.*, 2020, **203**, 112570.
- 71 L. T. Gien and H. J. Mackay, *J. Oncol.*, 2010, **2010**, 151750.
- 72 H. E. Bryant, N. Schultz, H. D. Thomas, K. M. Parker, D. Flower, E. Lopez, S. Kyle, M. Meuth, N. J. Curtin and T. Helleday, *Nature*, 2005, **434**, 913–917.
- 73 H. Farmer, N. McCabe, C. J. Lord, A. N. J. Tutt, D. A. Johnson, T. B. Richardson, M. Santarosa, K. J. Dillon, I. Hickson, C. Knights, N. M. B. Martin, S. P. Jackson, G. C. M. Smith and A. Ashworth, *Nature*, 2005, **434**, 917–921.
- 74 K. A. Menear, C. Adcock, R. Boulter, X. Cockcroft, L. Copley, A. Cranston, K. J. Dillon, J. Drzewiecki, S. Garman, S. Gomez, H. Javaid, F. Kerrigan, C. Knights, A. Lau, V. M. Loh, I. T. W. Matthews, S. Moore, M. J. O. Connor, G. C. M. Smith and N. M. B. Martin, *J. Med. Chem.*, 2008, **51**, 6581–6591.
- 75 E. D. Deeks, *Drugs*, 2015, **75**, 231–240.
- 76 M. Rose, J. T. Burgess, K. O'Byrne, D. J. Richard and E. Bolderson, *Front. Cell Dev. Biol.*, 2020, **8**, 564601.
- 77 Y. Y. Syed, *Drugs*, 2017, **77**, 585–592.
- 78 L. J. Scott, *Drugs*, 2017, **77**, 1029–1034.
- 79 S. M. Hoy, *Drugs*, 2018, **78**, 1939–1946.
- 80 A. Lee, *Drugs*, 2021, **81**, 1221–1226.

- 81 A. Markham, *Drugs*, 2021, **81**, 1343–1348.
- 82 C. K. Donawho, Y. Luo, Y. Luo, T. D. Penning, J. L. Bauch, J. J. Bouska, V. D. Bontcheva-Diaz, B. F. Cox, T. L. DeWeese, L. E. Dillehay, D. C. Ferguson, N. S. Ghoreishi-Haack, D. R. Grimm, R. Guan, E. K. Han, R. R. Holley-Shanks, B. Hristov, K. B. Idler, K. Jarvis, E. F. Johnson, L. R. Kleinberg, V. Klinghofer, L. M. Lasko, X. Liu, K. C. Marsh, T. P. McGonigal, J. A. Meulbroek, A. M. Olson, J. P. Palma, L. E. Rodriguez, Y. Shi, J. A. Stavropoulos, A. C. Tsurutani, G. D. Zhu, S. H. Rosenberg, V. L. Giranda and D. J. Frost, *Clin. Cancer Res.*, 2007, **13**, 2728–2737.
- 83 S. Boussios, P. Karihtala, M. Moschetta, C. Abson, A. Karathanasi, N. Zakyntinakis-Kyriakou, J. E. Ryan, M. Sheriff, E. Rassy and N. Pavlidis, *Invest. New Drugs*, 2020, **38**, 181–193.
- 84 S. Makin, *Nature*, 2021, **600**, S36–S38.
- 85 M. Onstad, R. L. Coleman and S. N. Westin, *Drugs*, 2020, **80**, 1525–1535.
- 86 B. Carney, G. Carlucci, B. Salinas, V. Di Gialleonardo, S. Kossatz, A. Vansteene, V. A. Longo, A. Bolaender, G. Chiosis, K. R. Keshari, W. A. Weber, T. Reiner, V. Di Gialleonardo, S. Kossatz, A. Vansteene, V. A. Longo, A. Bolaender, G. Chiosis, K. R. Keshari, W. A. Weber and T. Reiner, *Mol. Imaging Biol.*, 2016, **18**, 386–392.
- 87 L. N. Puentes, M. Makvandi and R. H. Mach, *J. Nucl. Med.*, 2021, **62**, 765–770.
- 88 R. A. Sankaranarayanan, S. Kossatz, W. Weber, M. Beheshti, A. Morgenroth and F. M. Mottaghy, *J. Clin. Med.*, 2020, **9**, 2130.
- 89 B. Carney, S. Kossatz and T. Reiner, *J. Nucl. Med.*, 2017, **58**, 1025–1030.
- 90 Z. Tu, W. Chu, J. Zhang, C. S. Dence, M. J. Welch and R. H. Mach, *Nucl. Med. Biol.*, 2005, **32**, 437–443.
- 91 D. Zhou, W. Chu, J. Xu, L. A. Jones, X. Peng, S. Li, D. L. Chen and R. H. Mach, *Bioorganic Med. Chem.*, 2014, **22**, 1700–1707.
- 92 D. Zhou, J. Xu, C. Mpoy, W. Chu, S. H. Kim, H. Li, B. E. Rogers and J. A. Katzenellenbogen, *Nucl. Med. Biol.*, 2018, **66**, 26–31.
- 93 M. Makvandi, A. Pantel, L. Schwartz, E. Schubert, K. Xu, C. J. Hsieh, C. Hou, H. Kim, C. C. Weng, H. Winters, R. Doot, M. D. Farwell, D. A. Pryma, R. A. Greenberg, D. A. Mankoff, F. Simpkins, R. H. Mach and L. L. Lin, *J. Clin. Invest.*, 2018, **128**, 2116–2126.
- 94 M. Makvandi, K. Xu, B. P. Lieberman, R. C. Anderson, S. S. Effron, H. D.

- Winters, C. Zeng, E. S. McDonald, D. A. Pryma, R. A. Greenberg and R. H. Mach, *Cancer Res.*, 2016, **76**, 4516–4524.
- 95 R. C. Anderson, M. Makvandi, K. Xu, B. P. Lieberman, C. Zeng, D. A. Pryma and R. H. Mach, *Nucl. Med. Biol.*, 2016, **43**, 752–758.
- 96 M. Makvandi, H. Lee, L. N. Puentes, S. W. Reilly, K. S. Rathi, C. C. Weng, H. S. Chan, C. Hou, P. Raman, D. Martinez, K. Xu, S. D. Carlin, R. A. Greenberg, B. R. Pawel, R. H. Mach, J. M. Maris and D. A. Pryma, *Mol. Cancer Ther.*, 2019, **18**, 1195–1204.
- 97 E. J. Keliher, T. Reiner, A. Turetsky, S. A. Hilderbrand and R. Weissleder, *ChemMedChem*, 2011, **6**, 424–427.
- 98 T. Reiner, E. J. Keliher, S. Earley, B. Marinelli and R. Weissleder, *Angew. Chem. Int. Ed.*, 2011, **50**, 1922–1925.
- 99 T. L. Andersen, S. D. Friis, H. Audrain, P. Nordeman, G. Antoni and T. Skrydstrup, *J. Am. Chem. Soc.*, 2015, **137**, 1548–1555.
- 100 T. C. Wilson, N. Pillarsetty and T. Reiner, *J. Label. Compd. Radiopharm.*, 2020, **63**, 419–425.
- 101 B. Salinas, C. P. Irwin, S. Kossatz, A. Bolaender, G. Chiosis, N. Pillarsetty, W. A. Weber and T. Reiner, *EJNMMI Res.*, 2015, **5**, 46.
- 102 F. Zmuda, G. Malviya, A. Blair, M. Boyd, A. J. Chalmers, A. Sutherland and S. L. Pimlott, *J. Med. Chem.*, 2015, **58**, 8683–8693.
- 103 S. Webster, K. M. O'Rourke, C. Fletcher, S. L. Pimlott, A. Sutherland and A.-L. Lee, *Chem. Eur. J.*, 2018, **24**, 937–943.
- 104 J. J. Molloy, K. M. O'Rourke, C. P. Frias, N. L. Sloan, M. J. West, S. L. Pimlott, A. Sutherland and A. J. B. Watson, *Org. Lett.*, 2019, **21**, 2488–2492.
- 105 F. Zmuda, A. Blair, M. C. Liuzzi, G. Malviya, A. J. Chalmers, D. Lewis, A. Sutherland and S. L. Pimlott, *J. Med. Chem.*, 2018, **61**, 4103–4114.
- 106 T. C. Wilson, M.-A. Xavier, J. Knight, S. Verhoog, J. B. Torres, M. Mosley, S. L. Hopkins, S. Wallington, P. D. Allen, V. Kersemans, R. Hueting, S. Smart, V. Gouverneur and B. Cornelissen, *J. Nucl. Med.*, 2019, **60**, 504–510.
- 107 M. Tredwell, S. M. Preshlock, N. J. Taylor, S. Gruber, M. Huiban, J. Passchier, J. Mercier, C. Génicot and V. Gouverneur, *Angew. Chem. Int. Ed.*, 2014, **53**, 7751–7755.
- 108 S. Preshlock, S. Calderwood, S. Verhoog, M. Tredwell, M. Huiban, A. Hienzsch, S. Gruber, T. C. Wilson, N. J. Taylor, T. Cailly, M. Schedler, T. L. Collier, J. Passchier, R. Smits, J. Mollitor, A. Hoepfing, M. Mueller, C.

- Genicot, J. Mercier and V. Gouverneur, *Chem. Commun.*, 2016, **52**, 8361–8364.
- 109 K. Buckley and R. B. Kelly, *J. Cell Biol.*, 1985, **100**, 1284–1294.
- 110 W. Löscher, M. Gillard, Z. A. Sands, R. M. Kaminski and H. Klitgaard, *CNS Drugs*, 2016, **30**, 1055–1077.
- 111 R. A. J. O. Dierckx, A. Otte, E. F. J. De Vries, A. Van Waarde and P. G. M. Luiten, *PET and SPECT of neurobiological systems*, Springer Nature Switzerland AG, 2nd edn., 2021.
- 112 R. Janz and T. C. Südhof, *Neuroscience*, 1999, **94**, 1279–1290.
- 113 J. G. Mendoza-Torreblanca, A. Vanoye-Carlo, B. V. Phillips-Farfán, L. Carmona-Aparicio and G. Gómez-Lira, *Eur. J. Neurosci.*, 2013, **38**, 3529–3539.
- 114 O. Bartholome, P. Van Den Ackerveken, J. S. Gil, O. de la B. Bonardeaux, P. Leprince, R. Franzen and B. Rogister, *Front. Mol. Neurosci.*, 2017, **10**, 1–15.
- 115 S. M. Bajjalieh, G. D. Frantz, J. M. Weimann, S. K. McConnell and R. H. Scheller, *J. Neurosci.*, 1994, **14**, 5223–5235.
- 116 R. Rossi, S. Arjmand, S. L. Bærentzen, A. Gjedde and A. M. Landau, *Front. Neurosci.*, 2022, **16**, 864514.
- 117 R. Janz, Y. Goda, M. Geppert, M. Missler and T. C. Südhof, *Neuron*, 1999, **24**, 1003–1016.
- 118 K. Heurling, N. J. Ashton, A. Leuzy, E. R. Zimmer, K. Blennow, H. Zetterberg, J. Eriksson, M. Lubberink and M. Schöll, *Mol. Cell. Neurosci.*, 2019, **97**, 34–42.
- 119 K. A. Stout, A. R. Dunn, C. Hoffman and G. W. Miller, *ACS Chem. Neurosci.*, 2019, **10**, 3927–3938.
- 120 M. Noyer, M. Gillard, A. Matagne, J. P. Hénichart and E. Wülfert, *Eur. J. Pharmacol.*, 1995, **286**, 137–146.
- 121 B. A. Lynch, N. Lambeng, K. Nocka, P. Kensel-Hammes, S. M. Bajjalieh, A. Matagne and B. Fuks, *Proc. Natl. Acad. Sci. U. S. A.*, 2004, **101**, 9861–9866.
- 122 M. Gillard, B. Fuks, K. Leclercq and A. Matagne, *Eur. J. Pharmacol.*, 2011, **664**, 36–44.
- 123 P. Von Rosenstiel, *Neurotherapeutics*, 2007, **4**, 84–87.
- 124 W. Van Paesschen, E. Hirsch, M. Johnson, U. Falter and P. Von Rosenstiel, *Epilepsia*, 2013, **54**, 89–97.
- 125 H. Klitgaard, A. Matagne, J. M. Nicolas, M. Gillard, Y. Lamberty, M. De Ryck,

- R. M. Kaminski, K. Leclercq, I. Niespodziany, C. Wolff, M. Wood, J. Hannestad, S. Kervyn and B. Kenda, *Epilepsia*, 2016, **57**, 538–548.
- 126 A. Matagne, D. G. Margineanu, B. Kenda, P. Michel and H. Klitgaard, *Br. J. Pharmacol.*, 2008, **154**, 1662–1671.
- 127 B. M. Kenda, A. C. Matagne, P. E. Talaga, P. M. Pasau, E. Differding, B. I. Lallemand, A. M. Frycia, F. G. Moureau, H. V. Klitgaard, M. R. Gillard, B. Fuks and P. Michel, *J. Med. Chem.*, 2004, **47**, 530–549.
- 128 A. M. Feyissa, *Neuropsychiatr. Dis. Treat.*, 2019, **15**, 2587–2600.
- 129 P. Bhutani, G. Joshi, N. Raja, N. Bachhav, P. K. Rajanna, H. Bhutani, A. T. Paul and R. Kumar, *J. Med. Chem.*, 2021, **64**, 2339–2381.
- 130 J. Mercier, L. Archen, V. Bollu, S. Carré, Y. Evrard, E. Jnoff, B. Kenda, B. Lallemand, P. Michel, F. Montel, F. Moureau, N. Price, Y. Quesnel, X. Sauvage, A. Valade and L. Provins, *ChemMedChem*, 2014, **9**, 693–698.
- 131 J. Mercier, L. Provins and A. Valade, *Drug Discov. Today Technol.*, 2017, **25**, 45–52.
- 132 Z. Cai, S. Li, D. Matuskey, N. Nabulsi and Y. Huang, *Neurosci. Lett.*, 2019, **691**, 44–50.
- 133 G. Becker, S. Dammicco, M. A. Bahri and E. Salmon, *Molecules*, 2020, **25**, 2303.
- 134 H. Cai, T. J. Mangner, O. Muzik, M. W. Wang, D. C. Chugani and H. T. Chugani, *ACS Med. Chem. Lett.*, 2014, **5**, 1152–1155.
- 135 H. M. Rashed, R. N. Shamma and H. A. El-Sabagh, *Eur. J. Pharm. Sci.*, 2018, **121**, 29–33.
- 136 M. H. Sanad, H. M. Eyssa, F. A. Marzook, A. B. Farag, S. F. A. Rizvi, S. K. Mandal, S. S. Patnaik, A. S. M. Fouzy, S. A. Bassem and F. Verpoort, *Radiochemistry*, 2021, **63**, 635–641.
- 137 S. Estrada, M. Lubberink, A. Thibblin, M. Sprycha, T. Buchanan, N. Mestdagh, B. Kenda, J. Mercier, L. Provins, M. Gillard, D. Tytgat and G. Antoni, *Nucl. Med. Biol.*, 2016, **43**, 325–332.
- 138 G. I. Warnock, J. Aerts, M. A. Bahri, F. Bretin, C. Lemaire, F. Giacomelli, F. Mievis, N. Mestdagh, T. Buchanan, A. Valade, J. Mercier, M. Wood, M. Gillard, A. Seret, A. Luxen, E. Salmon and A. Plenevaux, *J. Nucl. Med.*, 2014, **55**, 1336–1341.
- 139 C. Warnier, C. Lemaire, G. Becker, G. Zaragoza, F. Giacomelli, J. Aerts, M. Otabashi, M. A. Bahri, J. Mercier, A. Plenevaux and A. Luxen, *J. Med. Chem.*,

- 2016, **59**, 8955–8966.
- 140 S. Goutal, M. Guillermier, G. Becker, M. Gaudin, Y. Bramoullé, A. Luxen, C. Lemaire, A. Plenevaux, E. Salmon, P. Hantraye, O. Barret and N. Van Camp, *EJNMMI Res.*, 2021, **11**, 36.
- 141 N. B. Nabulsi, J. Mercier, D. Holden, S. Carré, S. Najafzadeh, M.-C. Vandergeten, S.-F. Lin, A. Deo, N. Price, M. Wood, T. Lara-Jaime, F. Montel, M. Laruelle, R. E. Carson, J. Hannestad and Y. Huang, *J. Nucl. Med.*, 2016, **57**, 777–784.
- 142 J. J. Weiss, R. Calvi, M. Naganawa, T. Toyonaga, S. F. Farhadian, M. Chintanaphol, J. Chiarella, M. Q. Zheng, J. Ropchan, Y. Huang, R. H. Pietrzak, R. E. Carson and S. Spudich, *Clin. Infect. Dis.*, 2021, **73**, 1404–1411.
- 143 R. S. O’Dell, A. P. Mecca, M. K. Chen, M. Naganawa, T. Toyonaga, Y. Lu, T. A. Godek, J. E. Harris, H. H. Bartlett, E. R. Banks, V. L. Kominek, W. Zhao, N. B. Nabulsi, J. Ropchan, Y. Ye, B. C. Vander Wyk, Y. Huang, A. F. T. Arnsten, R. E. Carson and C. H. van Dyck, *Alzheimer’s Res. Ther.*, 2021, **13**, 11.
- 144 K. B. Andersen, A. K. Hansen, M. F. Damholdt, J. Horsager, C. Skjærbæk, H. Gottrup, H. Klit, A. C. Schacht, E. H. Danielsen, D. J. Brooks and P. Borghammer, *Mov. Disord.*, 2021, **36**, 2057–2065.
- 145 M. K. Chen, A. P. Mecca, M. Naganawa, J. D. Gallezot, T. Toyonaga, J. Mondal, S. J. Finnema, S. F. Lin, R. S. O’Dell, J. W. McDonald, H. R. Michalak, B. Vander Wyk, N. B. Nabulsi, Y. Huang, A. F. T. Arnsten, C. H. van Dyck and R. E. Carson, *J. Cereb. Blood Flow Metab.*, 2021, **41**, 2395–2409.
- 146 M. Xiong, S. Roshanbin, J. Rokka, E. Schlein, M. Ingelsson, D. Sehlin, J. Eriksson and S. Syvänen, *Neuroimage*, 2021, **239**, 118302.
- 147 M. B. Thomsen, S. A. Ferreira, A. C. Schacht, J. Jacobsen, M. Simonsen, C. Betzer, P. H. Jensen, D. J. Brooks, A. M. Landau and M. Romero-Ramos, *Neurobiol. Dis.*, 2021, **149**, 105229.
- 148 R. H. Asch, S. E. Holmes, A. M. Jastreboff, M. N. Potenza, S. R. Baldassarri, R. E. Carson, R. H. Pietrzak and I. Esterlis, *Neuropsychopharmacology*, 2022, **47**, 543–552.
- 149 D. Bertoglio, J. Verhaeghe, L. Wyffels, A. Miranda, S. Stroobants, L. Mrzljak, C. Dominguez, M. Skinbjerg, J. Bard, L. Liu, I. Munoz-Sanjuan and S. Staelens, *J. Nucl. Med.*, 2022, **63**, 942–947.

- 150 L. Michiels, N. Mertens, L. Thijs, A. Radwan, S. Sunaert, M. Vandenbulcke, G. Verheyden, M. Koole, K. Van Laere and R. Lemmens, *J. Cereb. Blood Flow Metab.*, 2022, **42**, 303–314.
- 151 S. Li, Z. Cai, W. Zhang, D. Holden, S. fei Lin, S. J. Finnema, A. Shirali, J. Ropchan, S. Carre, J. Mercier, R. E. Carson, N. Nabulsi and Y. Huang, *Eur. J. Nucl. Med. Mol. Imaging*, 2019, **46**, 1952–1965.
- 152 C. C. Constantinescu, C. Tresse, M. Q. Zheng, A. Gouasmat, V. M. Carroll, L. Mistico, D. Alagille, C. M. Sandiego, C. Papin, K. Marek, J. P. Seibyl, G. D. Tamagnan and O. Barret, *Mol. Imaging Biol.*, 2019, **21**, 509–518.
- 153 S. Li, Z. Cai, X. Wu, D. Holden, R. Pracitto, M. Kapinos, H. Gao, D. Labaree, N. Nabulsi, R. E. Carson and Y. Huang, *ACS Chem. Neurosci.*, 2019, **10**, 1544–1554.
- 154 S. Patel, A. Knight, S. Krause, T. Teceno, C. Tresse, S. Li, Z. Cai, A. Gouasmat, V. M. Carroll, O. Barret, V. Gottmukkala, W. Zhang, X. Xiang, T. Morley, Y. Huang and J. Passchier, *Mol. Imaging Biol.*, 2020, **22**, 832–841.
- 155 M. Naganawa, S. Li, N. Nabulsi, S. Henry, M.-Q. Zheng, R. Pracitto, Z. Cai, H. Gao, M. Kapinos, D. Labaree, D. Matuskey, Y. Huang and R. E. Carson, *J. Nucl. Med.*, 2021, **62**, 561–567.
- 156 Z. Cai, S. Li, W. Zhang, R. Pracitto, X. Wu, E. Baum, S. J. Finnema, D. Holden, T. Toyonaga, S. F. Lin, M. Lindemann, A. Shirali, D. C. Labaree, J. Ropchan, N. Nabulsi, R. E. Carson and Y. Huang, *ACS Chem. Neurosci.*, 2020, **11**, 592–603.
- 157 C. Zheng, D. Holden, M.-Q. Zheng, R. Pracitto, K. C. Wilcox, M. Lindemann, Z. Felchner, L. Zhang, J. Tong, K. Fowles, S. J. Finnema, N. Nabulsi, R. E. Carson, Y. Huang and Z. Cai, *Eur. J. Nucl. Med. Mol. Imaging*, 2022, **49**, 1482–1496.
- 158 K. M. O'Rourke, *PhD Thesis, University of Glasgow*, 2018, 1–186.
- 159 A. Blair, *PhD Thesis, University of Glasgow*, 2014, 1–223.
- 160 F. Zmuda, *PhD Thesis, University of Glasgow*, 2016, 1–364.
- 161 N. L. Sloan, *PhD Thesis, University of Glasgow*, 2017, 1–203.
- 162 C. Pascali, S. K. Luthra, V. W. Pike, G. W. Price, R. G. Ahier, S. P. Hume, R. Myers, L. Manjil and J. E. Cremer, *Appl. Radiat. Isot.*, 1990, **41**, 477–482.
- 163 L. Dolci, F. Dolle, S. Jubeau, F. Vaufrey and C. Crouzel, *J. Label. Compd. Radiopharm.*, 1999, **42**, 975–985.
- 164 A. A. S. Tavares, J. Lewsey, D. Dewar and S. L. Pimlott, *Nucl. Med. Biol.*,

- 2012, **39**, 127–135.
- 165 M. C. Liuzzi, *PhD Thesis, University of Glasgow*, 2021, 1–182.
- 166 T. Reiner, J. Lacy, E. J. Keliher, K. S. Yang, A. Ullal, R. H. Kohler, C. Vinegoni and R. Weissleder, *Neoplasia*, 2012, **14**, 169–177.
- 167 G. M. Thurber, K. S. Yang, T. Reiner, R. H. Kohler, P. Sorger, T. Mitchison and R. Weissleder, *Nat. Commun.*, 2013, **4**, 1504.
- 168 V. Cepeda, M. Fuertes, J. Castilla, C. Alonso, C. Quevedo, M. Soto and J. Perez, *Recent Pat. Anticancer. Drug Discov.*, 2006, **1**, 39–53.
- 169 X. L. Cockcroft, K. J. Dillon, L. Dixon, J. Drzewiecki, F. Kerrigan, V. M. Loh, N. M. B. Martin, K. A. Menear and G. C. M. Smith, *Bioorganic Med. Chem. Lett.*, 2006, **16**, 1040–1044.
- 170 J. X. He, C. H. Yang and Z. H. Miao, *Acta Pharmacol. Sin.*, 2010, **31**, 1172–1180.
- 171 K. Ryan, B. Bolaños, M. Smith, P. B. Palde, P. D. Cuenca, T. L. VanArsdale, S. Niessen, L. Zhang, D. Behenna, M. A. Ornelas, K. T. Tran, S. Kaiser, L. Lum, A. Stewart and K. S. Gajiwala, *J. Biol. Chem.*, 2021, **296**, 100251.
- 172 T. Kinoshita, I. Nakanishi, M. Warizaya, A. Iwashita, Y. Kido, K. Hattori and T. Fujii, *FEBS Lett.*, 2004, **556**, 43–46.
- 173 T. Reiner, S. Earley, A. Turetsky and R. Weissleder, *ChemBioChem*, 2010, **11**, 2374–2377.
- 174 WO 2008/047082 A2, 2008, 1–40.
- 175 US 7,692,006 B2, 2010, 1–21.
- 176 S. Sengmany, E. Le Gall, C. Le Jean, M. Troupel and J. Y. Nédélec, *Tetrahedron*, 2007, **63**, 3672–3681.
- 177 E. Valeur and M. Bradley, *Chem. Soc. Rev.*, 2009, **38**, 606–631.
- 178 C. P. Irwin, Y. Portorreal, C. Brand, Y. Zhang, P. Desai, B. Salinas, W. A. Weber and T. Reiner, *Neoplasia*, 2014, **16**, 432–440.
- 179 G. Carlucci, B. Carney, C. Brand, S. Kossatz, C. P. Irwin, S. D. Carlin, E. J. Keliher, W. Weber and T. Reiner, *Mol. Imaging Biol.*, 2015, **17**, 848–855.
- 180 P. Demétrio de Souza França, S. Kossatz, C. Brand, D. Karassawa Zanoni, S. Roberts, N. Guru, D. Adilbay, A. Mauguen, C. Valero Mayor, W. A. Weber, H. Schöder, R. A. Ghossein, I. Ganly, S. G. Patel and T. Reiner, *Eur. J. Nucl. Med. Mol. Imaging*, 2021, **48**, 3618–3630.
- 181 A. Vanessa Saura, M. Isabel Burguete, F. Galindo and S. V. Luis, *Org. Biomol. Chem.*, 2017, **15**, 3013–3024.

- 182 S. Krajcovicova, J. Stankova, P. Dzubak, M. Hajduch, M. Soural and M. Urban, *Chem. Eur. J.*, 2018, **24**, 4957–4966.
- 183 R. Wodtke, J. Steinberg, M. Köckerling, R. Löser and C. Mamat, *RSC Adv.*, 2018, **8**, 40921–40933.
- 184 A. D. McNaught and A. Wilkinson, *IUPAC Compendium of Chemical Terminology Gold Book*, International Union of Pure and Applied Chemistry, 2nd edn., 1997.
- 185 R. N. Waterhouse, *Mol. Imaging Biol.*, 2003, **5**, 376–389.
- 186 T. Fujita, J. Iwasa and C. Hansch, *J. Am. Chem. Soc.*, 1964, **86**, 5175–5180.
- 187 K. Valkó, *J. Chromatogr. A*, 2004, **1037**, 299–310.
- 188 G. L. Trainor, *Expert Opin. Drug Discov.*, 2007, **2**, 51–64.
- 189 K. Valkó, S. Nunhuck, C. Bevan, M. H. Abraham and D. P. Reynolds, *J. Pharm. Sci.*, 2003, **92**, 2236–2248.
- 190 K. L. Valkó, *J. Pharm. Biomed. Anal.*, 2016, **130**, 35–54.
- 191 C. Pidgeon, S. Ong, H. Liu, X. Qiu, M. Pidgeon, A. H. Dantzig, J. Munroe, W. J. Hornback and J. S. Kasher, *J. Med. Chem.*, 1995, **38**, 590–594.
- 192 S. Ong, H. Liu and C. Pidgeon, *J. Chromatogr. A*, 1996, **728**, 113–128.
- 193 C. Y. Yang, S. J. Cai, H. Liu and C. Pidgeon, *Adv. Drug Deliv. Rev.*, 1997, **23**, 229–256.
- 194 W. K. Dong, H. J. Jeong, T. L. Seok, M. H. Sohn, J. A. Katzenellenbogen and Y. C. Dae, *J. Org. Chem.*, 2008, **73**, 957–962.
- 195 N. J. Taylor, E. Emer, S. Preshlock, M. Schedler, M. Tredwell, S. Verhoog, J. Mercier, C. Genicot and V. Gouverneur, *J. Am. Chem. Soc.*, 2017, **139**, 8267–8276.
- 196 F. Guibbal, P. G. Isenegger, T. C. Wilson, A. Pacelli, D. Mahaut, J. B. I. Sap, N. J. Taylor, S. Verhoog, S. Preshlock, R. Hueting, B. Cornelissen and V. Gouverneur, *Nat. Protoc.*, 2020, **15**, 1525–1541.
- 197 S. J. Lee, M. T. Morales-Colón, A. F. Brooks, J. S. Wright, K. J. Makaravage, P. J. H. Scott and M. S. Sanford, *J. Org. Chem.*, 2021, **86**, 14121–14130.
- 198 F. Zhu, M. Cizeron, Z. Qiu, R. Benavides-Piccione, M. V. Kopanitsa, N. G. Skene, B. Koniaris, J. DeFelipe, E. Fransén, N. H. Komiyama and S. G. N. Grant, *Neuron*, 2018, **99**, 781–799.
- 199 K. J. Makaravage, A. F. Brooks, A. V. Mossine, M. S. Sanford and P. J. H. Scott, *Org. Lett.*, 2016, **18**, 5440–5443.
- 200 X. Wu, S. Li, M. Zheng, J. Ropchan and Y. Huang, *J. Nucl. Med.*, 2019, **60**,

68 (Supplement 1).

- 201 M. C. Henry, H. M. Senn and A. Sutherland, *J. Org. Chem.*, 2019, **84**, 346–364.
- 202 H. Chen, X. Han, N. Qin, L. Wei, Y. Yang, L. Rao, B. Chi, L. Feng, Y. Ren and J. Wan, *Bioorganic Med. Chem.*, 2016, **24**, 1225–1230.
- 203 L. Roiser and M. Waser, *Org. Lett.*, 2017, **19**, 2338–2341.
- 204 H. Li, Y. Wang, L. Tang and L. Deng, *J. Am. Chem. Soc.*, 2004, **126**, 9906–9907.
- 205 H. Li, Y. Wang, L. Tang, F. Wu, X. Liu, C. Guo, B. M. Foxman and L. Deng, *Angew. Chem. Int. Ed.*, 2005, **44**, 105–108.
- 206 T. Marcelli, J. H. Van Maarseveen and H. Hiemstra, *Angew. Chem. Int. Ed.*, 2006, **45**, 7496–7504.
- 207 E. M. O. Yeboah, S. O. Yeboah and G. S. Singh, *Tetrahedron*, 2011, **67**, 1725–1762.
- 208 P. Chauhan and S. S. Chimni, *RSC Adv.*, 2012, **2**, 737–758.
- 209 A. J. Béchamp, *Ann. Chim. Phys.*, 1854, **42**, 186–196.
- 210 Z. Wang, *Comprehensive Organic Name Reactions and Reagents*, John Wiley & Sons, Inc., Hoboken, NJ, USA, 1st edn., 2010.
- 211 M. Orlandi, F. Tosi, M. Bonsignore and M. Benaglia, *Org. Lett.*, 2015, **17**, 3941–3943.
- 212 R. Porta, A. Puglisi, G. Colombo, S. Rossi and M. Benaglia, *Beilstein J. Org. Chem.*, 2016, **12**, 2614–2619.
- 213 P. Camps, D. Muñoz-Torrero and L. Sánchez, *Tetrahedron Asymmetry*, 2004, **15**, 2039–2044.
- 214 X.-F. Yang, C.-H. Ding, X.-H. Li, J.-Q. Huang, X.-L. Hou, L.-X. Dai and P.-J. Wang, *J. Org. Chem.*, 2012, **77**, 8980–8985.
- 215 The Royal Swedish Academy of Sciences, Press release: The Nobel Prize in Chemistry 2021, <https://www.nobelprize.org/prizes/chemistry/2021/press-release/>, (accessed 8 October 2021).
- 216 B. List, R. A. Lerner and C. F. Barbas, *J. Am. Chem. Soc.*, 2000, **122**, 2395–2396.
- 217 K. A. Ahrendt, C. J. Borths and D. W. C. MacMillan, *J. Am. Chem. Soc.*, 2000, **122**, 4243–4244.
- 218 S. Mukherjee, J. W. Yang, S. Hoffmann and B. List, *Chem. Rev.*, 2007, **107**, 5471–5569.

- 219 A. Erkkilä, I. Majander and P. M. Pihko, *Chem. Rev.*, 2007, **107**, 5416–5470.
- 220 D. W. C. MacMillan, *Nature*, 2008, **455**, 304–308.
- 221 J. Franzén, M. Marigo, D. Fielenbach, T. C. Wabnitz, A. Kjærsgaard and K. A. Jørgensen, *J. Am. Chem. Soc.*, 2005, **127**, 18296–18304.
- 222 Y. Hayashi, H. Gotoh, T. Hayashi and M. Shoji, *Angew. Chem. Int. Ed.*, 2005, **44**, 4212–4215.
- 223 B. S. Donslund, T. K. Johansen, P. H. Poulsen, K. S. Halskov and K. A. Jørgensen, *Angew. Chem. Int. Ed.*, 2015, **54**, 13860–13874.
- 224 L. Klier, F. Tur, P. H. Poulsen and K. A. Jørgensen, *Chem. Soc. Rev.*, 2017, **46**, 1080–1102.
- 225 G. J. Reyes-Rodríguez, N. M. Rezayee, A. Vidal-Albalat and K. A. Jørgensen, *Chem. Rev.*, 2019, **119**, 4221–4260.
- 226 H. Finkelstein, *Ber. Dtsch. Chem. Ges.*, 1910, **43**, 1528–1532.
- 227 J. O. Osby and B. Ganem, *Tetrahedron Lett.*, 1985, **26**, 6413–6416.
- 228 F. G. A. Stone and R. West, *Advances in Organometallic Chemistry*, 1st edn., 1966.
- 229 J. J. Zuckerman and A. P. Hagen, *Inorganic Reactions and Methods, Volume 5, The Formation of Bonds to Group VIB (O, S, Se, Te, Po) Elements (Part 1)*, 2009.
- 230 U. Grošelj, D. Seebach, D. M. Badine, W. B. Schweizer, A. K. Beck, I. Krossing, P. Klose, Y. Hayashi and T. Uchimaru, *Helv. Chim. Acta*, 2009, **92**, 1225–1259.
- 231 D. Seebach, U. Grošelj, D. M. Badine, W. B. Schweizer and A. K. Beck, *Helv. Chim. Acta*, 2008, **91**, 1999–2034.
- 232 D. Seebach, R. Gilmour, U. Grošelj, G. Deniau, C. Sparr, M. O. Ebert, A. K. Beck, L. B. McCusker, D. Šišak and T. Uchimaru, *Helv. Chim. Acta*, 2010, **93**, 603–634.
- 233 P. Dinér, M. Nielsen, M. Marigo and K. A. Jørgensen, *Angew. Chem. Int. Ed.*, 2007, **46**, 1983–1987.
- 234 I. Ibrahim, P. Hammar, J. Vesely, R. Rios, L. Eriksson and A. Córdova, *Adv. Synth. Catal.*, 2008, **350**, 1875–1884.
- 235 L. Zu, H. Xie, H. Li, J. Wang and W. Wang, *Adv. Synth. Catal.*, 2007, **349**, 2660–2664.
- 236 E. Dalcanale and F. Montanari, *J. Org. Chem.*, 1986, **51**, 567–569.
- 237 F. Xu, M. Zacuto, N. Yoshikawa, R. Desmond, S. Hoerrner, T. Itoh, M.

- Journet, G. R. Humphrey, C. Cowden, N. Strotman and P. Devine, *J. Org. Chem.*, 2010, **75**, 7829–7841.
- 238 H. Gotoh, H. Ishikawa and Y. Hayashi, *Org. Lett.*, 2007, **9**, 5307–5309.
- 239 A. V. Mossine, A. F. Brooks, V. Bernard-Gauthier, J. J. Bailey, N. Ichiishi, R. Schirmacher, M. S. Sanford and P. J. H. Scott, *J. Label. Compd. Radiopharm.*, 2018, **61**, 228–236.
- 240 M. A. Kavina, V. V. Sizov and I. P. Yakovlev, *Russ. J. Org. Chem.*, 2017, **53**, 873–878.
- 241 G. W. Gribble, *Chemosphere*, 2003, **52**, 289–297.
- 242 G. W. Gribble, *J. Chem. Educ.*, 2004, **81**, 1441–1449.
- 243 L. Wang, X. Zhou, M. Fredimoses, S. Liao and Y. Liu, *RSC Adv.*, 2014, **4**, 57350–57376.
- 244 P. Jeschke, *Pest Manag. Sci.*, 2010, **66**, 10–27.
- 245 L. Van Erven and M. J. Schlij, *Heart*, 2010, **96**, 1593–1600.
- 246 A. K. S. Salama and K. B. Kim, *Expert Opin. Pharmacother.*, 2013, **14**, 619–627.
- 247 E. B. Merkushev, *Synthesis*, 1988, **12**, 923–937.
- 248 T. D. Sheppard, *Org. Biomol. Chem.*, 2009, **7**, 1043–1052.
- 249 P. Knochel, W. Dohle, N. Gommermann, F. F. Kneisel, F. Kopp, T. Korn, I. Sapountzis and V. A. Vu, *Angew. Chem. Int. Ed.*, 2003, **42**, 4302–4320.
- 250 N. Kvasovs and V. Gevorgyan, *Chem. Soc. Rev.*, 2021, **50**, 2244–2259.
- 251 K. C. Nicolaou, P. G. Bulger and D. Sarlah, *Angew. Chem. Int. Ed.*, 2005, **44**, 4442–4489.
- 252 J. F. Hartwig, *Nature*, 2008, **455**, 314–322.
- 253 P. Ruiz-Castillo and S. L. Buchwald, *Chem. Rev.*, 2016, **116**, 12564–12649.
- 254 S. Bhunia, G. G. Pawar, S. V. Kumar, Y. Jiang and D. Ma, *Angew. Chem. Int. Ed.*, 2017, **56**, 16136–16179.
- 255 G. Evano, A. Nitelet, P. Thilmany and D. F. Dewez, *Front. Chem.*, 2018, **6**, 114.
- 256 J. R. Hanson, *J. Chem. Res.*, 2006, **5**, 277–280.
- 257 S. Stavber, M. Jereb and M. Zupan, *Synthesis*, 2008, **2008**, 1487–1513.
- 258 V. Snieckus, *Chem. Rev.*, 1990, **90**, 879–933.
- 259 T. Sandmeyer, *Ber. Dtsch. Chem. Ges.*, 1884, **17**, 1633–1635.
- 260 T. Sandmeyer, *Ber. Dtsch. Chem. Ges.*, 1884, **17**, 2650–2653.
- 261 H. H. Hodgson, *Chem. Rev.*, 1947, **40**, 251–277.

- 262 C. Galli, *Chem. Rev.*, 1988, **88**, 765–792.
- 263 X. Liu, X. Zhao, F. Liang and B. Ren, *Org. Biomol. Chem.*, 2018, **16**, 886–890.
- 264 R.-J. Tang, T. Milcent and B. Crousse, *J. Org. Chem.*, 2018, **83**, 930–938.
- 265 R. Narobe, S. J. S. Düsel, J. Iskra and B. König, *Adv. Synth. Catal.*, 2019, **361**, 3998–4004.
- 266 L. Lu, Y. Li and X. Jiang, *Green Chem.*, 2020, **22**, 5989–5994.
- 267 N. Rong, Y. Yuan, H. Chen, C. Yao, T. Li, Y. Wang and W. Yang, *Org. Chem. Front.*, 2021, **8**, 4479–4484.
- 268 S. Mal, M. Jana and S. Sarkar, *ChemistrySelect*, 2021, **6**, 11299–11330.
- 269 L. Niu, H. Zhang, H. Yang and H. Fu, *Synlett*, 2014, **25**, 995–1000.
- 270 S. Song, X. Sun, X. Li, Y. Yuan and N. Jiao, *Org. Lett.*, 2015, **17**, 2886–2889.
- 271 L. Li, W. Liu, H. Zeng, X. Mu, G. Cosa, Z. Mi and C.-J. Li, *J. Am. Chem. Soc.*, 2015, **137**, 8328–8331.
- 272 L. Li, W. Liu, X. Mu, Z. Mi and C.-J. Li, *Nat. Protoc.*, 2016, **11**, 1948–1954.
- 273 N. L. Sloan, S. K. Luthra, G. McRobbie, S. L. Pimlott and A. Sutherland, *RSC Adv.*, 2017, **7**, 54881–54891.
- 274 W. Liu, X. Yang, Y. Gao and C.-J. Li, *J. Am. Chem. Soc.*, 2017, **139**, 8621–8627.
- 275 G. J. P. Perry, J. M. Quibell, A. Panigrahi and I. Larrosa, *J. Am. Chem. Soc.*, 2017, **139**, 11527–11536.
- 276 C. Dong, K. Nakamura, T. Taniguchi, S. Mita, S. Kodama, S. Kawaguchi, A. Nomoto, A. Ogawa and T. Mizuno, *ACS Omega*, 2018, **3**, 9814–9821.
- 277 D. A. Petrone, J. Ye and M. Lautens, *Chem. Rev.*, 2016, **116**, 8003–8104.
- 278 N. Sloan and A. Sutherland, *Synthesis*, 2016, **48**, 2969–2980.
- 279 A. D. Marchese, T. Adrianov and M. Lautens, *Angew. Chem. Int. Ed.*, 2021, **60**, 16750–16762.
- 280 H. Saito, K. Yamamoto, Y. Sumiya, L. Liu, K. Nogi, S. Maeda and H. Yorimitsu, *Chem. Asian J.*, 2020, **15**, 2442–2446.
- 281 L. Tanwar, J. Börgel, J. Lehmann and T. Ritter, *Org. Lett.*, 2021, **23**, 5024–5027.
- 282 K. M. Wager and G. B. Jones, *Curr. Radiopharm.*, 2010, **3**, 37–45.
- 283 R. H. Seevers and R. E. Counsell, *Chem. Rev.*, 1982, **82**, 575–590.
- 284 S. Mushtaq, J. Jeon, A. Shaheen, B. S. Jang and S. H. Park, *J. Radioanal. Nucl. Chem.*, 2016, **309**, 859–889.

- 285 X. Shen, A. M. Hyde and S. L. Buchwald, *J. Am. Chem. Soc.*, 2010, **132**, 14076–14078.
- 286 S. D. Lepore and D. Mondal, *Tetrahedron*, 2007, **63**, 5103–5122.
- 287 J. Högermeier and H.-U. Reissig, *Adv. Synth. Catal.*, 2009, **351**, 2747–2763.
- 288 K. Ritter, *Synthesis*, 1993, **8**, 735–762.
- 289 A. B. Dürr, G. Yin, I. Kalvet, F. Napoly and F. Schoenebeck, *Chem. Sci.*, 2016, **7**, 1076–1081.
- 290 Y. Sumida, T. Sumida and T. Hosoya, *Synthesis*, 2017, **49**, 3590–3601.
- 291 K. Zhang, F. Christoffel and O. Baudoin, *Angew. Chem. Int. Ed.*, 2018, **57**, 1982–1986.
- 292 M. S. Hofmayer, F. H. Lutter, L. Grokenberger, J. M. Hammann and P. Knochel, *Org. Lett.*, 2019, **21**, 36–39.
- 293 T. Taeufer and J. Pospech, *J. Org. Chem.*, 2020, **85**, 7097–7111.
- 294 M. Rottländer and P. Knochel, *J. Org. Chem.*, 1998, **63**, 203–208.
- 295 K. W. Anderson, M. Mendez-Perez, J. Priego and S. L. Buchwald, *J. Org. Chem.*, 2003, **68**, 9563–9573.
- 296 F. Aulenta and H.-U. Reissig, *Synlett*, 2006, **18**, 2993–2996.
- 297 C. M. So and F. Y. Kwong, *Chem. Soc. Rev.*, 2011, **40**, 4963–4972.
- 298 A.-Y. Peng, B.-T. Chen, Z. Wang, B. Wang, X.-B. Mo, Y.-Y. Wang and P.-J. Chen, *J. Fluor. Chem.*, 2011, **132**, 982–986.
- 299 S. Shekhar, T. B. Dunn, B. J. Kotecki, D. K. Montavon and S. C. Cullen, *J. Org. Chem.*, 2011, **76**, 4552–4563.
- 300 X.-F. Wu, H. Neumann and M. Beller, *Chem. Eur. J.*, 2012, **18**, 3831–3834.
- 301 X.-F. Wu, H. Neumann and M. Beller, *Chem. Eur. J.*, 2012, **18**, 419–422.
- 302 G. A. Wiley, R. L. Hershkowitz, B. M. Rein and B. C. Chung, *J. Am. Chem. Soc.*, 1964, **86**, 964–965.
- 303 E. Bay, D. A. Bak, P. E. Timony and A. Leone-Bay, *J. Org. Chem.*, 1990, **55**, 3415–3417.
- 304 A. Thompson, G. Kabalka, M. Akula and J. Huffman, *Synthesis*, 2005, **4**, 547–550.
- 305 D. A. Watson, M. Su, G. Teverovskiy, Y. Zhang, J. García-Fortanet, T. Kinzel and S. L. Buchwald, *Science*, 2009, **325**, 1661–1664.
- 306 J. Pan, X. Wang, Y. Zhang and S. L. Buchwald, *Org. Lett.*, 2011, **13**, 4974–4976.
- 307 H. G. Lee, P. J. Milner and S. L. Buchwald, *Org. Lett.*, 2013, **15**, 5602–5605.

- 308 A. C. Sather, H. G. Lee, V. Y. De La Rosa, Y. Yang, P. Müller and S. L. Buchwald, *J. Am. Chem. Soc.*, 2015, **137**, 13433–13438.
- 309 A. C. Sather, H. G. Lee, J. R. Colombe, A. Zhang and S. L. Buchwald, *Nature*, 2015, **524**, 208–211.
- 310 Y. Imazaki, E. Shirakawa, R. Ueno and T. Hayashi, *J. Am. Chem. Soc.*, 2012, **134**, 14760–14763.
- 311 E. Shirakawa, Y. Imazaki and T. Hayashi, *Chem. Commun.*, 2009, **34**, 5088–5090.
- 312 J. Wannberg, C. Wallinder, M. Ünlüsoy, C. Sköld and M. Larhed, *J. Org. Chem.*, 2013, **78**, 4184–4189.
- 313 X. Han, B. M. Stoltz and E. J. Corey, *J. Am. Chem. Soc.*, 1999, **121**, 7600–7605.
- 314 S. M. Hickey, S. O. Nitschke, M. J. Sweetman, C. J. Sumby, D. A. Brooks, S. E. Plush and T. D. Ashton, *J. Org. Chem.*, 2020, **85**, 7986–7999.
- 315 L. Storace, L. Anzalone, P. N. Confalone, W. P. Davis, J. M. Fortunak, M. Giangiordano, J. J. Haley, K. Kamholz, H.-Y. Li, P. Ma, W. A. Nugent, R. L. Parsons, P. J. Sheeran, C. E. Silverman, R. E. Waltermire and C. C. Wood, *Org. Process Res. Dev.*, 2002, **6**, 54–63.
- 316 Y.-X. Bo, R. Xiang, Y. Xu, S.-Y. Hao, X.-R. Wang and S.-W. Chen, *Bioorg. Med. Chem.*, 2020, **28**, 115351.
- 317 K. F. McClure and S. J. Danishefsky, *J. Am. Chem. Soc.*, 1993, **115**, 6094–6100.
- 318 B. M. Trost and B. M. O'Boyle, *Org. Lett.*, 2008, **10**, 1369–1372.
- 319 S. Kitamura, K. L. Hvorecny, J. Niu, B. D. Hammock, D. R. Madden and C. Morisseau, *J. Med. Chem.*, 2016, **59**, 4790–4799.
- 320 D. Marcoux and A. B. Charette, *J. Org. Chem.*, 2008, **73**, 590–593.
- 321 C. B. Ziegler and R. F. Heck, *J. Org. Chem.*, 1978, **43**, 2941–2946.
- 322 L. K. Hwang, Y. Na, J. Lee, Y. Do and S. Chang, *Angew. Chem. Int. Ed.*, 2005, **44**, 6166–6169.
- 323 H. Wang, M. Yang, Y. Wang, X. Man, X. Lu, Z. Mou, Y. Luo and H. Liang, *Org. Lett.*, 2021, **23**, 8183–8188.
- 324 C. G. Cassity, A. Mirjafari, N. Mobarrez, K. J. Strickland, R. A. O'Brien and J. H. Davis, *Chem. Commun.*, 2013, **49**, 7590–7592.
- 325 B. D. Rabideau, K. N. West and J. H. Davis Jr., *Chem. Commun.*, 2018, **54**, 5019–5031.

- 326 Y. Toda, Y. Komiyama, A. Kikuchi and H. Suga, *ACS Catal.*, 2016, **6**, 6906–6910.
- 327 Y. Toda, S. Gomyou, S. Tanaka, Y. Komiyama, A. Kikuchi and H. Suga, *Org. Lett.*, 2017, **19**, 5786–5789.
- 328 Y. Toda, Y. Komiyama, H. Esaki, K. Fukushima and H. Suga, *J. Org. Chem.*, 2019, **84**, 15578–15589.
- 329 J.-J. Min, S. Biswal, C. Deroose and S. S. Gambhir, *J. Nucl. Med.*, 2004, **45**, 636–643.
- 330 Z. Cheng, M. Subbarayan, X. Chen and S. S. Gambhir, *J. Label. Compd. Radiopharm.*, 2005, **48**, 131–137.
- 331 D. Y. Kim, K. H. Yu, H.-S. Bom and J.-J. Min, *Nucl. Med. Mol. Imaging*, 2007, **41**, 561–565.
- 332 T. M. Shoup, D. R. Elmaleh, A.-L. Brownell, A. Zhu, J. L. Guerrero and A. J. Fischman, *Mol. Imaging Biol.*, 2011, **13**, 511–517.
- 333 D.-Y. Kim and J.-J. Min, *Nucl. Med. Mol. Imaging*, 2016, **50**, 185–195.
- 334 J. C. Poupon, A. A. Boezio and A. B. Charette, *Angew. Chem. Int. Ed.*, 2006, **45**, 1415–1420.
- 335 J. M. Zimbron, M. Dauphinais and A. B. Charette, *Green Chem.*, 2015, **17**, 3255–3259.
- 336 L. Zoute, C. Lacombe, J.-C. Quirion, A. B. Charette and P. Jubault, *Tetrahedron Lett.*, 2006, **47**, 7931–7933.
- 337 F. Stazi, D. Marcoux, J. C. Poupon, D. Latassa and A. B. Charette, *Angew. Chem. Int. Ed.*, 2007, **46**, 5011–5014.
- 338 D. Marcoux and A. B. Charette, *Adv. Synth. Catal.*, 2008, **350**, 2967–2974.
- 339 M. Ginisty, M. N. Roy and A. B. Charette, *J. Org. Chem.*, 2008, **73**, 2542–2547.
- 340 M.-N. Roy, J.-C. Poupon and A. B. Charette, *J. Org. Chem.*, 2009, **74**, 8510–8515.
- 341 H. Lebel, M. Davi, M.-N. Roy, W. Zeghida and A. Charette, *Synthesis*, 2011, **14**, 2275–2280.
- 342 Z. Lin, Z. Chen, G. Yang and C. Lu, *Catal. Commun.*, 2013, **35**, 1–5.
- 343 X. Nie, C. Lu, Z. Chen, G. Yang and J. Nie, *J. Mol. Catal. A Chem.*, 2014, **393**, 171–174.
- 344 L. D. Quin, *A Guide to Organophosphorus Chemistry*, John Wiley & Sons, Inc., 1st edn., 2000.

- 345 R. Martin and S. L. Buchwald, *Acc. Chem. Res.*, 2008, **41**, 1461–1473.
- 346 B. T. Ingoglia, C. C. Wagen and S. L. Buchwald, *Tetrahedron*, 2019, **75**, 4199–4211.
- 347 H. L. Ngo, A. Hu and W. Lin, *J. Mol. Catal. A Chem.*, 2004, **215**, 177–186.
- 348 T. Baumgartner and R. Réau, *Chem. Rev.*, 2006, **106**, 4681–4727.
- 349 E. Regulaska and C. Romero-Nieto, *Mater. Today Chem.*, 2021, **22**, 100604.
- 350 O. R. Evans, D. R. Manke and W. Lin, *Chem. Mater.*, 2002, **14**, 3866–3874.
- 351 K. Muthukumar, R. S. Loewe, A. Ambroise, S. Tamaru, Q. Li, G. Mathur, D. F. Bocian, V. Misra and J. S. Lindsey, *J. Org. Chem.*, 2004, **69**, 1444–1452.
- 352 P. H. Mutin, G. Guerrero and A. Vioux, *J. Mater. Chem.*, 2005, **15**, 3761–3768.
- 353 T. Amaya, Y. Abe, Y. Inada and T. Hirao, *Tetrahedron Lett.*, 2014, **55**, 3976–3978.
- 354 T. Amaya, I. Kurata, Y. Inada, T. Hatai and T. Hirao, *RSC Adv.*, 2017, **7**, 39306–39313.
- 355 C. M. Sevrain, M. Berchel, H. Couthon and P.-A. Jaffrès, *Beilstein J. Org. Chem.*, 2017, **13**, 2186–2213.
- 356 R. A. J. Smith, R. C. Hartley and M. P. Murphy, *Antioxid. Redox Signal.*, 2011, **15**, 3021–3038.
- 357 J. Zielonka, J. Joseph, A. Sikora, M. Hardy, O. Ouari, J. Vasquez-Vivar, G. Cheng, M. Lopez and B. Kalyanaraman, *Chem. Rev.*, 2017, **117**, 10043–10120.
- 358 W.-Q. Liu, C. Olszowy, L. Bischoff and C. Garbay, *Tetrahedron Lett.*, 2002, **43**, 1417–1419.
- 359 S. Oishi, S.-U. Kang, H. Liu, M. Zhang, D. Yang, J. R. Deschamps and T. R. Burke Jr., *Tetrahedron*, 2004, **60**, 2971–2977.
- 360 J. T. Suri, D. D. Steiner and C. F. Barbas III, *Org. Lett.*, 2005, **7**, 3885–3888.
- 361 W. Jiang, G. Allan, J. J. Fiordeliso, O. Linton, P. Tannenbaum, J. Xu, P. Zhu, J. Gunnet, K. Demarest, S. Lundeen and Z. Sui, *Bioorganic Med. Chem.*, 2006, **14**, 6726–6732.
- 362 A. Macchiarulo and R. Pellicciari, *J. Mol. Graph. Model.*, 2007, **26**, 728–739.
- 363 R. Jójárt, S. A. S. Tahaei, P. Trungel-Nagy, Z. Kele, R. Minorics, G. Paragi, I. Zupkó and E. Mernyák, *J. Enzyme Inhib. Med. Chem.*, 2021, **36**, 58–67.
- 364 W.-S. Huang, S. Liu, D. Zou, M. Thomas, Y. Wang, T. Zhou, J. Romero, A. Kohlmann, F. Li, J. Qi, L. Cai, T. A. Dwight, Y. Xu, R. Xu, R. Dodd, A. Toms, L. Parillon, X. Lu, R. Anjum, S. Zhang, F. Wang, J. Keats, S. D. Wardwell, Y.

- Ning, Q. Xu, L. E. Moran, Q. K. Mohemmad, H. G. Jang, T. Clackson, N. I. Narasimhan, V. M. Rivera, X. Zhu, D. Dalgarno and W. C. Shakespeare, *J. Med. Chem.*, 2016, **59**, 4948–4964.
- 365 P. Finkbeiner, J. P. Hehn and C. Gnamm, *J. Med. Chem.*, 2020, **63**, 7081–7107.
- 366 H. Tomori, J. M. Fox and S. L. Buchwald, *J. Org. Chem.*, 2000, **65**, 5334–5341.
- 367 T. Chen, Q. Tan, X. Liu, L. Liu, T. Huang and L.-B. Han, *Synthesis*, 2021, **53**, 95–106.
- 368 L. D. Freedman and G. O. Doak, *Chem. Rev.*, 1957, **57**, 479–523.
- 369 T. Hirao, T. Masunaga, Y. Ohshiro and T. Agawa, *Synthesis*, 1981, **1981**, 56–57.
- 370 T. Hirao, T. Masunaga, N. Yamada, Y. Ohshiro and T. Agawa, *Bull. Chem. Soc. Jpn.*, 1982, **55**, 909–913.
- 371 T. Hirao, T. Masunaga, Y. Ohshiro and T. Agawa, *Tetrahedron Lett.*, 1980, **21**, 3595–3598.
- 372 D. Prim, J.-M. Campagne, D. Joseph and B. Andrioletti, *Tetrahedron*, 2002, **58**, 2041–2075.
- 373 A. L. Schwan, *Chem. Soc. Rev.*, 2004, **33**, 218–224.
- 374 F. M. J. Tappe, V. T. Trepohl and M. Oestreich, *Synthesis*, 2010, **18**, 3037–3062.
- 375 C. S. Demmer, N. Krogsgaard-Larsen and L. Bunch, *Chem. Rev.*, 2011, **111**, 7981–8006.
- 376 G. Keglevich, R. Henyecz and Z. Mucsi, *Molecules*, 2020, **25**, 3897.
- 377 U. S. Kanchana, E. J. Diana, T. V. Mathew and G. Anilkumar, *ChemistrySelect*, 2021, **6**, 1579–1588.
- 378 M. Kalek and J. Stawinski, *Organometallics*, 2007, **26**, 5840–5847.
- 379 Y. Belabassi, S. Alzghari and J.-L. Montchamp, *J. Organomet. Chem.*, 2008, **693**, 3171–3178.
- 380 M. Kalek and J. Stawinski, *Organometallics*, 2008, **27**, 5876–5888.
- 381 M. C. Kohler, J. G. Sokol and R. A. Stockland Jr., *Tetrahedron Lett.*, 2009, **50**, 457–459.
- 382 M. Kalek, M. Jezowska and J. Stawinski, *Adv. Synth. Catal.*, 2009, **351**, 3207–3216.
- 383 E. L. Deal, C. Petit and J.-L. Montchamp, *Org. Lett.*, 2011, **13**, 3270–3273.

- 384 O. Berger, C. Petit, E. L. Deal and J.-L. Montchamp, *Adv. Synth. Catal.*, 2013, **355**, 1361–1373.
- 385 G. Keglevich, E. Jablonkai and L. B. Balázs, *RSC Adv.*, 2014, **4**, 22808–22816.
- 386 G. Keglevich, R. Henyecz, Z. Mucsi and N. Z. Kiss, *Adv. Synth. Catal.*, 2017, **359**, 4322–4331.
- 387 W. C. Fu, C. M. So and F. Y. Kwong, *Org. Lett.*, 2015, **17**, 5906–5909.
- 388 L.-L. Liao, Y.-Y. Gui, X.-B. Zhang, G. Shen, H.-D. Liu, W.-J. Zhou, J. Li and D.-G. Yu, *Org. Lett.*, 2017, **19**, 3735–3738.
- 389 C. Li, *Russ. J. Gen. Chem.*, 2020, **90**, 725–730.
- 390 S. Mahmoodzadeh and E. Dworatzek, *Front. Endocrinol.*, 2019, **10**, 310.
- 391 J. R. Hanrahan, M. Chebib and G. A. R. Johnston, *Interactions of flavonoids with ionotropic GABA receptors*, Elsevier Inc., 1st edn., 2015, vol. 72.
- 392 Y. Zhang, W. Chen, T. Tan, Y. Gu, S. Zhang, J. Li, Y. Wang, W. Hou, G. Yang, P. Ma and H. Xu, *Chem. Commun.*, 2021, **57**, 4588–4591.
- 393 G. Zhang, J. Wang, C. Guan, Y. Zhao and C. Ding, *Eur. J. Org. Chem.*, 2021, **2021**, 810–813.
- 394 K. S. Petrakis and T. L. Nagabhushan, *J. Am. Chem. Soc.*, 1987, **109**, 2831–2833.
- 395 Y. Uozumi, A. Tanahashi, S.-Y. Lee and T. Hayashi, *J. Org. Chem.*, 1993, **58**, 1945–1948.
- 396 J. Yang, J. Xiao, T. Chen and L.-B. Han, *J. Organomet. Chem.*, 2016, **820**, 120–124.
- 397 R. Henyecz, B. Huszár, V. Grenitzer and G. Keglevich, *Curr. Org. Chem.*, 2020, **24**, 1048–1054.
- 398 M. Al-Masum and T. Livinghouse, *Tetrahedron Lett.*, 1999, **40**, 7731–7734.
- 399 F. Y. Kwong and K. S. Chan, *Organometallics*, 2001, **20**, 2570–2578.
- 400 Y. Wang, C. W. Lai, F. Y. Kwong, W. Jia and K. S. Chan, *Tetrahedron*, 2004, **60**, 9433–9439.
- 401 P. N. M. Botman, J. Fraanje, K. Goubitz, R. Peschar, J. W. Verhoeven, J. H. Van Maarseveen and H. Hiemstra, *Adv. Synth. Catal.*, 2004, **346**, 743–754.
- 402 B. H. Lipshutz, D. J. Buzard and C. S. Yun, *Tetrahedron Lett.*, 1999, **40**, 201–204.
- 403 L. Ackermann, *Synthesis*, 2006, **10**, 1557–1571.
- 404 C. Amatore, A. Jutand and A. Suarez, *J. Am. Chem. Soc.*, 1993, **115**, 9531–

- 9541.
- 405 C. Amatore and A. Jutand, *Acc. Chem. Res.*, 2000, **33**, 314–321.
- 406 K. Fagnou and M. Lautens, *Angew. Chem. Int. Ed.*, 2002, **41**, 26–47.
- 407 A. H. Roy and J. F. Hartwig, *Organometallics*, 2004, **23**, 194–202.
- 408 F. Y. Kwong, C. W. Lai, M. Yu and K. S. Chan, *Tetrahedron*, 2004, **60**, 5635–5645.
- 409 R. Berrino, S. Cacchi, G. Fabrizi, A. Goggiamani and P. Stabile, *Org. Biomol. Chem.*, 2010, **8**, 4518–4520.
- 410 V. V. Grushin, *Organometallics*, 2000, **19**, 1888–1900.
- 411 C. A. Busacca, J. C. Lorenz, N. Grinberg, N. Haddad, M. Hrapchak, B. Latli, H. Lee, P. Sabila, A. Saha, M. Sarvestani, S. Shen, R. Varsolona, X. Wei and C. H. Senanayake, *Org. Lett.*, 2005, **7**, 4277–4280.
- 412 G. Mallesham, C. Swetha, S. Niveditha, M. E. Mohanty, N. J. Babu, A. Kumar, K. Bhanuprakash and V. J. Rao, *J. Mater. Chem. C*, 2015, **3**, 1208–1224.
- 413 Q. Fang, J. Li, S. Li, R. Duan, S. Wang, Y. Yi, X. Guo, Y. Qian, W. Huang and G. Yang, *Chem. Commun.*, 2017, **53**, 5702–5705.
- 414 L. Qiu, W. Hu, D. Wu, Z. Duan and F. Mathey, *Org. Lett.*, 2018, **20**, 7821–7824.
- 415 C. F. Bigge, J. T. Drummond, G. Johnson, T. Malone, A. W. Probert Jr., F. W. Marcoux, L. L. Coughenour and L. J. Brahce, *J. Med. Chem.*, 1989, **32**, 1580–1590.
- 416 M. Bayle-Lacoste, J. Moulines, N. Collignon, A. Boumekouez, E. de Tinguy-Moreaud and E. Neuzil, *Tetrahedron*, 1990, **46**, 7793–7802.
- 417 C. Thurieau, S. Simonet, J. Paladino, J.-F. Prost, T. Verbeuren and J.-L. Fauchere, *J. Med. Chem.*, 1994, **37**, 625–629.
- 418 S. S. Chauhan, A. Varshney, B. Verma and M. W. Pennington, *Tetrahedron Lett.*, 2007, **48**, 4051–4054.
- 419 A. N. Butkevich, M. L. Bossi, G. Lukinavičius and S. W. Hell, *J. Am. Chem. Soc.*, 2019, **141**, 981–989.
- 420 P. J. Fagan, M. D. Ward and J. C. Calabrese, *J. Am. Chem. Soc.*, 1989, **111**, 1698–1719.
- 421 L. S. Fowler, D. Ellis and A. Sutherland, *Org. Biomol. Chem.*, 2009, **7**, 4309–4316.
- 422 C. M. Reid, K. N. Fanning, L. S. Fowler and A. Sutherland, *Tetrahedron*, 2015, **71**, 245–251.

- 423 L. Gilfillan, R. Artschwager, A. H. Harkiss, R. M. J. Liskamp and A. Sutherland, *Org. Biomol. Chem.*, 2015, **13**, 4514–4523.
- 424 A. H. Harkiss, J. D. Bell, A. Knuhtsen, A. G. Jamieson and A. Sutherland, *J. Org. Chem.*, 2019, **84**, 2879–2890.
- 425 J. D. Bell, T. E. F. Morgan, N. Buijs, A. H. Harkiss, C. R. Wellaway and A. Sutherland, *J. Org. Chem.*, 2019, **84**, 10436–10448.
- 426 J. D. Bell, A. H. Harkiss, D. Nobis, E. Malcolm, A. Knuhtsen, C. R. Wellaway, A. G. Jamieson, S. W. Magennis and A. Sutherland, *Chem. Commun.*, 2020, **56**, 1887–1890.
- 427 C. Grison, P. Coutrot, C. Comoy, L. Balas, S. Joliez, G. Lavecchia, P. Oligier, B. Penverne, V. Serre and G. Hervé, *Eur. J. Med. Chem.*, 2004, **39**, 333–344.
- 428 A. Inoue, H. Shinokubo and K. Oshima, *J. Am. Chem. Soc.*, 2003, **125**, 1484–1485.
- 429 A. García-Rubia, R. G. Arrayás and J. C. Carretero, *Angew. Chem. Int. Ed.*, 2009, **48**, 6511–6515.
- 430 K. Gießler, H. Griesser, D. Göhringer, T. Sabirov and C. Richert, *Eur. J. Org. Chem.*, 2010, **2010**, 3611–3620.
- 431 R. J. Lundgren, B. D. Peters, P. G. Alsabeh and M. Stradiotto, *Angew. Chem. Int. Ed.*, 2010, **49**, 4071–4074.
- 432 D. Zhou, W. Chu, T. Voller and J. A. Katzenellenbogen, *Tetrahedron Lett.*, 2018, **59**, 1963–1967.
- 433 WO2017046737 A1, 2017, 1–247.
- 434 R. E. Meadows and S. Woodward, *Tetrahedron*, 2008, **64**, 1218–1224.
- 435 J. D. Hicks, A. M. Hyde, A. M. Cuezva and S. L. Buchwald, *J. Am. Chem. Soc.*, 2009, **131**, 16720–16734.
- 436 S. D. Schimler, R. D. J. Froese, D. C. Bland and M. S. Sanford, *J. Org. Chem.*, 2018, **83**, 11178–11190.
- 437 H. Yang, Y. Li, M. Jiang, J. Wang and H. Fu, *Chem. Eur. J.*, 2011, **17**, 5652–5660.
- 438 C. Zhu, F. Chen, C. Liu, H. Zeng, Z. Yang, W. Wu and H. Jiang, *J. Org. Chem.*, 2018, **83**, 14713–14722.
- 439 S. Mukhopadhyay and S. Batra, *Chem. Eur. J.*, 2018, **24**, 14622–14626.
- 440 M. Uemura, H. Yorimitsu and K. Oshima, *Tetrahedron*, 2008, **64**, 1829–1833.
- 441 H. Sato and S. Hosokawa, *Synthesis*, 2018, **50**, 1343–1349.
- 442 A. Pialat, B. Liéault and M. Taillefer, *Org. Lett.*, 2013, **15**, 1764–1767.

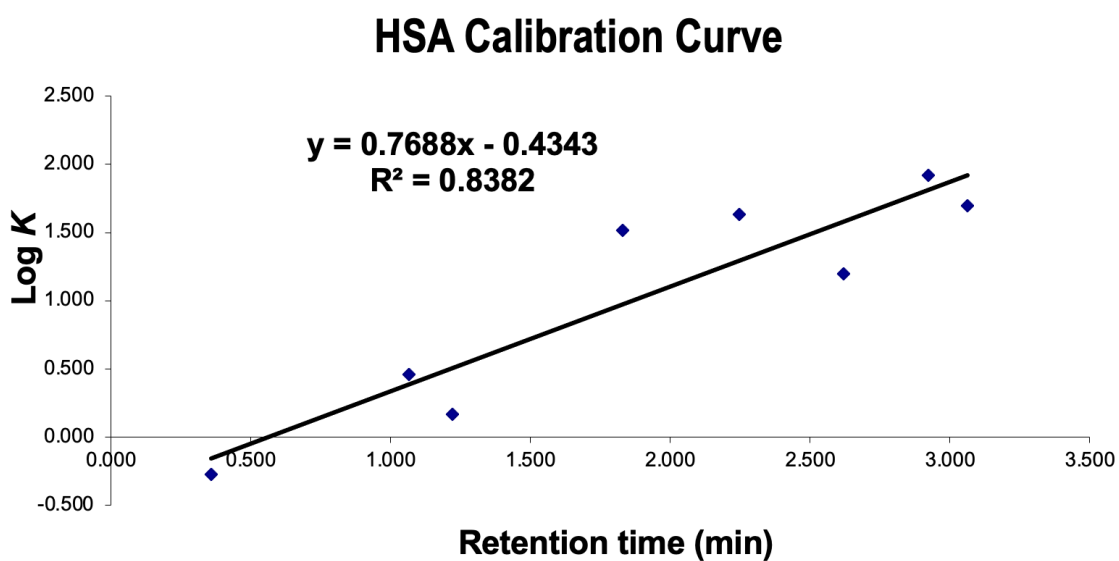
- 443 G. Hu, W. Chen, T. Fu, Z. Peng, H. Qiao, Y. Gao and Y. Zhao, *Org. Lett.*, 2013, **15**, 5362–5365.
- 444 M. Stankevič, J. Pisklak and K. Włodarczyk, *Tetrahedron*, 2016, **72**, 810–824.
- 445 J. Xu, P. Zhang, Y. Gao, Y. Chen, G. Tang and Y. Zhao, *J. Org. Chem.*, 2013, **78**, 8176–8183.
- 446 C. Shen, G. Yang and W. Zhang, *Org. Biomol. Chem.*, 2012, **10**, 3500–3505.
- 447 O. Berger and J.-L. Montchamp, *J. Org. Chem.*, 2019, **84**, 9239–9256.
- 448 D.-L. Zhu, S. Jiang, Q. Wu, H. Wang, L.-L. Chai, H.-Y. Li and H.-X. Li, *Org. Lett.*, 2021, **23**, 160–165.
- 449 G. Martorell, X. Garcías, M. Janura and J. M. Saá, *J. Org. Chem.*, 1998, **63**, 3463–3467.
- 450 X. Zhang, H. Liu, X. Hu, G. Tang, J. Zhu and Y. Zhao, *Org. Lett.*, 2011, **13**, 3478–3481.
- 451 W. S. Tay, Y. Li, X. Y. Yang, S. A. Pullarkat and P. H. Leung, *J. Organomet. Chem.*, 2020, **914**, 121216.
- 452 F. Däbritz, A. Jäger and I. Bauer, *Eur. J. Org. Chem.*, 2008, **2008**, 5571–5576.
- 453 H. Rao, Y. Jin, H. Fu, Y. Jiang and Y. Zhao, *Chem. Eur. J.*, 2006, **12**, 3636–3646.

5.0 Appendices

5.1 Appendix I – Raw Data Obtained from HPLC Determination of Physicochemical Properties

5.1.1 Percentage of Plasma Protein Binding (%PPB) *via* Human Serum Albumin (HSA) Chromatography

Compound	%PPB Literature	Log K	Tr 1	Tr 2	Tr 3	Retention time (min)
Nizatidine	35.0	-0.275	0.360	0.360	0.353	0.358
Bromazepan	60.0	0.165	1.217	1.223	1.227	1.222
Carbamazepine	75.0	0.460	1.067	1.067	1.063	1.066
Nicardipine	95.0	1.200	2.613	2.623	2.627	2.621
Warfarin	98.0	1.514	1.830	1.830	1.830	1.830
Ketoprofen	98.7	1.633	2.250	2.247	2.247	2.248
Indomethacin	99.0	1.695	3.063	3.060	3.063	3.062
Diclofenac	99.8	1.920	2.920	2.923	2.927	2.923



Compound	Tr 1	Tr 2	Tr 3	Retention Time (min)	Log K HSA.	% PPB HSA.
66	1.640	1.637	1.637	1.638	0.8250	87.85
67	1.440	1.443	1.437	1.440	0.6728	83.30
68	1.567	1.570	1.570	1.569	0.7719	86.39
69	1.477	1.477	1.473	1.476	0.7002	84.21
70	1.460	1.463	1.460	1.461	0.6889	83.84
71	1.773	1.773	1.770	1.772	0.9280	90.34
72	2.053	2.050	2.050	2.051	1.143	94.21
73	2.653	2.650	2.650	2.651	1.604	98.55

5.1.2 Membrane Permeability (P_m) and Membrane Partition Coefficient (K_m) via Immobilised Artificial Membrane (IAM) Chromatography

Compound	%	30	40	50	60
66	Tr 1	4.767	2.660	2.183	2.023
	Tr 2	4.790	2.660	2.183	2.023
	Tr 3	4.787	2.663	2.183	2.023
	Average	4.781	2.661	2.183	2.023

Compound	%	30	40	50	60
67	Tr 1		2.537	2.143	2.007
	Tr 2	4.160	2.533	2.147	2.007
	Tr 3	4.163	2.533	2.147	2.007
	Average	4.162	2.534	2.146	2.007

Compound	%	30	40	50	60
68	Tr 1	5.127	2.727	2.200	2.027
	Tr 2	5.120	2.727	2.203	2.027
	Tr 3	5.103	2.730	2.203	2.027
	Average	5.117	2.728	2.202	2.027

Compound	%	30	40	50	60
69	Tr 1	4.670	2.613	2.160	2.010
	Tr 2	4.667	2.610	2.160	2.010
	Tr 3	4.657	2.607	2.160	2.010
	Average	4.665	2.610	2.160	2.010

Compound	%	30	40	50	60
70	Tr 1	4.110	2.497	2.123	1.997
	Tr 2	4.120	2.497	2.123	1.997
	Tr 3	4.117	2.497	2.123	1.997
	Average	4.116	2.497	2.123	1.997

Compound	%	30	40	50	60
71	Tr 1	6.067	2.843	2.207	2.007
	Tr 2	6.070	2.840	2.207	2.007
	Tr 3	6.067	2.843	2.207	2.007
	Average	6.068	2.842	2.207	2.007

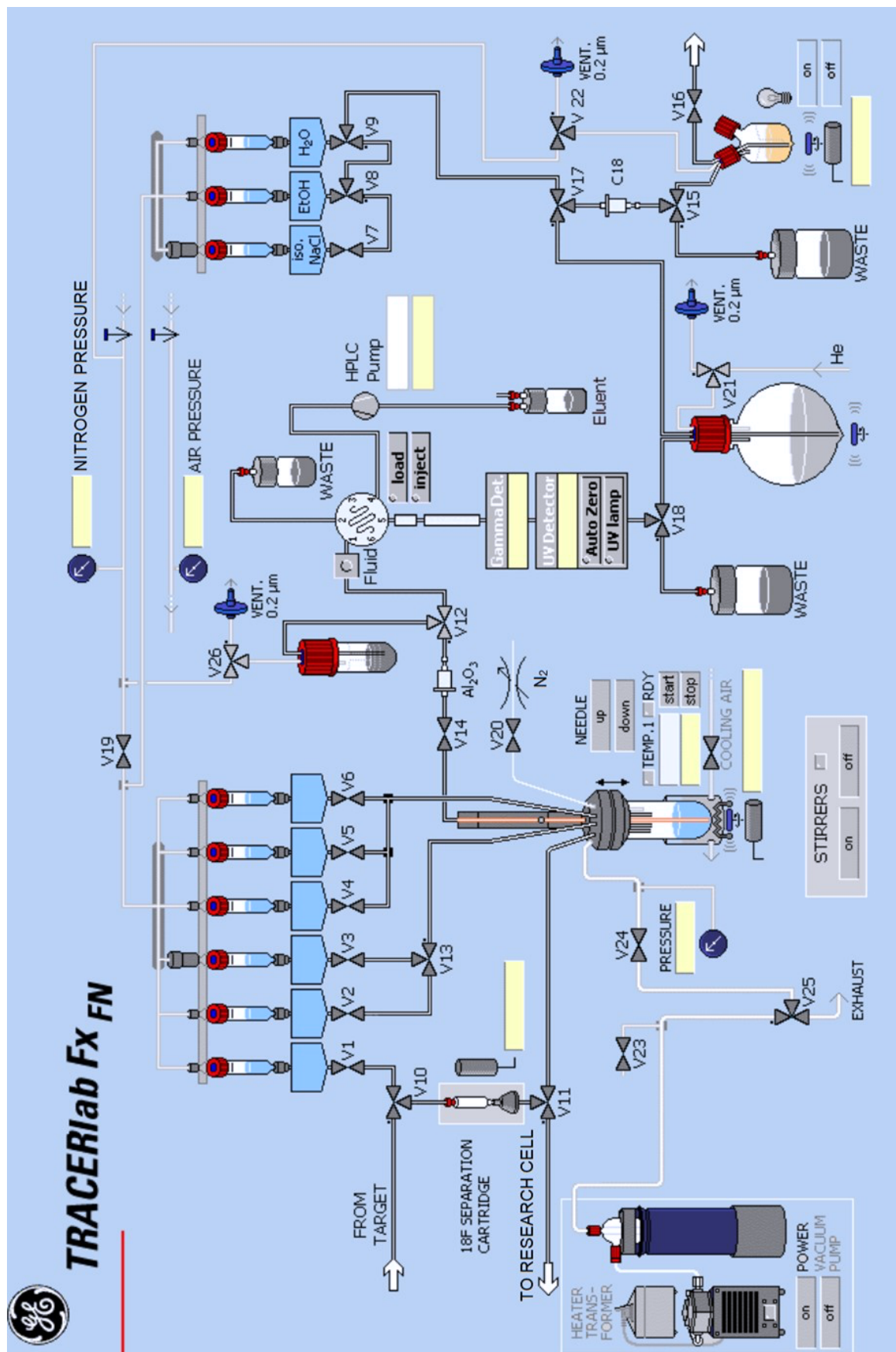
Compound	%	30	40	50	60
72	Tr 1	7.850	3.190	2.303	2.040
	Tr 2	7.837	3.187	2.303	2.040
	Tr 3	7.853	3.187	2.303	2.040
	Average	7.847	3.188	2.303	2.040

Compound	%	30	40	50	60
73	Tr 1	11.510	3.710	2.440	2.097
	Tr 2	11.527	3.707	2.440	2.097
	Tr 3	11.517	3.707	2.443	2.097
	Average	11.518	3.708	2.441	2.097

Citric Acid	1	1.883
	2	1.880
	3	1.881
	Average	1.881

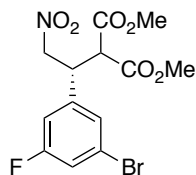
Compound	30	40	50	60	Retention Time (min)	k'	Vs	Vs/Vm	Km	Mw	Pm
67	4.162	2.534	2.146	2.007	6.587	2.5014	0.1481	0.0787	31.77	559.57	0.05677
70	4.116	2.497	2.123	1.997	6.523	2.4672	0.1481	0.0787	31.34	573.60	0.05463
69	4.665	2.610	2.160	2.010	7.709	3.0974	0.1481	0.0787	39.34	587.63	0.06695
71	6.068	2.842	2.207	2.007	10.820	4.751	0.1481	0.0787	60.34	574.58	0.10502
66	4.781	2.661	2.183	2.023	7.929	3.2145	0.1481	0.0787	40.83	559.57	0.07296
73	11.518	3.708	2.441	2.097	22.958	11.203	0.1481	0.0787	142.29	583.60	0.24381
68	5.117	2.728	2.202	2.027	8.657	3.6014	0.1481	0.0787	45.74	573.60	0.07974
72	7.847	3.188	2.303	2.040	14.701	6.8141	0.1481	0.0787	86.54	576.62	0.15009

5.2 Appendix II – Schematic of FX_{FN} Synthesiser

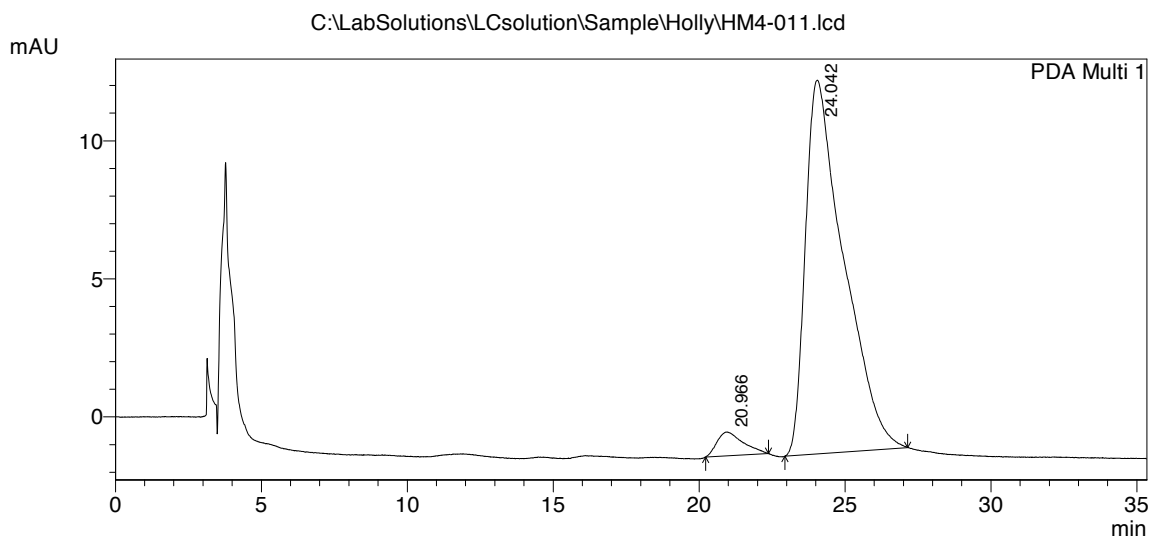


5.3 Appendix III – Chiral HPLC Traces

Dimethyl (1'*R*)-2-[1'-(3'',5''-difluorophenyl)-2'-nitroethyl]malonate ((*R*)-89)



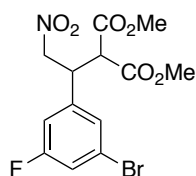
C:\LabSolutions\LCsolution\Sample\Holly\HM4-011.lcd
 Acquired by : Admin
 Sample Name : HM4-011
 Sample ID : HM4-011
 Injection Volume : 20 uL
 Data File Name : HM4-011.lcd
 Method File Name : 5% iPrOH-1mLmin.lcm
 Data Acquired : 12/06/2019 12:03:46
 Data Processed : 12/06/2019 12:39:08
 5% iPrOH, 1.0mL/min
 ODH



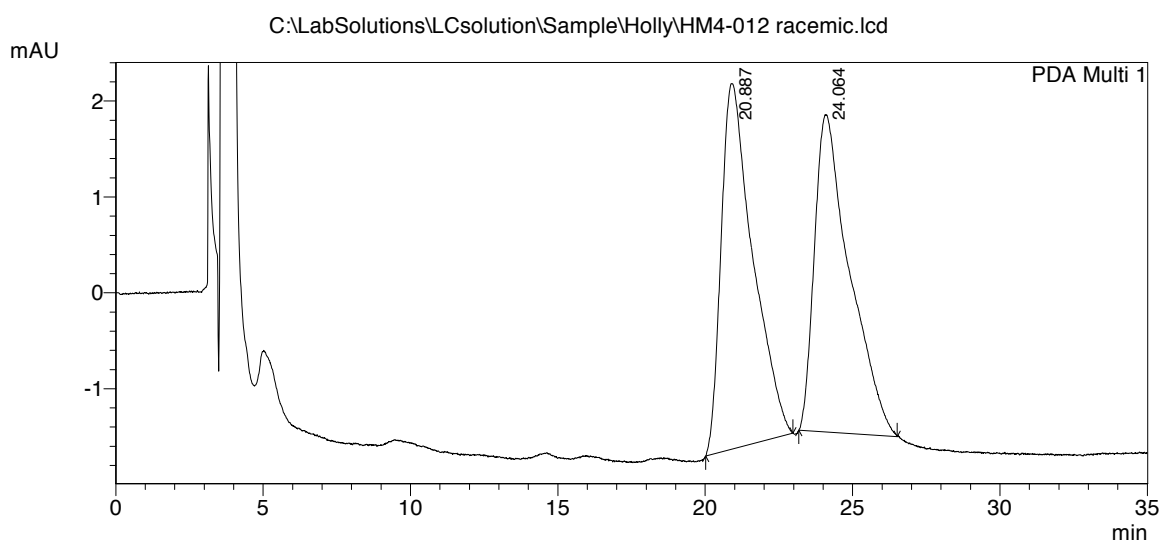
PDA Ch1 254nm 4nm

Peak#	Ret. Time	Area	Height	Area %	Height %
1	20.966	53645	863	4.163	5.994
2	24.042	1234959	13532	95.837	94.006
Total		1288604	14394	100.000	100.000

Dimethyl (±)-2-[1'-(3'',5''-difluorophenyl)-2'-nitroethyl]malonate (89)



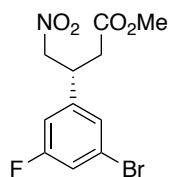
C:\LabSolutions\LCsolution\Sample\Holly\HM4-012 racemic.lcd
 Acquired by : Admin
 Sample Name : HM4-012 racemic
 Sample ID : HM4-012 racemic
 Injection Volume : 20 uL
 Data File Name : HM4-012 racemic.lcd
 Method File Name : 5%iPrOH-1mLmin.lcm
 Data Acquired : 12/06/2019 14:37:49
 Data Processed : 12/06/2019 15:12:50
 5% iPrOH, 1.0mL/min
 ODH



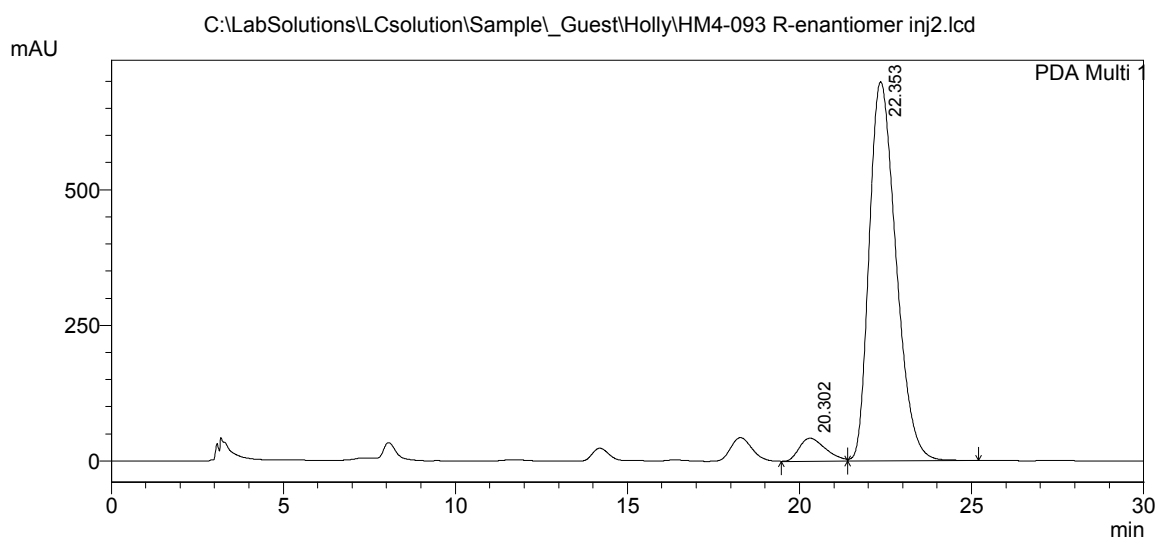
PDA Ch1 254nm 4nm

Peak#	Ret. Time	Area	Height	Area %	Height %
1	20.887	284521	3813	50.863	53.547
2	24.064	274863	3307	49.137	46.453
Total		559384	7120	100.000	100.000

Methyl (3*R*)-3-(3'-bromo-5'-fluorophenyl)-4-nitrobutanoate ((*R*)-98)



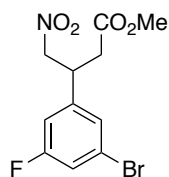
C:\LabSolutions\LCsolution\Sample_Guest\Holly\HM4-093 R-enantiomer inj2.lcd
 Acquired by : Admin
 Sample Name : HM4-093 R-enantiomer inj2
 Sample ID : HM4-093 R-enantiomer inj2
 Injection Volume : 20 uL
 Data File Name : HM4-093 R-enantiomer inj2.lcd
 Method File Name : AD-H_2%iPrOH-Hexane_1mL-min_30min.lcm
 Data Acquired : 23/09/2020 14:56:35
 Data Processed : 23/09/2020 17:18:16
 HM4-093 R-enantiomer inj2
 AD-H; IPA : Hex = 2 : 98 @ 1mL/min 30 min



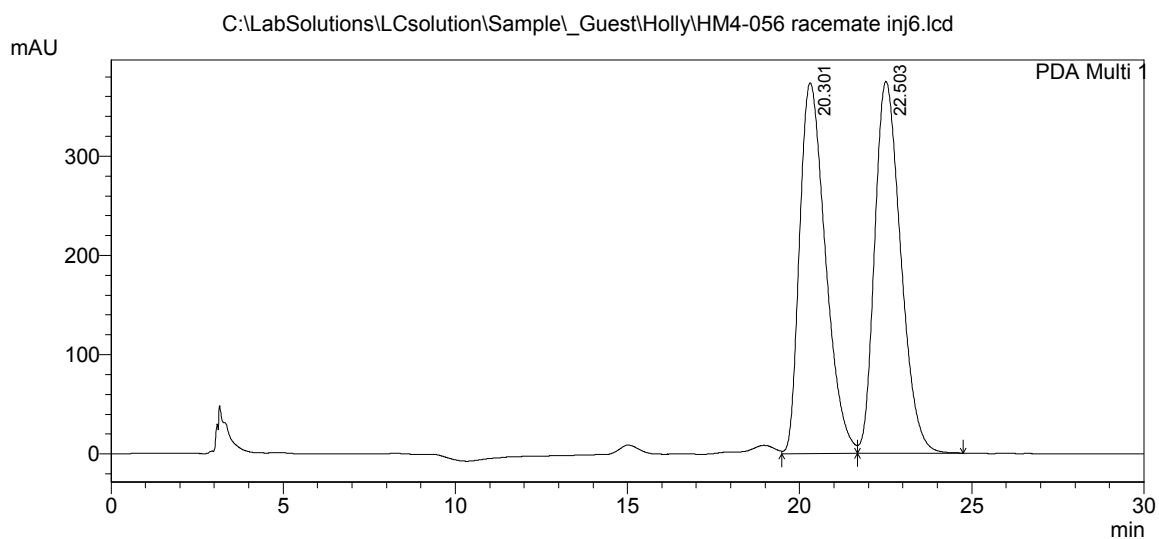
PDA Ch1 210nm 4nm

Peak#	Ret. Time	Area	Height	Area %	Height %
1	20.302	2249598	42341	5.608	5.712
2	22.353	37867036	698940	94.392	94.288
Total		40116634	741281	100.000	100.000

Methyl (±)-3-(3'-bromo-5'-fluorophenyl)-4-nitrobutanoate (98)



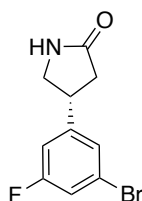
C:\LabSolutions\LCsolution\Sample_Guest\Holly\HM4-056 racemate inj6.lcd
Acquired by : Admin
Sample Name : HM4-056 racemate inj6
Sample ID : HM4-056 racemate inj6
Injection Volume : 20 uL
Data File Name : HM4-056 racemate inj6.lcd
Method File Name : AD-H_2%iPrOH-Hexane_1mL-min_30min.lcm
Data Acquired : 23/09/2020 16:08:48
Data Processed : 23/09/2020 16:38:50
HM4-056 racemate inj6
AD-H; IPA : Hex = 2 : 98 @ 1mL/min 30 min



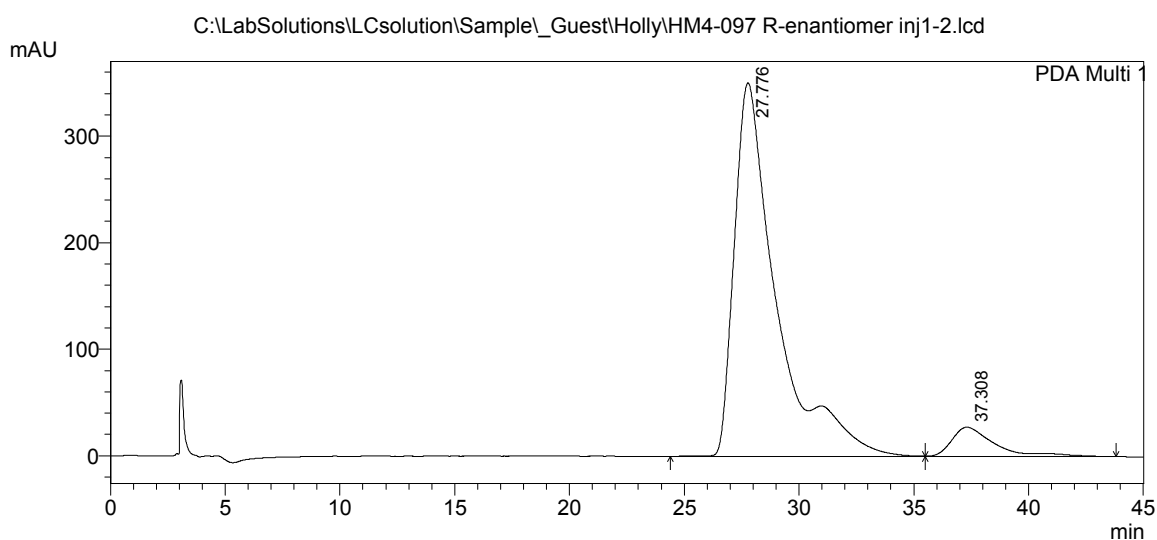
PDA Ch1 210nm 4nm

Peak#	Ret. Time	Area	Height	Area %	Height %
1	20.301	19520939	373575	49.771	49.925
2	22.503	19700943	374695	50.229	50.075
Total		39221882	748270	100.000	100.000

(4R)-4-(3'-Bromo-5'-fluorophenyl)pyrrolidin-2-one ((R)-83)



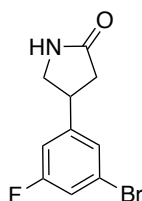
C:\LabSolutions\LCsolution\Sample_Guest\Holly\HM4-097 R-enantiomer inj1-2.lcd
Acquired by : Admin
Sample Name : HM4-097 R-enantiomer inj1
Sample ID : HM4-097 R-enantiomer inj1
Injection Volume : 20 uL
Data File Name : HM4-097 R-enantiomer inj1-2.lcd
Method File Name : AD-H_3%iPrOH-Hexane_1mL-min_45min.lcm
Data Acquired : 18/12/2020 12:15:17
Data Processed : 18/12/2020 16:08:20
HM4-097 R-enantiomer inj1
AD-H; IPA : Hex = 3 : 97 @ 1 ml/min 45 min



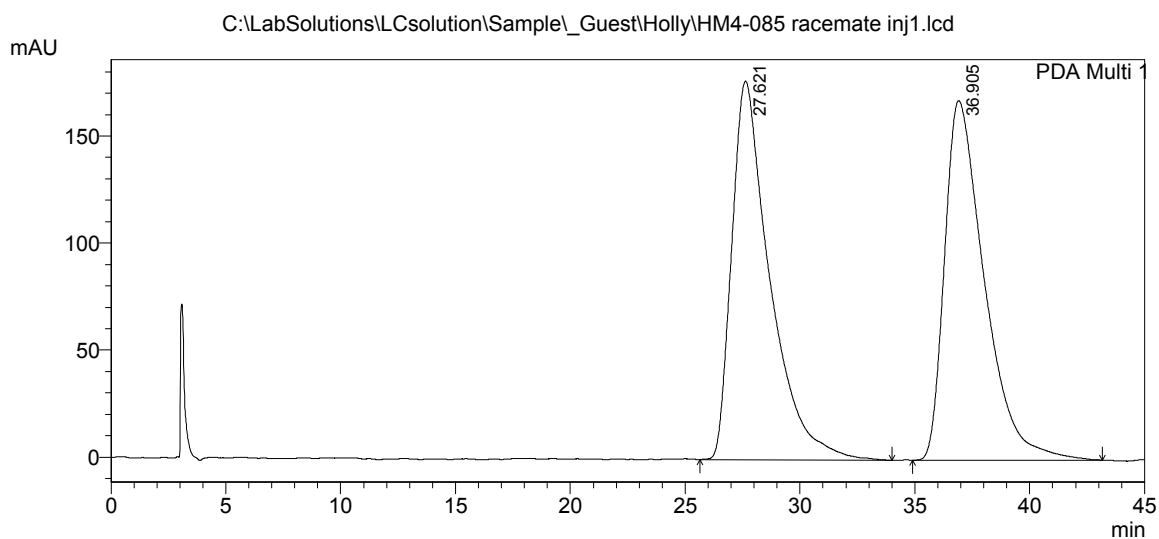
PDA Ch1 210nm 4nm

Peak#	Ret. Time	Area	Height	Area %	Height %
1	27.776	44466477	349325	92.469	92.717
2	37.308	3621372	27439	7.531	7.283
Total		48087849	376764	100.000	100.000

(±)-4-(3'-Bromo-5'-fluorophenyl)pyrrolidin-2-one (83)



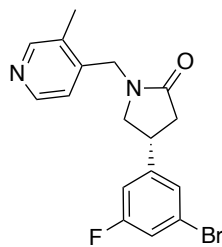
C:\LabSolutions\LCsolution\Sample_Guest\Holly\HM4-085 racemate inj1.lcd
Acquired by : Admin
Sample Name : HM4-085 racemate inj1
Sample ID : HM4-085 racemate inj1
Injection Volume : 20 uL
Data File Name : HM4-085 racemate inj1.lcd
Method File Name : AD-H_3%iPrOH-Hexane_1mL-min_40min.lcm
Data Acquired : 18/12/2020 11:25:53
Data Processed : 18/12/2020 12:20:46
HM4-085 racemate inj1
AD-H; IPA : Hex = 3 : 97 @ 1 ml/min 40 min



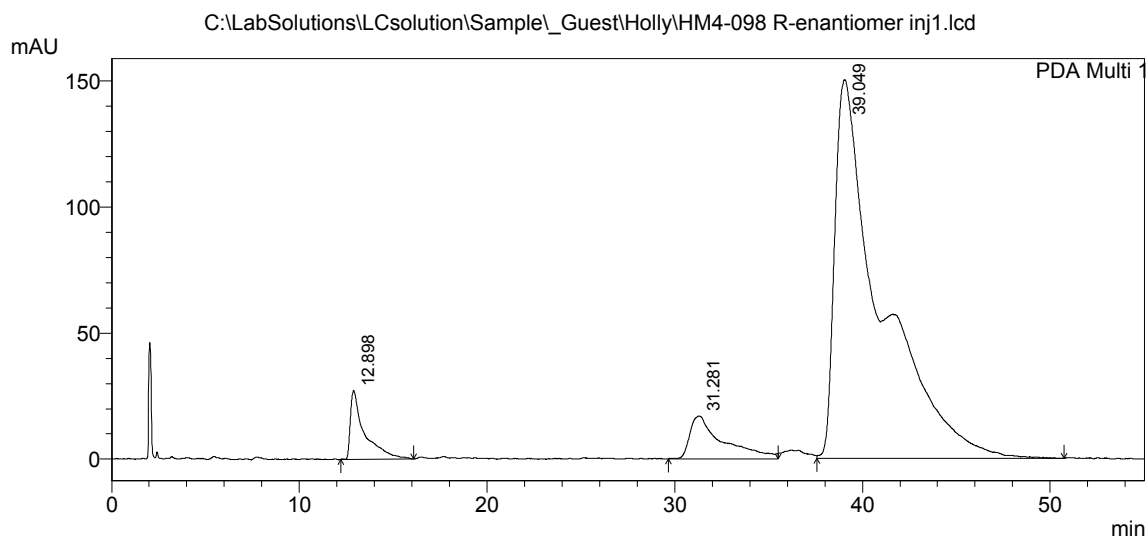
PDA Ch1 210nm 4nm

Peak#	Ret. Time	Area	Height	Area %	Height %
1	27.621	20445832	176929	50.219	51.279
2	36.905	20267282	168103	49.781	48.721
Total		40713113	345033	100.000	100.000

(4R)-4-(3'-Bromo-5'-fluorophenyl)-1-[(3''-methylpyridin-4''-yl)methyl]pyrrolidin-2-one ((R)-84)



C:\LabSolutions\LCsolution\Sample_Guest\Holly\HM4-098 R-enantiomer inj1.lcd
 Acquired by : Admin
 Sample Name : HM4-098 R-enantiomer inj1
 Sample ID : HM4-098 R-enantiomer inj1
 Injection Volume : 20 uL
 Data File Name : HM4-098 R-enantiomer inj1.lcd
 Method File Name : AD-H_8%*i*PrOH-Hexane_1.5mL-min_55min.lcm
 Data Acquired : 18/12/2020 14:53:27
 Data Processed : 18/12/2020 16:01:11
 HM4-098 R-enantiomer inj1
 AD-H; IPA : Hex = 8 : 92 @ 1.5 ml/min 55 min

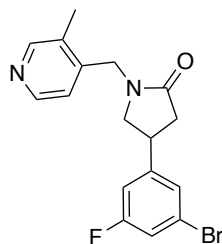


1 PDA Multi 1/210nm 4nm

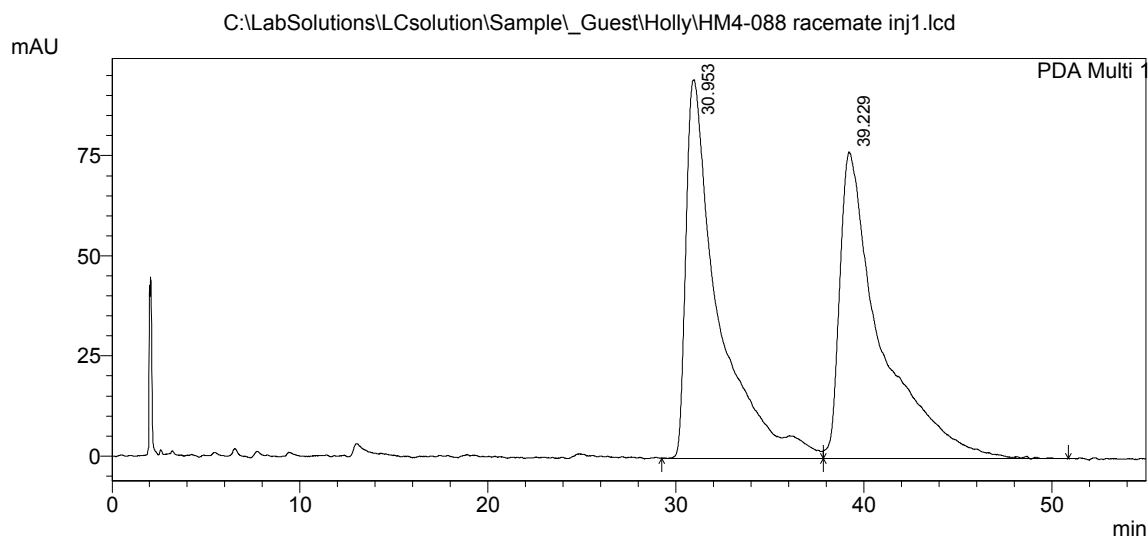
PDA Ch1 210nm 4nm

Peak#	Ret. Time	Area	Height	Area %	Height %
1	12.898	1436308	25415	4.938	13.214
2	31.281	2056643	16858	7.070	8.765
3	39.049	25596458	150059	87.992	78.021
Total		29089410	192332	100.000	100.000

(±)-4-(3'-Bromo-5'-fluorophenyl)-1-[(3''-methylpyridin-4''-yl)methyl]pyrrolidin-2-one (84)



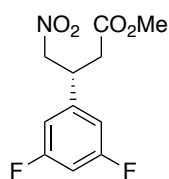
C:\LabSolutions\LCsolution\Sample_Guest\Holly\HM4-088 racemate inj1.lcd
 Acquired by : Admin
 Sample Name : HM4-088 racemate inj1
 Sample ID : HM4-088 racemate inj1
 Injection Volume : 20 µL
 Data File Name : HM4-088 racemate inj1.lcd
 Method File Name : AD-H_8%*i*PrOH-Hexane_1.5mL-min_45min.lcm
 Data Acquired : 18/12/2020 13:45:37
 Data Processed : 18/12/2020 14:40:38
 HM4-088 racemate inj1
 AD-H; IPA : Hex = 8 : 92 @ 1.5 ml/min 45 min



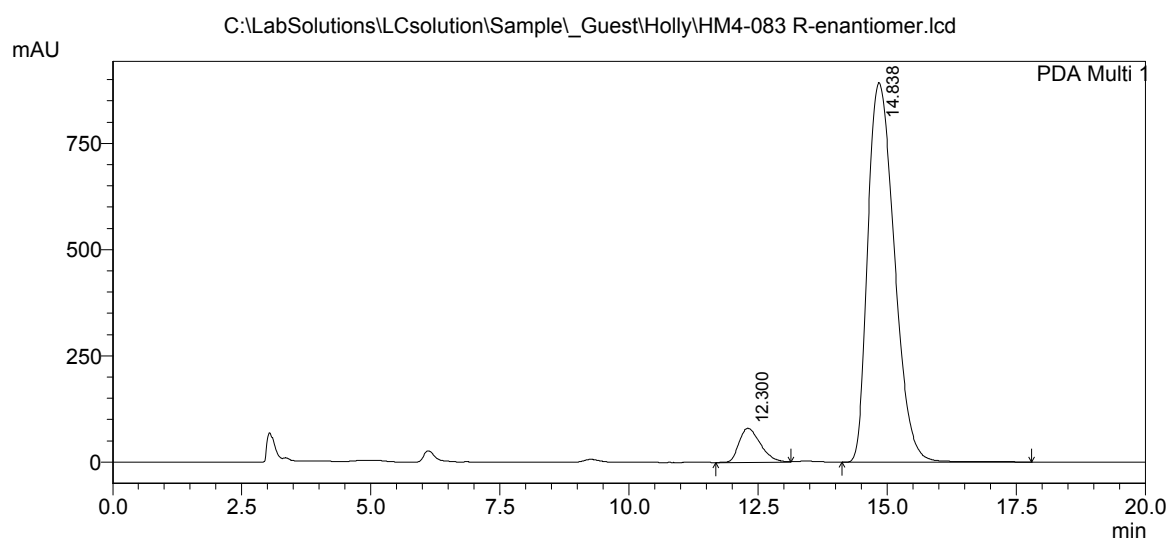
PDA Ch1 210nm 4nm

Peak#	Ret. Time	Area	Height	Area %	Height %
1	30.953	11331211	93949	49.477	55.280
2	39.229	11570971	76003	50.523	44.720
Total		22902182	169952	100.000	100.000

Methyl (3R)-3-(3',5'-difluorophenyl)-4-nitrobutanoate ((R)-103)



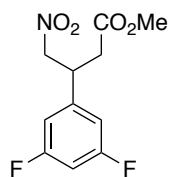
C:\LabSolutions\LCsolution\Sample_Guest\Holly\HM4-083 R-enantiomer.lcd
Acquired by : Admin
Sample Name : HM4-083 R-enantiomer
Sample ID : HM4-083
Injection Volume : 20 uL
Data File Name : HM4-083 R-enantiomer.lcd
Method File Name : AD-H_5%iPrOH-Hexane_1mL-min_20min.lcm
Data Acquired : 21/09/2020 15:00:29
Data Processed : 21/09/2020 17:02:30
HM4-083 R-enantiomer
AD-H; IPA : Hex = 5 : 95 @ 1mL/min for 20 min



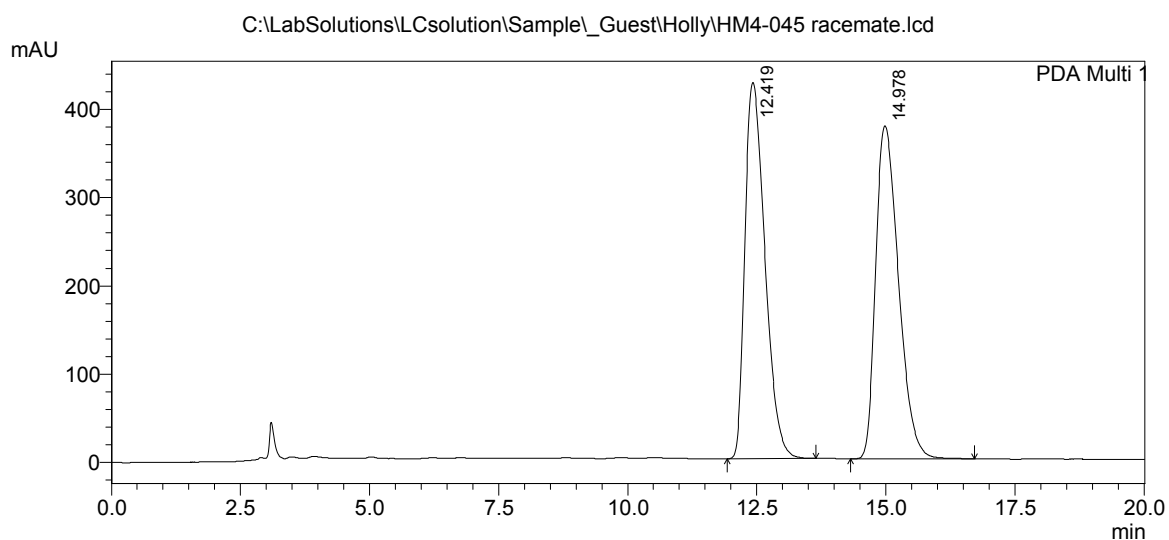
PDA Ch1 210nm 4nm

Peak#	Ret. Time	Area	Height	Area %	Height %
1	12.300	2344308	80172	6.816	8.236
2	14.838	32050660	893298	93.184	91.764
Total		34394969	973470	100.000	100.000

Methyl (±)-3-(3',5'-difluorophenyl)-4-nitrobutanoate (103)



C:\LabSolutions\LCsolution\Sample_Guest\Holly\HM4-045 racemate.lcd
Acquired by : Admin
Sample Name : HM4-045
Sample ID : HM4-045
Injection Volume : 20 uL
Data File Name : HM4-045 racemate.lcd
Method File Name : AD-H_5%iPrOH-Hexane_1mL-min_20min.lcm
Data Acquired : 21/09/2020 14:37:23
Data Processed : 21/09/2020 16:52:58
HM4-045 racemate
AD-H; IPA : Hex = 5 : 95 @ 1mL/min for 20 min

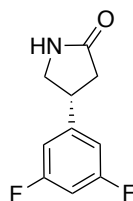


1 PDA Multi 1/210nm 4nm

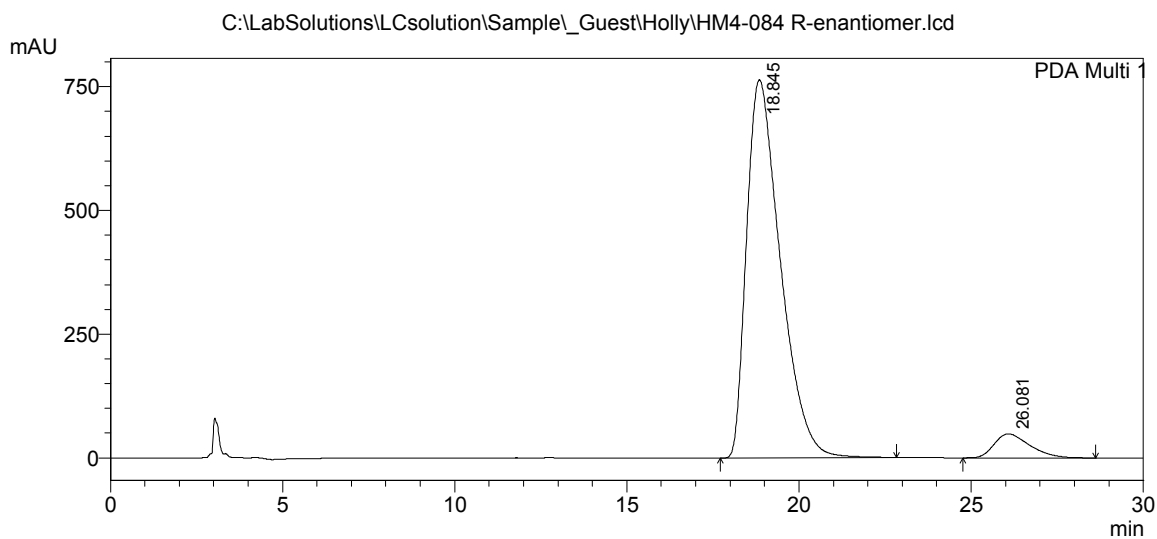
PDA Ch1 210nm 4nm

Peak#	Ret. Time	Area	Height	Area %	Height %
1	12.419	11512761	425916	49.770	53.047
2	14.978	11619386	376989	50.230	46.953
Total		23132147	802905	100.000	100.000

(4R)-4-(3',5'-Difluorophenyl)pyrrolidin-2-one ((R)-104)



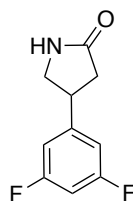
Acquired by : Admin
Sample Name : HM4-084 R-enantiomer
Sample ID : HM4-084 R-enantiomer
Injection Volume : 20 uL
Data File Name : HM4-084 R-enantiomer.lcd
Method File Name : AD-H_5%*i*PrOH-Hexane_1mL-min_30min.lcm
Data Acquired : 21/09/2020 16:04:56
Data Processed : 21/09/2020 17:09:50
HM4-084 R-enantiomer
AD-H; IPA : Hex = 5 : 95 @ 1mL/min for 30 min



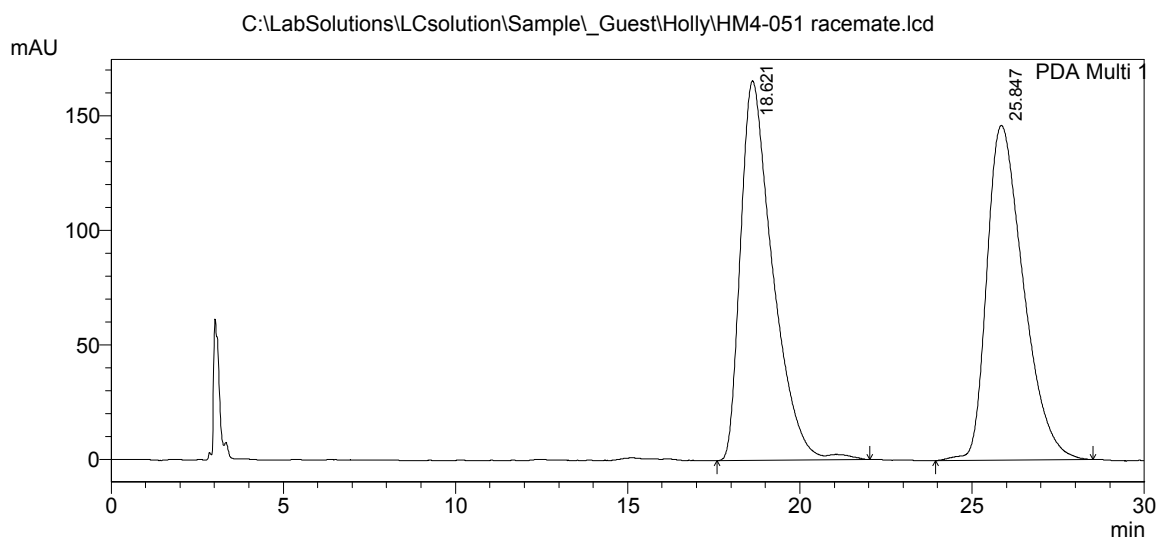
PDA Ch1 210nm 4nm

Peak#	Ret. Time	Area	Height	Area %	Height %
1	18.845	52112355	764235	93.708	94.021
2	26.081	3498905	48603	6.292	5.979
Total		55611260	812838	100.000	100.000

(±)-4-(3',5'-Difluorophenyl)pyrrolidin-2-one (104)



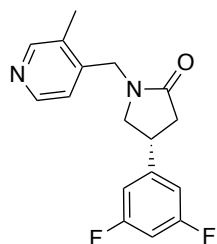
C:\LabSolutions\LCsolution\Sample_Guest\Holly\HM4-051 racemate.lcd
Acquired by : Admin
Sample Name : HM4-051 racemate
Sample ID : HM4-051 racemate
Injection Volume : 20 uL
Data File Name : HM4-051 racemate.lcd
Method File Name : AD-H_5%iPrOH-Hexane_1mL-min_30min.lcm
Data Acquired : 21/09/2020 15:26:07
Data Processed : 21/09/2020 17:05:10
HM4-051 racemate
AD-H; IPA : Hex = 5 : 95 @ 1mL/min for 30 min



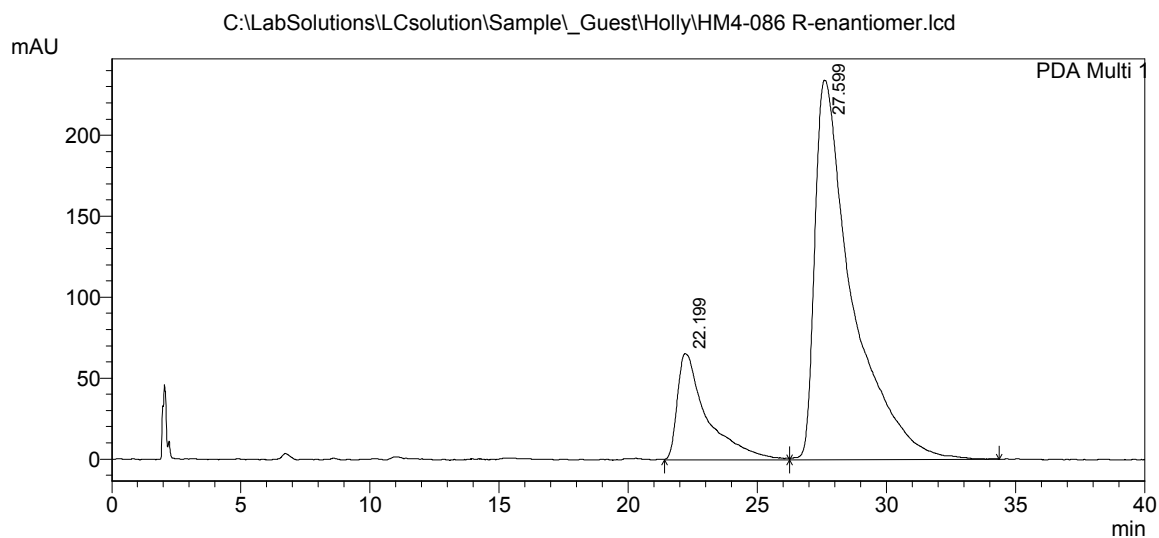
PDA Ch1 210nm 4nm

Peak#	Ret. Time	Area	Height	Area %	Height %
1	18.621	10707026	165585	49.838	53.127
2	25.847	10776588	146094	50.162	46.873
Total		21483614	311679	100.000	100.000

(4R)-4-(3',5'-Difluorophenyl)-1-[(3''-methylpyridin-4''-yl)methyl]pyrrolidin-2-one ((R)-24)



C:\LabSolutions\LCsolution\Sample_Guest\Holly\HM4-086 R-enantiomer.lcd
 Acquired by : Admin
 Sample Name : HM4-086 R-enantiomer
 Sample ID : HM4-086 R-enantiomer
 Injection Volume : 20 uL
 Data File Name : HM4-086 R-enantiomer.lcd
 Method File Name : AD-H_10%iPrOH-Hexane_1.5mL-min_40min.lcm
 Data Acquired : 25/09/2020 11:52:31
 Data Processed : 25/09/2020 12:48:08
 HM4-086 R-enantiomer
 AD-H; IPA : Hex = 10 : 90 @ 1.5 mL/min 40 min

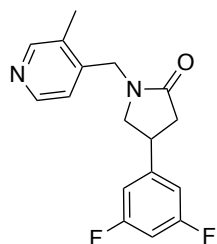


1 PDA Multi 1/210nm 4nm

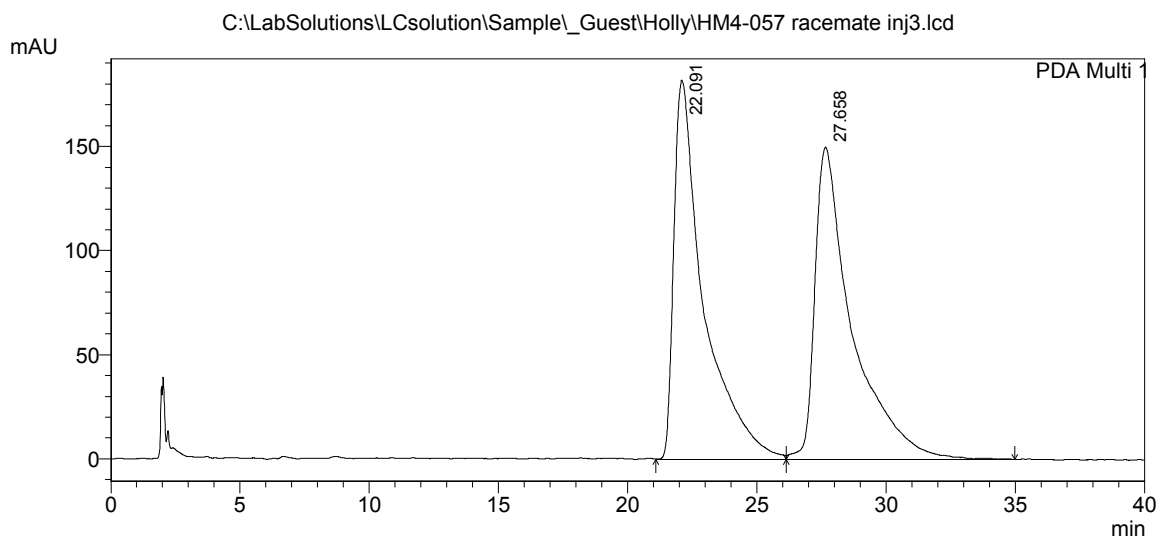
PDA Ch1 210nm 4nm

Peak#	Ret. Time	Area	Height	Area %	Height %
1	22.199	5270064	65819	18.299	21.927
2	27.599	23530368	234349	81.701	78.073
Total		28800432	300168	100.000	100.000

**(±)-4-(3',5'-Difluorophenyl)-1-[(3''-methylpyridin-4''-yl)methyl]pyrrolidin-2-one
(24)**



C:\LabSolutions\LCsolution\Sample_Guest\Holly\HM4-057 racemate inj3.lcd
 Acquired by : Admin
 Sample Name : HM4-057 racemate inj3
 Sample ID : HM4-057 racemate inj3
 Injection Volume : 20 uL
 Data File Name : HM4-057 racemate inj3.lcd
 Method File Name : AD-H_10%iPrOH-Hexane_1.5mL-min_40min.lcm
 Data Acquired : 25/09/2020 11:10:17
 Data Processed : 25/09/2020 11:56:22
 HM4-057 racemate inj3
 AD-H; IPA : Hex = 10 : 90 @ 1.5 mL/min 40 min



PDA Ch1 210nm 4nm

Peak#	Ret. Time	Area	Height	Area %	Height %
1	22.091	14525540	182076	49.299	54.822
2	27.658	14938711	150044	50.701	45.178
Total		29464251	332121	100.000	100.000